INTERNATIONAL SYMPOSIUM on
ADVANCED ENGINEERING & APPLIED MANAGEMENT
– 40th ANNIVERSARY in HIGHER EDUCATION (1970-2010)
4 – 5 November, 2010, Hunedoara, ROMANIA

[1] Camelia PINCA -BRETOTEAN, [2] Gelu-Ovidiu TIRIAN,
[3] Diana BISTRIAN, [4] Gladiola CHEȚE

DIMENSIONAL MATHEMATICAL MODEL TO OPTIMIZE THE PROCESSING MECHANISM OF TRANSLATIONAL ROTATING MOTION

[1.] UNIVERSITY POLITEHNICA OF TIMISOARA, FACULTY OF ENGINEERING FROM HUNEDOARA, ROMANIA

ABSTRACT:
The paper realized the analysis of the mechanisms eccentric cam with point of contact, the constructiv and functional point of view, consideringa mathematical model that allows a dimensional optimization. This paper reports the application of the Karush–Kuhn–Tucker method in the optimization process of a rotating cam dimensions. The problem was assessed both in analytical and numerical approaches.
KEYWORDS: Mechanism, cam, mathematical, model, dimensional, optimization

1. INTRODUCTION

Processing mechanisms of translational rotating motion are the cam and tachet mechanisms, [1], [2]. They belong to the upper bucket mechanisms and consist of a driver shaped element called cam, which is designed to transmit motion to another element of translational or oscillation motion, called tachet. Because movement can make any law by projecting properly any cam profile, these mechanisms are used in most areas of engineering (mechanical, textiles, fine mechanics, machine tools, internal combustion engines, and food engineering) which are necessary certain laws of motion technology or process required by mechanization and automation systems. It is recommended using these mechanisms because it has many advantages, such as: small dimensions, easy design, very good durability for complicated laws of motion, simple changes to the law of motion, relatively simple construction. The only disadvantage of these mechanisms is that superior coupling wear accidentally causing significant changes in the law of motion, noise, and vibration.

2. METHODOLOGY AND DISCUSSION

Rod push and cam mechanisms are part of the upper joints. They consist of a driver element having a profile, called cam and a driven element called rod push. The transmission from the driver element (cam) led to the component (rod push) is made by direct contact. This is a curve-shaped element, and it is well established and in close contact with the pusher motion. The pusher is made particularly by simple shapes: point-shaped planes, flat, circular (or roll), but may also have some curves and shapes. The laws of motion of the cam are usually those specific to the uniform movement, without acceleration. Standard laws of motion of pusher can be: linear, parabolic, co-sinusoidal, and sinusoidal; but there are also more complicated laws, such as power or exponential polynomials, etc. Because these mechanisms can perform any motion, by the appropriate design of the cam profile, they can be used in all engineering fields. Relative to the nature of the movement they are different: camshafts rotating basis related to the torque, the translational cam connected to the base by translational coupling, spinning translation cams, joint with a quadrilateral articulated rod. The pushers are the same: rotating (oscillating), translation or spinning translation [1], [2].

The main components of a cam mechanism and tachet are presented in fig.1. These three elements are denoted by 1, 2, 3; there are also three couplings: the A-rotation, B-top rotation and translation, the C-translation, [1], [2].

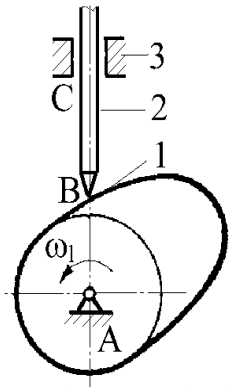

Fig.1 Components of cam mechanism with tachet
1-cam, 2-tachet, 3-layer; A-rotation, B-upper phase of rotation and translation, C-translatione.

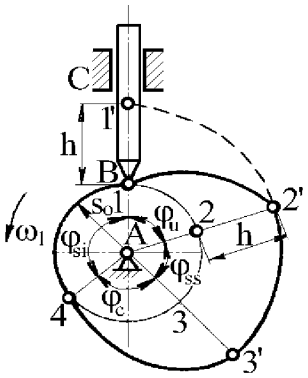

Fig.2 The phases of work of tha ca mechanism with tachet

A pusher moving from a position in a certain sense returns to the same position forming a kinematical cycle. This corresponds to a rotation of cam 360°.

The paper will analyze a cam mechanism and an eccentric translational tachet (point), which will create a dimensional optimization.

Phases of working mechanism are described in fig.2. They are:

- U - the climbing phase, when the pusher moves away from the rotation axis of the cam;
- SS - the upper stationary phase, when the pusher reaches the higher peak;
- C - the descent phase is the phase when the pushes gets closer to the rotation axis of the cam; and the lower stationary phase, when the pusher reaches its highest value.

In case of mechanisms with tachets reaching their highest values, the phase angle is the same with the cam angle.

If translational tip pushers, all operating parameters, established due to technological conditions are: h - the longest tachet pathway; the pusher cam angles covered by certain movements executed in accordance with technological requirements, called phase angles. Two of the phase angles are required: first of all, to climb the phase angle pusher away from the rotation axis of the cam, and the downhill phase angle, when the pusher approaches the rotation axis of the cam. Angles corresponding to the stationary phase are called stationary phase angles:

- superior stationary phase angle, when the pusher is situated to the maximum distance from the cam axis;
- angle of stationary phase, when the pusher is situated closer from the cam axis.

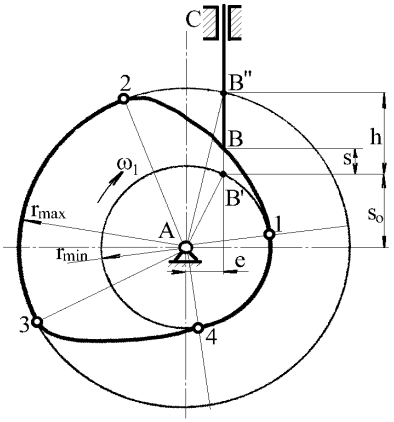

Fig. 3. The geometric parameters of the cam mechanism and eccentric tip translational tachet

When climbing, stroke size and phase angle influences on the pressure angle a lot, which is an important functional parameter. Pressure angle is defined as an acute angle formed between the load direction pusher motor speed and direction point of application of this force, which is identical to the relationship between the cam and the tachet.

Geometric parameters of cam mechanisms and eccentric tip translational tachet are shown in fig. 3.

Geometrical parameters of this mechanism are:

- S_o – the lowest distance from the contact point to the cam axis of rotation, measured on a parallel to the axis pusher;
- e - pusher eccentricity is the distance from the axis of rotation of the cam to the tachet.

Regarding the latter, cam gauge is determined using relations (1) and (2):

$$r_{\min} = \sqrt{s_o^2 + e^2} \quad (1)$$

$$r_{\max} = \sqrt{(s_o + h)^2 + e^2} \quad (2)$$

As shown in fig. 3 and equation (1), the cam minimum radius depends on *e* - the initial eccentricity and space. The calculation scheme to optimize the dimensions is shown in fig. 4.

The optimization problem is to minimize the radius "r_o". This is done in the presence of restrictions, which take account of maximum and minimum values of allowable pressure angles, the phase of lifting and lowering, respectively. Calculations were made following notations:

- S_1 - current area map of tachet lifting phase;
- S_3 - space to exit.

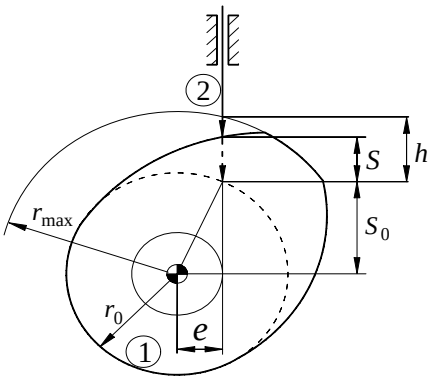

Fig. 4 Scheme of calculating the cam and tachet mechanisms

Lifting stage requires that the tangent of the angle of pressure, α, be lower or equal to the tangent of the biggest angle of pressure, α_{max}, namely:

$$\frac{\frac{dS_1}{d\varphi} - e}{S_0 + S_1} \le \tan(\alpha_{max}). \quad (3)$$

Descent phase requires that the tangent to the pressure angle be less than the smallest pressure angle tangent, α_{max}, namely:

$$\frac{\frac{dS_3}{d\varphi} - e}{S_0 + S_3} \ge \tan(\alpha_{min}). \quad (4)$$

The objective function describing the problem under consideration is the form given in equation (5):

$$f(S_0, e) = S_0^2 + e^2 \quad (5)$$

We obtain restrictions optimization problem (6) and (7) from relations (3) and (4).

$$g_1 = \frac{dS_1}{d\varphi} - e - (S_0 + S_1)\tan(\alpha_{max}) \le 0; \quad (6)$$

$$g_2 = (S_0 + S_3)\tan(\alpha_{min}) - \frac{dS_3}{d\varphi} + e \le 0, \quad (7)$$

Karush–Kuhn–Tucker (KKT) conditions [4], generalize the Lagrange method for finding the extrema of a function subject to a family of constraints. While Lagrange multipliers consider only equality constraints, KKT conditions allow for general inequality constraints [3], [5]. In [6], for example, has implemented and tested a modified version that outperforms every other tested method in terms of efficiency, accuracy, and percentage of successful solutions, over a large number of test problems.

Considering the problem of finding the extreme of a multivariate function " f " subject to a family of constraints χ_i, $1 \le i \le m$, where χ_i are inequalities of the form $g_i \le \nu_i$. Expressing the inequality constraints in the form $\chi_i \equiv g_i - \nu_i \le 0$, the Lagrange function is defined as:

$$L(x, \mu) = f(x) + \sum_{1 \le i \le m} \mu_i \left(g_i(x) - \nu_i \right). \quad (8)$$

A point x^* is said to be feasible point if it satisfies all the inequality constraints. Assume the vector $x^* = (x_1^*, \ldots x_n^*)$ minimizes the continuous function f subject to the constraints $\chi_i \equiv g_i(x) - \nu_i \le 0$, $1 \le i \le m$, than the vectors $\left(\nabla g_i(x^*)\right)_{1 \le i \le m}$ are linearly dependent, or there exists a vector $\mu^* = (\mu_1^*, \ldots \mu_m^*)$ which is an optimal solution for the original optimization problem satisfying the following KKT conditions

$$\nabla L(\mu^*, x^*) = 0 \quad \Leftrightarrow \quad \left(\frac{\partial L}{\partial x_i}(x^*) = 0 \right)_{1 \le i \le n} \quad (9)$$

$$\mu^* \left(g_i(x^*) - \nu_i \right) = 0, \quad g_i(x^*) \le \nu_i, \quad \mu_i \ge 0 \quad (10)$$

where ∇ is the gradient. The condition $\mu_i \ge 0$ implies non negative Lagrange multipliers and the relation $\mu^* \left(g_i(x^*) - \nu_i \right) = 0$ generates two cases

$$g_i(x^*) = \nu_i \quad (11)$$

$$g_i(x^*) < b_i \Rightarrow \mu_i = 0 \quad (12)$$

We consider the transmission function of growth (lifting) phase $S_1(\varphi) = h \sin(\varphi)$ and the transmission function of descending phase $S_3(\varphi) = h\left[1 - \sin(\varphi)\right]$, fig. 5.

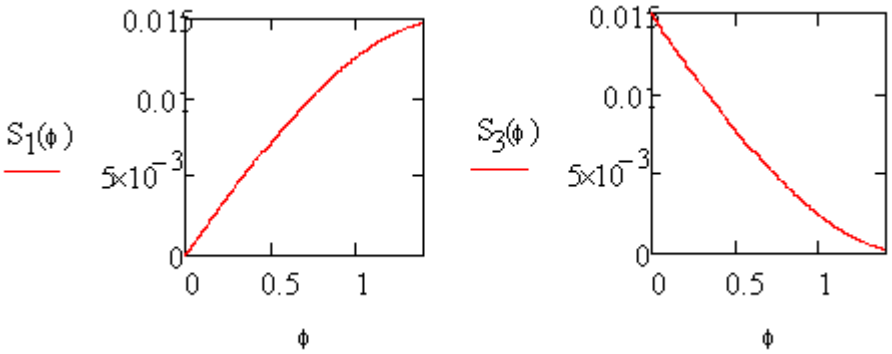

Fig. 5. The transmission function of lifting phase (left) and the transmission function of descending phase (right)

In the lifting phase, the tangent of the pressure angle must be less or equal then the tangent of the utmost pressure angle α_{max} and in the descending phase the tangent of the pressure angle must be grater or equal than the tangent of the least pressure angle α_{min}, leading to the inequalities:

$$\frac{dS_1}{d\varphi} - e \le (S_0 + S_1)\tan(\alpha_{max}) \text{ and } \left.\frac{dS_1}{d\varphi}\right|_{\varphi=\varphi_1} - e = (S_0 + S_1)\tan(\alpha_{max}) \tag{13}$$

$$\frac{dS_3}{d\varphi} - e \le (S_0 + S_3)\tan(\alpha_{min}) \text{ and } \left.\frac{dS_3}{d\varphi}\right|_{\varphi=\varphi_3} - e = (S_0 + S_3)\tan(\alpha_{min}) \tag{14}$$

We consider the objective function presented in relation (5) $f(S_0, e) = {S_0}^2 + e^2$, where e represents the eccentricity and S_0 is the initial space, which should be minimized subject to the following constraints:

$$\chi_1 \equiv h\cos(\varphi_1) - \tan(\alpha_{max})\left[S_0 + h\sin(\varphi_1)\right] - e \le 0 \tag{15}$$

$$\chi_2 \equiv e + h\cos(\varphi_3) + \tan(\alpha_{min})\left[S_0 - h\left(\sin(\varphi_3) - 1\right)\right] \le 0 \tag{16}$$

The KKT conditions state the following necessary conditions for a feasible point $x^* = (S_0^*, e^*, \varphi_1^*, \varphi_3^*)$ be a local optimal solution point:

$$\nabla f(x^*) + \sum_{i=1}^{2} \mu_i \nabla \chi_i(x^*) = 0, \tag{17}$$

$$\chi_1(x^*) \le 0, \quad \chi_2(x^*) \le 0, \tag{18}$$

in terms of a Lagrangean function defined as follows:

$$L(S_0, e, \varphi_1, \varphi_3, \mu_1, \mu_2) = f(S_0, e) + \mu_1\chi_1(S_0, e, \varphi_1, \varphi_3) + \mu_2\chi_2(S_0, e, \varphi_1, \varphi_3) \tag{19}$$

The necessary conditions given by equation (17) can be restated in a compact formulation as $\nabla_x L(x^*, \mu^*) = 0$. We define the vectors:

$$\nabla f \equiv 2\begin{bmatrix} S_0 \\ e \\ 0 \\ 0 \end{bmatrix}, \tilde{\chi}(S_0, e, \varphi_1, \varphi_3) = \begin{bmatrix} \chi_1(S_0, e, \varphi_1, \varphi_3) \\ \chi_2(S_0, e, \varphi_1, \varphi_3) \end{bmatrix}, H(S_0, e, \varphi_1, \varphi_3) = \begin{bmatrix} \nabla\chi_1 \\ \nabla\chi_2 \end{bmatrix},$$

where:

$$\nabla\chi_1 \equiv \begin{bmatrix} -\tan(\alpha_{max}) \\ -1 \\ -h\sin(\varphi_1) - h\cos(\varphi_1)\tan(\alpha_{max}) \\ 0 \end{bmatrix}, \nabla\chi_2 \equiv \begin{bmatrix} \tan(\alpha_{min}) \\ 1 \\ 0 \\ -h\sin(\varphi_1) - h\cos(\varphi_1)\tan(\alpha_{min}) \end{bmatrix}$$

The equations of the constrained optimization problem are translated in the following form:

$$\begin{aligned} &\nabla f\left(x^*\right)^T + \boxed{H}\left(x^*\right)^T \mu^* = 0, \\ &\tilde{\chi}\left(x^*\right)^T \mu^* = 0, \\ &\mu^* \geq 0, \end{aligned} \tag{20}$$

with $x^* = \left(S_0^*, e^*, \varphi_1^*, \varphi_3^*\right)$ and $\mu^* = \left(\mu_1^*, \mu_2^*\right)$.

To rezolve the optimization model for the mechanism considered these stages are known lifting height of the pusher:

$h = 0.015$ m – lifting height of the pusher;

$\varphi_1 = 80^\circ$ - angle of rotation of the cam corresponding lifting phase;

$\varphi_2 = 20^\circ$ - angle of rotation of the cam corresponding to the upper stationary phase;

$\varphi_3 = 80^\circ$ - angle of rotation of the cam corresponding to the descendent phase;

- transmission function for the ascendent phase, sinusoidal;
- transmission function for the desscendent phase, sinusoidal.

Starting the computation with the initial solution $S_0 = 0.02$, $e = 0.002$, $\varphi_1 = 0.6$, $\varphi_2 = 3.1$, $\mu_1 = \mu_2 = 0.1$, the feasible point is calculated as:

$$x^* = \begin{pmatrix} S_0^* = \mathbf{0.01398937243798}, \\ e^* = \mathbf{0.003998901367188}, \\ \varphi_1^* = \mathbf{1.599993896484375}, \\ \varphi_3^* = \mathbf{2.792587280273438} \end{pmatrix} \tag{21}$$

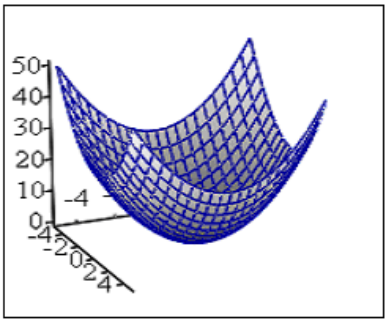

f

Fig. 6. The response surface of the objective function

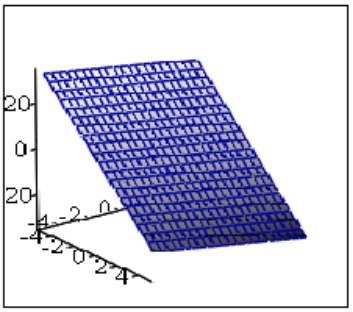

χ 1

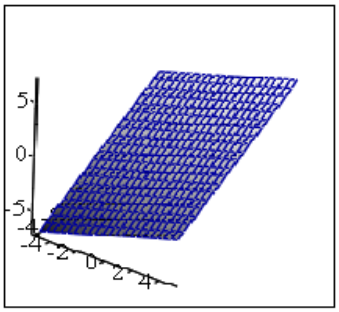

χ 2

Fig.7. The constrained planes for optimal angles $\chi_1\left(S_0, e, \varphi_1^*, \varphi_3^*\right)$ (left) and $\chi_2\left(S_0, e, \varphi_1^*, \varphi_3^*\right)$ (right)

The response surface determined by the objective function defined in (5) is depicted in fig. 6. Setting the optimal rotating angles to φ_1^* and φ_2^* respectively , the constrained surfaces become two constrained planes, which are presented in fig. 7.

3. CONCLUSIONS

This paper reports the application of the Karush–Kuhn–Tucker method in the optimization process of a rotating cam dimensions.

The problem was assessed both in analytical and numerical approaches. The mathematical states of the method is described and the Karush–Kuhn–Tucker conditions of the constrained optimization are translated into a structure containing the objective function, the matrix for the inequality constraints, lower and upper bounds for the feasible point. The strategy for numerically implementation was to transform the problem into an easier subproblem that can then be solved and used as the basis of an iterative process. By assuming that the bound constraints have been expressed as inequality constraints we obtained the subproblem by linearizing the nonlinear constraints.

REFERENCES

[1.] Antonescu P., s.a., Mecanisme, Editura Printech Bucureşti, 2000.
[2.] Bratu I., Rus A., Mecanisme. Aplicaţii , Editura Universităţii din Oradea, 2003
[3.] Conn A.R,. Gould, Ph. L. Toint."A Globally Convergent Augmented Lagrangian Pattern Search Algorithm for Optimization with General Constraints and Simple Bounds", SIAM Journal on Numerical Analysis, Volume 28, Number 2, pages 545–572, 1991.
[4.] Lewis, R. M., Torczon V., "A Globally Convergent Augmented Lagrangian Pattern Search Algorithm for Optimization with General Constraints and Simple Bounds", SIAM Journal on Optimization, Volume 12, Number 4, pages 1075–1089,2002.
[5.] Malacaria P., Han Chen: Lagrange Multipliers and Maximum Information Leakage in Different Observational Models. In Proc. PLAS 2008, ACM.
[6.] Schittkowski, K., "NLQPL: A FORTRAN-Subroutine Solving Constrained Nonlinear Programming Problems," Annals of Operations Research, Vol. 5, pp. 485-500, 1985.

INTERNATIONAL SYMPOSIUM on
ADVANCED ENGINEERING & APPLIED MANAGEMENT
– 40th ANNIVERSARY in HIGHER EDUCATION (1970-2010)
4 – 5 November, 2010, Hunedoara, ROMANIA

[1.]Mihaiela ILIESCU, [2.]Marian LAZĂR, [3.]Victor GRIGORE

RESEARCHES ON TRUE PULSE LASER MICRO-WELDING

[1.]UNIVERSITY POLITEHNICA OF BUCHAREST, MANUFACTURING DEPARTMENT, ROMANIA
[2-3.]S.C. OPTOELCTRONICA 2001, S.A., MĂGURELE, ROMANIA

ABSTRACT:
Microwelding represents an important machining method that, theoretically, requires special technological equipment. Also, the involved „working" parameters must be set to their appropiate values, depending on material's type, workpiece's thickness, welding's required characteristics, etc. [2].
Some preliminary research results on Nd: YAG laser microwelding are going to be presented above, for some specific type materials (alluminium alloy, stainless steel, copper-zinc alloy), while the technological equipment is a „combination" of two already existing ones: Trumf laser and Isel CNC machine.
KEYWORDS:
microwelding, preliminary research results

1. INTRODUCTION

Laser Beam Machining (LBM) is highly used in top industrial fields (aerospace, nuclear), because of, both, tough characteristics of the involved materials and required machining complexity (high geometrical precision, such as x100 or, x 10 μm).

The applicability of this machining method is due to laser beam's specific properties, such as: one direction; intensity; monochromatics; amplifying when passing through different environments, coherent light and high energy density.

Laser beam represents an „universal tool" used in micromachinig (welding, drilling, cutting, engraving, deposition, etc.) one of its important characteristics being the lack of direct physical contact tool – workpiece. As consequence, there are no machining forces on the workpiece and no wear of the tool [1]

When laser micromachinig ther is no absolute request for void equipment, thermal influenced zones can be neglected and thermal deformations are very small, while the machined materials can be tough, extra-tough or, fragile ones.

Microwelding represents an important machining method that, theoretically, requires special technological equipment. Also, the involved „working" parameters must be set to their appropiate values, depending on material's type, workpiece's thickness, welding's required characteristics, etc. [2]. Some preliminary research results on Nd: YAG laser microwelding are going to be presented above, for some specific type materials (alluminium alloy, stainless steel, copper-zinc alloy), while the technological equipment is a „combination" of two already existing ones: Trumf laser and Isel CNC machine.

2. METHOD AND EQUIPMENT

When laser machinig, there has to be defined two important parameters [1]:
- spot diameter obtained in lens focus:

$$d_0 = \frac{\frac{4}{\pi} f\lambda}{D} \qquad [\mu m] \qquad (1)$$

where: f is lens focal distance [mm]; D – lens opening [mm]; λ – wave length of emitted radiation [μm].

- power maximum density in lens focus.

$$W_P = \frac{P}{10^2 \lambda^2} \quad [W/cm^2] \tag{2}$$

where: P represents the power emitted by laser radiation [W].

There are also some other laser beam specific parameters that do influence the machining process, meaning:

- *power* – determines the penetration depth;
- *power density / intensity* – is dependent on cross section of the laser beam;
- energy – determines the volume of molten material and can be calculated by:

→ the product of power and laser – material intaraction time,

or

→ the product of power and pulse duration.

Laser (micro)machining is based on two main phenomena: material's melting and vaporisation when the laser beam impacts the work-piece surface by spot focusing. Each material has a specific value of density power when vaporisation starts, for example: alluminium – $W_{PS}=2Ý10^5 W/cm^2$, iron / steel – $W_{PS}=1,2Ý\ 10^5\ W/cm^2$ etc.

So, radiation penetration depth can be determined by:

$$h = v \cdot t_i \quad [mm] \tag{3}$$

where: v represents prelevation speed; t_i – pulse duration

$$h = v \cdot t_i \quad [mm] \tag{4}$$

This paper presents experimental results in laser microwelding , the equipment used being made of the following ones.

A. Laser central unit TruePulse 62 – see figure 1

This is a Nd: YAG laser type, that generates intense invisible radiations, with wavelength „close to" infrared radiations.

Some of its technical charactersitics, as mentioned by the producer, are presented in table 1.

Laser lenses can be used for radiation wavelength values from 1030 nm to 1064 nm.

Fig.1 Laser optical unit True Pulse [4]

Tabel 1 [4]

Characteristics	Values
- Rradiation wave length	1064 nm
- Medium power	65 W
- Pulse minimum power	250 W
- Pulse maximum power	5000 W
- Pulse minimum duration	0,2 ms
- Pulse maximum duration	50 ms
- Pulse maximum energy	50 J
- Maximum frequency of pulse repetition	900 Hz
- Laser beam quality	8 mm mrad

B. Isel-automation machining systems [5] - systems made of three main components: isy CAM software, ProNC software and Flatbed or Euromod basic units.

An image of its basic unit – used in experiments can be seen in fig. 2.

Fig.2 Isel Flatbed unit [5]

3. EXPERIMENTS

There are many factors that do influence laser micro-welding process, some being: material's type, laser beam power density, pulse duration and shape, shielding gas etc.

Even the process is rather complex, it has many advantages, the main ones dealing with: welding materials with different physical – chemical properties; welding in hard accessible zones and positions – by laser beam focusing with lenses; or, by allowing its pass through medium that are transparent with respect to laser radiation wavelength, etc.

Mainly, there are two micro-welding principles, one is *conduction* (the heat source generated by laser beam absorption is localised on work-piece surface, where melting starts - see fig. 3) and the other is *penetration* (melting temperature is above evaporation value and so, into the metal it is generated an absorbent cavity full of ionized metallic gas - see fig. 4).

The exepriments used penetration micro-welding so, high depth and very narrow welding belt could be obtained. The Nd:YAG laser was used in CW mode CW (continuous wave) . Images taken while micro-welding experiments are presented in fig. 5, 6 and 7 – there can be noticed both values of the laser beam parameters, and images of the welding belt of the work-piece.

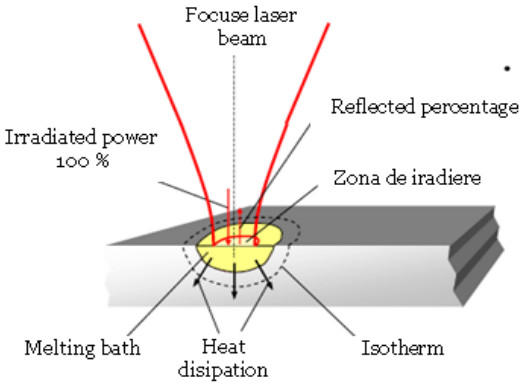

Fig. 3 Micro-welding by thermal conduction

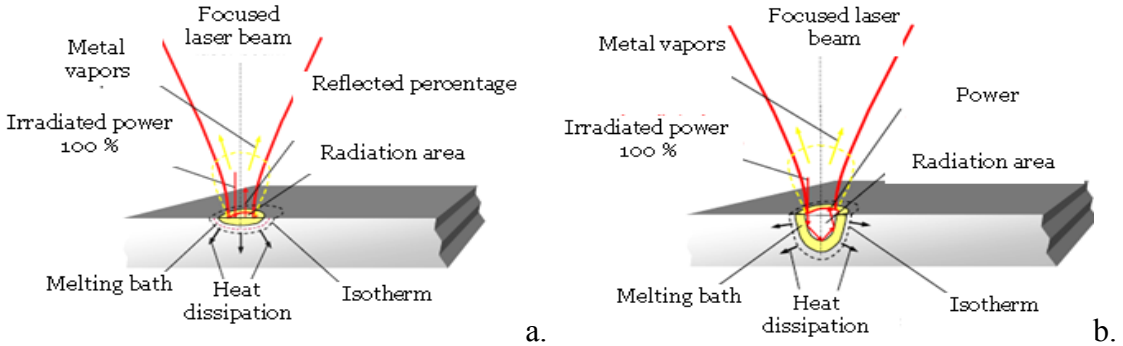

Fig. 4 Micro-welding by penetration

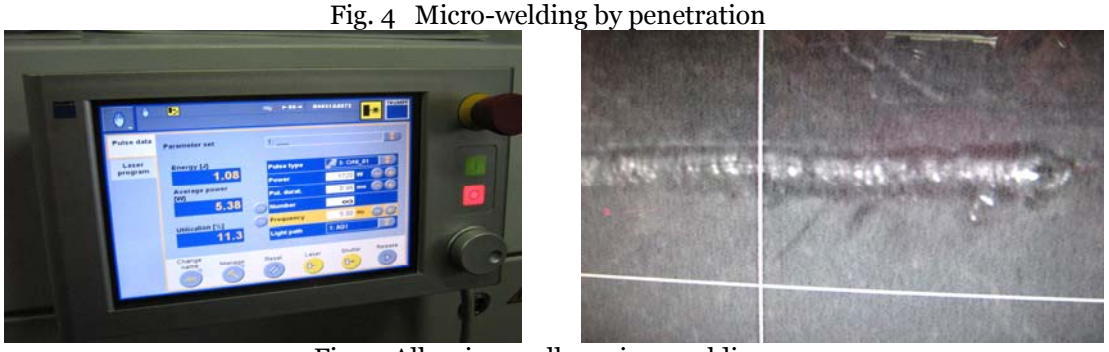

Fig. 5. Alluminum alloy micro-welding

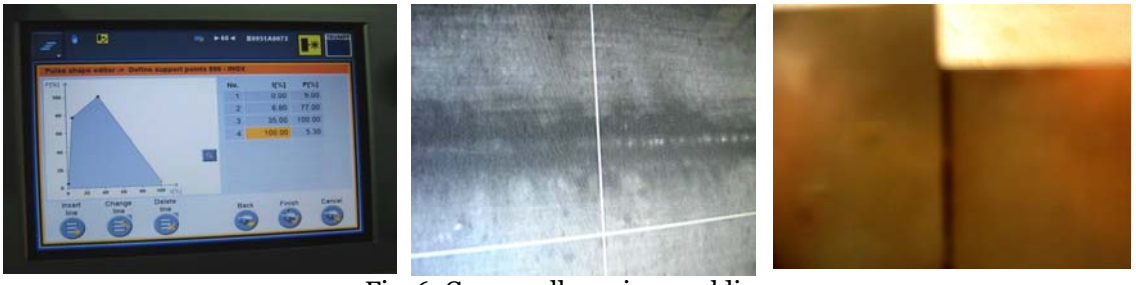

Fig. 6. Copper alloy micro-welding

Fig. 7. Stainless-steel micro-welding

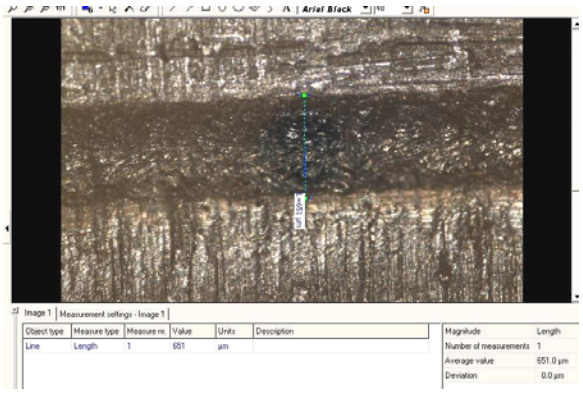

Alluminum alloy welding belt width: 651 μm

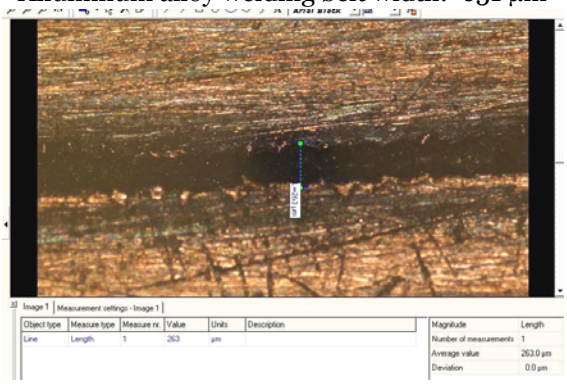

Copper alloy welding belt width: 263 μm

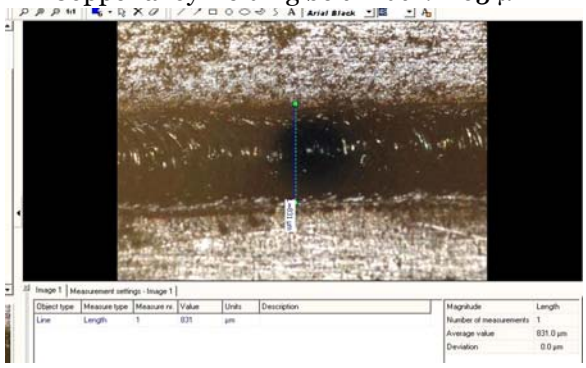

Stainless steel welding belt width: 831 μm

Fig. 8. Microscope images of the welding belts

It has to be pointed out the fact that even some orientative values of laser beam parametrs in micro-welding are presented in specific references, if considering them exactly, no good results are obtained. So, it was necessary to make experiments with specific materials and existing equipment – and the results to be further used in industrial application.

The laser head (on TruePulse 62) is the one generating radiation (for micro-), and the CNC machine (Isel Flatbed) allows computer aided welding - on various complex trajectories and high precision (1 μm) [3].

Images of microscope checking on the welding belts width (that points out the micro- charactersitic) are presented in figure 8.

4. CONCLUSION

Laser Beam Machining is highly used in top indutrial fields. When machinig materials, welding is an important method.

Some orientative values of laser beam parametrs in micro-welding are presented in specific references, but, no good results are really obtained, if considering.

It was necessary to make experiments with specific materials and existing equipment – and the results are further used in industrial application.. The material testec were:alluminum alloy, copper alloy and stainless steel.

Further research must be developped – based on design of experiments and specific software so that, if possible, regression models of micro-welding parameters and welding belt's characteristics, to be obtained.

The results presented by this paper are part of the Research Project on Innovation no. 229/2008.- Advanced Micro-Technologies on Laser Machining

REFERENCES:

[1.] Marinescu N., Nanu D., ş.a., „Procese de prelucrare cu fascicule şi jeturi", INOE, Bucureşti, 2000, ISBN 973-98742-6-6 ;
[2.] Yi Qin, „Micromanufacturing Engineering and Technology", William Andrew Inc., USA, 2008
[3.] Iliescu M., „Computer Aided Technolgies (CAD, CAM and CNC) Important Means in Developing an Inniovative Machinig Force's Measuring Mevice", Metalurgia International, no. 7/ /2010, ISSN 1582-2214
[4.] www. us.trumf.com, accessed, september, 2010
[5.] www.isel.com, accessed, september, 2010

INTERNATIONAL SYMPOSIUM on
ADVANCED ENGINEERING & APPLIED MANAGEMENT
– 40th ANNIVERSARY in HIGHER EDUCATION (1970-2010)
4 – 5 November, 2010, Hunedoara, ROMANIA

[1.]Carmen Inge ALIC, [2.]Cristina Carmen MIKLOS, [3.]Imre Zsolt MIKLOS

FINITE ELEMENT ANALYSIS OF A SEAT BELT BUCKLE DEVICE

[1-3.] UNIVERSITY „POLITEHNICA" TIMIŞOARA, FACULTY OF ENGINEERING HUNEDOARA, ROMANIA

ABSTRACT:
In the last years, there has been rapid and extensive progress in automotive technologies. These technical advances include devices that provide increased protection for the occupants of the vehicle in case of crash and systems that allow drivers to avoid collisions, or at least to mitigate their severity. Integrated systems for restraining the occupant, used in automotive applications, have shown to improve the safety of the occupant and to decrease the risk of injury during impacts of motor vehicles.
Although safety belts and air bags are always been considered among the primary safety devices, today the seat belt system is widely regarded as being the most important element of safety equipment in a vehicle.
In the first section of this paper, the most important elements of the safety equipment in a vehicle are described. The second section presents the modeling, analysis and evaluation techniques for the Seat Belt Buckle Assembly strength, used in order to ensure the safety of the occupants in conditions of impact. Proper design of the seat belt buckle assembly is crucial, as in case the seat belt buckle assembly can not endure the load that was derived by the motion of an occupant during an impact, the seat belt system can not play the role of a restraining system anymore. In order to perform this analysis and evaluate the strength, we examine the effectiveness of a latch plate as component of the seat belt buckle assembly, using the finite element analysis method.
KEYWORDS:
safety device, safety belt system, seat belt buckle assembly, finite element analysis

1. INTRODUCTION AND CONTEXT

Vehicle crashworthiness and occupant safety remain among the most important and challenging design considerations in the automotive industry. In the recent years, there has been rapid and extensive progress in automotive technologies, especially with respect to electronic sensing and control systems, which allowed engineers to develop a wide range of "high-tech" safety systems. These include devices that provide increased crash protection for vehicle occupants, and systems that may allow drivers to avoid collisions or, at least, to mitigate their severity. Some of these systems, described in Fig.1, are available as standard equipment on new vehicles, while others involve additional costs, as part of specific and optional equipment packages on certain vehicle models.

The most important safety devices are considered today the Safety belts and Air bags (Fig.2) which save thousands of lives each year (for example, according to the reports [5], the use of seat belts in 2009 saved an estimated of 12,713 lives). The air bag is a proven and effective safety device, but it doesn't replace a seat belt. Air bags are designed to work only with seat belts, because if an occupant doesn't wear his seat belt, he could be thrown into a rapidly opening frontal air bag and a movement of such force could injure or kill him. Consequently, the seat belt system is widely regarded today as being the most important element of safety equipment in a vehicle. When used according to [1], seat belts are approximately 45% effective at preventing fatal injuries and 67% effective at preventing serious injuries. Moreover, nearly all safety experts agree that buckling up dramatically increases the chances of surviving an accident, and those seat belts reduce the risk of death for a front seat car occupant by about 50 percent.

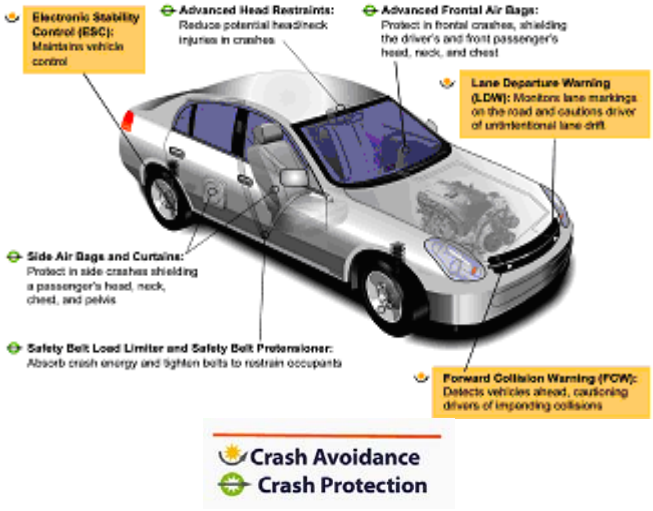

Fig.1 Safety technologies: Crash Avoidance and Crash Protection

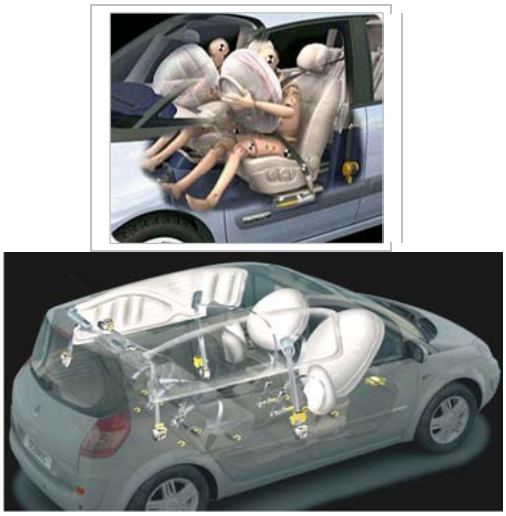

Fig.2 Safety belts and air bags

Despite this safety record, the performance of the belt systems is continuously being refined. Recent papers discuss the development of 4-point harnesses for use in production vehicles [2], [3], while devices such as pretensioners and belt load limiters [4] are becoming common features in contemporary vehicles.

The development and the evaluation of protection measures against the effects of accidents, require an accurate assessment of the operational behavior in the exploitation of safety systems, and involve a good knowledge of the tolerance of the human body, as well as its mechanical response to impact.

2. PRESENTATION OF THE STUDIED SAFETY BELT SYSTEM

2.1 Standard three-point safety belt system

The safety belt, also called seat belt, is part of an overall occupant restraint system. This is intended to reduce injuries by stopping the wearer from hitting hard interior elements of the vehicle or other passengers, respectively the so-called second impact [6], and by preventing the passenger from being thrown-out from the vehicle. A properly secured seat belt offers protection in head-on, side and rollover collisions, by securing in the life space of the vehicle. In fact, the belts system help spread out the energy of the moving body in a collision over the chest, pelvis, and shoulders.

a.

b.

c.

d.

Fig.3. Standard three-point seat belt system and its components

The standard three-point belts shown in Fig. 3a, attaches to the car in three places, two mount near the rear of the seat bottom and one towards the top of the side pillar, offering a maximum of comfort and convenience. The seat-belt latch plate clips into a buckle Fig.3b, which in the front seats of cars is usually placed at the end of a stiff stalk. A pretensioner Fig.3c, and a

retractor device Fig.3d, are included as part of the safety belt system. In the event of an impact, the safety belt system is designed to grip the belt and not allow the occupant to travel forward any more than they already are.

The seat belt buckle assembly, Fig.3b, must be able to withstand extremely high loads during a crash, and at the same time it must be easy to open even when heavily loaded. Moreover, the buckle assembly must withstand high accelerations in all direction without opening. This feature is critical when the seatbelt system includes a pretensioner, as such a pyrotechnic device pulls rapidly the buckle in one direction towards the floor and then the pulling force suddenly switches in the other direction. (Fig.4)

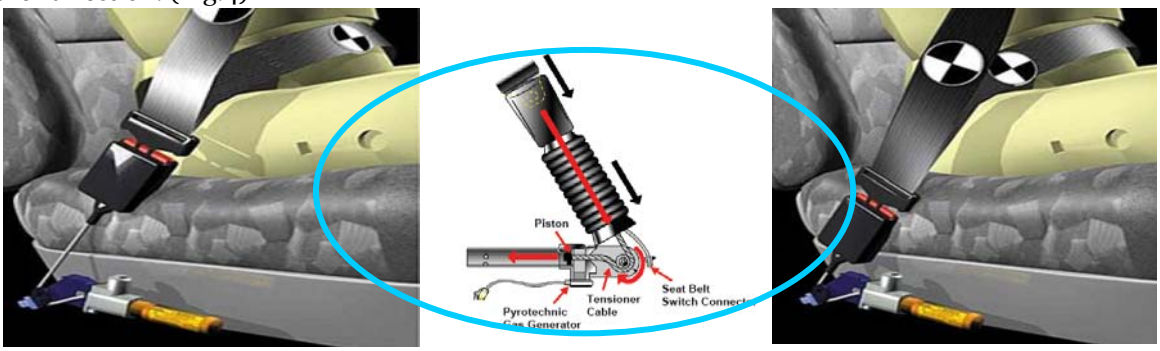

Fig.4 Functions and operating mode of a pyrotechnic pretensioner

2.2 Faulty Seat Belts

If the seat belt buckle can not endure the load that was derived by the motion of an occupant motion during a frontal impact, the seat belt can not do the role of a restraint system any more. Thus, proper strength of a seat belt buckle is essential in the case of a frontal impact.

In general, motor vehicle safety teams check the performance of their equipment to protect the occupant against unreasonable risk of accidents and of death or injury in an accident. In this context, a safety defect is defined as a problem that exists in a motor vehicle or in its equipments and that: poses a risk to motor vehicle safety; may exist in a group of vehicles of the same design or manufacture, or in items of equipment of the same type and manufacture.

Examples of defects considered safety-related to a vehicle occupant, are listed below:

- Critical vehicle components that break, fall apart, or separate from the vehicle, causing potential loss of vehicle control or injury to persons inside or outside the vehicle.
- Seats and/or seat backs that fail unexpectedly during normal use.
- Safety seats that contain defective safety belts, buckles, or components that create a risk of injury, not only in a vehicle crash but also in non-operational safety of a motor vehicle.
- Air bags that deploy under conditions for which they are not intended to deploy.

A typical auto crash is viewed as having “two collisions”: the "first collision" occurs when the vehicle impacts another vehicle or a fixed object; the "second collision" (following immediately, often after only milliseconds, the first collision) occurs when a vehicle occupant impacts the interior of the vehicle or is ejected and hits the ground (the literature notes also the existence of a “third impact”, between the internal organs and the frame of the body).

The purpose of a seat belt is to either prevent the second collision or to minimize its injury-producing potential. When it works properly, the seat belt is indisputably the most important safety device in an automobile, however when it works poorly or completely fails to work, the seat belt can cause serious injury and even death.

Seat belts can fail to restrain occupants due to both poor design and/or faulty manufacturing. Some of the more common defects include: Inertial unlatching & False latching, or/and the Failure of some component parts of the seat belt buckle. Consequently, the ways to unlatch a seat belt buckle in an accident, [7], can be: Overload; Inadvertent contact; False latch/Partial engagement; Inertial release. During a collision in such situations, the seat belt becomes unlatched and can allow the latch plate to pull out of the buckle. As a result, the occupant is essentially unbelted and unrestrained and, frequently, can be ejected from the car. If a seat belt system failure is suspected, the evidence that a seat belt failed because of design or manufacturing defects is often subtle and can be difficult to detect; since it is extremely difficult to prove that a seat belt failed without the physical evidence, it is important to preserve the failed seat belt system and to attach it to the technical expertise.

2.3 Presentation of the studied device

A safety belt buckle device, Fig.5a, is designed to coupling the seat belt that fixes to seat the occupant of the vehicle in order to limit its movement during a shock, and thus, during a strong deceleration, the occupant of a vehicle in motion is not projected in the moving direction as result

of the accumulated kinetic energy. Generally, the most current safety belts are equipped with buckles devices similar to those presented in Fig.5b and Fig.5c.

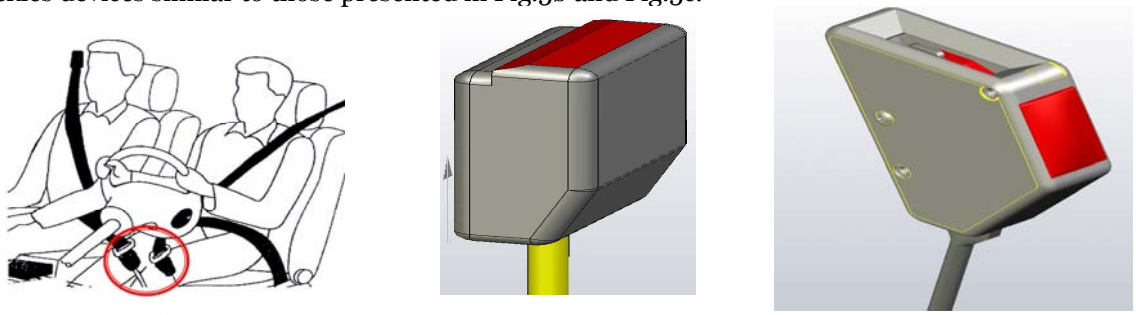

a. Studied area b. End-release buckle c. Side-release buckle

Fig. 5. Studied area and Types of safety belt buckle devices

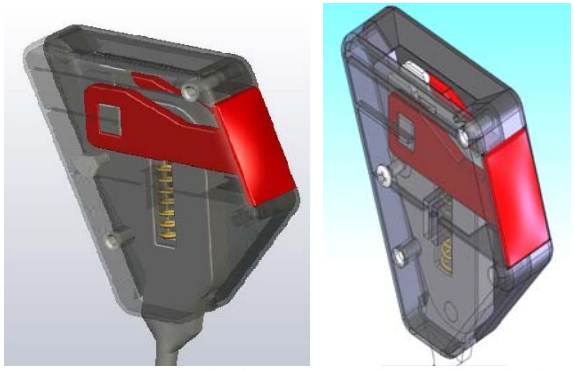

Fig.6. 3-D model of the studied coupling device

The 3D model of the studied coupling device (with side-release button) is shown in Fig.6.

2.4. Effort evaluation in pretensioned seat belt system

The static analysis of the cable–guide subassembly, Fig. 7a, followed by the solving of the equations equilibrium system (1), with F_1=400 daN and F_2=300 daN, give as result the forces in the belt system, F=635 daN. After the decomposition of this force, at A, C and E points, Fig.7b, we obtained the following values of forces:

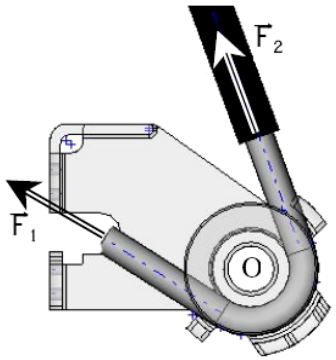

F_1=400 daN
F_2=300 daN

$$\begin{cases} \sum F_{ext} = 0 \\ \sum M_{F_{ext}} = 0 \end{cases} \quad (1)$$

$\Rightarrow$ F=635 daN.

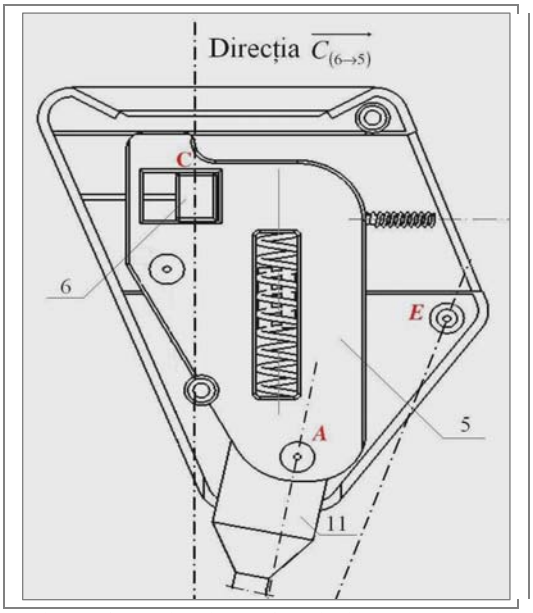

$\overline{A}_{11\to5}$ = 635 daN ;

$\overline{C}_{6-10}$ = 343 daN;

$\overline{E}_{1,2-5}$ = 350 daN.

Fig.7. Evaluation of the resultant force in the safety belt system and its components

2.5 Finite Element Analysis of the buckle latch plate

The belt buckle assembly must have the capacity to transmit the forces being put on the system. In case one of its component parts, in particular the latch plate, can not endure the load that was derived by the motion of an occupant during an impact, the safety belt system can not play the role of a restraining system anymore.

Therefore, the latch plates of the seat belts, although have different designs being manufactured by different companies, are an important element of the system. The importance of this element lies in its own security and is related to assure the functional role of the safety belts systems.

- **Material Proprieties:** the analyzed latch plate is made of steel grade CK55 (corresponding to OLC 55 X, STAS 880), whose properties are listed in Table 1a and 1b.

Table 1a. Mechanical properties in the quenched and tempered condition (+QT)

Mechanical properties	Mechanical properties for the ruling sections (see prEN10083-1:2002, Annex A) with a diameter (d) or for flat products thickness (t) of		
	d ≤ 16mm t ≤ 8mm	16mm < d ≤ 40mm 8mm < t ≤ 20mm	40mm < d ≤ 100mm 20mm < t ≤ 60mm
Re $_{min}$ (MPa)	550	490	420
Rm (MPa)	800-950	750-900	700-850
A min. (%)	12	14	15
Z min. (%)	30	35	40
KV min. (J)	-	-	-

Table 1b. Mechanical properties in the normalized condition – (+N)

	Mechanical properties for products with a diameter (d) or, for flat products thickness (t) of		
	d ≤ 16mm t ≤ 16mm	16mm < d ≤ 100mm 16mm < t ≤ 100mm	100mm < d ≤ 250mm 100mm < t ≤ 250mm
Re $_{min.}$ (MPa)	370	330	300
Rm min. (MPa)	680	640	620
A min. (%)	11	12	12

- **Geometric parameter and 3-D CAD model:** the geometry of the latch plate, shown in Fig.8, was based on these functional requirements and is in accordance with the configuration of the belt buckle.

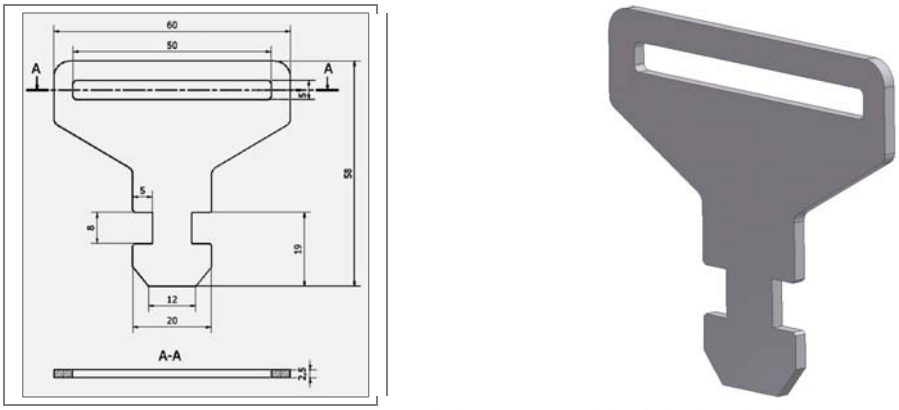

Fig.8. Geometric parameters and the 3-D model of the latch plate

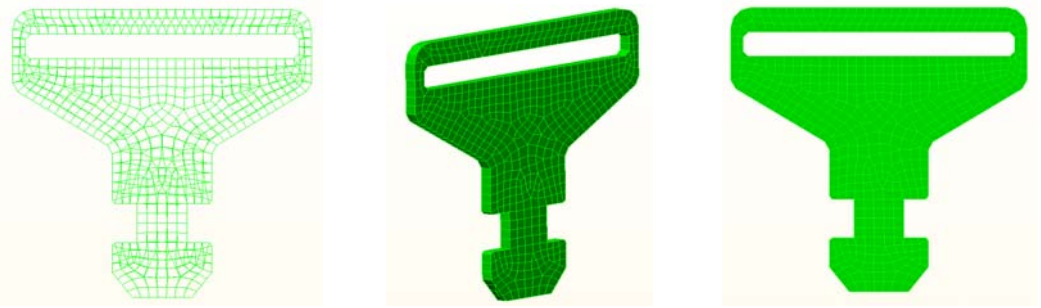

Fig.9. Discretization (meshing) of the latch plate model

- **Finite Element Analysis of the latch plate**

The finite element analysis performed using Algor software, involved the following steps:

- ❖ Conception of the 3-D CAD model of the latch plate (or transfer to Algor a CAD model designed in another modeling tools/dedicated software/, like Inventor, Mechanical Desktop, SolidEdge, in .stp format file), for creating the 3D geometry of the part/assembly to perform FEA.
- ❖ Save of the 3D CAD geometry in neutral format like IGES, STEP etc. Though some of the FEA packages allow importing the CAD geometry directly from some of the 3D CAD packages.
- ❖ Start of FEA package and import the CAD geometry into the FEA package.
- ❖ Defining Material Properties: modulus of elasticity, Poisson ratio, etc.
- ❖ Defining the displacement boundary conditions (Fig.10) and applying the mechanical loads (Fig.11);
- ❖ Discretization (meshing) of the model (Fig.9);
- ❖ Performing of the finite element analysis, respectively obtaining the solution of the finite element matrix equations (solved for the unknown displacements, given material properties, forces, boundary conditions and mesh size);
- ❖ Analysis and interpretation of the FEA results (Fig.12), and conclusions drawn from the analysis.

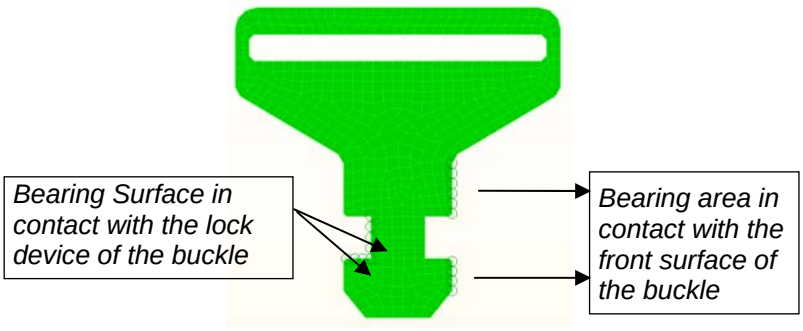

Fig.10. Boundary displacement constraint conditions

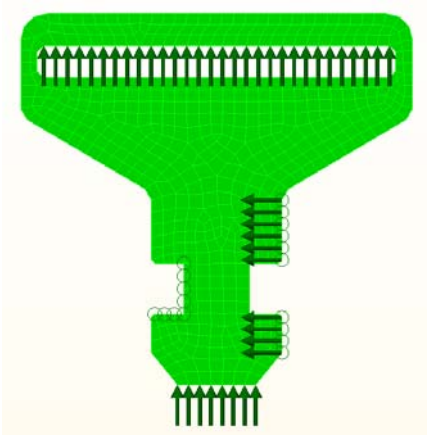

Fig.11. Applied of mechanical loads

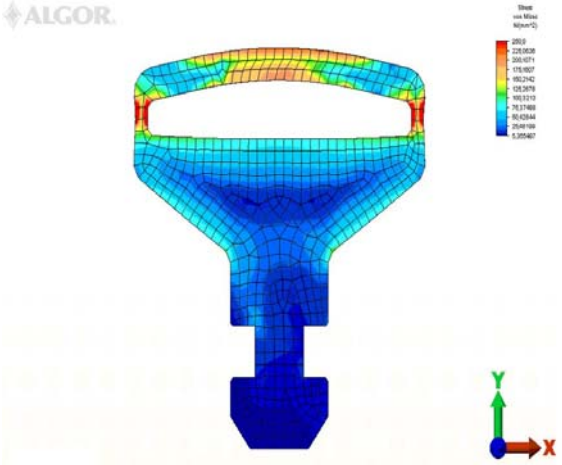

Fig.12. Finite Element Analysis of the safety belt latch plate. Distribution and values of Stress

3. INTERPRETATION AND CONCLUSIONS. FUTURES STUDIES

The CAD modeling and the Finite Element Analysis of the seat belt system (buckle assembly and latch plate), was carried out in order to verify the safety of the car occupants in impact conditions. The proper design of a seat belt buckle is essential for the situation of a frontal impact, because if the buckle assembly can not endure the load derived by an occupant motion during a frontal collision, the safety belt can not serve as functional restraint system.

The effectiveness of the component parts of the safety belt assembly was analyzed using the *Algore V Release* software, based on the Finite Element Method, and the results that we obtained reveal the correct design conception of the examined elements.

In our future studies, we are planning to do further development on the subject of analyzing the passive safety systems using FEA software. This work is motivated by the continuously increasing standards for protection measures against the effects of accidents. These require an accurate assessment of the operational behavior of the safety systems in exploitation, and involve a good knowledge of the tolerance of the human body, as well as its mechanical response to impact.

REFERENCES

[1.] Transport, Infrastructure and Communities Portfolio/Government of Canada, www.tc.gc.ca
[2.] High-Tech Vehicle Safety Systems. Canadian Association of Road Safety Professionals, http://www.carsp.ca/page/111/400
[3.] National Highway Traffic Safety Administration, http://www.nhtsa.gov/
[4.] Limiting performance analysis of a seat belt system with slack, Richard W. Kent, Sergey V. Purtsezov, Walter D. Pilkey, International Journal of Impact Engineering 34-8 (2007) 1382–1395.
[5.] Report/Lives Saved in 2009 by Restraint Use and Minimum Drinking Age Laws and Seat Belt Use in 2010 – Overall Results.
[6.] http://en.academic.ru/dic.nsf/enwiki/7248718
[7.] http://www.vehiclesafetyfirm.com/cm/crashworthiness/diagnosing-seatbelt-use.pdf
[8.] http://www.algor.com/news_pub/tech_reports/2004/interpretingresults/
[9.] Tichkiewitch, S. - Méthodologie et outils pour l'intégration dans la conception. "Conception et fabrication de produits mécaniques", Drăghici, G. şi Brissaud, D.(coord) Ed.Eurobit, Timişoara, 1999

INTERNATIONAL SYMPOSIUM on
ADVANCED ENGINEERING & APPLIED MANAGEMENT
– 40th ANNIVERSARY in HIGHER EDUCATION (1970-2010)
4 – 5 November, 2010, Hunedoara, ROMANIA

[1.]Amalia Ana DASCĂL, [2.]Daniel CARAULEANU

WHEELS AUTO MODELING USING FINITE ELEMENT METHOD

[1,2.]UNIVERSITY POLITEHNICA OF TIMISOARA, FACULTY ENGINEERING OF HUNEDOARA, ROMANIA

ABSTRACT:
The question always arises buying rims "steel or alloy wheels?". In addition to the rims look more appealing than those of alloy steel, there are technical reasons why it tends to use them: reduced weight, starting and braking, rigidity, rapid cooling. Although it can produce sheet steel or cast alloy wheels profile is adopted depending on the specifics of the construction vehicles and the stress faced by their wheels.
In this paper we studied the tensions that arise when a wheel is subjected to aerodynamic loading conditions, trying to play the best areas in which attention must be enhanced in order to prevent premature destruction. Using CATIA V5, we designed a concept of light and have undergone a finite element method using different forces and accelerations restrictions in areas where problems occur during use. Calculating the diagrams thus playing rim is observed when the material behavior is tensed and so we can correct the areas that present a danger of destruction.
At the end of the method could draw the conclusion which shows the success of the concept, but also design new technologies for observation and verification of parts or assemblies.
KEYWORDS:
wheels auto, finite element method, aluminum alloys, stress

1. INTRODUCTION

Although the design is changing rims, some classical models are still within the top preferences. Versions with 4 or 5 spokes or those with cross-spoke wheels are derived from racing cars. The conclusion is that it hides behind the form and function. The shape is derived from this calculation is to provide durability, low weight and hardness. On the other hand there and "trendy wheels" that change from one "season" to another. If these wheels to decide the importance of technical characteristics is the designer and engineer, [4]. Because these types of wheels have a relatively short life focuses on the methods of production as cheap and as fast. Unfortunately, to meet the above conditions, is unable to use the latest technology in the field. On the other hand, car manufacturers tend to include standard equipment alloy wheels. Since their invention in the '50s, alloy wheels have been used to improve machine performance.

In terms of material they are made, the wheels are magnesium alloy (the original version was produced) or aluminum alloy. The magnesium alloys are too fragile to be used on the streets. I'm pretty hard to maintain and limited in terms of resistance to harmful environmental factors. For example, the tendencies to oxidize magnesium have often varnished. Currently this type of wheels used on racing cars participating in such as Formula 1 races held in Indianapolis, etc.. which are continuously monitored by staff members. For normal use of the machines were designed aluminum alloy wheels having a greater resistance to common shocks from a road. They are made in different models, all weighing less than the steel version, [2].

2. METHODOLOGY

2.1. Jante alloy or steel?

When you think about when choosing a winter set of wheels to choose between alloy and steel wheels. Below we have listed some advantages and disadvantages to light:

Alloy wheels - is a plus in terms of aesthetics - have a very good precision manufacturing - are lighter than steel rims - have a greater strength and durability - helps to brake - Requires special care (especially in winter) to avoid damaging action skid materials, dust and mud;
Wheels of steel - Satisfy the requirements of drivers who want a winter set of wheels at the highest price - can be found in two types of finishes (black or metallic);
- Changing the layout is easy and relatively cheap by replacing the protective caps - are cheaper than alloy rims due to lower costs for materials and labor;

2.2. Influence rims

The question always arises buying rims "steel or alloy wheels?". In addition to the rims look more appealing than those of alloy steel, there are technical reasons why it tends to use them, fig. 1.

Fig.1. Appearance of some wheels

1. Lightweight compared to steel wheels. It is the most important asset of alloy rims. Items such as tires and brake system components in the vicinity of the wheel are the most affected by shocks (not protected by any damping system). The weight of these elements is much less requires less energy to be controlled.
2. Starting and braking. By reducing the total mass of the vehicle to facilitate both starting and braking.
3. Rigidity. A car equipped with alloy wheels will be much easier to control in a curve than on steel rims fitted. It is known that an alloy rim is more rigid than a steel, which will influence how it behaves tire mounted on it. This will, in turn, less malleable by the opposing forces of resistance acting on her great curves, which leads to a good response.
4. Rapid cooling. Due to high thermal conductivity property of the material they are made of alloy wheels to ensure rapid cooling of the wheel and brake components in their proximity.

2.3. Construction

In general running wheel disc pressed steel sheet, but in some cases logs are used and spoke cast or dragged in obtaining an adequate rigidity to the smallest weight. Merge wheel rim is made by welding, sheet metal disc by mechanical fasteners for spokes drawn, and if cast alloy wheels with lightweight wheels, disc and rim forming common body. Drive-wheel assembly is mounted on the hub with screws or bolts.

Configuration and rim profile is adopted depending on the specifics of the construction vehicles and the stress faced by their wheels.

Depending on constructive solutions adopted there are two types of wheels:

- wheels joints (fig.2.a) - used in the wheels of cars, light commercial vehicles, 4x2 wheeled steering wheels and engines of small power tractors;
- removable wheels with cylindrical or slightly conical profile (fig.2.b) - used wheels trucks, buses, vans and heavy wheels of large and medium power tractors.

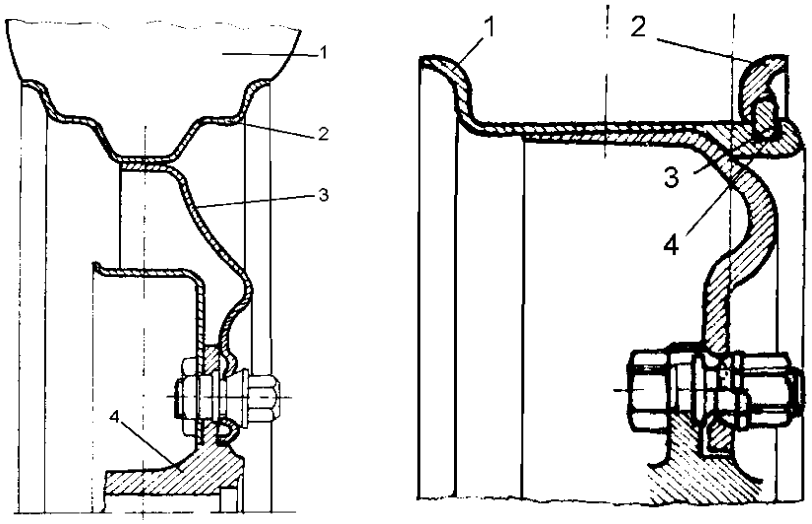

Fig.2. Constructive Solutions wheels

Joints with deep profile wheels have ears shoulder high profiled rim, providing a strong tire lateral stability. These buildings used tire edges are elastic and flexible, being allowed profiled rim mounting them directly.

If removable wheels, figure 2.b, less tapered profile, 5-15A taper creates the possibility of a better tire crosses. Installation is as simple as pushing the tire on the rim a border of fixed and removable border 2 fixation with flexible sealing ring 3 which is inserted into channel 4.

This construction allows easy mounting and dismounting tires and ensure takeover axial forces. For vehicles that are used for rear-wheel dual (double), disc wheel profile is designed to allow both wheels to the hub assembly, symmetrical about the plan to raise and support. If the rims for tubeless tires to be given to sealing surfaces must not show local irregularities or bulging, [1].

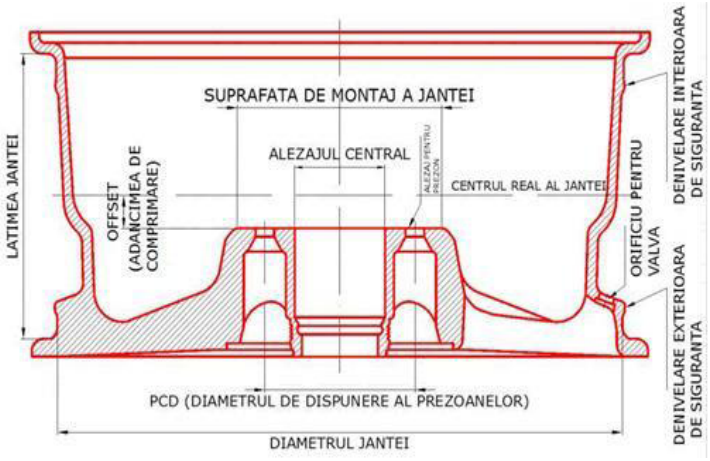

Fig.3. Elements of the rim

Symbolization. Ex. of symbolization: 5 ½ J x 49 ET 14H2 = 5 ½ inch rim width (inches), J = border rim shape feature point, x = rim in one piece, 14 = nominal rim diameter in inches (inches) H2 = rim profile; ET49 = depth Compression: 49m;

2.4. Compatibility wheel / tire – oversize

Oversize rim and tire, was conceived to enhance performance and appearance of your vehicle. It is accomplished by fitting larger diameter wheels and tires compared to the lower height. It is envisaged that following these changes to keep the overall diameter of the wheel to a maximum difference of 3% compared to the initial diameter. This is important because variations larger diameters would lead to traction problems, and finally to a modified fuel consumption. Also, the cars equipped with computer-assisted braking some confusion could arise, leading to accelerated brake failure.

The rule for dimensioning:

* Plus 1: Increase section width by 10 mm, reduces the appearance of 10 points. Increases rim diameter by 1 inch.
* Plus 2: Increase section 20 mm, decreases aspect with 20 points. Increases rim diameter by 2 inches

2.5. Aided design in CATIA V5.

CATIA (Computer Aided Three Dimensional Interactive Applications) product of Dassault Systemes is currently one of the most widely used integrated CAD / CAM / CAE in the world, with applications in various fields, including: mechanical engineering, aerospace, shipbuilding, automotive, robotics, agricultural machinery, chemical, food and more. To version 5 is available since 1999, every new update is introduced new modules and functionality, while improving existing ones.

CATIA V5 is the top information technology design technologies such as machine building and construction industry in different parts. CATIA V5 is the cornerstone in the integration of people, tools, methods and resources in an enterprise. Its unique model Product/Process/Resources results in a truly collaborative work environment that enhances creativity and flow of information, the definition of 3D products and processes.

Using an intuitive interface and flexible CATIA Part Design module makes it possible to design three-dimensional sound of different pieces most often encountered in the design of mechanical products, as, with CATIA Sketcher, the other modules of the program. The module offers a highly productive working environment, each piece designed with a number of parameters, both in its use and in how CATIA Knowledge Advisor for parameterization and automatic creation of families of parts, a set of dependencies between parts, etc.

3. ANALYSES

FINITE ELEMENTS ANALYSIS METHOD WITH WHEELS FEM incorporating CAD programs contain special procedures that allow optimization optimization through automatic calculation of optimal values for some design parameters so as to satisfy a set of conditions imposed on an objective function, defined by the user. Also, the designer can always return to the

geometric shape of the structure, the material of which it will be made and, of course, the loads that will be covered in this stage of development where the structure is only a virtual model. The first step in addressing a new analysis is its choice of the [Insert], but, implicitly, the execution module, the type of static analysis (Static-house) is the default. As an immediate result, shaft specifications are added element 'Static Case ". The expansion element "Static Case" (press the mouse icon with the symbol "to his left), its elements are displayed: Restrictions (Restraints), loads (Loads) solutions (Static Case Solution) and sensors (Sensors). They have very important roles in finite element analysis. Of course, the early analysis, sub-items do not contain values, the user must set restrictions and tests for the program to calculate solutions CATIA and activate the sensors. For example may be given three tests, Deformed Meshes, Von Mises stress and the estimated local error. They can be active and/or off simultaneously, the result of the analysis being presented on the screen, [3].

3.1. Command Masses

In general, instruments masses Masses are based on distribution theory, used to model the characteristics of purely inertial system, representing scalar fields table, a certain intensity, applied the model to be analyzed in a single point on an edge or a surface it. (Fig. 3).

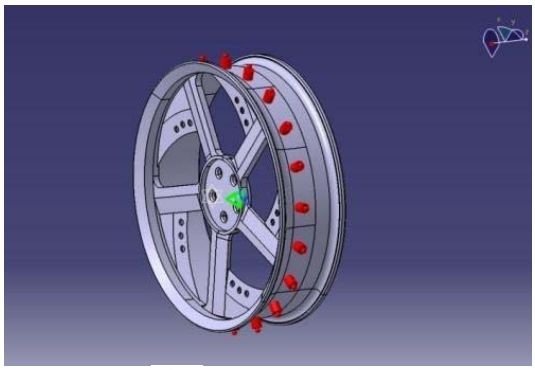

Fig. 3 Masses Order

3.2. Command Restraints

Restrictions should be defined to represent a structural interface between the model and analyzed subassembly or assembly to which it belongs. If the model is not properly constrained, will result in many numerical problems (singularity) and finite element analysis could not be done. Clamp restriction model requires a one-piece module created a solid modeling program. (Fig. 4).

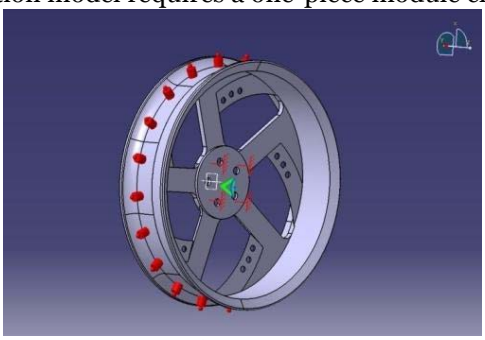

Fig.4.Order restraints

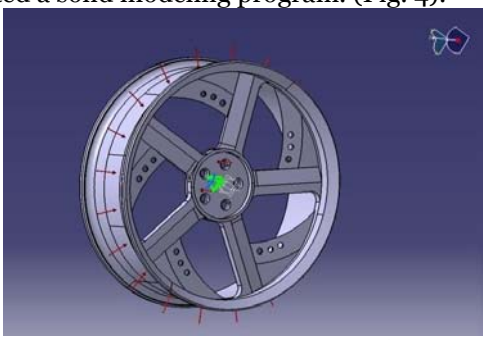

Fig.5 Pressure Control

3.3. Command Loads

Loads various instruments added load models will be analyzed by finite element method, essential step analysis process. These virtual loads simulating actual loads to which the model will be subjected during operation.

Pressure - this charge, expressed in N / m creates a uniform pressure applied on the given area so that the forces exerted directions are always perpendicular (Fig. 5).

Distributed Force - distributed forces are in fact equivalent static system with a resultant force of a real force, applied at a certain point of a model or virtual components (Fig. 6).

Acceleration - is concentrated loads type acceleration field (N/kg or m/s) with uniform intensity, applied in virtual models or parts examined (Fig. 7).

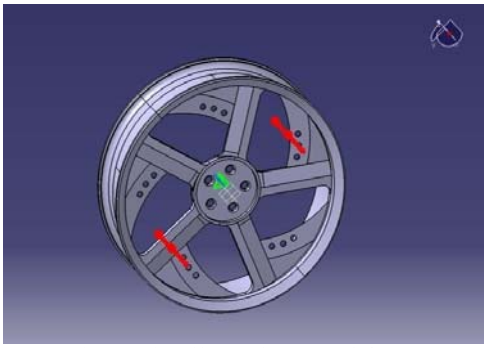

Fig.6 Distributed control force

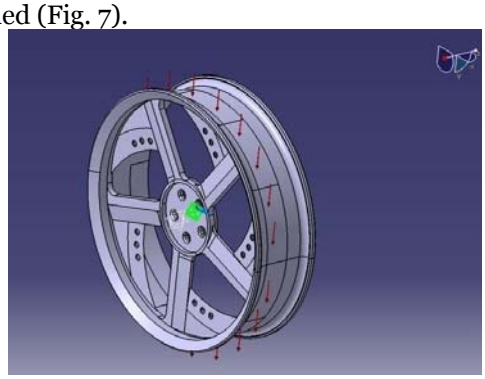

Fig.7 Aceleration command

4. CONCLUSIONS

Compute a tool meets the most important roles in the finite element analysis of a model: triggers this process, but only for the completely bound and showing loads. Thus, throughout the process, the user defines a set of parameters (material characteristics, limitations, strengths, etc..), Following the steps described above. Then, during calculation, the program transforms the conditions applied to interpret the model parameters, allowing users access to visual and numerical data.

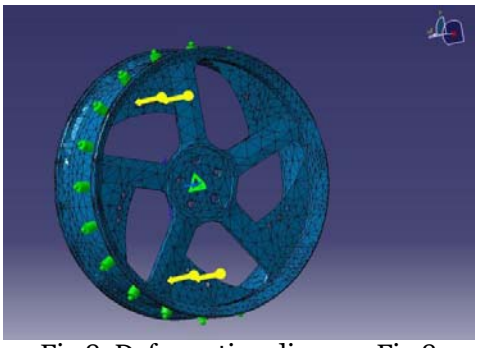

Fig.8. Deformation diagram

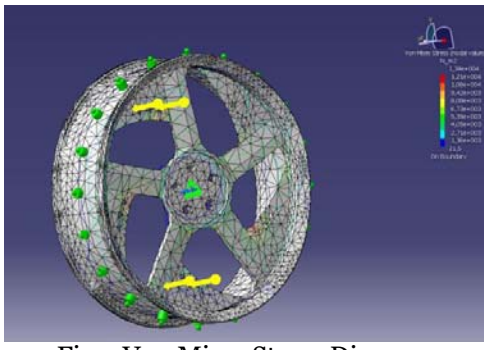

Fig.9 Von Mises Stress Diagram

Deformation - images provided by this tool are used to visualize the model analyzed in the distorted representation as a result of all the conditions imposed (material restriction loads) (Fig. 8). Von Misses Stress - images produced from the use of this tool shows Von Misses field model, representing in fact, a scalar field values derived from the volume density: strain energy and used to measure the tension created in the model (Fig. 9).

Displacement - tool is used to view the field trips (in mm) of network nodes as a result of the imposition of load restrictions and conditions on a model (Fig. 10).

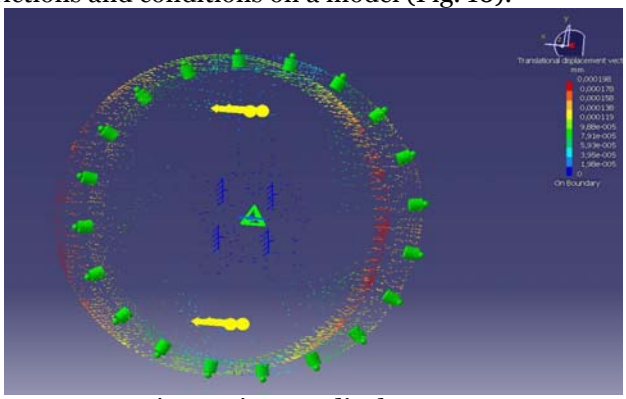

Fig.10 Diagram displacement

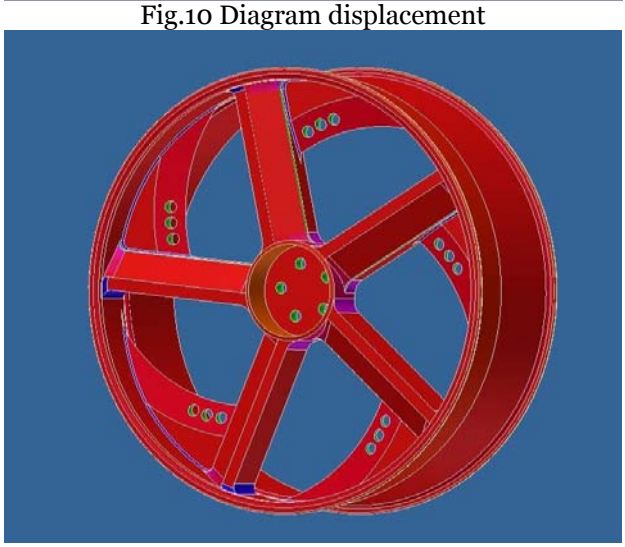

Fig. 11 Air dispersion diagram

Following analysis, the program discretized surface nodes and 14 253 4807 rim type TE4 elements that were used to play Deformed Mesh diagram. Consider having a rim made of aluminum 2710kg/m3 density and temperature variation of 2.36 K.

Getting the number of nodes and elements to apply a single restriction supportive axis forces Fx-182 N, N-0 Fy and Fz-413N, 2591 ± 001kg loads on a total of 14,421 lines that compose the song, they an X-axis inertial de6 mm, 9 mm Z axis and Y axis 7mm.

Applying finite element program calculates a rigidity of 2.82 N on the curve track construction, restrictions imposed on a single area, the constraints are on one surface which is divided into a number of 258 points.

Applying energy of 1925 J-006's with the song being in balance, the program plays the Von Misses stress diagram (loading values in network nodes) after the following table:

Table 1. Finite element analysis result

Components	Force applied	Restrictions	Arrears	Size relative error
Fx (N)	5.1822e+001	-5.1822e+001	3.3040e-012	2.6954e-013
Fy (N)	2.0000e+000	-2.0000e+000	1.6995e-012	1.3864e-013
Fz (N)	-1.4131e-003	1.4131e-003	-1.0375e-011	8.4638e-013
Mx (N/m)	-1.6294e-001	1.6294e-001	-2.1683e-012	4.3130e-013
My (N/m)	3.7634e+000	-3.7634e+000	3.4395e-012	6.8415e-013
Mz (N/m)	-4.7306e-004	4.7306e-004	-4.0315e-013	8.0192e-014

Following tests carried out we sought the advice of corporations specializing in design and manufacturing of car wheels, which are PIAA Corporation (USA) and Enke Corpoation (Japan), who helped design the tests based on which we performed. Their responses were:

PIAA Corporation - is a unique design with small defects in the layout STAS. Our tests show that a light produced by the initial appearance and size model for 17", 20", 21" inch would require producers of aluminum alloy. A problem would be hiding cover stud be bent in the wind very well so will lose the whole concept. Otherwise we want to congratulate you for design and design and wish you success in the future.

Enke Corporation - We are glad that you asked us to think and hope we can help. First we conducted a test I noticed that you made and I have attached chart to see the success of the rim. To explain the diagram as soon as possible: one is where the air has a very good aerodynamic curve, which means that the aerodynamic design point of view is correct, Area 2 is where the air is blocked so there will lose speed but that area is too small can be ignored. Instead hide stud should be done with great precision our advice a little curve max. 2-3 mm from the plane to remove the green rim.

This approach is useful for any product development needs of Class A-surfacing. CATIA V5 users can implement and practice the same technique, without adding any costly hardware. As a personal opinion I add, as a matter of fact, over time, the need to design a new model of the rim in a short period of time can be achieved only with computers, specialized software specifically with these dedicated engineers today.

REFERENCES:

[1.] UNTARU, M., Dynamics of motor vehicles on wheels, Didactics and Pedagogic Publishing House, Bucharest, 1981.
[2.] STOICESCU, AP, Design and drive performance cars, consumer, Technical Publishing House, Bucharest, 2007.
[3.] GHIONEA, I.G., Assisted design in Catia V5. Theoretical and applications, Ed Bren, Bucharest, 2007.
[4.] OPREAN, M., Modern car. Requirements, Constraints, Solutions, Romanian Academy Publishing House, Bucharest, 2003.
[5.] DASCAL, A. Body and supporting structures for road vehicles, Publishing House Cermi, 2008.

INTERNATIONAL SYMPOSIUM on
ADVANCED ENGINEERING & APPLIED MANAGEMENT
– 40th ANNIVERSARY in HIGHER EDUCATION (1970-2010)
4 – 5 November, 2010, Hunedoara, ROMANIA

[1.]Paolo BOSCARIOL

EXPERIMENTAL VALIDATION OF A SPECIAL STATE OBSERVER FOR A CLASS OF FLEXIBLE LINK MECHANISMS

[1.] UNIVERSITY OF UDINE – DIEGM,
Udine, ITALY

ABSTRACT:
This paper presents an experimental validation of a state observer for flexible-link manipulators (FLM). The design of this observer is based on an accurate dynamic model of the mechanisms, able to take into account the coupled rigid-flexible dynamics of the system.
Experimental results on a single-link manipulator affected by gravity force show that the proposed observer achieves a good estimation of the plant dynamics even if the displacement signal is not measured. The evaluation of the performance is done experimentally by comparing the estimated elastic displacement with the measures obtained on the field.
KEYWORDS:
flexible-link manipulators (FLM), mechanisms, dynamic model

1. INTRODUCTION

Dynamics and control of flexible-link mechanisms are topics of a widespread interest in the scientific literature. From the 70's, a large number of papers have been published: Dwivedy [1] cites 433 works from 1975 to 2005 on the modeling of this class of mechanism and Benosman [2] cites 119 papers up to 2003. This popularity is motivated by several advantages of flexible-link manipulators over their rigid counterpart, such as lower weight, higher operative speed and reduced power consumption. Nevertheless, specific solutions in terms of control must be used to reach satisfactory performance, high accuracy and stability.

Model-based control strategy for flexible manipulators, such as [3,4,5] by the same Author or [6] and [7], just to mention some recent works, requires the use of state observers to estimate the evolution of the dynamics of the plant. The estimation of the dynamics of such plant is essential, since complexity of the motion would otherwise require the use of a very large number of sensors. In this case the proposed state-space observer requires the measure of only the angular position of the mechanism and the instant value of the torque applied to the mechanism, so it does not require the use of other sensor such as strain gauge bridges or accelerometers. For example in [8] a strain gauge bridge is adopted to measure the elastic deformation of a four links FLM.

The test bench is a single-link flexible mechanism affected by gravity force. The performance of the proposed Kalman state observer is evaluated experimentally. The estimation of the state of the plant is based only on the measure of the angular position of the hub and on the torque signal, thus reducing the effects of measures such as strain gauge signal which are usually affected by noise. The accuracy of such system is evaluated experimentally by comparing the estimated state with the measure of the elastic displacements performed by a strain gauge transducer.

2. THE STUDY

In this section the dynamic model of a flexible-link mechanism suggested by Giovagnoni [9] will be briefly explained. The choice of this formulation among the several proposed in the last 30 years has been motivated by the high grade of accuracy provided by this model, which has been proved several times, for example in [10,11].

The main characteristics of this model can be summarized in four points:

1. finite element (FEM) formulation
2. Equivalent Rigid-Link System (ERLS) formulation [12]
3. mutual dependence of the rigid and flexible motion
4. capability of describing mechanisms with an arbitrary number of flexible and rigid links

First, each flexible link of the mechanism is subdivided into several finite elements. Referring to the Figure 1 the following vectors, calculated in the global reference frame {X,Y, Z}, can be defined:

- $\boldsymbol{r}_i$ and $\boldsymbol{u}_i$ are the vectors of nodal position and nodal displacement in the i-th element of the ERLS
- $\boldsymbol{p}_i$ is the position of a generic point inside the i-th element
- $\boldsymbol{q}$ is the vector of generalized coordinates of the ERLS

The vectors defined so far are calculated in the global reference frame {X,Y,Z}. Applying the principle of virtual work:

$$\delta W^{elastic} + \delta W^{external} + \delta W^{inertia} = 0$$

the following relation can be stated:

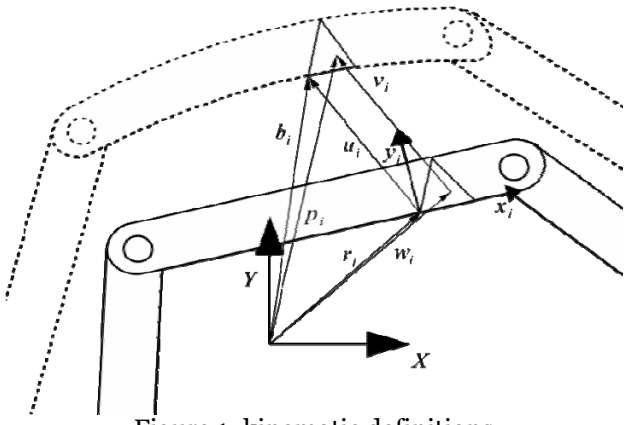

Figure 1: kinematic definitions

$$\sum_i \int_{V_i} \delta \mathbf{p}_i^T \ddot{\mathbf{p}}_i \rho_i dw + \sum_i \int_{V_i} \delta \check{\boldsymbol{\eta}}_i^T \mathbf{D}_i \check{\boldsymbol{\eta}}_i dw = \sum_i \int_{V_i} \delta \mathbf{p}_i^T \mathbf{g} \rho dw + (\delta \mathbf{u}^T + \delta \mathbf{r}^T)\mathbf{F} \qquad (1)$$

ε_i, $\boldsymbol{D}_i$, ρ_i and $\delta\varepsilon_i$ are the strain vector, the stress-strain matrix, the mass density of the i-th link and the virtual strains, respectively. $\boldsymbol{F}$ is the vector of the external forces, including the gravity, whose acceleration vector is g. Eq. 1 shows the virtual works of inertial, elastic and external forces, respectively.

From this equation, $\delta \boldsymbol{p}_i$ and $\ddot{\boldsymbol{p}}_i$ for a generic point in the i-th element are:

$$\delta \mathbf{p}_i = \mathbf{R}_i \mathbf{N}_i \mathbf{T}_i \delta \mathbf{r}_i$$

$$\ddot{\mathbf{p}}_i = \mathbf{R}_i \mathbf{N}_i \mathbf{T}_i + 2(\dot{\mathbf{R}}_i \mathbf{N}_i \mathbf{T}_i + \mathbf{R}_i \mathbf{N}_i \dot{\mathbf{T}}_i)\dot{\mathbf{u}}_i \qquad (2)$$

where $\boldsymbol{T}_i$ is a matrix that describes the transformation from global-to local reference frame of the i-th element, $\boldsymbol{R}_i$ is the local-to-global rotation matrix and $\boldsymbol{N}_i$ is the shape function matrix. Taking $\mathbf{B}_i(x_i, y_i, z_i)$ as the strain-displacement matrix, the following relation holds:

$$\check{\boldsymbol{\eta}}_i = \mathbf{B}_i \mathbf{T}_i \delta \mathbf{u}_i$$

$$\delta \check{\boldsymbol{\eta}}_i = \mathbf{B}_i \delta \mathbf{T}_i \mathbf{u}_i + \mathbf{B}_i \mathbf{T}_i \delta \mathbf{u}_i \qquad (3)$$

Since nodal elastic virtual displacements ($\partial \boldsymbol{u}$) and nodal virtual displacements of the ERLS ($\partial \boldsymbol{r}$) are independent from each other, from the relations reported above the resulting equation describing the motion of the system is:

$$\begin{bmatrix} \mathbf{M} & \mathbf{MS} \\ \mathbf{S}^T\mathbf{M} & \mathbf{S}^T\mathbf{MS} \end{bmatrix} \begin{bmatrix} \ddot{\mathbf{u}} \\ \ddot{\mathbf{q}} \end{bmatrix} = \begin{bmatrix} \mathbf{f} \\ \mathbf{S}^T\mathbf{f} \end{bmatrix} \qquad (4)$$

$\boldsymbol{M}$ is the mass matrix of the whole system and $\boldsymbol{S}$ is the sensitivity matrix for all the nodes. Vector $\mathbf{f} = \mathbf{f}(\mathbf{u}, \dot{\mathbf{u}}, \mathbf{q}, \dot{\mathbf{q}})$ accounts for all the forces affecting the system, including the gravity force. Adding a Rayleigh damping, the right-hand side of Eq. 4 becomes:

$$\begin{bmatrix} \mathbf{f} \\ \mathbf{S}^T\mathbf{f} \end{bmatrix} = \begin{bmatrix} -2\mathbf{M}_G - \alpha\mathbf{M} - \beta\mathbf{K} & -\mathbf{M}\dot{\mathbf{S}} & -\mathbf{K} \\ \mathbf{S}^T(-2\mathbf{M}_G - \alpha\mathbf{M}) & -\mathbf{S}^T\mathbf{M}\dot{\mathbf{S}} & 0 \end{bmatrix} \begin{bmatrix} \dot{\mathbf{u}} \\ \dot{\mathbf{q}} \\ \mathbf{u} \end{bmatrix} + \begin{bmatrix} \mathbf{M} & \mathbf{I} \\ \mathbf{S}^T\mathbf{M} & \mathbf{S}^T \end{bmatrix} \begin{bmatrix} \mathbf{g} \\ \mathbf{F} \end{bmatrix} \qquad (5)$$

Matrix $\boldsymbol{MG}$ accounts for the Coriolis contribution, while $\boldsymbol{K}$ is the stiffness matrix of the whole system. α and β are the two Rayleigh damping coefficients. System in (4) and (5) can be made solvable by forcing to zero as many elastic displacement as the generalized coordinates, in

this way ERLS position is defined univocally. Therefore removing the displacement forced to zero from (4) and (5) gives:

$$\begin{bmatrix} \mathbf{M}_{in} & (\mathbf{MS})_{in} \\ (\mathbf{S}^T\mathbf{M})_{in} & \mathbf{S}^T\mathbf{MS} \end{bmatrix} \begin{bmatrix} \ddot{\mathbf{u}}_{in} \\ \ddot{\mathbf{q}} \end{bmatrix} = \begin{bmatrix} \mathbf{f}_{in} \\ \mathbf{S}^T\mathbf{f} \end{bmatrix} \tag{6}$$

The values of the accelerations can be computed at each step by solving the system in (6), while the values of velocities and displacements can be obtained by an appropriate integration scheme (e.g. the Runge-Kutta algorithm).

It is important to focus the attention on the size and the rank of the matrices involved in (6), and also to the choice of the general coordinates used in the ERLS definition. Otherwise it might happen that a singular configuration is encountered during the motion of the mechanism [9]. In this case, (6) cannot be solved.

3. ANALISES, DISCUSIONS, APPROACHES and INTERPRETATIONS

In the first part of this section the experimental setup and the test bench single-link flexible manipulator are briefly described. Then the equations and the design of the proposed state observer are introduced. In the last part of the section the experimental results of the observer used with a PID position control are shown and discussed.

3.1. EXPERIMENTAL SETUP

The plant used to evaluate the effectiveness of the proposed predictive control strategy is a single-link flexible mechanism. It is made by a long and thin steel rod, actuated by a brushless motor. No reduction gears are used, so one end of the link is rigidly coupled to the motor shaft. The flexible link can rotate on the vertical plane, so the mechanism dynamics is heavily affected by the gravity force. The structural and dynamic characteristics of the flexible rod can be found in Table 1. Owing to the overall dimensions, the mechanism has a limited movement range (around ± 25 [deg]) from the vertical position. The motion of the link is governed trough an Indramat DKC-MKD brushless servo drive system. This drive is used as a torque generator, i.e. the instant value of the torque applied by the motor can be controlled by using an analog signal. Such a signal is supplied by a National Instruments PCI-6259 DAQ board, controlled by a Core 2 Quad PC.

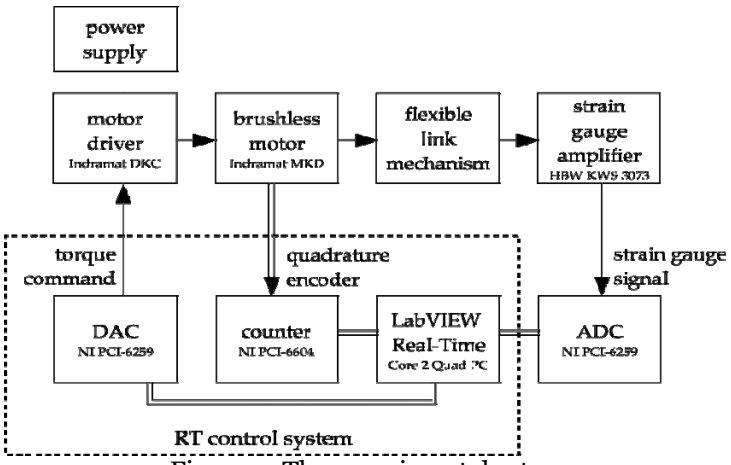

Figure 2: The experimental setup

Table 1: structural and dynamic characteristics of the flexible rod

	Symbol	Value
Young's modulus	E	230 × 109 [Pa]
Flexural stiffness	EJ	191.67 [Nm4]
Beam width	a	1 × 10−2 [m]
Beam thickness	b	1 × 10−2 [m]
Mass/unit length	m	0.7880 [kg/m]
Flexible Link length	l	1.5 [m]
Strain sensor position	s	0.75 [m]
First Rayleigh damping constant	α	4.5 × 10−1 [s−1]
Second Rayleigh damping constant	β	4.2 × 10−5 [s−1]

The angular position is measured by a 4000 cpr quadrature encoder is read with a National Instruments PCI-6602 board. The strain gauge signal is measured with the same PCI-6259 board used to generate the torque reference signal, as it is visible in Figure 3. The data acquisition and the control software runs over the LabVIEW Real-Time OS.

Figure 3: The flexible-link mechanism used for experimental tests

The dynamic model can be described with a good accuracy it with four finite elements. This discretization is sufficient to describe accurately the first four modes of vibration: 23 Hz, 63 Hz, 124 Hz, 206 Hz. Higher order modes can be neglected as they have low energy and high damping values.

3.2. DESIGN OF THE STATE OBSERVER

Most model-based control strategies can be applied only when a measure of the whole state $\boldsymbol{x}$ is available. In this application, there are only two measured values, so a state observer must be used. Here a Kalman asymptotic estimator has been chosen. An estimation of $\boldsymbol{x}(k)$ and $\boldsymbol{x}_m(k)$ (where $\boldsymbol{x}(k)$ is the state of the plant model and $\boldsymbol{x}_m(k)$ is the state of the measurement noise model) can be computed from the measured output $\boldsymbol{y}_m(k)$ as:

$$\begin{bmatrix} \hat{\mathbf{x}}(k \mid k) \\ \hat{\mathbf{x}}_m(k \mid k) \end{bmatrix} = \begin{bmatrix} \hat{\mathbf{x}}(k \mid k-1) \\ \hat{\mathbf{x}}_m(k \mid k-1) \end{bmatrix} + \mathbf{L}\left(\mathbf{y}_m(k) - \hat{\mathbf{y}}_m(k)\right)$$

$$\begin{bmatrix} \hat{\mathbf{x}}(k+1 \mid k) \\ \hat{\mathbf{x}}_m(k+1 \mid k) \end{bmatrix} = \begin{bmatrix} \mathbf{A}\hat{\mathbf{x}}(k \mid k) + \mathbf{B}\,\mathbf{z}(k) \\ \mathbf{A}\hat{\mathbf{x}}_m(k \mid k) \end{bmatrix} \tag{7}$$

$$\hat{\mathbf{y}}_m(k) = \mathbf{C}_m\hat{\mathbf{x}}(k \mid k-1)$$

The gain matrix $\boldsymbol{L}$ has been designed by using Kalman filtering techniques (see Franklin et al. [13])

The design of both the estimator and the prediction model is based on a linear state-space model of the FLM which has been obtained by applying the linearization procedure developed by Gasparetto in [14] to Eq. (6). The resulting state-space model can be rewritten as:

$$\begin{cases} \dot{\mathbf{x}}(t) = \mathbf{A}\mathbf{x}(t) + \mathbf{B}\mathbf{z}(t) \\ \mathbf{y}(t) = \mathbf{C}\mathbf{x}(t) \end{cases} \tag{8}$$

where $\boldsymbol{A} \in \mathrm{R}^{[26]} \times \mathrm{R}^{[26]}$, $\boldsymbol{B} \in \mathrm{R}^{[26]} \times \mathrm{R}^{[1]}$, $\boldsymbol{C} \in \mathrm{R}^{[2]} \times \mathrm{R}^{[26]}$ are time-invariant matrices. The state vector $\boldsymbol{x}$ includes all the nodal displacements and the angular position q, as well as their time derivatives:

$$\mathbf{x}(t) = [u_1, u_2, \ldots, u_{13}, q, \dot{u}_i, \dot{u}_2, \ldots, \dot{u}_{13}, \dot{q}]^T \tag{9}$$

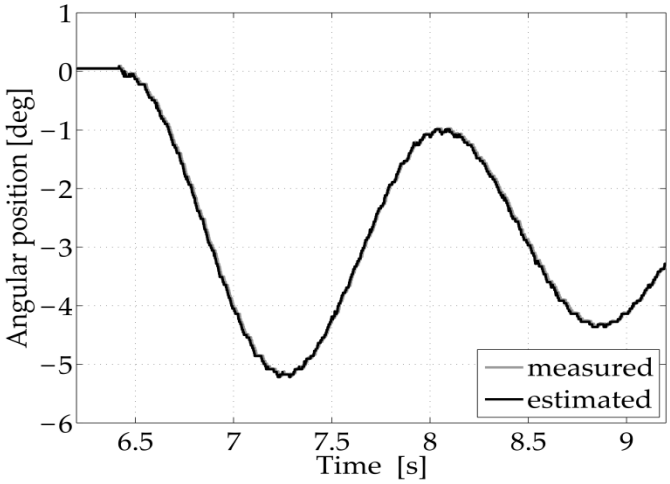

Figure 4: Experimental comparison of measured and estimated angular position

The output vector of the LTI system consists of two elements: $\mathbf{y}(t) = [u_6, q]^T$, being u_6 the rotational displacement at the midspan of the link. The input vector $\boldsymbol{z}(t)$ includes the torque applied to the link as single element.

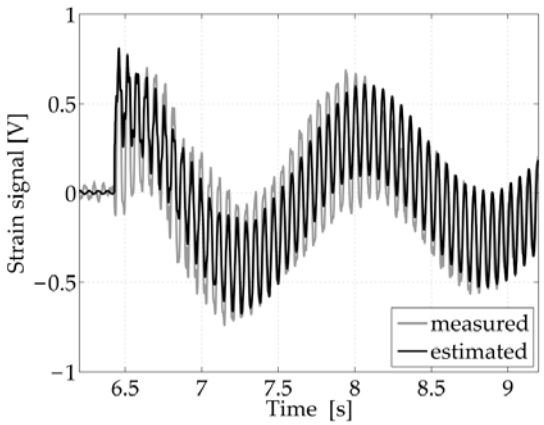

Figure 5: Experimental comparison of measured and estimated elastic displacement

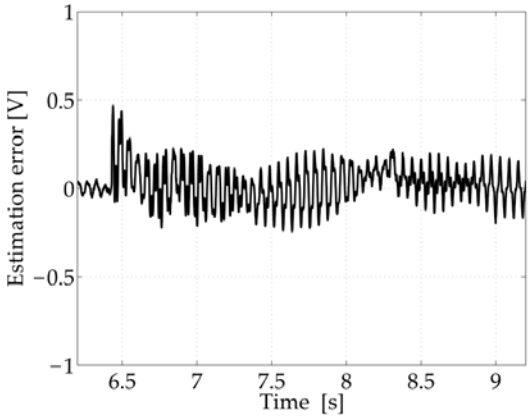

Figure 6: Elastic displacement: estimation error

A comparison of measured and estimated values of the link curvature is reported in Figures 3,4,5. As it can be seen, the value of the elastic displacement can be evaluated with a good accuracy. The angular position of the mechanism is controlled with a PID controller with gravity compensation. The block diagram of the closed-loop control system is provided in Figure 6.

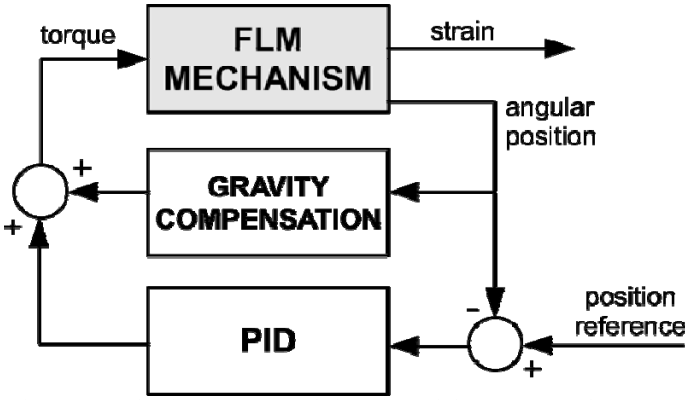

Figure 7: Block diagram of the closed-loop control system

It must be pointed out that the state observer has the availability of only the quadrature encoder signal and the nominal torque applied to the rod. In this way, the robustness of the closed-loop system can be improved, since the measure of the strain gauge signal is heavily affected by noise. Moreover, the reduced number of sensor make this control strategy suitable to most robotic manipulators for industrial use, since sensors such as accelerometers and strain gauge bridges are usually unavailable on these systems.

4. CONCLUSIONS

A state estimator for flexible-link mechanisms has been implemented and tested on a real single link mechanism. It has been proved experimentally that the state estimator used for all the experimental tests is capable of providing an accurate estimation of the plant dynamics with a very limited set of sensors. Such an estimator needs the measure of the angular position only and the torque applied by the brushless motor. For this reason, the proposed controller can be easily adapted to most of the industrial manipulators, which usually do not have sensors for measuring the elastic displacement of the links.

REFERENCES

[1.] DWIVEDY, S., EBERHARD, P., 2006. Dynamic analysis of flexible manipulators, a literature review. Mechanism and Machine Theory 41 (7), 749–777. 17

[2.] BENOSMAN, M., LE VEY, G., 2004. Control of flexible manipulators: A survey. Robotica 22 (05), 533–545.

[3.] Boscariol, P., Gasparetto, A., Zanotto, V., 14-17 April 2009. Vibration reduction in a flexible link mechanism through the synthesis of an mpc controller. In: Proceedings of the 5th IEEE Iternational Conference on Mechatronics (ICM2009). Malaga, Spain.

[4.] Boscariol, P., Gasparetto, A., Zanotto, V., January 2010. Active position and vibration control of a flexible links mechanism using model-based predictive control. Journal of Dynamic Systems, Measurement, and Control 132.
[5.] P. Boscariol, A. Gasparetto, V. Zanotto Model Predictive Control of a Flexible Links Mechanism Journal of Intelligent and Robotic Systems: Volume 58, Issue 2 (2010), Page 125-147
[6.] Hassan, M., Dubay, R., Li, C., Wang, R., 2007. Active vibration control of a flexible one-link manipulator using a multivariable predictive controller. Mechatronics 17 (6), 311–323.
[7.] Chalhoub, N., Kfoury, G., Bazzi, B., 2006. Design of robust controllers and a nonlinear observer for the control of a single-link flexible robotic manipulator. Journal of Sound and Vibration 291 (1-2), 437–461.
[8.] R. Caracciolo, A. Gasparetto, A. Trevisani and V. Zanotto. On the Design of State Observers for Flexible Link Mechanisms. In Proceedings of the 1st IASME International Conference on Advances in Mechanics and Mechatronics (483-144), Udine, Italy, March 2004
[9.] Giovagnoni, M., 1994. A numerical and experimental analysis of a chain of flexible bodies. Journal of Dynamic Systems, Measurement, and Control 116, 73–80.
[10.] Gasparetto, A., 2004. On the modeling of flexible-link planar mechanisms: experimental validation of an accurate dynamic model. Journal of dynamic systems, measurement, and control 126, 365.
[11.] Caracciolo, R., Richiedei, D., Trevisani, A., Zanotto, V., 2005. Robust mixed norm position and vibration control of flexible link mechanisms. Mechatronics 15 (7), 767–791.
[12.] Chang, L., Hamilton, J., 1991. The kinematics of robotic manipulators with flexible links using an equivalent rigid link system (ERLS) model. Journal of Dynamic Systems, Measurement, and Control 113, 48.
[13.] Franklin, G., Workman, M., Powell, D., 1997. Digital control of dynamic systems. Addison-Wesley Longman Publishing Co., Inc. Boston, MA, USA.
[14.] Gasparetto, A., 2001. Accurate modelling of a flexible-link planar mechanism by means of a linearized model in the state-space form for design of a vibration controller. Journal of Sound and vibration 240 (2), 241–262.

INTERNATIONAL SYMPOSIUM on
ADVANCED ENGINEERING & APPLIED MANAGEMENT
– 40th ANNIVERSARY in HIGHER EDUCATION (1970-2010)
4 – 5 November, 2010, Hunedoara, ROMANIA

[1.] Albano LANZUTTI

SMOOTH TRAJECTORY PLANNING ALGORITHMS FOR INDUSTRIAL ROBOTS: AN EXPERIMENTAL EVALUATION

[1.] DIPARTIMENTO DI INGEGNERIA ELETTRICA, GESTIONALE E MECCANICA
UNIVERSITA' DI UDINE, UDINE - ITALY

ABSTRACT:
An analysis of the experimental results of a new method for smooth trajectory planning for robot manipulators is presented in this paper.
The technique is based on the minimization of an objective function that is composed of two terms: the first one is proportional to the trajectory execution time, the second one is proportional to the integral of the squared jerk. The need for a smooth trajectory and the need for a fast execution can be adjusted by changing the values of two constants that weigh the two terms. The trajectory execution time is not set *a priori* and the kinematic constraints on the robot motion are taken into account. Cubic splines and fifth-order B-splines are used to compose the overall trajectory.
Two different trajectory planning techniques (the first one minimizes the maximum absolute value of the jerk along the whole trajectory, while the second one ensures only the continuity of the position, velocity and acceleration values) have been implemented with the aim to compare the outcomes of the tests.
The described methods are applied to a 3-d.o.f. Cartesian robot and the experimental tests are carried out by using an accelerometer mounted on the manipulator end-effector.
KEYWORDS:
Trajectory planning, Smoothness, Time-jerk optimization, Experimental validation

1. INTRODUCTION

One of the most important current robotic industrial requirements is the estimation and the reduction of the manipulators vibrational phenomena. Indeed, the demand for increasing productivity through fast and high precision motion is growing, thus the designers are forced to reduce the masses of the robot structures, resulting in a loss of structural rigidity and an increase of flexibility affecting also the dynamic response of the system.

A proper calibration of the manipulator control system and a dedicated action on the trajectory planning phase [**Eroare! Fără sursă de referință.**] can be considered as a solution of the problem.

The trajectory planning is a fundamental issue for robotics applications and automation in general. At high operating speeds, required in many current tasks, the possibility to generate trajectories that satisfy specific targets and requirements is a basic step to ensure optimal results. Robotic movements and trajectories that have smoothness properties are becoming more widely used in modern applications. Indeed, the planning of trajectories with a bounded value of the jerk is an important target, since this allows to reach higher task execution speeds, reduce the excitation of the resonant frequencies of the manipulator structure and improve the tracking accuracy.

The analysis of the scientific literature shows that the trajectory planning problem is based on the optimization of some objective function or of some parameters. Criteria that are based on minimum execution time, minimum energy or actuator effort, minimum jerk or hybrid optimality approaches can be found.

With the aim to increase the productivity in the industrial sector, the first trajectory planning techniques proposed were the minimum-time algorithms. Starting from unconstrained problems [**Eroare! Fără sursă de referinţă.**], this type of optimization is recently evolved in minimum time algorithms under kinematic constraints (i.e. maximum values for velocity, acceleration and jerk) [**Eroare! Fără sursă de referinţă.**].

A second important criterion for trajectory planning is focused on the minimization of the actuator effort, i.e. the minimization of the energy required to the manipulator actuators [**Eroare! Fără sursă de referinţă.**]. If the energy consumption is minimized instead of the execution time, the effort of the actuators and the stresses of the manipulator are reduced, moreover the resulting trajectory is easier to track. This type of optimization is then preferable in applications with limited capacity of energy source.

Another type of trajectory planning algorithms are based on the optimization of the jerk along the whole length of the path [**Eroare! Fără sursă de referinţă.-Eroare! Fără sursă de referinţă.**]. If this technique is used, the excitation of the resonant frequencies of the mechanical system is reduced. Thus, the stresses to the actuators and to the robot structure are intrinsically reduced, and the tracking errors decrease.

As mentioned in the foregoing, starting from the fundamental optimization techniques above described, hybrid optimality approaches are implemented.

For instance, hybrid time-energy-optimal trajectory planning algorithms can be found in [**Eroare! Fără sursă de referinţă.**]. With the aim to reach the advantages of the jerk reduction in fast trajectories, hybrid time-jerk optimal techniques are proposed [**Eroare! Fără sursă de referinţă.-Eroare! Fără sursă de referinţă.**]. These algorithms are based on different primitives that are used to interpolate the path (e.g. trigonometric splines in [**Eroare! Fără sursă de referinţă.**], polynomials of fourth and fifth order in [**Eroare! Fără sursă de referinţă.**]) and different optimization procedures (e.g. genetic algorithms are used in [**Eroare! Fără sursă de referinţă.**], SQP algorithm in [**Eroare! Fără sursă de referinţă.-Eroare! Fără sursă de referinţă.**]).

One of the most popular algorithms for planning smooth trajectories is described in [**Eroare! Fără sursă de referinţă.-Eroare! Fără sursă de referinţă.**]. Based on interval analysis, this technique minimizes the absolute maximum value of the jerk along a trajectory whose execution time is known and set *a priori*. Cubic splines are used to interpolate the via-points of the path and the output of the algorithm is a set of time intervals that produces the lowest jerk peak.

A minimum time-jerk trajectory planning technique is presented in [**Eroare! Fără sursă de referinţă.-Eroare! Fără sursă de referinţă.**]. Two algorithms based upon a minimization of an objective function that takes into account the speed and the smooth of the trajectory are presented. More in detail, the objective function is composed of a term that is proportional to the total execution time and of a term that is proportional to the integral of the squared jerk along the path, both weighted by two parameters.

A method based on the objective function defined in [**Eroare! Fără sursă de referinţă.-Eroare! Fără sursă de referinţă.**] and extended by considering also the power consumption of the actuating motors and the joints physical limits (so that the technique is a time-jerk-energy planning algorithm) is presented in [**Eroare! Fără sursă de referinţă.**].

In this paper, the two trajectory planning algorithms presented in [**Eroare! Fără sursă de referinţă.-Eroare! Fără sursă de referinţă.**] are considered. Unlike most jerk-minimization techniques, this method does not require a trajectory execution time set *a priori*, and takes into account the robot motion constraints. Thus, one can define the upper bounds on the absolute values of velocity, acceleration and jerk for each robot joint. In order to demonstrate the benefits of the used algorithms (i.e. reduced mechanical stresses and reduced vibrational phenomena), the trajectories so planned are input to a 3-d.o.f. Cartesian robot and the vibrations of its arms during their movements are evaluated by using an accelerometer.

With the aim of evaluating the results obtained with the minimum time-jerk technique, both the method described in [**Eroare! Fără sursă de referinţă.-Eroare! Fără sursă de referinţă.**] and a classical spline based planning algorithm have been implemented and experimentally tested on the Cartesian manipulator.

The paper is organized as follows : in section 2 the planning algorithms [**Eroare! Fără sursă de referinţă.-Eroare! Fără sursă de referinţă.**] and [**Eroare! Fără sursă de referinţă.-Eroare! Fără sursă de referinţă.**] and the main characteristics of the planning techniques under test are explained; the simulations and experimental results of the used techniques ,with a brief description of the experimental set-up, are analyzed in section 3.

2. THE TRAJECTORY PLANNING ALGORITHMS

2.1. MINIMUM TIME-JERK TRAJECTORY PLANNING ALGORITHM

The minimum time-jerk algorithm (described with many details in [**Eroare! Fără sursă de referință.-Eroare! Fără sursă de referință.**]) concerns trajectories *off-line* geometrically defined. Accordingly, a *path planner* at the top level generates the geometric paths (obstacle avoidance problems are solved at this level) as a sequence of nodes in the operative space which represent successive positions and orientations of the end-effector of the manipulator. The execution time of the planned trajectory is not set *a priori (*it is a result of the algorithm), and the upper bounds on velocity, acceleration and jerk (the kinematic constraints) are taken into account.

The generated trajectory is optimized in the sense of the best compromise between execution time and value of the jerk. In order to achieve this task, a hybrid objective function made of two terms having opposite effects is considered. The first term is proportional to the trajectory execution time, whereas the second term is proportional to the integral of the squared jerk. The two effects are weighted by the coefficients k_T and k_J respectively.

In order to represent the trajectories, two specific primitives are chosen.

The first primitive is a cubic spline (the algorithm is so called SPL3J) and the objective function is given by:

$$FOBJ = k_T \sum_{i=1}^{n-1} h_i + k_J \sum_{j=1}^{N} \sum_{i=1}^{n-1} \left[\frac{\left(\alpha_{j,i+1} - \alpha_{j,i}\right)^2}{h_i} \right] \tag{1}$$

where $\alpha_{j,i}$ is the acceleration of the j-th joint at the i-th via-point, n is the number of the via-points of the path, N is the number of robot joints and h_i is the time interval between two via-points (for more details [**Eroare! Fără sursă de referință.**]).

The second primitive is a fifth-order B-spline, degree p = 5 and order k = 2r = 6, (the algorithm is so called BSPL5J) and the objective function is given by :

$$FOBJ = k_T \sum_{i=1}^{vp+1} h_i + k_J \sum_{j=1}^{N} \int_0^{tf} \left(\sum_{k=1}^{n-2} CPJ_{j,k} \cdot N_{p-3,k}(t) \right)^2 dt \tag{2}$$

where vp is the number of via-points, n+1 is the number of control points (n = vp + 2(r-1)), $N_{i,p}(t)$ is the base function, $CPJ_{j,k}$ is the control point of the jerk and t_f is the total execution time of the trajectory (for more details [**Eroare! Fără sursă de referință.**]).

The solution of the optimization problem is a vector of time intervals h_i between two subsequent via-points that minimize the objective functions (1) or (2).

With a suitable choosing of the value of the two weights k_T and k_J, in both solver methods above described, a balance between speed and smoothness of the trajectory can be reached. The limit conditions are the minimum execution time (i.e. k_J = 0) and the minimum jerk value (i.e. k_T = 0). A criterion to make the choice of the two weights is reported in [**Eroare! Fără sursă de referință.**].

2.2. GLOBAL MINIMUM JERK TRAJECTORY PLANNING ALGORITHM

For a comparative analysis of the experimental results, the global minimum jerk trajectory planning algorithm (so called GMJ) presented in [**Eroare! Fără sursă de referință.-Eroare! Fără sursă de referință.**] has been implemented. In this technique, the execution time of the trajectory is set *a priori* and the manipulator kinematic constraints are not taken into account. Moreover, cubic splines are used to interpolate the sequence of points of the geometric path that is planned in *off-line* mode.

The algorithm can be summarized as follows.

If **h** is the vector of the time intervals between two consecutive via-points, and defined $j_{k,i}(\mathbf{h})$ as the value of jerk of the i-th spline at the k-th joint, the optimization problem of the GMJ algorithm is :

$$\min_{h \in \mathbf{R}^{+n}} \; \max \left\{ \left| j_{k,i}(\mathbf{h}) \right| : i = \mathbf{1}, \ldots, n; k = \mathbf{1}, \ldots, m \right\} \tag{3}$$

subject to:

$$\sum_{i=1}^{n} h_i = T \tag{4}$$

where n is the number of via-points, m is the number of robot joints and T is the trajectory execution time. The output of the algorithm is a set of time intervals h_i that minimizes the absolute maximum value of the jerk along the whole path.

2.3. COMPARATIVE ANALYSIS OF THE PLANNING TECHNIQUES PROPERTIES

With the aim of evaluating the trajectories obtained by running the three techniques above described (SPL3J, BSPL5J and GMJ), a fourth algorithm has been implemented. It is based on cubic splines (so as to ensure the continuity of position, velocity and acceleration values). The duration of the time intervals between two via-points is proportional to the trajectory execution time, that is set *a priori*, and the number of via-points (accordingly the algorithm is called PROP). The algorithm so implemented does not take into account the kinematic constraints of the manipulator. In Table I the main properties of the four algorithms are reported.

Table I : Main properties of the SPL3J, BSPL5J, GMJ and PROP algorithms

Algorithm	Primitive	Trajectory time	Optimization	Kinematic Constraints
SPL3J	cubic spline	calculated	jerk-time	Yes
BSPL5J	quintic B-spline	calculated	jerk-time	Yes
GMJ	cubic spline	imposed	max jerk	No
PROP	cubic spline	imposed		No

An important remark on the convergence time of the four techniques that have been used must be done: for all the tested trajectories, GMJ algorithm gives the solution after several hours, whereas SPL3J, BSPL5J and PROP algorithms take less than a minute to produce the solutions. This drawback is very important if, for example, the techniques will be used to plan trajectories for industrial applications where short times of solution are necessary.

4. EXPERIMENTAL EVALUATION OF VIBRATIONAL PHENOMENA

4.1. IMPLEMENTED TRAJECTORIES

Three different trajectories have been implemented in Matlab™ and then input to the Cartesian manipulator with the aim to test and validate the benefits of using smooth trajectory planning algorithms.

The target of the experimental tests is to compare the vibrational phenomena on the robot end-effector that are induced by the movements of its arms after applying the four techniques above described on the same geometric path. This means that the trajectories via-points and the execution time associated to each path are the same for each algorithm. In order to reach the second target, the three trajectories are first simulated with the SPL3J and BSPL5J (the values of k_T and k_J are set with the aim to get the same execution time) and the execution time so obtained is then input in the GMJ and PROP algorithms. In this way, with the same test starting conditions for the four techniques, a more strict evaluation of the vibrational phenomena can be conducted. The three trajectories are below described:

Trajectory #1 : the first path implements a pick-and-place movement. The k_T and k_J values are respectively 860 and 0.005 for SPL3J technique, 10 and 1 for BSPL5J and the execution time is 7.4 s. The via-points of the trajectory are reported in Table II and in Table III the simulated mean and maximum jerk values for each algorithm are included.

Table II : Trajectory #1 via-points

Via-points	X position [mm]	Y position [mm]	Z position [mm]
1	0	0	0
2	0	0	-170
3	10	12.9	-190
4	30	38.6	-200
5	175	225	-200
6	320	411.4	-200
7	340	437.1	-190
8	350	450	-170
9	350	450	0

Table III : Maximum and mean jerk values for the four algorithms

	max [mm/s³]			mean [mm/s³]		
	x	y	z	x	y	z
SPL3J	183.54	230.43	322.49	90.04	115.68	182.84
BSPL5J	178.90	231.13	376.55	74.90	96.16	178.77
GMJ	169.52	212.19	305.21	88.90	114.18	193.02
PROP	588.30	756.70	1105.20	264.32	340.06	533.65

Trajectory #2: the second example implements a "L-shaped" path. The k_T and k_J values are respectively 845 and 0.005 for SPL3J technique, 139 and 1 for BSPL5J and the execution time is 5 s. In Table IV the trajectory via-points are reported.
For each technique, the simulated maximum and mean jerk values are shown in Table V.

Table IV : Trajectory #2 via-points

Via-points	X position [mm]	Y position [mm]	Z position [mm]
1	0	0	0
2	270	0	20
3	290	0	40
4	290	20	60
5	290	290	80

Table V : Maximum and mean jerk values for the four algorithms

	max [mm/s³]			mean [mm/s³]		
	x	y	z	x	y	z
SPL3J	531.75	532.01	195.93	278.86	278.22	84.96
BSPL5J	615.39	696.89	189.58	244.31	215.50	64.04
GMJ	511.99	524.35	184.15	273.33	293.09	56.49
PROP	1259.40	1259.20	34.60	474.02	473.92	23.04

Trajectory #3 : the last trajectory is a square with five via-points, whose sequence is reported in Table VI. The k_T and k_J values are respectively 1280 and 0.5 for SPL3J technique, 10 and 1 for BSPL5J and the execution time is 14.5 s.

The simulated maximum and mean jerk values for the four algorithms are reported in Table VII.
As mentioned before, the SPL3J and BSPL5J algorithms optimize the trajectories in the sense of best trade-off between the execution time and the integral of the squared jerk, whereas the GMJ technique minimizes the absolute maximum value of the jerk along the path. Starting from these considerations, the lowest maximum values of the jerk and the lowest mean jerk values are expected if the GMJ and SPL3J/BSPL5J are used respectively.

Table VI : Trajectory #3 via-points

Via-points	X position [mm]	Y position [mm]	Z position [mm]
1	10	10	0
2	330	10	0
3	330	330	-170
4	10	330	-170
5	10	10	0

Table VII : Mean jerk values for the four algorithms

	max [mm/s³]			mean [mm/s³]		
	x	y	z	x	y	z
SPL3J	68.96	61.95	32.91	35.39	32.38	17.26
BSPL5J	86.44	69.30	36.82	30.25	27.66	14.70
GMJ	49.42	57.28	30.43	32.35	34.11	18.12
PROP	82.59	82.59	43.88	38.87	38.87	20.65

If Tables III, V and VII are considered, it is possible to find a confirmation to the above anticipations: the GMJ algorithm provides the lowest maximum jerk values if compared with the other three techniques, while SPL3J and BSPL5J feature the lowest mean jerk values. Then, it is possible to verify that the PROP method is the worst in terms of both the mean and the maximum jerk values.

4.2. EXPERIMENTAL SET-UP

The experimental tests, aimed to evaluate the vibrational phenomena during the execution of the three trajectories planned with the four algorithms, are made on a Cartesian manipulator (Figure 1), controlled using a real time external controller.

The 3-d.o.f. manipulator has three prismatic joints, whose kinematic bounds are shown in Table VIII, a workspace of 500x600x500 mm (X, Y and Z) and an accuracy of 0.1 mm.

Table VIII : Kinematic bounds of the Cartesian manipulator

Joint	Kinematic Bounds		
	Velocity [mm/s]	Acceleration [mm/s²]	Jerk [mm/s³]
1	225	700	2400
2	225	700	2400
3	225	700	2400

The joints are actuated by means of brushless servo-motors, coupled with the robot arms by using a cogged belt and equipped with resolver position sensors. Each motor is linked to the transmission belt by a reduction gearhead.

An embedded multifunction board, the Sensoray S626, is used in order to realize a link between the manipulator and the external control loop.

The position real time controller is set up on an AMD Athlon(tm) XP 2400 (1.99 GHz with 480 MB of RAM memory) by means of the xPC Target™ toolbox of Matlab™.

In order to evaluate the vibrational phenomena of the robot during the movements of its arms induced by the planned trajectories, an uni-axial accelerometer is mounted on the end-effector. The device has a maximum value of acceleration of ±5g and an accuracy of 1036 mV/g.

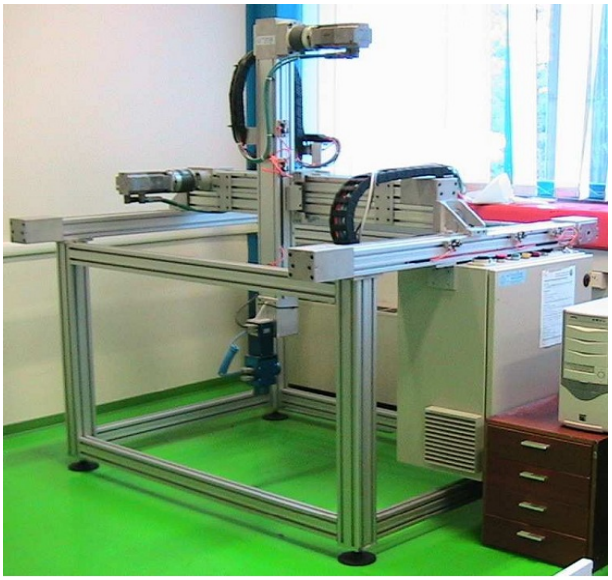

Figure 1 : Cartesian manipulator used for testing the trajectory planning algorithms

It is important to emphasize the fact that the evaluation of the vibrational phenomena is only focused on the performance of the four trajectory planning algorithms, since the performances of the real time controller are not considered as fundamentals for the experimental tests. Starting from this assumption, the only inputs that can be changed in a "simulated" industrial task are the trajectories parameters, in good accordance with the conditions found in industrial environments, where generally a user is not allowed to change the parameters of the machine controller.

4.3. EVALUATION OF THE TRAJECTORIES SMOOTHNESS

The smoothness of the three trajectories planned with the four algorithms is experimental tested by means an accelerometer mounted on the robot end-effector. The direction used to measure the vibration of the manipulator has been chosen by taking into account the mean values of the simulated jerk along the path. By considering this assumption and the Tables III, V and VII, the X cartesian direction has been chosen for trajectories #2 and #3, whereas the Z cartesian direction has been chosen for trajectory #1.

In Table IX the mean values of the measured accelerations are reported. If the PROP values are considered as reference, a mean improvement of 36% is obtained if SPL3J and GMJ techniques are considered, a mean improvement of 31% is obtained if BSPL5J algorithm is used.

Table IX : Measured accelerations mean value

	Accelerations mean value [m/s²]		
	SPL3J	BSPL5J	GMJ
Trajectory #1	0.12	0.12	0.13
Trajectory #2	0.40	0.43	0.37
Trajectory #3	0.48	0.55	0.47

The comparison between the four trajectory planning algorithms for all the paths implemented, confirms the effectiveness of the SPL3J, BSPL5J and GMJ techniques in reducing the vibrations if compared to the PROP method.

All the experimental tests demonstrate that the real behavior of the Cartesian manipulator is effectively represented by the simulations, since the simulated accelerations obtained by running the algorithms and input to the manipulator have a time course comparable with the accelerations measured by the accelerometer mounted on the end-effector. To confirm this, in Figures 2-5 a comparison between the simulated and the measured accelerations (for Trajectory #1) is reported.

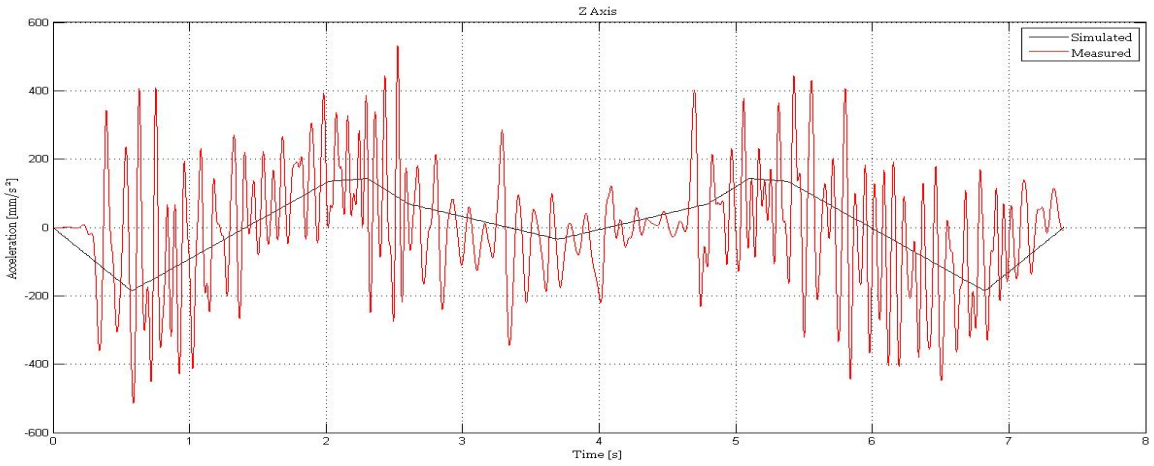

Figure 2 : Simulated vs. measured acceleration (Trajectory #1 - SPL3J)

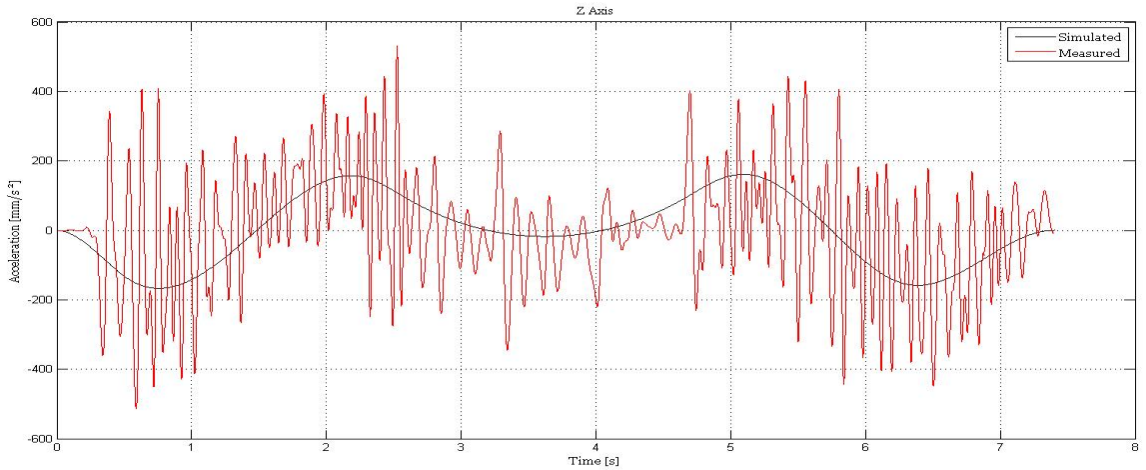

Figure 3 : Simulated vs. measured acceleration (Trajectory #1 - BSPL5J)

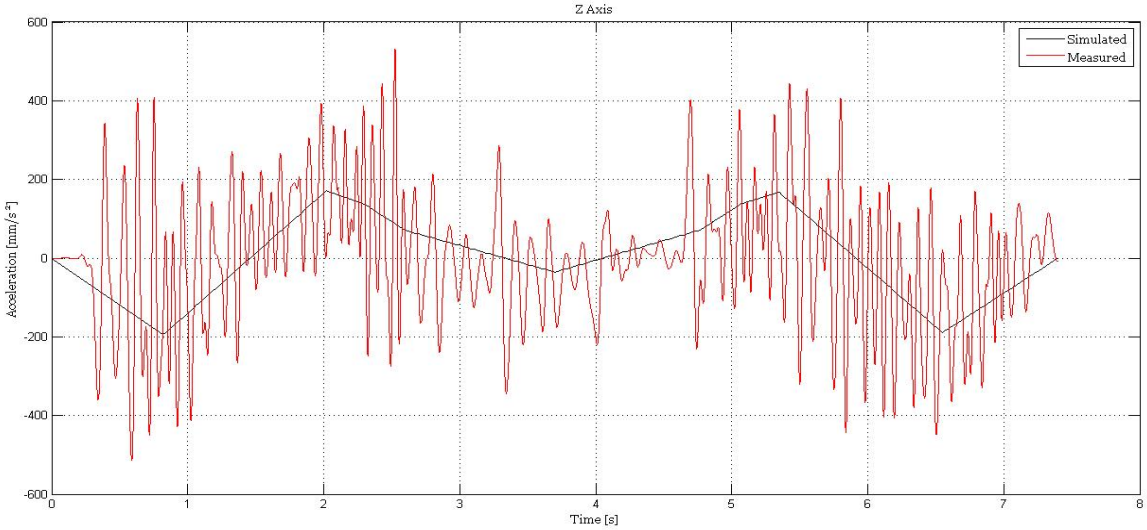

Figure 4 : Simulated vs. measured acceleration (Trajectory #1 - GMJ)

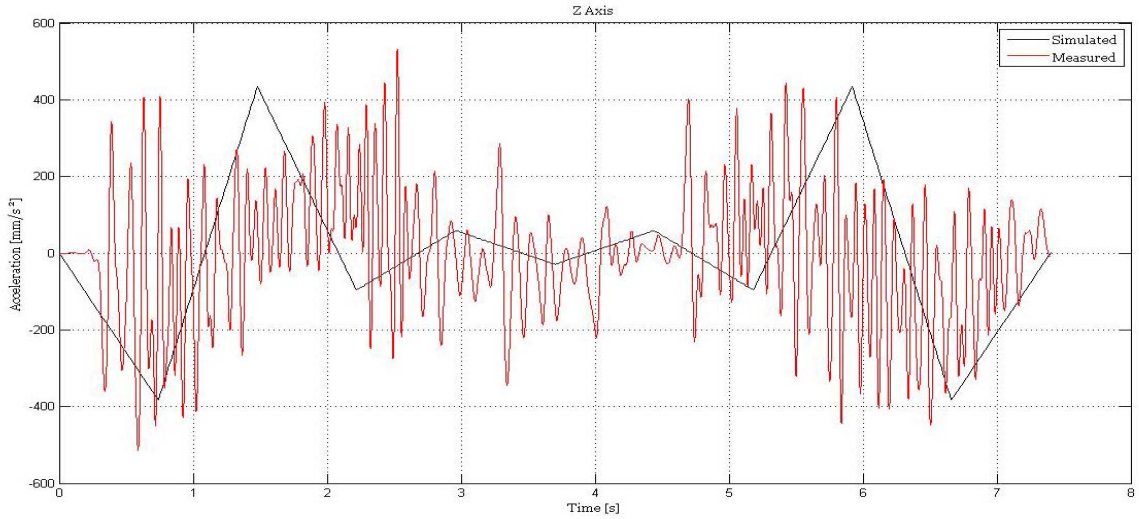

Figure 5 : Simulated vs. measured acceleration (Trajectory #1 - PROP)

5. CONCLUSIONS

In the present paper a minimum time-jerk trajectory planning technique has been experimental evaluated and validated. This method, that takes into account both the integral of the squared jerk along the trajectory and its execution time, is implemented by using two types of primitives : cubic splines (SPL3J) and fifth-order B-splines (BSPL5J). The kinematic constraints are considered in the optimization problem, and the execution time is not set *a priori*.

An accelerometer mounted on the robot end-effector has been used with the aim to measure the accelerations of the manipulator joints, in order to evaluate the vibrational phenomena of the Cartesian robot. Three test-trajectories have been implemented on a Cartesian manipulator and the experimental results have been compared with the results obtained with a global minimum jerk (GMJ) method, one of the most popular for planning smooth trajectories, and with a "classic" spline algorithm. The outcomes of the tests demonstrate the effectiveness of the smooth trajectory planning techniques, since the results prove the reductions of the vibrational phenomena of the robot arms during the trajectory execution.

REFERENCES

[1.] T. BROGARDH, Present and future robot control development – An industrial perspective, Annual Reviews in Control, 31 (1) (2007), 69-79.

[2.] A. PIAZZI and A. VISIOLI, Global minimum-time trajectory planning of mechanical manipulators using interval analysis, International Journal of Control, 71 (4) (1998), 631–652.

[3.] K. JOONYOUNG, K. SUNG-RAK, K. SOO-JONG, K. DONG-HYEOK, A practical approach for minimum-time trajectory planning for industrial robots, Industrial Robots : An International Journal, 37 (1) (2010), 51–61.

[4.] G. FIELD and Y. STEPANENKO, Iterative dynamic programming: an approach to minimum energy trajectory planning for robotic manipulators, Proc. of the IEEE International Conference on Robotics and Automation, 3 (1996), 2755–2760.

[5.] A. PIAZZI, A. VISIOLI, An interval algorithm for minimum-jerk trajectory planning of robot manipulators, Proceedings of the 36th Conference on Decision and Control, (1997), 1924–1927.

[6.] A. PIAZZI, A. VISIOLI, Global minimum-jerk trajectory planning of robot manipulators, IEEE Transactions on Industrial Electronics, 47 (1) (2000), 140–149.

[7.] H.XU, J.ZHUANG, S.WANG and Z.ZHU, Global Time-Energy Optimal Planning of Robot Trajectories, Proc. of the International Conference on Mechatronics and Automation, (2009), 4034–4039.

[8.] D. SIMON and C. ISIK, A trigonometric trajectory generator for robotic arms, International Journal of Control, 57 (3) (1993), 505–517.

[9.] P. HUANG, Y. Xu and B. LIANG, Global minimum-jerk trajectory planning of space manipulator, International Journal of Control, Automation and Systems, 4 (4) (2006), 405–413.

[10.] K. PETRINEC and Z. KOVACIC, Trajectory planning algorithm based on the continuity of jerk, Proc. of the 15th Mediterranean Conference on Control & Automation, (2007).

[11.] A. GASPARETTO and V. ZANOTTO, A new method for smooth trajectory planning of robot manipulators, Mechanism and Machine Theory, 42 (4) (2007), 455–471.

[12.] A. GASPARETTO and V. ZANOTTO, A technique for time-jerk optimal planning of robot trajectories, Robotics and Computer-Integrated Manufacturing, 24 (3) (2008), 415–426.
[13.] F. LOMBAI and G. SZEDERKENYI, Throwing motion generation using nonlinear optimization on a 6-degree-of-freedom robot manipulator, Proc. of IEEE International Conference on Mechatronics, (2009).
[14.] A. GASPARETTO, A. LANZUTTI, R. VIDONI and V. ZANOTTO, Trajectory planning for manufacturing robots: algorithm definition and experimental results, Proc. of ASME 2010 10th Biennial Conference on Engineering Systems Design and Analysis ESDA2010, (2010).

INTERNATIONAL SYMPOSIUM on
ADVANCED ENGINEERING & APPLIED MANAGEMENT
– 40th ANNIVERSARY in HIGHER EDUCATION (1970-2010)
4 – 5 November, 2010, Hunedoara, ROMANIA

[1]Aurelia TĂNĂSOIU, [2]Stelian OLARU

ON THE LIFETIME OF RAILWAY VEHICLE BEARING STRUCTURES AND COMPONENTS

[1-2]UNIVERSITY "AUREL VLAICU" ARAD, ROMANIA

ABSTRACT:
The paper presents a study on the lifetime of railway vehicle bearing structure components. A lifetime calculation is presented on the basis of static strain and stress measurements. The calculation is then compared to the experimental results of fatigue tests and the ensuing conclusions are presented.
KEYWORDS:
strain, stress, lifetime, Wohler curves

1.INTRODUCTION

Gondola wagons are used for bulk goods, the carbody being formed by a metallic structure covered with sheet metal. During travel teh lateral walls are heavily loaded such that a careful study is necessary for the resistance of the pillars that are part of the structure of the lateral walls.

The carbodies of gondola wagons contain two types of pillars within the structure of the lateral walls:

- Pillars fixed next to the pivot bearing beam;
- Pillars fixed next to the intermediary beams.

The strain and stress state was determined experimentally for two constructive options of the affixing of the pillars corresponding to the pivot bearing beam:

a. Without welding between the lower frame and the lateral pillar;
b. With welding between the lower frame and the lateral pillar.

The study aims to determine the optimal constructive option in regards to the resistance of the pillar joining with the chassis structure.

The testing was conducted on a number of 3 pillars (no. 1, 2, 3) without welding between the lower frame and the lateral pillar, and on a number of 2 pilars (no. 4, 5) with welding between the lower frame and the lateral pillar [1].

In order to conduct the testing, 5 pillars were manufactured such that they could be fixed to the testing device. The static testing were conducted on all 5 pillars in order to determine the strains and stresses.

2. EXPERIMENTAL STUDY OF THE LIFETIME

Analyzing the experimental results, it was observed that the maximum values of the stresses were measured at the points denoted by TER5 and TER6 (table 1), situated in an area that constitutes a remarkable stress concentrator.

The applied forces were determined experimentally with a force transducer with a measurement range of 0 – 10 tf, precision class 0,1 type C1 – HBM.

Table 1

Pillar no.	TER5 - σ[N/mm²]			TER6 - σ[N/mm²]		
	30kN	45kN	60kN	30kN	45kN	60kN
1	227	351	391	183	257	327
2	170	246	320	143	232	343
3	182	242	326	144	186	292
4	142	210	285	159	231	313
5	194	290	372	159	240	323

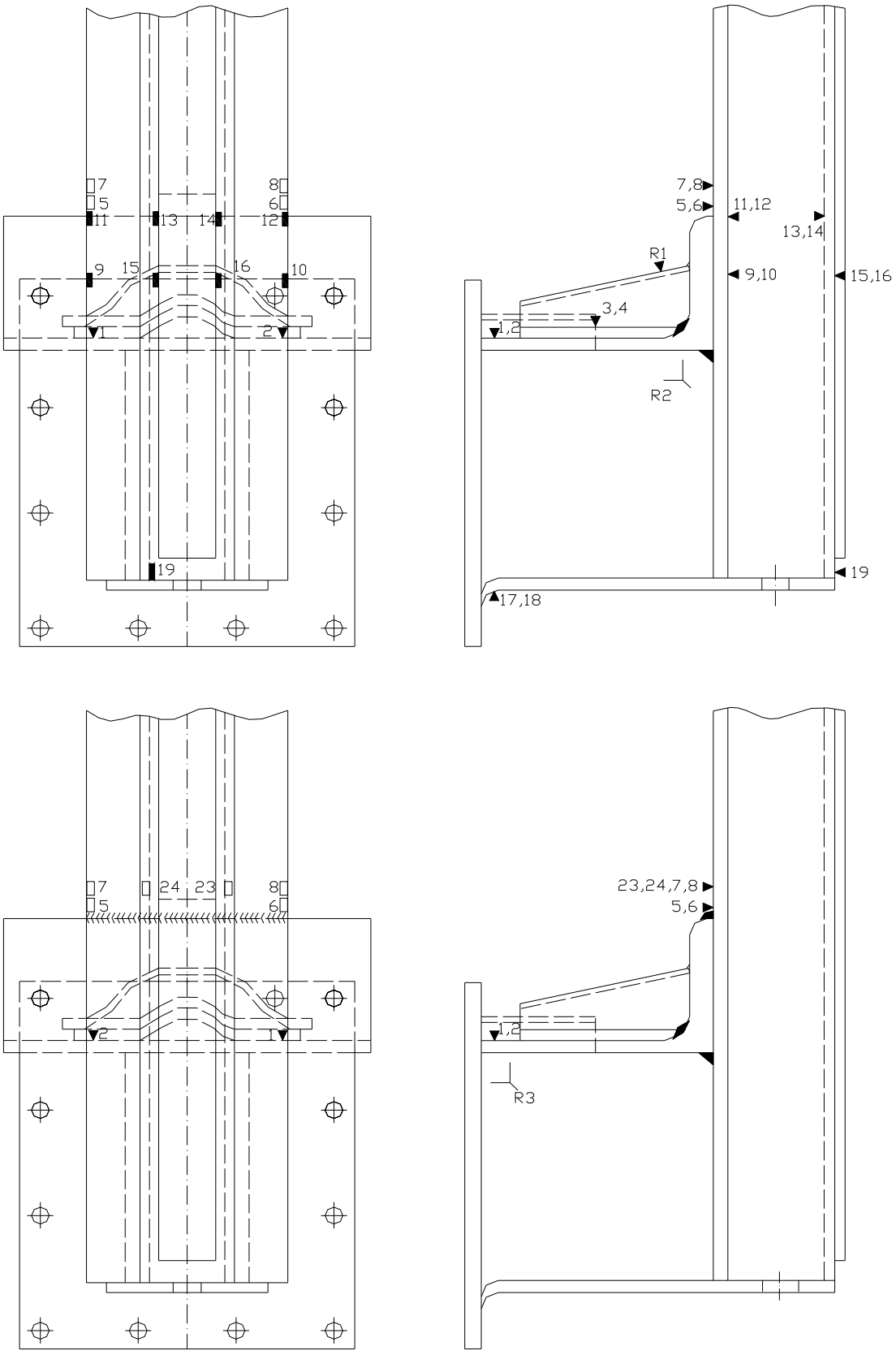

fig. 1a, 1b Placement of the electric resistive transducers

The estimation of the lifetime was done using the Wohler fatigue curves reccomended by the UIC (European Railway Association) in report ERRI B12/Rp60 [4]. The curves are shown in figure 2 and table 2.

Table 2.

Concentration class	Log a		Fatigue stress [N/mm²]
	m=3	m=5	
160	12,901	17,036	117
140	12,751	16,786	104
125	12,601	16,536	93
112	12,451	16,286	83
100	12,301	16,036	74
90	12,151	15,786	66
80	12,000	15,536	59
71	11,951	15,286	52
63	11,701	15,036	46
56	11,551	14,786	41
50	11,401	14,536	37
45	11,251	14,256	33
40	11,101	14,036	29
36	11,001	13,386	26

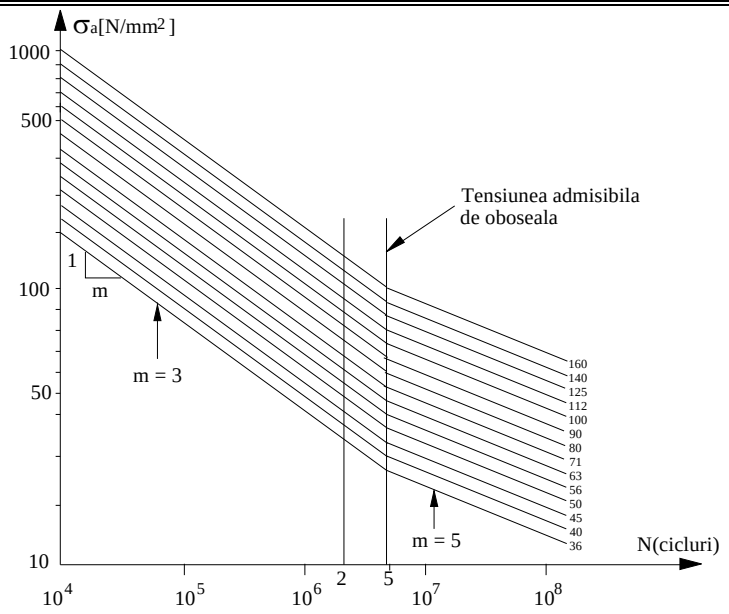

Figure 2.

Consequently, we have conducted the lifetime computation using adequeate Wohler curves [2] and the stresses determined experimentally for a load cycle of ± 15 kN, hence resulting the number of predicted cycles until the appearance of the first crack (Nf) in the area of transducers TER5, TER6 as being those in table no. 3.

Table 3.

No.	Pillar no.	Nf
Pillars without welding between the lower frame and the lateral pillar		
1.	1	387.648
2.	2	223.606
3.	3	454.926
Pillars with welding between the lower frame and the lateral pillar		
4.	4	862.622
5.	5	564.952

3.EXPERIMENTAL FATIGUE TESTING

Fatigue testing was conducted on a stand adequate to the desired goal, applying each pillar dynamic forces within a load cycle F_{med}= 45 kN, ΔF = ±15 kN and a frequency of 5,83 Hz. Throughout the trials, the time evolutions of the strains and stresses were followed closely.

The results of the lifetime estimation of each pillar for a dynamic excedent $2\Delta\sigma$ coresponding to a load $\Delta F = \pm 15$ kN are shown in table 4.

Table 4.

Pillar no.	Nf estimated [cycles]	Nf exp. [cycles]	Nr exp. [cycles]
1	387.648	445.000	740.000
2	223.606	235.000	390.000
3	454.926	483.000	818.000
4	862.622	960.000	1.101.600
5	564.952	830.00	970.000

The tests determined the number of cycles applied until the appearance of the first crack, „Nf" and the number of cycles applied until complete failure „Nr".

Figures 4 and 5 show the appearance of the fissure in the area of the stress concentrator, which was observed during the testing using the penetrating liquid method, together with the cracking or breaking manner of the pillar that have undergone fatigue testing.

During the trials it was observed that at points TER5 and TER6 the values of the stresses tend to decrease in value prior to the appearance of a crack due to the accentuated degradation of the material in the cracking section.

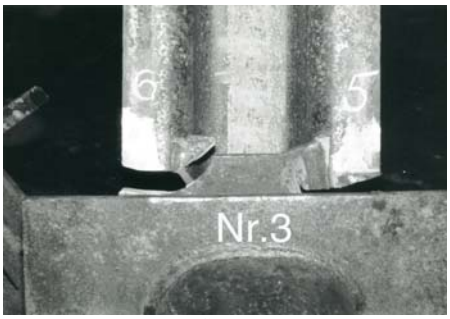

fig. 3

fig.4

4.CONCLUSIONS

Comparing the values for the estimated lifetime to the values of the lifetime up to the appearance of the first crack, a good accorandance is observed between the calculated and experimental results. This fact further confirms the correct assessment of the concentration class of the TER5 and TER6 areas, and therefore the correct choice of the used Wohler curves.

From the analysis of the experimental results it is observed that the lifetime for the pillars with welding between the lower frame and the lateral pillar is approximately 100% higher then that of the pillars without welding between the lower frame and the lateral pillar. Consequently, the solution used for pillars nr. 4 and nr. 5 should be used in the fabrication process of the wagons.

It is appreciated that the lifetime observed, estimated and determined experimentally by fatigue testing for the considered loads, is consistent in relation to the resistance of the lateral wall structure under the conditions of wagon use over a time of at least 25 years.

REFERENCES

[1.] Lăsleanu A., Copaci I. ş.a. – „Încercări la oboseală la stâlpii laterali ai vagoanelor gondolă – export URSS" – lucrare cercetare C.C.S.I.T.V.A. Vagoane Arad 1990.

[2.] Copaci Ion, Tănăsoiu Bogdan – *Durata de viaţa a elementelor elastice metalice, arcuri elicoidale folosite la suspensia vehiculelor feroviare,* Sesiunea de comunicări ştiinţifice cu participare internaţională „Cercetare ştiinţifică şi educaţie în forţele aeriene", pag. 238 -245 AFASES – 2008 Braşov 16 – 17 mai.

[3.] Aurelia Tanasoiu, Ion Copaci, Nicolae Ilias, Iosif Andras – Railway vehicle response to diferent testing scenarios and procedures, Al XVI-lea Seminar International de Stiinte Tehnice, "INTERPARTNER"23-29 sept. 2007, Alushta, Crimea, Ucraina.

[4.] ERRI B12 RP 60 - „Test to demonstrate the strength of railway vehicles", Utrecht, 1995

INTERNATIONAL SYMPOSIUM on
ADVANCED ENGINEERING & APPLIED MANAGEMENT
– 40th ANNIVERSARY in HIGHER EDUCATION (1970-2010)
4 – 5 November, 2010, Hunedoara, ROMANIA

[1]Corneliu BIRTOK-BĂNEASĂ, [2]Sorin Aurel RAȚIU, [3]Claudiu Alin BERTEAN

THE STUDY OF INFLOW IMPROVEMENT IN SPARK ENGINES BY USING NEW CONCEPTS OF AIR FILTERS

[1,2,3] "POLITEHNICA" UNIVERSITY OF TIMISOARA, FACULTY OF ENGINEERING HUNEDOARA, ROMANIA

ABSTRACT:
The article presents an experimental study conducted in the laboratory of Internal Combustion Engines belonging to the Road Motor Vehicles specialization within the Polytechnic University of Timisoara, the Faculty of Engineering of Hunedoara.
The purpose of this experiment consists in testing two concepts of air filters, conceived and made by one of the authors, filters which have been awarded at numerous invention rooms, both inside the country and abroad.
At the basis of the experimental measurements there is a stand that contains a spark engine - and its afferent apparatuses – conceived by the authors, stand which allows the determination of the pressure field on the inflow track into the engine. A series of pressure plugs were made downstream the air filter, and measurements were performed at different operating drives of the engine positioned on the stand.
The experimental results have been processed and compared with the ones obtained during the operation of the classical filter engine, provided by the builder. When the new filters are installed, one can observe a genuine improvement of the pressure drive on the inflow track.
KEYWORDS:
Air filter, spark engine, the inverted super absorbing filter, pressure field

1. INTRODUCTION

The correct filtration of the air flowing inside the cylinders of the internal combustion engine is essential for preserving the good engine's operation in time. The obstruction of various impurities' admission from the atmospheric air significantly lowers the wearing-out of the engine's moving parts. Unfortunately, in addition to its air filtration function, the air filter displays a significant gas-dynamic resistance of the absorbed air. If the air filter is not periodically cleaned and the car runs frequently in a dusty area, both the absorption pressure p_a and the filling coefficient η_V are dramatically decreased.

Currently, on the market there are several constructive air filters versions, which differ according to the filtering principle:

- filters with filtering cell;
- inertia filters;
- combined filters.

These air filters have the following disadvantages:

- the presence of the filtering element inside the box induces an enhanced gas-dynamic resistance of the absorbed air (generating the phenomenon of insufficient absorption);
- storage of impurities inside the filter affects the self-cleaning feature of the filtering element;
- the filtering element can not be visualized and it has to be dismantled for the impurity level to be checked;
- incapacity of the air filter to significantly increase the speed of the absorbed air;
- incapacity of the air filter to cool the absorbed air;
- impossibility of the air filter to create a slight effect of overfeeding during the functioning of the engine.

2. DESCRIPTION OF EXPERIMENTAL STAND

The basis for experimental measurements represents a stand containing a 4-stroke spark engine with 4 vertical cylinders in line, with a camshaft in the engine block, Dacia make, model 810.99, with carburettor and the afferent equipment, which enables the pressure field to set on the engine intake route (figure 1). A series of pressure plugs have been made downstream the air filter, and measurements have been made for different operation regimes of the engine installed on the stand, as well as for different super absorbing filters designed and made by the authors.

The positioning of the pressure plugs on the engine intake route is illustrated in figure 2.

The measurements have been made for the idle engine regime and for different revolutions. The values of the relative pressures in the intake route points where the pressure plugs were mounted have been measured, as seen in figure 2. The TESTO 510 (0-100hPa) digital manometer shown in figure 3 was used.

Moreover, to simulate motor vehicle movement, the measurements were made with an air-blower present, placed in front of the cooling radiator of the engine installed on the stand.

Fig. 1. Bird's-eye view of the experimental stand

Fig. 2. Placement and numbering of the pressure plugs

Fig. 3. TESTO 510 digital manometer

Fig. 4. Stand trial of the original classic filter

Data for the intake system equipped with original classic filter (figure 4), super absorbing filter with internal diffuser (figure 5), and supple super absorbing filter (figure 6) have been prevailed.

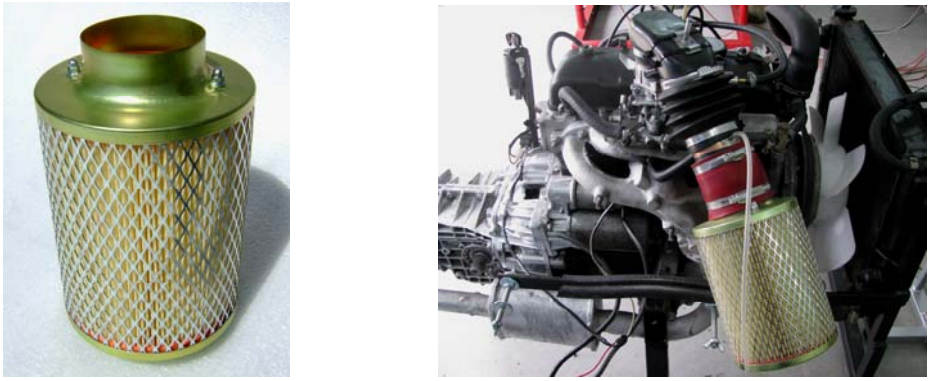

a. b.

Fig. 5. Super absorbing filter with internal diffuser: a – detail, b – mounted on the stand

a. b.

Fig. 6. Supple super absorbing filter: a – detail, b – mounted on the stand

3. RESULTS OF EXPERIMENTAL MEASUREMENTS

The results of the experimental measures for each concept are shown below, monitoring the pressure evolution for each plug, and then for each revolution, as well as the pressure distribution on the intake route up to the gallery entrance.

Due to the presence of pressure waves generated by the alternative movement of the pistons in the engine cylinders, and by the periodic opening and closure of the intake valves, the pressure values fluctuate on quite a wide range. Thus, after stabilizing the engine revolution, the (upper and lower) limit values of the pressures in the mounted plugs were registered and their average was calculated.

Original classic filter

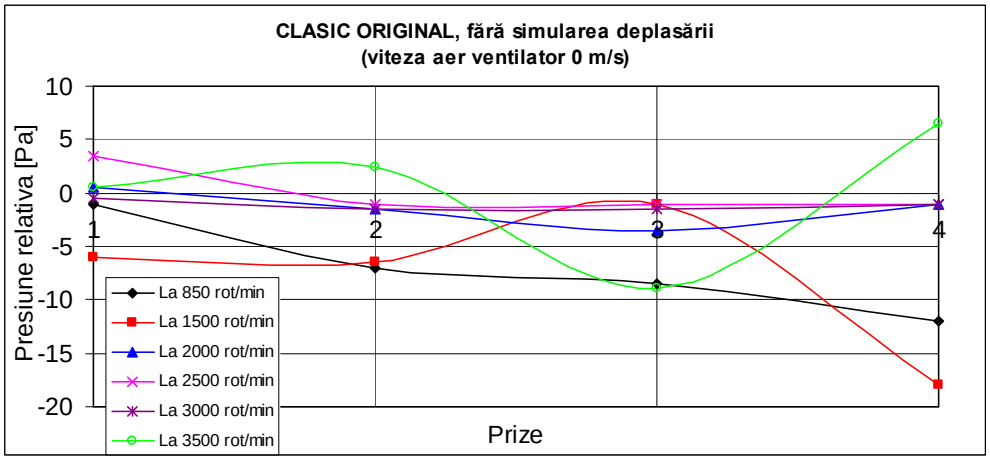

Fig. 7. Relative pressure variation along the intake route for each revolution, without movement simulation (0 m/s for air-blower air speed)

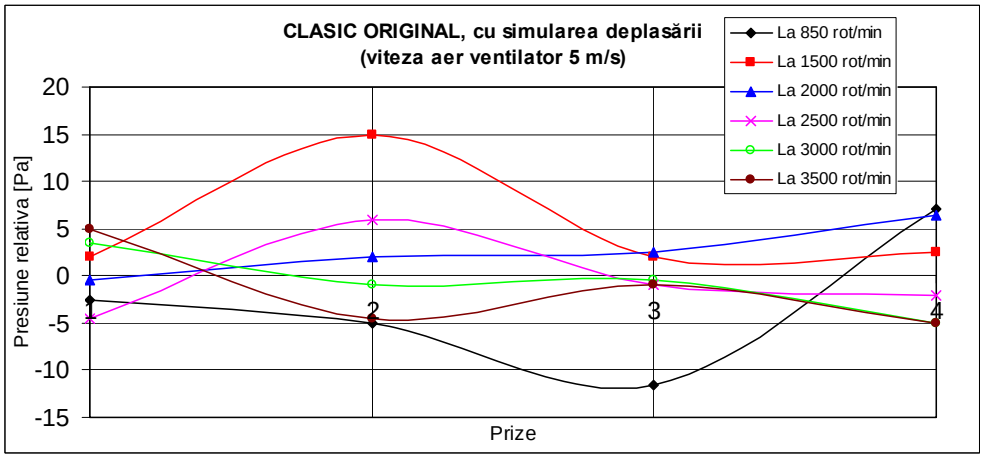

Fig. 8. Relative pressure variation along the intake route for each revolution, with movement simulation (5 m/s for air-blower air speed)

Super absorbing filter with internal diffuser

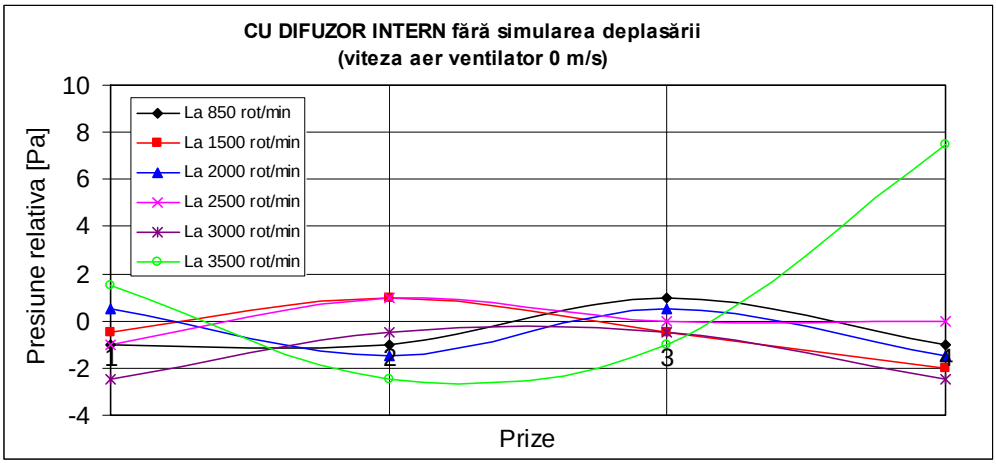

Fig. 9. Relative pressure variation along the intake route for each revolution, without movement simulation (0 m/s for air-blower air speed)

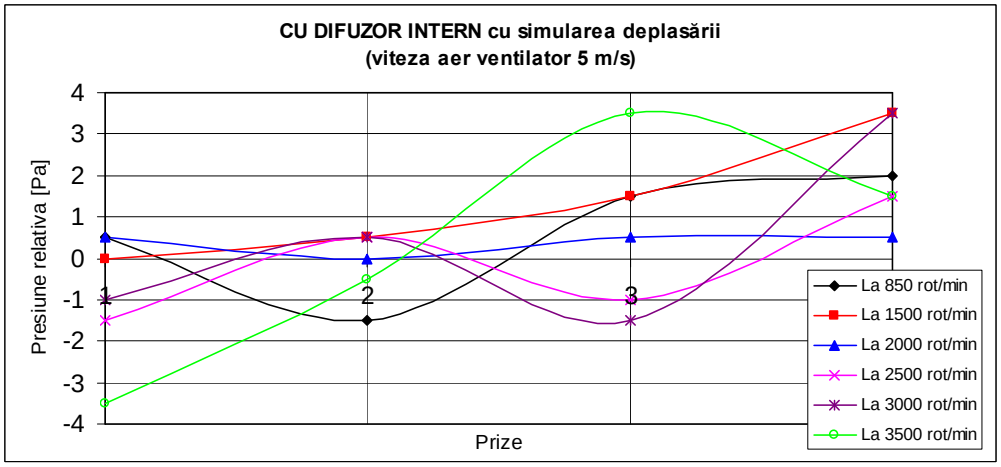

Fig. 10. Relative pressure variation along the intake route for each revolution, with movement simulation (5 m/s for air-blower air speed)

Supple super absorbing filter

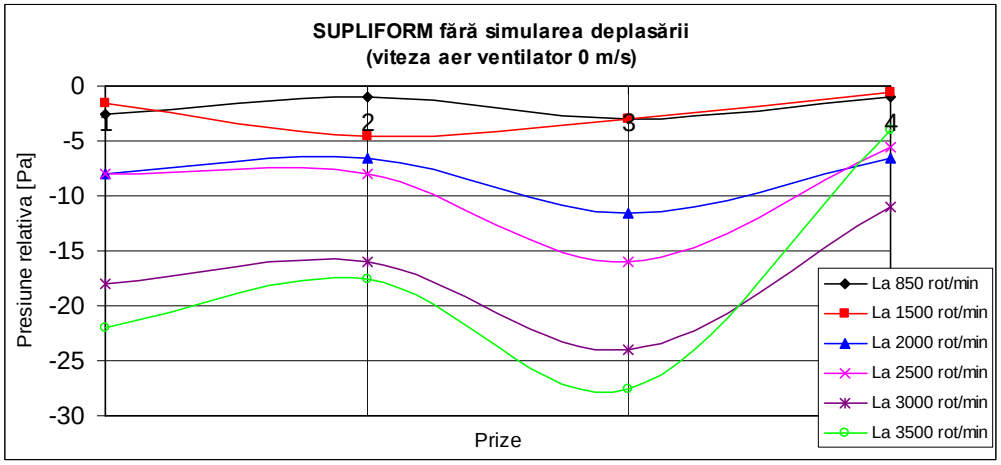

Fig. 11. Relative pressure variation along the intake route for each revolution, without movement simulation (0 m/s for air-blower air speed)

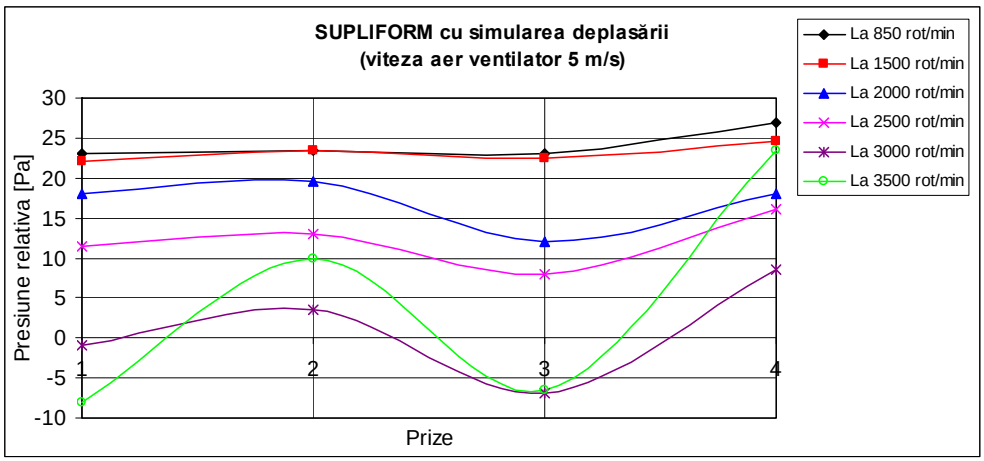

Fig. 12. Relative pressure variation along the intake route for each revolution, with movement simulation (5 m/s for air-blower air speed)

4. CONCLUSIONS

Monitoring the pressure evolution for each plug and for different engine revolutions, we can conclude the following:

- A slight overpressure effect produced by the super absorbing filter with internal diffuser along the entire revolution range, which is beneficial to the filling process;
- The overpressure effect is more evident for low revolutions for both filter concepts, and it diminishes as the revolution increases;
- The super absorbing filter with internal diffuser and the supple super absorbing one maintain the overpressure effect at high revolutions, too;
- The pressure fluctuation depending on the revolutions is less visible for the super absorbing filters with internal diffuser and broad area;
- Monitoring the pressure evolution on the intake route for different engine revolutions, one can see that for low revolutions the designed filters have a pressure fluctuation which is a lot weaker than the one induced by the original classic filter. For high revolutions the pressure evolution is somehow similar for all filters.

REFERENCES

[1.] Birtok-Băneasă, C. – *Studii privind îmbunătăţirea admisiei motoarelor cu ardere internă* – Proiect de diplomă 2010, coordonator: Şef lucrări dr.ing. Sorin RAŢIU, UNIVERSITATEA "POLITEHNICA" TIMIŞOARA, Facultatea de Inginerie Hunedoara;

[2.] Birtok-Băneasă, C. – *Creşterea randamentului volumetric al m.a.i. prin valorificarea undelor de presiune pe traseul de admisie – SDTA* – Simpozion Ştiinţific studenţesc, 22-23 mai 2009, HD-39-STUD, Hunedoara;

[3.] Birtok-Băneasă, C. – *Stand experimental pentru măsurarea câmpurilor de presiuni într-un filtru de aer inversat* – Simpozion Ştiinţific studenţesc, 23-24 mai 2008, HD-38-STUD, Hunedoara;

[4.] Birtok-Băneasă, C. – *Noi concepte privind proiectarea filtrelor de aer pentru motoarele cu ardere internă*, Simpozion Ştiinţific studenţesc, 18-19 mai 2007, HD-37-STUD, Hunedoara;

[5.] McComb, W.D. – *Turbulenţa fluidelor*, Editura Tehnică, Bucureşti, 1997 ;

[6.] Raţiu, S., Mihon,L. – *Motoare cu ardere internă pentru autovehicule rutiere* – Procese şi Caracteristici, Editura Mirton, Timişoara, 2008;

[7.] Raţiu, S. – *Motoare cu ardere internă pentru autovehicule rutiere* - Procese şi Caracteristici, Experimente de laborator, Editura Mirton, Timişoara, 2009;

[8.] Raţiu, S. ş.a. – *New concepts in modeling air filters for internal combustion engines,* The 20th International DAAAM SYMPOSIUM, 25-28th November 2009, Vienna, Austria;

[9.] www.corneliugroup.ro.

INTERNATIONAL SYMPOSIUM on
ADVANCED ENGINEERING & APPLIED MANAGEMENT
– 40th ANNIVERSARY in HIGHER EDUCATION (1970-2010)
4 – 5 November, 2010, Hunedoara, ROMANIA

[1.]Veronica ARGESANU, [2.]Imre-Albert FARKAS, [3.]Ioan LAZA, [4.]Mihaela JULA

SEALING DESIGN IN MACHINE BUILDING

[1-4.] UNIVERSITY "POLITEHNICA" TIMIŞOARA, FACULTY OF MECHANICS, TIMISOARA, ROMANIA

ABSTRACT:
The paper shows how the variation of the functional surfaces may be applied in the problem of design an area of sealing round a lid cover cork or similar object taking into interdependence form-function-technology. The proposed analysis method in the constructive generations of areas of sealing and the succession of analysis stages has the advantage of obtaining optimal types of the product which correspond to the purpose in the conditions of maximum economics.
The analysis criteria from technologic and behavior during using point of view has not been the object of the selection of the purpose types.
KEYWORDS:
machine building, sealing

1. GENERAL PROBLEMS REGARDING SEALS PROBLEMS – INTRODUCTIONS

The sealing are assemblies of machines parts, having the essential role to close as tight as possible a space that contains a pressurized environment as the separation of two or more pressurized environments that are under different pressures and also the air-tight protection of environments that contain lubrifiant against leakage or foreign objects.

A good operations sealing is an essential factor for the rehabilitee of the machines that use them. Because of that is necessary that all t he sealing problems are well analyzed and resolved with all the implications even from the first concept of those machines, installations and device's.

From the point of view of the surface shape, sealing can be plane, conical and spiral . the quality of fixing sealing in the majority of cases depends not only on the type of rubber used but also of the surface geometry.

The gasket quality of sealing is in the majority cases in function not only the rubber mixture chosen but in the same measure with the geometry of surfaces.

The choice of the right seals a very difficult issue especially if the work conditions are not ordinary and must be based on the detailed knowledge of all the intervening factors.

The knowledge of the theoretical and practical aspects of the sealing process is slowed by the fact that for every type of sealing there is a basic principle of closing a gap. These principles which allowed the selection of the optimal fixing, try to explain the process of closing a gap for maintaining a certain pressure in a certain space, also to specify the contributing factors to this process that influence the loss of fluid through leakage from the gap.

The sealing process is influenced by the kind and shape of the fixing material used, and the properties of the sealed environment, excepting the phenomena occurring in the sealing gap.

So far a general theory regarding sealing that also explains its aspects has yet to be published. The process of sealing through direct contact link to the pressured gap that needs to be covered can be well defined by the pressure gradient dp/dl, parameters that define the allure of the pressure drop on the length of the gap curve.

2. THE SHAPE-FUNCTION-TECHNOLOGY INDUSTRIAL DESIGN

Following the steps to achieve a process, starting from the logical scheme (fig. 1) taking as its starting point two aspects of problem analysis one will reach the desired function formulation and the other maintaining the desired proprieties or performances, represent the set that can represent all the criteria for an optimal product.

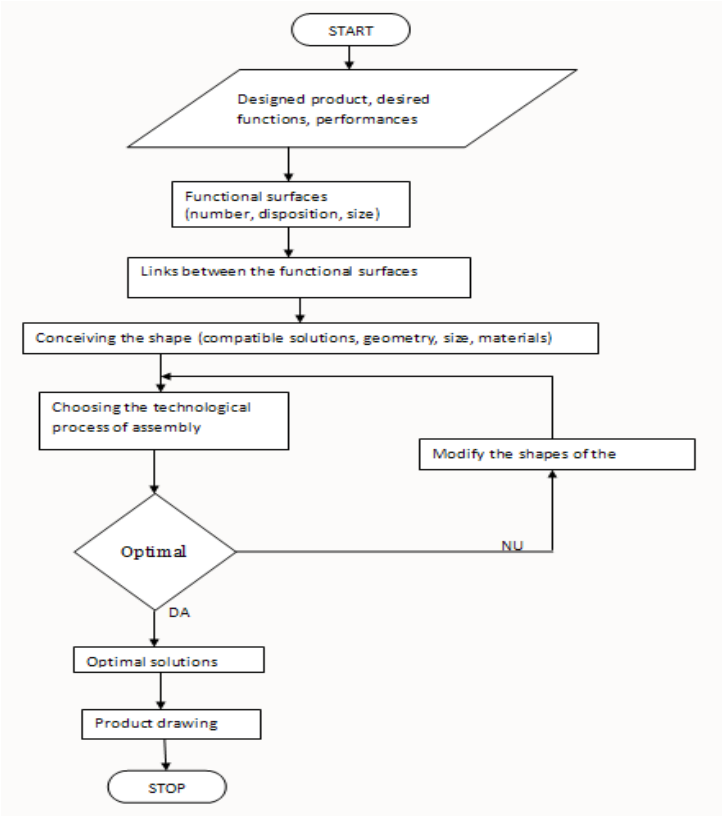

Fig. 1. Logical scheme

They are possible solutions for the sealing area. Varying structure, shape, materials, and choosing from the set of possible solutions after eliminating the possible imposed solutions, a set to match the desired optimal properties results.

Starting from the variation of functional surfaces the sealing area can be designed for ducts, lids or similar parts. The issue is drawn in fig. 2

Examining the problem on the basis of variation of the four variable parameters can show the suggestion drowning from figure 2 and 3. These don't have to be seen as final solutions but only as types of solutions that need to ulterior be worked at in detail after. (Fig.4)

FUNCTIONAL SURFACES
Parameter variation:
- Number
- Placement
- Size
- Geometrical shape

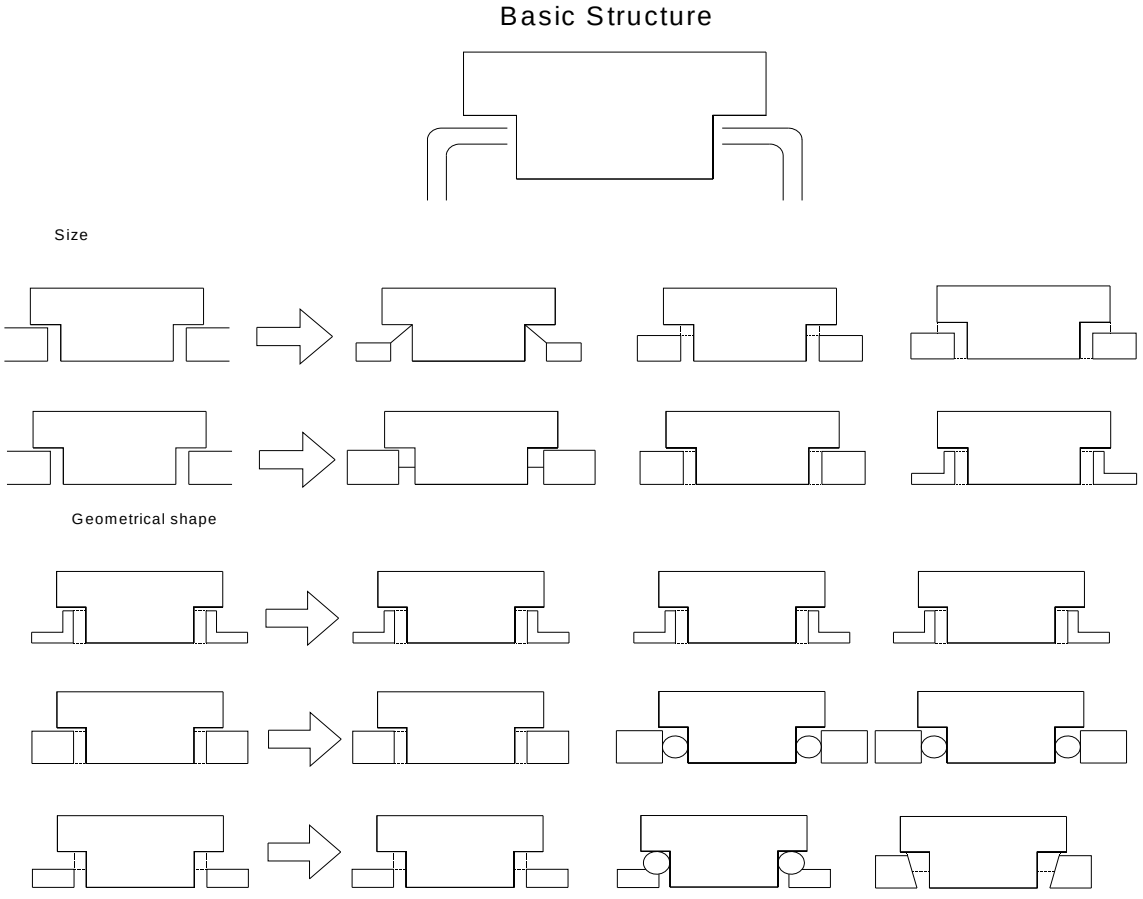

Number

Placement

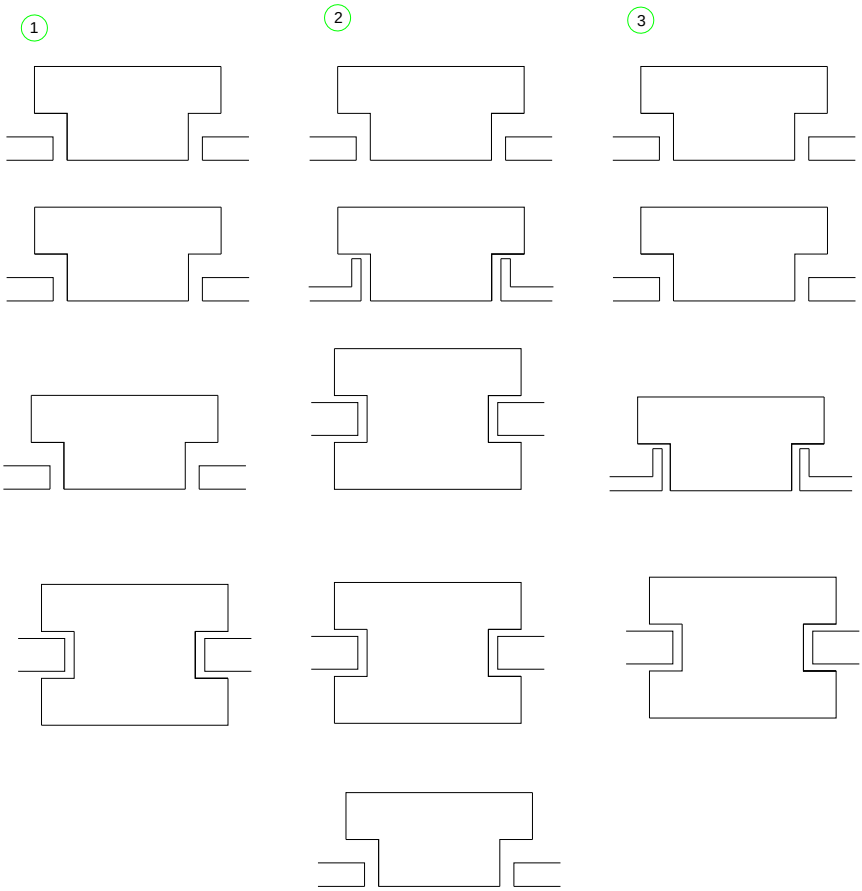

The parameter variation can be freely altered within the confines of the functionality of the surface. If one examines the whole array of solutions the evaluation of limits by individual parameters is required.

As general control of limitation it is necessary to examine the functional surfaces with both the highest and lowest use.

Such surfaces can be referred as minimal or maximal surfaces.

It is the choice of the designer to systematically apply the variation of principles or just apply the principle of maximal or minimal surface and adding few connections between the possibilities of the two cases. (Figure 5)

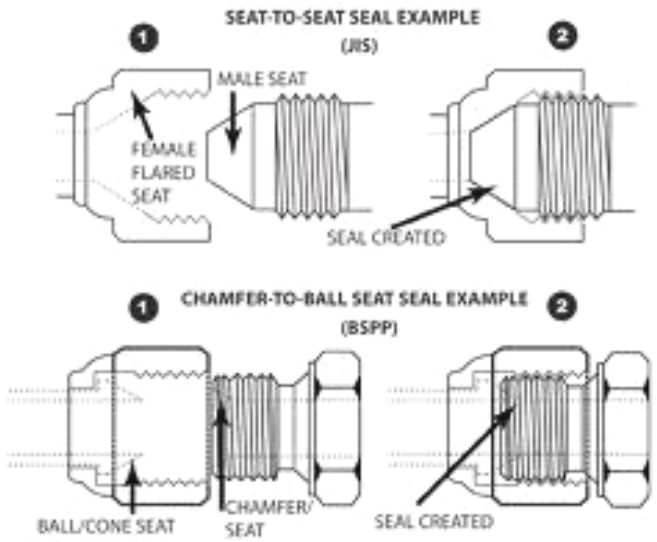

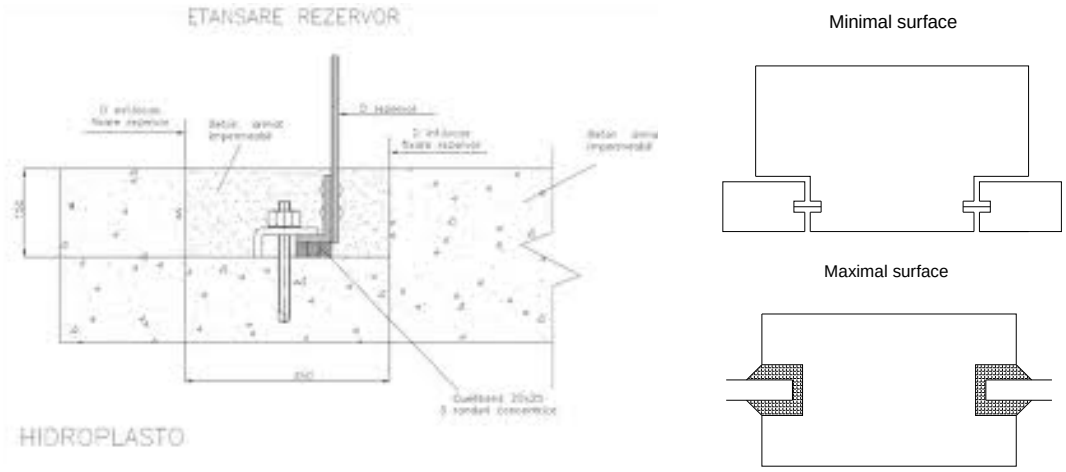

Fig. 5

Knowing the varieties, number, placement, shape and size is important in both cases.
The number of solutions after every analysis is presented in figure 6.

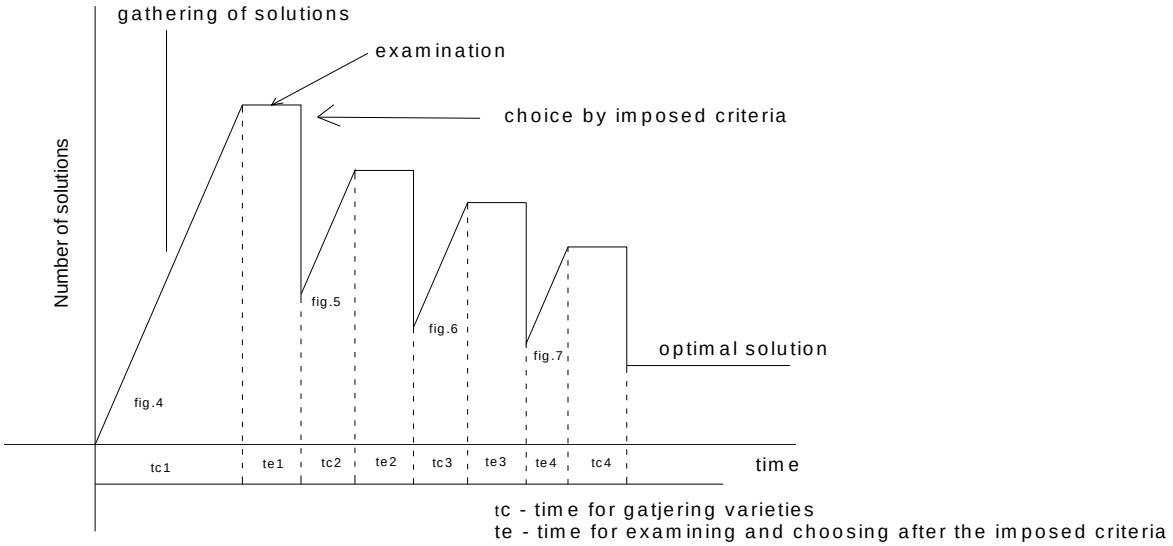

Fig. 6

The achievement of optimal varieties dependant of the domain of use results passing through the design stages presented in the paper.

3. CONCLUSION

The proposed analysis method in the constructive generations of areas of sealing and the succession of analysis stages has the advantage of obtaining optimal types of the product which correspond to the purpose in the conditions of maximum economics.

The analysis criteria from technologic and behavior during using point of view has not been the object of the selection of the purpose types.

REFERENCES

[1.] Eskild, Tealve : - A short course in industrial design, Hermes-Butterworts, London, 1979.
[2.] Cristea, V. s.a : - Etansari ET., Bucuresti, 1973.
[3.] K. Prilutskii, D. N. Ivanov, E. I. Zamolotskaya, A. N. Bessonnyi and A. I. Prilutskii - Modeling methods for perfecting sealing units of piston compressors at the design stage, September, 2004.
[4.] Fu Ying Zhang, Xi Mei Lu, Ping Wang, Qing Ping He, Efficiency-Reinforcement Design, Reciprocating Sealing Element, TRIZ Technology Evolution, August, 2009

INTERNATIONAL SYMPOSIUM on
ADVANCED ENGINEERING & APPLIED MANAGEMENT
– 40th ANNIVERSARY in HIGHER EDUCATION (1970-2010)
4 – 5 November, 2010, Hunedoara, ROMANIA

[1.] Renato VIDONI

A MULTI AGENT ROBOTIC SYSTEM FOR SIMULATION AND CONTROL OF A MANUFACTURING PROCESS

[1.] DIPARTIMENTO DI INGEGNERIA ELETTRICA,
GESTIONALE E MECCANICA UNIVERSITA' DI UDINE, UDINE – ITALY

ABSTRACT:
In this work the multi-agent technology is exploited in order to develop a Multi-Agent Robotic System with the aim to simulate and control a production chain and lay the bases for the introduction of the agent technology into a manufacturing industrial process.
In particular, a simplified washing-machine production system has been studied and agentified. More in detail, automatic production, negotiation, supplying of pieces and management of the production have been considered.
The overall simplified system has been implemented by means of the JADE (Java Agent Development Environment) platform, compliant with the FIPA (Foundation for Intelligent Physical Agents) specifications, and extensively tested in order to prove the robustness and effectiveness of the approach. The developed simplified system has been conceived in order to be easily expansible, thanks to its modularity and structure, and ready to be upgraded.
KEYWORDS:
manufacturing process, assembly line, Multi-Agents, robots

1. INTRODUCTION

Reconfigurable and adaptive production systems, which can provide companies with the proper level of agility and effectiveness, are necessary in order to satisfy fast changes of customers' needs and demands.

Markets are highly competitive and push manufacturing systems from a mass production to a mass customization fashion. A reduction of the product life-cycles, short lead times and high utilization of resources without increasing the costs are the main targets to satisfy.

In order to comply with these requests, Just In Time (JIT) techniques that allow to reduce waste of time and resources are adopted. Thus, the market is becoming more and more mutable and changeable and new technologies have to be adopted in order to react and adapt in a fast manner.

Such premises do not allow a centralized production because a high amount of work and a low flexibility of the structure will occur. Hence, production means need to become reconfigurable and founded on autonomous and intelligent modules, which dynamically interact with each other for the achievement of local and global objectives. Production processes have to provide the required level of agility, i.e. the ability to success in a rapidly changing outer environment, and embed adaptivity attributes. Moreover, in a flexible production system the goals are also the time-to-market reduction, the raise of the productivity level and the cost reduction.

Autonomous and intelligent agents - an agent is a system situated in some environment and capable of autonomous action in this environment in order to meet its design objectives [1] -, that model the production by means of a decentralized control unit and are suitable for high uncertainty and error ratios, can be the answer. Indeed, differently from the Computer Integrated Manufacturing, there is no need of a centralized approach and a unique complex process manager; only the communication and negotiation phases between agents for the use and control of machinery, resources and materials are needed.

The main advantages of this technology and approach are:

1. Decentralized and distributed decision (i.e. each agent keeps decisions autonomously).
2. Modular structure (i.e. agents are independent).

Agents can be used and exploited for:

1. *Simulation.* Agent frameworks are extensively used where the interactions between different entities have to be studied;
2. *Management and control.* An effective control system has to show flexibility, fault tolerance, reusability and low costs. As underlined in [2], agent technology is suitable for effectively reacting to the production changing and high volumes production.

In the last decade, the *scientific community* has *contributed* to the development of techniques and applications of Multi-Agent systems (MAS [1,3]).

A Multi-Agent System (MAS) consists of a group of agents that can potentially interact with each other [3]. By exploiting this feature several advantages such as reliability and robustness, modularity and scalability, decentralization, time-dependency, adaptivity, concurrency, parallelism and dynamism [4,5] can be reached. Bussman in [6] shows how a Multi-Agent system matches the requirements for agile and fast reaction to sudden and unpredictable changes in production demands and is suitable for high volumes production.

In literature, many works that deal with MAS can be found (e.g. [2]; [7]; [8]; [9]; [10]) but agent concepts and techniques are rarely applied and practically adopted in industry. Only few applications and a small part of the available technology has been successfully applied and is currently on the market. How underlined in ([2]; [11]), many works do not specify the working environment or the production plant, focusing only on the definition of a general or theoretical model. Usually, MAS has been applied in order to simulate process flows or decision activities by developing demonstrators, industrial process and chain production simulators, and small system prototypes ([8]; [12]; [13]; [14]; [15]).

At today, industrial companies rarely use Multi-Agents mechatronic systems in production and management. Most of the works are only simulations ([2]; [11]; [16]) while successful working applications is low. Among these, the flexible and distributed MAS control of a ship equipment, the Rockwell Automation, Inc. “MAST” simulation tool for material-handling and the application of MAS for production planning of SkodaAuto cars [11] can be cited.

With the purpose of standardizing agent technologies for the interoperation of heterogeneous software agents, “the Foundation for Intelligent Physical Agents” (FIPA) has become an IEEE Computer Society standards organization and has developed specifications for permitting the creation of a set of shared rules. Thanks to this efforts on standardization, FIPA-OS (FIPA-Open Source), JADE (Java Agent Development Environment) and ZEUS agent platforms compliant to the FIPA rules and directives have been created. The JADE agent platform [17], based on Java, has been chosen in this attempt in order to implement the agents and deploy the multi-agent environment.

In this work, the intelligent agent techniques will be adopted in order to study and develop a distributed framework in order to simulate and control an industrial process like the washing machine chain production.

The target is to model and identify the production chain and to realize a Multi-Agent-Robotic-System (MARS) able to simulate and control a fully autonomous assembly process that works by means of the cooperation of software and robotic agents. Such physical robotic agents moves on the environment in order to comply with specific requests as transport and station restocking like in a real factory.

2. THE STUDY: WASHING-MACHINES CHAIN PRODUCTION

Industrial manufacturing, robotized and autonomous operations and washing-machines chain production are addressed in this work. These fields suit well with the agent technology and theories.

The main target is to develop a MARS (Multi Agent Robotic System) with a high degree of flexibility that can be exploited as the base for a future intelligent and automatic system able to control the full chain production. Such a chain can be viewed, in a simplified scheme, as a collection of working stations.

Each station is in charge to assembly one (or a set of) component and pass the piece at the following station where the next correct component has to be assembled.

Each station is furnished with a small store of components (i.e. local store) that, in order to not stop the production, has to be correctly supplied and refurnished. Thus, each station can be viewed as an agent that is autonomous and reactive. Moreover, autonomous agents or robotic

agents can be applied in order to consider and substitute the human work (i.e. a human that drives a forklift truck for supplying an order).

In practice, when the autonomous agent that represents the *i*-th station realizes that the local store has to be refurnished, searches a free autonomous robotic agent that can supply its request both in terms of material quantity and time. After a negotiation phase and the entrust of the task, the chosen autonomous robotic agent goes to the central store, loads the components and brings them to the calling station. Some agents can be used as traders and facilitators in order to manage the communication or settle the conflicts and some others can record the robot data in order to give information to the stations like a yellow page service.

In this attempt, some simplifications have been made but the developed framework is implemented in order to be modular and easily expanded. A sketch of the chosen scenario is shown in Fig. 1.

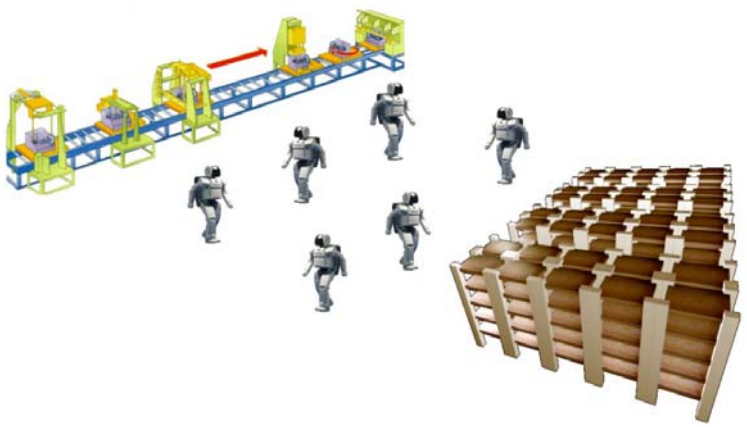

Fig. 1: Sketch of the scenario: assembly line, supply robots and main store

In this work the simplified supply chain has been modeled by means of four stations, each one in charge of assembly a specific part of the washing-machine:

- Station 1: motor and belt;
- Station 2: drum and washing tank ;
- Station 3: two bearings;
- Station 4: frame.

In a simplified view, the production follows the following operations:

- Station *i*, if the component is available in the local store, assembles the piece and, if Station *i+1* is free, pushes forward the assembly; if Station *i* does not have the piece to be mounted, searches and calls an autonomous robotic agent in order to be re-furnished. If an autonomous robotic agent is free, it is charged/entrusted to go the the central store, keep the lacking components and refurnish the calling station.
- When Station *i* has sent the current assembly to the station *i+1*, its internal state is set on “free” and it is able to receive and manage another piece.

All the works and operations have to be carried out in a parallel and not sequential manner. The flow-chart of the simplified process is presented in Fig. 2.

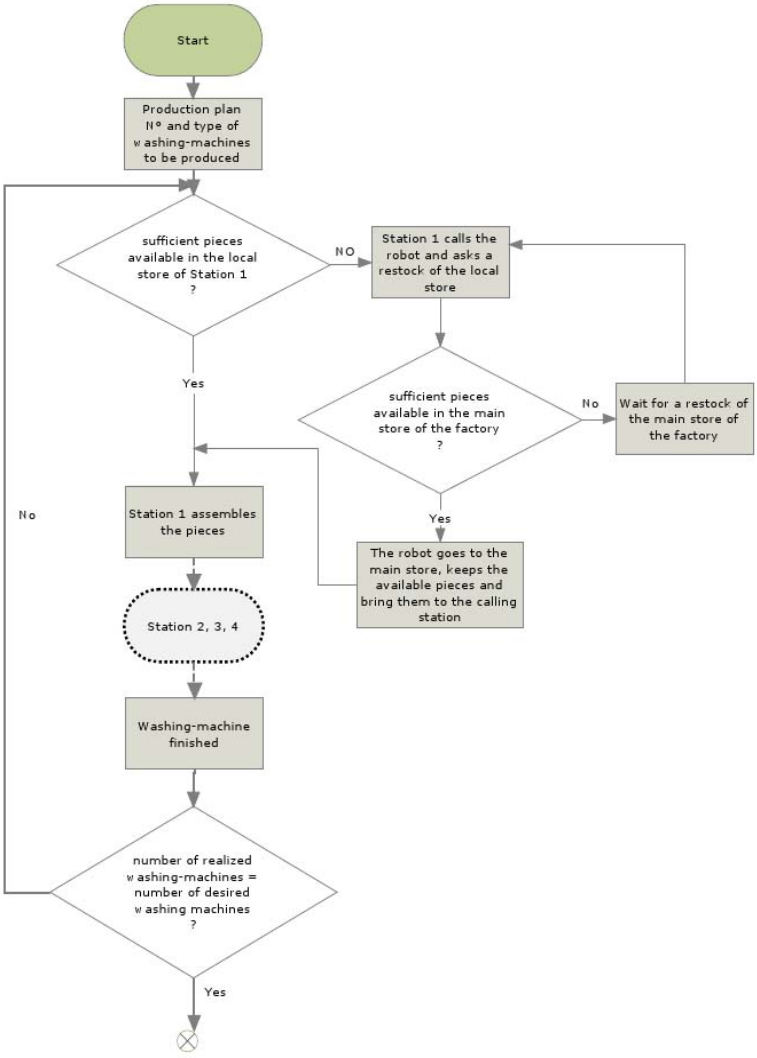

Fig. 2 : Flow-chart of the simplified process

3. THE MA(R)S SYSTEM

At least two kind of agents are necessary: one for the stations, *Station Agent*, and one for the autonomous robots, *Robot Agent*.

Moreover, a *Production Agent*, that is in charge to start and stop the process flow, and a *Supply agent*, that will manage and supply the main store when the stocks are ending, are necessary. Thus, by considering for sake of simplicity only one autonomous robotic agent, 7 agents are single out: 4 *Station Agents*, 1 *Production Agent*, 1 *Robot Agent* and 1 *Supply Agent*.

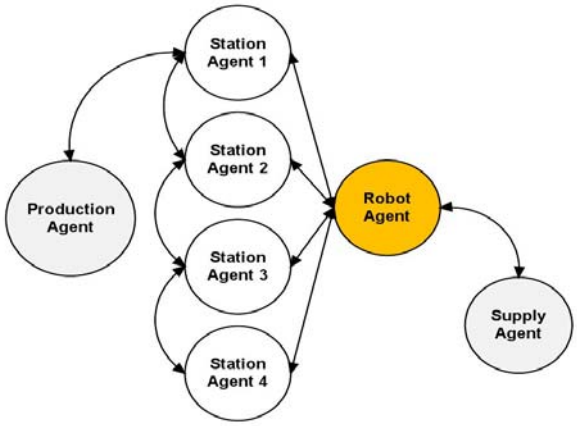

Fig. 3 : Agents of the framework

If all works properly, the *Production Agent* calls *Station Agent 1* that, after its assembly task, calls *Station Agent 2* and so on. If a component to be mounted is ending, the related station calls the *Robot Agent* that negotiates the components with the *Supply Agent* (see Fig. 3).

3.1 *Production Agent*

The *Production Agent* starts the production and sets the number of washing-machines that has to be produced.

First of all, it continuously searches all the available *Station Agents* by means of a cyclic behavior.

Inner this behavior, the *Station Agent 1*, i.e. the one related to the first station, is searched by means of a *CALL_FOR_PROPOSAL (CFP)-message* inner the *StationCommand* behavior.

If the *Production Agent* receives a *PROPOSE-message*, the *Station Agent 1* is ready to work; otherwise, if the replies are only *REFUSE-messages*, it means that there are no free agents or their name is not *Station Agent 1* and the behavior is repeated (general case). Within the *REFUSE-MESSAGE* the number of completed washing-machines is passed and, in the particular case of a number of completed pieces equal to the desired one, the production is completed.

If a *PROPOSE-message* is received, the *Production Agent* sends an *ACCEPT_PROPOSAL-message* with the current number of lacking washing-machines to the *Agent Station* that replied with a *PROPOSE-message*.

3.2 *Station Agent*

Each *Station Agent* has to know the number of available pieces in its local store, the part to assembly, how many and which *Robot Agents* and *Station Agents* are present in the framework and the name of the following station.

Each station has a certain number of available pieces in its local store and of elements that has to assembly (e.g. motor, bearings).

Moreover, each agent has to register itself into the *Directory Facilitator (DF)* that is a sort of "yellow page", in order to be found.

For this class, six behaviors are implemented:

· *ResearchRequest*, cyclic.

This behavior waits the *CFP-messages* from both the *Production* and the other *Station Agents* and sends a *PROPOSE-message* if it is free and is the correct station. Otherwise, a *REFUSE-message* is sent.

· *ArrangeResearch*, cyclic

This behavior starts with the *ACCEPT_PROPOSAL-message* of the *Production Agent* and sends an *INFORM-message* to the calling agent.

· *ProductionResearchRobotAgent*, one-shot.

It is called inner the *ArrangeResearch* behavior. If the local store is not empty, the correct piece is assembled and the *SearchStationAgent* behavior is called. If the local store has few pieces or it is empty the *ExecutionResearch* behavior is called.

· *ExecutionResearch*, generic.

It asks the lacking components to a suitable *Robot Agent*.

· *SearchStationAgent*, oneshot.

It is similar to the cyclic behavior of the *Production Agent*. It calls the *StationbystationCommand* generic behavior.

· *StationbystationCommand*, generic.

Similar to the *CommandStation* behavior. The next station is searched in order to pass the current washing-machine to be assembled.

If the local store is empty, a *REQUEST-message* is sent to the *Robot Agents*. A first research of the available robots is made; after that the lacking piece is requested by means of a *CFP-message*.

The negotiation is based on the time requested to supply the local store. The request is repeated until when at least one robot replies positively.

3.3 *Supply Agent*

It has two cyclic behaviors:

· *SupplyRequest*, cyclic.

In this behavior the supply requests from the *Robot Agents* are evaluated.

In this first version of the framework the main store is considered as ideal and, thus, the reply is always a *PROPOSE-message*.

· *SupplyOrder*, cyclic.

With this behavior the supply requests are satisfied and an *INFORM-message* is sent to the calling *Robot Agent* when the operation is ended.

3.4 *Robot Agent*

Each *Robot Agent* is able to supply a certain number of pieces and is registered into the *DF* in order to make visible its services. Moreover it represents a real autonomous robotic system (e.g. AGV, forklift truck).

The implemented behaviors are:

· *RequestOffer*, cyclic.

This behavior is used in order to supply the *CFP-messages* of the *Station Agents*. If the requested components are available and the robot is able to fulfill the order, it replies with a *PROPOSE-message* with the estimated time for making the operation. Otherwise a *REFUSE-message* is sent.

· *SupplyOrder*, cyclic.

This behavior reacts when the *Agent Station* accepts the proposal; it makes the restocking and sends an *INFORM-message* when a successful delivery is done.

· *SearchSupplyAgent*, one-shot.

It searches a *Supply Agent* in order to satisfy the order. It calls the *SupplyOrder* behavior.

· *SupplyOrder*, generic.

Similar to *StationCommand* behavior.

When a *Robot Agent* accepts a task, its state is set to “occupied” until when the requested components are not delivered.

In order to realize a framework that deals not only with software agents but also with physical agents, real robots have to be integrated into the framework. The software language, the communication channel and the physical sensors and actuators have to be set-up.

The hardware chosen in order to create a realistic simplified scenario is the *Lego Mindstorms NXT* shown in Fig. 4(a) [18].

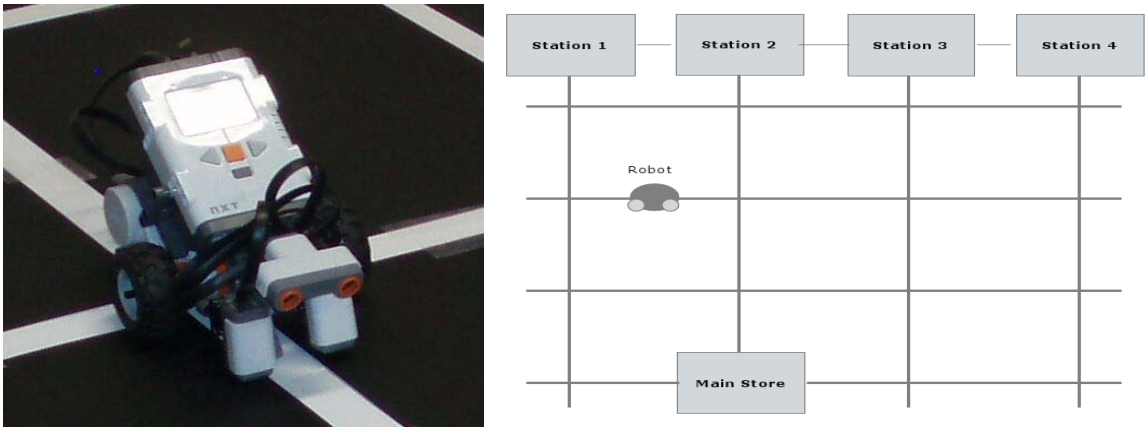

(a) (b)

Figura 4: the NXT robot (a) and the realized scenario (b)

This robot has been employed on a three wheeled (tricycle) configuration with two motors that control the two tractor wheels (see Fig.4(a)). The robot is equipped with different sensors. In particular, two classes of them have been used. Two light sensors have been installed and located at

the robot front in order to follow the chosen road and recognize the crosses. Indeed the travel area has been defined as a grid of roads to be followed. Also, an ultrasonic distance sensor has been included in the robotic system in order to evaluate if there are obstacles in a range between 10 and 15 cm. Java is the programming language that has been used to implement the overall system. In particular, in order to command and control the robot, the ICOMMAND API has been exploited and the leJOS firmware has been employed [18].

As depicted in Fig.4(b), the working stations are at the top while the main store is at the bottom of the plant. When a robot is called and accepts the work, it has to leave from the calling station or from the current position, go the central store and come back to the calling station. For each station a predefined path can be used or a shortest path searching algorithm can be exploited. In order to communicate, send orders and receive information with the real robot, a Bluetooth-connection is established between the Robot Agent and the NXT.

The overall system has been implemented on an Intel Pentium Dual Core T3400 @ 2.16 Ghz, RAM 4 GB PC hardware and extensively tested in order to fix bugs or unwanted behaviors. Different production orders have been sent to the *Production Agent* in order to simulate a realistic production.

4. CONCLUSIONS

In this work a Multi-Agent Robotic System has been studied, defined and realized in order to lay the bases for the optimization and management of an industrial process by means of the theories based on the autonomous agents.

As a scenario, a washing-machine assembly line has been evaluated. Human operators that work in order to restock the local stores of each working station have been considered as autonomous (robotic) agents.

Each working station has been modeled as an agent, and a simplified agentification of the process has been made. The overall framework and agents have been realized by means of the JADE platform that follows the FIPA standards and a NXT robot has been integrated into the system in order to simulate in a realistic manner the motion of a robotic agent and the communication process into the real-environment.

Future work will cover the extension of the framework in order to consider the main store management and the integration of different robotic systems with high navigation, motion and handling capabilities.

REFERENCES

[1.] Wooldridge, M. *An introduction to multiagent Systems*. Ed. JohnWiley & SonsLtd., Chichester, (2002).

[2.] Caridi, M. and Cavalieri, S., (2004), *Multi-agent systems in production planning and control: an overview*, Production Planning & Control, 15:2, 106-118.

[3.] Vlassis, N. *A concise introduction to multiagent systems and distributed artificial intelligence. Synthesis*, Lectures on Artificial Intelligence and Machine Learning. Morgan and Claypool Publishers. (2007).

[4.] Elamy, A. H. *Perspectives in agent-based technology*. AgentLink News, Vol. 18 pp. 19-22. (2005).

[5.] Parunak, H. V. D., (1998), *Practical and industrial applications of agent-based systems*. URL: http://agents.umbc.edu/papers/apps98.pdf.

[6.] S. Bussmann, K. Schild, *An agent-based approach to the control of flexible production systems*, In Proc. of the 8th IEEE Int. Conf. on Emergent Technologies and Factory Automation (ETFA 2001) (2001), pp. 481-488.

[7.] Hao, Q, Shen, W, Zhang, Z, (2005), *An Autonomous Agent Development Environment for Engineering Applications*, Int. J. of Advanced Engineering Informatics, 19(2):123-134.

[8.] Hao, Q. and Shen, W., (2006), *An agent-based simulation of a JIT material handling system*, in IFIP Int. Federation for Information Processing, 220: 67-78, Information Technology for Balanced Manufactiuing Systems, (Boston: Springer).

[9.] Sayda, A.F., and Taylor, J.H., (2007), *Toward A Practical Multi-agent System for Integrated Control and Asset Management of Petroleum Production Facilities,IEEE Int. Symposium on Intelligent Control (ISIC)*, Singapore, October 2007.

[10.] Dangelmaier, W, Heidenreich, J, Pape, U, () *Supply Chain Management: A Multi-Agent System for Collaborative Production Planning*, Proc. Of the IEEE Int. Conf. on e-Technology, e-Commerce and e-Service, 2005. (EEE '05).

[11.] Pechoucek, M., Marík, V, (2008), *Industrial deployment of multi-agent technologies: review and selected case studies*, Autonomous Agent and Multi-Agent Systems, 17:397–431.
[12.] Albert, M., Längle1, T., Wörn, H., Capobianco, M., Brighenti, A., (2003), *Multi-Agent Systems for Industrial Diagnostics,* Proceedings of 5th IFAC Symposium on Fault Detection, Supervision and Safety of Technical Processes 2003.
[13.] Hallenborg, K, (2007), *Decentralized scheduling of baggage handling using multi-agent technologies, in Multiprocessor Scheduling: Theory and Applications*, ed. Levner, Dec. 2007, Itech Education and Publishing, Vienna, Austria
[14.] Trullàs-Ledesma, J. and Ribas-Xirgo, L., (2008), *Integrating physical and software sub-systems in a manufacturing environment through agentification*, IX Workshop of Physical Agents 2008.
[15.] Xiaohua Liu, Jie Lin, Feng Wang, (2009), *Simulation system of Production Scheduling Multi-Agent-Based*, 2009 World Congress on Computer Science and Inf. Eng.
[16.] Burmeister, B, *Industrial Application of Agent Systems: Lessons Learned and Future Challenges*, L. Braubach et al. (Eds.): MATES 2009, LNAI 5774, pp. 1–3, 2009. © Springer-Verlag Berlin Heidelberg 2009.
[17.] Bellifemine, F., Caire, G., Poggi, A., Rimassa, G. JADE: *A software framework for developing multiagent applications. Lessons learned*. Information & Software Technology, Vol. 50(1-2) pp. 10-21, 2008.
[18.] leJOS, 2010. *Java for lego mindstorms*. Web available, http://lejos.sourceforge.net

INTERNATIONAL SYMPOSIUM on
ADVANCED ENGINEERING & APPLIED MANAGEMENT
– 40th ANNIVERSARY in HIGHER EDUCATION (1970-2010)
4 – 5 November, 2010, Hunedoara, ROMANIA

[1.] József SÁROSI

ACCURATE POSITIONING OF HUMANOID UPPER ARM

[1.] FACULTY OF ENGINEERING, UNIVERSITY OF SZEGED, HUNGARY

ABSTRACT:
Several control ways have been applied to control different humanoid or robot arms, manipulators, prosthetic and therapy devices driven by pneumatic artificial muscles (PAMs). The early control methods were based on classical linear controllers and then some modern control strategies have been developed (e. g. adaptive controller, sliding-mode controller, fuzzy controller, neural network controller and others) ([1], [2] and [3]).
This paper presents a humanoid upper arm and discusses its positioning using sliding-mode control.
KEYWORDS:
humanoid or robot arms, pneumatic artificial muscles, sliding-mode control

1. INTRODUCTION

Nowadays, pneumatic actuators have been considered as a substitute of conventional motors because of its high power/weight and power/volume ratios. The newest type of pneumatic actuator the McKibben muscle possesses all advantages of traditional pneumatic actuators without the main drawback such as low power to weight ratio. The main disadvantages are connected with the accuracy of control and nonlinearities of pneumatic systems [4].

The behaviour and structures of PAMs are well described in literature ([5], [6] and [7]).

Many researchers have studied to generate easier model of PAM to overcome difficulty in control because of it's nonlinearity, also some have tried to control robot using that model, but their studies are limited on simulation and their good performances are valid only being applied to simulation model. Physical implementation is more complicated problem [4].

Pneumatic artificial muscles show similarity to biological muscles, for this it's very effective to implement humanoid. The PAMs are one-way acting, we need two ones to generate bidirectional motion: one of them moves the load, the other one will act as a brake to stop the load at its desired position and the muscles have to change function to move the load in the opposite direction. This specific connection of the muscles to the load is generally named as an antagonistic setup.

The layout of this paper is as follows. Section 2 (The study) is devoted to display our test-bed and the LabVIEW program for positioning. Section 3 (Results and discussion) presents several experimental results. Finally, section 4 (Conclusions) gives the investigations we plan.

Fluid Muscles DMSP-10-250N-RM-RM (with inner diameter of 10 mm and initial length of 250 mm) produced by Festo company were selected for our newest study.

2. THE STUDY

In [8] and [9] can be found detailed descriptions of our test bed and former experimental results for positioning.

The newest setup for positioning a humanoid upper arm is shown in Figure 1. The PAMs were installed horizontally and can be controlled by MPYE-5-M5-010-B type proportional valve made by Festo.

Because of the difficulties caused by the nonlinear properties of pneumatic systems a LabVIEW based sliding mode control was designed. The purpose of positioning is to move the arm from a starting position to a desired position. With the use of sliding-mode control the positioning error can be minimized.

The positioning of the arm was measured with a BDF-6350-3-05-2500-65 type (produced by Balluff) rotary incremental encoder.

The signals from the encoder have to be acquired by the LabVIEW program so that they can be used by computer. The device is a NI 6251 card equipped with a PCI interface, to this a SCB 68 type I/O device has been attached with a special connecting cable, on the data acquisition card there are 16 16-bit analog inputs and two 16-bit analog outputs also there are 24 digital inputs and two 32-bit counters as well.

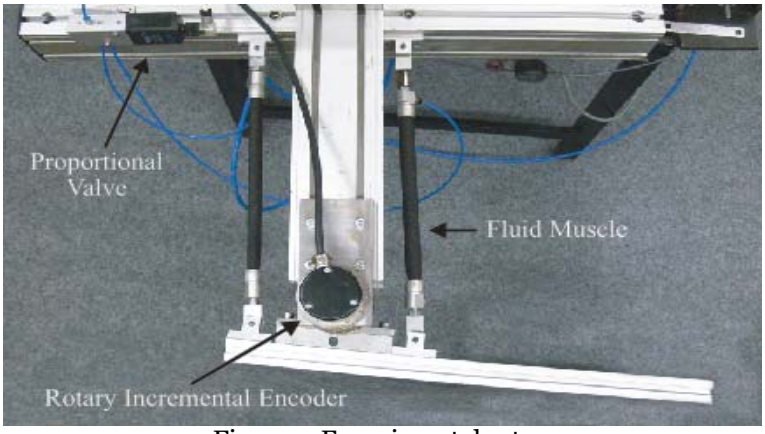

Figure 1. Experimental setup

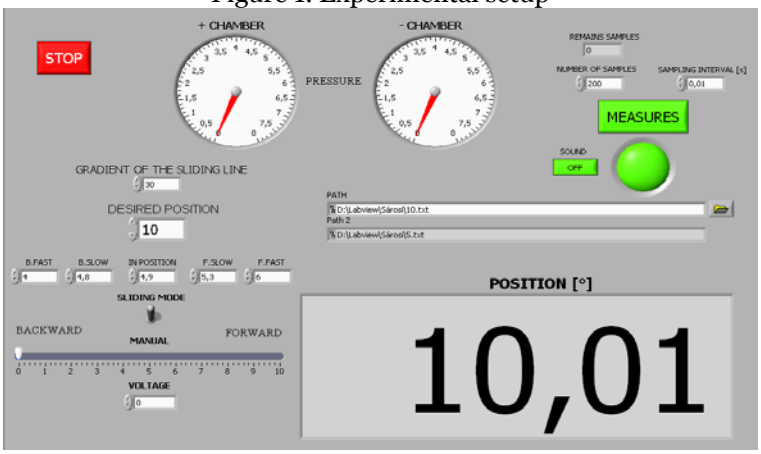

Figure 2 Front panel of LabVIEW program for positioning

The Figure 2 shows data acquisition and positioning that can be achieved in LabVIEW environment. Aside from the desired position the number of samples and the sampling time can also be set. The data can be saved into a text file.

3. RESULTS AND DISCUSSION

Positioning was first done in room temperature on the pressure of 6 bar. The desired positioning was set to 10°, the number of samples was set to 200, while the sampling rate was set to 10 ms, thus the measurement took 2 s. The quality of the positioning (overshot, steady state error) can be manipulated with the slope of the sliding line. When choosing the slope of the sliding line the optimum between two concurrent properties must be found (speed, accuracy). The more smaller the slope the more faster the trajectory reaches the sliding line, but it will take longer to set. For the slope of the sliding line a value of 30 was set.

Figure 3 shows the positioning as a function of time. It took about 1 s for the position to reach the set value. To show the accuracy of positioning the area around the desired position has been magnified (Figure 4). It has been observed that the value of the steady state error is quite favorable, 0,04°.

The measurements were repeated in 20° position. The desired positioning was set to 20°, the number of samples was set to 200, while the sampling rate was set to 10 ms, thus the measurement took 2 s, and the slope of the sliding line a value of 30 was set. Figure 5 shows the positioning as a function of time. It took about 1,2 s for the position to reach the set value. To show the accuracy of positioning the area around the desired position has been magnified (Figure 6). This Figure shows the accuracy of positioning is within 0,04°.

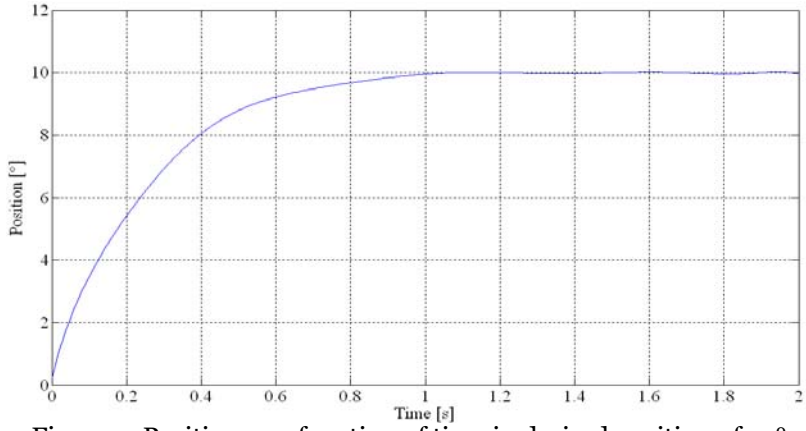

Figure 3. Position as a function of time in desired position of 10°

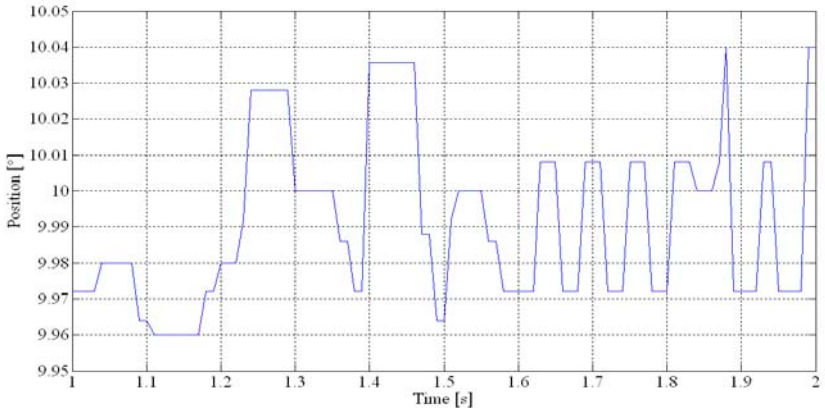

Figure 4. Position as a function of time in desired position of 10° (enlarged)

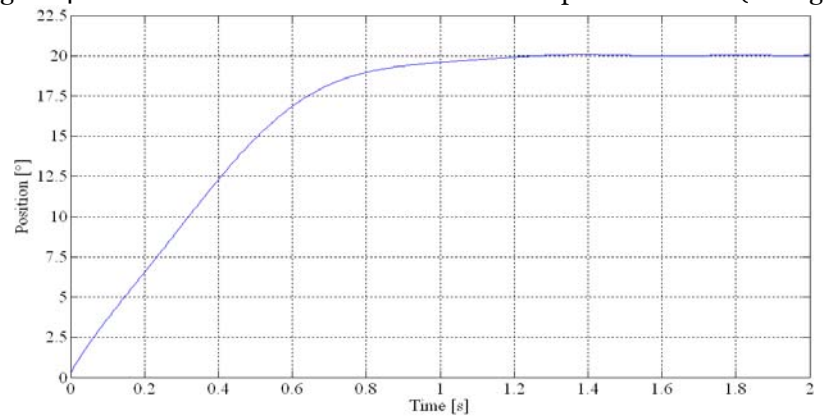

Figure 5. Position as a function of time in desired position of 20°

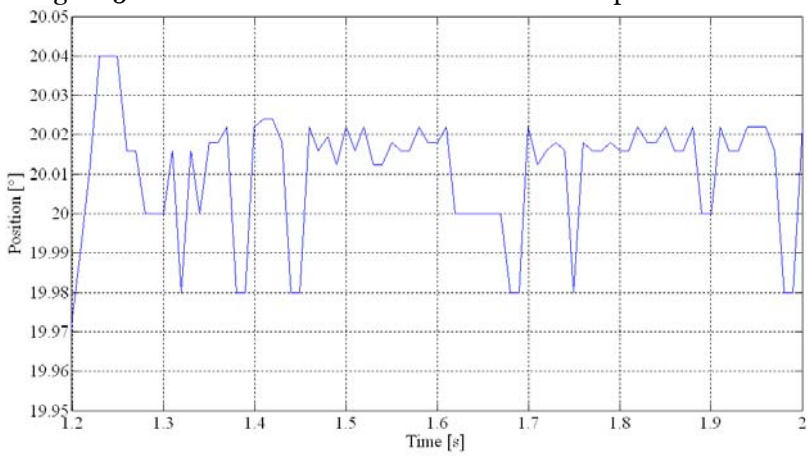

Figure 6. Position as a function of time in desired position of 20° (enlarged)

4. CONCLUSIONS

From these experiments we concluded is that the sliding-mode control can be used for precise robust control of positioning of a humanoid upper arm, for it is fast, robust to external interferences and the changing of internal parameters. Our plans include building a new arm with more muscles and more degrees of freedom for more complex movement and analyzing the data.

REFERENCES

[1.] Caldwell, D. G., Medrano-Cerda, G. A. and Goodwin M. (1995): Control of pneumatic muscle actuators, IEEE Control System Magazine, Volume 15 (1), pp. 40-48.
[2.] Situm, Z. and Herceg, Z. (2008): Design and control of a manipulator arm driven by pneumatic muscle actuators, 16th Mediterranean Conference on Control and Automation, Ajaccio, France, 25-27 June, 2008, pp. 926-931.
[3.] Zhu, X., Tao, G., Yao, B. and Cao, J. (2008): Adaptive robust posture control of parallel manipulator driven by pneumatic muscles with redundancy, Mechatronics, IEEE/ASME Transactions on, Volume 13 (4), pp. 441-450.
[4.] Choi T. Y., Kim J. J., and Lee J. J. (2006): An artificial pneumatic muscle control method on the limited space, SICE-ICASE International Joint Conference, Bexco, Busan, Korea, 18-21 October, 2006, pp. 4738-4743.
[5.] Daerden, F. and Lefeber, D. (2002). Pneumatic artificial muscles: actuator for robotics and automation, European Journal of Mechanical and Environmental Engineering, Volume 47, pp. 10-21.
[6.] Caldwell, D. G., Razak, A. and Goodwin, M. J. (1993): Braided pneumatic muscle actuators, Proceedings of the IFAC Conference on Intelligent Autonomous Vehicles, Southampton, United Kingdom, 18-21 April, 1993, pp. 507-512.
[7.] Tondu, B. and Lopez, P. (2000): Modeling and control of McKibben artificial muscle robot actuator, IEEE Control System Magazine, Volume 20, pp. 15-38.
[8.] Sárosi J., Gyeviki J., Szabó G. and Szendrő P. (2010): Laboratory Investigations of Fluid Muscles, International Journal of Engineering, Annals of Faculty of Engineering Hunedoara, 2010, Volume 8 (1), pp. 137-142.
[9.] Sárosi J., Gyeviki J., Véha A. and Toman P. (2009): Accurate Position Control of PAM Actuator in LabVIEW Environment IEEE, 7th International Symposium on Intelligent Systems and Informatics, Subotica, Serbia, 25-26 September, 2009, pp. 301-305.

INTERNATIONAL SYMPOSIUM on
ADVANCED ENGINEERING & APPLIED MANAGEMENT
– 40th ANNIVERSARY in HIGHER EDUCATION (1970-2010)
4 – 5 November, 2010, Hunedoara, ROMANIA

[1] Iosif DUMITRESCU, [2] Dumitru JULA, [3] Vilhelm ITU

STUDY OF IMPROVEMENT OF ROTATION MECHANISM BALL OF EsRc-1400 ROTOR EXCAVATOR

[1, 2, 3] UNIVERSITY OF PETROŞANI, ROMANIA

ABSTRACT:
The paper presents the study of the possibility of improvement of EsRc-1400 rotor excavator's rotation mechanism ball.

KEYWORDS:
EsRc-1400 Rotor, Rotation Mechanism Ball, Improvement

1. INTRODUCTION

Increasing mechanization of lignite strata and sterile rocks extraction from their stripping, involves modernization processes, as well as technological systems used in specific extraction conditions and technical furbishing of quarries.

Lignite quarries in Romania are equipped with technological flows provided with rotor excavators, conveyer belts, dumping machines, depositing and additional machines, providing a theoretical capacity of 200 000 m³/h, and transportation and dumping of 300 000 m³/h, respectively.

In Romanian lignite quarries 99 rotor excavators are in use, 53 dumping machines, 584 conveyer belts summing up 325 km and other depositing and additional machines.

EsRc rotor excavator is the basic machine in the lignite quarries in our country, approximately 70% of the excavations' volume being done with this type of machine.

Fig. 1 shows an overall view of EsRc-1400 excavator where the rotation mechanism between the lower platform on the track and the upper part with the cutting part, the lifting mechanism and the related metal structure can be seen.

Fig. 1. Overall view of EsRc -1400 rotor excavator

The upper platform of the excavator is positioned over the basic shaft and can rotate by the Ø 8650 mm support and rotation ball, and by two gears that match with a toothed wheel.

The toothed wheel and the lower rolling path of the ball are interlocked with the basic shaft, and the upper rolling path is interlocked with the rotating platform.

The platform rotation with all the upper structure leaning on it is made with the rotation mechanism.

2. DESIGN OF LONGITUDINAL BALL BEARING

Fig. 2 shows the overall solution for longitudinal ball bearings, which are the portent mobile structure that makes possible the rotation of the upper platform of the excavator as to the shaft and its handling mechanism, which stays fixed from a rotation point of view.

The lower rolling path, 3, made up of six segments fixed between them with bolts, is fixed, being mounted on the excavator shaft, and the upper rolling path, 10 fixed to the upper structure of the excavator, rotates along with it.

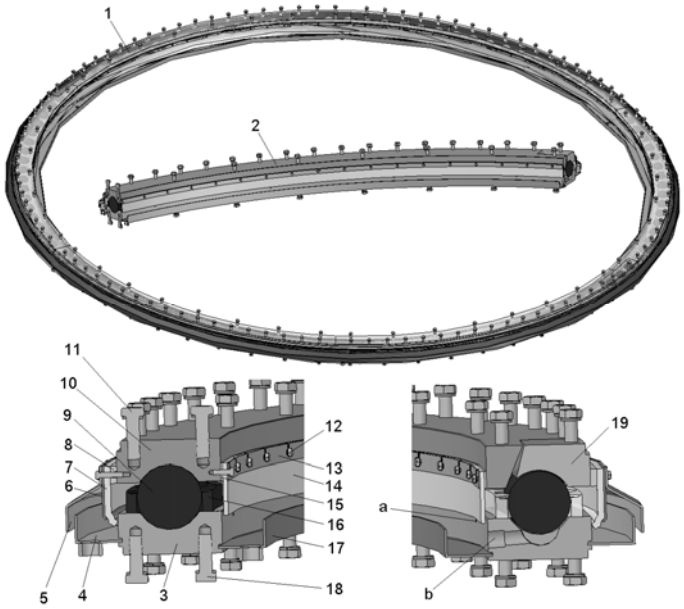

Fig.2. Longitudinal ball bearing with 8650 rolling diameter

A solution was adopted by which the rolling paths are obtained from segments, due to the large sizes.

The marks in this figure mean: 1 – longitudinal ball bearing, 8650 mm rolling diameter, made up of six segments; 2 – rolling segment; 3 – lower rolling path segment, fixed; 4 – outside chute to collect greasing oil; 5 – baffle; 6 – outside sleeve doubling; 7 – outside sleeve; 8 – outside spacing ring; 9 – Ø150 mm ball, 109 pieces; 10 – mobile segment for upper rolling path; 11- M30x100 special screw with Grower nut, 207 pieces; 12 – M12x30 screw with safety washer; 13 – inside ring; 14 – inner sleeve; 15 – inside spacing ring; 16 – cage for 3 balls, 35 pieces and a cage for 4 balls; 17 – inside chute to collect greasing oil; 18 – M30x85 special screw with Grower washer, 108 pieces; 19 – inspection part, 2 pieces; a – four.

M12x1,5 holes on each segment to supply oil under pressure; b – a G1 ¼ hole on each segment to remove oil.

Construction details of a segment running track component are presented below in Figure 3.

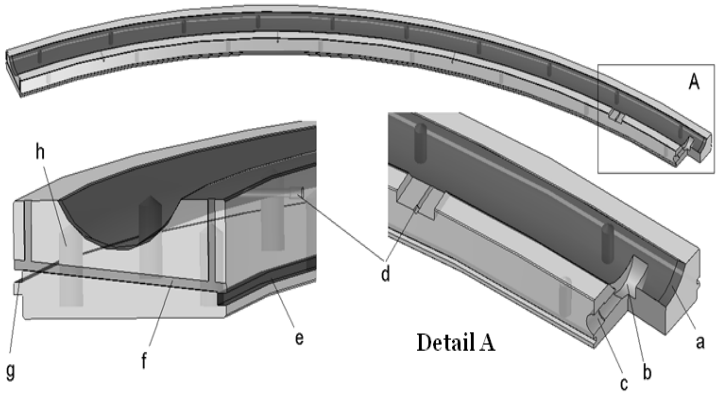

Fig.3. Lower rolling path segment a – 1,5x20 mm cut at the end of the segment; b – collecting duct; c – G 1¼ ” hole for oil removal; d – 4 M12x1,5 holes for oil supply under pressure; e – duct for positioning the lower chute; f – 12x8 mm ducts for oil removal from cage greasing; g – duct for positioning outside duct; h – 16 M30x50/60 holes.

3. PROPOSALS TO IMPROVE THE DESIGN OF LONGITUDINAL BALL BEARING

Following the analysis of the pressure longitudinal bal bearing presented above, it results that both operation life and static load are improved by increasing the number of balls of the bearing, without modifications of the rolling path and ball sizes.

Fig. 4 shows the modified bearing with 143 balls, made up of: 1 – lower ring, made up of 6 segments; 2 – cage with 4 balls; 3 – cage with 3 balls; 4 – 150 mm diameter ball. The numbers of cages were maintained for this bearing (35+1), only that the 3 ball were transformed in 4 balls cages, and the cage with 4 balls in 3 balls cage.

Fig. 5 shows the variation of the operation life of the two design variants, with doted line the 109 bearing.

This analysis was made because it assists in the execution of the 41MoCr11/STAS 791-80 alloyed steel rolling paths execution improvement and not steel for RUL2 bearings.

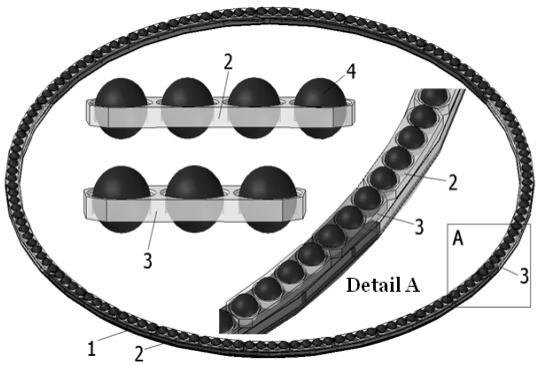

Fig. 4. Modified bearing with 143 balls

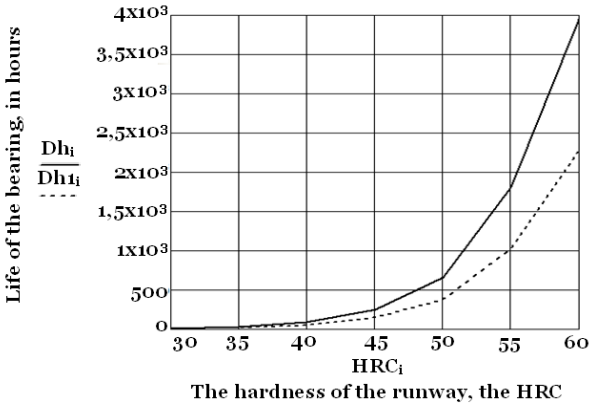

Fig. 5. Operation life variation module for the two longitudinal ball bearing constructive variants

The thermal treatment applied is superficial tempering of the rolling path, since on the opposite M30 end threaded holes required to mount the bearing on the metal structure of the excavator are executed.

As a result of superficial tampering, along the rolling path the hardness is uneven, leading to its uneven wear. Both for the axial bearing and for the toothed wheel cyclical change of the excavator position to the face is required, for an even wear of the rolling path segments, and of the toothed wheel segments, respectively.

Fig. 6 shows an improvement solution for the longitudinal ball bearing.

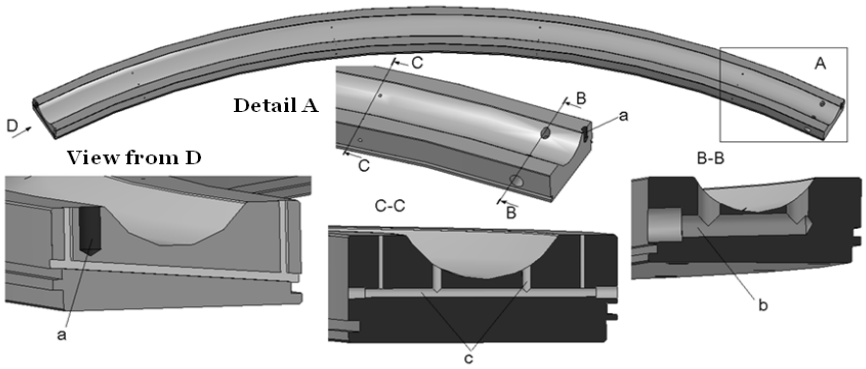

Fig. 6. Improvement solution of the lower rolling path segment

4. CONCLUSIONS

Increasing the number of balls with 34, from 109 to 143, an increase of the operation life is obtained by more than 70%. In absolute value it is 300 hours at 50 HRC hardness and reaches to 1650 hours at 60 HRC harness of the rolling path. From the above, it is required a thermal treatment of superficial tampering for a harness of more than 60 HRC and in a variation range along the rolling path as small as possible, for an even wear. The rolling paths are made from improved 41MoCr11/STAS 791-80 steel alloy and not RUL2 steel for bearings.

The design of the lower rolling path of the bearing can be improved by:

- removal of (1,5x20 mm) cuts at the end of the segments to have a continuous rolling path, without thresholds;
- bores at each end for Φ20x40 mm dowel pin (a), in view of centring segments between them, a solution also found in the toothed wheel;
- modification of the oil collecting solution on the rolling path (b) in order to keep up continuity of the rolling path;
- improving solution for grease supply under pressure for the rolling path (c), with the possibility of supply on the outer or inner side and easy decongestion of grooves, with greasing of the friction surface between the cage and the lower ring.

According to literature, it is recommended to grease with consistent grease, due to the way the proofing is done, mineral oil under pressure is required, which should remove abrasive particles from the rolling path. For the future, a study can be done and tests for using a greasing system with consistent grease.

REFERENCES

[1.] Găfiţeanu, M. şa – Organe de maşini, vol. I şi II, Editura Tehnică, Bucureşti, 1981 şi 1983.
[2.] Muscă G. – Proiectarea asistată folosind Solid Edge, Editura Junimea, Iaşi, 2006.
[3.] *** - Documentaţia tehnică a excavatorului cu rotor EsRc-1400.
[4.] *** - Colecţia de standarde de Organe de maşini, vol. I.b, I.c, Editura Tehnică, Bucureşti, 1983.

INTERNATIONAL SYMPOSIUM on
ADVANCED ENGINEERING & APPLIED MANAGEMENT
– 40th ANNIVERSARY in HIGHER EDUCATION (1970-2010)
4 – 5 November, 2010, Hunedoara, ROMANIA

[1.]Adina BUDIUL BERGHIAN, [2.]Teodor VASIU, [3.]Amalia DASCĂL

KINETIC AND STATIC ANALYSIS AT LOADED RUNNING OF MECHANISMS OF PARALLEL GANG SHEARS' TYPE ASSIGNED FOR CUTTING THE METALLURGICAL PRODUCTS

[1-3.] UNIVERSITY "POLITEHNICA" TIMISOARA, FACULTY OF ENGINEERING HUNEDOARA, ROMANIA

ABSTRACT:
In this study is presented the kinetic and static analysis of shear type mechanisms for cutting metallurgical products at the mill train of the semi-finished steel products Rolling Mill No. 1 – S.F.1 of S.C. MITTAL STELL S.A. HUNEDOARA, in conditions of disregarding the frictions existent in the kinetic couplings.

KEYWORDS:
mechanism, forces and moments of inertia forces, reaction

1. INTRODUCTION

The kinematical scheme for the mechanism of parallel gang shears assigned to cut metallurgical products is shown in Figure 1 and consists in: hand-hold 1, short driving rod 2, upper arm 3, long driving rod 4, lower arm 5 and upper slide 6. This type of mechanism works in phases i.e.: in the first phase is lowered the superior cutter up to the surface of the steel semi-finished product and then stopped and locked in this position moment when the inferior cutter, which performs the cutting of steel semi-finished product, starts to lift. After cutting has done the inferior cutter comes back to the initial position and then the upper arm is lifted in the initial position. All these movements are coordinated by the crankshaft, i.e. handhold 1 and are accomplished at a stroke of 360° of the handhold. From this reason, the kinetic analysis and kinetic and static analysis as well for this type of mechanism will be performed on phases of movement [1].

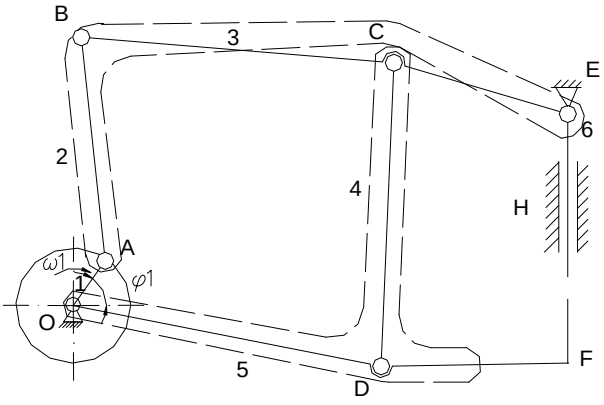

Figure 1. Kinetic Scheme of the 8000kN shear

2. KINETIC AND STATIC ANALYSIS OF THE DYAD ODC

2.1. Determination of the position for gravity centers of the elements to the dyad ODC

- long driving rod 4 (Figure 2).
- lower arm 5 (Figure 3)

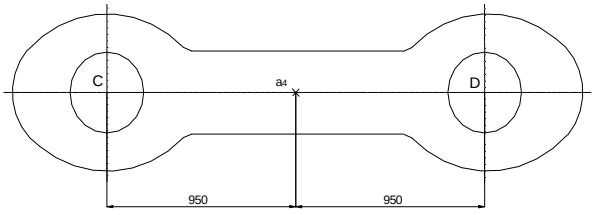

Figure 2. Gravity centre of the element (4) (long driving rod)

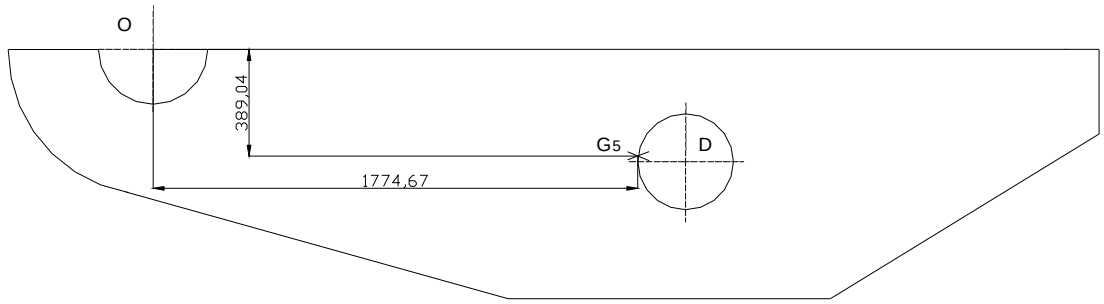

Figura 3. Gravity centre of the element (5) (lower arm)

2.2. The determination of the accelerations of the gravity centre and these directions

- accelerations of the gravity centre to the long driving rod (element4)[2]

$$a_{G4C} = G_4C\sqrt{\omega_4{}^4 + \varepsilon_4{}^2} \text{ the acceleration center } G_4 \text{ against the point C;} \quad (1)$$

$$\overline{a}_{G4} = \overline{a}_C + \overline{a}^n_{G4C} + \overline{a}^t_{G4C} \Rightarrow$$

$$a_{G4} = \sqrt{a_C^2 + a_{G4C}^2 - 2a_C a_{G4C}\cos s_4}\text{ , the acceleration center } G_4 \quad (2)$$

- accelerations of the gravity centre to the lower arm (element 5)

$$a_{G5D} = G_5D\sqrt{\omega_5{}^4 + \varepsilon_5{}^2} \text{ the acceleration center } G_5 \text{ against the point D;} \quad (3)$$

$$\overline{a}_{G5} = \overline{a}_D + \overline{a}^n_{G5D} + \overline{a}^t_{G5D} \Rightarrow$$

$$a_{G5} = \sqrt{a_D^2 + a_{G5D}^2 - 2a_D a_{G5D}\cos s_5}\text{ , the acceleration center } G_5 \quad (4)$$

The directions of the accelerations to the gravity centers G_4 respective G_5 and to the forces of inertia reacts on the elements (4) and (5) are determined from the polygon of the accelerations.

2.3 The calculus of the inertia forces and to the moments of the inertia forces reacts on the elements of the dyad ODC

The inertia forces and the moments of the inertia forces to the elements of the dyad ODC are caused with help of the relations [10], (m_4=2543 Kg, m_5=8597Kg) [1]:

$$\begin{aligned}\overline{F}_{i5} &= -m_5\overline{a}_{G5}\\ \overline{F}_{i4} &= -m_4\overline{a}_{G4}\end{aligned} \quad (5)$$

$$\begin{cases} J_{G4} = m_4\dfrac{l_4^{\,2}}{12} \\ J_{G5} = m_5\dfrac{l_5^{\,2}}{12} \end{cases} \Rightarrow \begin{cases} \overline{M}_{i4} = -J_{G4}\overline{\varepsilon}_4 \\ \overline{M}_{i5} = -J_{G5}\overline{\varepsilon}_5 \end{cases}$$

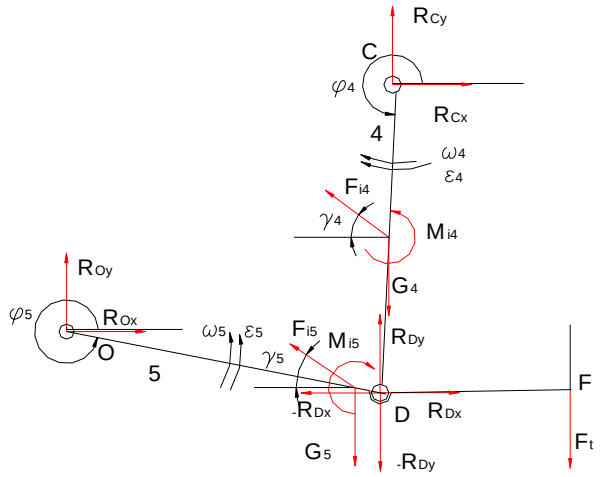

Figure 4. Loading Scheme of ODC dyad

2.4. Determination of reactions in kinetic couplings of dyad ODC without taking into account the frictions of kinetic couplings

Determination of reactions in couplings is performed having as base the loading scheme presented in Figure 4.

With the notations of figure 4. and in conditions when are known the weights of component elements (thus are known the weight forces too) can be written the following equations of equilibrium (m_4=2543; m_5=8597Kg) [1].

$$\begin{cases} \sum F_x(5)=0 \Rightarrow R_{Ox}+R_{Dx}-F_{i5}\cos\gamma_5=0 \\ \sum F_y(5)=0 \Rightarrow R_{Oy}+R_{Dy}-G_5+F_{i5}\sin\gamma_5-F_t=0 \\ \sum F_x(4)=0 \Rightarrow R_{Cx}-R_{Dx}-F_{i4}\cos\gamma_4=0 \\ \sum F_y(4)=0 \Rightarrow R_{Cy}-R_{Dy}+F_{i4}\sin\gamma_4-G_4=0 \\ \sum M_D(5)=0 \Rightarrow -R_{Ox}l'_5\sin(360-\varphi_5)-R_{Oy}l'_5\cos(360-\varphi_5)-M_{i5}+G_5Da_5\cos(360-\varphi_5)- \\ \quad -F_{i5}Da_5\sin[\gamma_5-(360-\varphi_5)]-F_tDF=0 \\ \sum M_D(4)=0 \Rightarrow -R_{Cx}l_4\sin(360-\varphi_4)-R_{Cy}l_4\cos(360-\varphi_4)+M_{i4}-G_4Ca_4\cos(360-\varphi_4)- \\ \quad -F_{i4}Ca_4\sin(360-\varphi_4-\gamma_4)=0 \end{cases} \quad (6)$$

in which: l_i -represent the loungers of kinematic elements; -a_i represented the positions to the gravity centers of the elements in report with one from couples the marginal, their values the by-pathes determinate in the previous paragraphs.

The unknown are $R_{Ox}; R_{Oy}; R_{Cx}; R_{Cy}; R_{Dx}; R_{Dy}$, and has been solved in MathCAD, and with solutions obtained can be calculated the values of reactions in couplings O, D, C:

$$\begin{aligned} R_O &= \sqrt{R_{Ox}^2+R_{Oy}^2} \\ R_C &= \sqrt{R_{Cx}^2+R_{Cy}^2} \\ R_D &= \sqrt{R_{Dx}^2+R_{Dy}^2} \end{aligned} \quad (7)$$

Graphic representation of reaction variation in coupling C, without friction, depending on variation of handhold angle φ_1 is shown in Figure 5.

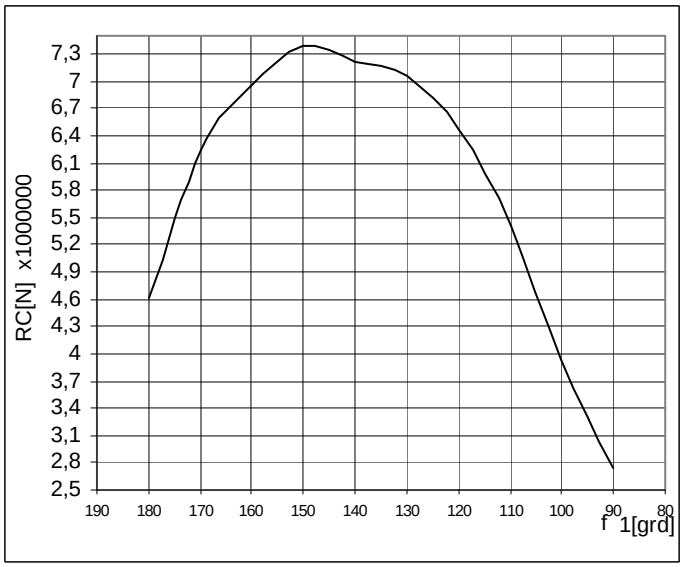

Figure 5. Variation of reaction in coupling C, without friction

3. Kinetic and static analysis of the dyad ABE

3.1. Determination of position for gravity centers of the elements to dyad ABE

-element (2) – short driving rod :

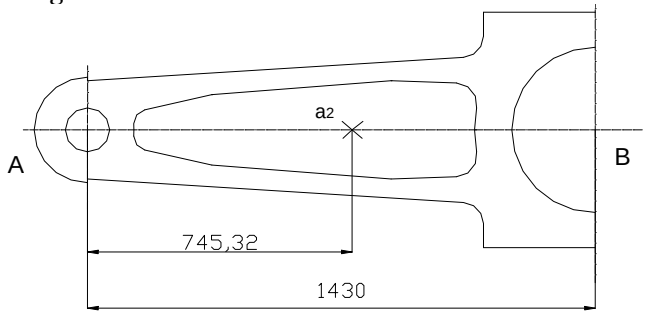

Figure 6. Gravity centre of the element (2) (short driving rod)

- element (3)- upper arm:

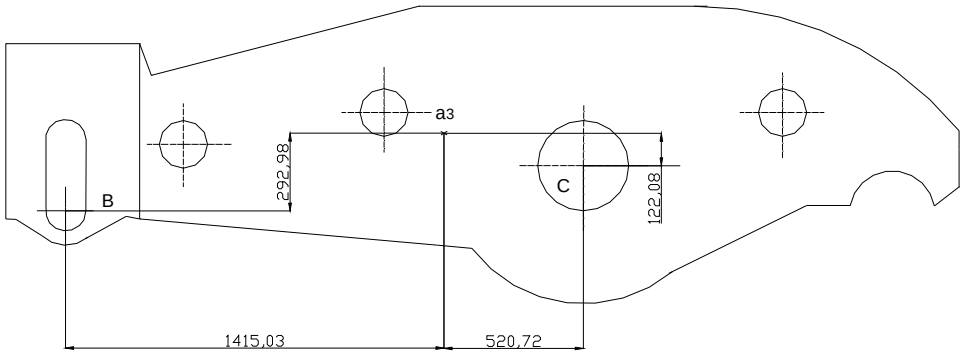

Figure 7. Gravity centre of the element (3) (upper arm)

3.2. The determination of the accelerations of the gravity centre and these directions

- accelerations of the gravity centre to the short driving rod

$a_A = OA\omega_1^2$, the acceleration of the point A; (8)

$a_{G2A} = G_2 A\sqrt{\omega_2^4 + \varepsilon_2^2}$, the acceleration center G_2 against the point A (9)

$\overline{a}_{G2} = \overline{a}_A + \overline{a}^n_{G2A} + \overline{a}^t_{G2A} \Rightarrow$

$a_{G2} = \sqrt{a_A^2 + a_{G2A}^2 - 2a_A a_{G2A}\cos s_2}$, the acceleration center G_2 (10)

- accelerations of the gravity centre to the upper arm (element 3):

$a_{G3B} = G_3 B\sqrt{\omega_3^4 + \varepsilon_3^2}$ the acceleration center G_3 against the point B; (11)

$\overline{a}_{G3} = \overline{a}_B + \overline{a}^n_{G3B} + \overline{a}^t_{G3B} \Rightarrow$

$a_{G3} = \sqrt{a_B^2 + a_{G3B}^2 - 2a_B a_{G3B}\cos s_3}$, the acceleration center G_3 (12)

3.3. The calculus of the inertia forces and to the moments of the inertia forces reacts on the elements of the dyad ABE

The inertia forces and the moments of the inertia forces to the elements of the dyad ABE are caused with help of the relations (m_2=425Kg, m_3=6 155Kg):

$$\overline{F}_{i3} = -m_3\overline{a}_{G3}$$
$$\overline{F}_{i2} = -m_2\overline{a}_{G2} \quad (13)$$
$$\begin{cases} J_{G2} = m_2\dfrac{l_2^2}{12} \\ J_{G3} = m_3\dfrac{l_3^2}{12} \end{cases} \Rightarrow \begin{cases} \overline{M}_{i2} = -J_{G2}\overline{\varepsilon}_2 \\ \overline{M}_{i3} = -J_{G3}\overline{\varepsilon}_3 \end{cases}$$

3.4. Determination of reactions in kinetic couplings of dyad ABE without taking into account the frictions of kinetic couplings

Determination of reactions in couplings is performed having as base the loading scheme presented in Figure 8:

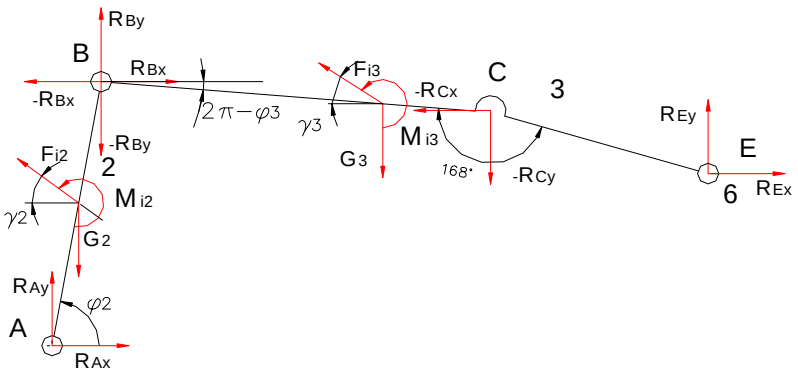

Figure 8. Loading Scheme of ABE dyad

With the notations of figure 13. and in conditions when are known the weights of component elements can be written the following equations of equilibrium: (m_2=425; m_3=6155Kg)[1]:

$$\begin{cases} \sum F_x(2)=0 \Rightarrow R_{Ax}+R_{Bx}-F_{i2}\cos\gamma_2=0 \\ \sum F_y(2)=0 \Rightarrow R_{Ay}+R_{By}-G_2+F_{12}\sin\gamma_2=0 \\ \sum F_x(3)=0 \Rightarrow -R_{Bx}-R_{Cx}+R_{Ex}-F_{i3}\cos\gamma_3=0 \\ \sum F_y(3)=0 \Rightarrow -R_{By}-R_{Cy}+R_{Ey}+F_{i3}\sin\gamma_3-G_3=0 \\ \sum M_B(2)=0 \Rightarrow R_{Ax}l_2\sin\varphi_2-R_{Ay}l_2\cos\varphi_2+G_2Ba_2\cos\varphi_2-F_{i2}Ba_2\sin(180^o-\gamma_2-\varphi_2)+ \\ \qquad +M_{i2}=0 \\ \sum M_E(3)=0 \Rightarrow -R_{Bx}l_3\sin(360^o-\varphi_3+4^o)+R_{By}l_3\cos(360^o-\varphi_3+4^o)+ \\ \qquad +M_{i3}+G_3Ea_3\cos(360^o-\varphi_3+8^o)-F_{i3}Ea_3\sin[\gamma_3-(360^o-\varphi_3)-8^o] \\ \qquad -R_{Cx}l''_3\sin(\varphi_3-\theta)+R_{Cy}l''_3\cdot\cos(\varphi_3-\theta)=0 \end{cases} \quad (14)$$

The set of equations is a linear one with 6 equations and 6 unknown $R_{Ax}; R_{Ay}; R_{Bx}; R_{By}; R_{Ex}; R_{Ey}$, and has been solved in MathCAD, and with solutions obtained can be calculated the values of reactions in couplings A; B; E:

$$\begin{aligned} R_A &= \sqrt{R_{Ax}^2+R_{Ay}^2} \\ R_B &= \sqrt{R_{Bx}^2+R_{By}^2} \\ R_E &= \sqrt{R_{Ex}^2+R_{Ey}^2} \end{aligned} \quad (15)$$

Graphic representation of reaction variation in coupling E, without friction, depending on variation of handhold angle φ_1 is shown in Figure 9:

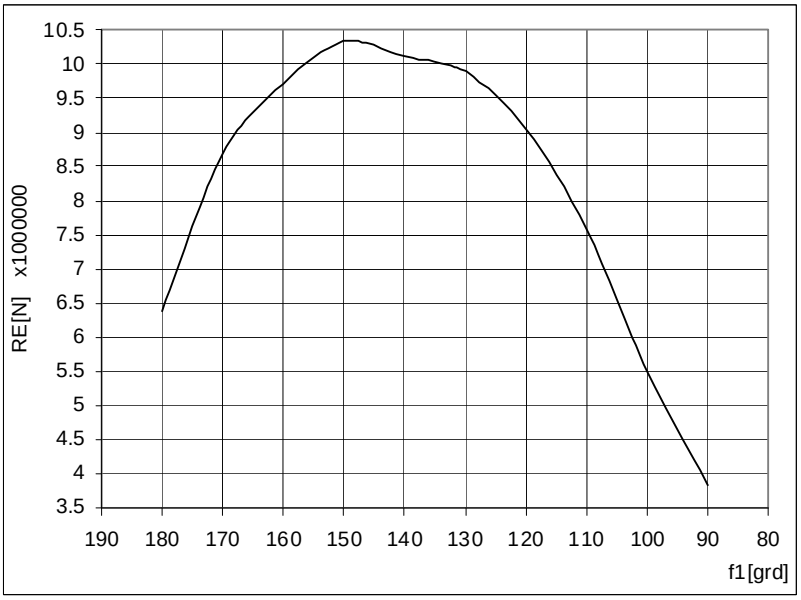

Figure 9.Variation of reaction in coupling E, without friction

4. CONCLUSIONS

The kinetic and static analysis of the mechanism of the guy scissors for cuting metallurgical products of 8000kN are accomplished without the taking in consider the frictions from couple kinematic for the case in which is cut (300x300) mm2 metallurgical product, from OLC20, to a temperature of 970°C. The reactions from couples kinematic have the values maxims when the relativ deepness of penetrate to the knifes in material is ε= 04.

BIBLIOGRAPHY

[1.] Budiul, Berghian, A, "Contributions on reliability improvement of shear type mechanisms assigned to cut metallurgical products", PhD Thesis (Doctor's Degree).
[2.] Conţiu, T.- "Culegere de probleme din Teoria mecanismelor şi a maşinilor", Editura Tehnică, Bucureşti, 1957;
[3.] Handra Luca, V. Stoica, I. A.- "Introducere în teoria mecanismelor", Vol. I, II, Editura Dacia, Cluj Napoca, 1982;

INTERNATIONAL SYMPOSIUM on
ADVANCED ENGINEERING & APPLIED MANAGEMENT
– 40th ANNIVERSARY in HIGHER EDUCATION (1970-2010)
4 – 5 November, 2010, Hunedoara, ROMANIA

[1.]Ion Silviu BOROZAN, [2.]Veronica ARGESANU, [3.]Raul Miklos KULCSAR, [4.]Ioan LAZA

ABOUT THE TENSIONING OF THE BELT DRIVES

[1-4.] UNIVERSITY "POLITEHNICA" TIMIŞOARA, FACULTY OF MECHANICS, TIMISOARA, ROMANIA

ABSTRACT:
The intensity of the initial tensioning effort must be correlated with the belt drive tensioning system and with the maximum torque to be transmitted.
In the particular case of the constant tensioning of belt drives, this correlation is analyzed and there is recommended the appropriate control methods.
The automotive industry is in continuous expansion and the competition for timing belt drive requires high standards of manufacturing. As a result, the belt drive not only requires a strict correlation but also a high durability if not, the effects could be dramatic.
KEYWORDS:
automotive industry, manufacturing, standards, control methods

1. INTRODUCTION

Rational limits of the initial tensioning.

The pulling capacity, the mechanical efficiency and the fatigue durability of a belt drive are conditioned by the correct evaluation and conservation time of the tensioning.

The initial tension effort intensity must be correlated with the maximum transmitted torque and tensioning system of the drive.

In case of a transmitted power $K_r P$ [kW], by z $\geq$ 1 number of parallel belts at a velocity v[m/s], the optimum level of tensioning results from the relation:

$$F_0^* = 10^3(K_r P/vz/2\varphi) \text{ [N]} \quad (1)$$

When setting –in repos state- the influence of the centrifugal forces that result in function must be compensated (not taking in consideration the elasticity of the drive-shaft system):

$$F_0 = F_0^* + m_1 v^2 \text{ [N]} \quad (2)$$

where: m1-belt linear weight

2. THE STUDY

Tension systems

The traction coefficient (Kutzbach invariant) from relation (1), defined as a proportion between the transmitted tangential force F_t and the double initial tensioning effort $2F_0$:

$$\varphi = F_t/2F_0 \quad (-) \quad (3)$$

depends on the exact tensioning situation of the belt and the proportion between the active efforts in the branches:

$$m = F_1^*/F_2^* = \exp(\mu\beta_{a1}) \quad (-) \quad (4)$$

where: $\mu = \mu_0/\sin(\alpha/2)$ -is the apparent friction coefficient (for $\alpha = 40^0$) at the V belts, and $\beta_{a1} \leq \beta_1$ [rad] representing the minimum (active) slip angle on the pulley with $d_{p1} \leq d_{p2}$.

Based on the command and adjust mode of the forced contact between the conjugated surfaces of the pulley and belt, we have the following constructive solutions for permanent tensioning.

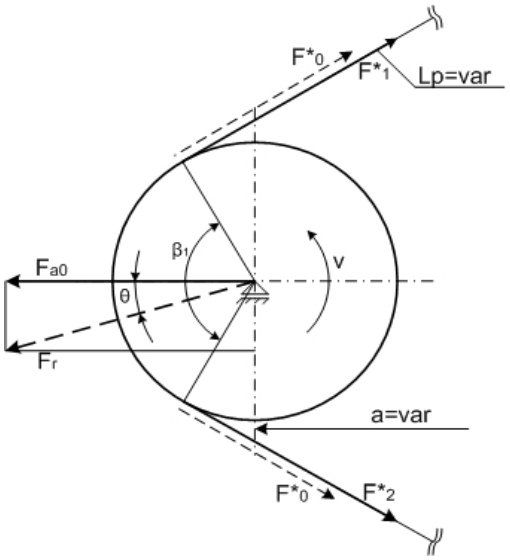

Fig. 1

The drive with a = constant, L_p =variable, tensioned by loading the driven side (pushed with a tightening pulley) exterior force F_{ac}, invariable in intensity and direction (Fig. 2).

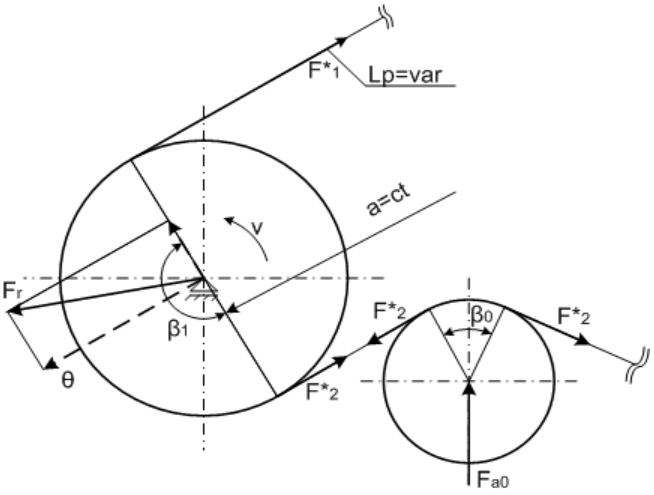

Fig. 2

$$F_{ac}=2F_0^*\sin(\beta_0/2)=2F_0^*\sin(\beta_0/2) \quad [N] \qquad (6)$$

$$\varphi=(m-1)/2m \quad [-]$$

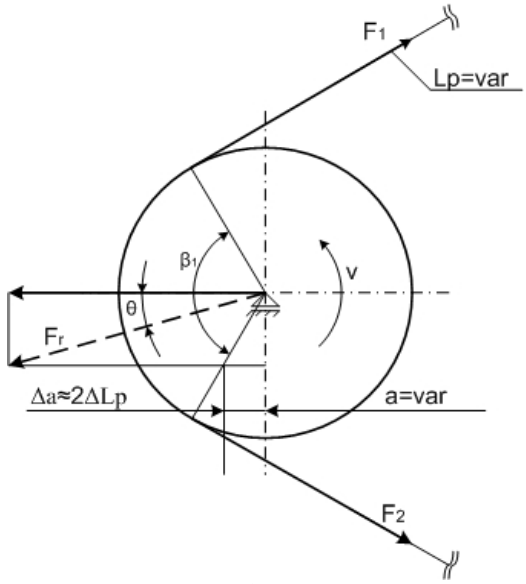

Fig. 3

Both methods accomplish the tensioning on the constructive way and, as a result, further operations of control and adjustment are no longer necessary.

The drive with a, L_p =constant, tensioned by forced fixing the belt with an initial elongation (Fig. 3):

$$\Delta L_p=\frac{F_0L_p}{E_tA_c}=\frac{F_tL_p}{2\varphi E_tA_c}=\frac{m-1}{2\varphi k_\beta}/(2.5-k_\beta) \quad (-) \qquad (7)$$

where, for L_p [mm], primitive length of the belt, E_tA_c [N] traction rigidity; k_β represents the correction factor of the wrapping angle.

In this case, according to relations (1, 2, and 7) each belt must be tensioned when fixing it with the effort:

$$F_0=500(K_TP/zv)(2.5-k_\beta)/k_\beta+m_1v^2 \quad [N] \qquad (8)$$

3. ANALYSES, DISCUSSIONS, APPROACHES AND INTERPRETATIONS

The measurement of the fixing and in use tensioning effort

For the drives with a, L_p =constant, the initial tensioning effort can be measured indirectly in two distinctive ways:

The measurement of the fixing elongation Δl_0 [mm] of a belt segment, of initial length l_0 [mm], situated on one of the free sides of the drive (Fig. 4):

$$F_0=(\Delta l_0/l_0)A_cE_t \quad [N] \qquad (9)$$

where: A_c [mm²] the belt's transversal section area; E_t [mm²] -the belt's equivalent elasticity module.

Examining the law of the propagation of errors (in the hypothesis of the use of a stress measuring device of first class precision) results that upon the precision of the measurement the determinant weight $\Delta E_t/E$.

$$\Delta F_0/F_0=\pm[(\Delta l_0/l_0)]+(\Delta E_t/E_t)+(\Delta A_c/A_c)]\cong\pm(\Delta E_t/E_t) \quad [-] \qquad (9a)$$

Consequently, this measurement method may be used only if the experimental dependence load-strain F (ΔL) is known.

The measurement of the sag of the belt f_n [mm] produced by a control force F_n [N] applied normal on the middle of one of the branches opening l [mm] (Fig. 4).

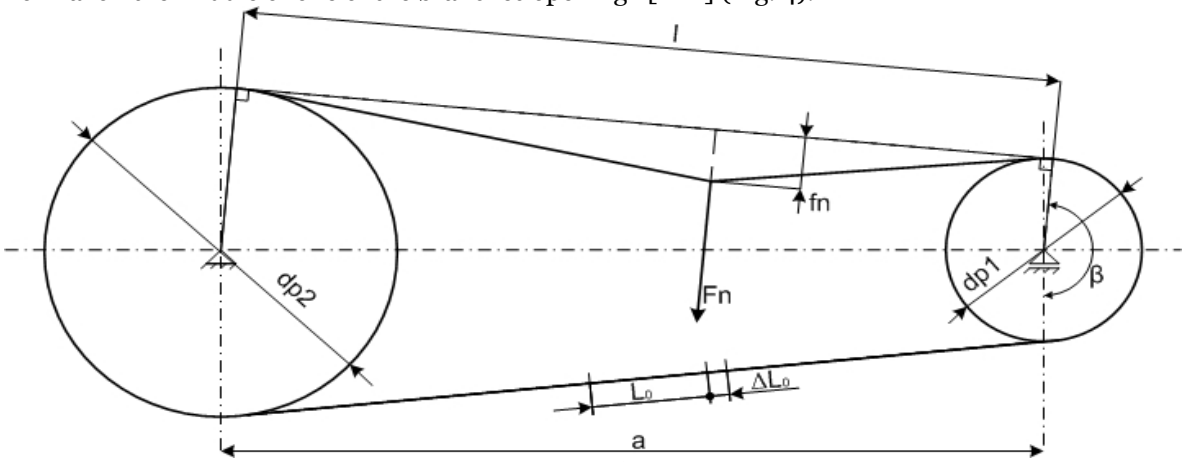

Fig. 4

The connection between control sizes f_n and F_n, the drive geometry and initial effort are shown in the following relation:

$$F_0\cong F_n/4\,(f_n/l)-2A_cE_t(f_n/l)^2(l/L_p) \quad [N] \qquad (10)$$

were: $l=a\sin(\beta_1/2)\cong a\{1-0.125[(d_{p2}-d_{p1})/a]^2\}$ [mm] is the length of the free side of the drive.

Perturbation analysis of the control force measurement shows the fact that the systematic errors can be minimized if $f_n/l\in[1/50\,;\,1/100]$ (because $l/L_p<1/2$ and $A_cE_t/F_0\leq 100$)

$$\Delta F_0/F_0=2(f_n/l)^2(l/L_p)A_cE_t/F_0\leq 0.02 \quad [-] \qquad (10a)$$

According to this theory there are recommended two alternatives:

a).Limitation of the f_n sad of the belt to the value $f_n=l/100$ [mm] (Gates method) in which the intensity of the control force is given by the relation:

$$F_n=[F_0+2A_cE_t(l/L_p)]10^{-4}/25 \quad [N] \qquad (10b)$$

b).Fixation of the control force at the value $F_n\cong 0.5A_c$ [N] (Optibelt method) in which the proportioned arrow f_n/l must realize the relation 10.

First approximation is initialized at the value:

$$(f_n/l)'=F_n/4F_0>(f_n/l)'' \quad [-] \qquad (10c)$$

And by successive iterations the proportionate arrow (f_n/l) is obtained for which $\Delta F_0/F_0\leq 0.01$.

The conduction law of measurement errors for both alternatives:

$$(\Delta F_0/F_0)\cong\pm(\Delta F_n/F_n+\Delta l/l+\Delta f_n/f_n)\cong\pm\Delta f_n/f_n \quad [-] \qquad (10d)$$

As a result, at the measurement of the arrow the absolute error must be limited to the value:

$$\Delta f_m\in\pm(0.1;0.5) \text{ mm.}$$

The Gates and Optibelt methods can be applied with any restrictions to any type of belt (round, flat or V). The belt's loosening imposes periodic control and correction of the initial tension by a conditioned program of endurance structure.

In case of a new belt the following stage control is recommended:

STAGE	0	I	II	III and the following
*Period of functioning	Installation (fixing)	0.5...5 hours	24...36 hours	500...1000 hours

*Inferior limits are accepted in case of a pronounced loosening!

4. CONCLUSIONS

The correct evaluation and periodic control of an initial tension are vital operations for the function of a belt drive in the projected parameters.

For the narrow V belts STAS 7192-81 specific parameters that complete the control and calculation of the initial tensioning have the following values:

Profile / Parameter	SPZ	SPA	SPB	SPC
m_1 [kg/m]	0.066...0.07	0.12...0.13	0.17...0.21	0.32...0.38
A_c [mm^2]	53	89	153	279
$F_n=0.5A_c$ [N]	25	50	75	125
$2A_cE_t10^{-4}$ [N]*	15	20	26	41

*Chords by polyestheric fibres.

Outside the specifications according to the shafts parallelism and belt pulleys alignment the execution and exploitation documentary must contain the minimum recommendations regarding the appropriate tension effort intensity and the control method.

REFERENCES

[1.] Gheorghiu, N., Transmisii prin curele trapezoidale- contributii la studiul teoretic si experimental al capacitatiide tractiune- Teza de doctorat, IPTV Timisoara, 1969/70.
[2.] Gheorghiu, N., Ionescu, N., Argesanu, V., Sistematizarea controlului tensionarii initiale la transmisiile prin curele, PRASIC-Brasov, mai 1982.
[3.] *** Antriebaentwurfshandbuch für Industriekeilriemen, Gates (Deutschland) GmbH.
[4.] *** Berechnungsunterlagendbuch für Optibelt-Keilriemen mit Kevlar-Aufbau, Arntz-Optibelt KG.
[5.] *** Blauri Schmalkeilriementriebe und Keilriementriebe-Groössenbestimmung Henn-Leistungen, A. Fr. Flender GmbH.
[6.] www.syncrotech.eu
[7.] www.gates.com
[8.] www.optibelt.de

INTERNATIONAL SYMPOSIUM on
ADVANCED ENGINEERING & APPLIED MANAGEMENT
– 40th ANNIVERSARY in HIGHER EDUCATION (1970-2010)
4 – 5 November, 2010, Hunedoara, ROMANIA

[1.]Cristina Carmen MIKLOS; [1.]Imre Zsolt MIKLOS; [1.]Carmen Inge ALIC

COMPUTER AIDED ANALYSIS OF A DIFFERENTIAL GEAR WITH SIMPLE SATELLITE

[1-3] UNIVERSITY POLITEHNICA OF TIMISOARA, FACULTY OF ENGINEERING FROM HUNEDOARA, ROMANIA

ABSTRACT:
In the present paper shows how to achieve structural and kinematic analysis of a differential gear with simple satellite, assisted by computer, using an application written in Matlab, based on the method of Willis. Differential gear with satellite is simply part of the chain of kinematic motion transmission from tilting mechanism from the Blooming type rolling trains.
KEYWORDS:
differential gear, planet gear, planet carrier, degree of mobility, kinematic analysis

1. INTRODUCTION

Differential gear who is studied in this paper is part of the handling - tilting mechanism, from the blooming type rolling train. Kinematical scheme of the handling - tilting mechanism is shown in figure 1.

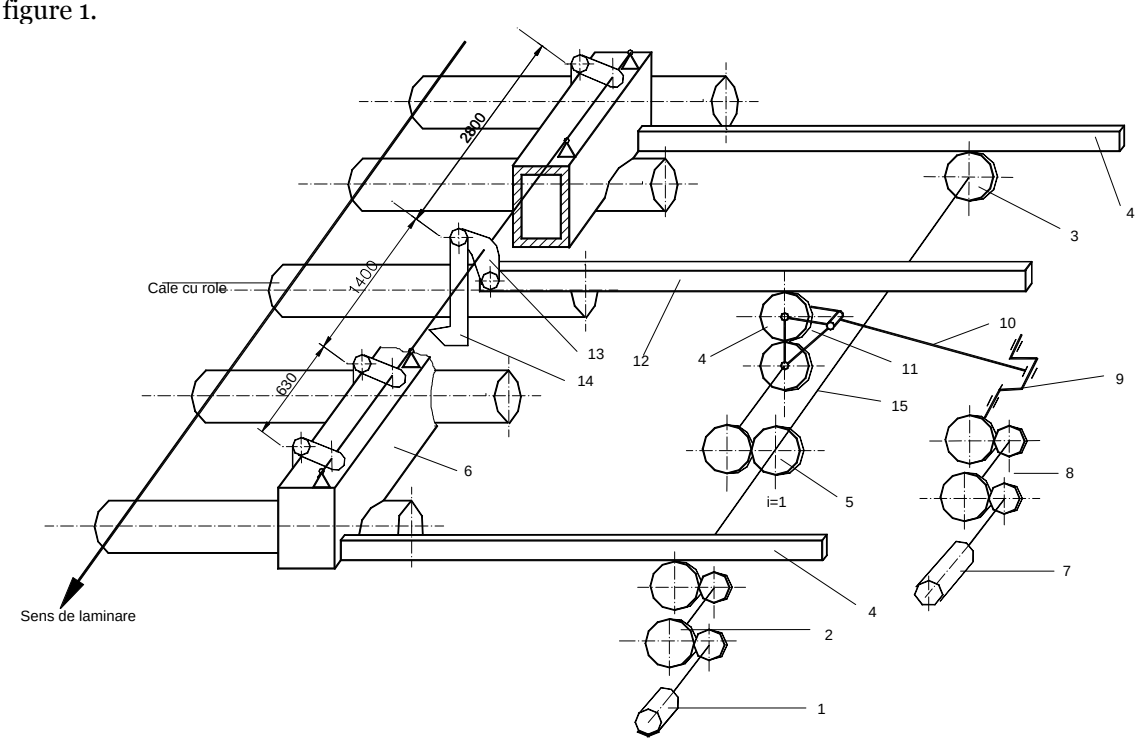

Fig.1. Kinematic scheme of the handling - tilting mechanism

From Figure 1 shows that the two mechanisms (handling and tilting) acting on interdependence. Handling mechanism is driven by electric motor (1), which through the gears (3) (pinion - rack) act handling ruler rods (4). It is noted that the rollover mechanism hooks (14) are mounted directly on handling ruler, so during the handling process they must move with them together, without performing the actual overthrow (hooks must remain stationary). This is ensured

by the gears train (5) that synchronizes the movement of the two mechanisms and through the differential gear (11) allows racks movement (12), together with handling ruler, so the rollover mechanism will remain stationary.

To achieve the overthrow blooms without there side move, of the handling drive motor is stopped by braking, and the differential gear drive motor is turned on. In this way is distributing movement on crankshaft (9) mounted on the gear output shaft (8), and through the connecting rod (10) at the housing differential gear (11), (which serves as a satellite port arm) impart him an oscillatory motion. By this motion, spur gear (4) (satellite) rotates clockwise and engage the tilting mechanism rack, which it gives a movement that allows the uplift hooks. Through a complete rotation of the mechanism tilting crankshaft is achieved also the uplift and descent their hooks.

2. ANALYSIS OF A DIFERENTIAL GEAR WITH SIMPLE SATELLITE

Geometric and kinematic input data's necessary for structural and kinematic analysis of the differential gear are taken from the tilting mechanism analysis results of the rolling train [4], [5].

Kinematic scheme of the differential gear who engages the tilting mechanism is shown in fig.2.

Differential gear is composed of central wheel **rc**, satellite **s**, planet carrier **b** (housing gear) and the rack **cr**. Central wheel and the satellite are cylindrical spur gear of the same size (r = 378 [mm]), and the same number of teeth Zc = Zs = 18, the modulus being m = 42 [mm].

Differential gear is considered a plan mechanism with number of family 3, has four moving parts (central wheel **rc**, satellite **s**, planet carrier **b** and rack **cr**), four kinematic lower joints on V class (three rotational and one translational - fig. 2) and two kinematic upper joints on IV class (the two points of engagement). Mechanism degree of mobility is:

$$M_3 = 3n - 2C_5 - C_4 = 3\cdot 4 - 2\cdot 4 - 1\cdot 2 = 2$$

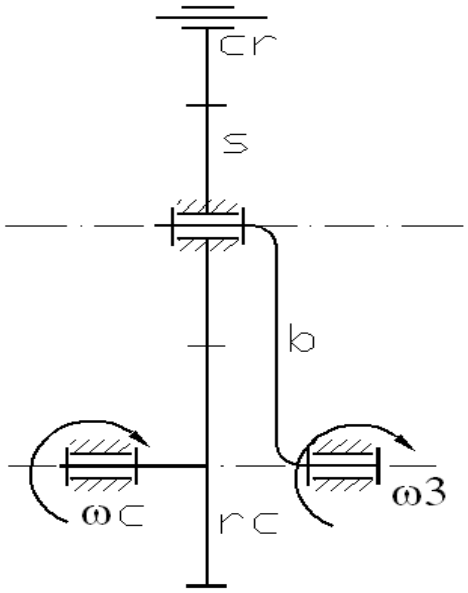

Fig.2. Differential gear kinematic scheme

With the conditions that the central wheel is braked (differential gear action time), the mechanism is reduced to three mobile elements (satellite **s**, planet carrier **b** and rack **cr**), three kinematic lower joints V class (two rotational and one translational - fig. 2) and two kinematic upper joints IV class. Mechanism degree of mobility is:

$$M_3 = 3n - 2C_5 - C_4 = 3\cdot 3 - 2\cdot 3 - 1\cdot 2 = 2$$

and so the mechanism is a planetary mechanism.

Universal method for kinematic study of the differential gear and planetary gear is stop planet carrier method or Willis method. For the kinematic study the real mechanism need to turn into an equivalent mechanism with fixed axes, whose study is already known. In order to understand the problems easier is used a new scoring system for the transmission ratio, who has three indices: i^{b}_{a-b}, where **i** is mechanism gear ratio, the higher index is fixed element to which motion is relate, in this case planet carrier **b**, and lower indices in order, are the driver element **a** and the driven element, **b**.

Stop planet carrier method is that the in imaginary mode to entire mechanism assembly is give an angular velocity $-\omega_3$ (or speed $-n_3$), opposite to the gear case angular velocity ω_3 (with planet carrier role) around its own rotational axis. In this way planet carrier (gear housing) will have zero angular velocity, planetary gear has become an ordinary gear, which can be studied by known methods.

$$i^{b}_{rc-cr} = \frac{\omega_c - \omega_3}{\omega_s - \omega_3} = -\frac{Z_s}{Z_c} = -1$$

During the tilting mechanism operating the central wheel is fixed (ω_c = 0), so the angular velocity of the satellite will have the following value:

$$\frac{-\omega_3}{\omega_s - \omega_3} = -1 \Rightarrow \omega_s - \omega_3 = \omega_3 \Rightarrow \omega_s = 2\cdot\omega_3$$

and the rack linear speed of movement will be:

$$V_{cr} = r \cdot \omega_s$$

The calculations above are provided from Răsturnător1000 program writted in Matlab, and the angular velocity of the satellite according to the position angle φ_1 of the crank tilting mechanism is shown in fig. 3 [4].

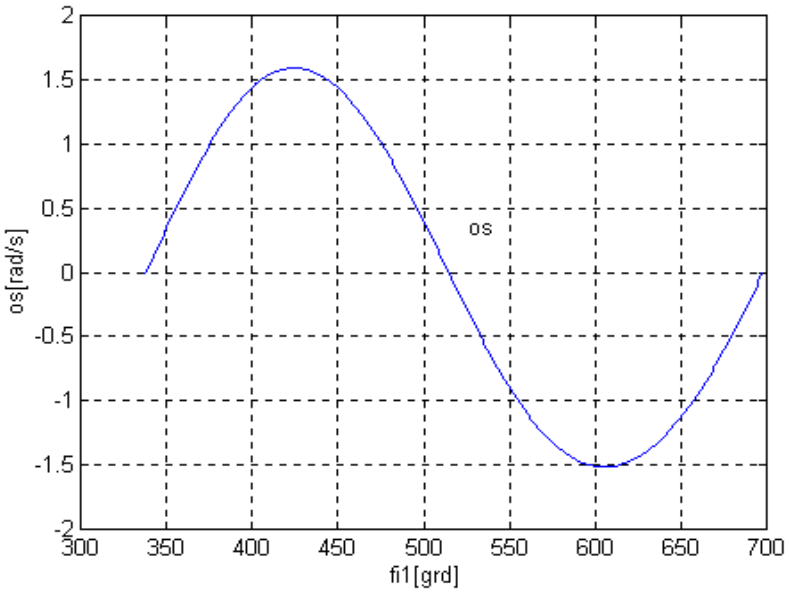

Fig.3. Satellite angular velocity

3. CONCLUSIONS

Differential gears with simple satellite structural and kinematic analysis, but also other types of construction, are achieved simply by applying the Willis method, and by using computer programs written in different programming languages. Before the kinematic analysis, according to fig.3 results a sinusoidal continuous variation of satellite angular velocity:

- satellite angular velocity from the differential gear ω_s is twice the gear case angular velocity with the conditions that during the tilting mechanism operating the central wheel is braked.
- angular speed ω_3 gear case varies between the following limits: 0,9 [rad/s] and 0,95 [rad/s].

REFERENCES

[1.] GHINEA, M., FIREȚEANU, V., Matlab, calcul numeric, grafică, aplicaţii. Editura Teora Bucureşti 1997.
[2.] MANOLESCU, N., KOVÁCS, FR., Teoria mecanismelor şi a maşinilor, Editura Didactică şi Pedagogică, Bucureşti, 1972
[3.] MIKLOS, I. Zs., Mecanisme. Analiza mecanismelor, Editura Mirton Timişoara, 2005
[4.] MIKLOS, I. Zs., Contribuţii cu privire la îmbunătăţirea performanţelor tehnologice ale mecanismelor de răsturnat la liniile de laminare, Teză de doctorat, Universitatea din Petroşani, 2001
[5.] ZAMFIR, V., MIKLOS, I. Zs., The kinetostatic analysis of the tilting mechanism at the 1000 mm rolling train, UPT's Scientific Bulletin, Vol. 44(58), Fascicle 2, 1999
[6.] * * * Instrucţiuni tehnologice pentru liniile de laminare Blooming 1300 şi 1000 mm, Combinatul Siderurgic Hunedoara, Uzina nr.4 – Laminoare, Vol. II, 1983

INTERNATIONAL SYMPOSIUM on
ADVANCED ENGINEERING & APPLIED MANAGEMENT
– 40th ANNIVERSARY in HIGHER EDUCATION (1970-2010)
4 – 5 November, 2010, Hunedoara, ROMANIA

[1] Camelia PINCA -BRETOTEAN, [2]Gelu-Ovidiu TIRIAN

CONSIDERATIONS ON THERMAL FATIGUE INTERNAL COMBUSTION ENGINES

[1.] UNIVERSITY POLITEHNICA OF TIMISOARA, FACULTY OF ENGINEERING FROM HUNEDOARA, ROMANIA

ABSTRACT:
This paper refers to the principle of thermal fatigue research on internal combustion engines, particularly for Dacia engine ignition engines.
Knowing the negative effects in case of any harm caused to the gears making up the internal combustion engines, in order to mitigate the causes of destruction caused by cracking, we must do some thorough, complex, theoretical, and experimental research on thermal fatigue, using new theoretical and experimental approaches. Research is done in three directions: to study the thermal component of part machineries, to study and perform experimental determination of variable fields of surface temperature of machine components, to perform experiments on thermal fatigue life samples subjected to different regimes of stress. The main objective of this paper is to solve complex problems of internal combustion engines by acquiring new, original, theoretical and experimental knowledge on the thermal fatigue phenomenon that occurs in part machinery enabling the transfer of heat from the combustion chamber to the cooling fluids for engines fitted to motor vehicles.
KEYWORDS:
Thermal, fatigue, internal, combustion, engine, cyclic

1. INTRODUCTION

Basic research on thermal fatigue of internal combustion engines is an important problem both from a theoretical or an experimental point of view, but also in economic terms.

Machine gears of motor vehicles participate in the working cycle. This cycle is characterized by temperature variations. Such variations are important for heat developed inside the combustion chamber and sent forwards to the cooling fluid. Thus, within certain parts of their gears, they create some temperature fields triggering cyclic tension. The rate of temperature change is very important in case of internal combustion engines fitted to motor vehicles; they create some variable and cyclical thermal fields up to a speed measured in seconds or even tenths of seconds, producing specific thermal fatigue cracks. These cracks appear after a certain number of thermal cycles; their number depends on the material machine gears are made of, as well as on the operating mode of the engine parameters. If the number of thermal cycles increases, it develops and increases heat exhaustion, and cause some specific surface cracks across the entire surface layer of the gears, negatively changing energy and economic indices of the engine.

Knowing the negative effects in case of any harm caused to the gears making up the internal combustion engines, in order to mitigate the causes of destruction caused by cracking, we must do some thorough, complex, theoretical, and experimental research on thermal fatigue, using new theoretical and experimental approaches. We must study and do important research on thermal fatigue, not only mitigating the raging crack, but also avoiding thermal shock, which is particularly dangerous during working of the engine. Classical methods of resistance calculation for machine gears inside internal combustion engines which are exposed to thermal fatigue do not consider the demands of certain items, which are caused by variations of temperature fields across the surface and within the surface layer. Such phenomena occur during the engine working, and it is being offset by increasing the allowable tension values.

Although scientific literature referring to the research on internal combustion engines is quite extensive, research do not refer particularly to the phenomenon of thermal fatigue within the superficial layer of fixed and mobile machine gear. The research of thermal fatigue of internal combustion engines, particularly of fixed and mobile machine gears, is less studied both on national and international level.

So far, there are no specialized publications covering thermal fatigue of internal combustion engines in detail, both theoretically and experimentally. Within the context of market economy, a new development in basic research of thermal fatigue of machine gear is necessary. This research should use the most modern and efficient solutions.

2. METHODOLOGY AND DISCUSSION

The main objective of this them of researches is to solve fundamental and complex problems of internal combustion engines by acquiring new, original, theoretical, and experimental knowledge on thermal fatigue occurring inside all machine gears that enable the transfer of heat from the combustion chamber to the cooling fluid inside internal combustion engines.

During internal combustion engines working, specific fatigue cracks appear within the surface layer of any item enabling the transfer of heat, and they grow slowly due to thermal cyclic variations of temperature fields, [1].

Thermal fatigue cracks appear on the surface and within the outside layers of the parts participating in the heat transfer. Thermal fatigue cracks specific that develops gradually because of cyclic temperature variations. These cracks appear and on the upper layers and on the surface of parts machineries (although in the most favorable operating conditions), limiting their use to situations which have negative effects on energy and economic indices of the engine[2],[3].

To study thermal fatigue of the organs that make up fixed and mobile internal combustion engines the following objectives must be achieved:

- to study the thermal behaviour of part machinery of vehicle engines participating in the transfer of heat from the combustion chamber cooling fluid during operation;
- to experimental and determine all variable fields and surface temperature of the upper layers of part machinery;
- to perform experimental research on fatigue resistance of samples subjected to different thermal regimes request.

The operation of an internal combustion engine is characterized by a set of values that define the operating system. The operating regime is defined by three fundamental dimensions: speed, load, and temperature characterizing the thermal regime of the engine. The thermal regime is the body temperature indicating the degree of enforcement mechanism for heating the engine. Thermal regime is indicated by the exhaust gas temperature "t_{ge}"or cooling fluid temperature "t_r" [2].

To achieve thermal regime we have built a trial bench to measure the temperature inside the combustion chamber and cylinder head wall temperature in the intake and exhaust valves, fig.1.

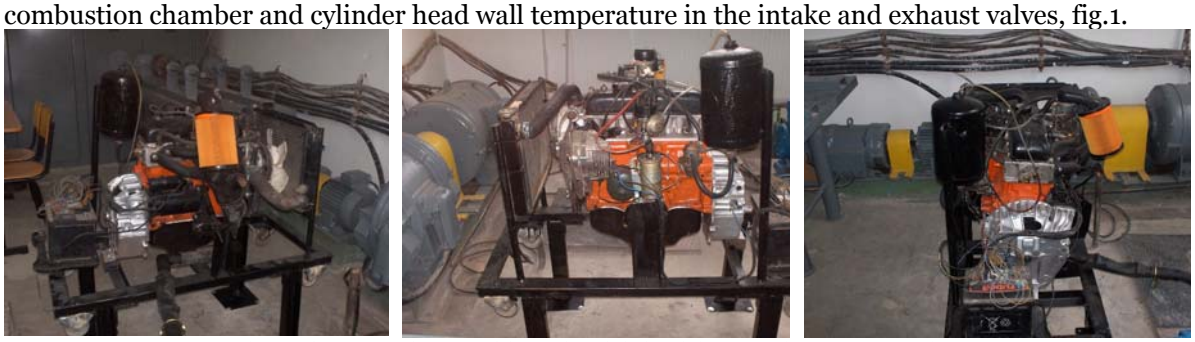

Fig.1 The experimental bench with ignition engine type Dacia

Experimental bench includes a Dacia spark ignition engine, with all related auxiliary facilities that allow normal functioning. The engine is mounted on a resistance structure which enables a rather good stiffness to the bench and eliminates engine vibration during operation, a phenomenon that would adversely affect experimental measurements.

The thermal study raises questions about [1], [2],[4], [5] how to: clarify the limit; evaluate heat passing through the pieces as part of the heat developed in the combustion chamber;

The main technical parameters considered for a thermal study of spark ignition engine are [1], [2], [4], [5]: gas temperature; pieces on the wall temperature chamber and the cooling fluid; heat transfer coefficient.

Of all these parameters, the temperature of the combustion chamber is necessary to determine how precisely it influences major heat transfer and thermal default application of part

machinery of the engine structure, both directly and through the coefficients of convection, radiation and conduction heat [1], [4]. Thus, the gas temperature in the engine combustion chamber is determined analytically and experimentally.

In terms of analytical research, gas temperature in the combustion chamber is determined based on the indicated chart, and the method involves choosing a number of sizes that varies a lot, which means obtaining the actual values who differ from the regular ones.

From the experimental point of view, gas temperature in the combustion chamber is determined by a chamber of thermo-vision, type T200 - the characteristics of the view field are of 25 x 19 mm focus distance, min 0.4 laser semi penetrating mm, 635 HM (red) laser wavelength, and 7.2 V ionic power battery. Following the transfer of heat from flue gases to the walls of the chamber, by convection and radiation transfer that occurs inside the internal combustion engines mechanical stress, thermal stresses appear in addition. Temperatures that vary over time in the combustion chamber are transmitted as oscillations to fixed and mobile part machinery composition engine. Heat taken from them during operation is transferred to a lesser extent during the gas engine fluid change. Depending on the quantity of heat generated by engine operation and the different thermal resistance which occur during heat transfer (thermal conductivity material, building sections, etc.), part machineries suffer from temperature fields. These fields are cyclic at very small intervals (seconds or tenths of seconds) and are responsible for the occurrence of thermal fatigue.

The reason why these varying temperature fields occur is explained as follows: during the intake stroke of a piston engine, the intake valve is open, and cool air intake cools off the intake drift; during the compression stroke both valves remain closed; at the beginning of the compression cylinder walls yield air heat. In the further compression, the phenomenon is reversed, heat flows from the compressed air cylinder walls during the discharge gas resulting from combustion exhaust valve opens, and exhaust gases warm up the gallery.

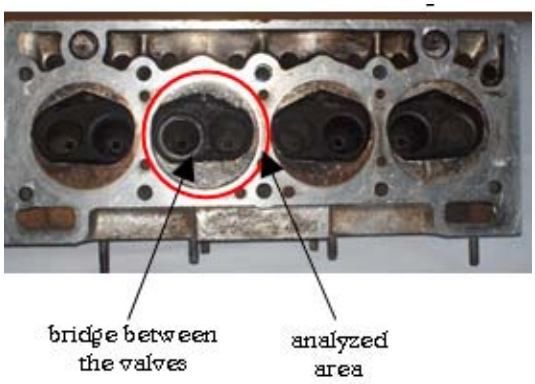

Fig.2 Studied area of Dacia engine cylinder head

Determination of the variable temperature field is the second objective of further research on thermal fatigue. Their experimental determination is made by mounting thermocouples in the wall of Dacia engine cylinder head areas of intake and exhaust valves fig. 2.

Thus, we have created a succession plan that includes next steps:

- Removing the entire engine cylinder head;
- Appropriate training to detect areas where the cylinder head and the temperature difference is high;
- Drawing and making channels in areas to be fitted thermocouples;
- Performance and installation works were thermocouples;
- Fitting the so prepared engine cylinder head assembly;
- Check thermocouples mounting and connecting them to systems of data acquisition;
- Measuring and recording changes in temperature fields;
- Assessing and obtaining experimental determinations of temperature charts;
- Highlighting areas where thermal fatigue occurs.

Following the analytical calculations, we observed that the center axle of the valve is subject to cyclical variations in temperature, fig. 3.

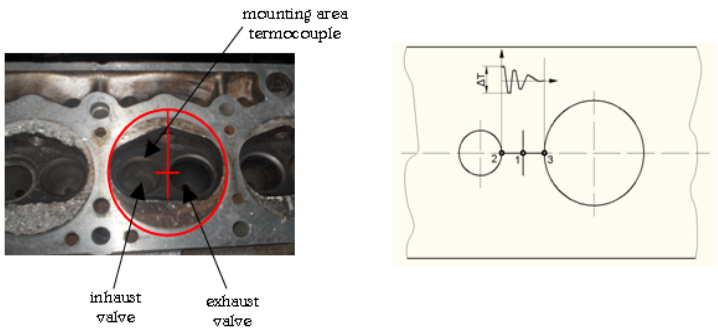

Fig.3 Location of the areas that appear schematized cyclical temperature changes

The center deck of valves - the zone is located in section 1 - the highest temperature occurs at the end of the combustion process. The highest temperature difference at the end of admission is between points 1 and 2, and between points 1 and 3 the difference still reaches the highest value at the end of the admission, but less than that between points 1 and 2. Temperature oscillation amplitude gets lower to reaching the cooling fluid. The highest amplitude of

these oscillations occurs during the engine operation in overload. The effect of these oscillations and the temperature difference is the appearance of thermal stress cracks generating specific thermal fatigue. This phenomenon is more pronounced inside spark ignition engine cylinder heads due to operation in very different thermal regimes. In general, engine parts fitted vehicles is more pronounced appearance of cracks due to operation in very different thermal regimes compared to engines operating in stable regimes, [2], [3].

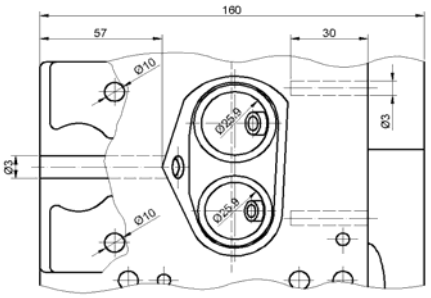

Fig.4 Position channels for mounting thermocouples

For sensing variable temperature fields were chosen thermocouple Pt, Rh-Pt, with a measuring domain of -50 ... 17500C, 0.01 mm diameter, and 6 V/0Cμby sensitivity. These thermocouples were installed near the outlet and inlet pipes and valves in the deck of under representation of fig. 4. These thermocouples are connected to a data acquisition system comprising a data acquisition card that allows recording data during engine operation. When using such a computer program experimental data are processed and converted into temperature charts. Through these diagrams temperature we are able to determine the evolution of thermal tensions causing thermal fatigue.

Further research will be done to study how thermal fatigue influence part machinery constituting the main engine, on an original design facility being registered by OSIM patent, No. A/00439/17.05.2010. This facility was originally designed for durability determinations in thermal fatigue tests as rings, made by hot rolled cylinders.

This facility suitable for experimental determination of thermal fatigue involves mounting some samples of various sizes and shapes on the main shaft of ignition engine, and which are subject to simultaneously heating in an oven at a temperature of 1000° C and cooled off in different environments. Samples are mounted tangentially on all generators of rigid disks mounted on the main axis of the plant. In fig. 5 we describe the intermediate and edgeways support discs provided with channels for assembling samples that may have cross-section shapes and sizes, and different lengths, but approximately equal sets.

Fig.5 Lateral and intermediate support discs provided with channels mounted on the main axis, prepared for sample mounting

Fig.6 Thermocouples crossed through the main axis of the facility to connect their data acquisition system

a - overview of the oven for sample heating

b - detail view of the oven profile

c - loop mounting resistors for electric sample heating oven

Fig.7 Oven to heat samples taken from fixed and mobile parts machinery of a ignition engine to determine thermal fatigue resistance

Thermocouples are mounted on two samples set opposite on the circumference of the supporting disc. These thermocouples response inertia correspond to thermal load cycle, whose conductors are rigid and sent to the reaming of the main shaft to the tension collector, and then to data acquisition system that allows simultaneous recording of temperature variations of experimental application. In Figure no. 6 we describe thermocouples that cross through the main axis to connect their facility data acquisition system. During experiments samples of different materials and quality are subject to cyclic thermal heating inside ovens and cooled off in different environments, fig.7 - carbonic snow, water, and air.

3. CONCLUSIONS

The main objective of the paper is determining the main directions and principles of experimental research work on thermal fatigue phenomenon that occurs in part machinery that participate in the transfer of heat from the combustion chamber to coolant engines fitted to motor vehicles.

Importance of carrying out such research derives from the fact that thermal fatigue of vehicles' engines is less studied both nationally and internationally. So far no specialized publications which deal in detail, theoretical and experimental thermal fatigue of internal combustion engines. Market economy requires a new development in fundamental research of thermal fatigue of motor part machinery, using the most modern and efficient worldwide technology solutions.

REFERENCES

[1.] Bățagă N., Brânzaş P, Iancu A.- Determinarea câmpului de temperatură pentru piesele de autovehicule solicitate termic, Metrologie aplicată, Nr.6,1970
[2.] Botean A.I. – Studiul solicitărilor termomecanice în motoarele cu ardere internă utilizând
[3.] metode moderne de cercetare – Raport final grant de cercetare, 2006
[4.] Popa B., Bățagă N., Mădărăşan T., Marinescu M.- Solicitarea termică în construcţia de maşini, Ed. Tehnică, Bucureşti, 1978
[5.] Tănase P.- Teoria modelării proceselor termoenergetice, Ed. Evrika, Brăila, 1996
[6.] Teberean I. – *Agenţi termodinamici şi maşini termice*, Editura Dacia, 1999

INTERNATIONAL SYMPOSIUM on
ADVANCED ENGINEERING & APPLIED MANAGEMENT
– 40th ANNIVERSARY in HIGHER EDUCATION (1970-2010)
4 – 5 November, 2010, Hunedoara, ROMANIA

[1.]Dinu DRĂGAN, [2.]Mircea Cristian ARNĂUTU,
[3.]Nicuşor Laurenţiu ZAHARIA, [4.]Ion SIMION

2100 HP DIESEL ELECTRICAL LOCOMOTIVE RUNNING TEST

[1.] ROMANIAN RAILWAY AUTHORITY – AFER, 393 CALEA GRIVIŢEI, BUCHAREST, ROMANIA

ABSTRACT:
The diesel – electrical locomotives are used from Romanian freight operators to run trains where electrical locomotives can't run. At Romanian Railways, one of diesel locomotives is 2100 HP Sulzer diesel – electrical locomotives.

KEYWORDS:
strain gauge, experimental stress analysis, Hottinger

1. INTRODUCTION

The early diesel – electrical locomotives manufactured in Romania under Sulzer license had leaf type springs at secondary suspension. During time, the operators wasn't satisfied about leaf type springs so it was necessary a replacement with other types of spring. One of the solutions was using of rubber springs. Because the dimensions of the rubber springs are others than leaf springs the frame of the bogie was modified so it was necessary to perform an experimental stress analysis with strain gages. According to the Railway standards, the tests can performed on bench test or with locomotive in circulation with a method accepted at Romanian Railways. Because in Romania are only wagon/passenger cars bench test, it was necessary to develop the test method necessary for testing the locomotive's bogie. This paper presents the method which was use for testing.

Figure 1 and figure 2 illustrate the two types of secondary suspension (leaf springs and rubber springs).

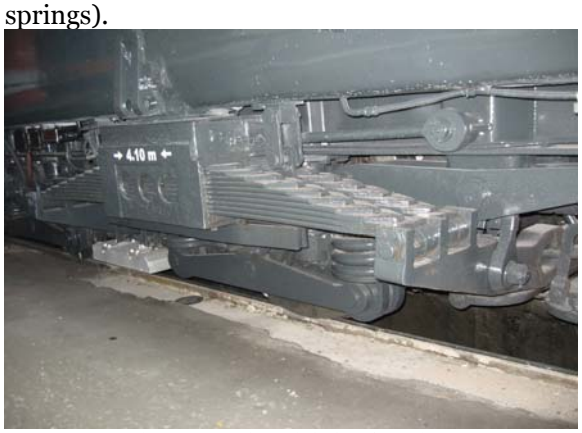

Fig. 1: Bogie with leaf spring


Fig. 2: Bogie with rubber spring

2. TESTS

The tests were performed in two steps:

- static tests,
- dynamic tests.

During the static test, were recorded the static stress σ_{st} due the locomotive's body action on the bogies.

Recording of the stress variation (dynamic components of the stress) $\Delta\sigma_+$ and $\Delta\sigma_-$ were made during locomotive's circulation on 100 km/h speed. Based on values of $\Delta\sigma_+$ and $\Delta\sigma_-$ were calculated outmost values of the stress with the equations:

$$\sigma_{\max} = \sigma_{st} + \Delta\sigma_+ \quad (1)$$

$$\sigma_{\min} = \sigma_{st} + \Delta\sigma_- \quad (2)$$

The medium value of the stress results from the equation:

$$\sigma_m = \frac{\sigma_{\max} + \sigma_{\min}}{2} \quad (3)$$

The amplitude of the stress results from the equation:

$$\sigma_v = \frac{\sigma_{\max} - \sigma_{\min}}{2} \quad (4)$$

The σ_v values were comparative with the values from Goodman – Smith diagrams presented in annex F.3 of the report ERRI B12/RP17. The allowable condition is:

$$\sigma_v \le \sigma_{vadm} \quad (5)$$

In the figure 3 is presented graphically how the tests were done.

The measurement points were located in the relevant areas of the modified bogie's frame.

The measurements were performed in 10 points. Hottinger LY11-10/120 strain gages were glued on the elements of the bogie with Hottinger Z70 adhesive. The strain gages were connected at measuring devices with cables.

The measurements were performed with Hottinger Centipede 100 Multipoint Measuring Unit (for the static tests) and Hottinger MGCplus (for the dynamic tests). The measuring devices Centipede 100 and MGCplus were connected to a laptop computer. The acquisition software used was Catman 4.5 (an Hottinger product).

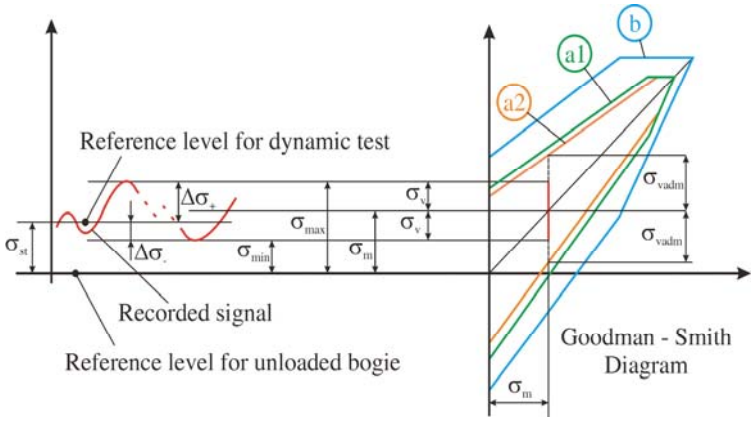

Fig. 3. Tests diagram

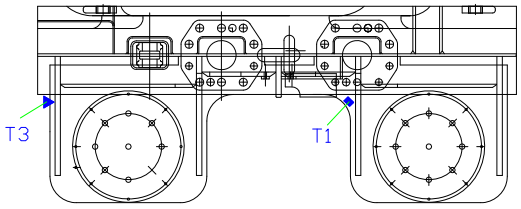

Fig. 4. Strain gauges T1 and T3

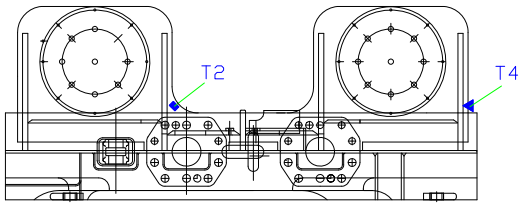

Fig. 5. Strain gauges T2 and T4

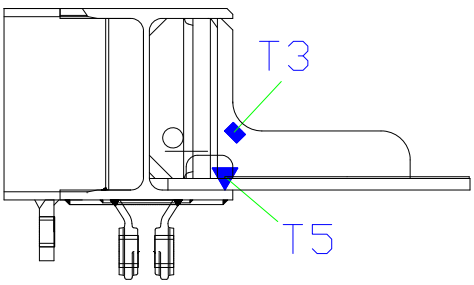

Fig. 6. Strain gauges T3 and T5

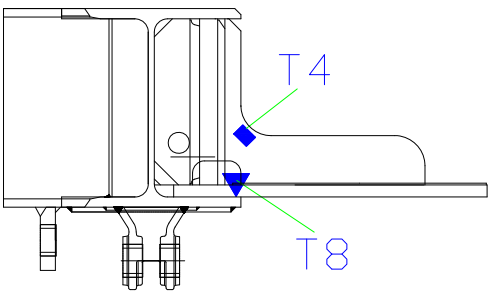

Fig. 7. Strain gauges T4 and T8

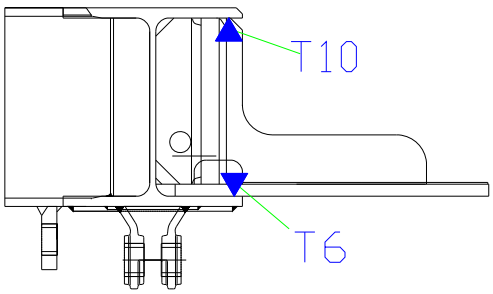

Fig. 8. Strain gauges T6 and T10

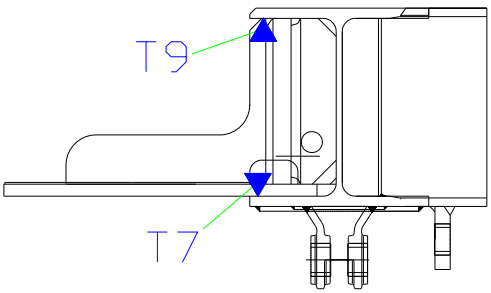

Fig. 9. Strain gauges T7 and T9

3. RESULTS

The dynamic diagrams of the measurement points are shown in figures 9÷14 (there are presented only the diagrams for the most stressed points static and dynamic).

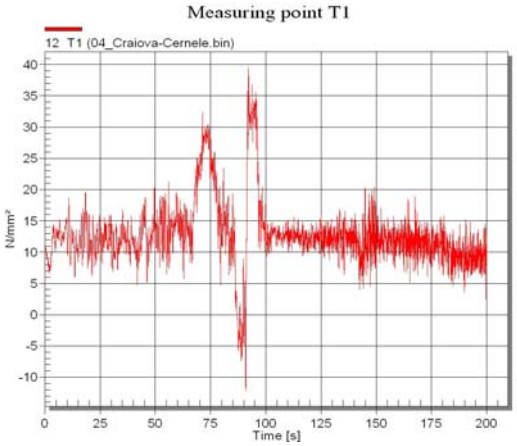

Fig. 10. T1 strain gauge stress

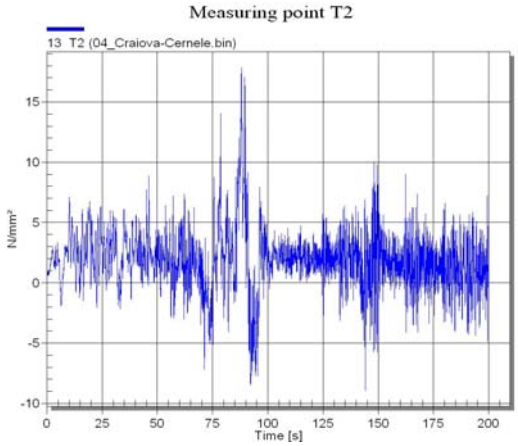

Fig. 11. T2 strain gauge stress

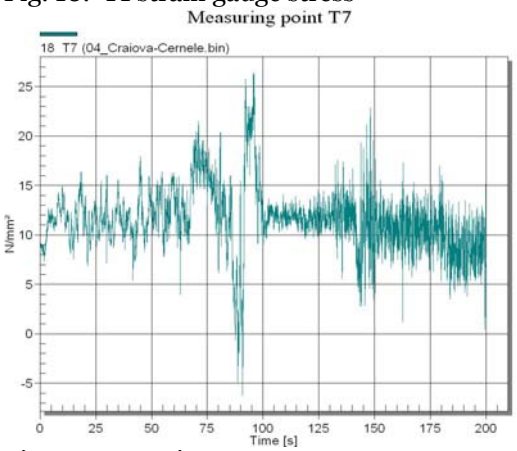

Fig. 12. T7 strain gauge stress

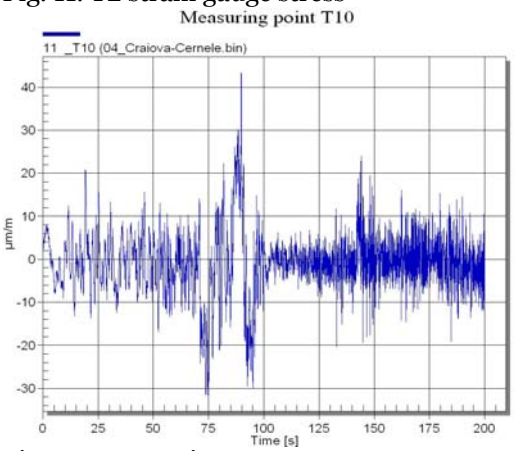

Fig. 13. T10 strain gauge stress

During the tests, the measuring tests were on curve “a2” and “a1” (from the Goodman – Smith diagram) – table 1.

Table 1: Position of the measuring points on Goodman - Smith diagram

SG	T1	T2	T3	T4	T5	T6	T7	T8	T9	T10
Curve	a2	a2	a2	a1	a2	a2	a2	a2	a2	a2

4. CONCLUSIONS

The results, was smaller than permissible stress, so we can concluded that the design solution used by manufacturer was good.

Based on test results, the designer can improve his design to increase the quality of the final product.

After the tests the new certification from the Railway Commission was obtain.

REFERENCES

[1.] Mănescu T. Ş., Jiga G. G., Zaharia N. L., Bîtea C. V., Noţiuni fundamentale de rezistenţa materialelor şi teoria elasticităţii, Editura „Eftimie Murgu", ISBN 978-973-1906-67-6, Reşiţa, 2010
[2.] Mănescu T. Ş., Jiga G. G., Zaharia N. L., Bîtea C. V., Noţiuni fundamentale de rezistenţa materialelor, Editura „Eftimie Murgu" Orizonturi tehnice, ISBN 973-8286-79-4, Reşiţa, 2008
[3.] Mănescu T. Ş., Copaci I., Olaru S., Creangă F.Ş, Tensometria electrică rezistivă în cercetarea experimentală, Editura Mirton, ISBN 973-661-892-5, Timişoara, 2006
[4.] Karl Hoffman: An Introduction to Measurement using Strain Gages, Hottinger Baldwin Messtechnik GmbH, Darmstadt, 2005
[5.] Mănescu T. Ş., Zaharia N. L., Experimental Stress Analysis at a Diesel – Electrical Locomotive Frame Bogie, Structural Analysis Of Advanced Materials Proceedings, page 123, ISBN 978-2-9534804-0-5, Tarbes, Franţa, 2009
[6.] ***ERRI B12/RP17 – Programe des essais à faire subir aux wagons à châssis et superstructure en acier (aptes à recevoir l'attelage automatique de choc et traction) et à leurs bogie à châssis en acier, Utrecht, 1997

INTERNATIONAL SYMPOSIUM on
ADVANCED ENGINEERING & APPLIED MANAGEMENT
– 40th ANNIVERSARY in HIGHER EDUCATION (1970-2010)
4 – 5 November, 2010, Hunedoara, ROMANIA

[1.]Mihaela JULA, [2.]Raul KULCSAR, [3.]Ionut BOROZAN, [4.]Imre-Albert FARKAS

STRUCTURAL AND FUNCTIONAL PARTICULARITIES AS A CRITERION FOR THE DESIGN OF TANGENTIAL BELT DRIVE

[1-4.] UNIVERSITY "POLITEHNICA" TIMIŞOARA, FACULTY OF MECHANICS, TIMISOARA, ROMANIA

ABSTRACT:
The tangential belt drive is a relatively inexpensive solution to increase productivity in the textile industry and it is made by assembling two friction transmissions with flexible elements into a functional hybrid system, namely an open flat belt drive with parallel shafts and velocity ratio i=1 as being the motor element for the actual tangential drive (reduced to the driving wheel), and the tangential transmission itself, consisting of the "n" consumers displayed cvasitangentially on one or both free sides of the flat belt drive (basic drive) being the driven element. The functionality of this drive is based on the friction force between the belt and driving pulley on one hand, and between the belt and the tangential pulleys on the other hand.
KEYWORDS: tangential belt drive, productivity

1. INTRODUCTION

Increasing productivity in the textile industry was made simultaneously in two ways:
- by increasing the processing speed;
- by increasing the number of processing stations which equips a single machine.

The simultaneous drive of the spindles of textile machinery requires the following additional conditions:
- the starting and the stopping of the spindles must be made simultaneously when starting or stopping the machinery;
- speed differences between two or more spindles to be within acceptable limits of the processing method (reflected by the uniformity of the produced wires in length and overall);
- stopping and starting a post should not affect the operation of the other posts;
- low cost.

These requirements have led to the emergence of a new transmission, the tangential drive which is a speed amplifier and uses a flat belt with both sides active.

The tangential drive is strictly applied in the textile industry, spinning machinery, twisting, texturing, elastic wrapping etc. and, more recently, in mail sorting.

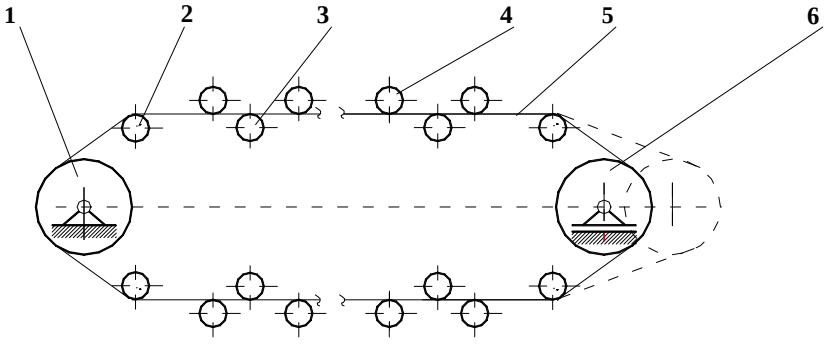

Fig.1a. 1. driving pulley; 2. deviation pulley; 3. pressure pulley; 4. tangential pulley; 5. tangential belt; 6. deviation (free) pulley.

It is made by assembling two friction drivs with flexible elements into a functional hybrid system, namely (fig.1a):

- ❖ an open flat belt drive with parallel shafts and velocity ratio i=1 as being the motor element for the actual tangential drive
- ❖ the tangential drive itself, consisting of the "n" consumers displayed cvasitangentially on one or both free sides of the flat belt drive, being the driven element.
- ❖ in the same direction and having the velocity ratio i=1. On its free sides there are disposed the driven tangential pulleys. The deviation pulley rotates free and doesn't transmit energy.

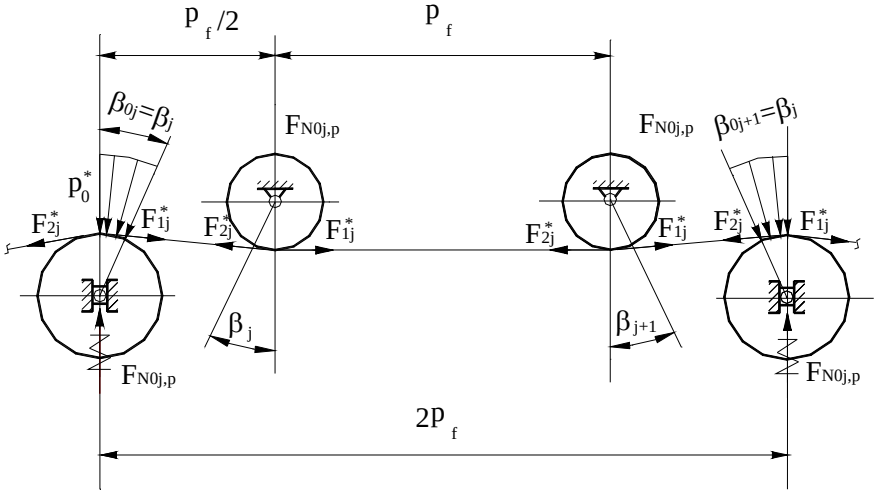

Fig.1b

The over all size of the drive and the tensioning of the belt is determined by this construction.

The dimensions of the drive are established in two steps:

a. the pulley diameter of the flat belt drive can be calculated by using one of the quasi empiric relations [1]:

$$d >> c_d\,(k_A P_m/\omega_m)^{1/3} \quad [mm] \in \{d_1\}_{STAS}$$
$$d_1 >> (d_{min}/h)_a \cdot h \quad [mm] \in \{d_1\}_{STAS} \qquad (1)$$

The option must satisfy the obvious equality:

$$\omega_m \cdot d_1 = \omega_f \cdot d_f \qquad (2)$$

where:

ω_f [rad/s] - angular velocity;

d_f [mm] – tangential pulley diameter (sizes required by the process and by construction/ design).

If equality (1) is not satisfied, parameters ω_m and d_1 are changed within rational limits (engine change or introducing an additional drive between the engine and the primary transmission).

b. The distance between the $d_{1,2}$ pulley axes of the primary transmission is evaluated from the following:

$$a \cong [n' + (2 \ldots 3)]\, p_f + d_1 \qquad (3)$$

by : n '= n or n' = 0,5 n –it is expressed the number of the tangential pulleys disposed entirely to a side or divided on both of the free sides (of useful length $l \cong n' \cdot p_f$).

pf [mm] is the optimal distance between two successive tangential pulleys (step) and it is set by the textile machine manufacturer according to its type, processed wire and processing technology;

c. Whereas the pressure pulleys have a diameter $d_p \geq d_f$, the step p_f and the distance between axes will be adjusted in the second approximation thus setting the actual drive overall dimensions;

d. The geometrical sizes being established and given the flat configuration of the twin transmission (see fig.1a), it is established graphically or analytically the primitive length of the belt (L_p) and the wraping angle on the driving pulley (β_1).

2. TANGENTIAL BELT DRIVE TENSIONING. RATIONAL LIMITS OF THE INITIAL TENSION

To achieve the friction force necessary for the energy transfer, the two drives will be tensioned individually, namely: the flat belt drive is permanently tensioned with a and L_p = variable; (fig.3) and the tangential belt drive itself will also be permanently tensioned with spring or, more rarely, roller locked (fig.3).

The first step is the stretching of the belt and takes place when the tangential pulleys are moved off. It must create the operating conditions of the whole drive. The force of initial tension is installed like in open belt drives with parallel shafts rotating in the same direction, with variable center distance, and corresponds to the total peripheral force to be transmitted by the driving pulley (fig.2).

The second step also involves two different stages:

- bringing the tangential pulleys into contact with the belt;
- the realization of an angle of contact on the tangential pulleys and providing for a permanent belt tension irrespective of its stretching by help of idler pulleys. A lamellar spring device ensures pressure of idlers on the belt (fig.3).

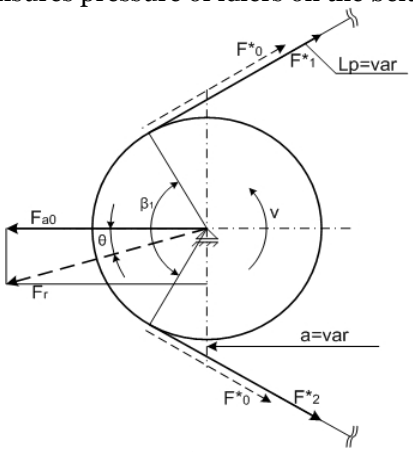

Fig.2

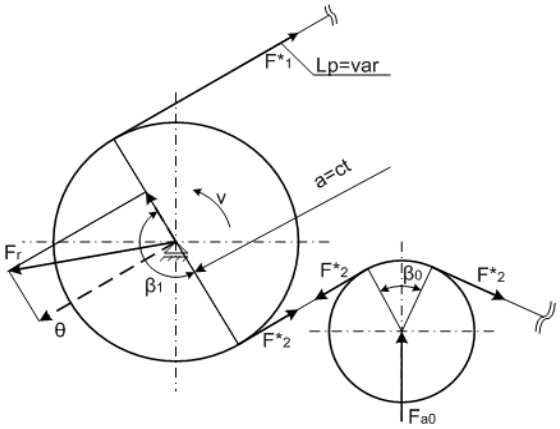

Fig.3

3. ANALISES, DISCUTIONS, APROACHES and INTERPRETATIONS

a. The pulling capacity, efficiency and fatigue resistance of a belt drive are conditioned by a proper assessment and by the conservation in time of the streching.

The force of initial tension is installed like in open belt drives with parallel shafts rotating in the same direction, with variable center distance, and corresponds to the total peripheral force to be transmitted by the driving pulley. On the driving pulley (1) Fig.1 the wrap angle $\beta>30^\circ$ corresponds to the case of classical belt drive studied by the specialized literature. Thus, the tensioning force is for the real values of the power and torque transmitted by a spindle on a textile machine [1];

$$P_m = c_1 \sum_{j=1}^{n} P_j \cong c_1 \cdot n \cdot P_j$$
$$F_t = \sum_{j=1}^{n} F_{tj};\ \ F_{tj} = \frac{2T_j}{d_j};\ \ T_j = \frac{P_j}{\omega_j} \qquad (4)$$

b. The actual tangential drive is achieved likely a belt drive a = ct, Lp = var strained by loading the conducted side of the drive (with an idler) with an external force having a invariable intensity and direction (fig. 3). The wrap angle on the tangential pulley (4) tends to zero as in friction drives when friction is of coulombian nature. In this case the Euler formula looses its validity. Pressure of the idler on the belt is recommended in the catalogues of Habasit and VIS tangential belt firms from the formulae:

$$F_{N0j,f} = 2.5 \cdot \frac{F_t}{n} \quad \text{(Habasit)} \qquad (5)$$

$$F_{N0j,f} = 2.2 \cdot \frac{F_t}{n} \quad \text{(VIS)} \qquad (6)$$

where:

Ft = peripheral force for the entire machine;

n = number of operating members.

As we can see, these formulae do not contain explicitly the coefficient of friction.

4. CONCLUSIONS

The overall size of a tangential belt drive is determined especially by the technological process. The tangential pulleys have a very small wrap angle (ßj<5°) that introduced in the Euler's formulae the relations are loosing their validity. This low value of the wrap angle βj of the belt on the tangential pulley (fig.1) allows us to describe the proper tangential belt drive with equations specific to cylindrical friction drives, that is, following the coulombian friction model. In this case, the higher the coefficient of friction, the lower is the pressing force on the belt corresponding to the tangential consumer (the spindle of the textile machine

REFERENCES

1. Jula M, Mădăras About the Necessary Pressing Force in Tangential Belt Drives., Buletinul ştiinţific al Universităţii „Politehnica" din Timişoara seria Mecanica, Tom 49(63), Fascicola 2, 2004.
2. *** Catalog VIS
3. *** Catalog Habalsit

INTERNATIONAL SYMPOSIUM on
ADVANCED ENGINEERING & APPLIED MANAGEMENT
– 40th ANNIVERSARY in HIGHER EDUCATION (1970-2010)
4 – 5 November, 2010, Hunedoara, ROMANIA

[1.] Sebastian DUMA, [2.]Mihaela POPESCU, [3.]Cosmin LOCOVEI

STUDIES REGARDING THE ACQUIREMENT OF HARDNESS STANDARD BLOCKS FOR TRANSMITTING THE VICKERS HARDNESS SCALE 200…800 HV_1

[1.] UNIVERSITY "POLITEHNICA" TIMIŞOARA, FACULTY OF MECHANICS, ROMANIA

ABSTRACT:
Abstract: In the present work the conditions that the hardness standard blocks must comply with are briefly presented in order to materialize the Vickers scales HV_1. Starting from these conditions the accent is placed on choosing the material, the primary and secondary treatment applied in order to comply with the imposed metrological requirements for the hardness standard blocks.
KEYWORDS:
Vickers, scales, hardness standard blocks, hardness testing

1. INTRODUCTION

The hardness standard blocks are measures with unique value. These are materializations of standardized hardness points. They are used to verify periodically the hardness determining devices, being a very important constituent of a high quality product.

2. THE STUDY - CONDITIONS IMPOSED BY THE VICKERS HARDNESS STANDARD BLOCKS

The test consists of the applying on the part a diamond penetrator with an F force and a given time, which has a pyramidal shape with a square base and with the angle between 2 sides of 136 °

At the Vickers test, the hardness characteristics is a plastic one that is determined with the ratio between the applied force F and the lateral surface of the remnant track – figure 1.

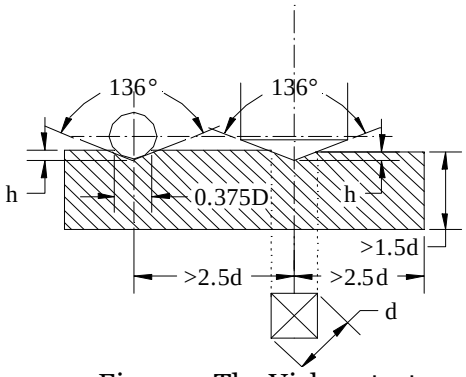

Figure 1. The Vickers test

The hardness standard blocks are made out of steel or metals and non-ferrous alloys with a homogenous and stable structure, as to ensure the uniformity and stability in time of the hardness.

Irregularities such as cracks, pores or non-metallic inclusions are not accepted. Grain size has to be fine and uniform.

The base surfaces of the hardness standard blocks must be:

- flat and parallel
- finely rectified
- without corrosion spots, scratches or other imperfections that might influence the hardness tests.

The hardness standard blocks must have a high uniformity of the hardness on the testing surface. The uniformity of the hardness is given by the fidelity error that must not cross a specified value. The maximum value accepted for the fidelity error depends on the method of hardness testing, the hardness scale, the hardness interval and the precision class. For the scales analysed in the present work the uniformity of the hardness must be high, $e_f \leq 1\%$.

For the Vickers method the error is calculated as following:

$$e_f = \frac{R}{\bar{d}} \cdot 100 \ [\%] \quad (1),$$

where

amplitude $R = d_{max} - d_{min}$

d_{max} – the maximum average diagonal obtained at the measuring of every indent made at calibration.

d_{min} – the minimum average diagonal obtained at the measuring of every indent made at calibration.

$\bar{d} = \frac{1}{n} \sum_{i=1}^{n} d_i$ (2) - the average of the n indents from where the periodical hardness is calculated

$d = \frac{d_I + d_-}{2}$ (3)- average indent diagonal

d_I, d_- - the diagonals of a print

3. ANALISES, DISCUSIONS APPROACHES AND INTERPRETATIONS EXPERIMENTAL RESULTS

The material chosen for experimentations is 100Cr6 steel (RUL 1). From previous experiments [1], [3], results that the analysed material may have a homogenous structure that ensures the uniformity and stability in time of the hardness. One of the primary conditions is the supplementary refinement of the steel by remelting with a void spring (RAV) and electrical remelting under cinder (REZ) and primary thermic treatment (annealing of globulization).

The chemical composition of the samples, after elaboration, is presented in table 1.

Table 1 The chemical composition of the sample's material

C [%]	Mn [%]	Si [%]	Cr [%]	P [%]	S [%]	Ni [%]
1,00	0,33	0,29	1,6	0,014	0,006	0,12

The whole experimental lot was quenched at 840°C, temperature obtained as optimum after previous experiments [3]. After this, the subzero treatment is applied (-183°). After the treatment each sample is metallographically prepared and structurally analysed, using electron microscopy and X-rays diffraction. The structure is homogenous in section and formed out of fine martensite, remnant carbides from initial status – globulisation, small carbides and uniformity spread and small quantities of residue austenite.

The hardness oh the samples is too high (approx 835HV_1) for a Vickers 200...800 HV_1 scale materialization.

Table 2 The results of the measuring of twenty samples of about 200, 250, 440 and 760 HV_1

No.	Material; Thermic treatment	Average diagonal $\bar{d}$, µm	Hardness HV_1	Fidelity error ef, %
1	100Cr6 Globulized	95.12	205	0.36
2		95.20	205	0.50
3		94.82	206	0.46
4		96.44	200	0.46
5		93.94	210	0.98
6	100Cr6 Quenched + Tempered at 700 °C	87.37	243	0.93
7		85.20	255	0.20
8		85.36	254	0.56
9		85.27	253	0.17
10		85.07	257	0.19
11	100Cr6 Quenched + Tempered at 400 °C	64.66	443	0.72
12		65.39	434	0.76
13		62.96	467	0.18
14		65.38	434	0.70
15		65.17	436	0.21
16	100Cr6 Quenched + Tempered at 160 °C	48.85	757	0.81
17		49.52	739	0.67
18		49.03	760	0.26
19		49.83	742	0.91
20		48.41	792	0.70

In order, to obtain a softer material, tenacious (with a sorbitic or a pearlitic globular structure), the tempering treatment has been applied right after quenching [2], [4]. The tempering temperatures experimented were 160, 400, 700 °C. After tempering, the Vickers HV_1 hardness has been determined for all tempered samples and for the samples that have not been treated with the secondary treatment. The sclerometrical determing was made by the calibration device for Vickers hardness determing currently in the endovment of the National Institute of Metrology.

In order, to confer the nominal hardness and to have the possibility to calculate the fidelity error, an each sample the hardness was measured in five points. In the following tables the experimental results are presented for the samples that led to acquiring a hardness of approx. 200, 250, 440 and 760 HV_1.

In table 2 the results of the measuring are presented for twenty samples of about 200, 250, 440 and 760 HV_1.

It is observed that all the samples are proper for the hardness standard blocks performing. (hardness uniformity is between the specified limits).

Each sample was metalographically prepared and structurally analysed using electron microscopy and X-rays diffraction.

In figure 2 a part (2θ = 31...39) of the diffraction spectrum is presented for the sample tempered at 700, 400°C and the sample globulised.

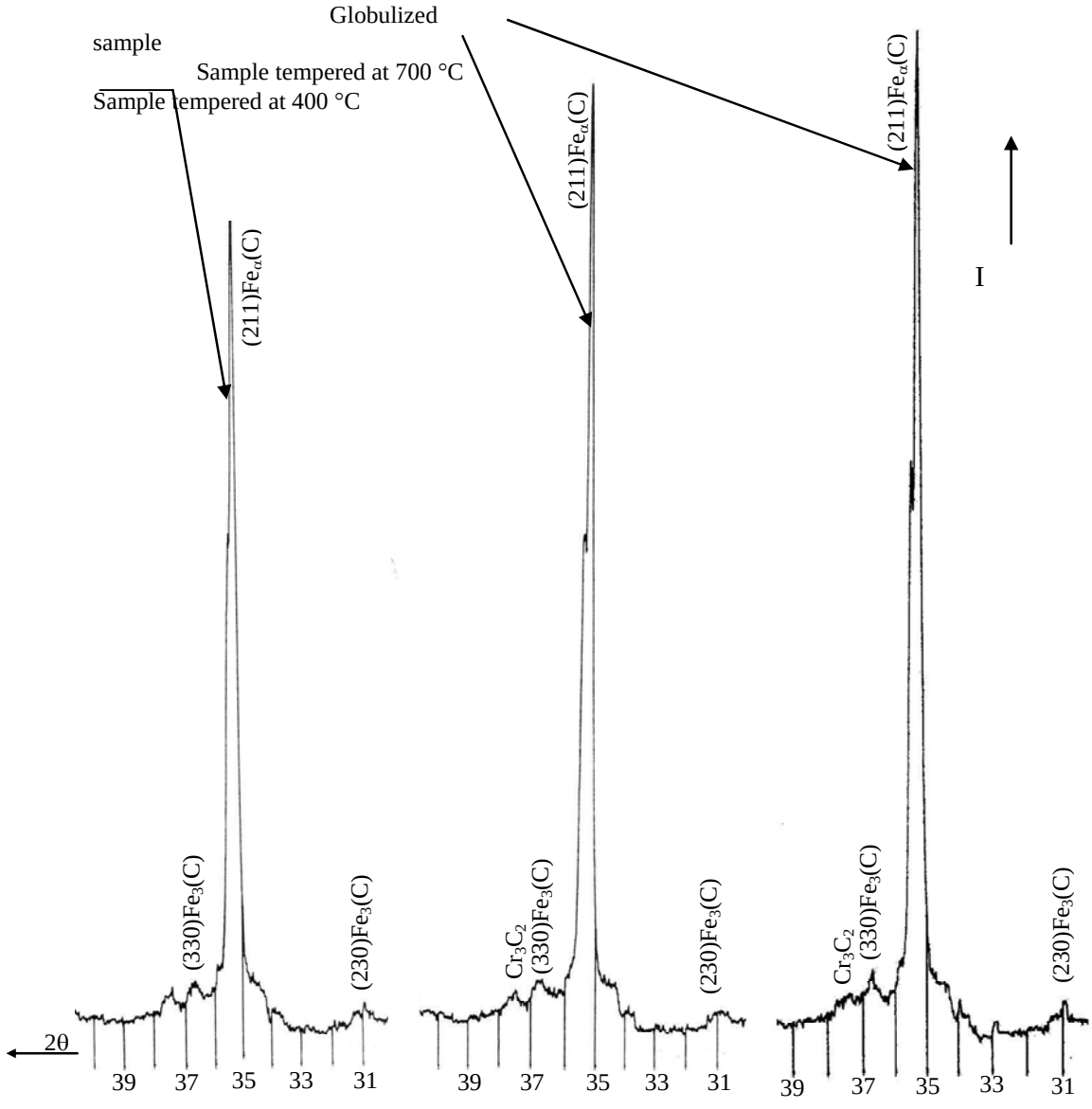

Figure 2. Part of the diffraction spectrum for samples tempered at 700°, 400° C and for the globulized sample

The structures obtained from electron microscopy are presented in figures 3, 4 and 5.

Analysing the resulting hardness values, X-rays diffractions and microstructures it can be observed that the growth of the tempering temperature is the bigger the carbide particles are and the lower internal tensions which leads to a decreasement of the hardness.

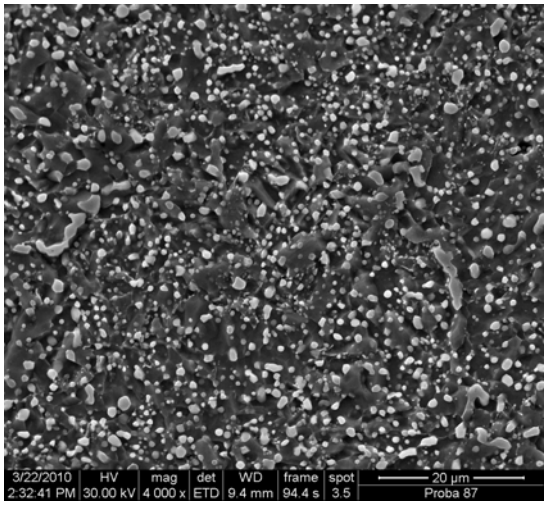

Figure 3. Microstructure of the annealed material (4000 X)

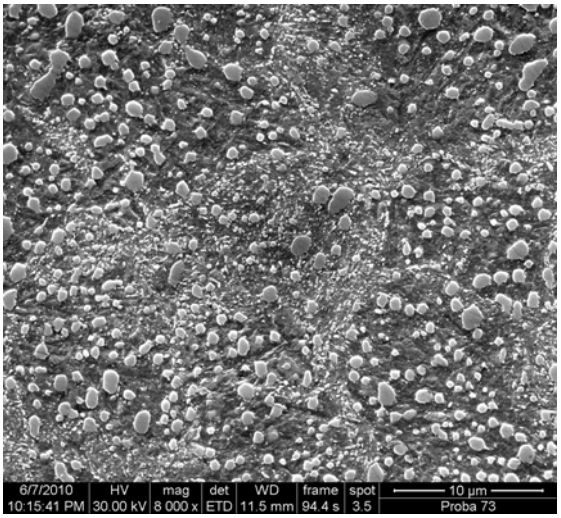

Figure 4. Structural aspect of the material after the tempering at 700 °C (8000 X)

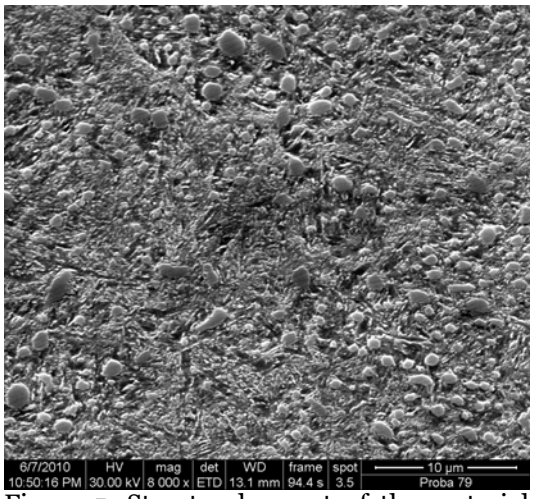

Figure 5. Structural aspect of the material after the tempering at 400 °C (8000 X)

4. CONCLUSIONS

To comply with the requirements of uniformity and stability in time imposed to the hardness standard blocks, some conditions must be respected. The most important are:

- using a premium quality steel, supplementary refined and received with high strictness bar by bar;
- the correct appliance of the primary and secondary thermic treatment (in this case: globulisations + quenching + subzero treating + tempering).

The appropriate elaboration of the 100Cr6 and the primary treatment following by quenching and subzero treating gives a uniformity and stability in time of the properties (especially hardness). The value of the hardness is established with the tempering treatment.

REFERENCES

[1] Duma. S.: *Studies regarding the acquirement of hardness standard blocks for transmitting the Knoop hardness scale 275…577 $HK_{0,2}$ and Brinell 416…589HBW 5/750* – Scientific Bulletin of the " POLITEHNICA" University of Timisoara, 2009, Tom 54(68) Fasc. 3, ISSN :1224-6077;

[2] Hazotte. A. (ed.): - *Solid State Transformation and Heat Treatment.* Wiley-VCH, Weinheim 2004, ISBN-10: 352731007X, ISBN-13: 9783527310074;

[3] Popescu, M., Duma, S., Locovei, C.: Experimental research concerning structural and hardness stability of 100Cr6 steel machine parts, 10th International Conference "Research and Development in Mechanical Industry" RaDMI 2010, 16 - 19. September 2010, Donji Milanovac, Serbia, ISBN 978-86-6075-018-3;

[4] Serban, V.A., Răduţă, A.: *Ştiinţa şi Ingineria Materialelor*, Editura Politehnica, Timişoara, 2010, ISBN: 978-606-554-044-6.

INTERNATIONAL SYMPOSIUM on
ADVANCED ENGINEERING & APPLIED MANAGEMENT
– 40th ANNIVERSARY in HIGHER EDUCATION (1970-2010)
4 – 5 November, 2010, Hunedoara, ROMANIA

[1.] Ľubomír ŠOOŠ

NEW METHODOLOGY CALCULATIONS OF RADIAL STIFFNESS NODAL POINTS SPINDLE MACHINE TOOL

[1.] SLOVAK TECHNICAL UNIVERSITY IN BRATISLAVA
FACULTY OF MECHANICAL ENGINEERING, BRATISLAVA, SLOVAKIA

ABSTRACT:
Spindle - bearings system of the machine tools play a major role in the fulfilling the required working accuracy and productivity. The number of spindles supported on angular contact ball bearings is increasing proportionally with increasing demands on the machine tool quality. It is caused by the fact that these spindle bearings in various combinations can to reach sufficient radial and axial stiffness and revolving frequency of the spindle-bearing system. The complex analysis stiffness of nodal points is difficult and complicate. In this paper is introduced as well simplified mathematical apparatus for evaluation of radial stiffness bearing knot.

KEYWORDS:
Spindle, Bearing, Machine Tools, Stiffness

1. INTRODUCTION

The number of spindles supported on angular contact ball bearings is increasing proportionally with increasing demands on the machine tool quality. It is caused by the fact that these bearings can be arranged in various combinations to create bearing arrangements which can be enabling to eliminate radial and also axial loads. The possibility of variation of the number of bearings, preload value, bearings dimensions and contact angle of bearings used in bearing arrangements create wide spectrum of combination to reach sufficient radial stiffness and revolving frequency of the spindle-bearing system, (Fig.1). The sufficient stiffness and revolving frequency of headstock are necessary criteria for reaching demanding manufacturing precision and machine tool productivity.

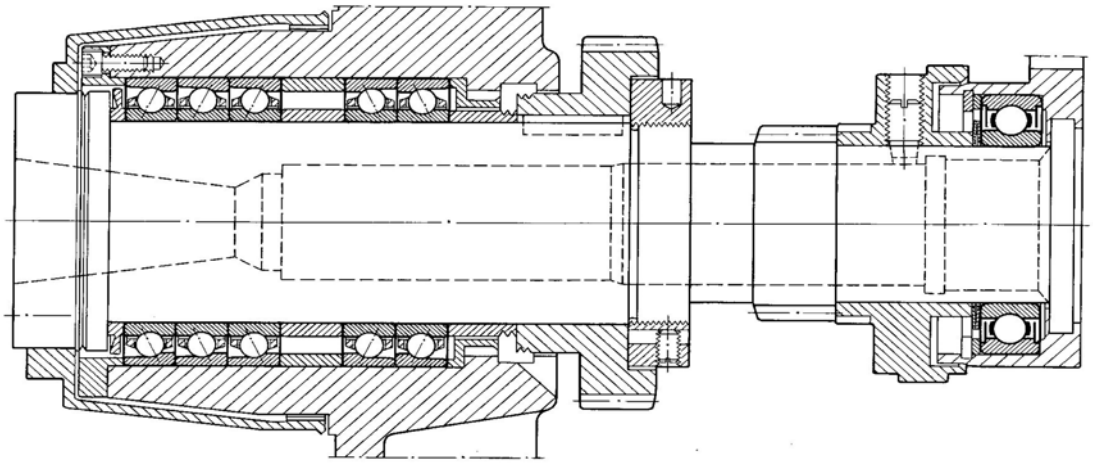

Figure 1: Horizontal machining centre, Thyssen-Hüller Hille GmbH , Germany
Work nodal – 3x71914 ACGB/P4 - 2x71914 ACGB/P4, Opposite side– 6011-2Z

2. THE CALCULATION OF RADIAL STIFFNESS OF NODAL POINTS

2.1 Assumptions of solution

According to the Hertz assumptions [2], there is dependence between the load "P" and deformation "δ" at the contact point of the ball with the plane, given by the relationship

$$P = k_{\delta}.\delta^{3/2} \tag{1}$$

1. the bearings in the nodal points are of the same type and dimensions, with exact geometric dimensions
2. the value of the contact angle is equal for all directionally-arranged bearings in the nodal point, which causes equal distribution of strain on these bearings
3. radial load is equally distributed onto all bearings of the nodal point

2.2 Stiffness of nodal points with directionally-arranged bearings

The calculation of the stiffness of a nodal point is based on the stiffness of the bearing itself [4], which is defined as

$$C_{r1} = \frac{d\ F_{r1}}{d\ \delta_{r0}} \tag{2}$$

As radial displacement δ_{ro} is a function of contact deformation δ_o of the ball with the highest load [3], the equation for calculating stiffness of radial beveled bearings will have the form of

$$C_{r1} = \frac{d\ F_{r1}}{d\ \delta_0} \cdot \frac{d\ \delta_0}{d\ \delta_{r0}} \tag{3}$$

When calculating stiffness, the distribution of load among the rollers must be determined, and the dependence between the load on the top ball and external load must be found. The distribution of load in the bearing can be derived from the static condition of balance [4]

$$F_{r1} = \frac{F_{r1}}{i} = \sum_{j=0}^{z} P_j.\cos(\alpha_j).\cos(j.\gamma) \tag{4}$$

where $\gamma = \frac{360}{z}$ is the spacing angle of balls.

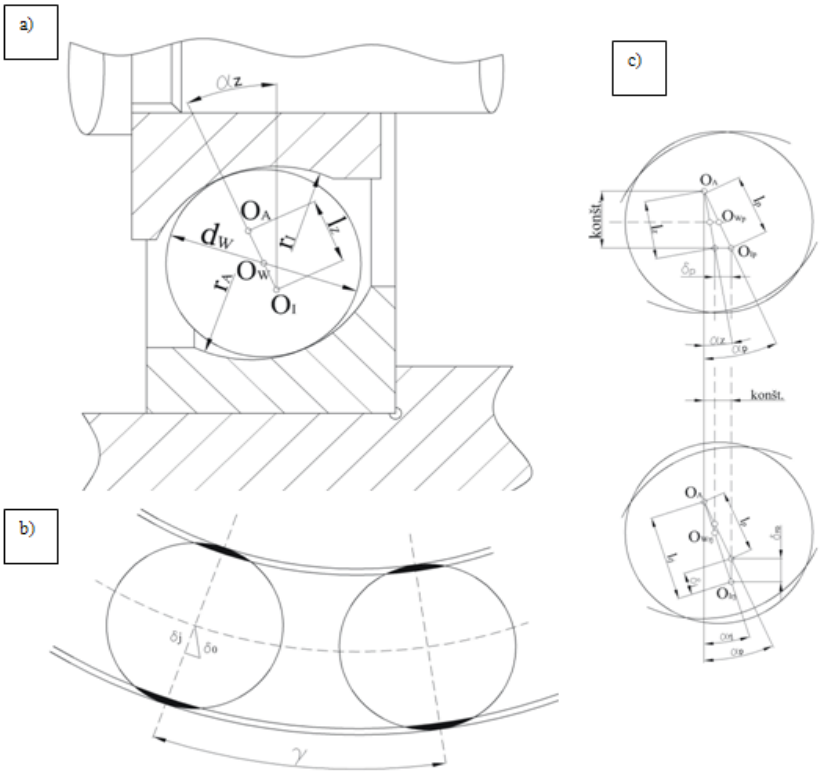

Figure 2: Built-in bearing scheme, a – unloaded, b – pre-stressed, c – radial loaded

The values of contact deformations δ_j and angles α_j differ from each other around the circumference of the bearing and can be expressed as follows, (Fig.2):

$$\delta_j = l_{rj} - l_p = \sqrt{\left[l_z.\sin(\alpha_z)+\delta_p\right]^2 + \left[l_z.\cos(\alpha_z)+\delta_{r0}.\cos(j.\gamma)\right]^2} - l_p \quad (5)$$

$$\cos(\alpha_j) = \frac{l_z.\cos(\alpha_z)+\delta_{r0}.\cos(j.\gamma)}{\sqrt{\left[l_z.\sin(\alpha_z)+\delta_p\right]^2 + \left[l_z.\cos(\alpha_z)+\delta_{r0}.\cos(j.\gamma)\right]^2}} \quad (6)$$

By loading the pre-stressed bearing by radial force is distance between center of balls O_AO_{ip} constant, (Fig.1 b, c).

$$l_p.\sin(\alpha_p) = l_{rj}.\sin(\alpha_{rj}) = konst. \quad (7)$$

The dependence between the deformation of the j-th ball and the top ball can be determined by the relation

$$\delta_j = \delta_0.\cos(j.\gamma) \quad (8)$$

By derivation of the equation (4) we get

$$\frac{d\ F_{r1}}{d\ \delta_0} = i.\sum_{j=0}^{z}\left[\frac{d\ P_j}{d\ \delta_j}.\cos(\alpha_j) - P_j.\sin(\alpha_j).\frac{d\ \alpha_j}{d\ \delta_j}\right].\frac{d\ \alpha_j}{d\ \delta_0}.\cos(j.\gamma) \quad (9)$$

The unknown derivatives in equation (9) can be calculated by derivation/simplification of the relations (1), (7), (8).

$$\frac{dP_j}{d\delta_j} = \frac{3}{2}k_\delta^{2/3}P_j^{1/3} \quad (10)$$

$$\frac{d\alpha_j}{d\delta_j} = -\frac{tg(\alpha_j)}{l_{rj}} \quad (11)$$

$$\frac{d\delta_j}{d\delta_0} = \cos(j.\gamma) \quad (12)$$

The dependence of the contact deformation and radial displacement, Fig. 1, can be determined from the relation

$$\frac{d\ \delta_0}{d\ \delta_{r0}} = \left(\frac{d\ \delta_j}{d\ \delta_0}\right)^{-1}.\frac{d\ \delta_j}{d\ \delta_{r0}} \quad (13)$$

where $\frac{d\ \delta_j}{d\ \delta_{r0}}$ is calculated from the equation (5)

by inserting equations (14) and (12) into equation (13)

$$\frac{d\delta_j}{d\delta_{ro}} = \frac{1}{2}.\frac{2(l_z\cos\alpha_z + \delta_{ro}\cos(j.\gamma))\cos(j.\gamma)}{\sqrt{(l_z\cos\alpha_z + \delta_{ro}\cos(j.\gamma))^2 + (l_z\sin\alpha_z + \delta_p)^2}} = \cos\alpha_j\cos(j.\gamma) \quad (14)$$

$$\frac{d\ \delta_0}{d\ \delta_{r0}} = \frac{1}{\cos(j.\gamma)}.\cos(\alpha_j).\cos(j.\gamma) = \cos(\alpha_j) \quad (15)$$

After inserting equations (15) and (9) into equation (3) we will get the resulting relation for the stiffness of a pre-stressed nodal point with directionally-arranged bearings.

$$C_r = i.\sum_{j=0}^{z}\left[\frac{3}{2}.k_\delta^{2/3}.P_j^{1/3}.\cos^2(\alpha_j) + P_j.\frac{\sin^2(\alpha_j)}{l_{rj}}\right].\cos^2(j.\gamma) \quad (16)$$

2.3 The stiffness of nodal point with bearings arranged according to the shape

When calculating the nodal point with bearings arranged according to the shape we divide the nodal point into part "1" and part "2" (Fig.1), with the *same* orientation of contact angles -nodes as directionally-arranged bearings, and the stiffness of the parts will be calculated as follows:

$$C_{r1} = i_1.\sum_{j=0}^{z}\left[\frac{3}{2}.k_\delta^{2/3}.P_j^{1/3}.\cos^2(\alpha_{1j}) + P_j.\frac{\sin^2(\alpha_{1j})}{l_{r1j}}\right].\cos^2(j.\gamma) \quad (17a)$$

$$C_{r2} = i_2 . \sum_{j=0}^{z} \left[\frac{3}{2} . k_{\delta}^{2/3} . P_j^{1/3} . \cos^2(\alpha_{2j}) + P_j . \frac{\sin^2(\alpha_{2j})}{l_{r2j}} \right] . \cos^2(j.\gamma) \qquad (17b)$$

for Fig. 1: numbers of balls: $i_1 = 3$, $i_2 = 2$, *contact angles* $\alpha_1 = \alpha_2 = 25^\circ$
By their subsequent addition we determine the total stiffness of the nodal point with

$$C_r = C_{r1} + C_{r2} \qquad (18)$$

In order to optimize the stiffness and load-bearing capacity for determined technological conditions, the manufacturers of machine tools have come out with a new, non-traditional solution of nodal points. By diminishing the contact angle of the bearing in Part 2, the axial stiffness of the nodal point is partially decreased, but at the same time the value of the radial stiffness and boundary axial load is increased.

2.4 Approximate calculation of stiffness

When evaluating the overall stiffness of a spindle, the designer must take into account the approximate calculation of the stiffness of the nodal points.

If all the rollers are loaded, and their number is more than 2 per bearing [4], the following equation can be applied:

$$\sum_{j=0}^{z} \cos^2(j.\gamma) = \frac{z}{2} \qquad (19)$$

If the bearing angle is loaded only in an axial direction by the pre-stressing force, then the load on the rollers is constant around the whole circumference and can be expressed, for the particular parts of the nodal point [8],, in the form

$$P_{1j} = \frac{F_p}{i_1 . z . \sin(\alpha_{p1})}; \; P_{2j} = \frac{F_p}{i_2 . z . \sin(\alpha_{p2})} \qquad (20)$$

The magnitude of the contact angles of spindle bearings is not greater than 26 degrees. In that case the value of the second expression in equations (17a) and (17b) is negligible.

Taking into consideration these assumptions, we will get the relationship for the approximate calculation of the radial stiffness of a bearing angle with directionally placed bearings.

$$C_r = \frac{3.10^{-3}}{4} . z^{2/3} . k_{\delta}^{2/3} . i^{2/3} . F_p^{1/3} . \frac{\cos^2(\alpha)}{\sin^{1/3}(\alpha)} \qquad (21)$$

and with bearings arranged according to shape:

$$C_r = \frac{3.10^{-3}}{4} . z^{2/3} . k_{\delta}^{2/3} . i_1^{2/3} . F_p^{1/3} . \frac{\cos^2(\alpha_1)}{\sin^{1/3}(\alpha_1)} . \left[1 + \frac{i_2^{2/3} . \cos^2(\alpha_2) . \sin^{1/3}(\alpha_1)}{i_1^{2/3} . \cos^2(\alpha_1) . \sin^{1/3}(\alpha_2)} \right] \qquad (22)$$

where the approximate value of the deformation constant is $k_{\delta} = \sqrt{1{,}25 . d_w}$, d_w – diameter of balls.

The pre-stressing value " F_p" can be calculated according to the standard STN 02 46 15. Some foreign manufacturers (fy SKF, FAG, SNFA ...) publish this value in their catalogues. The number of balls "z" and diameters of balls "d_w" of some types of bearings are quoted in literature, e.g. [7].

3. VERIFICATION OF MEASURED AND CALCULATED VALUES

The results obtained according to this mathematical model were compared with the values measured by means of the experimental device shown in Fig 3. This device was used to measure the deformation characteristics of nodal points with different combinations of arrangement, pre-stressing values, contact angles, loads and revolution frequencies. This new equation (22) for middle stiffness of the bearing arrangement "C_r" calculation was experimental verified, [1], [5], [6].

At Fig. 3 we have been compared experimental measure stiffness, exactly theoretical and middle calculated radial stiffness of the bearing arrangement B7216 AATB P4 O UL. Results are very good. At zero frequencies the values of radial stiffness are experimental higher than theoretical values, Fig.3. The dependence of stiffness on loading has a digressive (decreasing) course. The decrease is nearly linear, until a certain critical force "F_{kr}", at this point the least-loaded roller becomes unloaded. The deformation characteristic of the nodal point is influenced by the type of flange. The direction and gradation of the stiffness change under the given operation conditions depend on their construction.

At Fig. 4 and Fig. 5 is experimental stand for messing radial and axial stiffness.

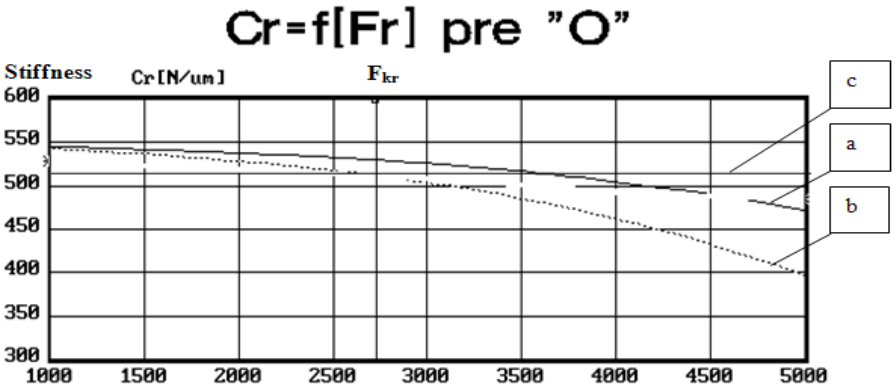

Figure 3 Radial stiffness of the bearing arrangement B7216 AATB P4 O UL, a - experimental, b – exactly theoretical, c – middle theoretical

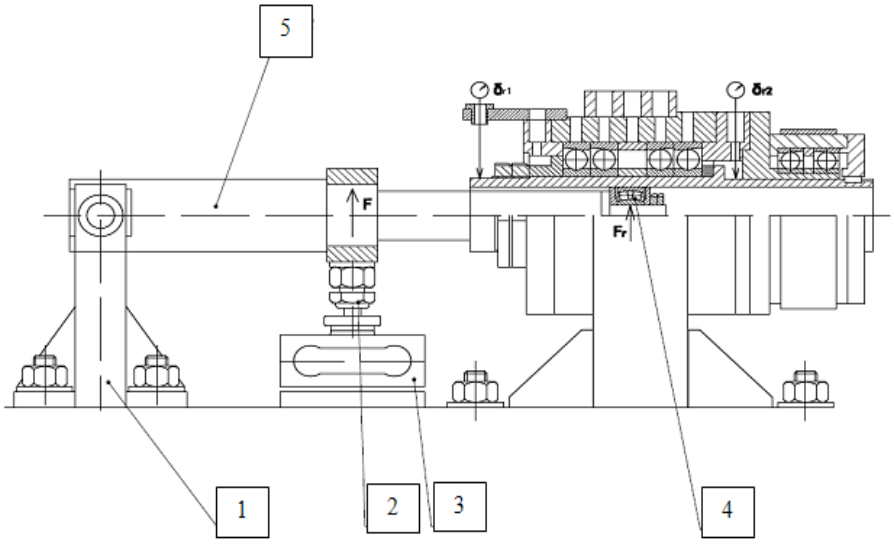

Figure 4 Cut of experimental stand, 1- holder, 2- to retighten screw, 3- dynamometer, 4- force bearing, 5- force arm

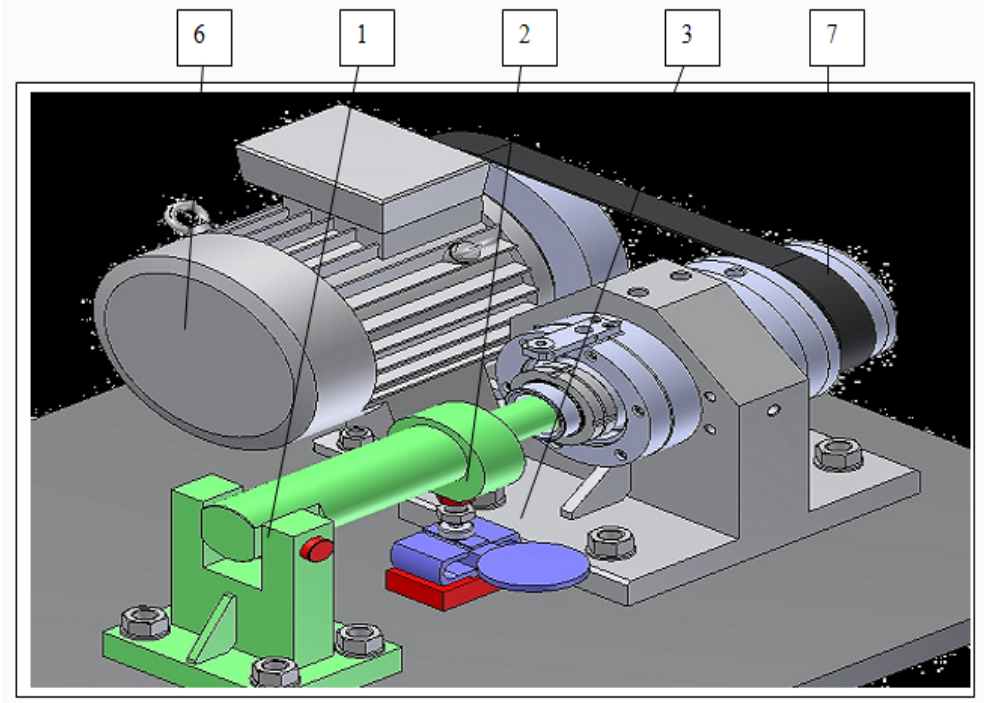

Figure 5.3D model of experimental stand, 1- holder, 2- to retighten screw, 3- dynamometer, 6- drive, 7- Poly V belt

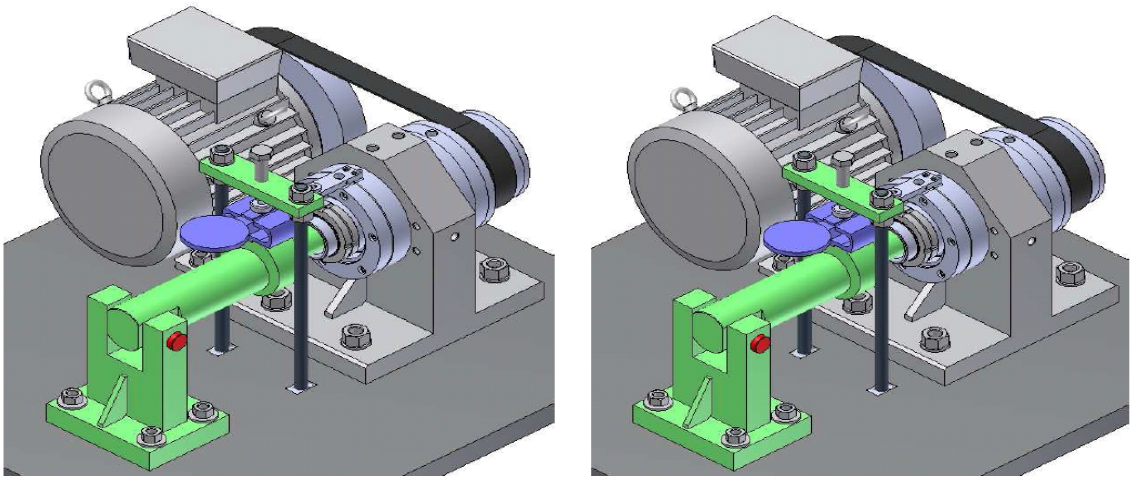

Figure 6.Different decisions measuring radial stiffness bearing knot

4. SUMMARY

In this paper are presented the regulations for selection and calculation of the radial stiffness of nodal points composed of radial ball bearings with beveled contact. The resulting radial stiffness of spindle nodes is a function of various factors. Its calculation, considering the operation conditions of the node, is quite complicated, and cannot be accomplished without the use of computer technologies.

The research results show that the change of the radial stiffness of pre-stressed nodes is relatively small at zero revolution frequencies, in dependence on loading, and can be mineralized.

In this field the results of the precise and the approximate mathematical model are practically equal. From the preceding it follows that in a preliminary design of mounting, a simplified mathematical model for calculating the stiffness of nodal points can be used, as derived in this article.

This contribution has arisen in assistances financial resources project KEGA nr. 3/7216/09.

LITERATURE

[1.] Šooš, Ľ.: Statika ložiskových uzlov vretien obrábacích strojov. [Kandidátska dizertačná práca]. STU Bratislava. 1992, 140 s.

[2.] Harris, T.A.: Rolling Bearing Analysis. New York - London - Sydney, 1966, 481s.

[3.] Balmont, V.B. - Russkich,S.P.: Rasčet radialnoj žestkosti radialno - upornogo podšipnika. Trudy instituta. M., Specinformcentr VNIPPa, 69, 1978, č.1, s..93 - 107.

[4.] Kovalev, M.P.- Narodeckiij,M.Z.: Rasčet vysokotočnych šarikopodšipnikov. 2 vyd. Moskva, Mašinostroenie 1980. 279s.

[5.] Šooš, Ľ.: Quality of design engineering: case of machine tools headstock. In: Quality Festival 2008 : 2nd International quality conference. - Kragujevac, May 13-15, 2008. - Kragujevac : University in Kragujevac, 2008. - ISBN 978-86-86663-25-2.

[6.] Lavorčík, L.- Šooš, Ľ.- Zoň, J.: Applied Software Technology of Designing a Bearing Housing Fitted with Rolling Bearing Arrangement. In..: "ICED 91". Zurich, August, 1991, s.1228 -1233.

INTERNATIONAL SYMPOSIUM on
ADVANCED ENGINEERING & APPLIED MANAGEMENT
– 40th ANNIVERSARY in HIGHER EDUCATION (1970-2010)
4 – 5 November, 2010, Hunedoara, ROMANIA

[1.]Paolo BOSCARIOL, [2.]Alessandro GASPARETTO,
[3.]Albano LANZUTTI, [4.]Renato VIDONI, [5.]Vanni ZANOTTO

NEUMESY: A SPECIAL ROBOT FOR NEUROSURGERY

[1-5.] UNIVERSITY OF UDINE – DIEGM. VIA DELLE SCIENZE 208, 33100 UDINE, ITALY

ABSTRACT:
In the last years a large number of new surgical devices have been developed so as to improve the operation outcomes and reduce the patient's trauma. Nevertheless the dexterity and accuracy required in positioning the surgical devices are often unreachable if the surgeons are not assisted by a suitable system. From a kinematic point of view, the robot must reach any target position in the patient's body being less invasive as possible with respect to the surgeon's workspace. In order to meet such requirements a suitable design of the robot kinematics is needed. This paper presents the kinematic design of a special robot for neurosurgical operations, named NEUMESY (NEUrosurgical MEchatronic SYstem).
NEUMESY is a six joints serial manipulator whose kinematic structure lets the robot to adapt to different patient's positions while minimizing the overall dimensions. Owing to the usual symmetry of a surgical tool, the kinematic dimension of the neurosurgical task is five, being given by one point and one direction on the space. Therefore the NEUMESY is kinematically redundant, leaving an extra DOF to the surgeon to choose a suitable robot configuration which minimally limits his movements during the surgical operations. The link lengths have been optimized in order to maximize the robot workspace with respect to the surgical task, while minimizing the links static deformations.
KEYWORDS: surgical devices, kinematic design, special robot, neurosurgical operations, NEUMESY

1. INTRODUCTION

The initial experimentation of robotic systems in surgery was undertaken during the early 1980s [6,7,3], and it basically consisted of adapting the industrial robot technologies already in existence. In the last decade, there has been a growing awareness, within the medical community, of the benefits offered by using robots in various surgical tasks. Traditional surgery involves making large incisions to access the part of a patient's body that needs to be operated on. Minimally Invasive Surgery (MIS), on the other hand, is a cost-effective alternative to open surgery. Basically, the same operations are performed using instruments designed to enter the body cavity through several tiny incisions, rather than a single large one. By eliminating large incisions, trauma to the body, post-operative pain, and the length of hospital stay are significantly reduced.

However, new problems connected to the use of robots in surgery have arisen, since there is no direct contact with the patient. For this reason, it is necessary to develop suitable tactile sensors to provide surgeons with the perception of directly operating on the patient. Such a result can be achieved by using force feedback systems, in which the force applied to patient's tissue is fed back to a robotic device (haptic master) directly operated by the surgeon.

We can categorize surgical robots based on their different roles during surgical treatment [4,5] Passive robots only serve as a tool-holding device once directed to the desired position. Semiactive devices perform the operation under direct human control. Active devices are under computer control and automatically perform certain interventions. Moreover, the surgical robot can have different levels of autonomy. To be specific, systems that are able to perform fully automated procedures are called autonomous. On the other hand, when the surgeon completely controls every single motion of the robot, this is called a tele-operated system or a master-slave system. Medical robotics has found fruitful ground especially in neurosurgical applications, owing to the accuracy required by the high functional density of the central nervous system [6,11,9].

In past decades, several different robotic neurosurgical devices have been created. A comprehensive survey can be found in [4]. In particular, in the 1980s Benabid and colleagues [1,2] experimented with an early precursor to the robot marketed as Neuromate [5] (Renishaw Mayfield, UK). Today's robot projects focus on three major areas of improvement [4]:

- ❖ increasing the overall accuracy of the classical stereotactic systems
- ❖ increasing the added-value of the equipment
- ❖ enhancing the capabilities of the surgeon

The Mechatronics Research Group (composed of researches of the University of Padova, University of Udine and University of Trieste, Italy) [10] with the assistance of the Neurosurgical Department of the University of Florence [11] has developed two master-slave robotic systems for minimally-invasive neurosurgical operations. The first robot (Figure 1), named LANS (Linear Actuator for Neuro Surgery) has been conceived specifically to perform biopsies and neurosurgical interventions by means of a miniaturized x-ray source (the PRS, Photon Radiosurgery System, by Carl Zeiss), whose emitting tip must be placed accurately inside the patient's brain tissues [12,13]. The LANS robotic system is composed of a haptic master module, operated by the surgeon, and a slave mechatronic module moving a PRS probe, or a biopsy needle, along a predefined emission axis in accordance with the master position imposed by the surgeon. In order to orient the LANS along the established emission axis, a NeuroMate robot is employed in a frame-based configuration which ensures the highest possible accuracy. The system has been designed assuming that during the surgical operation only the LANS (which is very accurate, and provides the surgeon with force feedback) is in active mode while the NeuroMate is powered off. This allows overcoming much of the problems associated with the complex nature of this surgical therapy. Moreover, very precise and repeatable movements of the biopsy needle and of the x-ray source can be obtained, thus improving the overall intervention outcomes.

DAANS (Double Action Actuator for NeuroSurgery, [14]) is the second robot (Figure 2) carried out by Mechatronics research group. The aim of the system is to provide another degree of freedom to the PRS source about the emission axis. The system allows extending the therapy with PRS also to irregular shape tumorous lesions, by integrating translation and spin movements of the source.

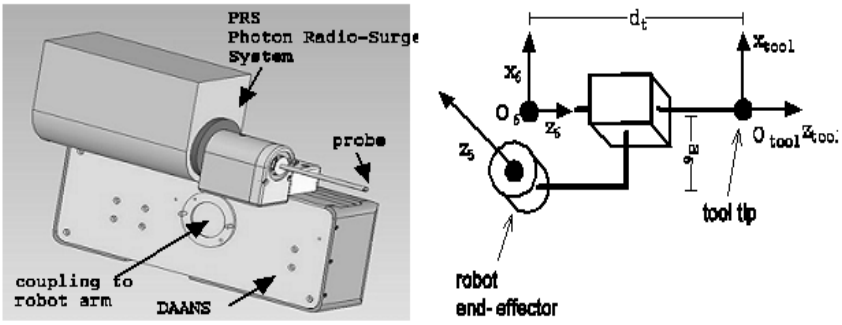

a. b.

Fig. 2 (a) The DAANS actuator and the PRS *x*-ray source
(b) Simplified kinematic structure of the DAANS

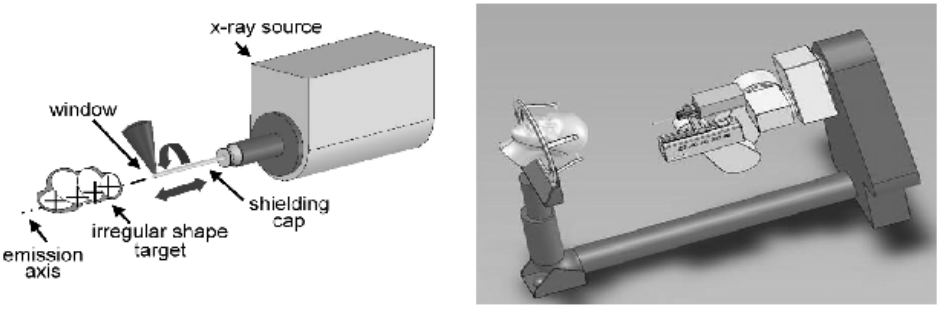

a b

Figure 4: (a) PRS and shielding caps (b) NEUROMATE and DAANS

Indeed, single isocenter radiosurgery procedures produce nearly spherical isodose distributions. In order to avoid unacceptable dose delivery to non target tissues, the high-dose region must be shaped to fit individual targets. The high-dose region can be manipulated into a variety of shapes that closely conform to a tumour shape by means of shielding caps and multiple targets dose delivery.

The caps are placed on the probe of the x-ray source as in Figure 4(a). Nevertheless, LANS and DAANS limit the NeuroMate mobility, owing to their geometrical dimension, which can interfere with the robot arm movements (Figure 4(b)). In this manner the NeuroMate workspace is reduced and some tool configuration are not reachable [12-14].
This paper presents the results of a preliminary analysis on the kinematic structure of a new surgical robot, named NEUMESY. The robot is able to maximize the performances of the therapy by means of the DAANS and PRS, increasing the workspace of the overall robotic system and allowing all possible tool configurations on the patient's head to be reached.

2. THE STUDY

Introducing a robot in an operating room must fulfil some elementary rules. From a kinematics point of view two type of constraints can be taken: medical requirements and robotics requirements [15].

2.1 Medical requirements:

For sterilization reasons no non-medical equipment must be closer than a fixed distance from the operating site. Thus the robot must collide neither with the patient, nor with the medical staff, nor with the surgical tools [15]. The requirement becomes quite complex in the frame-based applications, where the stereotactic frame (the mechanical structure the patient's head is fixed on) interferes with the robot movements. In order to satisfy this requirement, it is useful to define a virtual sphere (Figure 6) including the patient's head and the stereotactic frame. The robot must neither cross nor touch this sphere. The radius of the sphere depends on the stereotactic frame dimensions, while the center is on the patient's head. Moreover, the robot must minimally limit the surgeon's movements during the operation. To this end, the surgeon must be able to choose a suitable robot configuration for each tool position and the robot must adapt its workspace to the surgeon's requirements, which may change during the surgical task.

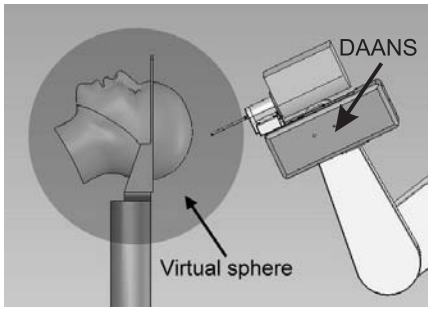

Fig. 6 The virtual sphere includes the patient's head and the stereotactic frame

2.2 Robotics requirements:

The robotics constraints concern the structure of the NEUMESY in order to satisfy the above medical constraints. The preliminary choice considers the robot kinematic structure. The advantages of a serial robot if compared to a parallel one are due to the larger workspace and the higher dexterity and manipulability. On the other hand a parallel manipulator is stiffer allowing higher accuracy in the tool positioning. According to the medical constraints, the robot has to be able to avoid the virtual sphere and it must minimally limit the surgeon's movements. Therefore, the solution adopted consists in a serial structure.

Nevertheless this choice requires a links length optimization so as to maximize both the workspace and the stiffness of the robot.

Moreover, since the neurosurgical tools have usually an axial symmetry, only two spatial points on the patient's head have to be stated by the surgeons. The first one is the Target Point (TP), the center of the cerebral lesion where the tool has to be placed, while the second one, is the Entry Point (EP), the hole through which the surgical instruments go into the skull. EP and TP state the Line of Action (LoA) along which the tools should be moved (Figure 7). Since the surgical operation fixes only five constraints on the space, a five DoF manipulator should be sufficient to a neurosurgical operation, nevertheless, a further DOF yields the kinematic redundancy which allows infinite configuration for the same surgical task, letting the surgeon choose the suitable one.

3. ANALISES, DISCUSIONS, APPROACHES and INTERPRETĂTIONS

3.1 Robot kinematics

The structure of the designed robot and its Denavit-Hartenberg description are displayed in Figure 7 and in Table 1, respectively. The first prismatic joint allows the robot to adapt to the patient's vertical position and change the robot configuration according to the surgeon requirements. The next three revolute joints form a spherical wrist whose position reduces the load and the elastic displacements on the robot links. Finally, two revolute joints allow orienting the end-effector while keeping the robot outside of the virtual sphere.

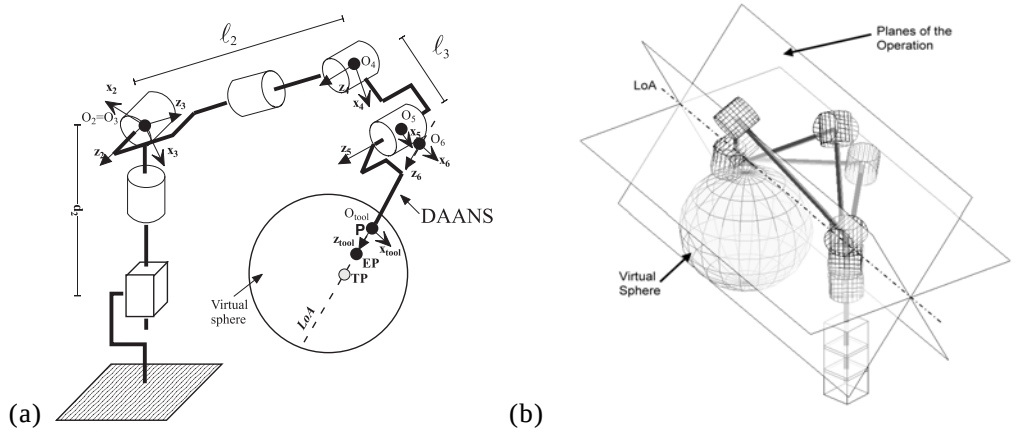

(a) (b)

Fig. 7 (a) The NEUMESY, the DAANS and the virtual sphere (b) Three robot configurations for the same TP and LoA

The robot features six DoFs while the kinematic dimension of the neurosurgical task is five, being given by one point and one direction on the space. Therefore the NEUMESY is kinematically redundant. As stated above, the redundancy can be used by the surgeon to choose a suitable robot configuration which minimally interferes with his movements. Indeed, the origins $O_2 \div O_6$ belong the the same plane on the sheaf (of planes) defined by the LoA. The plane is arbitrary but fixes the robot configuration and the constraints on the surgeon's movements. By choosing a different plane, the space required by the robot for the surgical operation changes and the surgeon's movement could be easier (Figure 8). The solution of the robot inverse kinematic will be presented in the next section

3.2 Solution of the inverse kinematic

For sake of simplicity, let $\mathbf{T}_i$ be the matrix ${}^{i-1}\mathbf{T}_i$, as well as $\mathbf{R}_i = {}^{i-1}\mathbf{R}_i$ the rotation matrix from the frame i to the frame $i-1$ and $\mathbf{p}_i = {}^{i-1}\mathbf{p}_i$ the origin of the frame i referred to the frame $i-1$. The inverse kinematic problem can be expressed as

$$ {}^{0}\mathbf{T}_6 = \breve{\mathbf{T}}\,{}^{6}\mathbf{T}_{tool}^{-1} =: \mathbf{T} = \begin{bmatrix} \mathbf{s} & \mathbf{n} & \mathbf{a} & \mathbf{p} \\ 0 & 0 & 0 & 1 \end{bmatrix} \tag{1} $$

where $\breve{\mathbf{T}} = \begin{bmatrix} \breve{\mathbf{s}} & \breve{\mathbf{n}} & \breve{\mathbf{a}} & \breve{\mathbf{p}} \\ 0 & 0 & 0 & 1 \end{bmatrix}$

Equation (1) can be rearranged as

$$ {}^{2}\mathbf{T}_6 = \mathbf{Q}_1 \tag{2} $$

where: ${}^{2}\mathbf{T}_6 = \mathbf{T}_3\mathbf{T}_4\mathbf{T}_5\mathbf{T}_6$ and $\mathbf{Q}_1 = \left({}^{0}\mathbf{T}_2\right)^{-1}\mathbf{T}$

Table 1 Denavit-Hartenberg parameters of the NEUMESY

i	${}^{i-1}\mathbf{T}_i$	σ_i	α_i	a_i	θ_i	d_i
1	${}^{0}\mathbf{T}_1$	1	0	0	0	q_1
2	${}^{1}\mathbf{T}_2$	0	$\frac{\pi}{2}$	0	q_2	d_2
3	${}^{2}\mathbf{T}_3$	0	$-\frac{\pi}{2}$	0	q_3	0
4	${}^{3}\mathbf{T}_4$	0	$\frac{\pi}{2}$	0	q_4	ℓ_2
5	${}^{4}\mathbf{T}_5$	0	0	ℓ_3	q_5	0
6	${}^{5}\mathbf{T}_6$	0	$\frac{\pi}{2}$	a_6	q_6	0
	${}^{6}\mathbf{T}_{tool}$	1	0	0	0	d_t

Equation (2) can be rewritten as:

$$ \mathbf{T}_3\mathbf{T}_4\mathbf{T}_5\breve{\mathbf{T}}_6 = \left({}^{0}\mathbf{T}_2\right)^{-1}\mathbf{T}\left(\mathbf{A}_6\right)^{-1} \tag{3} $$

Where: $\mathbf{T}_6 = \begin{pmatrix} \mathbf{R}_6 & \mathbf{0} \\ \mathbf{0}^T & 1 \end{pmatrix}$ and $\mathbf{A}_6 = \begin{pmatrix} 1 & 0 & 0 & a_6 \\ 0 & 0 & -1 & 0 \\ 0 & 1 & 0 & 0 \\ 0 & 0 & 0 & 1 \end{pmatrix}$

Comparing to each other the left and the right sides of (3), the following equations must hold:

$$\begin{aligned} \bar{\mathbf{a}} &= \mathbf{R}_3\mathbf{R}_4\mathbf{R}_5\mathbf{R}_6\mathbf{z} \\ \bar{\mathbf{p}} &= \mathbf{R}_3\mathbf{R}_4\mathbf{p}_5 + \mathbf{R}_3\mathbf{p}_4 \end{aligned} \tag{4}$$

where $\bar{\mathbf{a}}$ and $\bar{\mathbf{p}}$ are defined by: $\left({}^0\mathbf{T}_2\right)^{-1}\mathbf{T}\left(\mathbf{A}_6\right)^{-1} = \begin{pmatrix} \bar{\mathbf{s}} & \bar{\mathbf{n}} & \bar{\mathbf{a}} & \bar{\mathbf{p}} \\ 0 & 0 & 0 & 1 \end{pmatrix}$

and $\mathbf{z} = [0, 0, 1]^T$. Equations (4) can be further transformed into:

$$\begin{aligned} \mathbf{R}_4^{-1}\mathbf{R}_3^{-1}\bar{\mathbf{a}} &= \mathbf{R}_5\mathbf{z} \\ \mathbf{R}_4^{-1}\mathbf{R}_3^{-1}\bar{\mathbf{p}} &= \bar{\mathbf{p}}_5 + \mathbf{R}_4^{-1}\bar{\mathbf{p}}_4 \end{aligned} \tag{5}$$

After multiplying left and right sides to each other of the equations (5), it is possible to write:

$$\bar{\mathbf{p}}\cdot\bar{\mathbf{a}} = \bar{\mathbf{p}}_5\cdot\left(\mathbf{R}_5\mathbf{z}\right) + \left(\mathbf{R}_4^{-1}\bar{\mathbf{p}}_2\right)\cdot\left(\mathbf{R}_5\mathbf{z}\right) \tag{6}$$

where the right side of (6) is zero, since the vectors therein involved are orthogonal. Therefore from (6) the value of the q_1 can be determined, since the projection of $\bar{\mathbf{p}}$ into $\bar{\mathbf{a}}$ depends only on this joint variable. In particular: $q_1 = -\dfrac{d_t\breve{\mathbf{a}}\cdot\breve{\mathbf{n}} + a_6\breve{\mathbf{s}}\cdot\breve{\mathbf{n}} - \breve{\mathbf{p}}\cdot\breve{\mathbf{n}}}{\breve{n}_z} - d_2$ q. When $\breve{n}_z = 0$ the z_0-axis belongs to the operation plane. In this case, if the target point belongs to robot workspace, there are infinite solutions for q_1. Taking into account the module of $\bar{\mathbf{p}}$, there is:

$$\bar{\mathbf{p}}\cdot\bar{\mathbf{p}} = \mathbf{p}_4\cdot\mathbf{p}_4 + \mathbf{p}_5\cdot\mathbf{p}_5 + 2\left(\mathbf{R}_4\mathbf{p}_5\right)\cdot\mathbf{p}_4 \tag{7}$$

the left side of (7) being noted, since the module of $\bar{\mathbf{p}}$ depends only on joint variable q_1. In this way the value of q_5 can be determined from (7):

$$\sin q_5 = \frac{\bar{\mathbf{p}}\cdot\bar{\mathbf{p}} - \ell_2^2 - \ell_3^2}{2\ell_2\ell_3} \tag{8}$$

The equation (1) can be rearranged as ${}^1\mathbf{T}_5 = \mathbf{Q}_2$, where ${}^1\mathbf{T}_5 = \mathbf{T}_2\mathbf{T}_3\mathbf{T}_4\mathbf{T}_5$ and $\mathbf{Q}_2 = \mathbf{T}_1^{-1}\,\mathbf{T}\,\mathbf{T}_6^{-1}$. Considering the new vectors:

$$\begin{aligned} \tilde{\mathbf{s}} &= \mathbf{R}_2\mathbf{R}_3\mathbf{R}_4\mathbf{R}_5\mathbf{x} \\ \tilde{\mathbf{p}} &= \mathbf{R}_2\mathbf{R}_3\mathbf{R}_4\mathbf{p}_4 + \mathbf{R}_2\mathbf{R}_3\mathbf{p}_4 + \mathbf{p}_2 \end{aligned} \tag{9}$$

where $\tilde{\mathbf{a}}$ and $\tilde{\mathbf{p}}$ are defined by: $\mathbf{T}_1^{-1}\mathbf{T}\mathbf{T}_6^{-1} = \begin{pmatrix} \tilde{\mathbf{s}} & \tilde{\mathbf{n}} & \tilde{\mathbf{a}} & \tilde{\mathbf{p}} \\ 0 & 0 & 0 & 1 \end{pmatrix}$ and $\mathbf{x} = [1, 0, 0]^T$, rearranging (9) as

$$\left(\mathbf{R}_2\mathbf{R}_3\right)^{-1}\tilde{\mathbf{s}} = \mathbf{R}_4\mathbf{R}_5\mathbf{x}$$

$$\left(\mathbf{R}_2\mathbf{R}_3\right)^{-1}\left(\tilde{\mathbf{p}} - \mathbf{p}_2\right) = \mathbf{R}_4\mathbf{p}_5 + \mathbf{p}_4$$

and operating as in (5) it is possible to write:

$$\left(\tilde{\mathbf{p}} - \mathbf{p}_2\right)\cdot\tilde{\mathbf{s}} = \mathbf{p}_5\cdot\left(\mathbf{R}_5\mathbf{x}\right) + \left(\mathbf{R}_4^{-1}\mathbf{p}_4\right)\cdot\left(\mathbf{R}_5\mathbf{x}\right) \tag{10}$$

The left side of (10) depends only on joint variable q_6, while the right side is known, once q_1 and q_5 have been calculated. In this way (10) can be expressed in the form: $\mathrm{A}c_6 + \mathrm{B}s_6 = \mathrm{C}$,

where $A = a_6\breve{\mathbf{s}}\cdot\breve{\mathbf{s}} + d_t\breve{\mathbf{s}}\cdot\breve{\mathbf{a}} - \breve{\mathbf{s}}\cdot\breve{\mathbf{p}} + \breve{s}_z q_1$

$B = a_6\breve{\mathbf{s}}\cdot\breve{\mathbf{a}} + d_t\breve{\mathbf{s}}\cdot\breve{\mathbf{s}} - \breve{\mathbf{s}}\cdot\breve{\mathbf{p}} - \breve{a}_z q_1$

$C = -(\ell_3 + \ell_2 s_5)$

The solutions are: $q_6 = \text{atan2}(\pm\sqrt{A^2+B^2-C^2}, C) - \text{atan2}(B, A)$.

Equation (1) can be rearranged as: ${}^1\breve{\mathbf{T}}_5 = \mathbf{Q}_3$

where ${}^1\breve{\mathbf{T}}_5 = \mathbf{T}_2\mathbf{T}_3\mathbf{T}_4\breve{\mathbf{T}}_5$, $\mathbf{Q}_3 = \mathbf{T}_1^{-1}\,\mathbf{T}\,\mathbf{T}_6^{-1}\,\mathbf{A}_5^{-1}$, $\breve{\mathbf{T}}_5 = \begin{pmatrix}\mathbf{R}_5 & \mathbf{0}\\ \mathbf{0}^T & 1\end{pmatrix}$ *and* $\mathbf{A}_5 = \begin{pmatrix}\mathbf{I}_3 & \begin{matrix}\ell_3\\0\\0\end{matrix}\\ \mathbf{0}^T & 1\end{pmatrix}$

Considering the vectors:

$$\begin{aligned}\hat{\mathbf{a}} &= \mathbf{R}_2\mathbf{R}_3\mathbf{R}_4\mathbf{R}_5\mathbf{z}\\ \hat{\mathbf{p}} &= \mathbf{R}_2\mathbf{R}_3\mathbf{p}_4 + \mathbf{p}_2\end{aligned} \tag{11}$$

where $\hat{\mathbf{a}}$ and $\hat{\mathbf{p}}$ are defined by $\mathbf{Q}_3 = \begin{pmatrix}\hat{\mathbf{s}} & \hat{\mathbf{n}} & \hat{\mathbf{a}} & \hat{\mathbf{p}}\\ 0 & 0 & 0 & 1\end{pmatrix}$ and rearranging as above, it is possible to write:

$$\mathbf{R}_2^{-1}\hat{\mathbf{a}} = \mathbf{R}_3\mathbf{R}_4\mathbf{R}_5\mathbf{z} \tag{12}$$

$$\mathbf{R}_2^{-1}\left(\hat{\mathbf{p}} - \mathbf{p}_2\right) = \mathbf{R}_3\mathbf{p}_4 \tag{13}$$

From the projection of the equation (13) along $\mathbf{y} = [0, 1, 0]^T$, the value of c_3 can be determined as $c_3 = \dfrac{-d_2 + \hat{p}_z}{\ell_2}$ where $\hat{p}_z = (-\breve{a}_z)d_t + \breve{p}_z - q_1 - \breve{a}_z\ell_3 s_6 - a_6\breve{s}_z - c_6\ell_3\breve{s}_z$ while from the projection of the equation (13) along **z**, it is possible to write $\hat{p}_y c_2 = \hat{p}_x s_2$ where

$$\hat{p}_x = \breve{p}_x - \breve{a}_x(d_t + \ell_3 s_6) - (a_6 + c_6\ell_3)\breve{s}_x$$
$$\hat{p}_y = \breve{p}_y - \breve{a}_y(d_t + \ell_3 s_6) - (a_6 + c_6\ell_3)\breve{s}_y$$

In this way: $q_2 = \text{atan2}(\hat{p}_x, \hat{p}_y) + k\pi$ with $k = 0,1$

Finally, projecting (12) along **z**, the value of c_4 is determined as: $c_4 = \hat{a}_x s_2 - \hat{a}_y c_2$, where $\hat{a}_x = \breve{n}_x$ and $\hat{a}_y = \breve{n}_y$. Therefore: $q_4 = \text{atan2}(c_4, \pm\sqrt{1-c_4^2})$. There are four solutions for each pose defined by the matrix $\breve{T}$, which mainly differ to each other on the elbow configuration. During the surgical operation only the DAANS is in active mode while the NEUMESY is powered off. Therefore the requirement on the accuracy on the tool positioning concerns only the robot in the static configuration. At the same time, for safety reasons, the contacts between the robot and the virtual sphere have to be avoided.

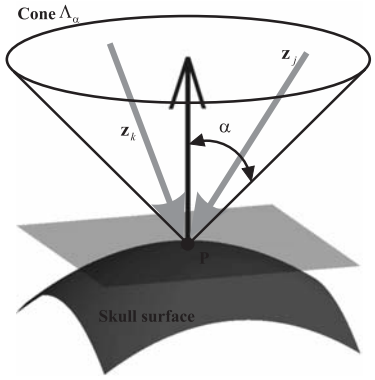

Figure 9. Cone Λ_α

The link lengths affect both the accuracy and the robot workspace owing to the NEUMESY kinematic structure and have to be appropriately chosen in order to satisfy the requirements stated above. The requirement on the robot workspace can be described by a reachabilty index which gives information about the number of points on the patient's skull being achievable along each desired tool configuration.

Let the skull surface S be discretized into N points $\mathbf{P}_i$ and the desired tool orientations at $\mathbf{P}_i$ be described by all the vectors $\mathbf{z}_k$ internal to the cone $\Lambda_\alpha(\mathbf{P}_i)$ with vertex at $\mathbf{P}_i$, angle α and axis coincident with the normal to the skull surface in $\mathbf{P}_i$ (Figure 9). Moreover, let the function $\text{IK}(\mathbf{P}, \mathbf{z})$ calculate the number of solutions for the inverse kinematic problem:

$$\begin{cases}\mathbf{P}_{tool} = \mathbf{P}\\ \mathbf{z}_{tool} = \mathbf{z}\end{cases}$$

subject to the constraint that all the robot links are external to the virtual sphere. The reachabilty index can be defined as:

$$\Phi_{\ell_2,\ell_3} = \frac{1}{N}\sum_{i=1}^{N}\Theta_\alpha(\mathbf{P}_i), \quad \mathbf{P}_i \in \mathrm{S}$$

where the function Θ_α returns 1 if, for each vector $\mathbf{z}_k$ belonging to the cone $\Lambda_\alpha(\mathbf{P}_i)$, the function $\mathrm{IK}(\mathbf{P},\mathbf{z})$ is nonzero. The function Θ_α returns 0 otherwise. The index Φ_{ℓ_2,ℓ_3} achieves the maximum (i.e. 1) when every point $\mathbf{P}_i \in \mathrm{S}$ is reachable along any direction internal to its cone $\Lambda_\alpha(\mathbf{P}_i)$.

Table 2 Parameters employed in the optimization problem

Parameter	Value
d_2	450 mm
a_6	55 mm
d_t	100 mm
q_1	$\in [0\ , 1200\ \mathrm{mm}]$
$q_i, i = 2..6$	$\in [-170°, +170°]$
α	$\frac{7}{18}\pi$
R	250 mm
$\mathbf{C}$	$[500\ \mathrm{mm},\ 0,\ 800\ \mathrm{mm}]^T$

In order to maximize the robot workspace, the skull surface is taken coincident with the virtual sphere. Therefore the generic point can be described as $\mathbf{P}_i = R\left[\cos\varphi_i\cos\theta_i, \cos\varphi_i\sin\theta_i, \sin\varphi_i\right]^T$ where R is the radius of the virtual sphere and φ_i and θ_i are the polar angles of the point. The angle α is chosen coherently with the tool orientation allowed during a neurosurgical task. A suitable value is $\alpha = 70^\circ$.

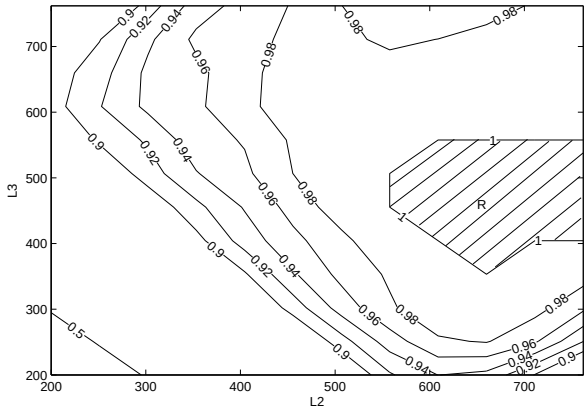

Figure 10: Level curves of Φ_{ℓ_2,ℓ_3} when the robot parameters of Table 2 are assumed

Figure 10 shows the level curves for Φ_{ℓ_2,ℓ_3} as a function of the link lengths l_2 and l_3 for the robot parameters in Table 2. It can be noticed that the index value is maximum inside the region R, while outside of this region $\Phi_{\ell_2,\ell_3} < 1$, which means that some tool configurations are not reachable by the robot.

Since both the index Φ_{ℓ_2,ℓ_3} and the arm stiffness depend on the link lengths, a suitable optimization problem must be defined so as to maximize the robot workspace while keeping the position errors, due to the links deformations, to a minimum.
The optimization problem can be stated as:

$$\max_{\ell_2,\ell_3>0} \quad \frac{1}{\left(\ell_2+\ell_3\right)^3}$$

$$\text{s.t.} \quad \Phi_{\ell_2,\ell_3}=1$$

$$\mathbf{P}\in \mathrm{S}\,\% \qquad \ell_2,\ell_3>0$$

where the cube at the denominator of the objective function takes into account the fact that the link stiffness at the end point is inversely proportional to the cube of link length. With reference to the values of Table 2, the maximum is reached at $\ell_2 = 660\ mm$ and $\ell_3 = 355\ mm$.

In order to highlight the performances of the NEUMESY for the chosen l_2 and l_3 values, let the function Θ_α be modified in $\bar{\Theta}_\alpha\left(\mathbf{P}_i\right)$, so that it returns not only a boolean value (0 or 1) but the mean number of solutions for each tool configuration defined by $\mathbf{P}_i \in \mathrm{S}$ and $\mathbf{z}_k \in \Lambda_\alpha(\mathbf{P}_i)$:

$$\bar{\Theta}_\alpha\left(\mathbf{P}_i\right)=\frac{1}{M}\sum_{\substack{\mathbf{z}_k\in\Lambda_\alpha(\mathbf{P}_i)\\ k=1..M}} \mathrm{IK}\left(\mathbf{P}_i,\mathbf{z}_k\right)$$

Figure 11 shows the $\bar{\Theta}_\alpha\left(\mathbf{P}_i\right)$ function for the values in Table 2. It can be noticed that there are on average more than ten admissible solutions for each tool configuration.

In order to have a clearer idea of the robot performances, it is convenient to give a spatial representation of the $\bar{\Theta}_\alpha\left(\mathbf{P}_i\right)$ index, by introducing a suitable surface $\mathrm{S}_{\bar{\Theta}_\alpha}$ defined as:

$$\mathrm{S}_{\bar{\Theta}_\alpha}=\{\mathbf{x}\in\mathbb{R}^3 \mid \mathbf{x}=\frac{1}{R}\bar{\Theta}_\alpha(\mathbf{P})\,\mathbf{P},\quad \mathbf{P}\in\mathrm{S}\}$$

where R is the radius of S.

Figure 12 shows the projections of the $\mathrm{S}_{\bar{\Theta}_\alpha}$ on the three principal planes. It can be noticed that the highest performances are achieved on the lateral sides of the virtual sphere, where there is the largest number of configurations allowing the robot to avoid the virtual sphere

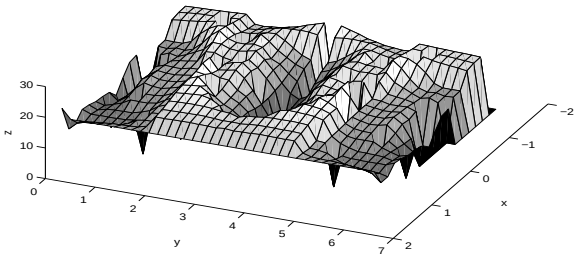

Figure 11: Performance index $\bar{\Theta}_\alpha\left(\mathbf{P}_i\right)$}

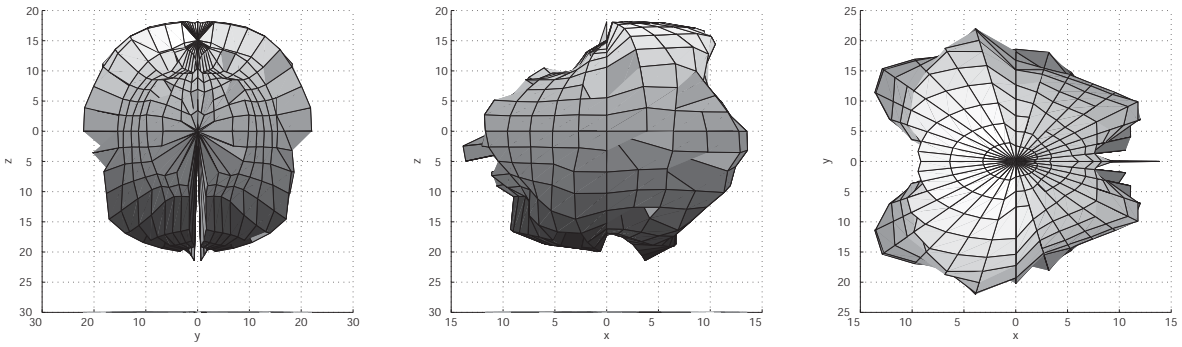

Figure 12: Projections of $\mathrm{S}_{\bar{\Theta}_\alpha}$ on the cartesian planes

4. CONCLUSION

In this paper a new robot for neurosurgery is presented. The robot, named NEUMESY, is a six joints serial manipulator designed as positioning device for a neurosurgical actuator previously built by our research group, able to move a low energy x-ray source for the treatment of cerebral lesions. The redundancy respect to the surgical task (5 DoFs, being given by one point and one direction on the space) gives an extra DoF allowing the surgeon to choose the suitable robot configuration which reduces the space required by the robot and maximizes the safety, keeping the robot links away from the patient's head.

The solution of the non-trivial inverse kinematic problem is produced and a kinematic simulator has been carried out in order to analyze the performances of the robot.

Finally, the links length has been optimized in order to satisfy the workspace requirements fixed by the neurosurgical task and reduce the static deformations of the robot arm.

Future works consist in the study of the trajectory planning using the benefits taken by the redundancy so as to limit the link vibrations and deformations during the surgical task.

REFERENCES

[1] Benabid AL, Cinquin P, Lavalle S, Le Bas JF, Demongeot J, de Rougemont J. Computer-driven robot for stereotactic surgery connected to CT scan and magnetic resonance imaging. Technological design and preliminary results. Appl Neurophysiol 1987;50:153-154.

[2] Benabid AL, Lavallee S, Hoffmann D, Demongeot J, Danel F. Potential use of robots in endoscopic neurosurgery. Acta Neurochir Suppl (Wien) 1992;54:93-97

[3] Faust R.A. Robotics in Surgery: History, Current and Future Applications. Nova Science Publishers, New York, 2007

[4] Haidegger T., L. Kovacs, G Fordos, Z. Benyo, P. Kazanzides. Future Trends in Robotic Neurosurgery. Proc. of 14th Nordic-Baltic Conf. on Biomedical Engineering and Medical Physics, 2008

[5] Haidegger, T. Tian Xia Kazanzides, P. Accuracy improvement of a neurosurgical robot system In Proc. Of BioRob 2008. 2nd IEEE RAS and EMBS Int. Conf. on Biomedical Robotics and Biomechatronics, 19-22 Oct. 2008, 836-841

[6] Kwoh Y.S., J. Hou, E.A. Jonckheere and S. Hayati A previous termrobotnext term with improved absolute positioning accuracy for CT guided stereotactic brain previous termsurgery. IEEE Trans Biomed Eng 35 (1988), pp. 153-160.

[8] McBeth P, Deon F. Louw M.D., Peter R. Rizun B.A.Sc.a and Garnette R. Sutherland M.D. Contact Information Robotics in neurosurgery. The American Journal of Surgery, Volume 188, Issue 4, Supplement 1, October 2004, Pages 68-75

[8] Nathoo N., Cavusoglu MC, Vogelbaum MA, Barnett GH. In touch with robotics: neurosurgery for the future. Neurosurgery. 2005 Mar;56(3):421-33

[9] Zamorano L, Li Q, Jain S, Kaur G. Robotics in neurosurgery: state of the art and future technological challenges. Int J Med Robot. 2004 Jun;1(1):7-22.

[10] http://www.mechatronics.it

[11] http://www.neurochirurgiafirenze.it

[12] G. Rosati, A. Rossi, and V. Zanotto Lans: a haptic system for minimally invasive radio-surgery *International Journal of Mechanics and Control*, 4(2):45U50, 2003

[13] A. Rossi, A. Trevisani, and V. Zanotto A telerobotic haptic system for minimally invasive stereotactic neurosurgery *Int. J. Medical Robotics and Computer Assisted Surgery*, Robotic Publications Ltd.,1(2):64-75, 2005

[14] A.Rossi, A.Gasparetto, A.Trevisani, and V.Zanotto A robotic approach to stereotacticradio-surgery Proc. Of the 7th Biennial *ASME Conference Engineering Systems Design and Analysis*, Manchester, UK, 19-22 July, 2004.

[15] Duchemin, G. Poignet, P. Dombre, E. Peirrot, F. LIRMM SCALPP: A 6-. dof robot with a non-spherical wrist for surgical applications *Advances in Robot Kinematics*, Kluwer Academic Publisher, 2000, 165-174

INTERNATIONAL SYMPOSIUM on
ADVANCED ENGINEERING & APPLIED MANAGEMENT
– 40th ANNIVERSARY in HIGHER EDUCATION (1970-2010)
4 – 5 November, 2010, Hunedoara, ROMANIA

[1.] Přemysl MATOUŠEK

ADAPTIVE CONTROL OF PNEUMATIC SERVOMECHANISM

[1.] TECHNICAL UNIVERSITY OF LIBEREC, FACULTY OF MECHANICAL ENGINEERING,
DEPARTMENT OF APPLIED CYBERNETICS, LIBEREC, CZECH REPUBLIC

ABSTRACT:
The pneumatic positional servomechanism is highly non - linear system and that is why its identification and control is more exacting than at hydraulic or electric servomechanisms. To be able to reach a better control process it is not enough only to identify the system and than set the parameters of the controller but the system also has to be identified continuously and simultaneously with the identification of the parameters of the controller which have to be re - set depending on the achieved mathematical model. This article briefly describes the two main parts that constitute an adaptive control. The first part describes a design of an optimal structure of mathematical model that allows the continuous identification. The second part describes a design of an adaptive space-state controller whereby the adaptive control is implemented.

KEYWORDS:
pneumatic system; identification; model; state – space

1. INTRODUCTION

The pneumatic servomechanism is a non - linear and integral system. The air is a gas characterized by its compressibility, concurrently the passive resistances arise during the motion of the piston, and these resistances cause the non - linearity. This is why it is not effective to take several measurements, identify the system and set the parameters of the controller on the basis of the resultant mathematical model, because at each motion of the piston we get different parameters of the mathematical model. And the controller adjusted to a concrete mathematical model would not control exactly. Thus the system has to be identified continuously to get the most accurate mathematical model that is corresponding to the given state of the system. At the same time it is necessary to re - set the parameters of the controller, depending on the achieved mathematical model. The pneumatic system and the wiring of the components is shown in figure 1.

2. PNEUMATIC SYSTEM

Pneumatic positional servomechanism consists of the cylinder with one - side piston rod with maximal stroke 960mm, proportional directional valve MPYE–5–1/8–HF–010-B, proportional pressure regulator VPPM–6L–L–1-618-0L10H-A4P-S1C1 and pressure regulator HEE-D-MINI-24 with the filter LF-D-5M-MINI. The position of the piston rod is measured by means the linear displacement encoder with the 1000mm measurement length.

The feeding is realized by the power supply 24V/2A. This voltage serves for feeding the pressure regulator, proportional pressure regulator and proportional directional valve and it is also regulated to 10V voltage, by which the linear displacement encoder is supplied. This displacement encoder is connected with the piston of the pneumatic drive. The voltage on the slider appropriate to the position of the piston is applied to connector block SCB - 68 of the data acquisition card, its analog inputs and outputs are from the range of 0 - 10V.

The air from the compressor is brought to the input of the pressure regulator, through which the air supply to the whole system is switched on or off. The pressure regulator is switched on by the 24V and to be able to switch it on by the digital output of the data acquisition card (5V), the

signal convert from 5V to 24V has to be ensured. This convert is ensured by the switching transistor.

Constant pressure in the system is ensured by means of proportional pressure regulator. This regulator is controlled by the 0 - 10V voltage, where 1V equals to 1bar. As the analog output of the data acquisition card is in the range of 0 - 10V, the proportional pressure regulator is controlled straight by the means of output voltage of the card. This is how the air regulation to the required constant pressure is ensured.

When the air pressure is set to the required value, the air is brought to the input of the proportional directional valve. The motion of the slide valve is also controlled by the 0 - 10V voltage because the proportional directional valve is connected in the same way as the proportional pressure regulator. The system further contains of two DMP 331 pressure sensors that measure the running pressure over and below the piston and they also generate the flow signal in the range of 4 – 20mA. To be able to connect the sensors to the data acquisition card two I/U converters are used. They bring the current signal to 0 – 10V voltage.

The data acquisition card is a part of the control system PXI - 1042Q and an external connector block SCB - 68 is attached to it. PXI system communicates with the PC by means of Ethernet interface and LabView software is used to the control of the system. Simplified electrical scheme is shown in the figure 2.

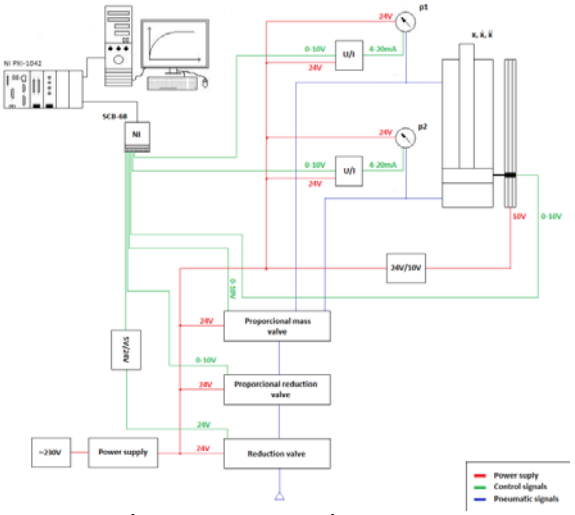

Figure 1: Pneumatic system

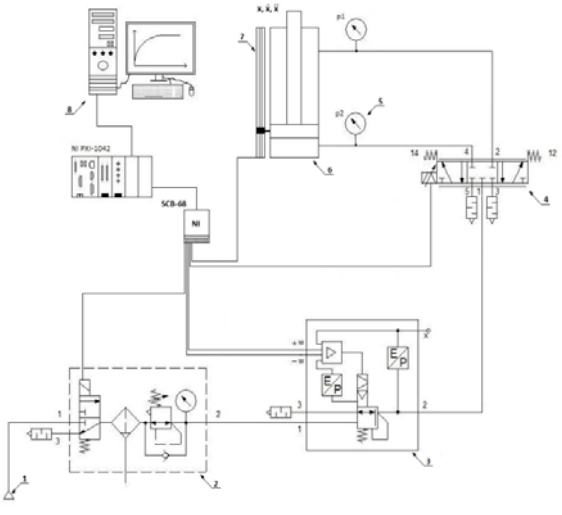

Figure 2: Simplified circuit

(1 – compressor, 2 – pressure regulator, 3 – proportional pressure regulator, 4 – proportional directional valve, 5 – pressure sensors, 6 - cylinder with one - sided piston rod, 7 - linear displacement encoder, 6 – control system)

3. IDENTIFICATION OF PNEUMATIC SYSTEM

To be able to realize the online identification of the pneumatic positional servomechanism, it is necessary to determine the order of the numerator and denominator of the system transfer. The system transfer was set by jumps in voltage excitation of various voltages, when the response of the system was recorded into the folder and was later identified in Matlab programme according to the quadratic criterion:

$$I_2 = \int [y(t) - y_m(t)]^2 = \sum_0^n (y(t) - y_m(t))^2 \qquad (1)$$

where $y(t)$ is the output of the system, $y_m(t)$ is the response of the model of the system.

The identification was realized with different structures of the model, when the most accurate transfer was achieved with the structures of the model in form:

$$G_1(s) = \frac{b_0}{a_2 s^2 + a_1 s}, G_2(s) = \frac{b_1 s + b_0}{a_3 s^3 + a_2 s^2 + a_1 s}, G_3(s) = \frac{b_2 s + b_0}{a_4 s^4 + a_3 s^3 + a_2 s^2 + a_1 s} \qquad (2, 3, 4)$$

where $a_4 - a_1$ are the coefficients of the numerator of the system transfer, $b_2 - b_0$ are the coefficients of the denominator of the system transfer.

In figure 3 there is the response of the pneumatic system for pressures of 3, 4 and 5 bars with the step change U = 4,6V voltage on the proportional directional valve and then in the figure 4 there is the progress of the system response $y_m(t)$ and the comparison of the mathematical models $G_1(s)$, $G_2(s)$ *and* $G_3(s)$ for pressure of 4 bar at this jump.

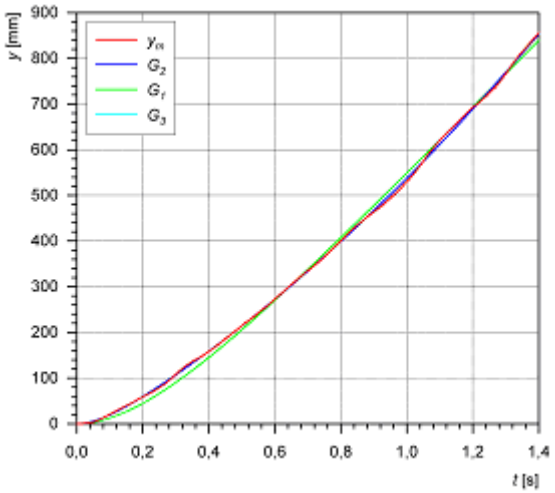

Figure 3: Response of the pneumatic system at 3, 4 and 5 bar pressures

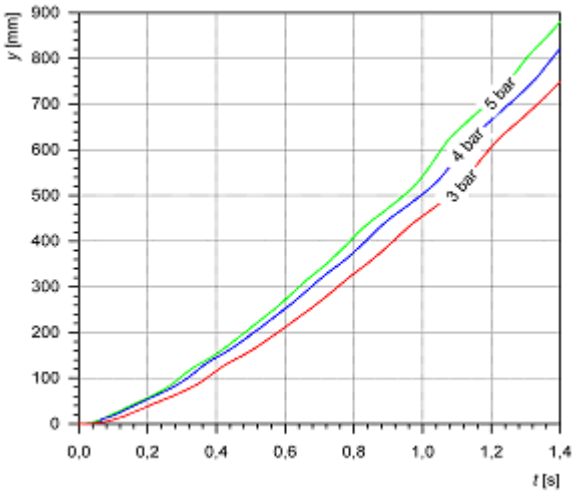

Figure 4: Comparison of the models $G_1(s)$, $G_2(s)$, $G_3(s)$

In the figure 4 there is noticeable that the differences among the models $G_1(s)$, $G_2(s)$, $G_3(s)$of the pneumatic system are minimal, but on the more detailed investigation it is clear that the transfer $G_2(s)$ reaches the most accurate reset and this is why it was finally chosen for the online identification of the system. It is needful to convert this transfer from the continuous to the discreet area to be able to realize the project of model structure, the convert from continuous to the discreet area was implemented by the Matlab software.

The model for online identification was chosen from three kinds, model ARX, ARMAX and Box - Jenkins. Model Box - Jenkins cannot be used for this identification, because its error differs from an order over against ARX and ARMAX models. The structure of ARX and ARMAX models results from the structure of discreet transfer that was achieved by the convert of the continuous model to the discreet model. Structure ARX model is used in [3 3 1] form, structure of ARMAX model in [3 1 3 1] form, where the difference equations are set by equation 5 and 6. The difference between the error of the ARX and ARMAX models during the identification of the system is nearly insignificant and it is shown in the figure 6. Finally, the ARX model was chosen for the online identification.

The signal from the linear displacement encoder is filtered, because it is extensively noisy. Kalman filter with the polynomials degree of 3 and number of samples 8 is used for the filtration. The comparison of the progress of the output signal ARX model with the structure that is defined by equation 6 and a measured signal $y_m(t)$ is shown in the figure 5.

$$(1 + a_1 z^{-1} + a_2 z^{-2} + a_3 z^{-3}) y(k) = (b_1 z^{-1} + b_2 z^{-2} + b_3 z^{-3}) u(k) + e(k) \quad (4)$$

$$(1 + a_1 z^{-1} + a_2 z^{-2} + a_3 z^{-3}) y(k) = (b_1 z^{-1} + b_2 z^{-2} + b_3 z^{-3}) u(k) + (1 + c_1 z^{-1}) e(k) \quad (5)$$

where $a_3 - a_1$, $b_3 - b_1$, c_1 are coefficients of the difference equations of ARX and ARMAX models, $u(k)$ is exciting signal, $y(k)$ the output of the model and $e(k)$ the error of the model.

In the figure 5 it is obvious, that the response of the pneumatic system $y_m(t)$ is nearly identical with the output of the ARX model and the error arised during the identification reaches at most 3,7mm and so it can be neglected during the next calculations.

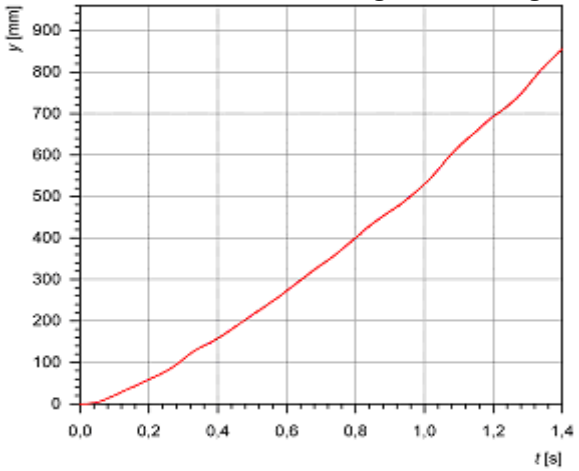

Figure 5: Identification of the system by ARX model

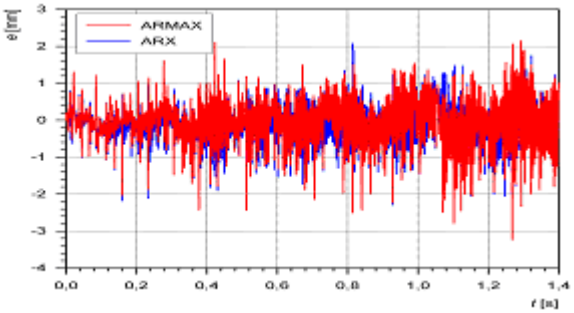

Figure 6: Difference of ARX and ARMAX models

4. STATE DESCRIPTIONS

The pneumatic system is regulated by the adaptive LQ controller, hence the discreet transfer of the ARX model has to be converted to state - space form (7). This conversion resides is based on the compilation of the state matrixes, when the observable canonical form was chosen for the state description. This canonical form reconstructs the response of the pneumatic system $y_m(k)$. The state vector consists of three state variables $x_1(k)$, $x_2(k)$, $x_3(k)$.

$$G(z) = \frac{b_4 z + b_0}{a_4 z^4 + a_3 z^3 + a_2 z^2 + a_1 z} \quad \rightarrow \quad \begin{matrix} x(k+1) = Mx(k) + Nu(k) \\ y(k) = Cx(k) + Du(k) \end{matrix} \qquad (6, 7)$$

where $x(k)$ is the state vector [n, l], $u(k)$ is the input vector [p, l], $y(k)$ is the output vector , M is the state matrix [n,n], N is the input matrix [n, p], C is the output matrix [l, n], D is the feedforward matrix [l, l].

4.1 REDUCED ORDER OBSERVER

The state vector consists of three variables where the first one is the measured response of the pneumatic system $y_m(k)$. The response of this system (position of the piston rod of the pneumatic cylinder) is measured by the linear displacement encoder and so it is not necessary to observe the variable $x_1(k)$ of the state vector. The two rest variables $x_2(k)$, $x_3(k)$ of the state vector are observed (8, 9). Not a full – state observer but the reduced order observer (designed by *D.G. Luenberger*) is used for the observation of the state vector.

$$\begin{bmatrix} x_1(k+1) \\ x_2(k+1) \\ x_3(k+1) \end{bmatrix} = \begin{bmatrix} y_m(k+1) \\ x_{E1}(k+1) \\ x_{E2}(k+1) \end{bmatrix} = \begin{bmatrix} M_{11} & M_{12} & M_{13} \\ M_{21} & M_{22} & M_{23} \\ M_{31} & M_{32} & M_{33} \end{bmatrix} \begin{bmatrix} y_m(k) \\ x_{E1}(k) \\ x_{E2}(k) \end{bmatrix} + \begin{bmatrix} N_1 \\ N_2 \\ N_3 \end{bmatrix} u(k) \qquad (8)$$

$$y(k) = [C_1 \quad C_2 \quad C_3] \begin{bmatrix} y_m(k) \\ x_{E1}(k) \\ x_{E2}(k) \end{bmatrix} + Du(k) \qquad (9)$$

During the project of the observer it is necessary to select the eigenvalues so that the error of the observe converges to zero. The dynamic qualities of the error of the observe are given by the eigenvalues $\lambda_{1,2}$, that's why the eigenvalues of the designed observer are zero. The observer was designed on the basis of equations 10, 11, 12, 13, 14 where $x_E(k)$ is the estimate $\hat{x}_E(k)$.

$$\overline{\hat{x}_E}(k+1) = M_E \overline{\hat{x}_E}(k) + H_E y_m(k) + N_E u(k) \qquad (10)$$

$$\hat{x}_E(k) = \overline{\hat{x}_E}(k) + Q y_m(k) \qquad (11)$$

$$M_E = F - QG \qquad (12)$$

$$H_E = H \quad QM_{11} \quad Q = G = Q \quad FG \qquad (13)$$

$$N_E = K - QN_{11} \qquad (14)$$

where $H = \begin{bmatrix} M_{21} \\ M_{31} \end{bmatrix}, K = \begin{bmatrix} N_{21} \\ N_{31} \end{bmatrix}, F = \begin{bmatrix} M_{22} & M_{23} \\ M_{32} & M_{33} \end{bmatrix}, G = [M_{12} \quad M_{13}]$.

The process of the state vector of the designed observer at jump in voltage U = 4,6V on the proportional directional valve is shown in the figure 7.

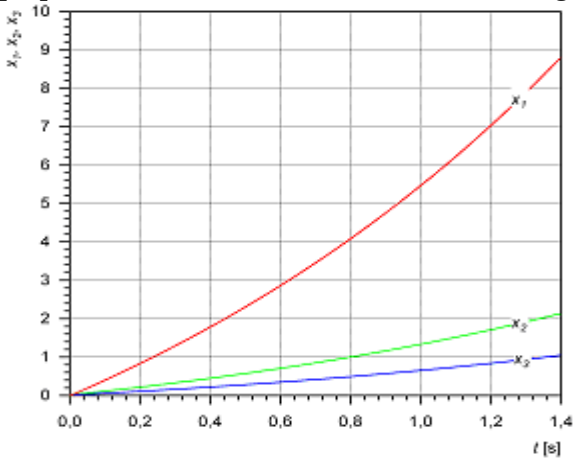

Figure 7: Simulation of the process of the state vector

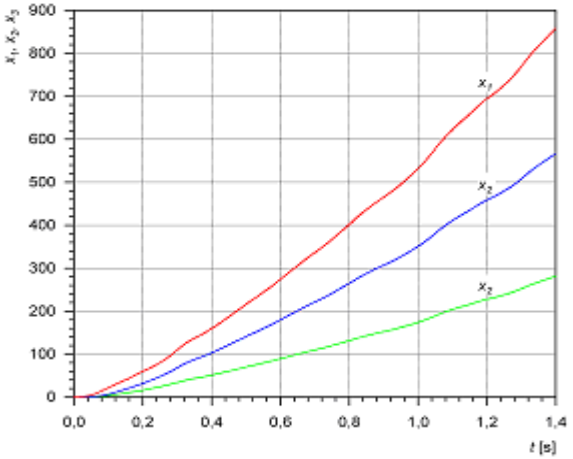

Figure 8: Real process of the state vector

In the figure 8 we can see the real process of the state vector of the designed observer. The calculation of the observer comes from the online identification of the pneumatic system by the ARX model. In each period of sampling we obtain new coefficients of the convert of the system. These coefficients are used for the construction of the new state matrixes that are necessary for the calculation of the state vector.

4.2 LQ CONTROLLER

The regulation of the piston position of the pneumatic system in the state space is implemented by means of LQ controller that is quadratically optimal for the linear systems. The controller minimizes the quadratic criterion for the discrete systems in the equation:

$$J(u(k)) = \sum_{k=1}^{N-1}(x^T(k)Qx(k) + u^T(k)Ru(k)) + x^T(N)Px(N) \quad (15)$$

where Q is a positive - definite Hermitian or real symmetric matrix, R is a positive - definite or real symmetric matrix.

For the calculation of LQ controller that regulates the position of the piston we used simplified quadratic criterion in this equation:

$$J(u(k)) = \sum_{k=1}^{N}(x^T(k)Qx(k) + u^T(k)Ru(k)) \quad (16)$$

where Q is a positive - semidefinite Hermitian or real symmetric matrix, R is a positive - semidefinite or real symmetric matrix.

The calculation of LQ controller comes from Riccati equation, when the condition of matrixes convergence $V = V(k) = V(k + 1)$ is kept:

$$V = Q + M^T VM - M^T VN(R + N^T SN)^{-1}N^T VM \quad (17)$$

and the resultant increase of the feedback of the state LQ controller is defined by this relation:

$$K = [R + N^T VN]^{-1}N^T VM \quad (18)$$

Our LQ controller should also equalize the influence of the constant failure and should follow the jump in voltage of the control quantity, so it is necessary to place a digital adder into the circuit. This adder increases the order of the system and the equation 8, 9 changes to form:

$$\begin{bmatrix} x(k+1) \\ x_4(k+1) \end{bmatrix} = \begin{bmatrix} M & 0 \\ CM & E \end{bmatrix}\begin{bmatrix} x(k) \\ x_4(k) \end{bmatrix} + \begin{bmatrix} N \\ CN \end{bmatrix}u(k) \quad (19)$$

$$y(k) = [C \quad 0]\begin{bmatrix} x(k) \\ x_4(k) \end{bmatrix} \quad (20)$$

where $x(k)$ is the state vector of variables $x_1(k)$, $x_2(k)$, $x_3(k)$ *and* $x_4(k)$ is the state variable that arised, because the adder was added to the system.

In the figures 9 and 10 there we can see the simulation of the regulation of the pneumatic system with the reduced order observer and LQ controller with the 0,2 m/s jump change of speed.

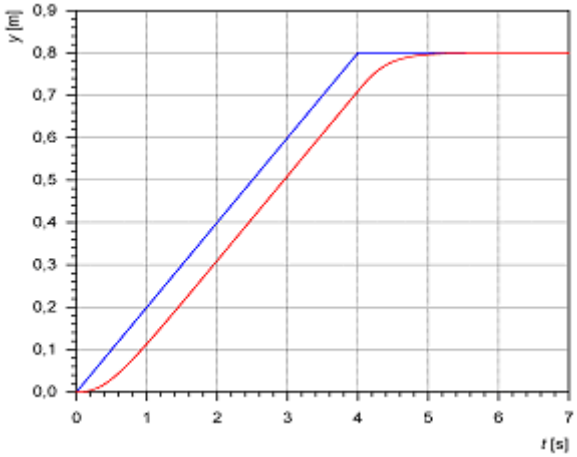

Figure 9: Simulated process of position

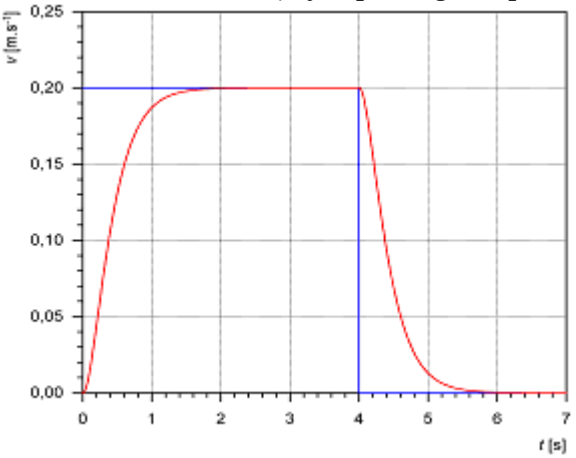

Figure 10: Simulated process of speed

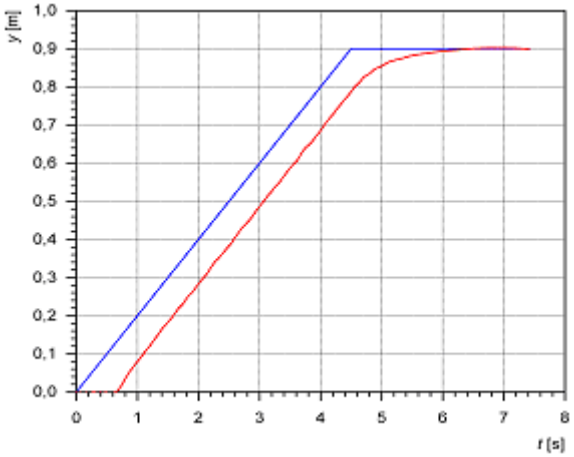

Figure 11: Real process of position

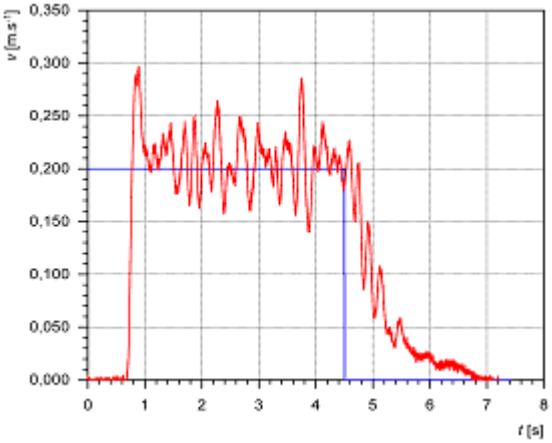

Figure 12: Real process of speed

In the figures 11 and 12 we can see the process of the regulation by means of LQ controller on the real pneumatic system to the speed step 0,2 m/s. During the regulation of the piston position at first the system is identified by ARX model. Then the state description of the system is made. As soon as the state matrixes are made the actual value of the state vector is calculated. The parameters of LQ controller are re - calculated after the completion of the calculation of the state vector. The output of LQ controller (an action interference) is observed on the directional valve.

5. RESULTS

The differences between the simulation and the real process of the regulation are evident from the figures 9 and 11. The differences between the smooth process of the simulation and the real process are caused mainly by the compressibility of the air and the passive resistances that have to be overcame during the motion of the piston. The passive resistances are also caused by the linear displacement encoder at which the stronger passive resistances arise in some places of the stroke. These resistances are probably caused by twisting the rod that connects the slider of the sensor with the end of the pneumatic piston inside the sensor case.

During the regulation by means of the state controller it is necessary to set the matrixes of weight coefficients accurately. If these matrixes are not set accurately the piston of pneumatic cylinder passes the required position at a high speed and after then it started to move to the required position at a low speed. When the matrix is set incorrectly the second most often behaviour of the piston occurs. It moves slowly to the required position from the beginning of setting the position. Another problem that we face at the pneumatic servomechanism is keeping the stable position. If we let the pneumatic servomechanism in a rest for a while, the air leakage occurs due to the untightness. This leakage deflects the piston from the equilibrium position so that the controller vibrates the piston around the required position.

The position at this pneumatic servomechanism is controlled only by means of the positional feedback and the LQ controller. At the hydraulic servomechanisms not only the positional feedback with the P controller is used for the control, but also the internal speed feedback with PI controller. We would like to eliminate an uneven speed of the piston motion of the pneumatic cylinder with the help of installation of the speed feedback as we can see it at hydraulic servomechanisms. Regulation of the position and the speed should not be implemented by the cascade connection of P and PI controllers but by two state LQ controllers that would be connected in cascade.

REFERENCES

[1] Strejc, V.: *Stavová teorie lineárního diskrétního řízení.* Academia, Praha 1978
[2] Modrlák, O.: *Úvod do diskrétní parametrické identifikace.* Skripta Liberec, 2004
[3] Modrlák, O.: *Základy analýzy a syntézy ve stavovém prostoru.* Skripta Liberec, 2004
[4] Balátě, J.: *Automatické řízení.* BEN-Technická literatura, Praha 2003

INTERNATIONAL SYMPOSIUM on
ADVANCED ENGINEERING & APPLIED MANAGEMENT
– 40th ANNIVERSARY in HIGHER EDUCATION (1970-2010)
4 – 5 November, 2010, Hunedoara, ROMANIA

[1.] Todor BAČKALIĆ, [2.] Maša BUKUROV

MODELLING OF THE SHIP LOCKING PROCESS IN THE ZONE OF SHIP LOCK WITH TWO PARALLEL CHAMBERS

[1.] FACULTY OF TECHNICAL SCIENCES, UNIVERSITY OF NOVI SAD, NOVI SAD, SERBIA

ABSTRACT:
Being aware of the waterway capacity, as a substantial characteristic of each traffic way, has a great importance to authorities that perform control and regulation of the vessel traffic. In specific real conditions and situations, for the purpose of the vessel traffic control, it is necessary to know specified limits of traffic density, which depends on corresponding parameters of observed system (ship lock zone). The vessel traffic control in the zone of ship lock is a complex system that is made of numerous subsystems. Determination of subsystems and their external and internal connections is conducted according to analysis of a real system. Simulation model is developed according to the analyzed model of vessel traffic process. Developed simulation model contain data on vessels which have passed through the observed system in defined time interval. Also, it contains statistic data on number of vessels and delays due to waiting queues for locking. An application of this model is possible in all cases of the waterway capacity determination by varying numerical data. Obtained results may be used as a planning and decision-making support in the process of the vessel traffic control in the zone of ship lock with two parallel chambers.
KEYWORDS:
ship lock, navigation, simulation, model

1. INTRODUCTION

Capacity is one of the most important characteristics of transportation systems. In analysis of traffic flows, the capacity should be distinguished from the traffic density. Capacity of the waterway is the maximal amount of cargo per time unit (day, month, and navigation period) for specific technical characteristics of waterway and fleet, as well as appropriated type of traffic organization. The waterway capacity can be measured according to two parameters: the amount of cargo per time unit (as a basic parameter) and the number of vessels per time unit (which is often applied in a real system).

The growth of traffic density on waterways initiated research of capacity determination and how to increase it. Each traffic system is complex system. Capacity determination of such system requires complex analysis of present state and existing problems, as well as possibilities to solve them. Magnitude of the waterway capacity, as a substantial characteristic of each traffic way, has a great importance for institutions and services that perform control and regulation of vessel traffic. Analytical methods for waterway capacity determination give average values of capacity [5]. In specific real situations, besides the vessel traffic safety [6], activities in vessel traffic control and decision-making processes require knowledge of traffic density limits, which depend on parameters of observed system.

Being aware of the capacity of certain waterway requires preliminary determination of influential factors and their effect on capacity quantity. Technological process of navigation is defined according to connections between elements and changes of the system state during navigation. After that follows model development and realization of simulation experiments. The capacity of the most difficult section of observed waterway determines capacity of the waterway as a

whole. It is possible to establish upper limit (maximal value) of waterway capacity as a whole by comparison of particular waterway section capacities, i.e. "bottle necks" based on capacity. When the traffic density on observed waterway reaches the limit values under certain technical and exploitation conditions, it is necessary to determine the waterway capacity for changed mode of exploitation (i.e. for changed technical characteristics and/or mode of exploitation). Some authors [9], [7] most attention give to determination of the ship lock capacity and its impact on the vessel traffic.

While studying problem of waterway capacity it is necessary to set apart natural and artificial sections of waterways. Natural waterways and canals can be divided into sectors: navigable sections and those that include objects on waterway (ship locks, inclined plane, boat lifts or other).

2. ORGANIZATION OF TRAFFIC AND TECHNOLOGICAL PROCESS OF NAVIGATION

The traffic organization on the waterway is represented by set of rules and activities for the control of navigation in the waterway, in order to perform rational utilization of waterway capacity and reduce time delays of vessels, with respect to existing navigational rules and the safety level of navigation. The traffic organization on the waterway or the section of waterway depends on [1]:

- technical and exploitation characteristics of the waterway and objects on the waterway
- technical and exploitation characteristics of fleet
- traffic density
- number of different types of vessels in fleet
- priority of specific vessels
- hydrological and meteorological conditions.

Each organization scheme is characterized by certain technological process of navigation (ship passing process or ship locking process). Also, for a certain type (scheme) of the vessel traffic organization there are different technological processes of navigation depending on vessel characteristics.

Technological process of navigation is presented by set of activities with defined phase change schedule. The phases are influenced by specific factors and limited by duration of time necessary to accomplish certain activity. Technological process of navigation depends on:

- an appropriate traffic organization scheme
- traffic density
- priority of vessels
- navigation conditions on the waterway
- technical and exploitation characteristics of objects on the waterway
- technical and exploitation characteristics of fleet
- hydrological and meteorological conditions.

There are following groups of technological processes depending on exploitation conditions on waterways' sections:

- technological process of navigation in two-way navigation sections
- technological process of navigation in one-way navigation sections
- technological process of navigation in zones of ship locks.

2.1. ORGANIZATION OF TRAFFIC IN THE ZONE OF SHIP LOCK

Organization of traffic on the waterway in the zone of ship lock, i.e. organization of ship locking process, is a compromise between the rational utilization of ship lock and reduction of vessels' delays in the zone of ship lock.

Organization of the vessel traffic on the waterway in the zone of ship lock depends on:

- number of locks (one or two parallel)
- number of lock chambers (one, two or more chambers in a row)
- way of ship locking process (one direction or both directions)
- technical characteristics of locks and approach canals
- traffic density
- technical characteristics of a fleet
- number of different types of vessels in a fleet
- priority level for certain vessels
- hydrological and meteorological conditions.

The factors listed above indicate a variety of organization ways, i.e. ability to determine a large number of traffic organization schemes, which depend on the degree of importance assigned to particular criterion.

From the standpoint of traffic organization and traffic density, there are three different types of navigation: free, restricted and regulated navigation [1]. The highest level is automated navigation (automated guidance). The navigation in two-way section corresponds to type of free navigation, since only restrictions in navigation are maximal allowed speed and distance between two vessels from the same direction. In other hand, navigation in a ship lock zone corresponds to type of regulated navigation.

During the ship locking process vessel changes position in real space and ship lock goes through certain phases, or states. Traffic organization scheme in a ship lock zone is influenced by adopted organization type. The technological process of the ship locking is analysed as a complex process in order to more clearly noticed specificity and mutual dependence between the state change of locks and movement of vessels. Long waiting of vessels at the entrance and vessels amassing must not be permitted.

2.2. THE TECHNOLOGICAL PROCESS IN THE ZONE OF SHIP LOCK

The technological process of ship locking is divided into two main subsets:

- from the aspect of ship lock
- from the aspect of vessels.

Phases, which ship lock and vessel go through during locking process, are defined by operations which must be executed. Duration of operations depends on several factors: the state of technical equipment, hydrologic and weather conditions, number and type of locked vessels, the intensity of the flow of requests for ship locking (traffic density) and other.

The technological process of ship locking was analyzed as a complex system. It consists of different phases through which pass: only vessels, only ship lock and phases for both - vessels and ship lock. Also, there are certain activities of the control of the ship locking process. Phases are represented by following activity flows:

- flow of vessel activities (ships and compositions),
- flow of ship lock activities (with or without vessels in the lock chamber),
- flow of control activities during the ship locking process.

Technological processes of ship locking can be classified according to:

- type and technical - exploitation characteristics of ship lock, approach canals and lock pools
- technical -exploitation characteristics of vessels
- organization mode of ship locking process.

From the standpoint of the ship locking process, according to the technical-exploitation characteristics, there are following systems:

- one lock (with one, two or more lock chambers in a row)
- two parallel locks (with one, two or more lock chambers in a row).

Technological processes of ship locking can be distinguished from the aspect of locking mode: one lock - one direction and one lock - both directions.

Depending on the technical-exploitation characteristics of the fleet and the locks, or possible number of vessels in the lock chamber during one cycle, there are following relationships between the lock and technological processes of ship locking:

- one lock chamber - one vessel (relevant)
- one lock chamber - one composition (relevant)
- one lock chamber - many vessels and compositions.

Taking into account assigned priority technological processes can be classified as:

- all vessels and compositions have equal priority, i.e. ship locking process without priority
- different priority levels for certain ships and compositions, i.e. ship locking process with priorities.

Table 1. Criterions for the classification of technological processes of ship locking

Type of the technological process of ship locking	Number of ship lock rows (1 or 2)	Number of lock chambers in a row (1, 2, ..., *n*)	Number of vessels in a lock chamber (1, 2, ..., *m*)	Ship lock is assigned to one or to both directions (one=1, both=2)	Number of ship priority levels (1, 2, ..., *p*)
11121	1	1	1	2	1
11122	1	1	1	2	2
...	...	...	...	...	...
22*m*21	**2**	**2**	***m***	**2**	**1**
...	...	...	...	...	...
2*nm*2*p*	2	*n*	*m*	2	*p*

Depending on the classification criterions above there are a lot of ship locks systems with the appropriate technological processes of ship locking (Table 1).

3. TECHNOLOGICAL PROCESS OF THE SHIP LOCKING IN THE ZONE OF SHIP LOCK SYSTEM WITH TWO PARALLEL LOCKS FOR BOTH DIRECTIONS

Technological process of the system with two parallel locks with two chambers in a row for more vessels in one cycle will be presented in the following schemes. Both locks are designed for both directions, giving greater importance to reduction of vessels delays in the ship lock zone (type 22*m*21, part marked in Table 1).

In Figure 1 are presented connections between segments of the technological process of navigation in the zone of a system.

In Figure 2 are presented activities of vessels at both levels (arrivals from the lower and upper level). In Figure 3 are presented some lock activities at ship locking process. In the Figures 4 and 5 are presented some activities of the ship lock control centre.

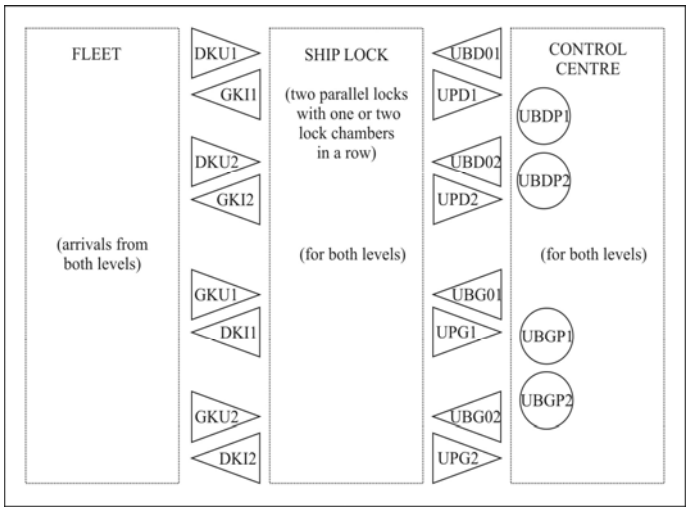

Figure 1. Connections between segments of the technological process in the ship lock zone

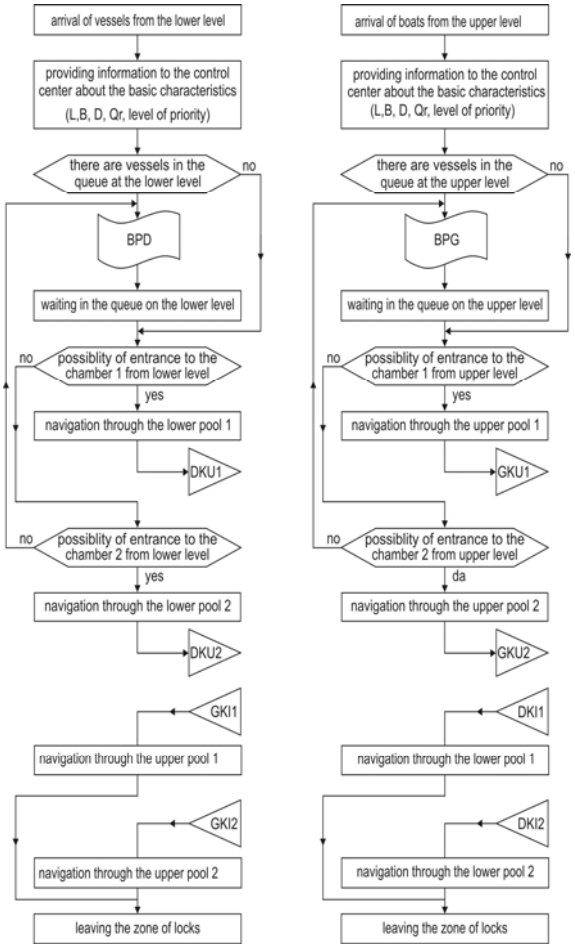

Figure 2. Activities of vessels at both levels

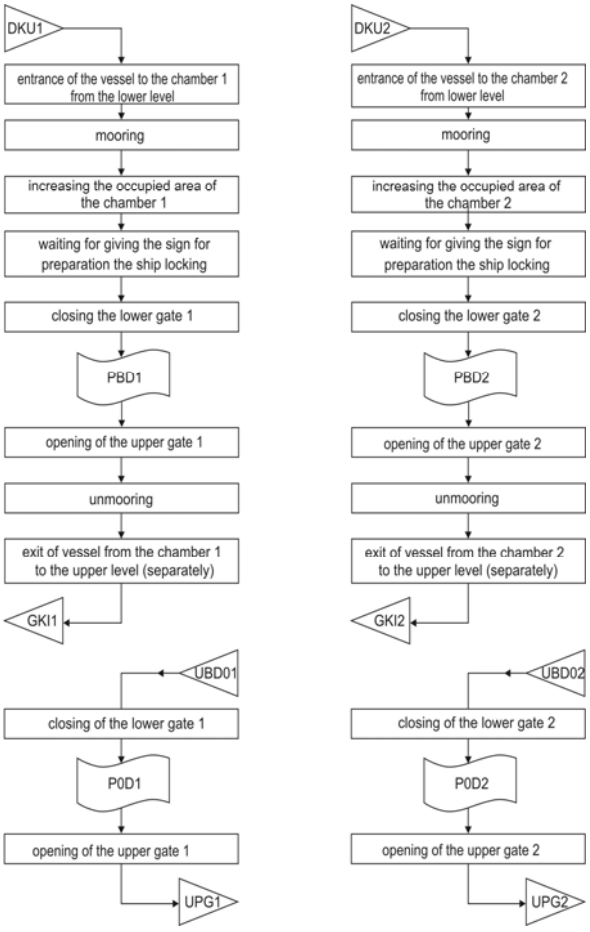

Figure 3. Ship lock activities at ship locking process (from lower to upper level)

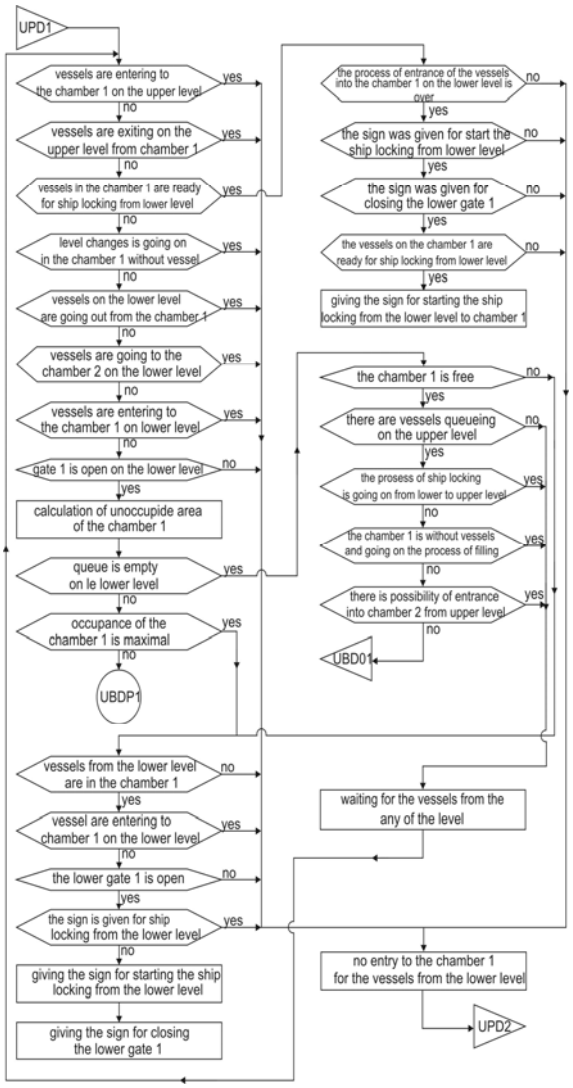

Figure 4. Activities of the ship lock control centre (locking from lower to upper level – lock1)

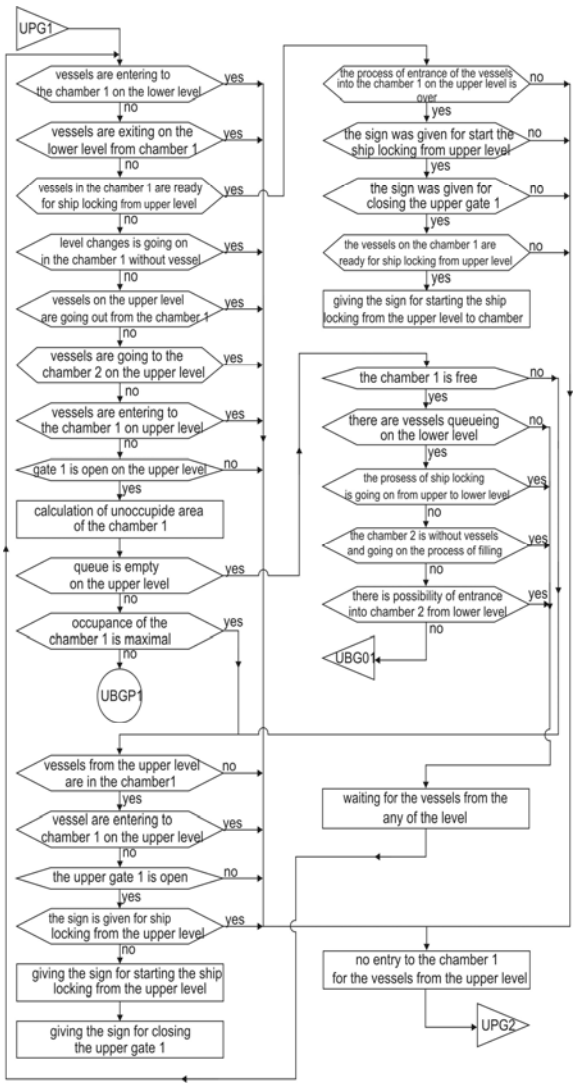

Figure 5. Activities of the ship lock control centre (locking from upper to lower level – lock1)

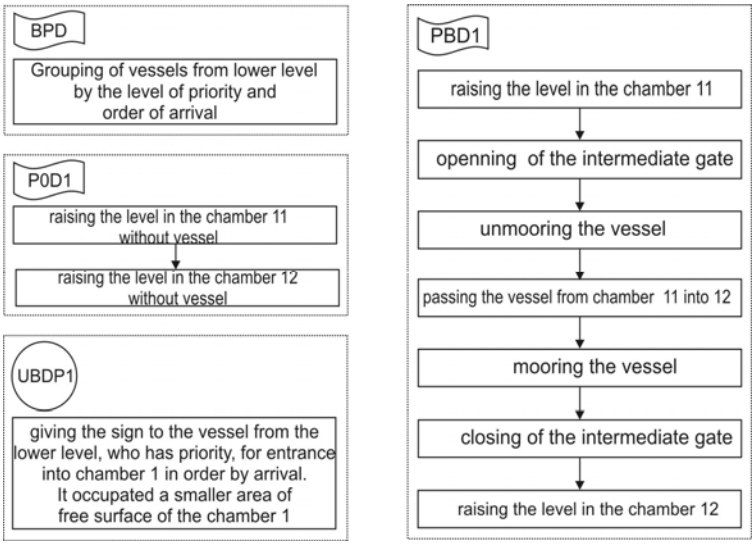

Figure 6. Description of some activities in the ship lock process

4. SIMULATION MODEL

4.1. DESCRIPTION OF THE SIMULATION MODEL

The developed simulation model is composed of nine sub-models:

- sub-model 1 - the ship locking process for vessels from the lower level
- sub-model 2 - the ship locking process for vessels from the upper level
- sub-model 3 - the control process of the ship lock 1 during locking from the lower level
- sub-model 4 - the control process of the ship lock 2 during locking from the lower level
- sub-model 5 - the control process of the ship lock 1 during locking from the upper level
- sub-model 6 - the control process of the ship lock 2 during locking from the upper level
- sub-model 7 – the control process of grouping of vessels in the queue at the lower level, depending on: the priority level, the order of arrival and area size ($L \times B$) that occupy the vessel in the lock chamber
- sub-model 8 - the control process of grouping of vessels in the queue at the upper level, depending on: the priority level, the order of arrival and area size ($L \times B$) that occupy the vessel in the lock chamber
- sub-model 9 - time sub-model (timer).

Ship locks are static elements in sub-models 1, 2, 3 and 4, while vessels are dynamic elements in sub-models 1 and 2. Control actions are dynamic elements in sub-models 3, 4, 5 and 6. In sub-models 7 and 8, control actions are dynamic elements, while queues (if were formed) are static elements.

Sub-model 1 is the locking process of vessels from the lower level to the upper level. It includes all operations and delays of vessels and locks from the moment vessel entrance into the ship lock zone at the lower level.

Sub-model 2 is the locking process of vessels from the upper level to the lower level. It includes all operations and delays of vessels and locks from the moment vessel entrance into the ship lock zone at the upper level.

Sub-models 3 and 4 describe control processes of ship locks 1 and 2 during locking from the lower level and include:

- control of vessels' entering in ship locks 1 and 2 from the lower level
- water level change in ship locks 1 and 2 without vessels, in cases when there is no queue at the lower level, lower gates 1 or 2 are opened, while vessels at the upper level wait in the queue.

Sub-models 5 and 6 describe control processes of ship locks 1 and 2 during locking from the upper level and include:

- control of vessels' entering in ship locks 1 and 2 from the upper level
- water level change in ship locks 1 and 2 without vessels, in cases when there is no queue at the upper level, upper gates 1 or 2 are opened, while vessels at the lower level wait in the queue.

Sub-models 7 and 8 describe control processes of vessels re-grouping in the queues at the lower and upper levels. Re-grouping depends on: priority level, order of arrival and area size ($L \times B$) which vessel occupies in the lock chamber. Sub-model 9 represents the duration of the simulation experiment.

4.2. EVALUATION OF THE SIMULATION MODEL

Evaluation of the developed simulation model included determination of the model validity and the model testing [2], [3]. Determination of the model validity was done up to the level of predictability. Predictive model validity is a stricter level of evaluation that is related to the model ability to be used to predict the situations that are not observed and studied on the real systems. That level was tested with simulation experiments. In the simulation experiments the traffic density was altered in both directions and system reactions were observed.

The model testing was done from the beginning of the real system modelling and includes:

- application of specialized language (GPSS) to realize the simulation program
- validity and accuracy testing of the simulation model (verification of static and dynamic properties of the model)
- correctness testing of the model to generate different distributions of input variables and system parameters.

Control of the simulation model has determined if there is a match between behaviour of program and model. The developed simulation model completely fulfils presented requirements and criterions, and such can be used in simulation experiments for capacity determination and change in density of traffic on certain real system.

5. CONCLUSION

Navigation in ship lock zones, as a part of system of navigation on inland waterways, apart other things, is characterized by limited capacity and the need to use information-control systems. Capacity presents one of the most important characteristic of each waterway, especially ship lock. The organization of traffic on the observed real system has significant influence on the capacity.

The developed simulation model of the technological process of ship locking gives a number of data, like vessel delays, transit times, resource utilizations, number of vessels in queues and others. The developed model can be applied to planning of vessel traffic control, since they give a possibility of choice of traffic organization that depends on certain conditions. Connections between elements of technological process in presented models have been copied from real system. This allows variation in densities and distribution of all incoming vessels' flows, as well as changes of technical characteristics of ship lock and vessels.

Application of developed simulation models is applicable for planning and decision making in ship locking control. Also, they can be applied to define type of organization of ship locking process. It is possible to do almost unlimited number of simulation experiments. More important, the model's fidelity enables to predict conditions for any future scenarios of interest (e.g., under increasing traffic volumes), and to answer various other "what-if" questions [8].

High-fidelity simulation models of ship locking process consisting of the entire vessel classes as well as level of priority, weather and waters conditions can be easily developed. Significant extensions of model can be made by adding new segments. Such extended simulation model includes the following: application of control rules, ability to monitor the influence of large vessels on waterway capacity.

Also, further research should focus on problems how to define optimal density of traffic for given conditions. To solve this problem it is necessary to introduce the term "level of service" (as a qualitative measure). Determination of the optimal density requires application of certain optimization methods in order to achieve certain levels of service with defined conditions and relevant parameters.

REFERENCES

[1] Bačkalić, T.: Traffic control on artificial waterways with limited dimensions as function of their capacity, (in Serbian), PhD thesis, University of Novi Sad, Serbia, 2001

[2] Biles, W.E., Sasso, D., Bilbrey, J.K.: Integration of simulation and geographic information systems: modeling traffic flow in inland waterways, Proceedings of the 36th conference on Winter simulation, ISBN:0-7803-8786-4, Washington D.C., USA, December 2004

[3] Bush, A., Biles, W.E., DePuy, G. W.: Iterative optimization and simulation of barge traffic on an inland waterway, Proceedings of the 35th conference on Winter simulation, ISBN: 0-7803-8132-7, New Orleans, Louisiana, USA, December 2003.

[4] Filipowicz, W.: Vessel Traffic Control Problems, Journal of Navigation, ISSN: 0373-4633, The Royal Institute of Navigation, Vol. 57, No. 1, 2004, pp. 15-24

[5] Griffiths, J.D.: Queueing at the Suez Canal, The Journal of the Operational Research Society, Palgrave Macmillan Journals on behalf of the Operational Research Society, Vol. 46, No. 11 (Nov., 1995), pp. 1299-1309

[6] Ince A.N., Topuz E.: Modelling and simulation for safe and efficient navigation in narrow waterways, Journal of Navigation, ISSN: 0373-4633, The Royal Institute of Navigation, Cambridge University Press, Vol. 57, No. 1, 2004, pp. 53-71.

[7] Ramanathan, V., Schonfeld, P.: Approximate Delays Caused by Lock Service Interruptions, Transportation Research Record 1430, Jan. 1994, pp. 41-49

[8] Smith, L.D., Sweeney, D.C., Campbell, J.F.: A simulation model to evaluate decision rules for lock operations on the Upper Mississippi river, Proceedings of 40th Hawaii International Conference on Systems Science (HICSS-40 2007) Waikoloa, HI, USA, 3-6 January 2007

[9] Wang, S.L., Schonfeld, P.: Demand Elasticity and Benefit Measurement in a Waterway Simulation Model, Transportation Research Record: Journal of the Transportation Research Board, Transportation Research Board of the National Academies, ISSN: 0361-1981, Volume 2033 / 2007, pp. 53-61, 2008

INTERNATIONAL SYMPOSIUM on
ADVANCED ENGINEERING & APPLIED MANAGEMENT
– 40th ANNIVERSARY in HIGHER EDUCATION (1970-2010)
4 – 5 November, 2010, Hunedoara, ROMANIA

[1.] József SÁROSI

INVESTIGATION OF POSITIONING OF FLUID MUSCLE ACTUATOR UNDER VARIABLE TEMPERATURE

[1.] FACULTY OF ENGINEERING, UNIVERSITY OF SZEGED, HUNGARY

ABSTRACT:
Some researchers have mentioned that temperature creates an important part in the accuracy of positioning of pneumatic artificial muscles (PAMs). However, in literature investigations for measuring temperature inside and outside the PAMs have not been found. This paper presents our robust motion control of these muscle actuators under different temperatures using sliding-mode control.
KEYWORDS:
muscle actuators, variable temperature

1. INTRODUCTION

The working principle of the pneumatic artificial muscles is well described in literature ([1], [2], [3], [4], [5] and [6]).

There are a lot of advantages of these muscles like the high strength, good power-weight ratio, low price, little maintenance needed, great compliance, compactness, inherent safety and usage in rough environments. However, problems with the control of the highly nonlinear pneumatic systems have prevented their widespread use [7]. For this, a fast and robust control necessary to achieve the desired motion. Several control ways have been applied to control different humanoid or robot arms, manipulators, prosthetic and therapy devices driven by pneumatic artificial muscles. The early control methods were based on classical linear controllers and then some modern control strategies have been developed (e. g. adaptive controller, sliding-mode controller, fuzzy controller, neural network controller and others) [8].

The layout of this paper is as follows. Section 2 (The study) is devoted to display our test-bed and the LabVIEW programs. Section 3 (Results and discussion) presents several experimental results. Finally, section 4 (Conclusions) gives the investigations we plan.

Fluid Muscles DMSP-10-250N-RM-RM (with inner diameter of 10 mm and initial length of 250 mm) produced by Festo company were selected for our newest study.

2. THE STUDY

A good background of our test bed and former experimental results of positioning can be found in [9] and [10].

The PAMs were installed horizontally and can be controlled by MPYE-5-M5-010-B type proportional valve made by Festo. Our robust position control method based on sliding-mode control. The linear displacement of the actuator was measured using a LINIMIK MSA 320 type linear incremental encoder with 0,01 mm resolution.

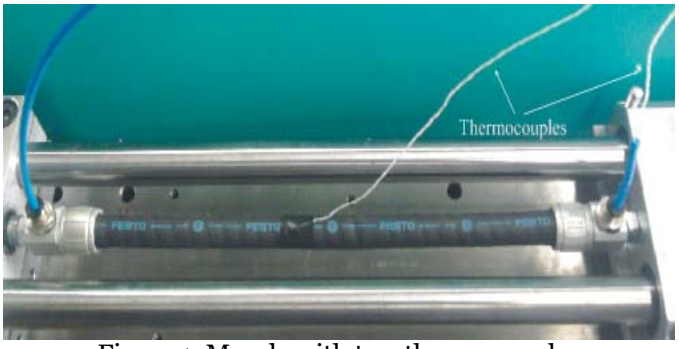

Figure 1. Muscle with two thermocouples

To measure temperature inside and outside the muscle the test-bed was completed two thermocouples type K (Figure 1). Figure 2 shows the block diagram of this positioning system with proportional valve.

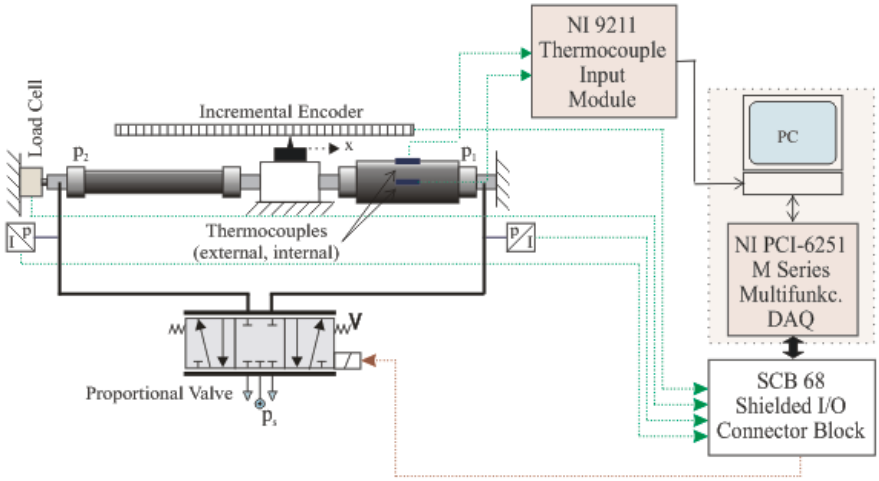

Figure 2. Block diagram of positioning system with proportional valve

The Figure 3 shows data acquisition and positioning that can be achieved in LabVIEW environment. Aside from the desired position the number of samples and the sampling time can also be set. The data can be saved into a text file.

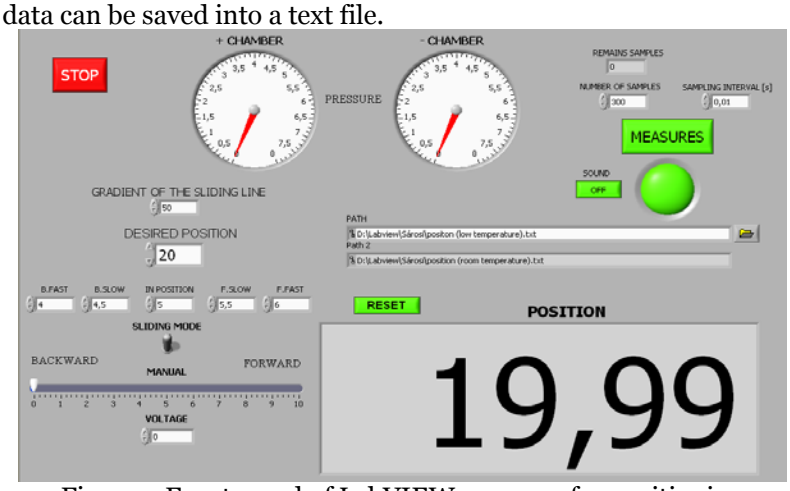

Figure 3 Front panel of LabVIEW program for positioning

The Figure 4 shows the front panel of the LabVIEW program created for temperature measurement. Here the number of samples and sampling time can also be set. During the periodic and automatic working of the muscles the contraction and rate of release can be adjusted with the frequency of the sine wave. The temperature inside and on the surface of the muscle can be read on the indicators on the screen also it is shown as a number. The measured results are saved in a text file for later processing.

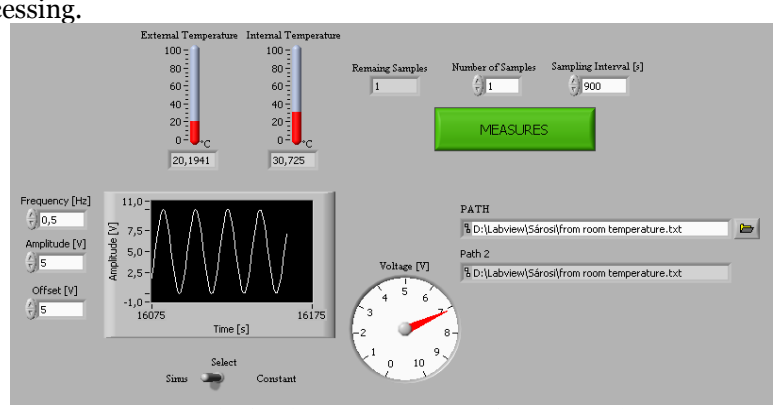

Figure 4. Front panel of LabVIEW program for measuring temperature

3. RESULTS AND DISCUSSION

Positioning was first done in room temperature on the pressure of 6 bar. The desired positioning was set to 20 mm, the number of samples was set to 300, while the sampling rate was set to 10 ms, thus the measurement took 3 s.

Figure 5 shows the positioning as a function of time. It took about 1,85 s for the position to reach the set value. To show the accuracy of positioning the area around the desired position has been magnified (Figure 6). This Figure shows the accuracy of positioning is within 0,01 mm.

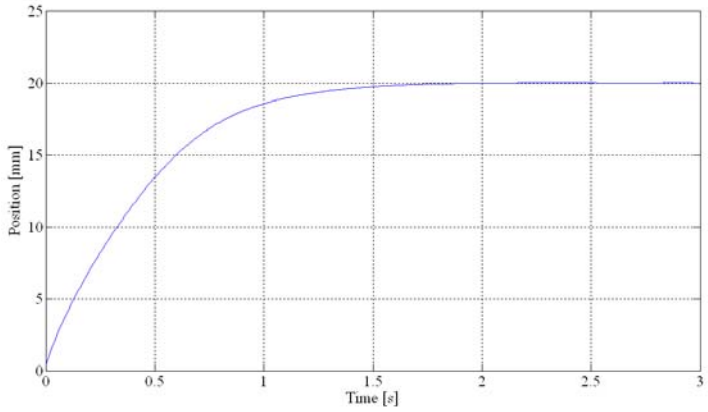

Figure 5. Position as a function of time

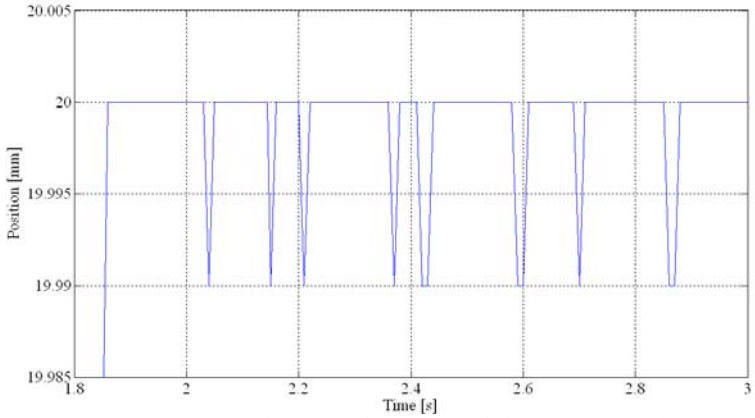

Figure 6. Position as a function of time (enlarged)

The periodic working of the muscles was achieved with a 0,5 Hz frequency sine wave. The measurement took 900 s during which the sampling time was 0,25 s, the acquired data is shown in Figure 7. While the surface temperature reached about 28 °C, the internal temperature oscillated a lot during contraction and release, for this reason a spline approximation was used for the internal temperature (Figure 8).

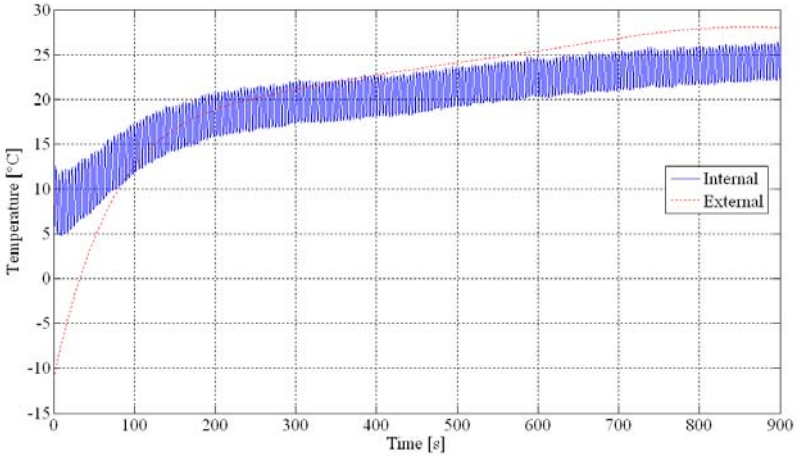

Figure 7. Temperature as a function of time

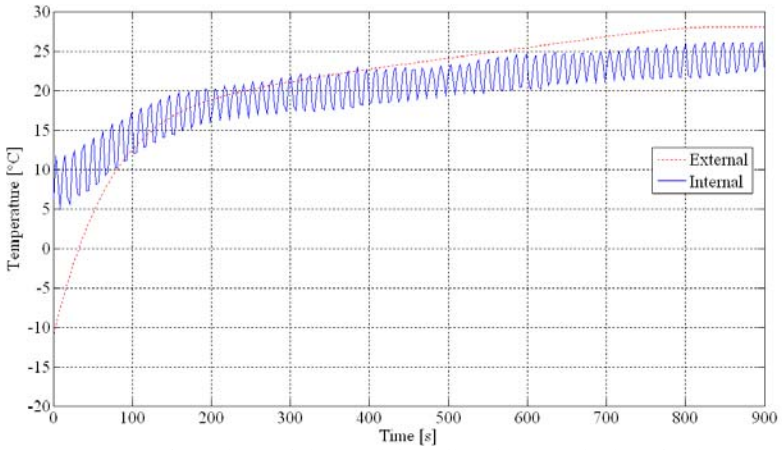

Figure 8. Temperature as a function of time with spline interpolation for internal temperature

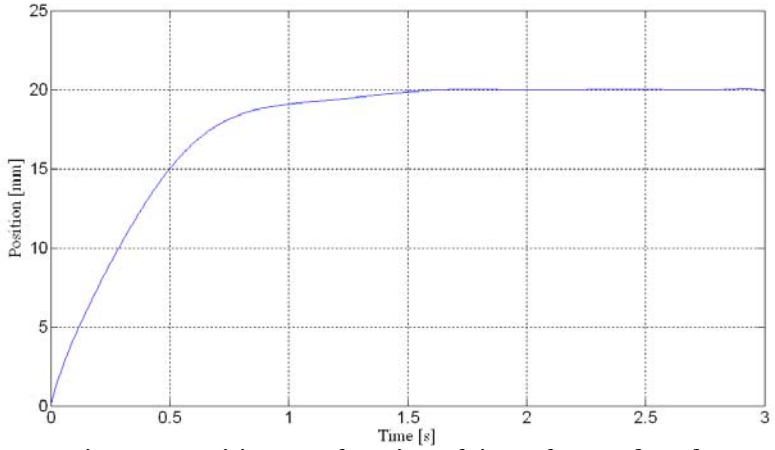

Figure 9. Position as a function of time after work cycle

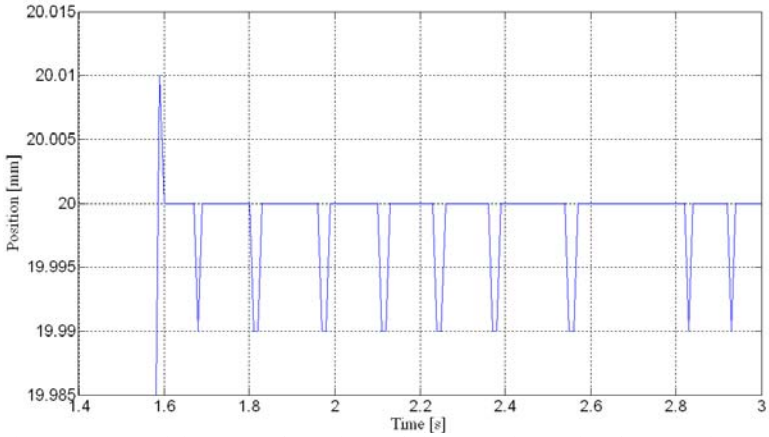

Figure 10. Position as a function of time (enlarged) after work cycle

After a constant temperature was reached positioning was measured on the pressure of 6 bar, too. The result of it is shown in Figure 9. It shows the desired position was reached within 1,6 s. To show the accuracy of positioning the area around the desired position has been magnified (Figure 10.). The accuracy of positioning remained within 0,01 mm.

4. CONCLUSIONS

From these measurements the conclusion is that the sliding-mode control is rather robust for accurate positioning and the accuracy and time of positioning is more favorable at higher temperature. We plan these investigations will be repeated with different muscles.

REFERENCES

[1.] Daerden, F. (1999): Conception and realization of pleated artificial muscles and their use as compliant actuation elements, PhD Dissertation, Vrije Universiteit Brussel, Faculteit Toegepaste Wetenschappen Vakgroep Werktuigkunde, pp. 5-33.

[2.] Daerden, F. and Lefeber, D. (2002): Pneumatic artificial muscles: actuator for robotics and automation, European Journal of Mechanical and Environmental Engineering, Volume 47, pp. 10-21.

[3.] Caldwell, D. G., Razak, A. and Goodwin, M. J. (1993): Braided pneumatic muscle actuators, Proceedings of the IFAC Conference on Intelligent Autonomous Vehicles, Southampton, United Kingdom, 18-21 April, 1993, pp. 507-512.

[4.] Balara, M. and Petík, A. (2004): The properties of the actuators with pneumatic artificial muscles, Journal of Cybernetics and Informatics, Volume 4, pp. 1-15.

[5.] Chou, C. P. and Hannaford, B. (1996): Measurement and modeling of McKibben pneumatic artificial muscles, IEEE Transactions on Robotics and Automation, Volume 12 (1), pp. 90-102.

[6.] Tondu, B. and Lopez, P. (2000): Modeling and control of McKibben artificial muscle robot actuator, IEEE Control System Magazine, Volume 20, pp. 15-38.

[7.] Caldwell, D. G., Medrano-Cerda, G. A. and Goodwin M. (1995): Control of pneumatic muscle actuators, IEEE Control System Magazine, Volume 15 (1), pp. 40-48.

[8.] Situm, Z. and Herceg, Z. (2008): Design and control of a manipulator arm driven by pneumatic muscle actuators, 16th Mediterranean Conference on Control and Automation, Ajaccio, France, 25-27 June, 2008, pp. 926-931.

[9.] Sárosi J., Gyeviki J., Szabó G. and Szendrő P. (2010): Laboratory Investigations of Fluid Muscles, International Journal of Engineering, Annals of Faculty of Engineering Hunedoara, 2010, Volume 8 (1), pp. 137-142.

[10.] Sárosi J., Gyeviki J., Véha A. and Toman P. (2009): Accurate Position Control of PAM Actuator in LabVIEW Environment IEEE, 7th International Symposium on Intelligent Systems and Informatics, Subotica, Serbia, 25-26 September, 2009, pp. 301-305.

INTERNATIONAL SYMPOSIUM on
ADVANCED ENGINEERING & APPLIED MANAGEMENT
– 40th ANNIVERSARY in HIGHER EDUCATION (1970-2010)
4 – 5 November, 2010, Hunedoara, ROMANIA

[1.] Ala'a M. DARWISH

STABILIZATION OF EMPTY UNDERGROUND CIRCULAR STORAGE TANKS AGAINST UPLIFTING UNDERGROUND WATER FORCES

[1.]DEPARTMENT OF BUILDING AND CONSTRUCTION ENGINEERING,
UNIVERSITY OF TECHNOLOGY, BAGHDAD, IRAQ

ABSTRACT:
Circular swimming pools or, in general, underground tanks can be mobilized due to two coincide factors: the first is when they are emptied for maintenance, while the second factor is when underground water level rises up to be close to the natural ground surface.
Under such circumstances an underground circular tank will be subjected to a buoyancy force equal to the weight of the displaced underground water minus the weight of the tank.
In this research eleven prototype models were tested to simulate the mentioned case. The base diameter of each model was different than the other, with an increment of 1cm each time. Water head required to float each model was recorded.
Test result shows that: Stabilizing of an empty underground circular tank can be reached by extending it's base diameter.
Finally, the equation of calculating the required base extension was derived.
KEYWORDS:
circular tank, swimming pool, underground tank, buoyancy, stabilization, state of-the art design approach

1. INTRODUCTION

During a maintenance process for a circular reinforced concrete swimming pool, it was found that there were some visible cracks along its circumference. These cracks were situated exactly between the pool walls and its surrounding shoulders. Moreover, after excavating few holes in the burying soil around the pool in order to fix its piping system, it was noticed that there were some movements/ disorientations in the piping fittings which had made the maintenance process a bit more complicated.

After verifying the mentioned case a complete analysis was done to find the cause of these engineering defects. The analysis result indicated that the pool was suffering from a noticeable amount of uplifting buoyancy force due to the rising of the surrounding water table level.

Going through the literature of the subject, it was found that; no concern had been paid to fix a swimming pool against uplifting pressure. This might be due to their shallow depth, normally 2 to 4 meters, in addition to the rare condition of the augmentation of buoyancy forces.

Taking the general case of deeper buried circular tanks (actually cylindrical tanks), it was found that some tanks are based upon reinforced concrete piles which can resist the calculated uplifting forces (Westbrook 1984). But, "Piles penetrating into a stratum having a confined hydrostatic head will be subjected to uplift, possibly sufficient to raise them from their end bearing. Seepage around piles in un-watered excavation may reduce skin friction to less than the hydrostatic uplift", (Chellis 1992). While (Darwish 2008) had complained about using piled foundation for this

purpose arguing that "Even if the piles are not lifted up, they are still subjected to repetitive high tensile stresses. These tensile stresses may be grater than the pile's concrete tensile strength and cracks near the pile heads can be expected. Crack formation across the entire cross section of a pile head will lead to an increasing tendency for corrosion of its reinforcing steel. Usually, sub-soil can support an underground tank without using any pile, because it is overburdened by the weight of the excavated soil which is normally greater than the weight of the filled tank. But if the tank becomes empty, during the rise of the underground water level, such soil even if it is hard as rocky soil can do little to resist tank floatation".

(Darwish 2008) had also solved the problem of anchoring empty underground storage rectangular tanks against underground- water-induced floatation by using two parabolic profile cables passing through the long side walls of a tank and anchored to sub-grade soil at their ends. While this solution is appropriate for rectangular and square cross-section underground tanks, it is not so for underground cylindrical tanks.

To study the case of unstable pools and, in general, underground circular tanks, prototypes of a steel circular tank with variable base diameters were used to simulate the case and to find a reasonable solution. The solution was based upon finding a balancing weight which can counter the net uplifting buoyancy forces. By changing the diameter of the prototype tank base, it was found that: with each increment of base extension there was an increase of the water head required to float the tank. Contentment was reached that the weight of the surrounding soil situated directly, as a ring of soil, over the tank base extension can manage to counter the net buoyancy force tending to lift the buried tank.

In spite of the complication of each case due to the variable water head height, the shape of the slipping surface, friction between the tank walls and the surrounding submerged/non-submerged soil and the length of the base extension, an equation was derived to calculate the required length of the base extension which can stabilize any tank with an average safety factor of +17%.

2. EXPERIMENTAL WORK

2.1 Materials

2.1.1 Transparent square plastic container having the dimensions of 50cm×50cm and a depth of 20cm.

2.1.2 Clean sand with the following properties:

- Specific weight = 2.61
- Dry density = 1.8 gm/cm^3
- Wet density = 1.42 gm/cm^3
- Submerged density = 0.42 gm/cm^3
- Angle of repose = 35°

2.1.3 Four water inlets to the container, one on each side, to discharge a controllable amount of water near the inner face of the container base, see Fig.1.

2.1.4 Four measuring stickers, one on each corner of the container.

2.1.5 A changeable base cylindrical steel pan having an outer diameter of 20cm, depth of 10cm, and a wall/ base thickness of 1mm. Its weight was 732gm.

2.1.6 Variable Steel bases, all with a thickness of 1mm, were used through the test. Their diameters start from 20cm to 30cm with an increment of 1cm. The first four columns of Table -1 show Notations, diameters and weights of the pan and its different bases.

2.1.7 Two dial gauges were attached to indicate any upward movement in the level of the buried pan.

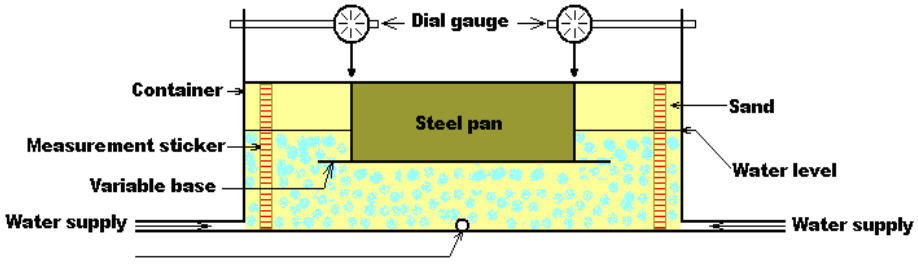

Fig.1 Testing device

2.2 Testing procedure

The container was filled with wet sand for half of its depth, the cylindrical steel pan #0 was placed on the sand and then the container was completely filled with wet sand. Water was allowed to seep slowly through the four inlets with a rising speed of 10cm/h.This rate was chosen to let the water surface to be at the same level allover the area of the container and to facilitate recording the rise of water by the four measuring stickers that were placed at the four inner sides of the container. Zero level was fixed at 10cm above the level of the inner face of the base. Mean value of water level was considered in the next calculations. Two dial gauges were attached to the container walls to measure any perpendicular movement might occur in the level of the steel pan.

The following observations were noted:

- The cylindrical pan was stable in its place until the height of water recorded 3.7cm. Suddenly, the pan was lifted and it continued to rise directly with the increase of water level.
- The same test was repeated using pan #1 which had a base extension of 1cm instead of pan#0 with no base extension to monitor the effect of increasing the diameter of the base of a buried tank on its stability against floating. After supplying the container with the same rate of water through the four water inlets, the steel pan remained stable until the level of water reached 4.3cm, then the pan started to rise and it continued to move upward directly with the rise of water level.
- The same procedure was repeated with pans #2, #3 and #10 on turn. The results are listed in table-1. It shows the theoretical water head required to lift the weight of each pan with respect to the actual recorded head of water.

Table -1 Theoretical and Actual head of water required to mobilize each pan

Notation	Base diameter (cm)	Weight (gm)	Theoretical head (cm)*	Actual head of water (cm)
Pan #0	20	732	2.33	3.7
#1	21	758	2.41	4.3
#2	22	784	2.50	5.3
#3	23	812	2.58	6.0
#4	24	841	2.68	6.8
#5	25	871	2.77	7.5
#6	26	902	2.87	8.1
#7	27	935	3.00	8.6
#8	28	968	3.10	9.1
#9	29	1003	3.20	9.6
#10	30	1040	3.30	10.0

* Only the weight of the pan was considered.

3. RESULTS& COMMENTS

One of the well known principles is that: the water floating force equals the weight of the displaced water by a submerged body. By applying this concept to pan #0, with no base extension, it indicates that a water level of 2.33cm is enough to push it up, but during the test the pan remained stable when water level reached this point. Pan #0 started to move up only when water level reached 3.7cm. The mentioned difference means that an extra force is required to lift the empty pan. The explanation is simply that the pan was not free to float and the extra force was required to overcome the friction between the outer surface of the pan's wall and the surrounding sand, see Fig.2-a.

Repeating the same testing procedure but with pan #10, with a base of 30cm diameter, the pan remained stable until the water level reached 10cm in depth. Taking into account that the displaced water was approximately the same for the two pans #0 and #10, in other word the required uplifting force should be very close, but test results showed that this is not true. The main difference between the two pans was the extended base of pan #10. This extension showed that it was active in stabilizing pan#10 against floating. It required (10-3.7 = 6.3cm) of an extra head of water to initialize its upward movement. While pan #0 required an extra force to overcome the friction between the outer surface of the pan's wall and the surrounding sand, pan #10 did not require such extra force because there was no direct slipping between the pan's wall and the surrounding sand. Actually, the base extension had shifted the slip surface away from the pan's wall, see Fig.2-b.

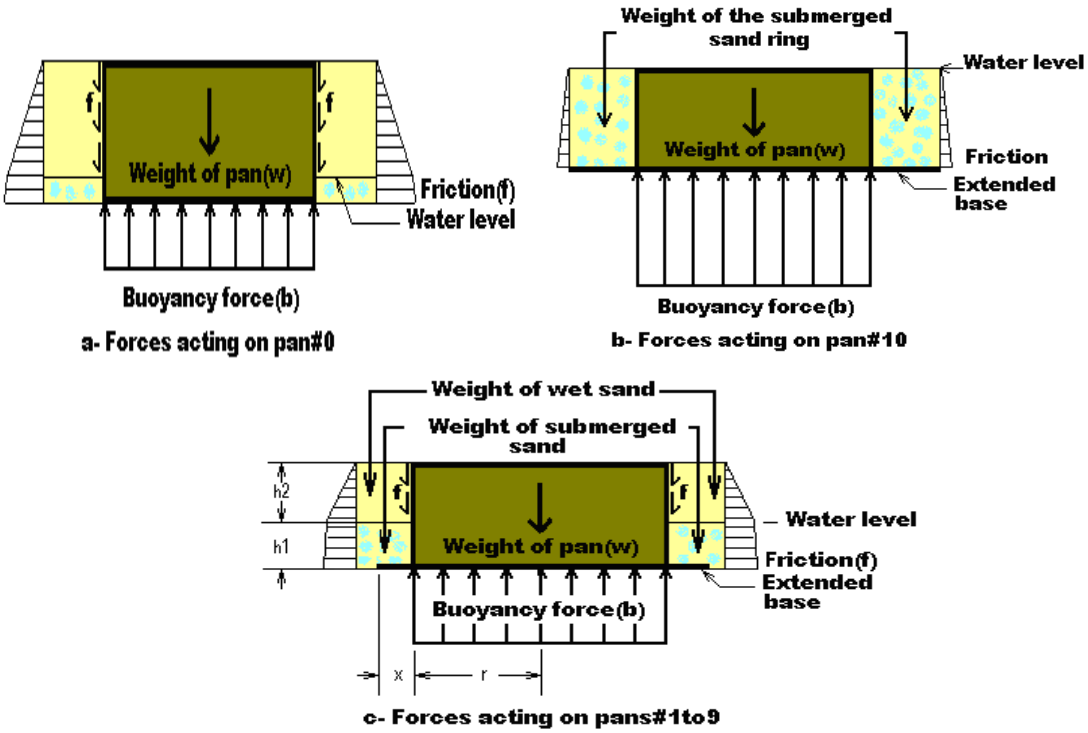

Fig.2 Forces distribution on testing pans

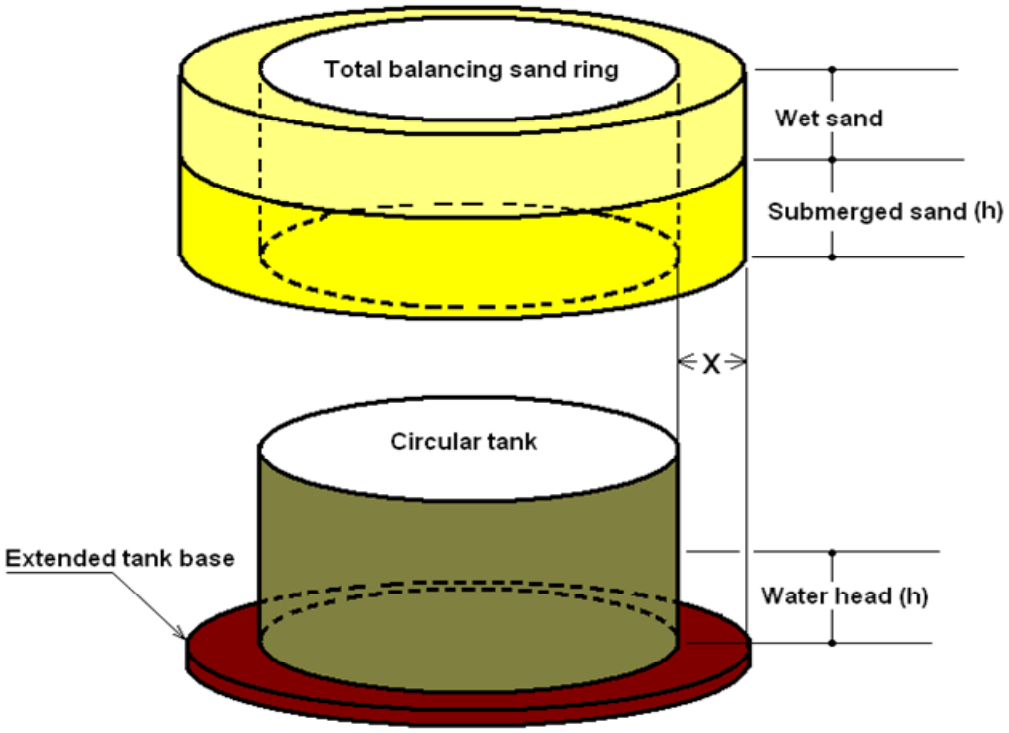

Fig.3 The balancing sand ring

By calculating the weight of the submerged ring of sand around the pan, see Fig.3, which was situated directly over the base extension, a hollow 10cm high cylinder with an interior diameter of 20cm and an exterior diameter of 30cm, it was found that it's weight equals:

$$(15^2 - 10^2) \times \pi \times 10 \times 0.42 = 1650 gm$$

While the uplifting force of the extra head of water equals:

$$10^2 \times \pi \times 6.3 = 1980 gm$$

By reducing the difference of weight between the two pans (1040-732= 308gm), the net extra uplifting force will be:

$$1980 - 308 = 1672\text{gm}$$

The difference between the weights of the surrounding submerged sand ring and the net uplifting force is equal to:

$$1672 - 1650 = 22\text{gm}$$

This force was required to overcome the friction between the submerged sand particles along the slip surface. It is worth to compare between that force and the force required to overcome the friction in the case of pan #0 which was equal to:

$$10^2 \times \pi \times (3.7 - 2.33) = 430\text{gm}$$

It is clear that, pan #0 required an extra uplifting force of 430gm to overcome friction compared to 22gm required by pan #10 for the same purpose, that is justified due to the decrease of friction coefficient by the effect of submerging.

During the test, the procedure was repeated using different pans with a base extension increment of 0.5cm each time as mentioned in table-1, pan#1 with a base extension of 0.5cm to pan#9 with a base extension of 4.5cm. The mean level of water head required to mobilize each pan was recorded and listed in table-1.

It should be noted that these nine pans were different in boundary conditions than pans#0&#10, while pan#0 was mobilized immediately after overcoming the soil friction with its walls and pan#10 was mobilized after it was surrounded completely by submerged sand, in the case of these nine pans, see Fig.-2-c, there were the following factors influencing their bouncy:

- Generation of a mechanical resistance for floating due to the base extension.
- The surrounding soil was partially submerged.
- The slip surfaces were started from the end of the base extension upwards.
- The slip surface was not identical around each pan; it came close to the upper part of the pan's wall from one side and shifted away from another side. In other word no specific slip surface angle could be defined.

A further calculation was done for each case based upon the bouncy force minus both of the weight of the pan and the weight of the composite, submerged& non-submerged, soil ring with a base equal to the extension of the base. Percentage of the actual extra water heads are shown in table-2.

Table-2 Percentage of the difference between actual/ theoretical floating water head

Notation	Weight of stabilizing soil ring (gm)	Equivalent head (cm)	Theoretical head (cm)	Total required head (cm)	Actual Water head (cm)	Head difference percentage %
Pan #0	0000	0.00	2.33	2.33	3.7	+58%
#1	0320	1.00	2.41	3.41	4.3	+26%
#2	0543	1.73	2.50	4.23	5.3	+25%
#3	0820	2.61	2.58	5.19	6.0	+16%
#4	1023	3.25	2.68	5.93	6.8	+15%
#5	1185	3.77	2.77	6.54	7.5	+15%
#6	1323	4.21	2.87	7.08	8.1	+14%
#7	1448	4.61	3.00	7.61	8.6	+13%
#8	1538	4.90	3.10	8.00	9.1	+14%
#9	1594	5.07	3.20	8.27	9.6	+16%
#10	1650	5.25	3.30	8.55	10.0	+17%
						Σ = +17%*

*Pan #0 was not included.

Excluding pan#0 with no base extension, the average actual water head required to mobilize the rest of pans having different base extensions is +17% greater than the theoretical required head, with a minimum of +13% for pan#7. As mentioned earlier, this increment is required to overcome friction forces which have different surface modes. Due to the accuracy in calculating buoyancy forces and all the weights of the pans and the surrounding soil rings, it could be concluded that protecting an underground circular tank against flotation can be done by adapting a weight of submerged/ non-submerged soil ring equal to the buoyancy force minus the weight of the pan/ tank. According to the required weight of the soil ring the length of the extension(x), see Fig.2-c, in any underground tank base can be determined by the following equation. This solution can guarantee an average safety factor of +17%:

$$V\gamma_w - w = \{(r+x)^2\pi - r^2\pi\}h_1\gamma_{sub} + \{(r+x)^2\pi - r^2\pi\}h_2\gamma_s$$

where: V = Volume of tank
γ_w = Density of water
w = Weight of tank
r = Outside diameter of the tank
x = Length of the tank's base extension
h_1= Underground water head measured from tank base level
γ_{sub} = Submerged soil density
h_2 = Height between soil top surface and underground water level
γ_s = Density of soil

The simplified form of the above equation can be written as follows:

$$2rx + x^2 = \frac{V\gamma_w - w}{\pi(h_1\gamma_{sub} + h_2\gamma_s)}$$

4. CONCLUSIONS

The following points can be concluded:

- Circular underground tanks are subjected to floating due to buoyancy forces created by the rise of water table level.
- Circular underground tanks constructed in soils having high water table levels should be stabilized against uplifting.
- Increasing the diameter of the base of an underground tank can increase its stability against floating.
- The required increment in the radius of the base of an underground circular tank can be safely taken equal to the thickness of a surrounding soil ring having a submerged/ non submerged weight, according to the highest expected underground water level, equal to the buoyancy force minus the weight of the tank.
- The mathematical derived equation for calculating the required base extension x is given as follows:

$$2rx + x^2 = \frac{V\gamma_w - w}{\pi(h_1\gamma_{sub} + h_2\gamma_s)}$$

REFERENCES

[1.] Chellis, R.D. (1992). Foundation Engineering, Chapter 7, McGraw-HILL Book Company, USA.
[2.] Darwish, A.M. "Anchoring of empty underground tanks against underground-water-induced floatation by using arched cable system", The IES Journal Part A: Civil & Structural Engineering, Vol. 1, No. 3, The Institution of Engineers, Singapore, August 2008.
[3.] Westbrook, R. (1984). Structural Engineering Design in Practice, 1st ed, Longman Inc., New York, USA.

INTERNATIONAL SYMPOSIUM on
ADVANCED ENGINEERING & APPLIED MANAGEMENT
– 40th ANNIVERSARY in HIGHER EDUCATION (1970-2010)
4 – 5 November, 2010, Hunedoara, ROMANIA

[1.]Gergely DEZSŐ, [2.]Gyula VARGA, [1.]Ferenc SZIGETI

INVESTIGATION THE CORRELATION BETWEEN TECHNOLOGICAL PARAMETERS AND THE WEAR IN CASE OF DRILLING WITH MINIMAL LUBRICATION

[1.]COLLEGE OF NYÍREGYHÁZA, 4400, NYÍREGYHÁZA, HUNGARY
[2.]UNIVERSITY OF MISKOLC, 3515, MISKOLC, HUNGARY

ABSTRACT:
College of Nyíregyháza and University of Miskolc has a common research project on environmentally conscious technologies. In the work published in this paper our purpose was to investigate the effects of technological parameters on the process of drilling and tool wear under outer minimal lubrication conditions.
Method of factorial experiment planning was applied for evaluation of experimental results. Relationships were determined between technological parameters and measured tool wears.
Physical model of twist drill was developed for calculating stress state and compare results with experimental wear measurements. This model shows good agreement with experiments and gives account of places of highest strain.
In this paper we demonstrate a formula describing the corner wear (VB_{Corner}) and flank wear (VB_{Flank}) as function of three quantity: feed (f), length of drilling (L_0) and volume of the lubricant (V_{oil}).
KEYWORDS:
environmentally technologies, parameters, drilling, tool wear, minimal lubrication conditions

1. INTRODUCTION

The stress and temperature distribution in the tool during the drilling process basically influences the lifetime of the drill and the rentability of machining by its effect to wear and vibrational state. That's why complex investigation of drill by experimental way and modelling is reasonable for it allows of determining relationship between tool wear, thermal state and stress state.

Finite element modelling of the twist drill was performed assuming minimal volume lubrication circumstances. We took into account that practical realization the principle of minimizing the environmental pollution in the European Union gradually got into the foreground even in production engineering [1, 2, 3, 9].

2. AIM OF EXPERIMENTS

Aim of our investigations was to develop a model for relationship between the wear and stress state of the twist drill, being suited for determining most loaded areas during the drillin process.

We used factorial experiment design for evaluating our experimental results on minimal lubrication drilling, so that we determine relationship between technological parameters of drilling and wear values.

In the modelling experimental data were used as input parameters.

We applied experiences of Department of Production Engineering at University of Miskolc when designing our experiments [4].

3. CIRCUMSTANCES OF EXPERIMENTS

At our experiments we used the following circumstances:
Machine tool: Universal milling machine, type: MU-250
Adjusted parameters:
Revolution number of main spindle: $n = 2250 rev/\min$,
Feeds: $f = 0{,}18 mm/rev$ and $f = 0{,}35 mm/rev$
Cutting speed: $v_c = 72{,}06 m/\min$
Cutting tool: twist drill (with right hand side flute) having inner cooling channels (Ø 10,2 K20 Gühring WRDG DIN 6537)
diameter: Ø10,2 mm,
material and coating: K20 carbide (monolith) twist drill with TiAlN coating.
Specimen material: cast iron, (EN-GJL-200 (MSZ EN 1561))
length of the holes: 30 mm,
Lubrication equipment: „NOGA MINI COOL"
Adjusted volumes: $\dot{V}_{oil} = 0 cm^3/h$, $\dot{V}_{oil} = 10 cm^3/h$, and $\dot{V}_{oil} = 28 cm^3/h$.
Oil: OMV cut XU (without chlorine).
Realization of minimum volume of lubrication was done by outer admission of the lubricants to the superficies of the twist drill by vaporizer type „NOGA MINI COOL" (we controlled two different volume per hour values: $\dot{V}_{oil} = 10 cm^3/h$ and $\dot{V}_{oil} = 28 cm^3/h$). Furthermore we have elaborated our experiments without using any coolants or lubricants. This was the dry machining, that is the dry drilling.

4. EVALUATION OF MEASURED WEAR RESULTS

Each measurement was repeated at least three times when the same parameter setup during executing our experiments. The evaluation was done by using mathematic statistics.

For characterisation of wear of the twist drill we have chosen the corner wear (VB_{Corner}) and flak wear (VB_{Flank}) [5, 6, 7]. The flank wear was measured on the direction radius at 3,5 mm from centre line on the main cutting edge, wear width into the direction of flank. By using of Factorial Experiment Design 12 experiments were elaborated (Table 1.).

The result of the experiments can be seen on Figure 1 and 2 for the values of corner and flank wear when the volume of coolants and lubricants were $\dot{V}_{oil} = 10 cm^3/h$, $\dot{V}_{oil} = 28 cm^3/h$, and for dry drilling.

On the figures can be seen that the wear of the twist drill was smaller at the case of higher value of coolants and lubricants ($\dot{V}_{oil} = 28 cm^3/h$).

Table 1. Codes of specimen and technological and experimental data applied

Number	Feed, *f*, mm/ford	Length of drilling, L_0, m	Oil volume, $\dot{V}_{oil}$, cm³/h
1	0,18	0,03	0,0
2	0,35	0,03	0,0
3	0,18	30,0	0,0
4	0,35	30,0	0,0
5	0,18	0,03	10,0
6	0,35	0,03	10,0
7	0,18	30,0	10,0
8	0,35	30,0	10,0
9	0,18	0,03	28,0
10	0,35	0,03	28,0
11	0,18	30,0	28,0
12	0,35	30,0	28,0

The evaluations of the experiments were done by the full Factorial Experiment Design.
Equations (2) and (3) valid when the drilling length varies in between $L_0 = 5m$ and $L_0 = 30m$, the volume of coolants and lubricants from $\dot{V}_{oil} = 10\, cm^3/h$ till $\dot{V}_{oil} = 28\, cm^3/h$, and the feed from $f = 0{,}18 mm/rev$ till $f = 0{,}35 mm/rev$.

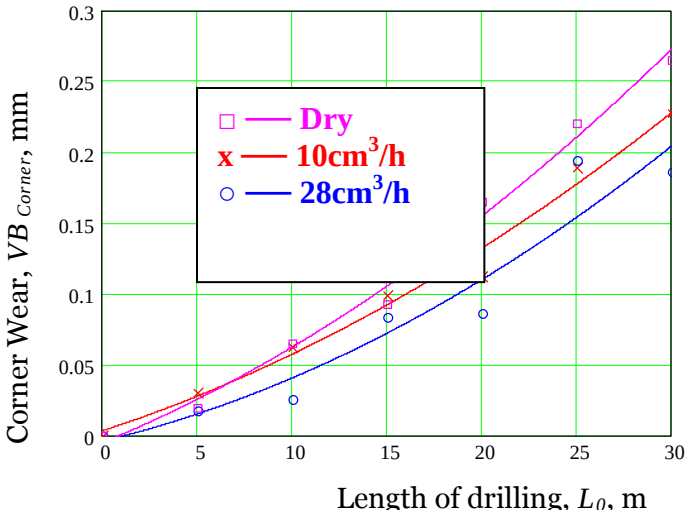

Figure 1. VB_{Corner} - Measured values of corner wear,

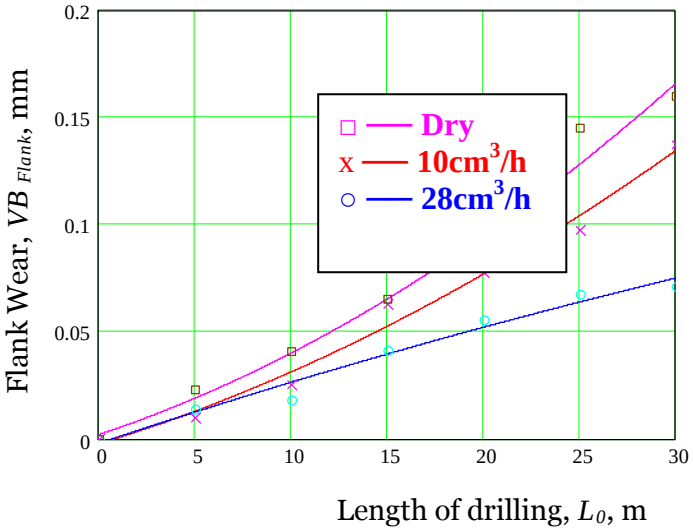

Figure 2. VB_{Flank} - Measured values of corner wear,

$$VB_{Corner} = k_0^{Corner} + k_1^{Corner} f + k_2^{Corner} L_0 + k_3^{Corner} \dot{V}_{oil} + k_{12}^{Corner} f \cdot L_0 + k_{13}^{Corner} f \cdot \dot{V}_{oil} + k_{23}^{Corner} L_0 \cdot \dot{V}_{oil} + k_{123}^{Corner} f \cdot L_0 \cdot \dot{V}_{oil} \quad (2)$$

$k_0^{Corner} = -0.0146$ $\quad k_1^{Corner} = 0.031$

$k_2^{Corner} = 5.789 \cdot 10^{-3}$ $\quad k_3^{Corner} = 2.118 \cdot 10^{-4}$

$k_{12}^{Corner} = 6.85 \cdot 10^{-3}$ $\quad k_{13}^{Corner} = -2.288 \cdot 10^{-3}$

$k_{23}^{Corner} = -1.41 \cdot 10^{-4}$ $\quad k_{123}^{Corner} = 3.268 \cdot 10^{-4}$

$$VB_{Flank} = k_0^{Flank} + k_1^{Flank} f + k_2^{Flank} L_0 + k_3^{Flank} \dot{V}_{oil} + k_{12}^{Flank} f \cdot L_0 + k_{13}^{Flank} f \cdot \dot{V}_{oil} + k_{23}^{Flank} L_0 \cdot \dot{V}_{oil} + k_{123}^{Flank} f \cdot L_0 \cdot \dot{V}_{oil} \quad (3)$$

$k_0^{Flank} = -2.686 \cdot 10^{-3}$ $\quad k_1^{Flank} = -0.04$

$k_2^{Flank} = 3.065 \cdot 10^{-3}$ $\quad k_3^{Flank} = 2.804 \cdot 10^{-4}$

$k_{12}^{Flank} = 8.575 \cdot 10^{-3}$ $\quad k_{13}^{Flank} = 8.497 \cdot 10^{-4}$

$k_{23}^{Flank} = -9.007 \cdot 10^{-5}$ $\quad k_{123}^{Flank} = -1.046 \cdot 10^{-4}$

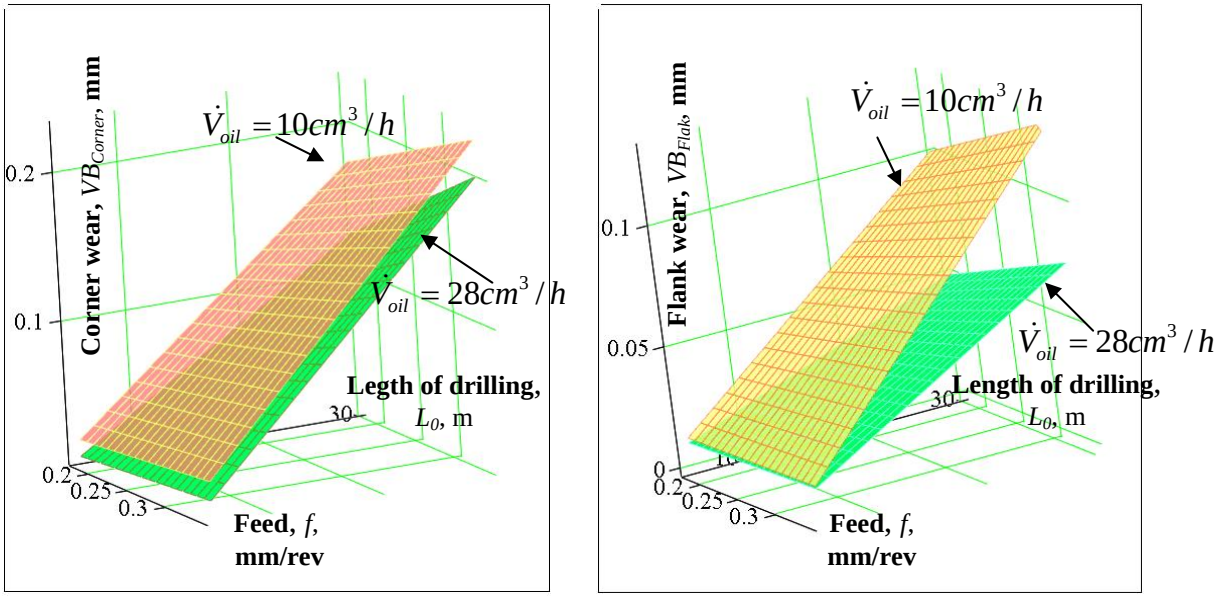

a) b)

Figure 3. Measured wear values of twist drill, a) corner wear, b) flank wear

5. MODELING

The thermal- and stress state of the drill was investigated by physical modelling. Our goal was to describe a model, which is simple as much as possible and stands in good accordance with observed wear picture.

The cutting force acting on edges was set as equal to the feed force per edge [8]. Material properties were of the K20 hard metal data.

We performed calculation for the sharp and the partly worn state of the tool. The worn state was modelled by rounding of the edges with 0,1mm and 0,2mm radii. The gradient of the stress far from the top in the drill was negligible, that's why we studied only 20mm long working part of the drill. So we avoided the superfluously large number of finite elements, and we managed to refine the mesh where it was necessary, i.e. where the gradient of physical quantities was large.

In our calculations both known mesh refinement methods were applied. The adaptive *h* refinement made the mesh denser where the target function changed rapidly, this decreasing the error of the finite element approximation. In our case, this resulted in refinement around edges and corners. The other method for improving the finite element mesh was the p-refinement, which increased the range of polynomial basis functions without changing of the original mesh, so making the approximating function much more flexible where the gradient of the target function was large. The software used realized these two types of refinement in two separate steps. Mechanical stress was used as target function for mesh refinement.

Finite element meshes of sharp and two worn drills are shown in Figures 4 and 5. Figure 4 demonstrates the finite element mesh and stress results for the sharp twist drill, Figure 5 shows the shape of a worn twist drill when the effect of the wear is represented by radius 0,1mm.

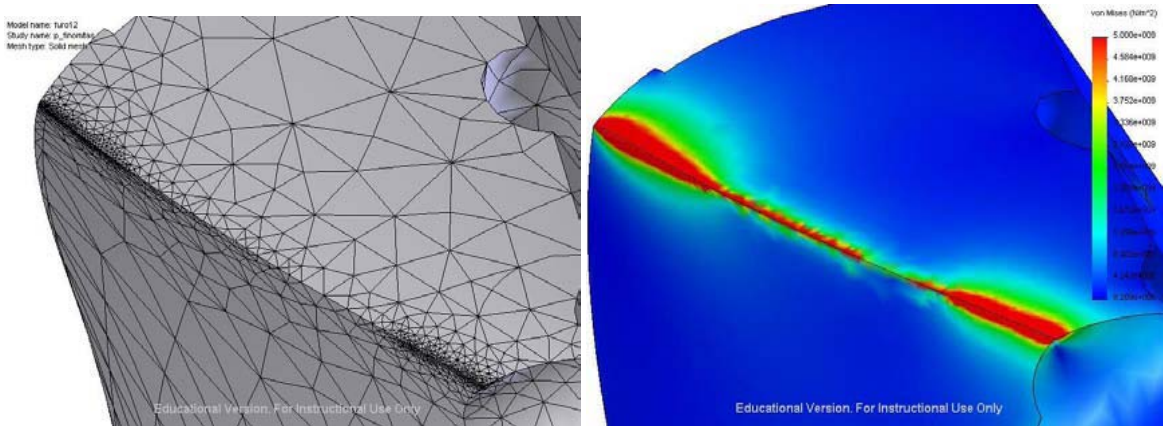

Figure 4. Mesh and stress state of sharp twist drill

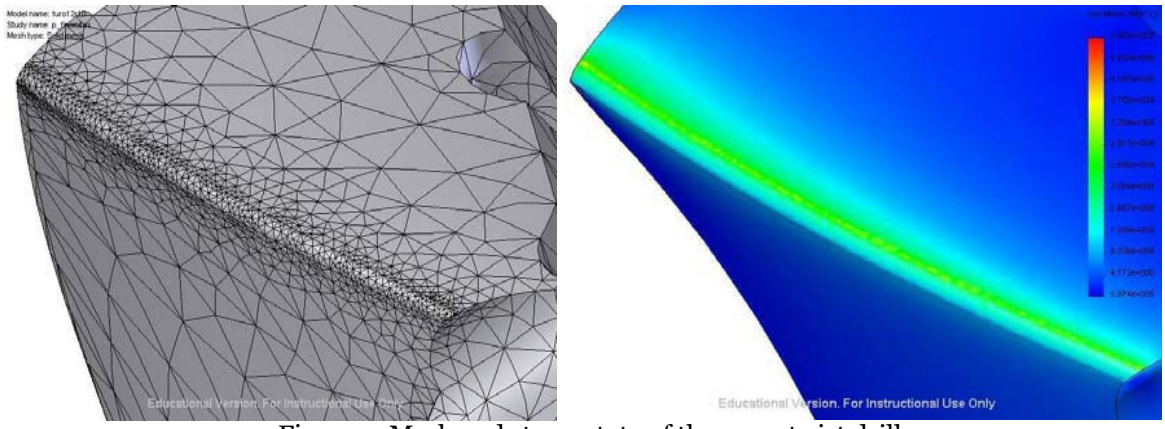

Figure 5. Mesh and stress state of the worn twist drill

6. CONCLUSIONS

This paper gave some remarks of successful implementation of dry and different near dry machining and for different experimental parameters.

- Formulas are derived by means of factorial experiment design describing the corner wear (VB_{Corner}) and the flank wear (VB_{Flank}) as function of three quantities: feed (f), length of drilling (L_o) and volume of the lubricant (V_{oil}).
- The feed of the twist drill and the applied volume of coolants and lubricants have significant effects to the wear of the twist drill.
- At the case of using similar volumes of coolants and lubricants, the measured values of flank wears (VB_{Flank}) were always smaller than the values of corner wears (VB_{Corner}).
- Modelling showed that wear changes significantly the stress state.
- In the first short period of drilling the maximum of the stress is at the chisel edge.
- Then as the wear increases, the stress distribution has been significantly changed spreading along the edge.

ACKNOWLEDGEMENTS
This work was supported as preferred research in 2010 by Scientific Committee of College of Nyíregyháza.

REFERENCES

[1.] WEINERT, K.: Trockenbearbeitung und Minimalschmierung. Springer Verlag Berlin 2000.
[2.] IGAZ, J., PINTÉR J., KODÁCSY J.: Minimálkenés. Gépgyártás XLVII. évf. 2007. 4.sz pp.: 22-31
[3.] KODÁCSY J., - NYÍRI J.: A fúrási folyamat összehasonlító vizsgálata különböző hűtés- kenési eljárásokkal. Gépgyártás XLVII. évf. 2007. 2-3.sz pp.: 27-29
[4.] DUDÁS, I., VARGA GY., CSERMELY, T., TOLVAJ, I. Umweltgerechte Zerspanungstechnik - Reduzierung und Ersatz von Fertigungshilfsstoffen beim Bohren (STD - 2EC jelű, ERB CIPACT 930167 témaszámú), Európai Közösség által finanszírozott kutatási projekt, Miskolci Egyetem, Gépgyártástechnológiai Tanszék, 4. Jelentés, 1995, pp.: 27.
[5.] VARGA, GY., DUDAS, I.: Modelling and Examinations of Environmentally Friendly Machining Processes, Proceedings of the 9th International Research/Expert Conference on Trends in the Development of Machinery and Associated Technology, TMT 2005, Antalya, Turkey, 26-30 September, 2005. pp.: 121-124. ISBN: 9958-617-28-5.
[6.] KANAI, M., KANDA, Y: Statistical Charasteristics of Drill Wear and Drill Life for the Standardized Performance Tests, Annals of the CIRP, 1978, Vol. 27, No. 1, pp.: 61-66
[7.] SZIGETI, F., VARGA, GY., PÉTER, L., SZÁZVAI, A.: Examination of outer and inner lubrication with minimum volume of lubricants when drilling of grey cast iron, Proceedings of the 7th International Multidisciplinary Conference, Baia Mare, Romania, 2007. p. 687-93,
[8.] DUDÁS I.: Gépgyártástechnológia I., A gépgyártástechnológia alapjai, Műszaki Kiadó, 2004, pp.583. ISBN 963 16 4030 2
[9.] DUDÁS, I.: Gépgyártástechnológia III. Miskolci Egyetemi Kiadó, Miskolc, 2003. p. 539.

INTERNATIONAL SYMPOSIUM on
ADVANCED ENGINEERING & APPLIED MANAGEMENT
– 40th ANNIVERSARY in HIGHER EDUCATION (1970-2010)
4 – 5 November, 2010, Hunedoara, ROMANIA

[1.] Jarmila ORAVCOVÁ, [2.] František LACKO, [3.] Peter KOŠŤÁL

DEVIATIONS OF WORKPIECE CLAMPING AS FACTOR HAVING INFLUENCE ON ACCURACY OF A SURFACE MACHINED

[1-3.] SLOVAK UNIVERSITY OF TECHNOLOGY, FACULTY OF MATERIALS SCIENCE AND TECHNOLOGY,
INSTITUTE OF PRODUCTION SYSTEMS AND APPLIED MECHANICS, TRNAVA, SLOVAKIA

ABSTRACT:
The paper deals with some questions regarding workpiece clamping in fixtures from the point of view of production inaccuracies. These inaccuracies consist of deviation of medium economical accuracy, deviation of seating and deviation of the fixture. The final achievable workpiece accuracy depends on the components of the mentioned deviations. The paper describes influence of the support point choice on deviation extend of the surface machined. Way for workpiece seating deviation calculation is given in the paper when the workpiece seats on various supporting points.
KEYWORDS:
seating deviation, non-identity deviation, clamping deviation, basic positioning surface, basic dimensional surface, supporting element

1. INTRODUCTION

We usually meet great amount of products different in shape and in their dimensions within engineering production praxis. The requirements on workpiece accuracy, and such way also on workpiece seating are permanently higher. For that reason it is important to appreciate suitability of the clamping equipment design for each actual case. Among various factors influencing the final achievable accuracy of the surface machined belong primary inaccuracies brought into production process.

2. DEVIATIONS INFLUENCE ON DIMENSIONAL ACCURACY OF THE SURFACE MACHINED

Various requirements concerning accuracy of the individual surfaces machined are set by designer for components production. Possibility to achieve the required dimensional accuracy for the concrete component depends on more factors. The important factor having influence on accuracy of the surface machined is way of workpiece positioning and its clamping in fixture. Another factor is the accuracy of fixture positioning within machine tool. The accuracy of the final dimension also depends on values of cutting parameters chosen for machining, on stiffness of the entire system and on accuracy of mutual position between tool and workpiece. The said factors generate great amount of deviations, which can be divided into following three deviation groups:

- deviation of medium economical accuracy $\boldsymbol{s}$,
- seating deviation $\boldsymbol{\varepsilon}$,
- fixture device deviation $\boldsymbol{\varepsilon_p}$

The required dimension accuracy $\boldsymbol{v}$ given by dimension tolerance $\boldsymbol{T_v}$ prescribed in drawing is stipulated by the formula:

$$T_v \geq \sqrt{\varepsilon^2 + s^2} + \varepsilon_p \qquad (1)$$

Value of the deviation of medium economical accuracy $\boldsymbol{s}$ is usually obtained by practical experiences and is elaborated for individual technological machining techniques of various

surfaces. Requirement for economical production is considered within this deviation, because to close tolerances can cause inadequately high production costs connected with surface machined and to cause increase of the final product price.

So as to find out the deviation of the fixture device $\boldsymbol{\varepsilon_p}$ for the concrete workpiece it is to find out the individual components which are part of the total deviation. The deviation of the fixture device consists of sum of the clamping deviation ε_{py}, the deviation of fixture positioning within machine tool ε_{po}, the deviation of tool adjustment ε_{pn} and of the dividing device deviation ε_{pd}. So value of the fixture device deviation can be calculated as:

$$\varepsilon_p = \varepsilon_{py} + \varepsilon_{po} + \varepsilon_{pn} + \varepsilon_{pd} \tag{2}$$

The seating deviation is to be taken as:

$$\varepsilon = \varepsilon_n + \varepsilon_s \tag{3}$$

where

ε_s - means the deviation (value) by which the produced dimension is modified as influence of workpiece seating through support surface,

ε_n - means the non-identity deviation of the basic positioning surface against basic dimensional surface, when it is to be taken as:

$$\varepsilon_n = \sum_{i=1}^{n} T_{zi} \cos\beta_i \tag{4}$$

where

T_{zi} - means tolerance of the distance between positioning and basic dimensional surface

$cos\beta_i$ – means angle between perpendicular line of the positioning surface and perpendicular line of the surface machined.

3. SUPPORTING ELEMENT INFLUENCE ON DEVIATION OF THE DIMENSION PRODUCED

An important decision step is choice of the clamping and positioning surfaces of the workpiece. In the end, this step influences achievement of the required dimensional accuracy of the surface machined. It is to take into consideration the basic dimensional surface, i.e. the surface from which the distance required machined surface is given on the drawing, when making decision, which surface should be taken as positioning surface.

The most common cases of workpiece seating in the fixture are when the positioning workpiece surface is:

- plane,
- external cylindrical surface,
- cylindrical opening.

When a prismatic component is positioned on two parallel stepped planes (Fig. 1), the deviation of supporting elements ε_e occurs because of allowed workpiece inaccuracies an because of shape of fixture supporting elements. The component of the deviation ε_e into direction of the dimension produced is ε_s. In this case means:

$$\varepsilon_s = L_1 \tan\varepsilon_e \tag{5}$$

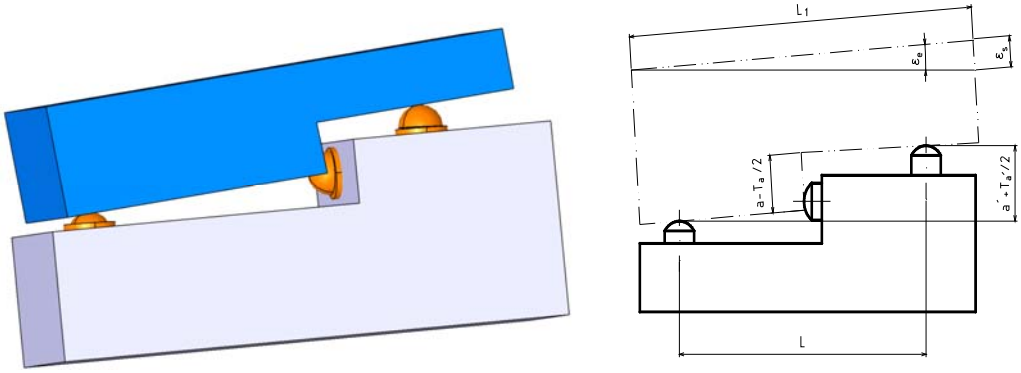

Fig. 1 Prismatic component on two paralel stepped planes

When positioning is made through cylindrical opening, the line contact between supporting elements and workpiece comes into existence. Value of the deviation ε_s is given as:

$$\varepsilon_s = \varepsilon_e = \Delta + T_d + T_{d'} \tag{6}$$

When a cylindrical surface is positioned in a prismatic support, the supporting contact is made through two straight lines. The value of the deviation ε_s depends on the dimensional basis. The said basis can be axis of the positioning surface or creating line of the rotary profile (Fig.2). For the first mentioned case means:

$$\varepsilon_s = \frac{T_d \cos\gamma}{2\sin\frac{\alpha}{2}} \tag{7}$$

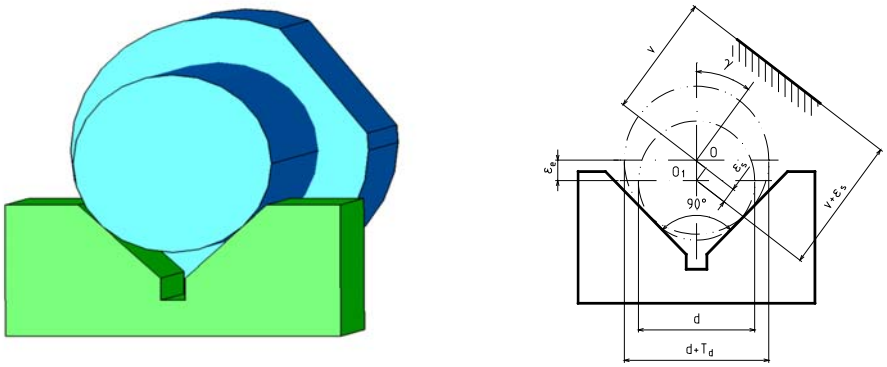

Fig. 2 Cylindrical surface in a prismatic support, when basis the axis is

The influence of the maximal deviation of machined surface distance on the surface angle of inclination and on choice of the basic dimensional surface is shown on workpiece positioned in prism. The results are summarised in the table 1.

Table 1

Positioning deviation ε_{max} for φ40h8 and prism angel **α=90°** [mm]			
Inclination angle of the surface machined γ	Basic dimensional surface		
	More distanced creating line of the positioning surface	Axis of the positioning surface	Les distanced creating line of the positioning surface
0°	0,008077	0,027577	0,047077
15°	0,007137	0,026637	0,046137
30°	0,004382	0,023882	0,043382
45°	0,000000	0,019500	0,039000
60°	0,005711	0,013788	0,033288

4. CONCLUSION

The proper design and construction of some clamping or fixing devices is not so simple task. Such equipment should meet many various requirements, which can influence its proper function an utilization. That is why it is to take into consideration and to analyze which requirements are the most important ones and in this connection decide which deviations should be minimalised primary.

Acknowledges

OPVaV-2008/2.2/01-SORO – 26220220055 – Laboratory of flexible manufacturing systems with robotized manipulation supported by no drawing production

This article was created with the support of the OP Research and development for the project **Laboratory of flexible manufacturing systems with robotized manipulation supported by no drawing production ITMS 26220220055,** co-financing from the resources of European Regional Development Fund.

Operačný program VÝSKUM a VÝVOJ

Support research activities in Slovakia/ Project is co-financing from resources EU

Európska únia
Európsky fond regionálneho rozvoja

REFERENCES

[1.] Charbulová, Marcela - Mudriková, Andrea - Danišová, Nina: Fixture devices for production systems. - Vega č. 1/0163/10. In: AMO Conference. - ISSN 1313-4264. - 10. International conference, 27 - 29 June 2010 AMO 10, 27 June - 01 July 2010 CEEPUS (2010), s. 1-6

[2.] Charbulová, Marcela - Mudriková, Andrea: Clamping Devices for Intelligent Production Systems. In: AMO Conference. - ISSN 1313-4264. - Vol. 3. 9. International Conference Advanced Materials and Operations : Scientific Reports. Project CII-BG-0203-02-0809 CEEPES. Bulgaria, Kranevo 24-28 June 2009. - Sofia : Technical University of Sofia, 2009, s. 597-601

[3.] Charbulová, Marcela: Modular clamping systems. In: Annals of Faculty of Engineering Hunedoara - Journal of Engineering. - ISSN 1584-2673. - Tom V, Fasc 3 (2007), s. 49-54

[4.] Košťál, Peter - Velíšek, Karol - Zvolenský, Radovan: Intelligent Clamping Fixture in General. In: Lecture Notes in Computer Science. - ISSN 0302-9743. - Vol. 5315 : Intelligent Robotics and Applications. First International Conference, ICIRA 2008, Wuhan, China, October 15-17, 2008. Part II (2008). - ISBN 978-3-540-88516-0, s. 459-465

[5.] Košťál, Peter - Velíšek, Karol: Flexible manufacturing cell´s clamping fixture. In: Proceedings of the 9th Biennial ASME Conference on Engineering Systems Design and Analysis (ESDA2008) : Haifa, Israel, 7.-9.7.2008. - : ASME, 2008. - ISBN 0-7918-3827-7. - CD Rom

[6.] Matúšová, Miriam - Hrušková, Erika: Element selection algorithm of modular fixture system. In: Annals of Faculty of Engineering Hunedoara - Journal of Engineering. - ISSN 1584-2673. - Tom V, Fasc 3 (2007), s. 36-40

[7.] Matúšová, Miriam - Javorová, Angela: Modular clamping fixtures design for unrotary workpieces. In: Annals of Faculty of Engineering Hunedoara - Journal of Engineering. - ISSN 1584-2673. - Tom VI, Fasc 3 (2008), s. 128-130

[8.] Mudriková, Andrea - Hrušková, Erika - Horváth, Štefan: Areas in flexible manufacturing-assembly cell. - článok vyšiel v časopise: Annals of Faculty of Engineering Hunedoara - Journal of Engineering, ISSN 1584-2673, Tome VI, Fascicule 3, 2008, str. 123-127. In: Scientific Bulletin. - ISSN 1224-3264. - Vol. XXII (2008), s. 293-298

[9.] Mudriková, Andrea - Velíšek, Karol - Košťál, Peter: Clamping fixtures used for intelligent assembly systems. In: ISCCC 2009 : Proceedings of the 2009 International Symposium on Computing, Communication and Control, October 9-11, 2009, Singapore. - Singapore : International Association of Computer Science and Information Technology Press, 2009. - ISBN 978-9-8108-3815-7. - S. 9-15

[10.] Oravcová, Jarmila - Košťál, Peter - Riečičiarová, Eva: Active parts of clamping devices. In: Annals of The Faculty of Engineering Hunedoara. - ISSN 1584-2665. - Tom VIII, Fas. 1 (2010), s. 235-236

[11.] Velíšek, Karol - Košťál, Peter - Zvolenský, Radovan: Clamping Fixtures for Intelligent Cell Manufacturing. In: Lecture Notes in Computer Science. - ISSN 0302-9743. - Vol. 5315 : Intelligent Robotics and Applications. First International Conference, ICIRA 2008, Wuhan, China, October 15-17, 2008. Part II (2008). - ISBN 978-3-540-88516-0, s. 966-972

INTERNATIONAL SYMPOSIUM on
ADVANCED ENGINEERING & APPLIED MANAGEMENT
– 40th ANNIVERSARY in HIGHER EDUCATION (1970-2010)
4 – 5 November, 2010, Hunedoara, ROMANIA

[1.]Tamás ENDRŐDY, [2.]Adrián SZŐNYI

ANALYSING THE 2-7 DOF HUMANOID ROBOT ARM CONSTUCTIONS AND THE POSSIBILITIES OF CONTROLLING/LEARNING THEIR MOVEMENTS

[1] UNIVERSITY SZENT ISTVÁN & UNIVERSITY OF SZEGED, HUNGARY
[2] FACULTY OF MECHANICAL ENGINEERING OF TECHNICAL AND ECONOMICAL UNIVERSITY OF BUDAPEST, HUNGARY

ABSTRACT:
Previously the authors mainly dealt with the construction and modelling of **2 DOF** (Degree of Freedom) and 2 links Humanoid robot arms which were operated in agonist-antagonist mode by 2 pairs of **PAM** (Pneumatic Artificial Muscle) elements to a target point in plane. The presented constructions were modelled and controlled by modifying the angles between shoulder-upper arm (α_{u0}) at the shoulder and between the upper arm -forearm (β_{f0}) at elbow artificial articulations. The kinematic systems fairly determine the trajectories of their structure joints, thus if the trajectory and derivatives are given - generally an inverse dynamic task has to be solved.
This lecture deals with the construction of **2-7 DOF** and **3-4 links** robot arms modelling and comparing to each other their advantages-disadvantages. The authors operate the links of the robot arm with the flexor—extensor agonistic-antagonistic pairs of **PAM** elements, also developed and analysed adaptive/learning algorithms for them.
By developing the humanoid robot arm constructions — modelling and mimicking the very complex structured and controlled human arm one can be successful only by significantly simplifying the structures of the human muscles, tendons, articulations and bones. Similarly one can be successful in guiding and learning the limbs' movements if we make simplifications in modelling the functionalities of the human brain.
KEYWORDS:
Humanoid robot arm, kinematic constructions, **PAM**, controlling movements, Folium model, tripod

1. INTRODUCTION

After some experiences having the manageable working points for any agonist-antagonistic pair of **PAM** (Pneumatic Artificial Muscle) elements, automatic/crude and adaptive/heuristic models have been made for driving the artificial wrist articulation of the robot arm through efficient series of points (line/arc segments) to the target point by harmonically controlling the flexor and extensor pneumatic muscles of the upper- and forearm [**1.**], [**3.**], [**4.**].

The punctiform considered elbow articulation can move on a circle with radius $\mathbf{R=l_{upper\ arm}}$ and centre $\mathbf{S_o}$ (shoulder) of a **2 DOF** humanoid robot arm; while the wrist point is guiding from a starting point to the plane target point by modifying the angles between shoulder-upper arm (α_{uo}) at the shoulder and between the upper arm-forearm (β_{fo}) at elbow artificial articulations. The punctiform wrist can move on any given trajectory inside a semicircle with radius $\mathbf{R=l_{upper\ arm} + l_{upper\ arm}}$ and $\mathbf{S_o}$ centre by series of generated short lines/circle arcs up to the target point. Thus the wrist can go round arbitrary obstacles in plane.

Instead of the more expensive stepping-motor and servo-motor actuators the angle-measuring sensors, mass flow rate valve and on-off proportional pressure valves were used which were programmable by the height or number of electronic pulses. The electronic pulses-pressure steps controlling mode was chosen by agonist-antagonist operated **PAM** elements. Thus the human brain controlled flexor-extensor muscles were mimicked in the **pulses-steps** operating mode. A complex controlling equipment and its virtual models were developed with crude and

adaptive/heuristic learning algorithms for controlling the movement trajectories of the wrist of the robot arm [**3.**].

There are many publications with agonist-antagonist pairs of **PAM** elements controlled by stepping-motors and servo-motor actuators e.g. at the Robot-laboratory of the Johns Hopkins University [**5.**], where they can also solve the guiding process from a starting wrist-point to the target-point in a plane, modifying the **angle1** and **angle2** by **a, b** and **c** parametres defining the position, velocity and acceleration by given functions. This example can also show the difficulties in controlling the punctiform wrist articulation via a given trajectory and its derivatives (**Picture 1**). This example gave a test and learning task possibilities following a given trajectory and its derivatives in the case of using stepping-motors. One can give 3 parametres for the position, velocity and acceleration -using the ($\mathbf{T-T_o}$) time slice every time- to go to the target point by changing the angles at the "shoulder" and the "elbow". The task is more difficult if one would like to follow a trajectory, etc.

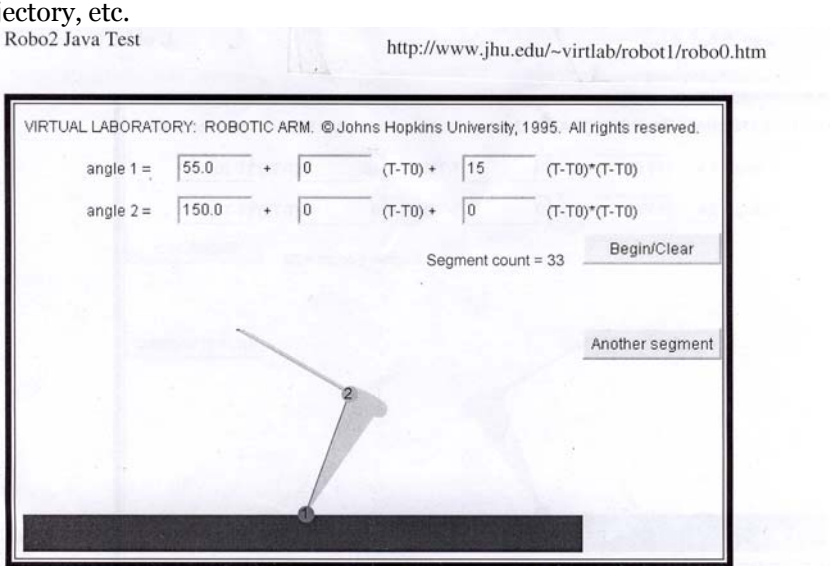

Picture 1. A test example: one can practice and learn how he can follow a given trajectory with its derivatives by giving 3 parametres and using the ($\mathbf{T-T_o}$) time slice every time

The humanoid robot arm generally has shoulder, elbow, wrist artificial articulations and -at the other end of the hand- a holder modellizing the human articulations and fingers/thumb.

It is well-known that the humanoid robot can possess more than **1 DOF** at any articulation by the artificial bones and muscles of its kinematic systems. Any way at the industrial robot generally every link/tag has only **1 DOF**.

Thus ***at the shoulder*** -as at an origo- one can realise ***1, 2 or 3 flexing DOF the upper arm around x,y and z axes***, besides sometimes it has a ***1 twisting DOF*** around the axe of the upper arm;

- at other end of the upper arm -***at the elbow*** origo articulation- one can realise ***1 flexing DOF*** *for* ***the forearm*** around the perpendicular axe to the upper arm, besides it can have ***1 twisting DOF around the axe of the forearm*** (around the radius);
- at wrist **1 flexing DOF** for the hand around the perpendicular axe to the forearm;
- finally at the other end of the hand there is a holder by the thumb and the fingers, but this later one can be operated by other typed tools, not by PAM elements.

These twisting DOFs can be operated and analysed separately from the other flexing DOFs at the shoulder, elbow and wrist. In the case of 3 DOF flexing around parallel axes it can lose the unambiguous trajectory moving of the hand's holder point from starting to target point.

This lecture mainly deals with constructing 3 or more DOF kinematic systems, humanoid robot arms, their virtual models and their guiding/learning movements. Our basic motivation was that we should define several kinds of kinematic (mechanical) constructions without building up them but their virtual model could be operated for the given tasks and could be tested ([**3.**]; see also: Balara, M. et al., (2004), [**6.**]; Fagg, A. H.,et al., 1999, [7.]).

Having designed these robot arm constructions (and all of their parts) kinematically we gave the adequate constraints in every artificial articulation in order to be able to assemble the whole robot arm afterwards. ***Thus every motion type, controlling and/or learning their typical movements should be studied/analysed without building up all of our constructions*** to spare a lot of time, money and material.

2. ROBOT ARM CONSTRUCTIONS

The artificial shoulder articulation can be modellized by a ball-and-socket joint (spherical joint) or 3 cylindrical flexing joints and 1 twisting joint around the upper arm-axe.

The elbow can be modellized by 1 cylindrical flexing joint.

Finally the artificial wrist can be realised virtually by 1 cylindrical flexing joint and 1 other twisting joint around the forearm-axe which operates the forearm and hand equally. Keeping the notations for the artificial articulations' angles at shoulder (**α**) and at elbow (**β**), we can choose (**γ**) at wrist for the angle between the axes of the hand and forearm. Thus, at the beginning of the movements to guard the unambiguous solution, one can transform the arm's holder point by (**Δγ = 0**), that is the forearm and the hand will move together. One can move the **Inventor-made virtual robot arm models** directly and also by ***VBA Macro program***. So, this lecture deals with guiding and controlling movement-strategies in the following cases:

- guiding the wrist or holder point of the robot arm from a starting to the target point,
- guiding the wrist/holder point movements via given trajectory and its derivatives.

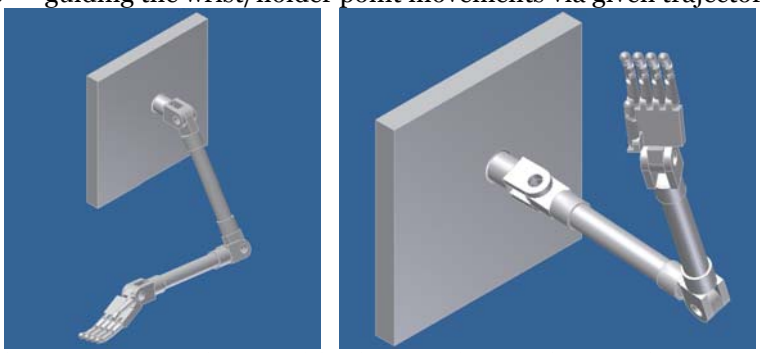

Figure 1. A 6 DOF humanoid robot arm in two characteristic states

There are some moving/controlling strategies but all of them can be characterised by a kind of inverse dynamic controlling process. The Figure 1 shows a 6 DOF robot arm which was analysed by object oriented VBA Macro programs, too. We tested its movements step by step at some given trajectories. In this robot arm we wanted to modellize **1-1 flexing DOF** by cylindrical joints at the shoulder, elbow and wrist artificial articulations.

Figure 2 shows a **5 DOF** humanoid robot arm (which had not flexing DOF at the wrist, that is **Δγ = 0**) in two characteristic states: at the starting state of its wrist and at end state with its wrist at the target point of a plane.

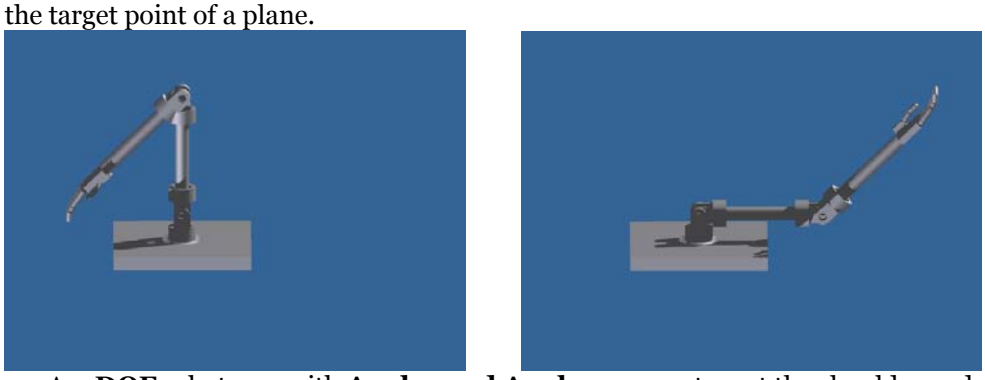

Figure 2. A **5 DOF** robot arm with **Angle1 and Angle2** parametres at the shoulder and elbow articulations were identified for the control VBA Macro program

The controlling Macro program is the following:

```
Sub Move()
Dim AssemblyDocument As AssemblyDocument
Dim Angle1Param, Angle2Param As Parameter
Dim AssCompDef As AssemblyComponentDefinition
Dim CY1 As Integer
Set AssemblyDocument = ThisApplication.ActiveDocument
Set AssCompDef = AssemblyDocument.ComponentDefinition
Set Angle1Param = AssCompDef.Parameters.Item("Angle1")
Set Angle2Param = AssCompDef.Parameters.Item("Angle2")
For CY1 = 1 To 45
Angle1Param.Value = 90 / 180 * 3.14 – 2* CY1 / 180 * 3.14
AssemblyDocument.Update
Angle2Param.Value = 45 / 180 * 3.14 + 2 * CY1 / 180 * 3.14
AssemblyDocument.Update
Next        End Sub
```

Figure 2 shows how these Inventor made kinematic models could be controlled by identifying the **I.1.** (constraint) = **Angle1** and the **II.1.** (constraint) = **Angle2** parameters of this **5 DOF** robot arm after modificated them by the above VBA macro program. We can see the results only for the Angle1 and Angle2 parameters. We also mention that only **2 flexing DOF** must be used out of the **3 flexing DOF** around the same (parallel) direction axes to preserve the unambiguous solution. In the **6 DOF** case the **3rd one** at the wrist, e. g. the **III.1.** (flexing constraint) has to be fixed at the first motion step. At the shoulder and wrist articulations **1-1 twisting DOF** (**I.2.** and **II.2.** constraints) can be realised around the axes of the links (actual pieces of the arm), the twisting angles are addable sum. At the shoulder we can use **1 other flexing DOF** by a cylindrical joint (**I.3.** constraint) to realise the **3rd DOF** at the shoulder. But it is more useful if one has a **7 DOF** robot arm with **3 flexing DOF** around the **x,y** and **z** axes besides the **1 twisted DOF** around the axe of the upper arm at the shoulder.

There are some other applications of the robot arms: e.g. Figure 3 shows a virtual kinematic model (**5 DOF** Reha-robot arm) for rehabilitating movements for somebody who has arm, muscles, tendons, articulations, but after a stroke or spinal/cerebral injury needs motion-rehabilitation by a kind of robot control. This model was also tested with some VBA macro programs by circular moving steps for any planar target points.

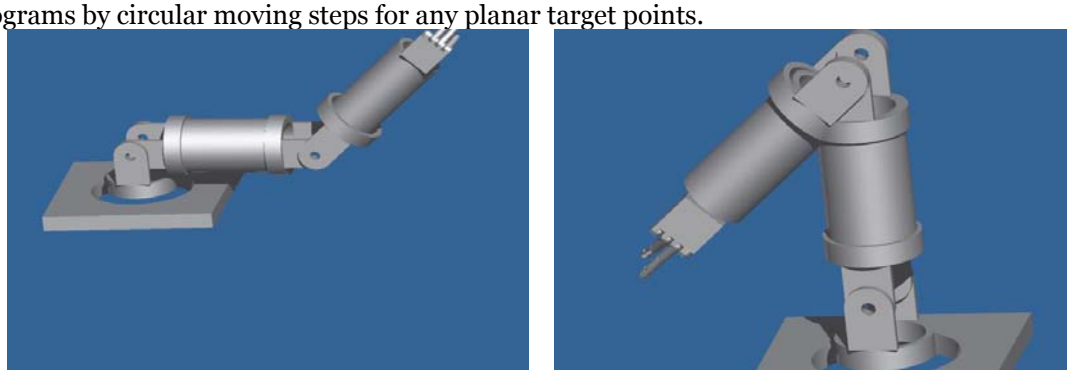

Figure 3. This Reha-robot arm also can be controlled by the same VBA Macro program

Figure 4 shows two experimental arm-prosthesis constructions: **4 DOF** prosthesis for replacing the upper and forearm and the other one with **3 DOF** for a person who partially lost this upper arm, too.

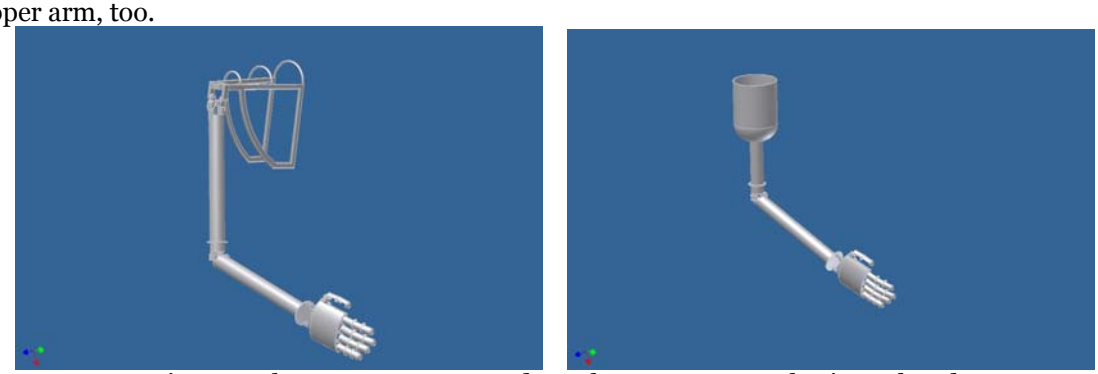

Figure 4 There are a **4 DOF** and another **3 DOF** prosthesis analysed

3. APPLICATION STEWART-PLATFORM STRUCTURE DEVELOPING A 3 DOF ROBOT ARM ARTICULATION

The *Stewart-platform* (known as 'hexapod' too) has **6 DOF**, and it has high payload-to-weight ratio (alike PAMs) since the payload is carried by several links in parallel (Ronen Ben-Horin, 1996, [**14**.]). Generally it is used as a base of the motion in the flight or automobile simulators, too (Picture 2).

We can similarly use a **3 DOF** tripod **PAM** controlled structure as a more simple variation of Stewart-platform. This

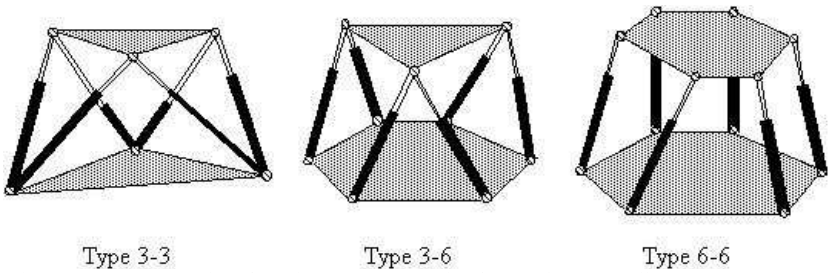

Picture 2. Examples for the Stewart-platform 'hexapod'

compact kinematic structure is analogue the **3 DOF** spherical joint at the artificial shoulder articulation of the **6** or **7 DOF** controlled by **PAM**s humanoid robot arms analysed above. It can replace the **2** or **3 flexing/twisting DOF** articulation with **2** or **3** cylindrical joints or **1** spherical joint.

Picture 3 shows the developed tripod-platform virtual model flexing/twisting around **x, y** and **z axes** in **CCW (+)** and **CW (-)** directions, which shows also its efficiency.

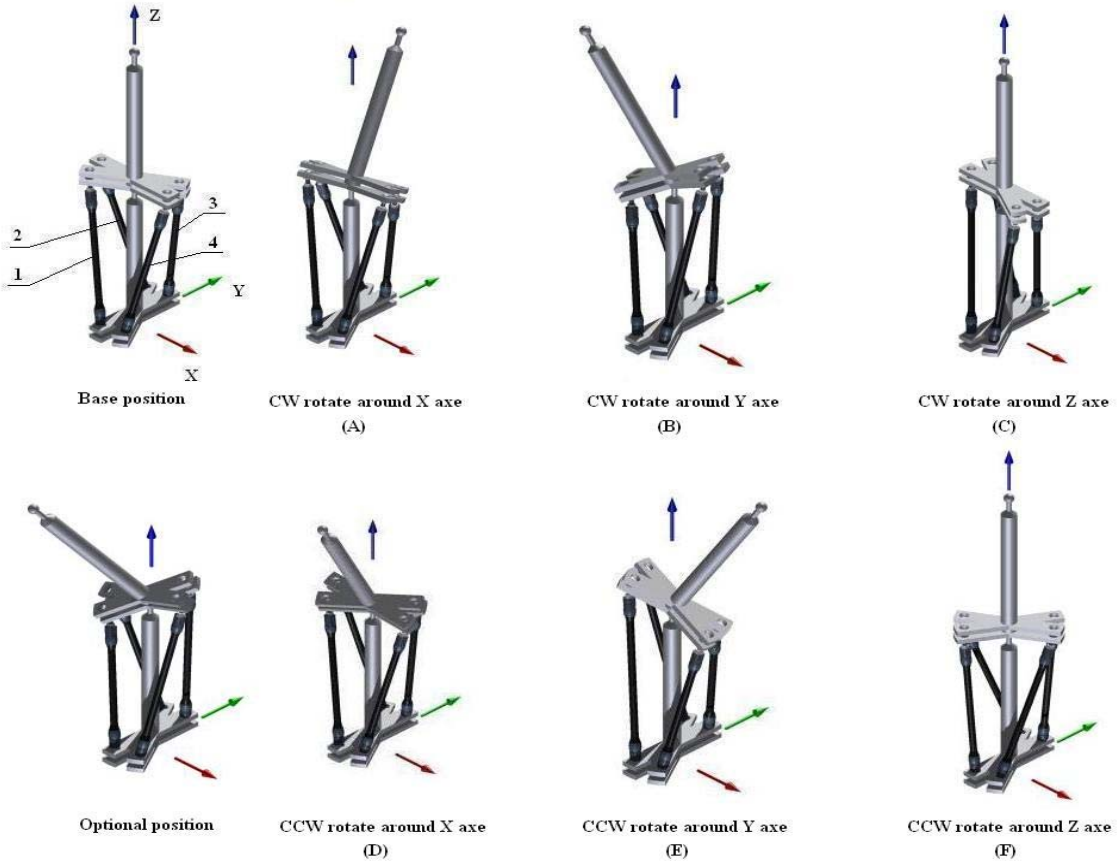

Figure 5. The basic solution of the developed **Stewart** tripod-platform by **PAM** actuators

This Table 1 shows the logical conditions with **C**=contraction and **L**=lengthening the named **PAM** elements for operating the rotation of the platform around the **x,y** and **z** axes**.** The main information which comes from this table, is that the structure **does not need 4 PAM** elements for moving the platform in 3 different ways -for having **3** different **flexing/twisting DOF**. If any one of this table-rows will be cleared, all the columns will be different. This means that three PAM could give constraints for the **3 flexing/twisting DOF** structure. The reason why it is better using **4** muscles here is that during the motions all the agonistic-antagonistic PAM elements have a twin/pairing element which gives more stability and balance for this developed tripod Stewart-type platform. The even-number of muscles give the easier way to solve the inverse kinematic task, too. Thus all the muscles need to be supported by another one operating in flexor or extensor mode. Many researches progressed this agonistic-antagonostic habit and finally used positioning by muscle pairs. The precise positioning is possible by using the sliding mode with the chosen PAM elements (Chin-I Huang et al., 1998, [**11.**]; and [**3.**]; [**4.**]; [**2.**]; [**15.**]).

Table 1 The state-table of the basic motions of this Stewart tripod-platform

	Motion					
PAM	A	B	C	D	E	F
1	L	C	L	C	L	C
2	C	C	C	L	L	L
3	C	L	L	L	C	C
4	L	L	C	C	C	L

4. MOVING-STRATEGIES FOR 2-7 DOF ROBOT ARM

The authors would like to expound some fundamental robot arm moving-strategies which can solve inverse dynamic controlling programming task but we analysed only the unambiguous flexing DOF cases:

- 1st possibility: One can determine the inverse transformation (more generally inverse Jakobi) $T_{j\,i} = T_{ij}^{-1}$ matrix which is simple enough to apply, but only in the 2 DOF cases and besides when only the starting and the target point are given for the robot arm holding point. If the trajectory is also given, we must apply the inverse transformation matrix for $P_i(x_i, y_i, z_i)$ points backward from the target point up to the starting point- densely enough (n-times) along the trajectory. But first we can choose the 2 DOFs (articulations/links) which are most important in the task to solve. In this method we can get a lot of difficulties even in the 2 DOF cases also if we have to solve the task with given 1st and 2nd derivatives of the trajectories and/or the robot arm possesses not only (parallel) flexing DOFs. To solve this task, e. g. the object oriented Inventor VBA Macro programming system is suitable for this aim: writing the controlling program.
- 2nd possibility: We can use the ***Inventor CAD system*** itself to produce the inverse dynamic programs to control movement-steps: by defining the "trajectory-rail/track" (for the robot arm holder point) as a continuous polyline which consists of any number of lines/arcs, segments with equal tangents between them constraint; otherwise we can use the so-called transitional constraint between the cylindrical/spherical holder (virtually) and a series of surface-pairs producing the composed trajectory. One can store data in a table at **n** pieces of the trajectory before the robot arm has to go along these $\mathbf{P_i(x_i, y_i, z_i)}$ connecting points, the angles $(\boldsymbol{\alpha_i, \beta_i})$ of the shoulder and the elbow articulations for these places. That is the angles $(\boldsymbol{\alpha_i, \beta_i})$ will be needed in the expected applications to control the robot arm along the given trajectory from the starting to the target point.
- 3rd possibility: We can design/make also adaptive/heuristic control programs ***considering the given trajectory and the position-errors in every i-th steps*** between the starting and the target point Endrődy T. et al., 2009, [**1.**];. These adaptive control algorithms could be added with a kind of heuristic learning and/or remembering possibilities and if the adaptive/ heuristic learning control algorithms do not work (e.g. stopped further of the target point, one must use a kind of direct/crude algorithm to finish the process going to the target point. There are some direct and heuristic/adaptive moving algorithms on the **Figure 6** and **Figure 7**.

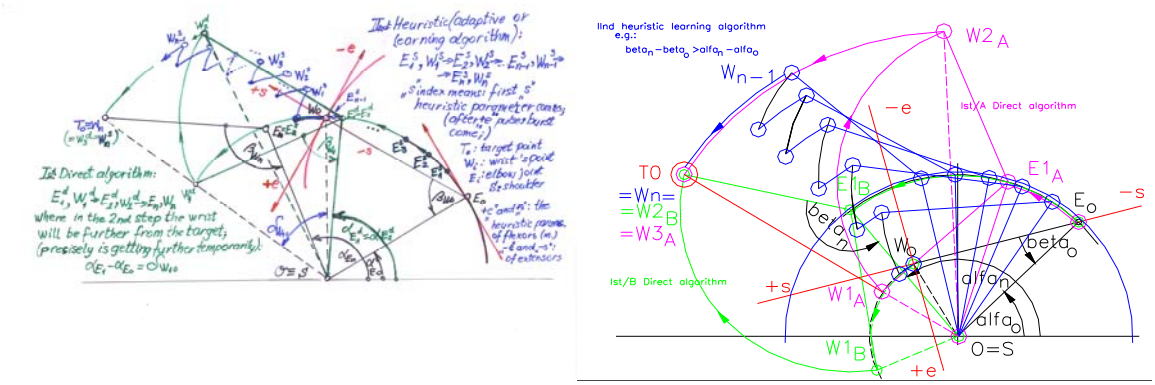

Figure 6 Direct and heuristic algorithms for controlling PAM elements of the upper- and forearm by electronic pulses controlled pneumatic valves

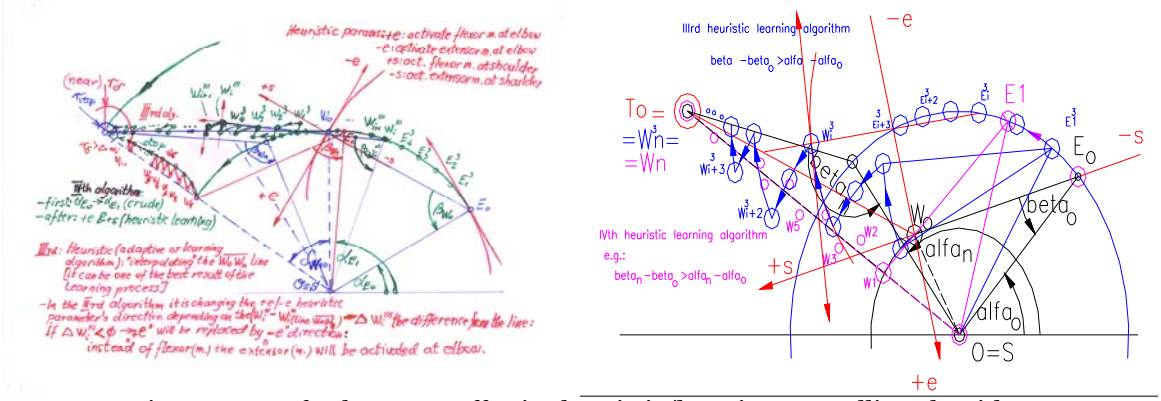

Figure 7. Two further more effective heuristic/learning controlling algorithms

In every controlled step the errors between the expected and the actual arrived i-th point of the trajectory can be corrected for the following experiences. For this aim the actual difference can be analysed between the wanted and the actual wrist/holder point supplementing the predicted

deviation of the holder position of the robot arm to produce better and better controlling program (Fagg,. A. H., 1997, [**9.**]).

- ❖ 4th possibility: One can use Stewart typed tripod platform or other planarly actuated parallel robot construction for replacing e.g. a **3 DOF** spherical joint at the shoulder artificial articulation (see Figure 5). At this type solution one can enjoy the kinematic and dynamic advantages of the parallel robot constructions, which are the following:
- higher payload-to weight ratio (alike PAM elements) in the consequence of the payload is carried here by several link in parallel,
- higher accurancy without cumulative joint error,
- simpler solution of the inverse dynamic equations, etc. (Ronem Ben-Horin, et al., 1996, [**14.**]).
- ❖ 5th and the best possibility (but can be entirely realised only in the future):

The best controlling system for humanoid robot arm (upper arm-forearm-hand) could mime the human brain neuronal networks' controlling process for the muscles, tendons and bones of the human limbs by a neural network e.g. the MLPNN structure with an inverse dynamic model and artificial muscle PAM elements (see: Ahn, K.A. and Anh, H. P. H. (2009), [**8.**]).

According to our present knowledge the required limbs' conscious movements are controlled first of all by motor cortex' nuclei given commands via the spinal cords' efferent neuronal networks. The eyes and visual cortex' neuronal networks watch the movements of the arm's articulations along the wanted trajectory. The visual system generates error-series along the trajectory between the actual and required positions, velocity, accelerate (Figure 8). This schema came from Smagt, van der P. (1998, [**12.**]) and it was added by the authors. Besides from the periphery, the neuronal network of Cerebellaris folium/folia gets information by the afferent fibres about the state of the tones and positions of the muscles, tendons, articulations and bones. Thus the nervous system can predict the position, error of the positions, the tensil forces and moments/torques, too. The Cerebral Motor-cortex nuclei can give the main commands for the muscles in cosequence of the actual learned knowledge made by the Cerebellar Foliums' networks. The learning process based the percepted and predicted position,velocity and acceleration errors during all of the motions. This is a very complex process, thus only the main information paths could be emphasized here.

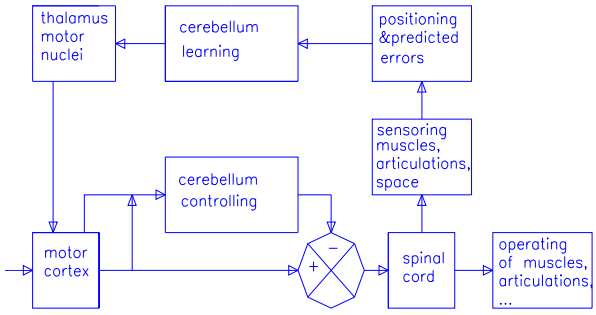

Figure 8. Controlling the human limbs' motion by the Motor cortex, Cerebellaris folium/folia and Spinal cord

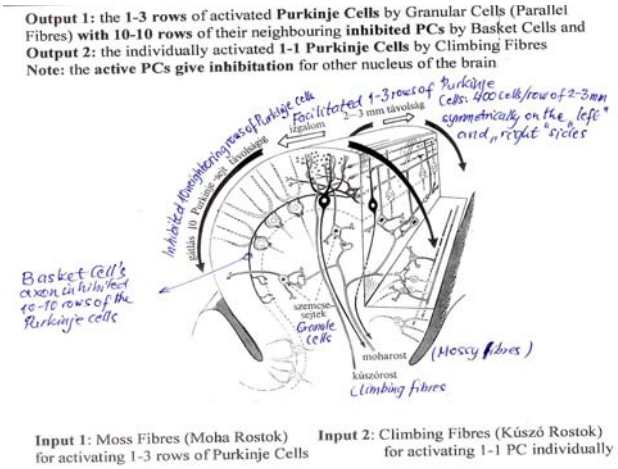

Figure 9. The main neuronal network of a typical Cerebellaris Folium by Pr. Szentágothai, J.

The cerebellum has homogenous folium-structures and deep nuclei for connecting other parts of the brain. The folium-networks have special "inverse neuronal structures", as Prof. J. Szentágothai said: it is similar to an organist who presses all the keys except the one which gives the sounds (Szentágothai, J., 1977, [**13.**]). Thus every folium can control by its inverse structure the agonistic-antagonistic and synergic mode operated muscles in an adequate way, because as well-known, the limbs and the articulations of the arm **need inverse dynamic control**. Besides the cerebellar folium-neuronal-structures can learn from the sensed and predicted positions, parameters of the limbs for the sophisticated movements. The "output" Purkinje neurons of folium bring inhibiting distributed commands via the cerebellar deep nuclei for spinal cord and via thalamus nuclei for cortex, so the folium-structures have very effective fluencies in controlling and learning the sophisticated movements of the arm. We developed a new controlling/learning neural system flowchart (Figure 10) which hopefully can use the advantages of the Folium's inverse structure to operate efficiently the needed inverse dynamic control process [**16.**]).

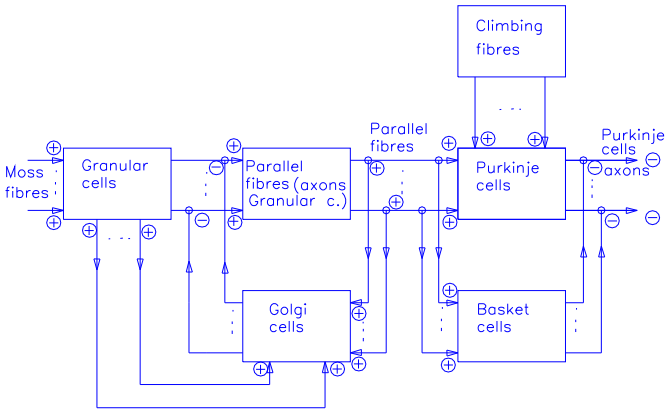

Figure 10. The neural model of the folium with feed-back and feed-forward control possibilities

5. CONTROLLING THE ROBOT ARM'S CIRCULAR STEPS BY PAM ELEMENTS

Till now we have not analysed how the robot arm-links can be moved along an arc separately/one-by-one and together along a kind of boved trajectory in the case of **2 flexing DOF** arm by the **PAM** elements. These **PAM** elements can contract linearly in different extent. The **PAM**s operate only in one direction (pulling) so it must be used together with its agonist or antagonistic pair, similarly to the muscles in the human body. Last years we made a few test-bed constructions to analyse its highly nonlinear character (e. g. **F** [N], **Δl** [mm] and **p** [bar, Pa]), its other important parameters: its exact longitudinal (± 0.01mm) sliding control process and defined maximal contractions (e. g. ± 10 %). After fixing the angle domain (e. g. 0-90°) at every flexing articulation for moving a link of the robot arm, one can define (for the rotational torque) the measures of the actual force-arm [mm], the point of application of the force and the direction line of the force, that is the fixing places of the artificial muscle elements. One of the main problems at any **2 DOF** robot arm-controlling process is how the given trajectory function of the holder point can be interpolated by little arcs from the starting point up to the target point (see: the **Figure 6** and **Figure 7**, or more detailed: the publication [**3.**]). First we have to find better and better interpolating by arcs „in second order" for α_i and β_i at the elbow and the shoulder articulations. Then at any movement strategies controlling algorithms mentioned, it is more simple to map the α_i, β_i [°] angles to the controlled contractions of the agonistic-antagonistic pairs of **PAM** elements at the shoulder and elbow artificial articulations.

6. CONCLUSIONS

The earlier cerebellar models demonstrated the possibilities of the role of the folium in solving the inverse dynamic control tasks of the robot arm movements. The main possibility came by the Purkinje cells generated inhibitory output.

One must take into consideration that the new light mass-weight artificial muscles (**PAM**s) changed the traditional robot control methods. Recently large contradictions came between the earlier cerebellum models and understanding its role in the motor cortex-cerebellum-spinal cord neuronal networks for the controlling and learning processes of the human limbs' movements. It seems more important to define inverse and forward models, too. We ought to modellize not only the motor apparatus, sensory organs but also the external world from which the actual movement controlling tasks come. The mimesis of the cerebellum could get more attention in present-day research.

REFERENCES

[1.] T. Endrődy, J. Gyeviki, J. Sárosi and Adrián Szőnyi, Constructions of humanoid robot arm, controlling and learning the movements of their joints, Synergy 2009 Conference, Gödöllő, Hungary, 30 August - 3 September, 2009, p 6

[2.] Sárosi, J., Gyeviki, J., Endrődy, T., Szabó, G. and Szendrő, P. (2009), Characteristics of the pneumatic artificial muscles, Synergy2009 Conference, Gödöllő, Hungary, 30 August - 3 September, 2009, p 6

[3.] Endrődy, T., Gyeviki, J., Sárosi, J., Véha, A., and Toman, P. (2008), Automatic and learning model of a planar humanoid robot arm controlled by 2 pairs of antagonistic PAMs moving to a target, ICoSTAF, Szeged, Hungary, 5-6 November, 2008, pp. 367-375

[4.] Toman, P., Gyeviki, J., Endrődy, T., Sárosi, J. and Véha, A. (2008), Design and fabrication of a test-bed aimed for experiment with pneumatic artificial muscle, International Conference on Science and Technique in the Agri-food Business, Szeged, Hungary, 5-6 November, 2008, pp. 361-366

[5.] http://www.jhu.edu/~virtlab/robot1/robo0.htm, Johns Hopkins University's Robot-laboratory, 1995
[6.] Balara, M. and Petík, A. (2004), The properties of the actuators with pneumatic artificial muscles, Journal of Cybernetics and Informatics, Volume 4, pp. 1-15.
[7.] Fagg, A. H., Barto, A.G., Zelevinsky, L. (Univ. of Massach., Dep. of Comp. Sci), Houk, J.C., Northwestern Univ., Dep. of Physio.: Using Crude Corrective Movements to Learn Accurate Motor Programs for Reaching,1999, pp.20-24
[8.] Ahn, K. A. and Anh, H. P. H. (2009), Design and implementation of an adaptive recurrent neural networks (ARNN) controller of the pneumatic artificial muscle (PAM) manipulator, pp.1-13.
[9.] Fagg, A. H., Zelevinsky, L., Barto, A. G. and Houk, J. C. (1997), Using Crude Corrective Movements to Learn Accurate Motor Programs for Reaching, Ch 6, NIPS*97 Workshop,1997, pp. 20-24.
[10.] M. Kawato Hikaridai, (1997), Multiple Internal Models in the Cerebellum, Ch5, NIPS*97 Workshop, 1997, pp. 17-19.
[11.] Chin-I Huang, Chih-Fu Chang, Ming-Yi Yu, Li-Chen Fu, Sliding-Mode Tracking Control of the Stewart Platform, 1998, p. 8
[12.] Smagt, van der P. (1998), Cerebellar control of robot arms, Inst. of Robotics and System Dynamics German Aerospace Center/DLR, Connection Science 10, pp.301-320.
[13.] Szentágothai, J. (1977), Funkcionális anatómia (Functional anatomy), Medicina publish., pp. 206-212., pp. 1426-1439., pp. 1484-1490.
[14.] Ronen Ben-Horin, Moshe Shoham and Shlomo Djerassi, Kinematics, Dynamics and construction of a planarly actuated parallel robot, Dep. of Mechanical Engineering Technion – Israel Institute of Technology, Haifa, 1996, p.2
[15.] P. Tomán, J. Gyeviki, T. Endrődy, J. Sárosi, A. Véha, Z. Szabó (2009),Sliding mode control of a robot arm driven by pneumatic muscle actuators, Journal of Engineering Annals of Faculty of Engineering Hunedoara, Tome VII (year 2009),Fascicule 4, (ISSN 1584-2665), pp.95-100
[16.] T. Endrődy: Developing product and prototype in integrated CAD/CAM system by application of complex modelling, effective communication, data- and knowledge base, PhD Dissertation, Eötvös Loránd University Budapest, Faculty of Informatics, Budapest, 2005, p. 174

INTERNATIONAL SYMPOSIUM on
ADVANCED ENGINEERING & APPLIED MANAGEMENT
– 40th ANNIVERSARY in HIGHER EDUCATION (1970-2010)
4 – 5 November, 2010, Hunedoara, ROMANIA

[1.]Flavius Lucian PATER, [2.]Ludovic Dan LEMLE

A DYNAMIC PROCESS MODEL BASED ON A FUNCTIONAL EQUATION

[1.] UNIVERSITY "POLITEHNICA" TIMIŞOARA, DEPARTMENT OF MATHEMATICS, ROMÂNIA
[2.] UNIVERSITY "POLITEHNICA" TIMIŞOARA, FACULTY OF ENGINEERING HUNEDOARA, ROMÂNIA

ABSTRACT:
In this paper, we present some new and original proofs of known results related with unitary operators acting on $B(H^2)$ algebra.
A.M.S.(2010) Subject Classification: *47A20*
KEYWORDS:
reproducing kernel, multipliers algebra, anti-unitary operator, polar decomposition

1. INTRODUCTION

First, let us remind some of the results well known in the literature.

Definition 1.1 *We define the Bergman's space* $H^2(B_d)$ *such that*

$$H^2(B_d) = \{ f \text{ analytic} \mid \int_{B_d} | f(z) |^2 \, dm(z) < \infty \}$$

where m represents a Lebesgue measure on B_d.

Theorem 1.2 *Let H a Hilbert space, then an operator* $T \in B(H)$ *is of rank 1 if and only if there exist* $\eta \in H$ *such that*

$$T(\xi) = (\xi \otimes \overline{\eta})(\xi) = \langle \xi, \eta \rangle \xi \ , \ (\forall)\xi \in H .$$

Definition 1.3 *For any operator* $T \in B(H)$ *given by*

$$T = \sum_{k=1}^{N} x_k \otimes y_k$$

for N fixed and $x_k, y_k \in H$ *with* $(x_k \otimes y_k)u := \langle u, x_k \rangle y_k$ *, we put associated the* $\tau(T) = \sum_{k=1}^{N} \langle x_k , y_k \rangle$ *. The linear form* τ *is called* ***trace***.

Proposition 1.4 We have $\tau(T) = \sum_{j \geq 1} \langle Te_j , e_i \rangle$ *for any orthonormal base* $(e_j)_{j \geq 1}$ *in H. Moreover, if* $R \in B(H)$, *we have* $\tau(TR) = \tau(RT)$

Let B_d be the unit ball from the complex space $\mathbf{C}^d$, $d = 1, 2, \ldots$ i.e.

$$B_d = \{ z = (z_1, z_2, \ldots, z_d) \in \mathbf{C}^d : \|z\| < 1 \},$$

where by $\|z\|$ we denoted the usual norm associated of inner product from $\mathbf{C}^d$:

$$\|z\|^2 = |z_1|^2 + |z_2|^2 + \ldots + |z_d|^2$$

Let P be the algebra of all holomorphic polynomials f . Each $f \in$ P have an expending in a Taylor series of form

$$f(z) = a_0 + a_1 z_1 + \ldots a_n z_n$$

and we can define the norme $\| f \|$ for this polynomial as the norm in l^2 there sequence of Taylor coefficients.

(1.1) $$\|f\|^2 = |a_0| + |a_1| + \ldots + |a_n|$$

We consider the case $d > 1$ and we denoted by P the algebra of all complex holomorphic polynoamials f which depends of $z = (z_1, z_2, \ldots, z_d)$. Each polynomial f has a unique expansion in a finite series

(1.2) $$f(z) = f_0(z) + f_1(z) + \ldots f_n(z),$$

where f_k is the homogeneous polynomial of degree k.

Now, we'll introduce a seminorm on P . Let be the homogeneous polynomial of degree k:

$$f(z) = \sum' a_{i_1 \ldots i_d} z_1^{i_1} \cdot \ldots \cdot z_d^{i_d}$$

where the degree of f is given by max($i_1 + \ldots + i_d$).

Let $E = \boldsymbol{C}^d$ be the linear space over $\boldsymbol{C}$ of dimension d having the inner product:

$$< z, w >= z_1 \overline{w}_1 + z_2 \overline{w}_2 + \ldots + z_d \overline{w}_d .$$

We build the following spaces $E^{\otimes_k}$ thus:

$E^0 = \boldsymbol{C}$

$E^1 = E$

…

$$E^{\otimes k} = \underbrace{E \otimes E \otimes \ldots \otimes E}_{k} = \{\varphi : E' \times \ldots \times E' \mapsto C\}$$

where E' is duality space of E. We have

$E^k = \{ \varphi \in E^{\otimes_k} : \varphi(f_{\tau(1)}, f_{\tau(2)}, \ldots, f_{\tau(k)}) = \varphi(f_1, \ldots . f_k), (\forall) f_i \in E', i = 1,\ldots,k \}$,

where $\tau \in S_k$ and S_k is the group of permutation.

First, we'll prove that the elements of H^2 can be identified with the elements of the symmetric Fock space over E, $F_+(E) = E^0 \oplus E^1 \oplus E^2 \oplus \ldots$, the sum from the right member denoting an infinite direct sum of Hilbert spaces (see [1], [3]). Also related work was done by ([2], [4], [5], [6], [7]).

Proposition 1.5. *For each $f \in P$, let $Jf \in F_+(E)$, (see [1]).*

$$Jf = (\xi_0, \xi_1, \ldots)$$

Where the sequence $\{\xi_k,\}_k$ is the Taylor coefficients for $k \leq n$ and for $k > n$, $\xi_k = 0$. Then J is a unique extension at an antiunitary operator from H^2 at $F_+(E)$.

Proposition 1.6. *Each element from H^2 may be considered like an analytic function in B_d, having the following form:*

$$f(z) = \sum_{k=0}^{n} < z^k, \xi_k > \quad , z = (z_1, \ldots, z_d) \in B_d,$$

where the norm $\|\cdot\|$ from H^2 is given by $\|f\|^2 = \sum_k \|\xi_k\|^2 < \infty$. Such function satisfyies the following increasing condition

$$|f(z)| \leq \frac{\|f\|}{\sqrt{1 - \|z\|^2}},$$

for any $z \in B_d$.

2. ON SOME UNITARY REPRESENTATIONS ON $B(H^2)$ ALGEBRA

Proposition 2.1. *Let A be a closed, normed $B(H^2)$ sub-algebra, generated by the multiplication operators de M_f , $f \in P$.*

Each element of A is a multiplication operator M_f for any $f \in M$, which is extending continuously to the closed unit ball $\overline{B}_d$ and there exists a natural homeomorphism from $\overline{B}_d$ to the space σ(A) of all complex homeomorphisms of A, $x \to w_x$,defined by

$$w_x(M_f) = f(x) \ , \ ||x|| \leq 1$$

For each $f \in M$ we have

$$\lim_{n \to \infty} \| M_f^n \|^{1/n} = \sup_{\|x\| \leq 1} |f(x)|$$

Proof. As the application $f \in M \to M_f \in B(H^2)$ is a isometric representation of the multipliers algebra on H^2 which carries the unit of M in the unit from $B(H^2)$, is enough to work on M . That means to consider A the closure in M of the polynomial algebra, practically needing to identify the space of maximal ideals.

Due to the inequality $||f||_\infty \leq ||f||_M$ from proposition 1.6, one can deduct that for every polynomial f and any $x \in \boldsymbol{C}^d$ satisfying $||x|| \leq 1$, we have

$$|f(x)| \leq \sup_{z \in B_d} |f(z)| = ||f||_\infty \leq ||f||_M$$

This implies there exist a unique complex homomorphism $w_x \in A$, satisfying:

$$w_x(f) = f(x), (\forall) f \in P$$

For all $g \in A$ we have now a continuous natural extension $\tilde{g}$ of g to the closed unit ball by putting

$$\tilde{g}(x) = w_x(g), \quad ||x|| \leq 1$$

$x \to w_x$ is a continuous application of the unit ball $\boldsymbol{C}^d$ on its image from $\sigma(A)$. In order to show its surjectivity, let w be an element of $\sigma(A)$. Then $(\forall) y \in \boldsymbol{C}^d$ we can consider the linear functional

$$\hat{y}(z) = < z, y >, \quad z \in \boldsymbol{C}^d$$

The application $y \to \hat{y}$ is an anti-linear application of $\boldsymbol{C}^d$ onto the space of linear functionals of P and we have $||\hat{y}||_M \leq ||y||$. Indeed suppose $y \neq 0$. Then the linear function

$$u(x) = \hat{y} / ||y|| = < x, y > / ||y||$$

belongs to the coordinate system of $\boldsymbol{C}^d$. Proposition 1.9 implies $||u||_M \leq 1$, hence $||\hat{y}||_M \leq ||y||$. So $y \to w(\hat{y})$ defines an antilinear functional on $\boldsymbol{C}^d$ satisfying

$$|w(\hat{y})| \leq ||\hat{y}||_M \leq ||y||, (\forall) y \in \boldsymbol{C}^d$$

It follows there exist a unique vector x in the unit ball of $\boldsymbol{C}^d$ such that

$$w(\hat{y}) = < x, y >, \quad y \in \boldsymbol{C}^d$$

Hence, $w(f) = w_x(f)$ for each linear functional f. As w and w_x are continuous unitary homeomorphisms of A, as P is the algebra generated by the linear functions and by constants and as P is dense in A it can be deduced that $w = w_x$ and so we've identified the maximal ideals space of A with the closure of the unit ball of $\boldsymbol{C}^d$. From the elementary theory of commutative Banach algebras we deduce that for every $f \in A$,

$$\lim_{n \to \infty} ||f^n||_m^{1/n} = r(f) = sup\{|w(f)| : w \in \sigma(A)\} = sup\{|\tilde{f}(x)| : ||x|| \leq 1\} = ||f||_\infty$$

q.e.d.

The d – shift considered as d – tuple of multiplication operators onto H^2 is not always convinient for calculations. We'll need the following equivalent definition of $(S_1, \ldots, S_d)$ as being operators „created" on the symetric Fock space $F_+(E)$.

Proposition 2.2 *Let $e_1, \ldots, e_d$ be an orthonormal base for a Hilbert space E of dimension d. Define the operators $A_1, \ldots, A_d$ on $F_+(E)$ by*

$$A_i \xi = e_i \xi, \quad \xi \in F_+(E)$$

where by $e_i \xi$ denote the projection of $e_1 \otimes \xi \in F(E)$ onto the symetric subspace $F_+(E)$. Let $z_1, \ldots, z_d$ an orthogonal system of coordinates $z_i(x) = < x, e_i >$, $1 \leq i \leq d$. Then it exists an unique unitary operator $W : H^2 \to F_+(E)$ such that $W(1) = 1$ and

(2.1) $$w(z_{i_1}, \ldots, z_{i_n}) = e_{i_1} \cdot \ldots \cdot e_{i_n}, \quad n \geq 1, i_k \in \{1,2,\ldots,d\}$$

In particular, the d – tuple of operators $(A_1, \ldots, A_d)$ is unitary equivalent with the d – shift.

Proof. For any $x \in E$ satisfying $||x|| < 1$ define an element $v_x \in F_+(E)$ by

$$v_x = 1 \oplus x \oplus x^2 \oplus x^3 \oplus \ldots$$

It is obvious that $||v_x||^2 = (1 - < x, y >)^{-1}$ for $||x||, |y|| < 1$ and more general

$$< v_x, v_y > = (1 - < x, y >)^{-1}, \quad ||x||, ||y|| < 1$$

We deduced this using $< z^k, w^k >_{E^k} = < z, w >_{E}^k$. $F_+(E)$ is generated by the set $\{ v_x : ||x|| < 1 \}$. Let $\{ u_x : ||x|| < 1 \}$ the set of H^2 functions definite în 1.11 and let * the canonical conjugation unique on E defined by $e_i^* = e_i$, as

$$(a_1 e_1 + \ldots + a_d e_d)^* = \bar{a}_1 e_1 + \ldots + \bar{a}_d e_d$$

then, we have

$$< u_x, u_y > = (1 - < y, x >)^{-1} = (1 - < x^*, y^* >)^{-1} = < v_{x^*}, v_{y^*} >$$

For any x, y from the unit open ball of E. By Proposition 2.1 [3] there exists an unique unitary operator $W : H^2 \to F_+(E)$ such that $W(u_x) = v_{x^*}$, $||x|| < 1$. $W(1) = W(u_0) = v_0 = 1$. Let $x \in E$, $||x|| \leq 1$

and let f_x be the linear functional on E defined $f_x(z) = < z, x >$. We have $\| f_x \|_{H^2} \leq 1$ and from that $\| f_x^n \|_{H^2} \leq 1$ for $n = 0,1,2,\ldots$. Hence for any $0 \leq r < 1$ and any $z \in B_d$ we have

$$u_{rx}(z) = (1- < z, r x >)^{-1} = \sum_{n=0}^{\infty} r^n < z, x >^n = \sum_{n=0}^{\infty} r^n f_x^n(z) \in H^2$$

Similarly $v_{rx^*} = \sum_{n=0}^{\infty} r^n (x^*)^n \in F_+(E)$.

Taking $W(u_{rx}) = V_{rx^*}$ and comparing the coeficients of r^n, we obtain

$$W(f_x^n) = (x^*)^n \ , \ for\ n=0, 1,\ldots$$

It can be deduced that

(2.2) $$W(f_{x_1} ,\ldots, f_{x_n}) = x_1^* x_2^* \ldots x_n^*$$

For any $x_1, x_2, \ldots, x_n \in E$. Indeed, by puting

(2.3) $$L(x_1, x_2, \ldots, x_n) = W(f_{x_1} ,\ldots, f_{x_n})$$

$$R(x_1, x_2, \ldots, x_n) = x_1^* x_2^* \ldots x_n^*$$

for $x_1, x_2, \ldots, x_n \in E$, it can be observed that L and R are symetric n – antilinear aplications which are equal when $x_1 = x_2 = \ldots = x_n \in B_d$. Hence $L = R$ and (2.1) is true. (2.2) is obtained by taking $x_k = e_{i_k}$ in (2.3).

(2.2) obviously implies $WS_i = A_i W$ for i= $1..d$ so the d – tuples $(S_1, \ldots, S_d)$ and $(A_1, \ldots, A_d)$ are unitary equivalent.

REFERENCES

[1.] Arveson, W. (1997). Subalgebras of C* - algebras III; multivariable operator Theory (preprint).
[2.] Coburn, L.A. (1973). Singular integral operators and Toeplitz operators on odd spheres, Ind. Univ. Math J 23, 433-439.
[3.] Pater, F., Juratoni, A., Bundău, O.(2008). O., On some reproducing kernel property for C^d orthonormal basis. Bulletin for Applied Computer Mathematics, B.A.M., ISSN 0133-3526, Hungary.
[4.] Popescu, G. (1991). Von Neumann inequality for $(B(H)^n)_1$, Math Scand 68, 292-304.
[5.] Rudin, W. (1976). Principles of Mathematical Analysis, 3rd edition, McGraw Hill.
[6.] Segal ,I.E. (1956). Tensor algebras over Hilbert spaces, Trans. Amer. Math. Soc, 106 –134.
[7.] Sz-Nagy , B. and Foias, C. (1970). Harmonic analysis of operators on Hilbert spaces, American Elsevier, New York.

INTERNATIONAL SYMPOSIUM on
ADVANCED ENGINEERING & APPLIED MANAGEMENT
– 40th ANNIVERSARY in HIGHER EDUCATION (1970-2010)
4 – 5 November, 2010, Hunedoara, ROMANIA

[1.]Flavius Lucian PATER, [2.]Liana Rodica PATER

A DYNAMIC PROCESS MODEL BASED ON A FUNCTIONAL EQUATION

[1.] UNIVERSITY "POLITEHNICA" TIMIŞOARA, DEPARTMENT OF MATHEMATICS, ROMÂNIA
[2.] "TIBISCUS" UNIVERSITY OF TIMIŞOARA, FACULTY OF ECONOMICAL SCIENCES, ROMÂNIA

ABSTRACT:
In this article is presented a new approach to some fundamental techniques of solving dynamic programming problems with the use of functional equations.
A.M.S.(2010) Subject Classification: 37J99
KEYWORDS:
dynamic programming, optimum, recurrence, resources, activity

1. INTRODUCTION

Dinamic programming represents a group of techniques and methods of optimization which helps solving large categories of problems of the form:

(1) $\max R(x_1,x_2,\ldots,x_n)=g_1(x_1)+g_2(x_2)+\ldots+g_n(x_n)$

with the restrictions:

(2) $x_1+x_2+\ldots+x_i+\ldots+x_n=Z$
$x_i\geq 0$

knowing that $g_1,g_2,\ldots,g_n$ are mostly exponential type functions:

(3) $g(x)=A+Be^{-cx}$

This mathematical theory treats especially the resources usage problem (people, materials, machines, etc.) with the purpose of their optimal recovery (see [1, 6, 8, 9]).

The notions used in dinamic programming are the following:

- *resources*: any means or reserves that can be mobilized and employed in order to achieve a productive activity;
- *activity*: any posible use of a resource;
- *profit:* partially or wholly the result obtained by the use of resources.

Profit can be measured with different units but by convention it is assumed that:

- profits are measured with the same unit of measurement in all activities;
- an activity-profit resource allocation is independent of all other activities;
- total profit obtained in the end is the sum of individual profits of the business.

Other important concepts are:

- *utility-function*: function of the type g (x) mentioned above and which is measured by size of profit made in relation to the resources allocated;
- *target-function*: function of the type R (x_1, x_2 ,..., x_n) (see [1]), which is the total amount of profit that can be achieved by allocating resources;
- *restrictions*: functions as those of (2) and limiting the use of resources;
- *allocation*: the allocation of resources in a given activity.

Of course, within optimization issues you may encounter different types of functions R (respectively g) which are required to be maximized (or minimized), as appropriate.

2. A DYNAMIC PROCESS MODEL

In the case of "regular" functions, the optimization process takes place in a possible domain, which is bounded by restrictions, so the most commonly used technique is based on Lagrange

multipliers, which we will denote by λ (see [7]). Assuming that the functions g_i in (1) are also regular functions, we form an auxiliary function S(λ;X) as follows:

(4) $S(\lambda; x_1,x_2,...,x_n)= g_1(x_1)+g_2(x_2)+...+g_n(x_n)- \lambda (x_1+x_2+...+x_i+...+x_n-Z)$

In this way we've included the first restriction from (2) in (1) and we've obtained a problem without restrictions. Because g_i are regular functions, obtaining the optimum is done by imposing the condition:

(5) $$\frac{\partial S(\lambda, X)}{\partial x_i} = 0$$

where $x \in E_n$. In this way we get equations of the form:

(6) $g_i'(x_i) - \lambda = 0$ (i=1,2,...,n)

Solving the above equation depending on λ:

(7) $x_i=h_i(\lambda)$

we determine λ by replacing all x_i values in (2) with their coresspondents from (6):

(8) $h_1(\lambda)+h_2(\lambda)+...+h_n(\lambda)=Z$

from where λ could be easily obtained, which will allow us to immediately find the values x_i, by using relations like (6).

As an example suppose we have a quadratic programming problem which asks the following:

(9) $\max R(X)= a_1x_1^2+a_2x_2^2+...+a_nx_n^2$

where $a_i>0$, and satisfies :

(10) $x_1+x_2+...+x_i+...+x_n=Z$
$x_i \geq 0$

The auxiliary function S has the form:

(11) $S(\lambda;X)= a_1x_1^2+a_2x_2^2+...+a_nx_n^2-\lambda(x_1+x_2+...+x_i+...+x_n-Z)$

Deriving S(X) with respect to x_i we'll obtain:

(12) $$\frac{\partial S(\lambda, X)}{\partial x_i} = 2 \cdot a_i \cdot x_i - \lambda$$

And by writing according to (5):

(13) $2 \cdot a_i \cdot x_i - \lambda = 0$

hence (14) $2 \cdot a_i \cdot x_i = \lambda$ and in consequence

(15) $$x_i = \frac{\lambda}{2 \cdot a_i}$$

Replacing (15) in (10) it results:

(16) $$\sum_{i=1}^{n} \frac{\lambda}{2 \cdot a_i} = Z \text{ or } \frac{\lambda}{2} \sum_{i=1}^{n} \frac{1}{a_i} = Z \text{ so that } \lambda = \frac{2 \cdot Z}{\sum_{i=1}^{n} \frac{1}{a_i}} \text{ and}$$

(17) $$x_i = \frac{Z / a_i}{\sum_{i=1}^{n} \frac{1}{a_i}} .$$

This allows us to find the maximum value of R:

(18) $$R = \sum_{i=1}^{n} a_i x_i^{\,2} = \frac{Z^2}{\sum_{i=1}^{n} \frac{1}{a_i}}$$

Unfortunatelly the method described above cannot be used for the general case. Because of this there were introduced new research methods and mathematical techniques, our original method, subject of this article, being one of them. In this way, solving the particular problem of maximizing the function:

(19) $R(X)- g_1(x_1)+g_2(x_2)+...+g_n(x_n),\ X \in E_n$,

inside the real domain delimited by:

(20) $$\sum_{i=1}^{n} x_i - Z, \quad x_i \geq 0$$

means to approach a series of allocation processes, where n can take any pozitive, integer value and x_i any non-negative value. The allocation process is done by passing from one activity to another so

it has a dynamic character. If the maximum of R(x) depends on n and Z, then the dependence will become clearer if we introduce a series of functions $f_n(Z)$ defined as follows:

(21) $n=1,2,3,\ldots$ (integers)

$Z \geq 0$,

$$f_n(Z)= \max_{x_i} R(x_1, x_2, \ldots, x_n),$$

$$x_i \geq 0, \sum_{i=1}^{n} x_i = Z$$

The third relation in (21) could be interpreted by defining $f_n(Z)$ as the maximum value of the realized profit. This is done by allocating most conviniently the total resources Z to all the n activities. It is important to notice though that sometimes the functions $f_n(Z)$ take some particular values. Hence, if there isn't any resource allocation, respectively $Z=0$ and $x_i=0$ then $f_n(0)=0$, $(n=1,2,3,\ldots)$, which is, in fact, a consequence of $g_i(0)=0$. But if n=1, that means $R(Z)=g_1(Z)$, so $f_1(Z)=g_1(Z)$.

If $f_n(Z)$ is the maximum profit that can be obtained by dividing Z optimally to n activities, then as a consequence we could say that $f_{n-1}(Z_1)$ is the maximum profit that can be obtained by dividing the resource Z_1 optimally to n-1 activities. Between $f_n(Z)$ and $f_{n-1}(Z_1)$ there exists a recurence which can be emphasized as follows:

Suppose a resource x_n is spread to activity n such that

(22) $0 \leq x_n \leq Z$.

But according to (22), x_n can take any integer value between 0 and Z. Suppose now, x_n is a random value, constant for the moment, which satisfies the condition (22). In this way the available resource quantity to be spread to the other n-1 activities is:

(23) $Z_1=Z-x_n$

If we accept that $f_{n-1}(Z_1)$ has the significance given above, then we can write:

(24) $R(Z)=g_n(x_n)+f_{n-1}(Z_1)$,

Which is equivalent with writing:

(25) $R(Z)=g_n(x_n)+f_{n-1}(Z-x_n)$

In order to obtain the maximum value R(Z) can take, meaning $f_n(Z)$, it will be assumed that x_n take all posible values between 0 and Z, then considering that value for which R(Z) is maximum, this being equivalent with writing:

(26) $$\max R(Z) = f_n(Z) = \max_{0 \leq x_n \leq Z} [g_n(x_n) + f_{n-1}(Z - x_n)]$$

In this way we can obtain the basic functional equation from dinamic programming that could be completely formulated as below:

(27) $$f_n(Z) = \max_{0 \leq x_n \leq Z} [g_n(x_n) + f_{n-1}(Z - x_n)]$$

for $n=2,3,\ldots$

when $Z \geq 0$

and $f_1(Z)=g_1(Z)$

3. CONCLUSIONS

The relations (27) leads to the optimality principle which can be presented as follows:

An optimal policy has the property that whatever the initial state and the initial decision, the resulting decisions (available at the moment) must constitute an optimal policy regarding the state implied by the first decision. At this point, some conclusions can be drawn:

- The optimization process has a decision character because at each step, a new decision has to be made regarding the next steps.
- The optimization process has a sequential character, meaning it takes place in a number of steps.
- The optimization process has a economic policy character (optimal policy) because is being realized based on a strategy with the ultimate goal the optimum economical result.

One can observe, though, the first relation in (27) is a recurrence relation which is in the same time a teoretical method used to obtain the series $\{f_n(Z)\}$ inductively, once $f_1(Z)$ is know. It is obvious that $f_1(Z)$ determines $f_2(Z)$, then $f_2(Z)$ leads to $f_3(Z)$and so on. From here one can conclude that the optimization process using the dinamic programming method is defined by analyzing descendingly the n-th activity towards the first one then is resolved going ascendingly from the first one to the last one.

REFERENCES

[1.] Bell P., C., Newson E., F. (1992). Statistics for business, The Scientific Press, San Francisco.
[2.] Boldur Gh., Raţiu-Suciu Camelia, Ciobanu Gh., Stancu I. (1975). Cercetare operaţională cu aplicaţii în economie, ASE, Bucureşti.
[3.] Boldur-Lăţescu, Gh., Săcuiu I., Ţigănescu E. (1979). Cercetarea operaţională cu aplicaţii în economie, E. D. P., Bucureşti.
[4.] Leontief W. (1970). Analiza input-output, Ed. Ştiinţifică, Bucureşti.
[5.] Mendenhall W., Reinmuth J., E., Beaver R., Duhan D. (1986) Statistics for management and economics, Duxbury Press, Boston.
[6.] Popa H., L., Străuţi G., Vasu M., Pater F. (2001). Managementul şi ingineria sistemelor de producţie, Ed. Politehnica, Timişoara.
[7.] Rafiroiu M. (1980). Modele ale cercetării operaţionale aplicate în construcţii, Ed. Tehnică, Bucureşti.
[8.] Raţiu-Suciu C. (1997). Modelarea şi simulare proceselor economice, E. D. P., Bucureşti.
[9.] Turban E., Meredith J. (1991). Fundamentals of Management Science, Irwin, Boston.

INTERNATIONAL SYMPOSIUM on
ADVANCED ENGINEERING & APPLIED MANAGEMENT
– 40th ANNIVERSARY in HIGHER EDUCATION (1970-2010)
4 – 5 November, 2010, Hunedoara, ROMANIA

[1.]Amalia Ana DASCĂL, [2.]Adina BUDIUL BERGHIAN

FOR MEASURING AN AMENDMENT DUROMETER BRINELL HARDNESS AT HOT

[1,2.]UNIVERSITY POLITEHNICA OF TIMISOARA, FACULTY ENGINEERING OF HUNEDOARA, ROMANIA

ABSTRACT:
The paper presents the theoretical studies and experimental results obtained from the mechanical attempts of hardness at heat, made on a Brinell hardmeter, using original heating precincts of the test-bars. Thermal-resistant steel types had been used for testing, which practically are submitted at high functional temperatures. Therefore, the precincts and the annex elements as well as the obtained results are shown. They can be applied practically in order to determine the life length of component parts made of this steel.

KEYWORDS:
mechanical test, Brinell hardness, heat chamber, high temperature

1. INTRODUCTION

When choosing a method for testing hardness at high temperatures should take into account a number of reasons, such as: if the surface resistance element can be explored by traces of hardness, the nature of the material under test, the field likely hardness, precision sought the test medium heat (heating chamber, control system and keep warm).

It should be noted that, until now, high temperature hardness tests are not covered by national or European regulations. Few research found in literature, [1], aimed at establishing correlations between characteristics of hardness, high temperature and other mechanical properties of material produced at the same temperatures (eg. correlation between hardness and tensile strength and resilience to high temperatures). Appropriate test methods Brinell and Vickers methods rather than dynamic methods. Brinell and Vickers methods are used can be used to design devices that adapt to a normal oven (chamber) heating.

Of static methods for determining hardness at high temperatures may be used as durometer Brinell method allows selection of a specific task using a touch and penetrated by a certain diameter, thereby realizing different values of the degree of demand.

In establishing the test parameters and specimen dimensions were considered in data requirements [3]. Given the recommendations set out and acknowledging that hardness steels studied at high temperatures may be more than 150 but greater than HB d ≤ 6 mm and≤150 HB, the average diameter of the footprint adopt d diameter ball Steel a ≥ 2,5· 6 = 12 mm, b ≥ 4 · 6 = 24 mm, D = 10 mm resulting to minimum thickness of the specimen s_{min} = 8 mm (Table A.1. of [3]). Using this geometry and considering that it made three prints for each high temperature test, samples were taken for dimensions of L x l x s = 60 x 40 x 10.

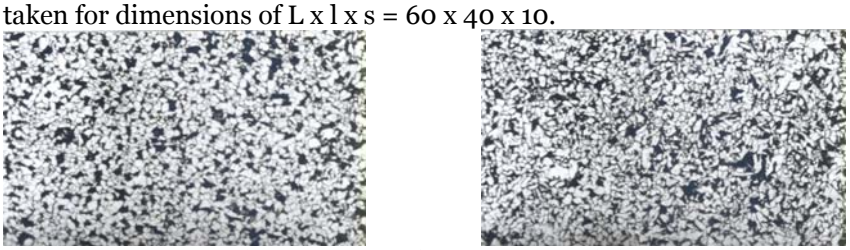

Fig.2. OLT35K and OLT 45K steel structures and the delivery status

The samples were analyzed for hardness in terms of metallographic, the state of delivery, and then after heat treatment and initial structures are shown in Figure 1, the marks of steel that have been performed hardness tests at high temperatures. Nital reagent used was 2%, and samples were studied at a magnification of 100 times.

Metallographic study showed that OLT 35k steel (left) has a structure with grain perlite ferito real-scoring 7-6 according to SR ISO 643-93, and the sample of OLT 45K (left) has a slightly heterogeneous structure ferito-perlite (islands have large grains). Structures correspond to the normative status of delivery specified in the manufacturer of the metal.

2. METHODOLOGY

According to literature [1], the main requirement to carry out proper test under conditions of high temperature hardness is equal between the test sample temperature and temperature head penetrator.

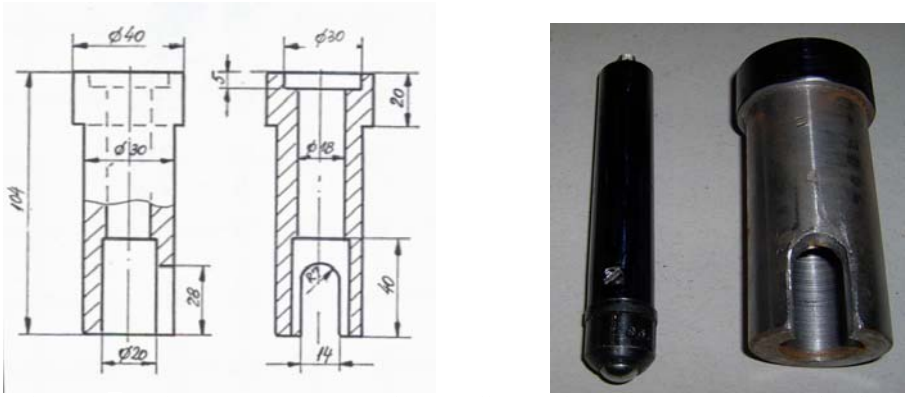

Figure 1. Variants penetrator rod extending rod and heat protection for flat

In order to perform Brinell hardness test was performed by heating specimens in a chamber that was adjusted to a pH durometer - C-02/02. The principle scheme is shown in enclosure made [9]. Temperature samples on site and hence temperature is adjusted by computer.

To ensure equality and head penetrator specimen temperature (in our case - steel ball) was used variant penetrator execution of an extension rod and to achieve thermal protection of the rods, through an appropriate head bush durometer Brinell.

These variations are shown in Figure 2 and Figure 1. Within the thermal protective sleeve were placed rings of asbestos, which provides thermal protection and sealing the area between the working chamber and head load Brinell apparatus.

3. RESULTS

The paper presents experimental tests on two brands of heat-resistant steel, the kind used in making steam pipes, namely: OLT 35k and OLT45K.

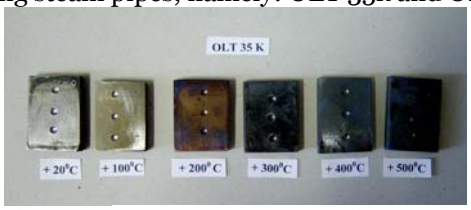

Figure 2. Lot samples OLT 35k, unused material, tested at high temperatures

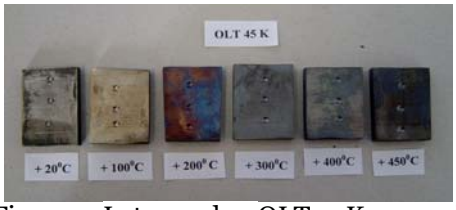

Figure 3. Lot samples OLT 45K, unused material, tested at high temperatures

Normalized specimens were tested at room temperature and at elevated temperatures up to 500°C. In Figure 2 are 35k specimens of OLT and in Figure 3, specimens of OLT 45K, where hardness tests at high temperatures: 20°C, 100°C, 200°C, 300°C, 400°C, 500° C.

After the samples were tested was conducted to measure two perpendicular diameters of each finger, and average diameter was calculated from tables [3] resulted Brinell hardness value.

4. CONCLUSIONS

The results of measurements, calculated values of hardness and size are presented in Tables 1 and 2, for each brand of steel.

The hardness values listed in tables were drawn curves of hardness variation depending on test temperature for each brand of steel, shown in Fig.3

The data obtained for hardness tests and analysis of the graph in Fig. 5 it is noted that the tested steels, the toughness shows a similar variation in tensile breaking strength Rm, Brinell hardness increases with increasing temperature up to 200°C, then begins to decline.

Table 1. Brinell hardness at high temperatures, steel 35k OLT, after normalization

Nr. crt.	Temperature test [°C]		Diameter, [mm] Footprint 1	2	3	Media	Brinell hardness, [HBS] Footprint 1	2	3	Media
1	+20	d_1	5,14	5,18	5,16	5,18	134	132	133	132
		d_2	5,18	5,22	5,20		132	130	131	
		d_m	5,16	5,20	5,18		133	131	132	
2	+100	d_1	4,71	4,67	4,69	4,676	162	165	164	164,33
		d_2	4,73	4,61	4,65		161	170	167	
		d_m	4,72	4,64	4,67		161	167	165	
3	+200	d_1	4,54	4,51	4,61	4,533	175	178	170	176
		d_2	4,48	4,52	4,55		180	177	174	
		d_m	4,51	4,51	4,58		178	178	172	
4	+300	d_1	4,78	4,80	4,76	4,765	157	156	158	158
		d_2	4,75	4,78	4,74		159	157	161	
		d_m	4,476	4,79	4,74		158	156	160	
5	+400	d_1	4,92	4,86	4,98	4,923	148	152	144	147,66
		d_2	4,95	4,90	4,93		146	149	147	
		d_m	4,935	4,88	4,955		147	150	146	
6	+450	d_1	5,17	5,17	5,18	5,156	133	133	132	133,66
		d_2	5,14	5,10	5,20		134	137	131	
		d_m	5,15	5,13	5,19		134	135	132	

Brinell hardness at high temperatures, OLT 45K steel, after normalization

Nr. crt.	Temperature test [°C]	d	Diameter, [mm] Footprint 1	2	3	Media	Brinell hardness, [HBS] Footprint 1	2	3	Media
1	+20	d_1	5,25	5,24	5,30	5,263	128	129	126	127,66
		d_2	5,25	5,28	5,26		128	127	128	
		d_m	5,25	5,26	5,28		128	128	127	
2	+100	d_1	4,65	4,82	4,79	4,705	167	154	156	162,66
		d_2	4,57	4,71	4,69		173	162	164	
		d_m	4,61	4,76	4,74		170	158	160	
3	+200	d_1	4,52	4,47	4,46	4,520	177	181	182	177
		d_2	4,58	4,56	4,54		172	174	175	
		d_m	4,55	4,51	4,50		174	178	179	
4	+300	d_1	4,73	4,75	4,73	4,738	161	159	161	160,33
		d_2	4,76	4,63	4,78		158	164	157	
		d_m	4,745	4,71	4,755		160	162	159	
5	+400	d_1	4,92	4,92	5,05	4,94	148	148	140	146,33
		d_2	4,90	4,92	4,94		149	148	146	
		d_m	4,91	4,92	4,99		148	148	143	
6	+450	d_1	5,34	5,22	5,21	5,245	124	130	130	128,66
		d_2	5,30	5,20	5,20		126	131	131	
		d_m	5,32	5,21	5,205		125	130	131	

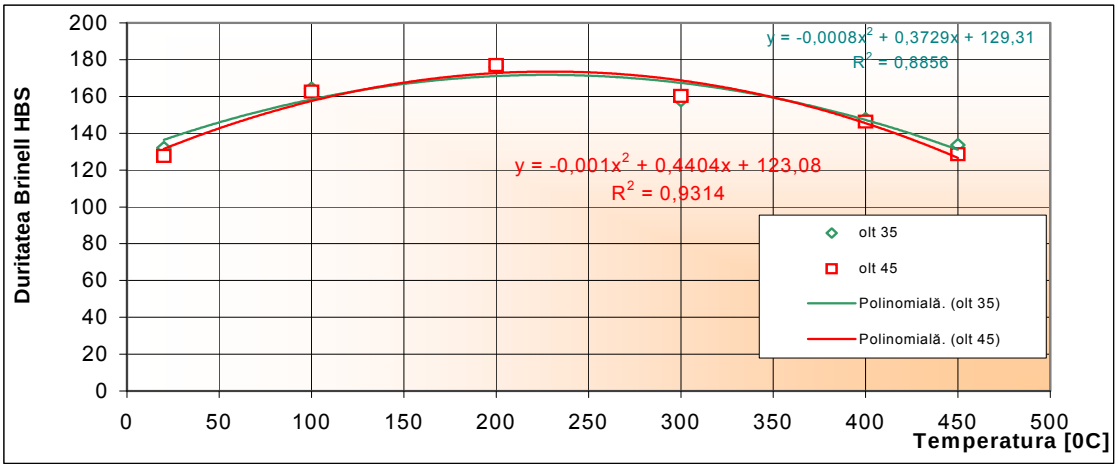

Fig.3. Variation curves of hardness versus temperature, for steels tested

This makes us conclude that one can determine the tensile breaking strength of steel, knowing its toughness and vice versa. Moreover, the literature gives relations between the two features.

REFERENCES

[1.] Borzdîk, AM, Methods goriaceh mehaniceschih ispîtanii metallov, Moscow, 1962.
[2.] Weber, F., Strength of materials, laboratory guide, Mirton Publishing House, Timisoara, 2000.
[3.] SR EN 10003-1:1997, Metallic materials. Brinell hardness test. Part 1: Test method.
[4.] Marchidan, DI Ciopec, M., Temperature - steps, methods and instruments, Scientific and Encyclopedic Publishing House, Bucharest, 1977.
[5.] Mocanu, R.D., and others, Testing materials, vol. I. Destructive testing of metals, Technical Publishing House, Bucharest, 1982.
[6.] Nădăşan, st., Etc., tests and analysis of metals, Technical Publishing House, Bucharest, 1965.
[7.] Răşănescu, I., Transfer phenomena, Didactic and Pedagogic Publishing House, Bucharest, 1984.
[8.] Dascăl, A., Contribution to study the behavior of steels at elevated temperatures, PhD thesis, Timisoara, 2004.
[9.] Dascăl, A., Behaviour of steel hardness test baking at high temperatures, Annals of the Faculty of Engineering of Hunedoara, Tom IV, Fasc.3, 2002.

INTERNATIONAL SYMPOSIUM on
ADVANCED ENGINEERING & APPLIED MANAGEMENT
– 40th ANNIVERSARY in HIGHER EDUCATION (1970-2010)
4 – 5 November, 2010, Hunedoara, ROMANIA

[1.] Siniša KUZMANOVIĆ, [2.] Milan RACKOV

THE INFLUENCE OF AXIAL LOAD AT OUTPUT SHAFT OF UNIVERSAL WORM AND HELICAL-WORM GEAR UNITS ON THEIR THERMAL POWER CAPACITY

[1, 2] UNIVERSITY OF NOVI SAD, FACULTY OF TECHNICAL SCIENCES, SERBIA,

ABSTRACT:
Universal worm and helical-worm gear units are among the mechanisms that operate with a relatively low level of efficiency for which their thermal power capacity is paid extremely high attention. Value of thermal power limit for gearboxes with free input shaft is particularly defined in the catalogue, enabling their correct choice, i.e. enables the timely assessment of the needs of taking certain procedures in order to overcome problems that may arise due to excessive heating of reducers. Thermal power capacity of motor gear reducer is taken into account when defining a range, i.e. when combining (connecting) the motor and gearbox which is made according to the catalogue, so that the problem is not noticeable to the customer. Today, in an era of tough competition, it is necessary to consider the impact of external overhung and axial loads applied to output shaft on the thermal power capacity of gearbox, so that it could be eventually taken into account when gear reducer is selected. This paper deals with the problem of reducing of thermal power capacity of gearboxes due to external loads of output shaft, i.e. it deals with additional heating due to increased power loss in the bearings. At the end it is concluded (as expected) that the effect of those loads is negligible and there is no need to take them into account when selecting the gear unit, because it does not achieve any effect.

KEYWORDS:
worm and helical-worm gear units, thermal power capacity

1. INTRODUCTION

When choosing a universal worm and helical-worm gear reducer, service factor is selected from the catalogs of almost all manufacturers of gearboxes according to the service nature (uniform, medium and heavy), operating time during a day (0 to 24 hours), starting frequency – number starting during an hour (from 0 upwards), ambient temperature, the effective operating of reducer in an hour (so called ED factor), permissive overhung and axial loads of the output shaft (and input shaft for gear reducers with solid shaft) and thermal power capacity, accounting that the electric motor drives gearbox. However, when the large overhung and axial loads are applied, in this case only axial load on the output shaft, it comes to additional heat generating of gear reducer and thus reducing its thermal capacity. This can cause excessive heating of gear unit (usually above 80°C, or even 100°C), which may, mainly due to changes in size, have bad influence on their operating. Therefore, in this paper it is necessary to consider the influence of external axial load on the thermal capacity of the worm and helical-worm gear unit and, perhaps, suggest ways to not occur problems due to excessive heating of gearbox.

2. THE AIM OF THE STUDY

The main objective of this paper is to point out the importance of thermal capacity of worm and helical-worm gear units, as well as the influence of the external axial load on the output shaft to the value of this capacity.

3. PROBLEM INTERPRETATIONS

Universal worm and helical-warm gear units can be delivered with motor or with free input shaft. If they are delivered with electric motors, they can be delivered with special motors, so called geared motors, or with standard (IEC) motors. What electric motors will be used depends on the attitude of the manufacturers company as well as specific demands of the customer [1].

If gear units are delivered with free input shaft, they can have usual solid input shaft and with IEC motors interface.

Large manufacturers usually use special motors, which are characterized by special flanges, special diameters of output shafts, stronger bearings and better sealing solution, so they have a number of advantages (easier, cheaper and more compact design, the possibility of achieving higher gear ratios, greater permitted force of the motor shaft and better tightness). Since they are buying large quantities of such motors, they get them quickly and at almost a price of standard motors, so that this procedure is completely payable to manufacturer. In addition, these manufacturers usually have their own factory of electric motors, so that they do not have practically this problem.

Small and medium manufacturers of gear units usually use standard IEC motors, although it is not the rule, mainly because of lower cost and short delivery time, and all the benefits of special motors they try to compensate by suitable way of installing motor to the gear unit. Since it is difficult to make up a lot of advantages of special motor, in practice there are different construction solutions of installing gear unit with standard IEC motors that are directly, or with IEC motors interface, connected for the housing of gear unit.

Gear units with standard IEC motors are delivered by large manufacturers, who use special geared motors, especially when customers require. For example, when customer wants to install motors on purchased gear units by himself. It is usually case when they think they can do cheaper or faster service of their motors, or in case of export of gear units in the country, where there are factories of electric motors, which wants with a large taxes on motors to protect their products from foreign competition, and customers are payable to buy electric motors, so they buy gear units with free input shaft motor, usually, with IEC motors interface, which allow them much easier and more secure mounting IEC motors, so that there is no possibility to install motor incorrectly.

Regardless of the type of the applied electric motor, it must consider that power losses originated in the gearbox must be delivered to the surroundings [1]:

$$P_L = P_{in}(1-\eta) = Q \le Q_o = \alpha\, A\, \Delta\Theta \qquad (1)$$

where: P_L – losses in the gearbox,
P_{in} – input power of gear reducer,
η – efficiency of gear reducer,
Q – heat flux caused by originated losses,
Q_o – maximum heat flux that can be transmitted to the ambient,
α – coefficient of heat transmission,
A – the surface area of housing of gear reducer that can exchange heat,
$\Delta\Theta$ – temperature difference, where $\Delta\Theta = \Theta - \Theta_o$,
where: Θ – the temperature of surface of reducer housing, usually it is considered that maximum temperature is Θ = 80...100°C [1] and Θ_o – temperature of ambient where the gearbox operates.

From equation (1) it follows that the value of the thermal power capacity (P_Q) is [3]

$$P_{in} \le P_Q = \frac{\alpha\, A\, \Delta\Theta}{1-\eta} \qquad (2)$$

This means that thermal power limit is the greatest power in the input at which, in a permanent operating, obtained losses in the gearbox can be transferred around without excessive heating of gear reducer (Fig.1).

It should take into account that the speed of heating depends exclusively on operating regime, input power, thermal inertia of gear reducer (of its mass) and selected cooling method. So, when choosing gear, among other requirements it must be met the following condition: $P_{in} \le P_Q$.

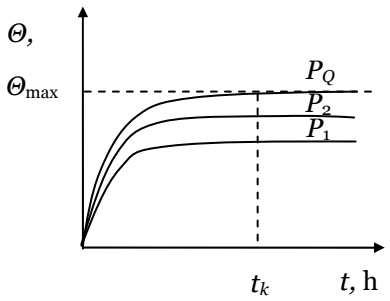

Figure 1. Graphical review of heating gear reducers depending on the input power (where t – time of heating, t_k – critical time when maximum permissive temperature is achieved (Θ_{max}), Θ – temperature of the gearbox housing, P – input power of gearbox)

When developing a catalog of geared motor, i.e. when the manufacturers compose the assembly of driving and gear unit (geared motor), they concern to fulfill this condition, and they account that the normal temperature of outside air is Θ_o = 20°C. When gear reducer operates at higher ambient temperatures, the value of thermal power capacity is corrected by special coefficient.

However, when selecting gearbox with free input shaft, the customers are referred by manufacturers (in their catalogs) to detailed procedure of gearbox selection, so that problem must be considered by customers (designers) that make procedure for gearbox installation, in order to avoid possible accidents that may occur in the overheated gearboxes.

4. DESCRIPTION OF WAYS OF SOLVING PROBLEMS

When selecting gear reducer with free input shaft, it must be provided:

$$T_N \geq T_{out} f_B \tag{3}$$

where: T_N – nominal torque,
T_{out} – output torque,
f_B – minimum value of the service factor.

When selecting motor gear reducer it is indirectly defined by service factors [2, 4, 5]

$$f_{B\text{perm}} \geq f_B \tag{4}$$

where: $f_{B\text{perm}}$ – permissive value of service factors given in the catalogs for each motor power, speed and size of reducer (it is determined by expression $f_{B\text{perm}} = T_N / T_{out}$),
f_B – service factor defined according to the type of loading, operating time in hours during a day, the number of cycles during an hour, the ambient temperature, the effective operative duration during an hour and, eventually, the desired life of gearbox.

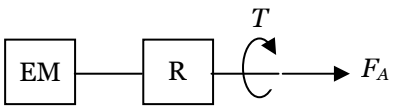

Figure 2. Schematic review of a loading of the output shaft of geared motor (EM – electric motor, R – reducer, F_A – axial load)

So, the choice of gear reducer with solid input shaft is based on its load torque (T_N), or motor service factor (equat.5), as well as the permissive values of radial ($F_{Ri\ \text{perm}}$) and axial ($F_{Ai\ \text{perm}}$) loads of the free input shaft of gearbox (for gearboxes with solid input shaft) and radial ($F_{Ro\ \text{perm}}$) and axial ($F_{Ao\ \text{perm}}$) loads of the output shaft (for both types of gear units), Fig.2.

Additionally, the choice of gear reducer is also based on thermal capacity (equation 2), where it should take into account that thermal capacity depends on the ambient temperature, as well as on the size (and sometimes the shape and position of mounting) of gear reducer. Its values can be obtained as a table or a diagram (Fig.3).

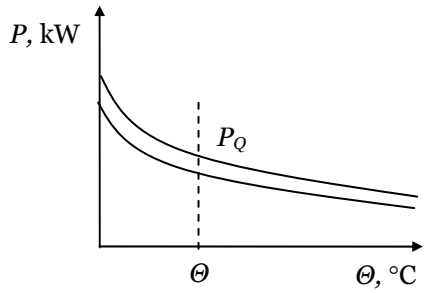

Figure 3. Graphic display of thermal capacity for particular size of gear reducer

Thermal capacity is a little different for geared motor and gear reducer with solid shaft (with classic input or with input for IEC motors), because the fan of electric motor of geared reducer provides some greater air circulation and thus better cooling of reducer, while, due to the heating of electric motor, gearbox is subjected to somewhat larger heating from the motor. Sometimes these cooling and heating quantities can be canceled, and sometimes unfortunately not, so they should be separately shown in the diagram (or table).

In order to reduce the production cost of electric motors, it is going on a maximum reduction of material consumption, which causes faster heating of the motor, so that today insulation material of class F is installed in motors (which allow their heating up to 150°C). Of course, the fan of electric motor does not allow reaching this temperature, but certainly because of higher temperatures of motor it comes to a stronger heating of gear unit, especially if the motor has bigger number of starting during an hour, and particularly if it is a motor with a brake which additionally heats the reducer.

Manufacturers of gear reducers are aware of this problem and take into account the thermal capacity of their gearboxes and try to increase it. They usually manage this by increasing the surface area of housing (i.e. by placing ribs on the surface of housing of gear unit), or by increasing the coefficient of heat transmission by defining of such forms of housing that will provide better air circulation around it, which is driven by a fan of electric motor (this is only applied for geared motor), or by placing a special fan (by manufacturers) on the worm shaft of worm and helical-worm gear reducer.

Operating regime of gear units has also major impact on their thermal capacity. For example, service nature, operating time and number of starting can strongly affect on the heating and thus the thermal capacity of gear reducer. Especially different combinations of these parameters can strongly affect on the heating which is considered by service factor. The calculation of their actual impact is quite complex and can not be accurately described by mathematics, but very accurate values can be obtained by concrete measurements.

In the case that condition is not satisfied (equation 2), it is necessary to adopt a larger (stronger) gearbox, with a larger surface area participating in the exchange of heat, or it is need to use the system for cooling oil. For smaller sizes of gear reducers it is cheaper to select larger gearbox, while in medium and large size of reducer it is rational to use oil cooling system. The system consists of filter, circulating pumps, overflow and several classic valves, piping and heat exchanger with fan and electric motors.

The existence of an external axial load on the output shaft, which permissive limit values can be found in the catalogs of manufacturers of gear reducers, causes additional load of bearings of gearbox and the occurrence of additional friction in them (whose approximate value amounts $F_{\mu A} = \mu F_{A\text{perm}}$ – friction in the bearing due to the external axial force) and it causes additional heating of gear unit. Since there is no additional overhung load, bearing will be subjected to maximum permissive axial force according to the catalog.

Additional losses of power in the bearing (P_L) can be calculated by the equation:

$$P_L = 1.05 \text{ x } 10^{-4}\, M\, n \tag{5}$$

where: n – number of revolution of output shaft, min^{-1}
M – total frictional moment of bearing

Total frictional moment of bearing (M) depends on several frictional moments as follows:

$$M = M_0 + M_1 + M_2 + M_3 \tag{6}$$

where: M_0 – load independent frictional moment, Nmm
M_1 – load-dependent frictional moment, Nmm
M_2 – axial load-dependent frictional moment, Nmm
M_3 – frictional moment of seals, Nmm

The frictional moment (M_0) is not influenced by bearing load but by the hydrodynamic losses in the lubricant and depends on the viscosity and quantity of the lubricant and also the rolling velocity. It dominates in high-speed, lightly loaded bearings and is calculated using:

$$M_0 = 10^{-7}\, f_0 \left(\nu n\right)^{2/3} d_m^3 \tag{7}$$

if $\nu n \geq 2000$ or using

$$M_0 = 160 \times 10^{-7}\, f_0\, d_m^3 \tag{8}$$

if $\nu n < 2000$, where: d_m – mean diameter of bearing (for particular bearing $d_m = 0.5\,(d + D) = 0.5\,(30 + 72) = 51$ mm)
f_0 – a factor depending on bearing type and lubrication (for particular bearing $f_0 = 1$)
ν – kinematic viscosity of the lubricant at the operating temperature, mm^2/s (for operating temperature $\Theta = 40$°C)

The load dependent frictional moment (M_1) arises from elastic deformations and partial sliding in the contacts and predominates in slowly rotating, heavily loaded bearings. It can be calculated from:

$$M_1 = f_1\, P_1\, d_m \tag{9}$$

where:
f_1 – a factor depending on bearing type and load

for particular bearing and load: $f_1 = (0.0006 \ldots 0.0009)\left(\dfrac{F_{R\text{perm}}}{C_0}\right)^{0.55}$ (10)

P_1 – the load determining the frictional moment, N, for particular bearing and load:

$$P_1 = 3\, F_{A\text{ perm}} - 0.1\, F_{R\text{ perm}} = 3\, F_{A\text{ perm}} \quad (F_{R\text{ perm}} = 0) \tag{11}$$

Frictional moment (M_2) which depends mostly on the axial load can be calculated as follows:

$$M_2 = f_2\, F_{A\text{ perm}}\, d_m \tag{12}$$

where: f_2 – a factor depending on bearing design and lubrication (for particular bearing design and lubrication $f_2 = 0.006$)

The frictional moment (M_3) of the seals for a sealed bearing can be estimated and for particular bearing it is calculated as $M_3 = 18$ Nmm.

For a smaller size of gear reducer (with shaft height $h = 80$ mm) orientation values of frictional moments and additional losses of power in worm and helical-worm reducer are calculated and shown in Table. 1.

Table 1. Results of calculation of a typical worm gear reducer without a fan with shaft height 80 mm

Thermal capacity – P_Q, W	1500	920	280
Permissive axial force of output shaft – $F_{A\,\mathrm{perm}}$, N	5520	7800	7800
Speed ratio – u	5.4	26	79
Revolution number of output shaft – n, min^{-1}	259	54	18
Load independent frictional moment – M_0, Nmm	7.66	6.7	6.07
Load-dependent frictional moment – M_1, Nmm	289.14	494.14	494.14
Axial load-dependent frictional moment – M_2, Nmm	1689.12	2386.8	2386.8
Frictional moment of seals – M_3, Nmm	18	18	18
Total frictional moment of bearing – M, Nmm	2003.92	2905.63	2905.01
Additional power losses in gear reducer – P_L, W	54.5	16.47	5.49
Percent ratio of power losses – $\frac{P_L}{P_Q}\cdot 100$, %	3.63	1.79	1.96

Based on carried out calculation it follows that the additional power losses in the gearbox, with the maximum permissive axial load of the output shaft, amounts about up to 3.63%. For lower speed ratio, power loss is less, not bigger than 2%. The power loss is bigger than only overhung load subjects the output shaft, but it is not so high and many manufacturers of gear reducer completely ignore it. When making the instruction for selecting gearbox, manufacturers of gear reducers, ignore the influence of external loads on the thermal capacity of gear unit and thus considerably simplify their selection of gear reducer.

5. CONCLUSION

Based on the conducted analysis it can be seen that the external axial loads of the output shaft of worm and helical-worm gear reducers have a small influence on the change of thermal capacity, usually about 2%, or for higher output speed up to 3.6%. Therefore, manufacturers of gear reducers ignore it with a full right, i.e. they do not take external forces into account when selecting gearbox and do not make correction in thermal capacity. This power loss would be more important for higher transmitted power with high output speed, when this 3.6% power loss is not negligible value, but it is a very rare case.

REFERENCES

[1] KUZMANOVIĆ, S., *Universal Gear Reducers with Cylindrical Gears*, University of Novi Sad, Faculty of Technical Sciences, Novi Sad, 2009. (in Serbian)
[2] Catalog SEW Eurodrive, Movimot Gearmotors, Edition 04/2004
[3] SKF General Catalogue, 2007
[4] Catalog Nord, Constant speeds, G1000/2008, Getriebebau Nord, Hamburg
[5] Catalog Siemens, Flender Gear Units, Catalog MD 20.1-2009

INTERNATIONAL SYMPOSIUM on
ADVANCED ENGINEERING & APPLIED MANAGEMENT
– 40th ANNIVERSARY in HIGHER EDUCATION (1970-2010)
4 – 5 November, 2010, Hunedoara, ROMANIA

[1.]Krassimir E. GEORGIEV

ADVANCED DESIGN OF MECHATRONIC WORKSTATIONS FOR TECHNOLOGICAL CONTACT OPERATIONS

[1.]BULGARIAN ACADEMY OF SCIENCE, INSTITUTE OF MECHANICS,
MECHATRONIC SYSTEMS DEPARTMENT, SOFIA, BULGARIA

ABSTRACT:
The objective of this paper is to outline the necessity of understanding vertical and horizontal system integration in advanced mechatronic systems. A Methodology, theoretical aspects and some practical results of creating and research of distributed mechatronic environment are presented, based on robotic assembly systems and 3D virtual models. A global algorithm for simulation and advanced design is presented as well.
KEYWORDS:
advanced mechatronic systems, system integration, global algorithm, simulation

1. INTRODUCTION

The flexibility of a mechatronic system can be obtained either by making its mechanical and electronic part as universal as possible or by constructing a large set of simple models which will be interchanged whenever the task of the system changes. In the latter case the mechanical and electronic structure of the system can be tailored exactly to the needs of the task at hand.

In both cases the control of such system is implemented in software. The software should be structured as a library of procedures and functions possibly concurrent, which will be used as software blocks for construction of the control system.

Virtual product models, together with adapted development methods and processes are the key to an integrated view of development, manufacturing and usage of products as they promise a significant increase of efficiency, quality and flexibility of product development.

For ROBOTIC and MECHATRONIC systems the coupling of subsystems could be realized on three different levels – physical modeling, mathematical modeling and behavioral modeling. At physical description and modeling a system is represented by physical models, for example as a multibody system, containing rigid bodies, joints and coupling force elements. The mathematical description and modeling is a representation of a system by mathematical equations which can be derived from the physical model description, e.g. the equations of motion of a multibody system.

The simulation results of the mathematical model description are considered as the behavioral model description - the trajectories of position and velocity of the bodies. Then coupling of models in the behavioral model description is referred to as simulator coupling, modular modeling and simulation or virtual assembly of them. The simulation of the global system is realized by time discrete linker and scheduler which combines the inputs and outputs of the corresponding subsystems and establishes communication between the subsystems to discrete time instants. Therefore it is possible to use different software packages for each subsystem and then to link the solvers together. Now the general modeling and design of MS may be presented in form with respective levels of task simulation and planning (distributed mechatronic environment).The modular description of systems allows for independent and parallel modeling of the internal dynamics of each subsystem. The inputs and outputs of the physical model are also physic quantities such as forces or motion of the bodies.

Here the main goal is to present a modular –block concept, mechatronical approach and 3D virtual environment for real time computer control, complex simulation and interactive user's design solutions of mechatronic (robotic) systems for contact operations.

2. DESIGN APPROACH AND MODELING OF DESIGN ALTERNATIVES

The full dynamic model is presented in previous author's publications and here we shortly note that, the models derived, based on the Lagrange's equations have the advantage that they are in closed form concerning the geometrical, inertial and functional parameters of the mechanical system. The joint reactions are excluded and considering the immense computational power of today's computers one can successfully explore various aspects of the dynamic modeling of the robotized system. This enables us to carry out dynamic synthesis of the technological movements and to build a strategy for dynamic behavior. Based on the derived equations we can compute the appropriate joint torque of the regional structure of the assembly robot, considering the predefined generalized coordinates $q_i = q_i(t)$ and the finite increments of the generalized coordinates $o_i = |q(t_i) - q(t_i - 1)|$, in order to minimize to total system energy and power consumption. Using MATLAB and Solid Works environments, we can derive effective solutions for the corresponding parameters m_i, l_i, h_i, J_{sk}^i as well as get results applicable in the practice in order to achieve higher velocities and minimal duration of the technological assembly.

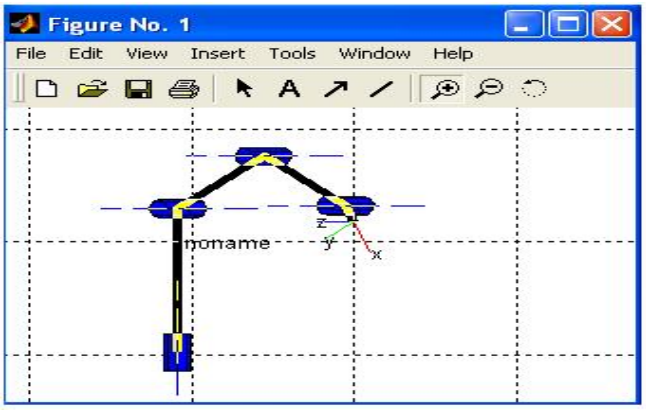

Fig. 1. Matlab simulation of robotic regional structure

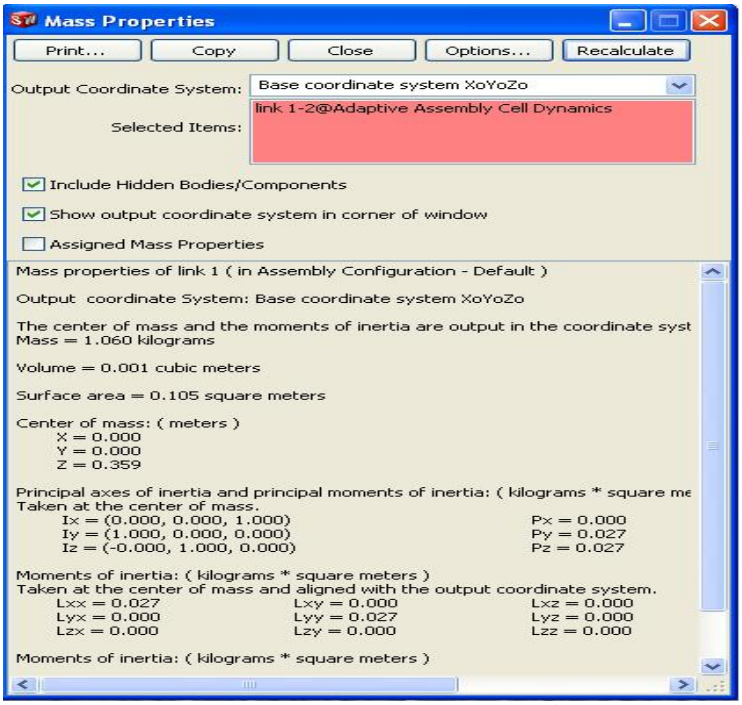

Fig.2. Solid works simulation of mass/inertia properties of robot links

Using the original author's idea of designing the system from modular structures with 3R active joints and adaptive sockets (accommodating the concept of local dynamic compliance), we are able to combine higher speed, thus obtaining solutions to the extremely difficult assembly tasks of prismatic details without chamfers. After the virtual 3D model is built (using Solid Works environment) it is possible to conduct various simulations. This enables us to research the model, carry out different scenarios to see what will be the behavior of the real adaptive assembly cell. The results from the kinematic simulations are presented further in the paper. However the question of the validity of the model is always open. Even in the user's guide of the simulation product is written that one shouldn't rely solely on the obtained results. That is why it was necessary to validate the results. For this purpose a mathematical kinematic computer model was built and researched using Matlab v6 combined with the specialized software toolbox Robotics Toolbox. The kinematic model was introduced using Denavit-Hartenberg convention. The direct and inverse kinematics was solved and the results were exported to the 3D robot model .Based on respective simulations we obtain the following results: at lower values of angular velocity of driving shaft and higher spring stiffness the driving robot torques are extremely low and the influence of initial contact between the assembled details is minimal. This fact is

confirming at the investigation of robot joint reactions at the computer simulations. The ultimate purpose is to achieve a system performance superior to what can be achieved by traditional development and design cycle. The author's idea follows this approach and mechatronics principles to close the open kinematic chains, using control and information loops. Then is possible to estimate different parameters of RS, to compliance them and to achieve complex properties: Adaptively, reconfiguratible structure, energy efficiency and high performance.

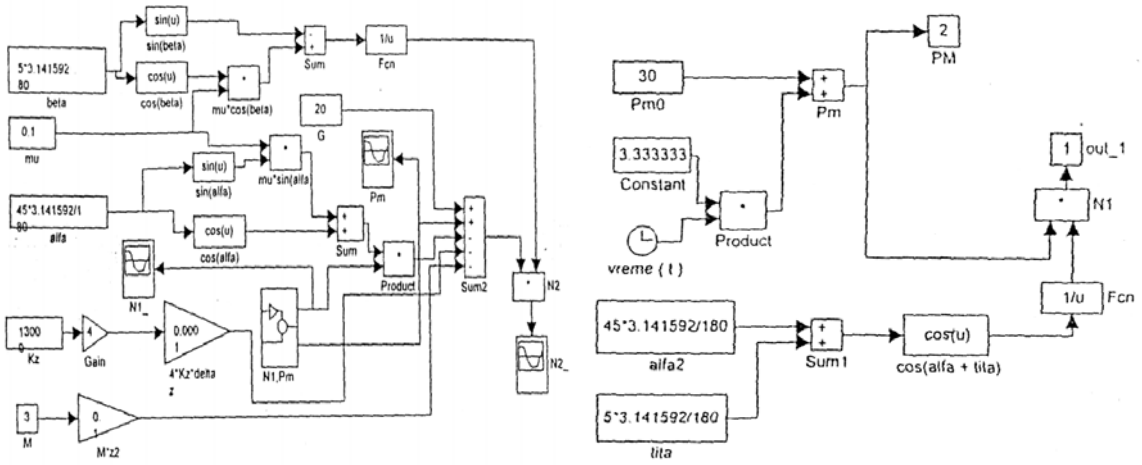

Fig.3 Simulink modeling of contact stages, during adaptive assembly

Therefore for the 6 R robotic structure the axis models are represented with the modules (blocks)- controller, motor, gearbox (including gear elasticity, damping and bearing friction) and mechanical part The calculated parameters are involved in the 3D kinematic model of the robotic system, using Solid Works 2005 - Cosmos Motion 2005. It is also possible to simulate the space contact at the adaptive assembly, using appropriate data of materials and dry friction forces. The respectively modular component of distributed mechatronic environment is shown on fig 4.

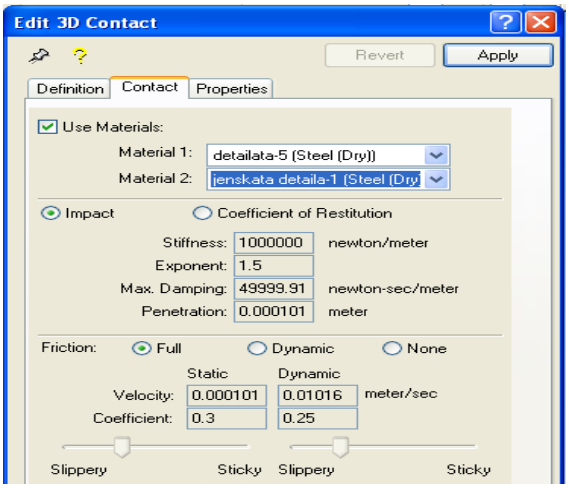

Fig 4 .Module of 3D contact interaction

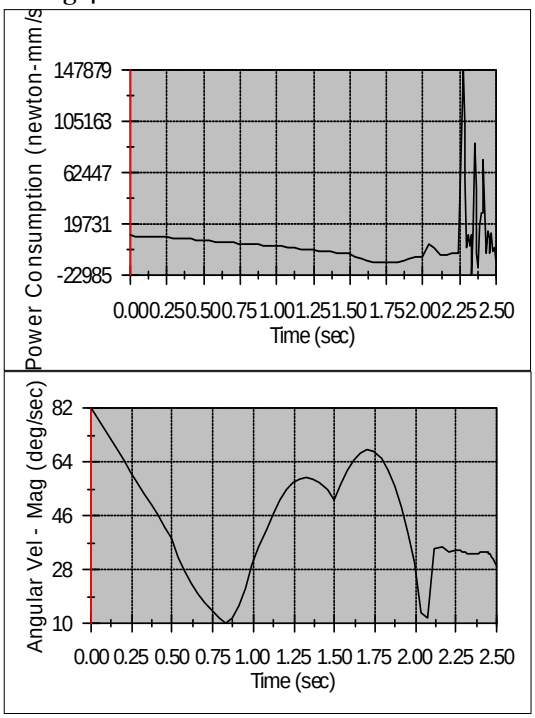

Fig. 5. Power consumption and angular joint velocity

The mechatronic environment consists of different number modular components and mechatronics procedures. Each procedure consists of 5 steps:

- Initial synthesis of 3D kinematical models
- Preliminary metrical synthesis
- Preliminary synthesis of control functions, direct and inverse dynamic tasks
- Using multivariant analysis and varying the important characteristics to obtain optimal design of building modules
- Final synthesis of the control functions (optimization) accounting for the full dynamic models

The full process of modeling and design we denote as synthesis by using analysis.
The modular component structure of environment supports a rapid exchangeability of models and allows spreading out modeling tasks and skills to different researchers in order to achieve sophisticated integration of capable models, reduce

developing time and costs. The given examples show both the necessity for applying a mechatronic design and simulation environment. This way the feasibility of highly complex systems can be studied by the combined efforts of numerical computation, simulation and CAD design (fig.5,6,7) . Effective system modeling needs of distributed simulation environment and respective subfunctions and subconfigurations $F^{i}{}_{J}$, $C^{i}{}_{J}$ (fig.7), concerning to database of different components: Sockets, actuators sensors, controllers, etc.

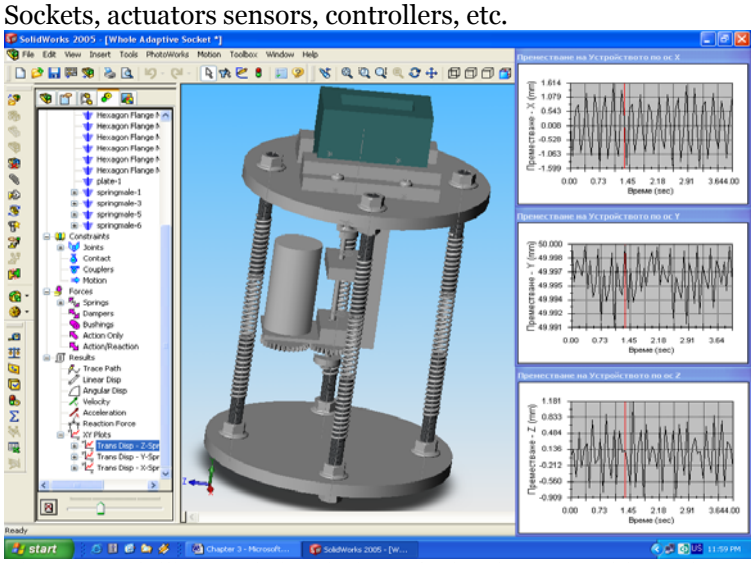

Fig.6 Modelling and simulation of adaptive assembly socket

In accordance with the above mentioned principles a virtual model of an adaptive assembly socket is realized and it is further more developed to a whole The three dimensional model of the device is built using Solid Works 2005 environment assuming that all main dimensions of the real model are exactly reproduced. The correct construction and mating of all the details in the assembly allows us to create a virtual assembled model of the adaptive assembly socket and a family sockets.

Furthermore a 3D model of a whole robotized unit is developed. The goal is to investigate and research the process of adaptive assembly using the developed devices. There have been various simulations with different parameters of local micro motion.

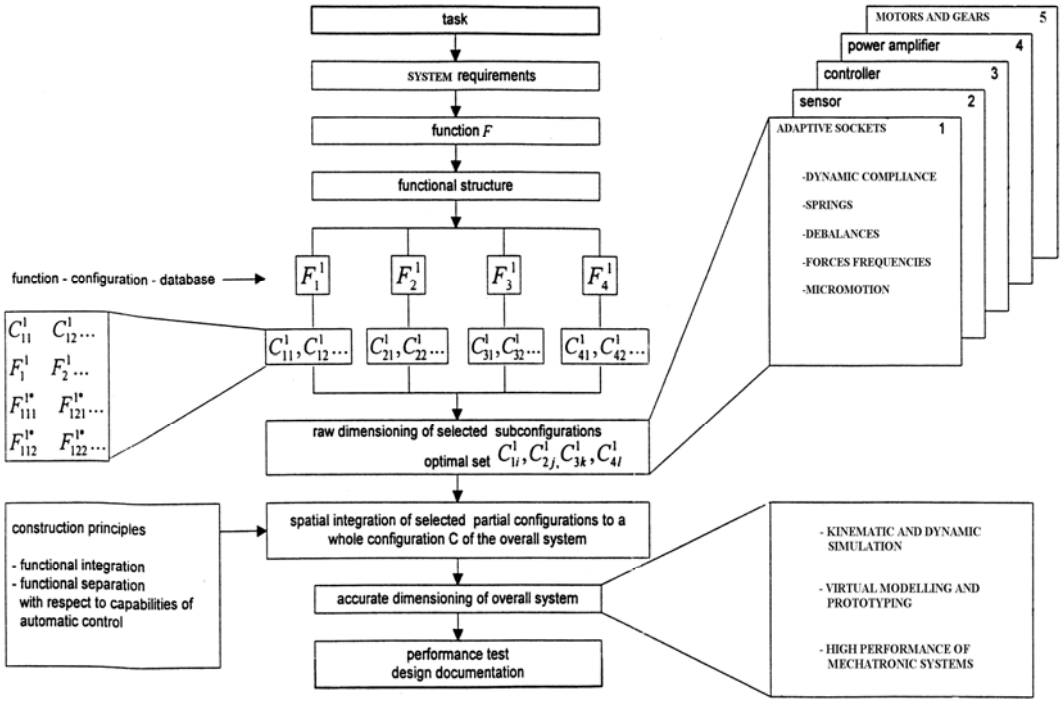

Fig.7. Design and simulation algorithm
(subfunctions and subconfigurations of complex robotic system)

Based on this methodology and interactive mechatronic environment, a real structure and solutions of adaptive robotic system are obtained. Real positioning accuracy and speed are improved, more than 15 % and the development time reduced more than 40%. Emphasis has been put on lightweight design and simulation, reconfiguration and different controller solutions. A raw draft of a controller or topological optimization can already be done with quite simple mathematical descriptions at an early stage of development. The model development can be performed in steps and adding of sensors will not affecting the modeling procedure of the submodel. The massive computational resources now available make it possible to treat the full

parametric description of a much more general class of robotic units ,so the researcher can think much more freely of generic design and control strategies which should lead to a maximum level of productivity of new ideas and technology evaluated by complete simulations. The next step is to use elaborate ways of modeling and description methods to cover all subtasks of this system in an integrative matter.

3. SENSOR BASED TASKS- MODELING AND SIMULATION

Let us first summarize the similarities and differences between non-contact sensor based tasks and force based tasks.

The task-function approach applies to both problems. The implementation of a control law involves two levels:

- High level consist of specifying the task to be performed and of choosing the vector of signals to be regulated in order to fulfill the user's objectives (choice of so called task function)
- Low level consists of writing and computing a control law (actuator torques):

$$T = M(q)\ddot{q} + N(q,\dot{q},t), \dim(q) = \dim(M) = n \quad (1)$$

where: T is the vector of applied actuator torques; M is the kinematic energy matrix; N gathers gravity, coriolis, centrifugal and friction forces; q, $\dot{q}$ - constitute the natural state vector of the system.

It may be shown that an efficient way to specify the objective that researcher wishes to reach with the robot consists of defining an output n-dimensional function e (q,t), called task to be regulated to zero during a time interval [o,T], starting from initial position q_o. A realistic approach to practical design and simulation of control laws is suggested in the form:

$$T = -K\hat{M}\left(\frac{\partial \hat{e}}{\partial q}\right)^{-1} \underline{G}\left(\mu \underline{D}\, e + \frac{\partial \hat{e}}{\partial q}\dot{q} + \frac{\partial \hat{e}}{\partial t}\right) + \hat{N} - \hat{M}\left(\frac{\partial \hat{e}}{\partial q}\right)^{-1} \quad (2)$$

where: symbol ^ points out that models (approximations, estimates) are used instead of the true terms. In this general expression all the terms except μ, D, G are allowed to be functions of q and t (here f comes from the difference of e, G and D are positive matrices; K and μ are positive scalars, all to be tuned by the researcher). Some terms ($\hat{M}, \hat{N}$) depend mainly on the used robots, while others also depend on the considered tasks, sampling period of the control laws. The performance of the feedback control loops is very sensitive to the sampling rates and propagation delays between measurements and control emission. Their value must be guaranteed in order to tune the gains of the loop.

At the equilibrium i.e. in the absence of motion the model reduces to:

$$T_{eq} = G(q_{eq}) + T_c = G(q_{eq}) + J^T(q_{eq})F_{eq} \quad (3)$$

where: J is the Jacobian matrix associated with the gripper. The differences between two classes of tasks – contact and noncontact come in part, from the physical characteristics of real contacts. For example – friction forces have to be modeled so as to estimate their contribution to the measured contact force. Then we may say that virtual contacts are easier to control than real contacts (assembly, grinding and polishing). Some knowledge of the interaction matrix is needed in the case of non-contact sensors and in both cases fine control of sensor-based tasks may require the use of dedicated estimation algorithms. Problem solutions very commonly rely on decomposition into smaller more easily understood solutions, ie the braking down of a problem into soluble parts. The whole process of investigation and creation can be represented in the form of splitting, effectively component solutions and integration after that via electronical (information) means. Physical integration is possible as well, for example intelligent actuators with sensors and etc.

4 . CONCLUSIONS

- To improve the reliability of Complex robotic systems ,make them faster and reduce the costs we have to use mechatronic environment for design and investigation,
- mechatronic modular-parameric approach to the horizontal and vertical integration and CAD integrated solutions (3D solutions)
- Sensor based control via aggregation of sensor data
- Virtual prototyping of mechanics and control via iterative mechatronic procedures (including so called hardware in the loop simulations)

This is perhaps the most efficient and modern way to the creation and application of High-performance intelligent manufacturing systems in the industry.

REFERENCES

[1.] ISSI T., Mechatronics , Moscow, 1988 (in Russian).
[2.] HONEKAMP R.et al., Structuring approach for complex mechatronic systems, Proceedings of ISATA, Florenz, VI.1997.
[3.] GEORGIEV Kr., Robotic systems for adaptive assembly, D.Sc.Thesis, 2003, 278 p., Sofia, BAS.
[4.] GEORGIEV Kr., Mechatronic assembly system with reconfiguration, Journal of Techical .Ideas, BAS, Sofia, 2005,(1).
[5.] HOLLERBACH J., Kinematics and dynamics for control in "Robotics Science", MIT,Cambridge, 1989.
[6.] GALABOV V., Synthesis of mechanisms for robotics ,Sofia ,TU edition ,1992 ,263 pages
[7.] PAVLOV V., Design of industrial robots, Sofia, 1993, 207 pages.
[8.] GEORGIEV K., Hybrid mechatronic systems for adaptive assembly and welding , Cd Proceedings of 12th international symposium MECHATRONIKA 2009 , ISBN 978-80-8075-209-5 ,Slovakia, 2009
[9.] GEORGIEV K., Accuracy analysis of MICROpositioning robotic systems, Proceedings of 7th International Conference on Biomechanics, Mechatronics and Robotics, Lepaya-Latvia, May 2010) , pp 59-63, ISBN 978-9934-10-027-7
[10.] GEORGIEV K, Synthesis and analysis of hybrid mechatronic systems for contact tasks, Proceedings of 13th international symposium MECHATRONIKA 2010, Slovakia, pp. 62-66
[11.] GEORGIEV K., KOTEV V., TIANKOV T, Callibration methodology for micro-nano robotic systems, Proceedings of 13th international symposium MECHATRONIKA 2010, Slovakia, Tr. Teplice, 2010, pp. 67-70, Proceedings registered at IEEE Xplore: DVD: (ISBN 978-80-8075-451-8; CFP1057K-DVD)PRINT: (ISBN 978-80-8075-457-0

INTERNATIONAL SYMPOSIUM on
ADVANCED ENGINEERING & APPLIED MANAGEMENT
– 40th ANNIVERSARY in HIGHER EDUCATION (1970-2010)
4 – 5 November, 2010, Hunedoara, ROMANIA

[1.] Juraj HUDÁK, [2.] Miroslav TOMÁŠ

ANALYSIS OF FORCES IN DEEP DRAWING PROCESS

[1.] DEPARTMENT OF TECHNOLOGIES AND MATERIALS, TECHNICAL UNIVERSITY OF KOŠICE,
FACULTY OF MECHANICAL ENGINEERING, KOŠICE, SLOVAKIA

ABSTRACT:
Presented contribution deals with force parameters research (drawing and blankholding) in deep-drawing process of flat bottomed cylindrical cup. Experimental research was realised using steel sheets for enamelling KOSMALT produced by U.S.Steel Košice, Ltd. Deep drawing process of this steel is complicated due to contradictory requests from the view of steel structure: good drawability and good enameling. At the present, there are new ways how to ensure requested properties from both views [6].
KEYWORDS: force parameters, research, deep-drawing processes

1. INTRODUCTION

Production of pressings is realized using forming machines, which ones act by force onto initial blank through forming die. Therefore they change its initial flat shape onto semi-finished or final product. Forming processes force parameters knows enable to technologists – forming processes designers and forming machines designers to dimension forming machine and forming die components. Besides, experimental research of forming forces allows process optimization, because they are complicated multi-factors systems. [1,2,3,5].

There are two types of sensors used in the field of force parameters research of deep-drawing processes – mechanical and electrical [3,4]. Experimental research of forces in deep-drawing processes is based on principle of non-electrical parameters measurement by electric way. Force parameters measurement (drawing and blankholding), is realized through elastic deformation element – dynamometer, which one is equipped by 4 tensometric sensors connected to Wheatston's bridge.

Experimental research of forces in deep-drawing processes is long-time realized in the Department of technologies and materials. In the past there was used measuring and monitoring system created by dynamometers (drawing and blankholding), voltage stabilizer, tensometric apparatus UM 131 and oscillograph for forces recording in force-time coordinates. Necessity of computer processing measured values required innovation of measured and monitoring system, where tensometric apparatus was developed and produced by INSPECT, Ltd. This tensometric apparatus has three canals for force recording and 1 canal for path recording and allows researching not only force-time relations, but also force-path relations.

Presented contribution deals with force parameters research (drawing and blankholding) in deep-drawing process of flat bottomed cylindrical cup. Experimental research was realised using steel sheets for enamelling KOSMALT produced by U.S.Steel Košice, Ltd. Deep drawing process of this steel is complicated due to contradictory requests from the view of steel structure: good drawability and good enameling. At the present, there are new ways how to ensure requested properties from both views [6].

2. METHODS OF EXPERIMENTAL WORK

Experimental measuring system

Research of forces in deep-drawing process was realised using with experimental measuring system machine-die-pressing consists subsystems:

1. double action hydraulic press Fritz Müller BZE 100
2. experimental drawing die with blankholder
3. pressing
4. measuring and monitoring subsystem for forces recording

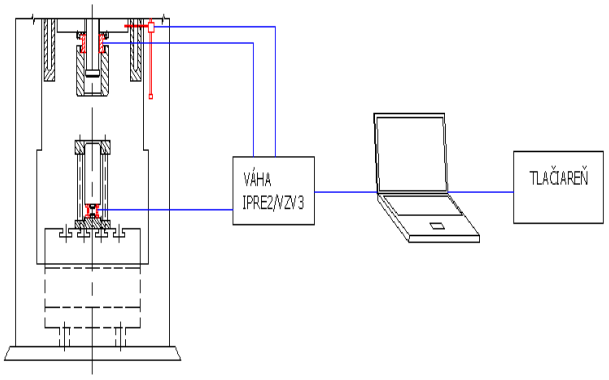

Fig. 1 Scheme of experimental measuring system. Cup, experimental material and experimental forming die

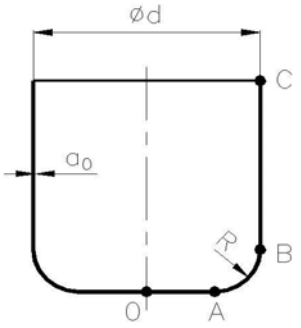

Fig. 2 Experimental flat bottomed cylindrical cup

Research of force parameters in deep-drawing process was realized on flat bottomed cylindrical cup without flange (Fig. 2). These cups were deep-drawed in experimental drawing die with blankholder (punch diameter Ø 73,5 mm, die diameter Ø 76mm, punch radius r_p = 5 mm, die radius r_t = 6 mm). Drawing of pressings with outside diameter Ø 76 mm were realised from initial blank diameters Ø 125 mm, Ø 134 mm, Ø 139 mm a Ø 145 mm.

As an experimental material there was used cold rolled drawing quality steel sheet for enamelling KOSMALT 190.21 with thickness 0,8 mm produced by U.S.Steel Košice, Ltd. Directional values of mechanical properties, normal anisotropy ratio and strainhardening exponent are shown in Table 1.

Table 1 Material formability values of KOSMALT 190.21, a_0=0,8 mm

direction [°]	$R_{po,2}$ [MPa]	Rm [MPa]	A_{80} [%]	r	r_m	Δr	n	n_m	Δn
0°	181	287	44,7	1,910	1,802	0,727	0,203	0,212	-0,006
45°	186	304	38,2	1,438			0,215		
90°	183	289	44,7	2,422			0,215		

Drawing punch and die of experimental modelling die were fastened onto press ram first and on press bed last mentioned by blankholder and drawing dynamometers. Blankholding force in drawing process was implied by rods to which act drawing cushion placed in the press bed. Blankholder dynamometer, fastened onto drawing die in the press ram, records overall force, drawing dynamometer records drawing force only. Final blankholding force is then calculated as a difference between overall force and drawing force. Path reader was placed in the left press shoe, where press ram movement was transferred onto slider movement of digital ruler SD-60.

Measuring subsystem for scanning and recording of drawing forces

Measuring subsystem for drawing forces recording consists:

1. dynamometers - drawing and blankholding (Fig. 3a)
2. path reader – digital ruler Mitutoyo SD-60 (Fig. 3b)
3. tensometric apparatus IPRE2/VZV3 (Fig. 3c)
4. notebook PC – Pentium III (Fig. 3c)
5. joining cables CANNON 9F/9M and RS232 cable

Tensometric apparatus (called weighing-machine by producer) IPRE2/VZV3 is set to continuous force measurement (weighting) and synchronised path reading from digital ruler SD-60. Electronics allows from 1 to 3 dynamometers reading and path reading. Also shows measured values of each dynamometer or path reader on display. It is also possible to set required sensor on display and set sampling frequency by which are measured and recorded data send to PC. Communication between tensometric apparatus and PC is realised through RS232 interface and apparatus is connected to PC by serial port. Data are send to PC in text file in ASCI code and allows simple importing to Excel. All communication and data sending is realised by Hyperterminal, which is standard part of MS Windows operating systems.

a) b) c)

Fig. 3 Components of measuring subsystem for recording forming forces
a) – drawing force dynamometer, b) path reader Mitutoyo SD-60,
c) tensometric apparatus IPRE2/VZV3 interconnected with PC

3. REACHED RESULTS AND INTERPRETATION

Graphic courses of drawing and blankholding forces at deep-drawing of flat bottomed cylindrical cup without failure are shown in Fig. 4 to Fig. 6 for each initial blank diameter. Graphic course of drawing and blankholding forces at deep-drawing of flat bottomed cylindrical cup from initial diameter where broken cup occurs is shown in Fig. 7

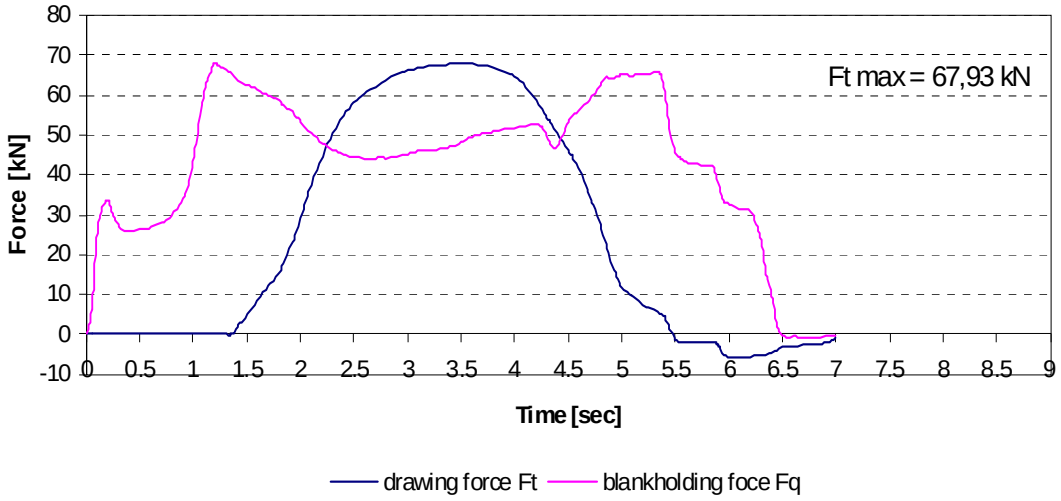

Fig. 4 Course of drawing and blankholding forces, D_0 = 125 mm, m = 0,608

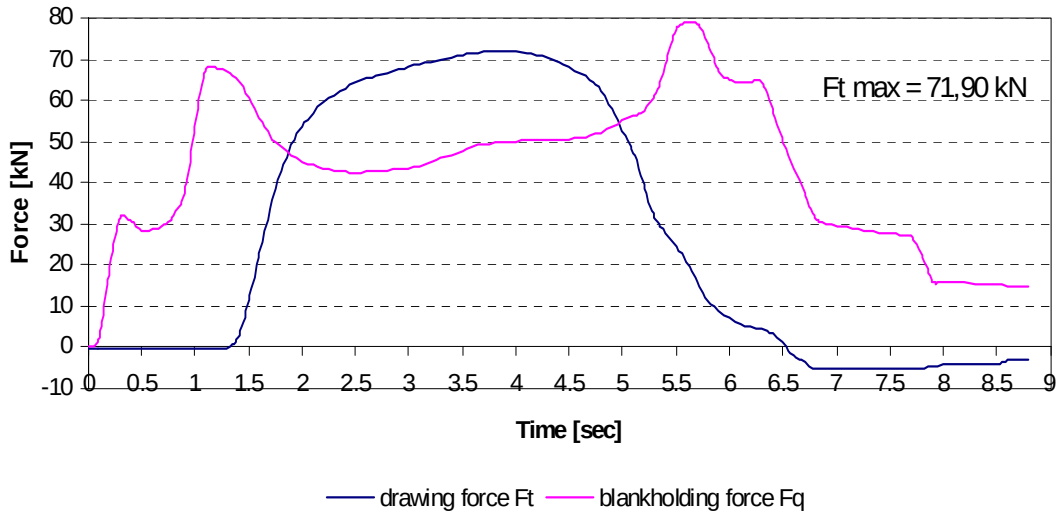

Fig. 5 Course of drawing and blankholding forces, D_0 = 134 mm, m = 0,567

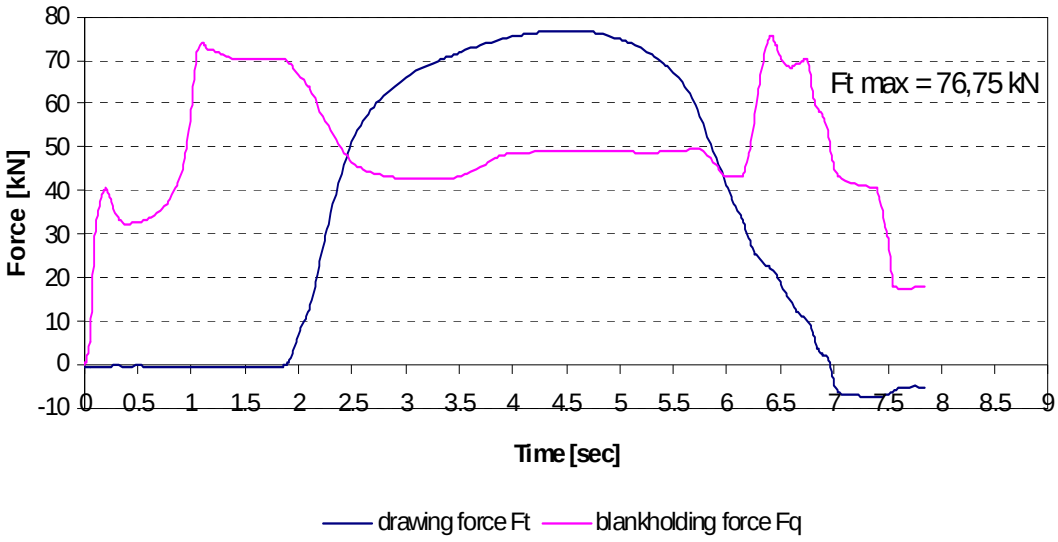

Fig. 6 Course of drawing and blankholding forces, D_o = 139 mm, m = 0,547

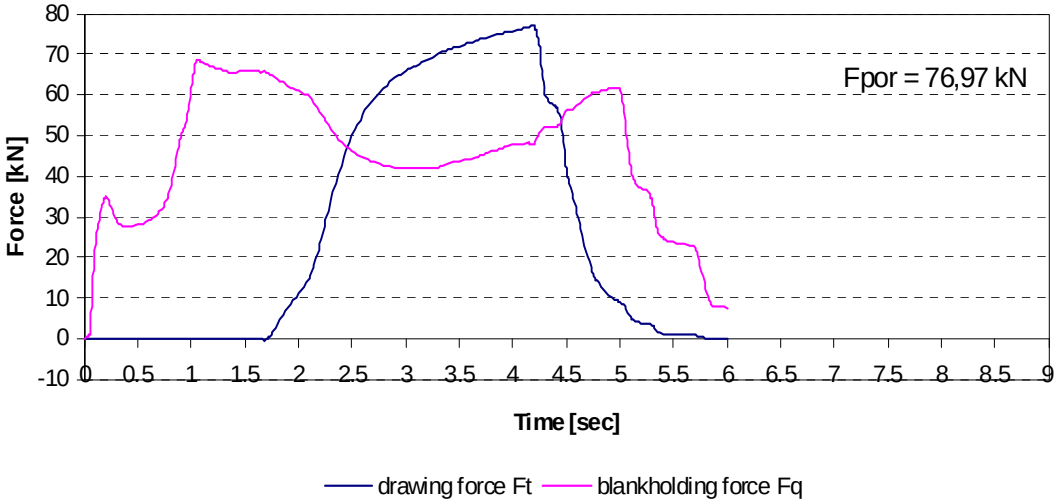

Fig. 7 Course of drawing and blankholding forces at cup breaking D_o = 145 mm, m = 0,524

Courses of drawing force at deep-drawing of flat bottomed cylindrical cup without flange from initial blanks, where no cup breaking occurs are typical for limit drawing case – drawing from flange. Drawing force increases rapidly at first stage next grows up slowly until drawing force maximum and then decreased. There is clearly seen maximum drawing force increasing with drawing ratio m decreasing. The area below drawing force line also increases. As a limit drawing ratio could be considered here drawing ratio m = 0,547 because of maximal drawing force (F_t max = 76,75 kN) is nearly to cup breaking force (F_{por} = 76,97 kN). Limit drawing ratio was observed at deep-drawing of initial blank diameter D_o = 139 mm, while cup breaking force was reached at deep drawing of initial blank D_o = 145 mm, where drawing ratio is m = 0,524.

Course of blankholding force has a dynamic character at the first stage, when blankholding touch down the drawing die. After rising up to 70 kN approx. drawing process begins and blankholding force decreases rapidly. Blankholding force decreasing could be explained as a response of press hydraulic system to press ram force movement, but there is also blankholding area decreasing due to drawing-in to die. Blankholding is then stabilised on 50 kN approx. When maximal drawing force is reached and is decreased, blankholding force increased again to initial value and next drops down after cup is drawn.

Dynamical processes at the beginning and at the end of cup drawing presents response of used machine, where there was used double action hydraulic press Fritz Müller BZE 100 equipped with drawing cushion placed in the press bed. Deep-drawing was realised using Vantol S lubricant.

Course of drawing and blankholding force at deep-drawing process when cup broke shows the same character in the first stages, as it is in deep-drawing of unbroken cup. After maximum drawing force is reached, drawing force sharply decreased. Maximum drawing force is called cup breaking force in this case. Cup breaks at the bottom to cup wall transition – at the cup radius, whereby bottom is tear off from cup wall.

4. CONCLUSIONS

From realised experiments follows:

1. course of drawing force at flat bottomed cylindrical cup without flange deep drawing process with blankholder respond to limit drawing case of deep-drawing from flange,
2. decreasing the drawing ratio caused maximal drawing force growth until dup breaking force,
3. course of blankholding force has a dynamic character at the start and at the end of deep-drawing with stabilized course when cup is drawn. This dynamic character represents response of press hydraulic system on deep-drawing process.

Realised measuring subsystem for drawing and blankholding forces recording allows realising power parameters research of deep-drawing process in dependence force-time with sampling frequency up to 0,01 s^{-1}. When path reader Mitutoyo SD-60 is used also, sampling frequency decreased up to 0,1 s^{-1}, what suit to static processes only. For that reason we consider to buy path reader with sampling frequency up to 0,01 s^{-1}, but also modification of tensometric apparatus is needed.

The advantage of measuring and monitoring subsystem is possibility to use it on whatever machine. The main restriction is the maximal allowed loading of used dynamometers, over crossing which leads to its plastic deformation.

The matter of this contribution is a part research project APVV-0629-06 [7], which is solved on Department of technologies and materials, Faculty of Mechanical Engineering, Technical university of Košice.

REFERENCES

[1] BLAŠČÍK, F. – POLÁK, K.: Teória tvárnenia. Alfa Bratislava, 1987
[2] SPIŠÁK, E. – BEŇO, J. – TOMÁŠ, M. – VIŇÁŠ, J.: Teória konvenčných technológií. TU v Košiciach, Strojnícka fakulta: 2009, 162 s. ISBN 978-80-553-0201-0
[3] BAČA, J. – BÍLIK, J. – ŽATKOVIČ, J.: Experimentálne metódy v tvárnení. Bratislava, Vydavateľstvo STU Bratislava, 2000
[4] KLEMENTEV, I. – KYŠA, R: Elektrické meranie mechanických veličín, ALFA Bratislava, 1990
[5] BÍLIK, J. – BALÁŽOVÁ, M. – KRŠIAKOVÁ, Ľ.: Vlastnosti a tvárniteľnosť plechov z ocele DP 450. Kovárenství, září 2010/38, s. 45-48, ISSN 1213-9289
[6] NIŽNÍK, Š. – ZAVACKÝ, M. – JANÁK, G. – FURMAN, Ľ.: Nové možnosti tvorby vodíkových pascí v hlbokoťažných IF oceľových plechoch určených pre smaltovanie. Acta Metallurgica Slovaca, roč. 13, č. 3 (2007), s. 336-344, ISSN 1335-1532
[7] SPIŠÁK, E. a kol.: Dizajn moderne koncipovaných ocelí na základe charakteristík lisovateľnosti. APVV-0629-06

INTERNATIONAL SYMPOSIUM on
ADVANCED ENGINEERING & APPLIED MANAGEMENT
– 40th ANNIVERSARY in HIGHER EDUCATION (1970-2010)
4 – 5 November, 2010, Hunedoara, ROMANIA

[1.] Peter KOŠTÁL, [2.] Imre KISS, [3.] Petar KERAK

THE INTELLIGENT FIXTURE AT FLEXIBLE MANUFACTURING

[1.] SLOVAK UNIVERSITY OF TECHNOLOGY, FACULTY OF MATERIALS SCIENCE AND TECHNOLOGY,
INSTITUTE OF PRODUCTION SYSTEMS AND APPLIED MECHANICS, TRNAVA, SLOVAKIA
[2.] UNIVERSITY POLITEHNICA TIMISOARA, FACULTY OF ENGINEERING HUNEDOARA, HUNEDOARA, ROMANIA

ABSTRACT:
Development of new generation production machines and systems demand that they are equipped by adequate fixture devices. These fixture devices are developed with machine together, to don't decrease their production facilities and their time and performance utilizations. Efficiency of fixture device in automatized production systems underlie using efficiency of entire production systems.
The majority of actual production is small or middle batch character. Thence, using of flexible production systems has lot of advantages. Their new generation fixture devices different from classical fixtures not only by design but also by its properties.
KEYWORDS:
intelligent fixture, flexible manufacturing, clamping, intelligent manufacturing

1. INTRODUCTION

Before 70th years of last centuries the mass production respond to basic requirements of market, but after this get started consumer affect the market. The producer must adapt to consumers requests and get started production of some variants of its products. This changeover has significant impact to mass production. Producers who can produce the wild range variants of its product have domination at market.

This trend in production continues to present time. Today market is characterized by strategy of consumer's individualization. This strategy is oriented to consumer's requests. Consumers want new products and time has a fundamental task to its satisfaction. The production was broadened, innovation cycle is shortened, the products have new shape, material and functions. At this strategy the traditional understand of costs lost in importance. Most important is a time and improving is its shortening. The production strategy focused to time need change from traditional functional production structure to production by flexible manufacturing cells and lines. Production by flexible cells (FMS) is a most important manufacturing philosophy in last years. This philosophy is based on similarity:

- similarity of manufactured parts,
- similarity of process plans.

Recognize the similarity of manufactured parts allow grouping them to groups by machines required to its manufacturing. By manufacturing of this group of parts we achieve economical effect near to mass production.

The manufacturing cell is an open manufacturing unit with transparent manufacturing processes. Flexible manufacturing cells represent a today trend to manufacturing innovations and productivity increasing.

The clamping fixture provides clamping of workpiece on machine desk, so as the workpiece have the right position toward a tool. This position must be retaining in machining time too.

Fixture using increasing the production quality, the productivity and decreasing the production costs. In some cases are fixtures using necessary. The fixture design is dependent on the

batches of production. In small batches we use the fixtures designed from modular system and in large batches we can use the dedicated fixtures.

The clamping fixture providing these basic functions:

- workpiece positioning on the desk of machine,
- to prevent of workpiece deformation when cutting and clamping forces are acting,
- tool support (in some cases).

These functions are provided by positioning, clamping and supporting elements (active elements) of fixture. These elements can be placed on standalone unit or on some units or can bee mounted to machine or some its part.

Automated technological system must ensure required product quality by theirs properties and parameters without human action. Consequently all subsystems automated technological systems are participated to provide for required quality with different but function dependent deals. For automated technological system production quality requirement assurance are needed correct decomposition functions between individual subsystems ATS, their time and position synchronization. In this process are needed respect dynamic shows and compatibility bilateral inputs and outputs of technological process in ATS.

2. FLEXIBLE MANUFACTURING

The flexible manufacturing cells are characterized by high level of manufacturing process automation. They are used mainly in middle batch production (500 – 2000 pieces of products) and for middle products range (5 – 100 types of products).

The supplementary devices are used mainly to manipulation with workpieces and tools:

- workpiece storage and device for workpiece changing,
- storage, controlling and changing of tools,
- quality control.

A part of complex automated manufacturing process is an automation of technological process control, automated transportation, handling, feeding, interchange of workpieces, tools and automated waste cleaner. There are many technological sites existing, which match given requirements. Besides obvious computer techniques for controlling the manufacturing machines, automatically working bins, loaders, conveyors, manipulators and industrial robots are implemented step by step. As industrial production is growing constantly, besides implementing of the classical automated means, which were mentioned above, manufacturing systems with intelligent control are being installed.

Exploitation of automated manufacturing systems is conditional by effectiveness of all subsystems, from which is the automated manufacturing system created. All subsystems are often developed together with certain automated system, not to decrease parameters of whole system.

3. INTELLIGENT CLAMPING FIXTURE AT GENERAL

The majority of actual production is small or middle batch character. Thence, using of flexible production systems for these types of production has a lot of advantages. The flexible production systems must has a flexible clamping fixtures too. This new generation fixture devices different from classical fixtures not only by design but also by its properties.

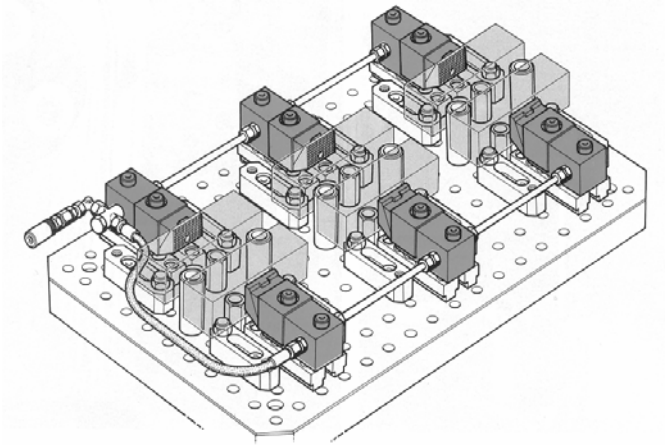

Fig. 1: Hydraulically operated clamping fixture

In standard production are mechanical peripheries (for example fixtures) controlled and monitored by operators. In automated production must these mechanical peripheries working in automated mode too. It means, that they must have not only own driving mechanism (hydraulic, pneumatic, electrical), but must have control and monitoring units too. The examples of hydraulic controlled clamping mechanism is at Fig. 1.

In time of working cycle these devices working automatically, without operator intervention and cooperate with other devices of production system.

During a automated work cycle are control and monitoring execute by sensors. The control based on sensors and controlled driving mechanism is base conditions for intelligent clamping fixture realize.

These intelligent clamping fixtures apart from the base functions provide same "intelligent" functions too:

- control of forces and torques acting to workpiece,
- monitoring of clamping operations and particular elements of fixture by sensors,
- other purpose oriented functions as clamping jaw change, or change of industrial robots end effectors

The aims of force and torque controlling are increasing of clamping operations reliability, decrease of workpiece deformation and decrease of workpiece surface damage possibility.

The clamping forces are proportional to pressure in pneumatic or hydraulic cylinder. This means, that we can monitor the clamping forces by monitoring of pressure in the cylinder. For pressure monitoring are used pressure sensors on base of tenzometers. For exact measure of clamping forces we can use force sensors build in clamping jaws.

The monitoring of clamping operations and particular elements of fixture enable the continuous diagnostic of clamping system. In base of this diagnostics can predict the possible future damages of fixture and we can disposal them before come the dropout in production, or ensue the bigger damage on the fixture system, tools or workpiece.

4. INTELLIGENT CLAMPING FIXTURE DESIGN

At our department is under realization the intelligent clamping fixture for flexible manufacturing cell. The basic condition to this clamping fixture is fellows:

- clamped workpiece has dimensions up to 60 mm,
- this fixture must be operated pneumatically (simply to change the clamping force by pressure),
- possibility of clamping jigs change,
- this fixture must give information to control system about:
  - air pressure,
  - position of clamping jigs (open or closed),
  - workpiece occurrence in clamping space,
  - clamping jig occurrence at jig holder,

When we will equip the clamping fixture by sensors, we achieve to capability collaboration between clamping fixture and flexible manufacturing cell.

The moving of clamping jigs holder are solved by pneumatic cylinders. Synchronization of this moving are realized by gears. Position of clamping jigs can be detected by magnetics sensors on side of fixture body. The position of clamping jig holder is detected by two magnetic sensors on side of fixture body.

The CAD model of our intelligent clamping fixture is shown in Fig. 2. These clamping fixtures can be used in a various field of small batch production:

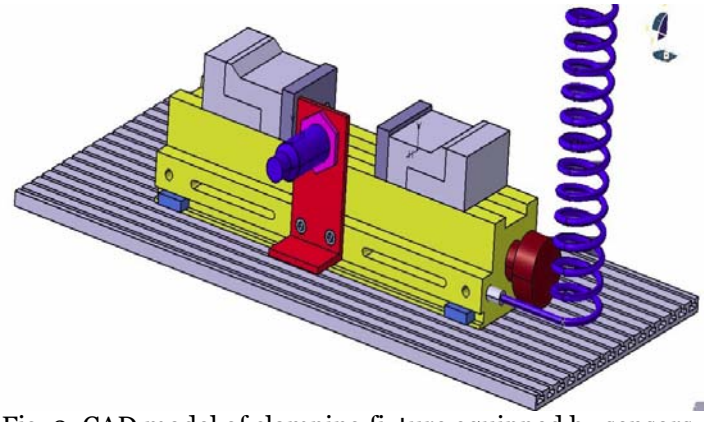

Fig. 2: CAD model of clamping fixture equipped by sensors

- clamping for NC, CNC machines,
- clamping for robotized production,
- clamping for measure systems,
- clamping for special automatized operations.

5. CONCLUSION

The cell manufacturing become in last years one of most important manufacturing type. This conception is based on relation between manufacturing cell – workpiece. Flexible manufacturing cells allows manufacturing the small numbers of part from huge range of types and achieve good economical effects near by large batch or mass production. The manufacturing cells structure has

connected the machines and save the production time, space and production costs too. Function of machines is coordinated and the material flow can be quick.

Use of intelligent fixtures helps increase reliability of manufacturing operations. Production with intelligent fixtures is more flexible. These fixtures are more expensive and more complex as classical fixtures, because has own automated clamping, positioning, control and monitoring units.

The intelligent devices helps prevent the production disorders in automated production systems.

Application of intelligent fixtures eliminates the hard manual works. Also can save manpowers and increase the productivity.

The aim advantage of intelligent fixture using is their capability reacts to production program exchange. Adaptability of these systems is base of higher generation of automation.

Acknowledgment:
This paper was created thanks to the national grants: VEGA 1/0163/10 – Clamping fixtures in intelligent production systems

REFERENCES

[1.] Danišová, Nina: Application of intelligent manufacturing system in the flexible assembly cell. In: Annals of Faculty of Engineering Hunedoara - Journal of Engineering. - ISSN 1584-2673. - Tom V, Fasc 3 (2007), s. 41-45

[2.] Charbulová, Marcela: Modular clamping systems. In: Annals of Faculty of Engineering Hunedoara - Journal of Engineering. - ISSN 1584-2673. - Tom V, Fasc 3 (2007), s. 49-54

[3.] Košťál, Peter - Velíšek, Karol - Zvolenský, Radovan: Intelligent Clamping Fixture in General. In: Lecture Notes in Computer Science. - ISSN 0302-9743. - Vol. 5315: Intelligent Robotics and Applications. First International Conference, ICIRA 2008, Wuhan, China, October 15-17, 2008. Part II (2008). - ISBN 978-3-540-88516-0, s. 459-465

[4.] Matúšová, Miriam - Javorová, Angela: Modular clamping fixtures design for unrotary workpieces. In: Annals of Faculty of Engineering Hunedoara - Journal of Engineering. - ISSN 1584-2673. - Tom VI, Fasc 3 (2008), s. 128-130

[5.] Mudriková, Andrea - Hrušková, Erika - Horváth, Štefan: Areas in flexible manufacturing-assembly cell. - článok vyšiel v časopise: Annals of Faculty of Engineering Hunedoara - Journal of Engineering, ISSN 1584-2673, Tome VI, Fascicule 3, 2008, str. 123-127. In: Scientific Bulletin. - ISSN 1224-3264. - Vol. XXII (2008), s. 293-298

[6.] Mudriková, Andrea - Hrušková, Erika - Velíšek, Karol: Logistics of material flow in flexible manufacturing and assembly cell. - registered in ISI Proceedings. In: Annals of DAAAM and Proceedings of DAAAM Symposium. - ISSN 1726-9679. - Vol. 19, No.1. Annals of DAAAM for 2008 & Proceedings of the 19th International DAAAM Symposium "Intelligent Manufacturing & Automation: Focus on Next Generation of Intelligent Systems and Solutions", 22-25th October 2008, Trnava, Slovakia. - Vienna : DAAAM International Vienna, 2008. - ISBN 978-3-901509-68-1, s. 0919-0920

[7.] Mudriková, Andrea - Velíšek, Karol - Košťál, Peter: Clamping fixtures used for intelligent assembly systems. In: ISCCC 2009: Proceedings of the 2009 International Symposium on Computing, Communication and Control, October 9-11, 2009, Singapore. - Singapore: International Association of Computer Science and Information Technology Press, 2009. - ISBN 978-9-8108-3815-7. - S. 9-15

[8.] Velíšek, Karol - Košťál, Peter - Zvolenský, Radovan: Clamping Fixtures for Intelligent Cell Manufacturing. In: Lecture Notes in Computer Science. - ISSN 0302-9743. - Vol. 5315: Intelligent Robotics and Applications. First International Conference, ICIRA 2008, Wuhan, China, October 15-17, 2008. Part II (2008). - ISBN 978-3-540-88516-0, s. 966-972

INTERNATIONAL SYMPOSIUM on
ADVANCED ENGINEERING & APPLIED MANAGEMENT
– 40th ANNIVERSARY in HIGHER EDUCATION (1970-2010)
4 – 5 November, 2010, Hunedoara, ROMANIA

[1.] Miroslava KOŠTÁLOVÁ

ASSEMBLING AND VERIFICATION DESIGN CORRECTNESS OF PRESS TOOLS BY HELP OF SYSTEM CATIA

[1.] SLOVAK UNIVERSITY OF TECHNOLOGY IN BRATISLAVA, FACULTY OF MATERIALS SCIENCE AND TECHNOLOGY, INSTITUTE OF PRODUCTION TECHNOLOGIES, DEPARTMENT OF FORMING, SLOVAKIA

ABSTRACT:
The paper deals with application of CATIA software in press tools construction for sheet metal forming. For development trends is characteristic utilization of scientific research in area of technological forming method with output on optimization, standardization and normalization. Software CATIA enables creation of catalogue of pressed parts, parametric creation of pressed tools, quickly design of required press tool and verification of correctness press tool design.

KEYWORDS:
combination press tool, verification, designing, kinematics

1. INTRODUCTION

Information technologies are means, which provides help to users in concrete disciplines in determination of optimal problems solving out of possible variants. In the area suggestion and construction of new products means set of informative technolologies in the first place abbreviation of development period and possibility of complex product description in term of its geometry and mechanical properties. Information about tool acquired on base the creation of 3D models is more complex than 2D drawing documentation. It is possible to use 3D dates in the preparation area and it makes possible consecutive immediate interconnection construction with production. It is first of all qualitative and it is quite principled change to the development of new product. It is characteristics for developments trends application results of scientific research in the area CA technology in designing of tools with output on optimization, standardization and normalization of segments and constructive groups of tools. It makes possible to apply standardization of constructive tools systems and consecutive quick design ground of tool, with the correspondent complement of functional parts. The tools for sheet metal forming in term of construction are very individual, production of each of pressed part requires dedicated tool.

Resource at tools construction is job description of production, it essentially influence on selection of operational and constructive parts of stamping dies, for design of tool are necessary construction-technological calculus, choice of suitable type of tool is realized on base request of automation.

2. FEATURE OF PRESS TOOL MODELLING BY SOFTWARE CATIA

The base for suggestion of press tool is computer model, which is created in development places of work. At data transmission between various places of work with the same system is secured full compatibility and transmission of various parameters, technological oriented entity and alike. CAD software have function for recovery of random damaged dates.

The main reasons, which guide to decide to use 3D system in construction works:

- enhancement of productivity in construction works
- reduce of mistakes in documentation
- improve documentation, especially bigger clearness at using of axonometric views, which are easy deduced from 3D model

- parametrization of each components, tools.
- the check is rises on models, not on drawing
- consistent structure of assemblies
- excessively effective tool to eliminating crashes

The possibilities of tools construction by software CATIA:

- construction of tool with possibility of its next modification
- creation of standard tool by part choosing from several modular systems (HASCO, FIBRO, RABOURDIN, STEINEL)
- creation own database of tools, components,
- catalogization of constituent components
- creation of full parametric model

3. SOLUTION OF CHOSEN TYPE OF TOOL

Technical characterization of press tool

The basic parameter for design type of tool was request of mass production of pressing, with designation as bottom. It was suggested combination press die that realizes operations blanking and drawing for one press stroke. According number of pressed parts of the same sort manufactured for one stroke it belongs in category of single-impression tools. In term of construction it is tool with guide by help of pins and guide bushings. Sheet strip will be used as semiproduct that will be manually put in tool on stepper backstop and back guiding pins. After first stroke is strip manually by operator moved and positioned on stepper backstop. Finished pressing is at the same time ejected through front chute in prepared container at shifting of strip. The scrap is removed in form of remains of strip, which operator put to palette after processing of last piece.

Operating characteristic of tool

- by type of feeding and collating of semiproduct - tool with manual feeding
- by type of pressing removal - tool with backward pressing displacement and its self-acting removal
- by type removal of scratch - removed in form strip remnant or strap

Solution of tool kinematics

On the fig. 1 is start of kinematics tool motion, when is tool in top dead centre. Than top part of tool moves down and after 30 mm it occurs touch of stripper with material and next after one mm occurs touch between cutting punch and material. Stripper is compressed through springs. The cutting punch stepwise intrudes into material and after cut compresses cutting punch blankholder and by consecutive compression draws bottom until achievement of bottom died center, when the tool returns into its initial position. End of tool motion is on the fig. 2.

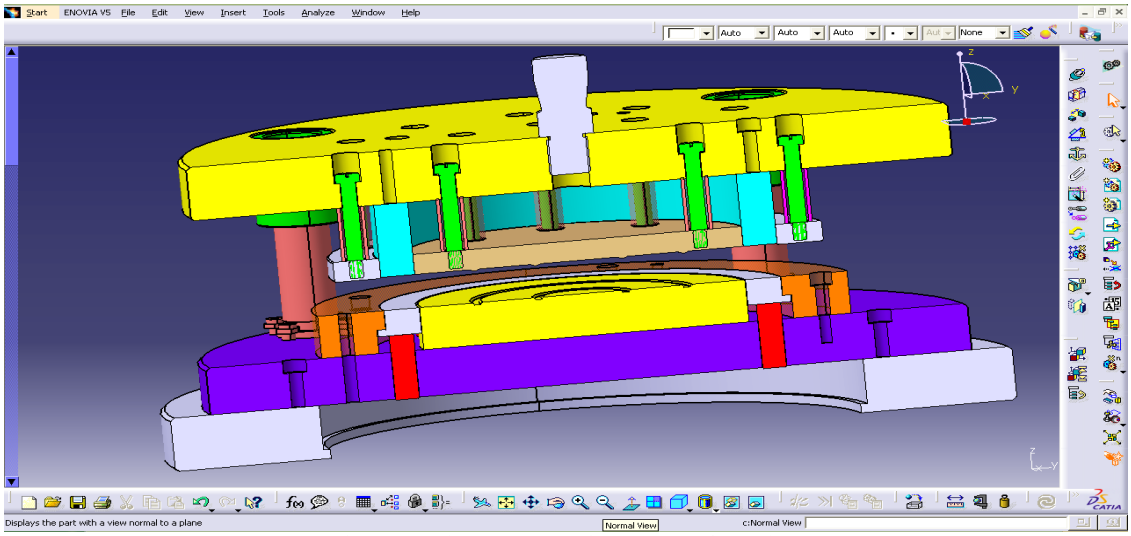

Figure 1 The press tool at start of motion

It was possible to trace tool motion from top die center to bottom die center after simulation running. It was utilized for description tool kinematics module Digital Mockup.

The module has appliances for design and control of digital prototype of press tool and for simulation of its functionality, it draws possible kinematics collision.

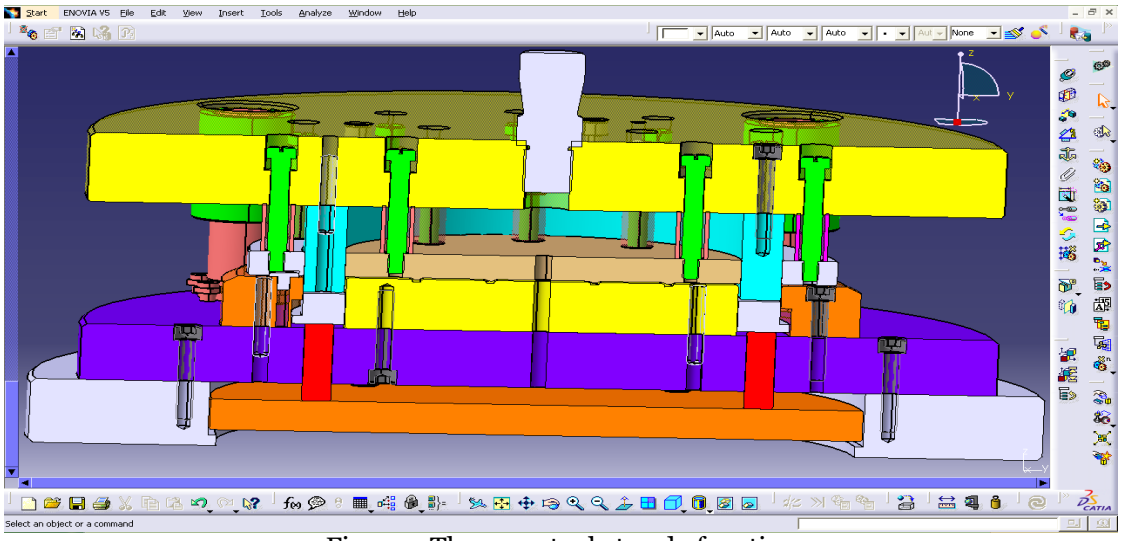

Figure 2 The press tool at end of motion

Verification of technologic parts of tool by help of analysis

It was required from constructional aspect allowance between cutting punch and stripper 0,5 mm. This request was checked by collision analyze, which establishes collision between components, eventually touch of components. On the fig. 3 is displayed contact between cutting punch and stripper with orange color, and at table on the right side is value of clearance equal 0 mm. The analyze mention on necessity of dimensions modification.

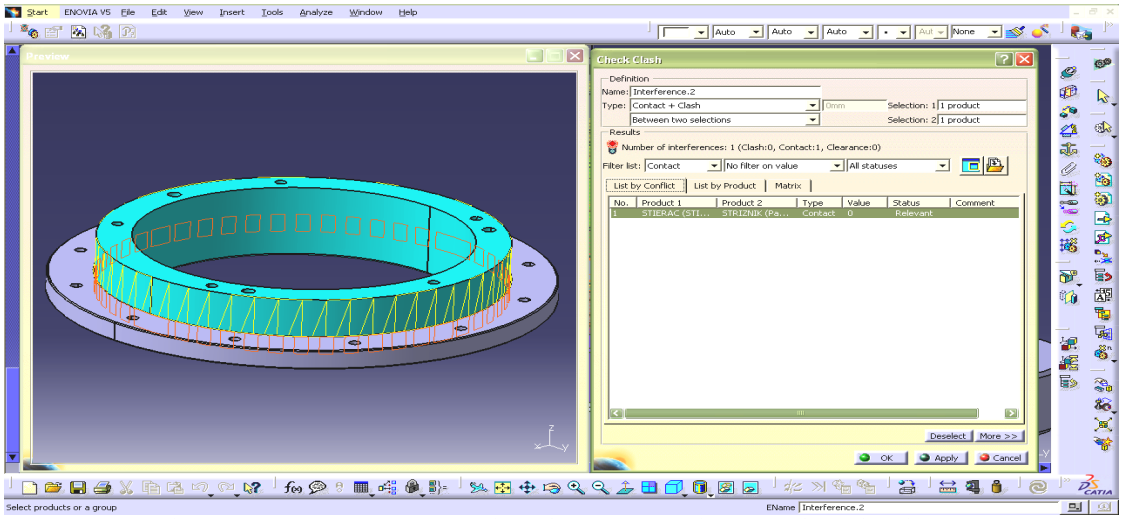

Figure 3 Contact representations between cutting punch and stripper

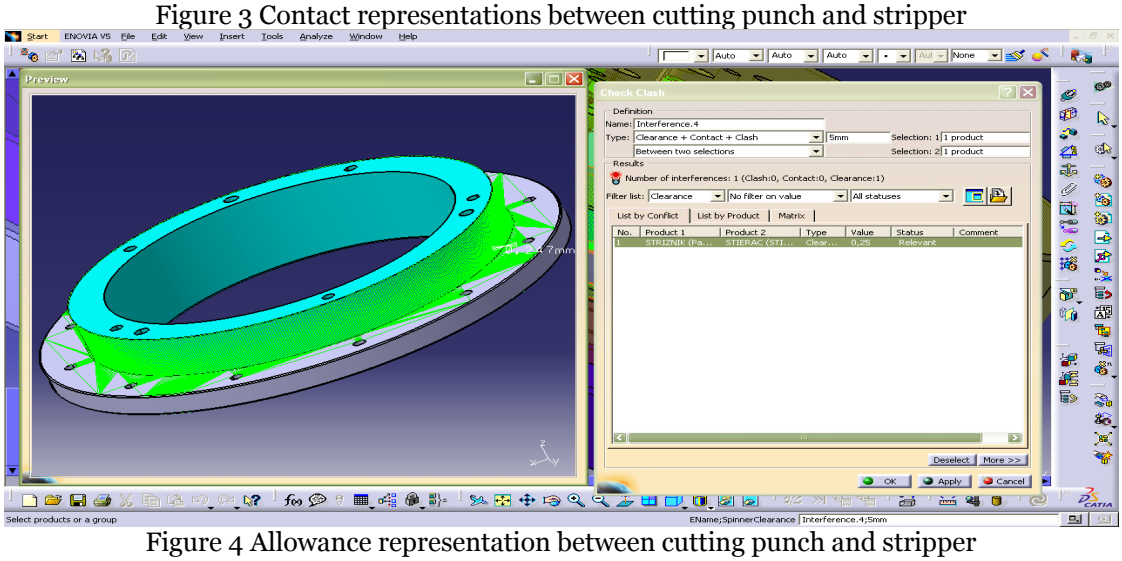

Figure 4 Allowance representation between cutting punch and stripper

Analysis of overhangs is on fig. 4. It results from analyze, that value of allowance corresponds to required value, in due window is value 0,25 mm and status Relevant, the allowance is displayed by green color. For creating analyze of overhangs and various collisions it was used modules Compute a Clash and Compute Clearance.

4. CONCLUSION

In respect of demand production of various shapes of pressed parts, the press tool represents very often the complicated kinematics system. By help of specialized functions of CATIA software constructer can in whichever state of production to analyze kinematics functions and to search possible clashes. It is possible to move with kinematics parts of tool and to check false clashes between various parts. The tool is possible to check by dynamic section by moveable plane and so it is possible quickly control 2D section. After verification precision of digital model it is possible automatic generation of NC programs for production. Such manner is saved time and material in preliminary stage of feeding production.

ACKNOWLEDGEMENTS

The paper was created with thanks of national grant VEGA 1/0060/08

REFERENCES

[1] KURIC, I., Košturiak, J., Janáč, A., Peterka, J., Marcinčin, J. Počítačom podporované systémy v strojárstve. Žilina : EDIS, 2002, s. 11-39 ISBN 80-7100-948-2
[2] POLÁK, K. Strihanie. Bratislava, SVTL 1967
[3] ZEMAN K. Prípravky, obrábecí a tvárecí nástroje. Nástroje pro tváření., Praha: ČVUT 1988
[4] KAPUSTOVÁ, M. – BÍLIK, J. Využitie výpočtovej techniky v oblasti tvárnenia. In Trendy technického vzdelávaní 2000, Olomouc, s. 161-164
[5] KOŠŤÁL, Peter - Mudriková, Andrea: Material flow in flexible manufacturing and assembly. In Computing and Solutions in Manufacturing Engineering, September 25-27, 2008, Brasov, Romania. In: Academic Journal of Manufacturing Engineering. - ISSN 1583-7904. - Supplement, Issue 1 (2008), s. 185-191
[6] KOŠŤÁL, Peter - Mudriková, Andrea: Uniwersalny system produkcyjny z wykorzystaniem komputerowo sterowanych urzadzeń. In: Nowoczesne, niezawodne i bezpieczne systemy mechanizacyjne dla górnictwa. - Gliwice : Centrum Mechanizacji Górnictwa KOMAG, 2008. - ISBN 978-83-60708-23-1. - S. 429-437
[7] KOŠŤÁLOVÁ, Miroslava - Kapustová, Mária: Designing variable parts of shearing tools by help of computer technique. In: Scientific Bulletin. - ISSN 1224-3264. - Vol. XXI / nadát. International Multidisciplinary Conference. 7th. Baia Mare, Romania, May 17-18, 2007 (2007). - Baia Mare : North University of Baia Mare, s. 359-362
[8] KOŠŤÁLOVÁ, Miroslava - Kapustová, Mária: Model construction of tools for sheet metal forming. In: KOD 2006 : Zbornik radova / nadát. Simpozijum sa medunarodnim učešcem. 4. Konstruisanje, oblikovanje i dizajn. Palic, 30-31. maj 2006. - Novi Sad : Fakultet tehničkih nauka, 2006. - ISBN 86-85211-92-1. - S. 271-272
[9] KOŠŤÁLOVÁ, Miroslava: Suitable forming tools types for robotized workplace.In: RaDMI 2006 : Proceedings on CD-ROM / nadát. International Conference. Budva, Montenegro, 13-17.Sept. 2006. - Trstenik : High Technical Mechanical School of Trstenik, 2006. - ISBN 86-83803-21-X. - S. 1-5
[10] KOŠŤÁLOVÁ, Miroslava: Designing variable parts of forming tools. Modelovanie variabilných častí tvárniacich nástrojov. In: CO-MAT-TECH 2006. 14. medzinárodná vedecká konerencia (Trnava, 19.-20.10.2006). - Bratislava : STU v Bratislave, 2006. - ISBN 80-227-2472-6. - S. 576-579
[11] KOŠŤÁLOVÁ, Miroslava: Model construction of shearing tools.In: CO-MAT-TECH 2005 : Proceedings/ International Scientific Conference, 13th, Trnava, Slovak Republic ,20-21 October 2005. - Bratislava : STU v Bratislave, 2005. - ISBN 80-227-2286-3. - S. 578-581

INTERNATIONAL SYMPOSIUM on
ADVANCED ENGINEERING & APPLIED MANAGEMENT
– 40th ANNIVERSARY in HIGHER EDUCATION (1970-2010)
4 – 5 November, 2010, Hunedoara, ROMANIA

[1.] Pavol ČEKAN, [2.]Anh NGUYEN THE, [3.]Ervin LUMNITZER

APPLICATION OPPORTUNITIES VIBRATION ANALYSERS

[1-3.] TECHNICAL UNIVERSITY IN KOŠICE, FACULTY OF MECHANICAL ENGINEERING, DEPARTMENT OF ENVIRONMENTAL STUDIES AND INFORMATION ENGINEERING, KOŠICE, SLOVAKIA

ABSTRACT:
This contribution dwell on apportionment accelerometer to categories. Characteristic any choises class accelerometers and allocation baseline allegation for choice adequate type. Alternative correct arection accelerometers in alone process of metering vibes.
KEYWORDS:
accelerometer, signal, vibration, sensor

1. EXORDIUM

At the present time quality of environment human is constantly invade whereby several factors, which negatively effects arrogate in large criterion also vibes. We know, that vibes let us say vibration in common is move physical system, which over deviation get back always into the stability location. Fot all that for metering vibes most often use as electromechanical converter of mechanical vibration on electrical signal (analyzer),which works on principle Newton´s intensity canon and piezoelectrical effect. By piezoelectrical effect is intensity on output directly in proportion to power and acceleration vibes, result from also name analyser – accelerometer.

2. ALLOTMENT ANALYSERS OF ACCELERATION VIBRATION (ACCELEROMETS)

Accelerometer is apparatus, which mete vibrations or acceleration in move compages (construction, parts of machines tec.). Intensity induce vibes or change move (acceleration) affect on substance analyse, which then compress piezoelectrical element generating electrical charge commensurable to compression. Because is electrical charge commensurable to intensity and substance of analyzer is constant, is so electrical charge also commensurable to acceleration.

Analyzers mechanic vibration (accelerometers) by principle activity we can separate on:

- **Active (generatorical)**, which are generic on their output electrical module e.g. piezoelectricaland electrodynamical;
- **Pasive, exigent of power energy**, which are modulation of any electrical modulate, or parameter of electrical circuit.

From these two basic groups analysers are used most often on metering of vibes:

- Piezoelectric (PE),
- Piezoelectrical with inbuilt electronic (IEPE),
- Piezorezistíve (PR),
- Capacitive (VC). [3]

3. CHARACTERISTIC SOME CHOICES TYPES OF ANALYSERS

On the basis listed above knowledges, opportunites use analysers and their technical parameters we can characteristic following types:

a) Model 7251A piezoelectric accelerometer IEPE

The Endevco model 7251A is a small piezoelectric accelerometer with integral electronics is shown on figure 1, designed specifically for measuring vibration on most structures. The unit is

hermetically sealed against environment contamination, offers high output sensitivity, and wide bandwidth. This new light weight (10.5 *gm*) design effectively minimizes mass loading effects.

Figure 1. Piezoelectric accelerometer IEPE model 7251A

The model 7251A features Endevco's Piezite type P-8 crystal element, operating in annular shear mode, which exhibits low base strain sensitivity and excellent output stability over time. This accelerometer incorporates an internal hybrid signal conditioner in a two-wire system, which transmits its low impedance voltage output through the same cable that supplies the constant current power. Signal ground is connected to outer case of the unit and, when used with the supplied isolated mounting screw, it is electrically isolated from ground. The centrally located mounting bolt permits 360° cable orientation, a very desirable feature in many applications. A model number suffix indicates sensitivity in *mV/g*; i.e., 7251A-10 features output sensitivity of 10 *mV/g*. Tablet 1. usher specification hereof scanner. [2]

Tablet 1. Specification [2]

Sensitivity (typical)	-10; 10 *mV/g* -100;100*nV/g*
Frequency response (± 1 *dB*)	2 to 10 000*Hz*
Shock limit	5000*g* pk
Temperature range	-67° *F* to + 257°*F* (-55°*C* to +125°*C*)
Weight	10,5 grams (0,37 oz)
Mounting	Insulated mounting screw or adhesive

b) Model 7264G Piezoresistive accelerometer

The Endevco model 7264G is a very low mass piezoresistive accelerometer (figure 2) weighing only 1.4 gram. This accelerometer is designed for crash testing, rough road testing and similar applications that require minimal mass loading and a broad frequency response. This acelerometermeets SAEJ211 and SAEJ2570 specifications for instrumentation for impact testing. It is equivalent in form and fit to the Endevco model 7264C-2K in that the location of the center of seismic mass is the same.

Figure 2 Piezoresistive accelerometer model 7264G.

The model 7264G utilizes a unique and advanced micromachined sensor which includes integral mechanical stops and damping. This monolithic sensor offers improved ruggedness, stability and reliability over previous designs. The model 7264G has suitable damping to minimize phase shift over the useful frequency range and attenuate resonance. With a frequency response extending down to dc (steady state acceleration), this accelerometer is ideal for measuring long duration transient shocks.

This accelerometer has a two active arm full bridge circuit with two fixed resistors to facilitate shunt calibration. Full scale output is 400 *mV* with 10 *V*dc excitation. It is also available with less than 1% transverse sensitivity ("T" option) and less than ±25 *mV* zero measured output ("Z" option).Tablet 2. usher specification hereof scanner.[2]

Tablet 2. Specification [2]

Sensitivity	(at 100 *Hz* & 10 *g*) (min/typ/max) *mV/g* 0.15/0.20/0.30
Frequency response *Hz*	(± 2.5% max, ref. 100 *Hz*) 0 to 2000 (± 4.0% max, ref. 100 *Hz*) 0 to 4000
Transverse sensitivity %	max 3 (1 optional)
Thermal sensitivity shift (max)	From +10 ˚*C* to +30 ˚*C* %/˚*C* typ ±0.06 From +50 ˚*F* to +86 ˚*F* %/˚*F* typ ±0.1

c) Acceleration Sensor AS – 020

The acceleration sensor AS-020 is used for measurement of vibration acceleration. Acceleration sensors operate in accordance with the piezo-electric compression principle (see figure 3).

Figure 3
Acceleration sensor
AS-020

Inside the sensor, a spring/mass damping system is formed by a piezo-ceramic disk and an internal sensor mass. When introducing vibrations into this system, the mass exerts an alternating force on the ceramic disk, and due to the piezo-electric effect, electric charges are caused which are proportional to acceleration. An integrated charge amplifier increases the output signal to a usable signal level. Tablet 3 usher specification hereof scanner.[1]

Tablet 3. Specification [1]

Transmission factor	100 *mV/g* ±5 % 10,2 *mV/m/s2* ± 5 %
Sensitivity deviation due to Temperature	- 22 °*C* - 3 % + 22 °*C* 0 % + 65 °*C* + 2,5 % + 120 °*C* + 5,5 %
Measuring range	± 80 *g* (UB = -24 *V*...-30 *V*) ± 40 *g* (UB = -20 *V*) ± 20 *g* (UB = -18 *V*)
Frequency range	4 ... 10 000 *Hz* (± 0,5 *dB*) 1,5 ... 15 000 *Hz* (± 3 *dB*)

4. EXAMPLES INSTALLATION OF ACCELEROMETER IN THE PROCESS OF METERING VIBES

Accelerometer we can install by six methods in the seriately duality to accomplish results of metering (see figure 4).:

a) The mechanical screw (needs a preparations on all kinds catch are mostly in accessories accelerometers, sometime their is advisable specify in the order) (see figure 4a);
b) The elecric isolate screw (this metod we apply if we get signal, although the measure point is not energizing) (see figure 4b);
c) The gripping by parametral magnet (this is the simplest gripping and is use in normal metering most useles) (see figure 4c);
d) The affixion of sensor with bee-wax (see figure 4e) or with fast toughen glue (see figure 4d);
e) The metering to screw by hand sonde (see figure 4f).

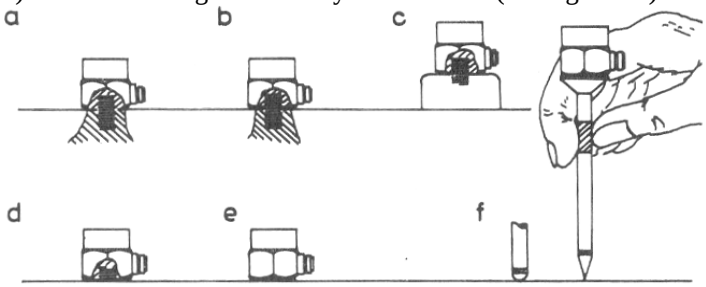

Figure 4 The style of gripping accelerometer. a – gripp by steel screw, b – gripp by electric isolate screw on isolate plate, c – gripp by permanent magnet, d – affix by the fast-gel glue, e – afix by bee-wax, f – screw by hand sonde with various types of tip

On (figure 5) is schematic exemples odvise installation of accelerometer and cable in process metering vibes.

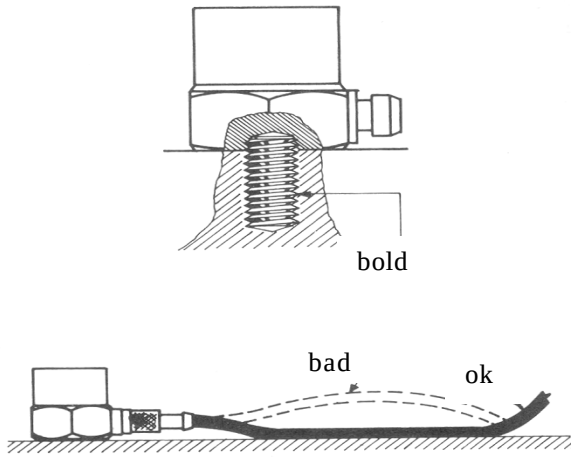

Figure 5 The instal accelerometer and cable at measure of vibes

On measure of vibes is important deliberate all positive requests at choice the favourable type soft sensor. Basal request, important especially on measuring of vibes easiest objevte is, that substanciality used sensor could not affected the vibes of measure point. On normal valuation is valid one princip, that sensor must by minimal 10 times easier as measure object and at the same time is necessary by care on the places, which have small consistence.[3]

5. CONCLUSION

The vibes as well as another factors are inseparatable component of environment for human. Summarize is therefore necessarily accentuate importace of measure vibe as negative factor of environment. Provide full elimination or cut down negative effects of vibes and contribute for upgrade of environment for human.

Acknowledgement
This paper was supported by projects KEGA 3/7426/09 Creation of didactic details and publishing of university textbook „Physical factors of environment - valuation and assessment" for main field 2nd and 3rd level of study environmental focused studying programs.

REFERENCES

[1.] Brüel&Kjaer Vibro [citing 2010-10-1]. Availableoninternet: <http://www.bkvibro.com>.
[2.] Endevco [citing 2010-10-1]. Available on internet: <http://www.endevco.com>.
[3.] ZAJAC, Jozef – TOMAŠVIČ, Peter – STAŠ, Anton: Znižovanie hluku a vibrácií v strojárskych prevádzkach: Bratislava: ALFA, 1990. 224 s. ISBN 80-05-00674-8

INTERNATIONAL SYMPOSIUM on ADVANCED ENGINEERING & APPLIED MANAGEMENT
– 40th ANNIVERSARY in HIGHER EDUCATION (1970-2010),

INTERNATIONAL SYMPOSIUM on
ADVANCED ENGINEERING & APPLIED MANAGEMENT
– 40th ANNIVERSARY in HIGHER EDUCATION (1970-2010)
4 – 5 November, 2010, Hunedoara, ROMANIA

[1.] Adalbert KOVÁCS

THE LAGRANGE INTERPOLATION FORMULA FOR ANALYZING FLUID MOVEMENT IN NETWORK PROFILES

[1.] UNIVERSITY "POLITEHNICA" OF TIMISOARA, DEPT. OF MATHEMATICS, TIMIŞOARA, ROMANIA

ABSTRACT:
The paper presents two calculus algorithms for the study of the compressible fluid's stationary movement through profile grids on an axial–symmetric flow–surface. The first method is based on an iterative formula developed by the authors to calculate the complex conjugate velocity (using the CVBEM algorithm). The second method solves the fundamental integral equation in real values by a priori building up the velocity potential's integral equation (BEM method). In this case it is presented the necessity of using the Lagrangian interpolation formula through five points for the calculation of the derivatives of the velocity potential. In both cases the consecutive approximations can be organized simultaneously or successive with respect to parameters ς (fluid's density) and h (thickness variation of fluid stratum).

KEYWORDS: hydrodynamic networks, boundary element method, Lagrange interpolation, complex velocity, velocity potential, Fredholme integral equation

1. INTRODUCTION

We study the direct problem from the hydrodynamics of networks for the stationary subsonic movement of the compressible fluid through profile grids on an axial-symmetric flow-surface, in variable thickness of stratum.

The movement is completely defined by the following equations [6]:

- Continuity equation for the compressible fluid:

$$div(\varsigma \cdot h \cdot \bar{v}) = 0 \tag{1}$$

- Potential (irrational) movement equation:

$$rot\ \bar{v} = 0 \tag{2}$$

- Characteristic equation of state of compressible fluid:

$$\varsigma = \varsigma(p) \tag{3}$$

where:
- ς and p are the fluid's density and pressure, respectively;
- $\bar{v}$ is the fluid's absolute velocity;
- h is a function of the thickness variation of fluid stratum.

Additionally to equations (1), (2), (3), while studying the direct problem, the following boundary value conditions are also considered:

a. The upstream and downstream velocities ($\vec{V}_{1\infty}$ and $\vec{V}_{2\infty}$, respectively) of the fluid are considered to be known;
b. The relative velocity on a flow-surface, thus also on the base profile L_0, is a tangential velocity. The transport velocity $\vec{u}$ is tangent to the circle that contains the current point of L_0. Hence, the considered flow-surface is a flow-surface for the absolute motion, thus we have:

$$(\vec{v} \cdot \vec{n})\big|_{L_o} = (\vec{w} + \vec{u}) \cdot \vec{n}\big|_{L_o} = (\vec{w} \cdot \vec{n})\big|_{L_o} = 0 \tag{4}$$

where: - $\vec{n}$ is the normal versor to the flow-surface;
- $\vec{w}$ is the fluid's relative velocity.

c. For ensuring unique solution, it is assumed that in the motion without detachments an equivalent condition with the Jukovski-Ciaplighin hypothesis is fulfilled, e.g. the equality of velocities in two points A' and A'' symmetrically situated on the trailing edge, thus we have [6]:

$$\left|\vec{v}_{A'}\right| = \left|\vec{v}_{A''}\right| \tag{5}$$

2. PREZENTING THE PROBLEM. THE COMPLEX VELOSITY OF MOVEMENT

The fundamental equations from the CVBEM method [3] in the problem of the compressible fluid's movement on a axial-symmetric flow–surface, in variable thickness of stratum are [6, 7, 8]:

$$\begin{aligned} \overline{w}(z) &= \overline{V}_m + \int_{L_0} H(z,\xi)\overline{w}(\xi)d\xi + i\iint_{D_0^-} H(z,\xi)\hat{q}(\xi)d\xi d\eta \\ F(z) &= \overline{V}_m \cdot z + \Gamma \cdot G(z,\xi_A) + \int_{L_0} H(z,\xi)F(\xi)d\xi + i\iint_{D_0^-} G(z,\xi)\hat{q}(\xi)d\xi d\eta \end{aligned} \tag{6}$$

where: $\overline{w}(z) = v_x - iv_y$ – is the complex conjugate velocity of motion; $F(z) = \varphi + i\psi$ is the complex potential of motion, where φ is the velocity potential and ψ is the flow rate function; A – is a fixed point on the base profile L_0; t – is the grid step; Γ – is the circulation around L_0; $\overline{V}_m = \frac{1}{2}\left(\overline{V}_{1\infty} + \overline{V}_{2\infty}\right)$ – is the asymptotic mean velocity;

$$\begin{aligned} H(z,\xi) &= \frac{1}{2ti} ctg\frac{\pi}{t}(z-\xi) \\ G(z,\xi) &= \frac{1}{2\pi i}\ln\sin\frac{\pi}{t}(z-\xi) \\ \hat{q}(\xi) &= 2\frac{\partial\overline{w}}{\partial\xi} = -\left(v_x\frac{\partial\ln p^*}{\partial\xi} - v_y\frac{\partial\ln p^*}{\partial\eta}\right), p^* = \frac{\varsigma\cdot h}{\varsigma_0}, \\ v_x &= \frac{\partial\varphi}{\partial x} = \frac{1}{p^*}\frac{\partial\psi}{\partial y}, \\ v_y &= \frac{\partial\varphi}{\partial y} = -\frac{1}{p^*}\frac{\partial\psi}{\partial x} \end{aligned} \tag{7}$$

$D_{0^*}^-$ – bounded simple convex domain, defined as: $D_{0^*}^- : \left[-\frac{t}{2}<\xi<\frac{t}{2}, -\left(t+\frac{l}{2}\right)<\eta<\left(t+\frac{l}{2}\right)\right]$ (8)

where l – is the projection of L_0 profile's frame on the Oy axis.

Based on the results of [5], [6] in the practical calculus of the complex conjugate velocity $\overline{w}(z)$, given by (6), the following iteration formula can be applied:

$$\overline{w}(z) = \overline{V}_m + \overline{w}_0^{(n)}(z) + \overline{w}_{\Delta q^*}^{(n-1)}, \quad n = 1,2,... \tag{9}$$

where: $\overline{w}_0^{(n)}(z) = \frac{1}{2it}\int_{L_0}\overline{w}^{(n)}(\xi)\cdot H(z,\xi)d\xi$

$$\begin{aligned} &\overline{w}_{\Delta q^*}^{(n-1)} = i\iint_{D_{0^*}^-}\Delta q^{*(n-1)}\cdot H(z,\xi)d\xi d\eta \\ &\Delta q^{*(n-1)}(\xi) = -\Delta v_x^{(n-1)}\frac{\partial\ln p^{*(n-1)}}{\partial\xi} - \Delta v_y^{(n-1)}\frac{\partial\ln p^{*(n-1)}}{\partial\eta} \\ &p^{*(n-1)} = \frac{(\varsigma\cdot h)^{(n-1)}}{\varsigma_0} \\ &\varsigma^{(n-1)} = \varsigma_0\left(1 - \frac{k-1}{2}\frac{\left(\overline{w}^{(n-1)}\right)^2}{c_0^2}\right)^{\frac{1}{k-1}}, \text{ where } k \text{ is the adiabatic constant} \\ &\left|\overline{w}^{(n-1)}\right|^2 = \left(v_x^{(n-1)}\right)^2 + \left(v_y^{(n-1)}\right)^2 \\ &c_0 \text{ – is the sound velocity} \end{aligned} \tag{10}$$

The successive approximation methods can be applied on (9) simultaneously over ς and h, or successively over ς and h. In the first approximation step it is assumed that $\varsigma = \varsigma_0 = const.$ and $h = const.$, hence $q^{*(0)}(\xi) = \Delta q^{*(0)}(\xi) = 0$, and (6) is solved without the double integral. For the velocity $\overline{w}^{(1)}(z) = v_x^{(1)} - iv_y^{(1)}$ thus obtained it is possible to determine $\varsigma^{(1)}, p^{*(1)}$. Next, $\Delta q^{*(1)}$ is calculated, and $\overline{w}^{(1)}_{\Delta q^*}$, is obtained from (10). Furthermore, we proceed similarly with the second approximation step, etc. Another possibility for solving the fundamental equations (6) is given by the BEM method [6], i.e. solving the equations in real variables, using the results of [7]. For doing so, we consider the integral equation of the complex potential $F(z) = \varphi + i\psi$, and transform it into an integral equation with real variables, i.e. we build the integral equation of the velocity potential $\varphi(x,y)$.

3. THE LAGRANGE INTERPOLATION POLYNOMIAL IN DETERMINING THE VELOCITY POTENTIAL OF MOVEMENT

3.1. The Lagrange Interpolation Polynomial

The problem of constructing a continuously defined function from given discrete data is unavoidable whenever one wishes to manipulate the data in a way that requires information not included explicitly in the data. The relatively easiest and in many applications often most desired approach to solve the problem is *interpolation* [2], where an approximating function is constructed in such a way as to agree perfectly with the usually unknown original function at the given measurement points. In the practical application of the finite calculus of the problem of interpolation is the following: given the values of the function for a finite set of arguments, to determine the value of the function for some intermediate argument[2].

A chronological overview of the developments in interpolation theory, from the earliest times to the present date could be found in. In this section we focus our attention on the theory of the *lagrange interpolation polynomial* [2], since, as we have already mentioned in the proof of proposition 3.3, its usage arises also in our calculus algorithm for the study of the compressible fluid's stationary movement through profile grids on an axial–symmetric flow–surface in variable thickness of stratum.

The problem of interpolation consists in the following [2: Given the values yi corresponding to xi, i = 0, 1, 2, . . . , n, a function f(x) of the continuous variable x is to be determined which satisfies the equation:

$$y_i = f(x_i) \text{ for } i = 0,1,2,\ldots,n \quad (11)$$

and finally $f(x)$ corresponding to $x = x'$ is required. (i.e. x' different from x_i, $i = \overline{1,n}$.)

In the absence of further knowledge as to the nature of the function this problem is, in the general case, indeterminate, since the values of the arguments other than those given can obviously assigned arbitrarily.

If, however, certain analytic properties of the function be given, it is often possible to assign limits to the error committed in calculating the function from values given for a limited set of arguments. For example, when the function is known to be representable by a polynomial of degree n, the value for any argument is completely determinate when the values for $n + 1$ distinct arguments are given.

Consider the function $f : [x_0, x_n] \to R$ given by the following table of values [2]:

x_k	x_0	x_1	...	x_n
$f(x_k)$	$f(x_0)$	$f(x_1)$	...	$f(x_n)$

x_k are called *interpolation nodes*, and they are not necessary equally distanced from each other. We seek to find a polynomial $P(x)$ of degree n that approximates the function $f(x)$ in the interpolation nodes, i.e.:

$$f(x_k) = P(x_k); k = 0,1,2,\ldots,n \quad (12)$$

The **Lagrange interpolation method** finds such a polynomial without solving the system (12).

Theorem 3.1. Lagrange Interpolating Polynomial

The Lagrange interpolating polynomial *is the polynomial of degree* n *that passes through* (n + 1) *points* $y_0 = f(x_0), y_1 = f(x_1), \ldots y_n = f(x_n)$. *It is given by the relation ([2]):*

$$P(x) = \sum_{j=0}^{n} P_j(x) \quad (13)$$

where:
$$P_j(x) = y_j \prod_{k=0, k\neq j}^{n} \frac{x - x_k}{x_j - x_k} \tag{14}$$

Written explicitly:
$$\begin{aligned} P(x) = &\frac{(x-x_1)(x-x_2)...(x-x_n)}{(x_0-x_1)(x_0-x_2)...(x_0-x_n)} y_0 + \\ &+ \frac{(x-x_0)(x-x_2)...(x-x_n)}{(x_1-x_0)(x_1-x_2)...(x_1-x_n)} y_1 + \\ &+ \frac{(x-x_0)(x-x_1)...(x-x_{n-1})}{(x_n-x_0)(x_n-x_1)...(x_n-x_{n-1})} y_n \end{aligned} \tag{15}$$

For illustrating the usability of the Lagrange interpolation method through five points for our calculus algorithm for the study of the compressible fluid's stationary movement through profile grids on an axial–symmetric flow–surface in variable thickness of stratum, namely, for calculating the tangential velocity $v_\tau = \frac{d\varphi}{ds}$ (see section 3, proposition 3.3, equation (24)).

3.2. Solving the Integral Ecuation of Velocity Potential

Our purpose is to solve the fundamental equations (6) (obtained from the CVBEM method) using (BEM) in real variables. For doing so, we consider the fundamental integral–equation of the complex potential $F(z) = \varphi + i\psi$ and transform it into an integral equation with real variables, i.e. we build the integral equation of the velocity potential $\varphi(s)$ ($\psi(s)$ is the flow rate function).

Theorem 3.2. *[6], [8] In the subsonic motion of the compressible fluid through the profile grid, on an axial–symmetric flow–surface, in variable thickness of stratum, the velocity potential* $\varphi(s)$, $s \in L_o$ *is the solution of the integral equation (16):*
$$\varphi(s) + \int_{L_o} \varphi(\sigma) \frac{dM(s,\sigma)}{d\sigma} d\sigma = b(s) + \iint_{D_{o^*}^-} \bar{q}(\sigma) N(s,\sigma) d\xi d\eta \tag{16}$$

where:
$s(x_o, y_o)$ and $\sigma(\xi,\eta)$ are the curvilinear coordinates of the fixed point A on the L_o base profile;
$$b(s) = 2\left(x_o V_{mx} + y_o V_{my}\right) + \Gamma M(s,\sigma_A) + \int_{L_o} [\psi(s) - \psi(\sigma)] \frac{dN}{d\sigma} d\sigma$$

$$M(z_o,\zeta) = \frac{1}{\pi} arctg \frac{th\frac{\pi}{t}(\eta - y_o)}{tg\frac{\pi}{t}(\xi - x_o)} \tag{17}$$

$$N(z_o,\zeta) = \frac{1}{\pi} \ln \sqrt{\frac{1}{2}\left[ch\frac{2\pi}{t}(\eta - y_o) - \cos\frac{2\pi}{t}(\xi - x_o)\right]}$$

v_{mx}, v_{my} - are the components of the asymptotic mean velocity v_m.

Proposition 3.1. *[7],[8] In the case of an axial-subsonic movement of a perfect and compressible fluid through profile grids, the flow rate function is determined from the boundary condition (6):*
$$\psi(s) = u_o \cdot \int_o^s p^*(s) \left(\frac{R}{R_o}\right) ds, \qquad u_o = \omega R_o, \tag{18}$$

where: ω is the angular rotation velocity of the profile grid; R_o defines the origin of the axis system related to the turbine's axis.

Equation (16) is an integro–differential equation. In this section, we will show a possibility of solving this equation applying the *method of successive approximation* (the iteration method), using also the result from [6] about the order of the term containing the double integral expression:
$$\varphi_{\bar{q}}(s) = \iint_{D_{0^*}^-} \bar{q}(\sigma) N(s,\sigma) d\xi d\eta \tag{19}$$

Proposition 3.2. *[6], [8] In the case of the subsonic movement of the compressible fluid through the profile grid on an axial–symmetric flow–surface, in variable thickness of stratum, the integral equation of the velocity potential* $\varphi : D_{0^*}^- \to \Re$ *is solvable by applying the method of successive approximations w.r.t. the parameter* $p^* = \frac{\varsigma \cdot h}{\varsigma_o}$.

Proof. For isentropic processes , by the Bernoulli–equation, we obtain:

$$\varsigma = \varsigma_0\left(1-\frac{\gamma-1}{2}\frac{v^2}{c_0^2}\right)^{\frac{1}{\gamma-1}}, v^2 = v_\tau^2 + v_n^2, v_\tau = \frac{d\varphi}{ds}, v_n = \frac{1}{p^*}\frac{d\psi}{ds} \tag{20}$$

where: γ is the adiabatic constant; c_o is the sound velocity in the zero velocity point; v_τ and v_n are, respectively, the tangential and normal velocities on L_o.

In the first approximation it is assumed that $\varsigma = \varsigma_o$ = constant and $p^* = p^{*(0)}$ = constant. Thus, from (7), it results that $q^{(0)}(\sigma) = 0$. Hence, in the integral equation (4) the double integral (19) is neglected and results the following Fredholme integral equation of second type, with continuous nucleus:

$$\varphi^I(s) + \int_{L_0}\varphi^I(s)\frac{dM(s,\sigma)}{d\sigma}d\sigma = b^I(s) \tag{21}$$

From solving equation (21) we obtain φ^I , and furthermore from (18), (20), (24) ψ^I, ς^I are obtained. Finally, using the relation:

$$p^* = \frac{\varsigma\cdot h}{\varsigma_0}, \qquad \bar{q}(\sigma) = -grad\varphi\cdot grad\ln p^* \tag{22}$$

a p^{*I} and $\bar{q}^I(\sigma)$ are determined.

In the second iteration $p^* = p^{*I}$ is assumed and for the determination of $\varphi^{II}(s)$ the following Fredholme integral equation of second type, with continuous nucleus, will be solved:

$$\varphi^{II}(s) + \int_{L_0}\varphi^{II}(\sigma)\frac{dM(s,\sigma)}{d\sigma}d\sigma = b^{II}(s) + \iint_{D_0^-}q^I(\sigma)N(s,\sigma)d\xi d\eta \tag{23}$$

where a φ^I and $b^{II}(s)$ are previously calculated from (18) and (17), respectively.

From solving equation (23), we obtain φ^{II} . Furthermore, from (18), (20), (24) and (22) ψ^{II}, ς^{II}, p^{*II} and $\bar{q}^{II}(\sigma)$ are obtained, respectively. Next, the third approximation might be done by assuming $p^*=p^{*II}$, and so on.

Proposition 3.3. *[7], [8] Having given the values of the velocity potential on each element of the* L_0 *profile's division, the tangential velocity* v_τ *may be calculated in each division element of the* L_0 *basic profile's boundary by the formula, given by the Lagrange interpolation method through five points:*

$$v_{\tau i} = \frac{d\varphi}{ds}(s_i) = \frac{2}{3\Delta s_i}(\varphi_{i+2}-\varphi_{i-2}) - \frac{1}{12\Delta s_i}(\varphi_{i+4}-\varphi_{i-4})$$

$$h = \Delta s_i = s_{i+1} - s_{i-1}, \tag{24}$$

$$i = 1,3,5,\ldots,2n-1,$$

where n denotes the number of division elements and by s_i we refer to the i^{th} element of the division of L_o.

To ensure the practical functionality of proposition 3.2, i.e. to indicate the solving method of the Fredholme integral equation of second type obtained in each approximation step (equation (18), (23)), let us formulate and prove two more propositions.

Based on the results obtained by employing the interpolation formula through five points (24), we further determine the velocities $v_{\tau i}$ and with the size of the complex velocity w_i. Using such obtained values, in [8] we give an efficient algorithm for deriving the fluid's complex velocity through profile grids.

4. CONCLUSION

We have shown some practical aspects of the usage of the calculus algorithm for the study of the compressible fluid's stationary movement through profile grids, on an axial–symmetric flow–surface, in variable thickness of stratum, namely :

- the usage of the boundary element method with real values;
- the applicability of the successive approximation method w.r.t. the parameters ς (fluid's density) and h (thickness variation of fluid stratum) for solving the integral equation of the velocity potential;
- the usage of the Lagrangian interpolation formula through five points for calculating the derivatives of the velocity potential.

Regarding practical applicability of our algorithm, our plans for the near future are:

- make more test cases w.r.t. several input (geometrical and hydrodynamical) values of the velocity potentials taken from practical experiments involving profile grids;
- study the possibility of applying the algorithm (i.e. the approximation methods) for the calculation of other fluid–characteristics.

REFERENCES

[1] P. Benerji and R. Butterfield: The Boundary Element Method in Applied Sciences (in Russian), MIR, Moskow, 1984.
[2] B. P. Demidovici and I. A. Maron: The Mathematical Basis of Numeric Calculus (in Russian). Nauka, Moskow, 1970.
[3] T.V. Hromadka II: The Complex variable boudary element method. Springer Verlag, Berlin, 1984.
[4] A. Kovács: Boundary element method for analyzing fluids movements in network profiles, Proc. of 8th Int. Symposium of Hungarian Researches on Computational Intelligence and Informatics, Budapest, Hungary, Nov. 15-17, 2007, pp. 139-150.
[5] A. Kovács: Über die Stabilierung und Bestimmung einer Iterationsformel für einen konexen unendlichen Bereich. Proc. of the 8th Symposium of Mathematics and its Applications, Timisoara, Romania, Nov. 4-7, 1999, pp. 88–92.
[6] A. Kovács: Mathematische Modelle in der Hydrodynamik der Profilgitters. Monographical Bookles in Applied and Computer Mathematics PAMM, Budapest, MB-19, 2001.
[7] A. Kovács and L. Kovács: The Lagrange Interpolation Formula in Determining the Fluid's Velocity Potential through Profile Grids. Bulletins for Applied Mathematics, Proc. of 2005 PAMM's Annual Central Meeting T.CVII/2005, Nr.2252, Balatonalmádi, Hungary, May 26-29, 2005, pp. 126-135.
[8] A. Kovács and L. Kovács: On the Calculus Algorithm of the Fluid's Velocity Potentials Through Profile Grids. Annals of the Faculty of Engineering Hunedoara-Journal of Engineering, Tome VII, Fasciule 3, pp. 232-237.
[9] G. V. Viktorov and I. V. Vutchikova: The Calculus of Fuid–Flow through Profile Grids on an Axial–Symmetric Flow–Surface with Variable Thickness of Stratum (in Russian), Izd. ANSSSR, MJG, vol. 5, 1969, pp. 96–102.
[10] G. N. Poloji: The Theory and Applications of P-analytic and (P,Q)-analytic Functions (in Russian). Nauka Dumka, Kiev, 1973.

INTERNATIONAL SYMPOSIUM on
ADVANCED ENGINEERING & APPLIED MANAGEMENT
– 40th ANNIVERSARY in HIGHER EDUCATION (1970-2010)
4 – 5 November, 2010, Hunedoara, ROMANIA

[1.]Diana STOICA

DISCRETE ASYMPTOTIC BEHAVIORS OF STOCHASTIC SKEW-EVOLUTION SEMIFLOWS IN HILBERT SPACES

[1.]UNIVERSITY "POLITEHNICA" TIMISOARA, FACULTY OF ENGINEERING OF HUNEDOARA, ROMANIA

ABSTRACT:
The paper presents the properties of exponential stability and instability in mean square for discrete stochastic skew-evolution semiflows in Hilbert spaces. Some characterizations which generalize classics results obtained in deterministic case are also provided.
KEYWORDS:
Discrete stochastic skew-evolution semiflows, stability and instability in mean square

1. INTRODUCTION

In this article we consider the stochastic skew-evolution semiflows, which can be considered a generalization of skew-product introduced by Arnold L. in [1], and present the proprieties of discrete exponential stability.

The problem of existence of stochastic cocycle over the stochastic semiflows is presented in many papers (see [2], [3], [6] and [8]).

Some of the results for uniform asymptotic behaviors in mean square of stochastic cocycles generated by stochastic differential equations was studied in the papers of D. Stoica [11,12].

We considered H a real Hilbert spaces. Let B(H) be a Banach space of all linear and bounded maps $A : H \to H$. We denote the sets $T = \{(m,n) \in N^2, m \geq n \geq 0\}$.

Assume $(\Omega, \Im, \mathbf{P})$ is a complete probability space with a normal filter $\{\Im_t\}_{t\geq 0}$, i.e. $\Im_0$ contains the null sets in $\Im$ and $\Im_t = \bigcap_{s>t} \Im_s$, for all $t \geq 0$, and let us consider a real valued $\{\Im_t\}$ - Wiener process $\{W(t)\}, t \geq 0$.

Let be $F : [0,T] \times \Omega \to H$ a stochastic process, and then $E(F) = \int_\Omega F(\Omega)\, dP(\omega)$ represent the mean of stochastic process F, where P is the probability measure. If $F \in C\left([0,T], L^2(\Omega, H)\right)$ then $\int_0^T E \,||\, F(t) \,||^2 \, dt = E\int_0^T ||\, F(t) \,||^2 \, dt$.

For an process Wiener W(t) in rapport with the filter $\{\Im_t\}$ we have

$$E\left\| \int_0^T F(t)\, dw(t) \right\|^2 = E\int_0^T ||\, F(t) \,||^2 \, dt .$$

Definition 1. Let be H a Hilbert space. A discrete stochastic semiflow on H is a random field $\varphi : (T \times \Omega, B(H) \times \Im) \to (\Omega, \Im)$ satisfying the following proprieties:

(1) $\varphi(n,n,\omega) = \omega$, for all $n \geq 0$ and $\omega \in \Omega$;

(2) $\varphi(m,n,\varphi(n,p,\omega)) = \varphi(m,p,\omega), \quad \forall (m,n),(n,p) \in T, \forall \omega \in \Omega$.

Definition 2. A discrete stochastic cocycles on H, over an discrete stochastic semiflow $\varphi : (T \times \Omega, B(H) \times \Im) \to (\Omega, \Im)$, is a random field $\Phi : (T \times \Omega, B(H) \times \Im \times B(H)) \to L(H)$, with the following proprieties:

(1) $\Phi(n,n,\omega)=I$, (Identity operator on H), $\forall n\geq N$, and $\omega\in\Omega$,

(2) $\Phi(m,n,\varphi(n,p,\omega))\Phi(n,p,\omega)=\Phi(m,p,\omega)$, $\forall(m,n),(n,p_0)\in T$, and $\omega\in\Omega$.

Definition 3. The mapping $\Theta: T\times Y\to Y$, defined by

$$\Theta(m,n,\omega,x)=(\varphi(m,n,\omega),\Phi(m,n,\omega)x)$$

where $Y=\Omega\times H$ is called the discrete stochastic skew-evolution semiflow on Y, and we denoted by $\Theta=(\varphi,\Phi)$.

Example 1. Let $\Theta_0(m,\omega,x)=(\varphi_0(m,\omega),\Phi_0(m,\omega)x)$ be the discrete skew-product of the metric discrete dynamical system $\varphi_0(m,.)$, $\forall m\in N$ on Ω, generated by de Wiener shift, introduced by Arnold in [1]. Then the mapping $\Theta=(\varphi,\Phi)$, defined by

$$\varphi(m,n,\omega)=\varphi_0(m-n,\omega)$$

$$\Phi(m,n,\omega)=\Phi_0(m-n,\omega),\quad \forall\,(m,n)\in T,\ \omega\in\Omega.$$

is a discrete stochastic skew-evolution semiflow, which generalizes the notation of classical discrete skew-product, considered by Arnold L. in [1].

A typical example of discrete skew-evolution semiflow is generated by the solution operator at time $t=n$ for a stochastic linear differential equation.

2. UNIFORMLY EXPONENTIALLY STABILITY AND INSTABILITY IN MEAN SQUARE

In this section we give the integral characterizations of uniform exponential stability and instability in mean square of discrete stochastic skew-evolution semiflows in Hilbert spaces. The main results are generalizations of the characterizations obtained in deterministic case, and presented of many authors including the papers [4], [9] and [10].

Definition 5. The discrete stochastic skew-evolution semiflow Θ is said to be uniformly exponentially stable in mean square if for some positive random variables $N(\omega)\geq 1, a(\omega)\in(0,1)$ one has

$$E\,\|\Phi(m,p,\omega)x\|^2\leq N(\omega)a(\omega)^{m-n}E\,\|\Phi(n,p,\omega)x\|^2, \tag{1}$$

for all $(m,n),(n,p)\in T,(x,\omega)\in Y$.

Definition 6. The discrete stochastic skew-evolution semiflow Θ is said to be uniformly exponentially instable in mean square if for some positive random variables $N(\omega)\geq 1, a(\omega)\in(0,1)$ one has

$$N(\omega)a(\omega)^{m-n}E\,\|\Phi(m,p,\omega)x\|^2\geq E\,\|\Phi(n,p,\omega)x\|^2, \tag{2}$$

for all $(m,n),(n,p)\in T,(x,\omega)\in Y$.

Theorem 7. Let be $\Theta=(\varphi,\Phi)$ a discrete stochastic skew-evolution semiflow. Then $\Theta=(\varphi,\Phi)$ is uniformly exponentially stable in mean square if and only if there are random variables $D(\omega)\geq 0$, such that:

$$\sum_{k=n+1}^{\infty}E\,\|\Phi(k,p,\omega)x\|^2\leq D(\omega)E\,\|\Phi(n,p,\omega)x\|^2, \tag{3}$$

for all $(n,p)\in T,(x,\omega)\in Y$.

Proof. *Necessity*. Let be a discrete stochastic skew-evolution semiflow $\Theta=(\varphi,\Phi)$ uniformly exponentially stable in mean square. Then, for $N(\omega)\geq 1, a(\omega)\in(0,1)$ we have from Definition 5, that

$$E\,\|\Phi(m,p,\omega)x\|^2\leq N(\omega)a(\omega)^{m-n}E\,\|\Phi(n,p,\omega)x\|^2,$$

for all $(m,n),(n,p)\in T,(x,\omega)\in Y$. Write this relationship for $k=n+1,n+2,\cdots,L$ and then we sum these relations member with member and we have:

$$\sum_{k=n+1}^{L}E\,\|\Phi(k,p,\omega)x\|^2\leq N(\omega)\sum_{k=n+1}^{L}a(\omega)^{m-n}E\,\|\Phi(n,p,\omega)x\|^2 \text{ for all } (n,p)\in T,(x,\omega)\in Y.$$

Passing to the limit for $L \to \infty$ and we obtained

$$\sum_{k=n+1}^{\infty} E \| \Phi(k,p,\omega)x \|^2 \le D(\omega) E \| \Phi(n,p,\omega)x \|^2$$

where $D(\omega) = N(\omega)\dfrac{a(\omega)}{1-a(\omega)}$, for all $(n,p) \in T, (x,\omega) \in Y$.

Sufficiency. For $(n,p) \in T$ and $(x,\omega) \in Y$ we denote by $S_{n+1} = \sum_{k=n+1}^{\infty} E \| \Phi(k,p,\omega)x \|^2$ and from hypothesis we have

$$E \| \Phi(m,p,\omega)x \|^2 \le S_m \le \left(\frac{D(\omega)}{D(\omega)+1}\right)^{m-n-1} S_{n+1} \le \left(\frac{D(\omega)}{D(\omega)+1}\right)^{m-n} (D(\omega)+1) E \| \Phi(n,p,\omega)x \|^2$$

for all $(m,n),(n,p) \in T, (x,\omega) \in Y$. So we have the relation

$$E \| \Phi(m,p,\omega)x \|^2 \le N(\omega)a(\omega)^{m-n} E \| \Phi(n,p,\omega)x \|^2,$$

where $N(\omega) = \dfrac{D(\omega)}{D(\omega)+1}$, and $a(\omega) = \max\{1,(D(\omega)+1)\}$, for all $(m,n),(n,p) \in T, (x,\omega) \in Y$, and we obtain that the discrete stochastic skew-evolution semiflow $\Theta = (\varphi,\Phi)$ is uniformly exponentially stable in mean square.

Theorem 8. Let be $\Theta = (\varphi,\Phi)$ a discrete stochastic skew-evolution semiflow. Then $\Theta = (\varphi,\Phi)$ is uniformly exponentially instable in mean square if and only if there are random variables $D(\omega) \ge 1$, such that:

$$\sum_{k=0}^{n} E \| \Phi(k,p,\omega)x \|^2 \le D(\omega) E \| \Phi(n,p,\omega)x \|^2, \tag{4}$$

for all $(n,p) \in T, (x,\omega) \in Y$.

Proof. *Necessity*. Let be a discrete stochastic skew-evolution semiflow $\Theta = (\varphi,\Phi)$ uniformly exponentially instable in mean square. Then, for $N(\omega) \ge 1, a(\omega) \in (0,1)$ we have from Definition 6, that

$$N(\omega)a(\omega)^{m-n} E \| \Phi(m,p,\omega)x \|^2 \ge E \| \Phi(n,p,\omega)x \|^2,$$

for all $(m,n),(n,p) \in T, (x,\omega) \in Y$. Write this relationship for $k = \overline{0,n}$ and then we sum these relations member with member and we have:

$$\sum_{k=0}^{n} E \| \Phi(k,p,\omega)x \|^2 \le N(\omega) \sum_{k=0}^{n} a(\omega)^{n-k} E \| \Phi(n,p,\omega)x \|^2 \le D(\omega) E \| \Phi(n,p,\omega)x \|^2 \quad \text{for all}$$

$(n,p) \in T, (x,\omega) \in Y$, where $D(\omega) = \max\left\{2, \dfrac{N(\omega)}{1-a(\omega)}\right\}$ and we obtain the relation (4).

Sufficiency. For $(n,p) \in T$ and $(x,\omega) \in Y$ we denote by $S_m = \sum_{k=0}^{m} E \| \Phi(k,p,\omega)x \|^2$ and from relation (4) we obtain

$$\left(\frac{D(\omega)}{D(\omega)-1}\right)^{m-n} S_n \le S_m \quad \text{for all } (m,n) \in T, (x,\omega) \in Y$$

From this relation we obtain

$$\left(\frac{D(\omega)}{D(\omega)-1}\right)^{m-n} E \| \Phi(n,p,\omega)x \|^2 \le D(\omega) E \| \Phi(m,p,\omega)x \|^2,$$

and if we denote $N(\omega) = D(\omega)$, and $a(\omega) = \frac{D(\omega)-1}{D(\omega)}$, for all $(m,n),(n,p) \in T$, $(x,\omega) \in Y$, and we obtain that the discrete stochastic skew-evolution semiflow $\Theta = (\varphi, \Phi)$ is uniformly exponentially instable in mean square.

REFERENCES

[1.] L. Arnold, Stochastic Differential Equations: Theory and Applications, New York: Wiley, (1972)
[2.] A. Bensoussan, F. Flandoli, Stochastic inertial manifold, Stochastic Rep. 53 (1995), no. 1-2, 13–39.
[3.] F. Flandoli, Stochastic flows for non-linear second-order parabolic SPDE, Ann. Probab. 24 (1996),no. 2, 547–558.
[4.] M. Megan, A. L. Sasu, and B. Sasu, On uniform exponential stability of linear skew-product semiflows in Banach spaces , Bulletin of the Belgian Mathematical Society - Simon Stevin, 9 (2002) 143–154.
[5.] M. Megan, C. Stoica, On Uniform Exponential Trichotomy of Evolution Operators in Banach Spaces, Integral Equations and Operator Theory, 60 (2008) 499–506.
[6.] S. E. A. Mohammed, T. Zhang, H. Zhao, The stable manifold theorem for semilinear stochastic evolution equations and stochastic partial dfferential equations, Memoirs of the A.M.S., 196(917) (2008)
[7.] G. Da Prato, J. Zabczyc, Stochastic Equations in infinite dimensions, University Press, Cambridge, 1992.
[8.] Skorohod, A.V., Random linear operators, Riedel, 1984.
[9.] C. Stoica, M. Megan, Discrete Asymptotic Behaviors for Skew-Evolution Semiflows on Banach Spaces, arXiv:0808.0378v2 [math.CA].
[10.] V.M. Ungureanu, Representations of mild solutions of time-varying linear stochastic equations and the exponential stability of periodic systems, Electronic Journal of Qualitative Theory of Differential Equations 4 (2004), 1–22.
[11.] D.Stoica, Exponential stability for stochastic cocycle, Ann. Tiberiu Popoviciu Semin. Funct. Equ. Approx. Convexity, 7 (2009), 111-118
[12.] D.Stoica, Uniform exponential dichotomy of stochastic cocycles, Stochastic Process. Appl., 12(2010), 1920-1928

INTERNATIONAL SYMPOSIUM on
ADVANCED ENGINEERING & APPLIED MANAGEMENT
– 40th ANNIVERSARY in HIGHER EDUCATION (1970-2010)
4 – 5 November, 2010, Hunedoara, ROMANIA

[1]Nicuşor Laurenţiu ZAHARIA, [2]Tiberiu Ştefan MĂNESCU,
[3]Mihaela Dorica STROIA, [4]Tiberiu MĂNESCU jr.

DYNAMIC COEFFICIENT DETERMINATION AT A TANK WAGON

[1] ROMANIAN RAILWAY AUTHORITY – AFER, 393 CALEA GRIVIŢEI, BUCHAREST, ROMANIA
[2-4] "EFTIMIE MURGU" UNIVERSITY REŞIŢA, 1-4 TRAIAN VUIA SQUARE, REŞIŢA, ROMANIA

ABSTRACT:
The tank wagons are widely used by railway freight operators to load and transport products like oil, gases, crude oil, mineral and vegetal oils, acids, alcohol, bitumen, water etc.
KEYWORDS:
dynamic coefficient, tank wagon, strain gages, rosettes, experimental stress analysis

1. INTRODUCTION

This paper present determination of dynamic coefficient based on the stress analysis results, of the strength structure of a tank wagon designed for chemical/mineral products. Before the tank wagon was allowed to circulate a series of tests had to be carried out, among which stress analysis, in accordance with international standards, as follows:

- EN 12663 – Structural requirements of railway vehicle bodies;
- UIC leaflet 577 (UIC = Union Internationale des Chemins de fer);
- ERRI B12/RP17 report (ERRI = European Rail Research Institute).

The tests which are presented in this paper were performed at Romanian Railway Authority – AFER on Stress Analysis Bench Test (fig. 1) and at Railway Test Centre Făurei (fig. 2).

Fig. 1. The tank wagon on AFER's Stress Analysis Bench Test

Fig. 2. Railway Test Centre Făurei

2. TESTS AND MEASURING POINTS

The following tests were performed in accordance with the above mentioned standards:

A. Static (Stress Analysis Bench Test):
1. 2 MN compressive force at buffer level (CT);
2. 2 MN compressive force at coupler level (CA);
3. 1.5 MN compressive force below buffer (CT50);
4. 0.4 MN compressive force applied diagonally at buffer level (CD);

5. 1 MN tensile force in coupler area (TA);
6. tank load under pressure (SV);
7. lifting at one end of the vehicle (RID);
8. lifting the whole vehicle (RID4).

B. dynamic (Railway Test Centre Făurei):

9. impact tests (T).

Horizontal loads (A1...A5) were applied at one end of the wagon by means of hydraulic cylinders. The other end of the wagon was leaned at buffer level, coupler level respectively. The vertical load (A6) was obtained by water filling at nominal capacity. The A7 test was performed by lifting the loaded wagon from under the buffer beam until the adjacent bogie got off the railways, with the other bogie still leaned. The A8 load was obtained by fully lifting the wagon from under its lateral support. Combination of horizontal forces with vertical loads were performed.

In figure 3 is show how the forces were applied in case of compressive force at buffers level combined with vertical load.

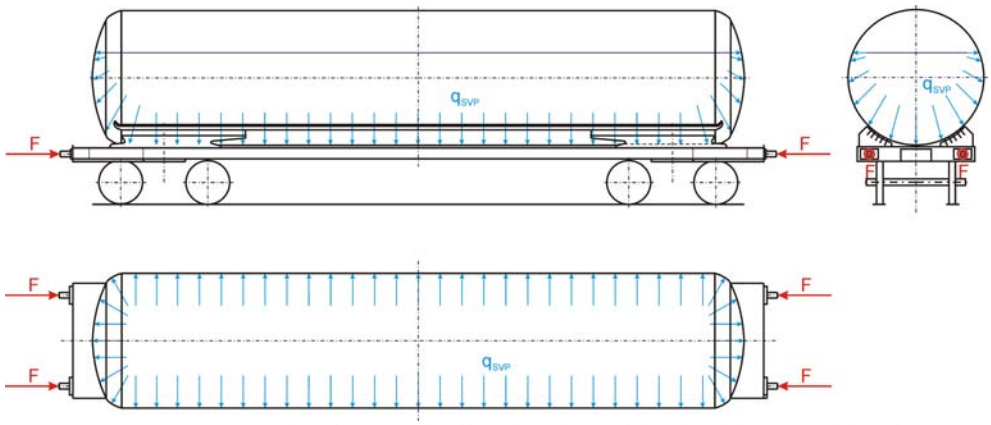

Fig. 3. Compressive force at buffers level combined with vertical load

Table 1. Static tests limits [N/mm²]

			Welding free area	Welding area
Horizontal loads (σ_{aH})			355	309
Vertical load (σ_{aV1})	Class	A	277	
		B	150	
		C	133	
		D	110	
Vertical load (σ_{aV2})			182	166

Static tests allowable limits are shown in table 1.

The dynamic (shock) tests were performed by ramming the tank wagon, stationary on horizontal straight railways, and a wagon set up according to ERRI B12/RP17, launched down a slope (fig. 4 , fig. 5 and fig. 6).

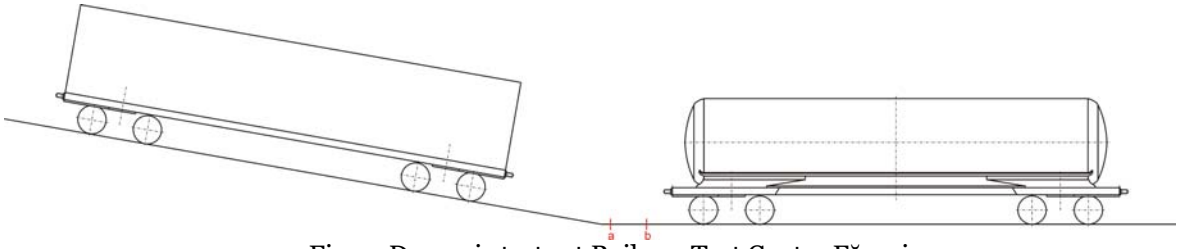

Fig. 4. Dynamic tests at Railway Test Centre Făurei

Fig. 5. The tested wagon and the ramming wagon

Fig. 6. The tested wagon and the laboratory coach

The test was performed in two stages:

1. Ten shocks at speeds growing until the sum of the forces against the two buffers reached 2.5 MN, while monitoring the relationship between the forces and the speed;
2. Another 20 shocks at the speed corresponding to 2.5 MN, namely 13.5 km/h, while recording the cumulative residual strains ε_{rc} and the maximum stress values as shown in figure 7.

The ram forces $F_1+F_2=F$ were measured with load cells located under the buffers, as shown in figure 11.

Fig. 7. The residual strains

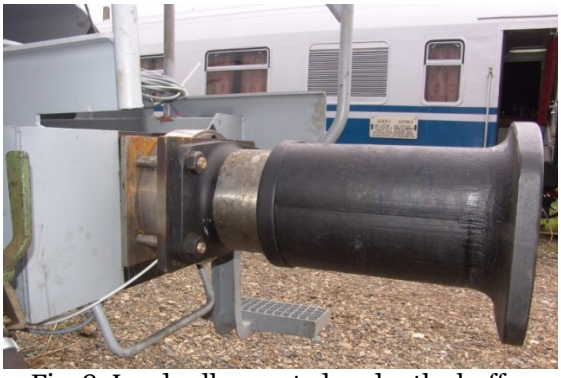

Fig. 8. Load cell mounted under the buffer

The speeds were determined by taking into account the time it took the first axle of the moving wagon to run the distance of 1 m between reference points a and b (fig. 4).

Acceptance criteria:

- cumulative residual strains ε_{rc} on shock completion should be less than 2,000 μm/m;
- ε_{rc} should become steady after 30 shocks;
- the wagon equipment should remain operational.

The measurement points were located in the relevant load areas, which are:

- the chassis;
- the cradle (connection between the chassis and the tank);
- the tank.

The measurements were performed at 67 measurement points, out of which 12 rosettes. The following devices and material was used: Hottinger CENTIPEDE, MGCplus, LY11-10/120 strain gauges, RY91-6/120 (0°-45°-90°) rosettes and Z70 bonding material, all of them produced by HBM. The diagrams of the measurement point location on the frame and the tank are shown in figure 9 and 10.

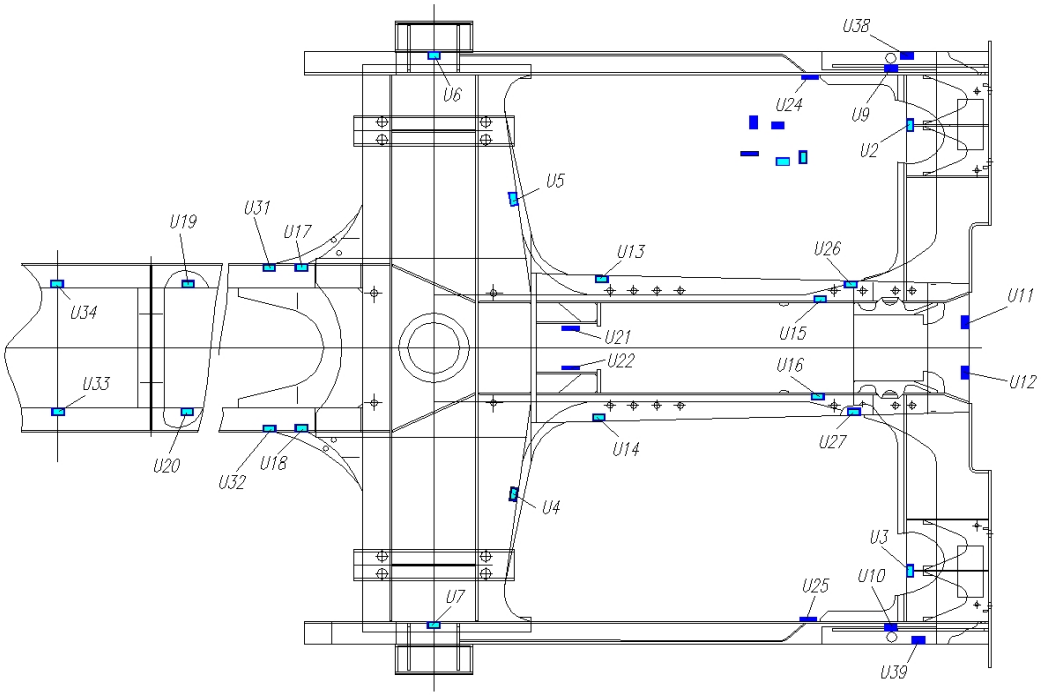

Fig. 9. Measuring points on chassis

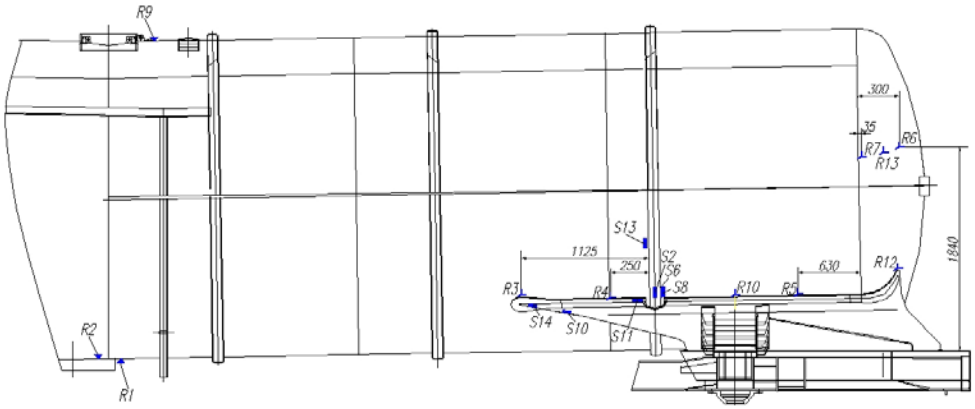

Fig. 10. Measuring points on tank and cradle

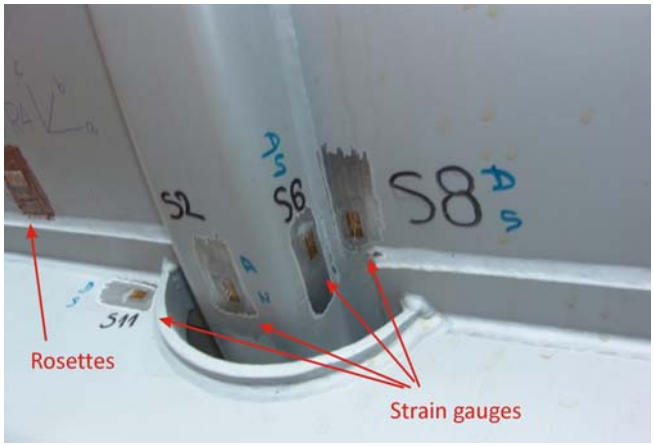

Fig. 10. Measuring points - strain gauges and rosettes (photo)

3. RESULTS

For the static tests, the measured stress was below the limits in table 1 except the following:

- During tests A1 and A3, the limit was exceeded by 3.7 % at measurement point U2; at the symmetrical measurement point U3 the measured stress was 291 N/mm², respectively 279 N/mm², less than σ_{aH}, which indicates that the accepted limit was exceeded because of asymmetrical load application;
- During test A1, at rosette R8 a specific strain ε_1 was measured, which exceeded the accepted limit by 4.9%

The highest cumulative residual strains $\varepsilon_{rc,}$ during dynamic test, were found at measurement points U2, U3, located on the buffer beam, behind the buffers, and S2. The measured values were: $\varepsilon_{rc,U2}$=776 μm/m, $\varepsilon_{rc,U3}$=821 μm/m and $\varepsilon_{rc,S2}$=-577 μm/m.

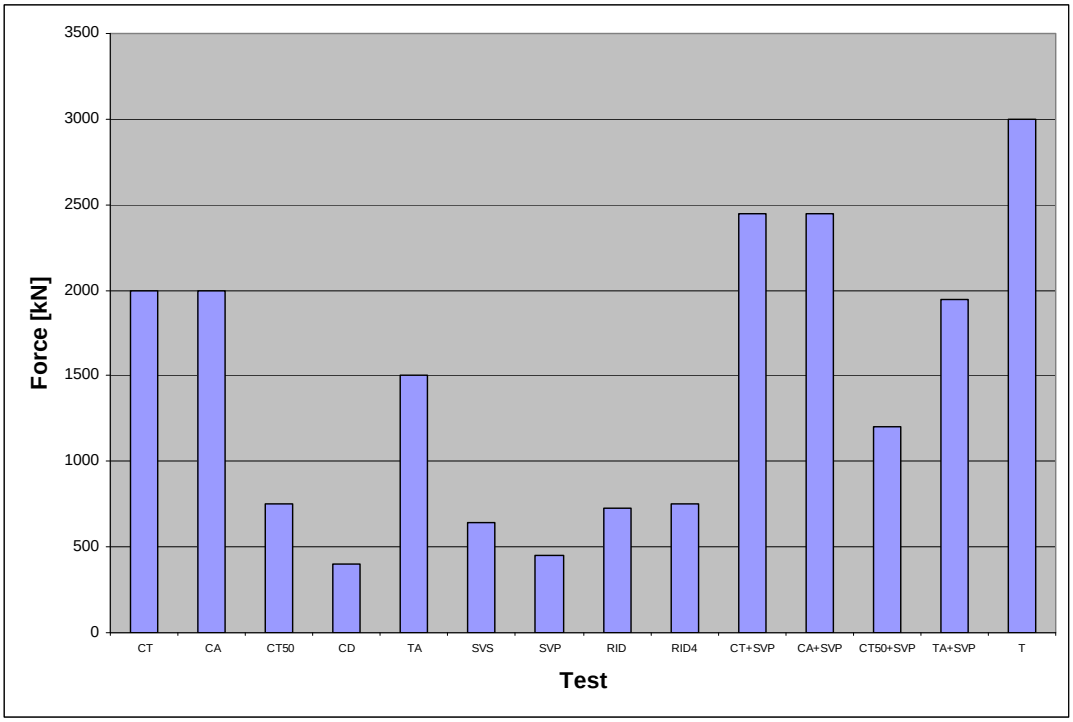

Fig. 11. The results for all test

The number of measuring points used at dynamic test is smaller than those used at static test, because of limited number of channels of measuring devices. One of choosing criteria is based on results of combined horizontal force at buffers level combined with vertical load (CT+SVS). This static test, simulate (because of buffer forces) dynamic (shock at ramming at wagons sorting) or quasi-static forces on buffers during circulation.

In figure 11, are presented the results (stress in N/mm²) for the tank wagon for entire test program.

The results grouped on main tank elements – chassis (U), cradle (C), tank (R) for CT+SVS and T test are presented in figure 12 and 13.

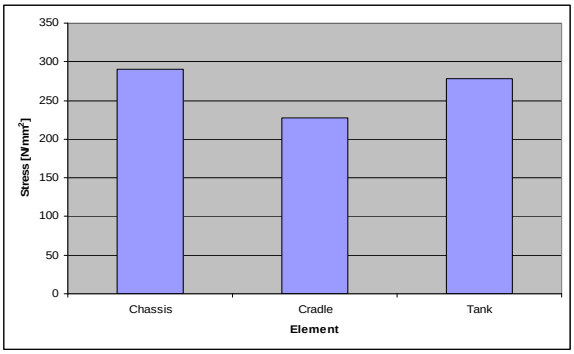

Fig. 12. The results at CT+SVS test

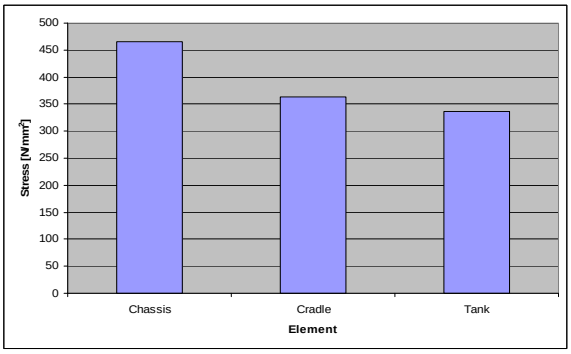

Fig. 13. The results at T test

Based on dynamic shock test results an evaluation of dynamic coefficient (by reference to CT+SVS test) – figure 14. Dynamic forces appear because of accelerations, vertical oscillatory movement of the wagon etc. From figure 14, the maximum stress at chassis level, is at U3 measuring point witch is glued behind the buffer. On the cradle, the maximum stress is at S2 measuring point witch is glued on one of tank's reinforcing ring. The maximum stress on the tank is at rosettes R3 witch is glued on the front of the tank

From expression $F_{dynamic}=\Psi \cdot F_{static}$, where Ψ is the dynamic coefficient. According to some authors, $\Psi=1,3$.

The maximum value of the dynamic coefficient is 5,13 at rosettes R13 and the minimum value is 1,07 at S9 strain gauge.

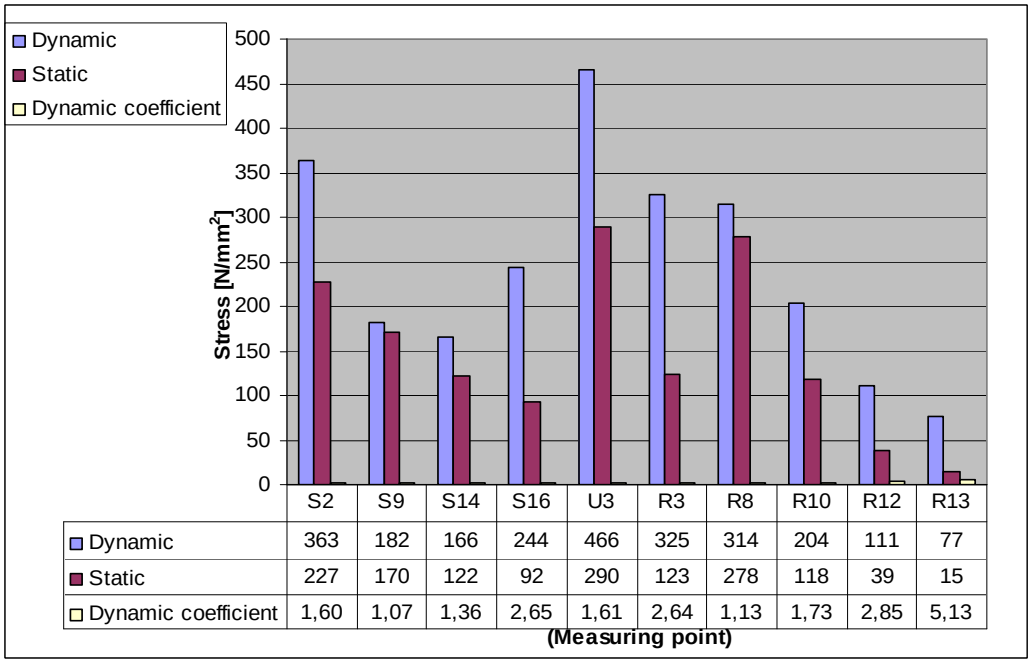

	S2	S9	S14	S16	U3	R3	R8	R10	R12	R13
Dynamic	363	182	166	244	466	325	314	204	111	77
Static	227	170	122	92	290	123	278	118	39	15
Dynamic coefficient	1,60	1,07	1,36	2,65	1,61	2,64	1,13	1,73	2,85	5,13

Fig. 14. Dynamic coefficient

The figure 14 show larger values of dynamic coefficient than 1,3 value, during a test witch simulate a real condition service of the tank wagon, but the dynamic coefficient it is not an evaluation condition of the wagon's conformity with reference documents. More, according to some UIC (International Railway Union) studies, the ramming speed is smaller than 10 km/h while the maximum ramming test speed was 13,5 km/h.

4. CONCLUSIONS

After the test, based on Testing Report from experimental stress analysis and other tests the tank wagon was certificate to circulate on European Railways (the client of the tank wagon was from Western Europe).

REFERENCES

[1.] Zaharia N. L., Contribuţii privind optimizarea structurilor portante ale vagoanelor cisternă de cale ferată în vederea creşterii sarcinii pe osie şi micşorarea tarei vehiculelor – teză de doctorat, conducător ştiinţific prof. dr. eur. ing. Mănescu T. Ş, Universitatea „Eftimie Murgu" Reşiţa, 2010
[2.] Mănescu T. Ş., Jiga G. G., Zaharia N. L., Bîtea C. V., Noţiuni fundamentale de rezistenţa materialelor şi teoria elasticităţii, Editura „Eftimie Murgu", ISBN 978-973-1906-67-6, Reşiţa, 2010
[3.] Mănescu T. Ş., Jiga G. G., Zaharia N. L., Bîtea C. V., Noţiuni fundamentale de rezistenţa materialelor, Editura „Eftimie Murgu" Orizonturi tehnice, ISBN 973-8286-79-4, Reşiţa, 2008
[4.] Mănescu T. Ş., Copaci I., Olaru S., Creangă F.Ş, Tensometria electrică rezistivă în cercetarea experimentală, Editura Mirton, ISBN 973-661-892-5, Timişoara, 2006
[5.] Karl Hoffman: An Introduction to Measurement using Strain Gages, Hottinger Baldwin Messtechnik GmbH, Darmstadt, 2005
[6.] Simion I., Melinte F., N. L. Zaharia, The Application Of Electrical Strain Gages For Stress Analysis On A Tank Wagon, 24th Danubia–Adria Symposium on Developments in Experimental Mechanics, pag. 183÷185, ISBN 978-973-739-456-9, Sibiu, 2007
[7.] ***EN 12663 – Structural requirements of railway vehicle bodies, 2000
[8.] ***UIC leaflet 577 – Sollicitations des wagons, 2004
[9.] ***ERRI B12/RP17 – Programme des essais à faire subir aux wagons à châssis et superstructure en acier (aptes à recevoir l'attelage automatique de choc et traction) et à leurs bogie à châssis en acier, Utrecht, 1997

INTERNATIONAL SYMPOSIUM on
ADVANCED ENGINEERING & APPLIED MANAGEMENT
– 40th ANNIVERSARY in HIGHER EDUCATION (1970-2010)
4 – 5 November, 2010, Hunedoara, ROMANIA

[1] Ştefan MAKSAY, [2] Diana STOICA

CONSIDERATIONS ON THE RECTANGLE TRUNCATED BIDIMENSIONAL NORMAL MODELING

[1,2] UNIVERSITY "POLITEHNICA" TIMISOARA, FACULTY OF ENGINEERING HUNEDOARA, ROMANIA

ABSTRACT:
In this article, which generalizes the paper [1], we started from the expression of the classic normal distribution density white two variables, we made a few considerations about the process of experimental data, by means of the distribution density that generalizes the bidimensional classical normal law. The bidimensional distribution densities are rectangle truncated [2], obviously keeping the properties of a density. The new expressions of the density, having one or more extra parameters, can better approximate the experimental data.
A.M.S.(2000) Subject Classification: 33B15; 00A71;
KEYWORDS:
Modeling truncated, normal distribution density, coefficient of correlation

1. INTRODUCTION

In this article, which generalizes the paper [1], we started from the expression of the classic normal distribution density with two variables [3], we made a few considerations about the process of experimental data, by means of the distribution density that generalizes the bidimensional classical normal law. Thus, we further on present a few distinct modeling variants.

The first two expressions for the distribution density will introduce one, respectively two parameters, fact that permits an optimal modeling of the experimental data.

This article proposes to model the experimental data presented in the next table, which shows the coordinates of points in the space with tree dimensions, where the first two lines represent the independent variables x and y, and the tree lines represent the dependent variable u.

var =

	1	2	3	4	5	6	7	8	9	10	11	12	13	14	15
1	0.483	1.06	1.144	1.389	1.574	1.605	1.891	2.039	2.501	2.606	2.728	2.776	2.824	2.887	3.973
2	2.093	2.132	2.153	2.227	2.38	2.706	2.782	3.002	3.083	3.107	3.67	3.836	4.071	4.329	4.514
3	0.03	0.064	0.073	0.105	0.18	0.196	0.231	0.229	0.229	0.215	0.149	0.1	0.084	0.05	0.02

Further on we note

$$mx := mean(x) \qquad my := mean(y) \qquad mu := mean(u),$$

$$sx := stdev(x) \qquad sy := stdev(y) \qquad su := stdev(u),$$

where *mean* and *stdev* represent the mean value and respectively the standard deviation of the corresponding variable. For the given measurements, we have

$$mx = 2.0986 \qquad my = 3.0724 \qquad mu = 0.1304$$

$$sx = 0.8795 \qquad sy = 0.8042 \qquad su = 0.0748.$$

Note by *fclas(x,y)* the classic normal distribution density with two variables [3]

$$fclas(x,y) := \frac{1}{2\cdot\pi\cdot sx\cdot sy}\cdot\exp\left[\frac{-1}{2}\cdot\left[\frac{(x-mx)^2}{sx^2}+\frac{(y-my)^2}{sy^2}\right]\right]. \qquad (1)$$

2. PRACTICAL CASE

Instead of the classic distribution density (1) we consider the function:

$$\text{ftrunc1}(x,y,cx,cy)=\begin{cases} K\cdot\dfrac{1}{2\pi\cdot sx\cdot xy}\exp\left[-\dfrac{1}{2}\cdot\left[\dfrac{(x-mx)^2}{sx^2}+\dfrac{(y-my)^2}{sy^2}\right]\right], & (|x-mx|<cx\cdot sx)\wedge(|y-my|<cy\cdot sy) \\ 0, \quad \text{in rest} \end{cases} \qquad (2)$$

where K, *cx* and *cy* are positives constants.

For the function *ftrunc1* to be a distribution density we impose the conditions

$$\text{ftrunc1}(x,y,cx,cy)\ge 0 \quad \text{and} \quad \int_{-\infty}^{\infty}\int_{-\infty}^{\infty}\text{ftrunc1}(x,y,cx,cy)\,dx\,dy=1,$$

hence results the value for K

$$K:=\frac{1}{\int_{mx-cx\cdot sx}^{mx+cx\cdot sx}\int_{my-cy\cdot sy}^{my+cy\cdot sy}\text{if}\left[[(|x-mx|<cx\cdot sx)\wedge(|y-my|<cy\cdot sy)],\frac{1}{2\cdot\pi\cdot sx\cdot sy}\cdot\exp\left[\frac{-1}{2}\cdot\left[\frac{(x-mx)^2}{sx^2}+\frac{(y-my)^2}{sy^2}\right]\right],0\right]dy\,dx}$$

We remark the fact that for $cx\to\infty$ and $cy\to\infty$, the function *ftrunc1(x,y,cx,cy)* coincides with the function *fclas(x,y)*.

The constants *cx* and *cy* will be determined by imposing the condition of minimizing the sum of the difference squares between of the value of theoretic function *ftrunc1(x,y,cx,cy)* and experimental value of independent variable u, that is we minimize the function *F(cx,cy)*

$$F(cx,cy):=\sum_{i=1}^{n}\left(\text{ftrunc1}\left(x_i,y_i,cx,cy\right)-u_i\right)^2$$

In order to achieve this, we will use the next program, written in language MathCAD.

ORIGIN ≡ 1

x := (0.4829 1.0601 1.1437 1.3885 1.574 1.6049 1.8914 2.0392 2.5008 2.6057 2.7279 2.776 2.824 2.8866 3.9726)

y := (2.0933 2.1323 2.1534 2.2267 2.3801 2.7062 2.7818 3.0022 3.0829 3.1074 3.6696 3.836 4.0711 4.3291 4.5142)

u := (0.03 0.0639 0.0733 0.1055 0.1802 0.1956 0.2314 0.2294 0.2288 0.2149 0.1492 0.1003 0.0836 0.0501 0.02)

$x:=x^T$ $y:=y^T$ $u:=u^T$

n := length(x) i := 1 .. n nrdivx:= 5 nrdivy:= 7

dxi := 1 dxf := 2.

dyi := 1 dyf := 3

```
prog1 := | px ← nrdivx
         | py ← nrdivy
         | for j ∈ 1 .. px + 1
         |     cx_j ← dxi + (j − 1)·(dxf − dxi)/px
         |     for k ∈ 1 .. py + 1
         |         cy_k ← dyi + (k − 1)·(dyf − dyi)/py
         |         K ← 1 / ∫_{mx−cx_j·sx}^{mx+cx_j·sx} ∫_{my−cy_k·sy}^{my+cy_k·sy} if[[[(x − mx)^2 < (cx_j·sx)^2] ∧ [(y − my)^2 < (cy_k·sy)^2]], fclas(x, y), 0] dy dx
         |         fCT_{j,k} ← Σ_{i=1}^{n} [if[[[(x_i − mx)^2 < (cx_j·sx)^2] ∧ [(y_i − my)^2 < (cy_k·sy)^2]], K·fclas(x_i, y_i), 0] − u_i]^2
         | fmin ← min(fCT)
         | for j ∈ 1 .. px + 1
         |     for k ∈ 1 .. py + 1
         |         indx ← j
         |         indy ← k
         |         break if (fCT_{j,k} − fmin) = 0
         |     break if (fCT_{j,k} − fmin) = 0
         | [cx_j  cy_k  fCT  (indx  indy  fmin)]
```

prog1 = (2 1.8571 {6,8} {1,3})

$cxf := prog1_{1,1}$ $cxf = 2$

$cyf := prog1_{1,2}$ $cyf = 1.8571$

$fCT := prog1_{1,3}$

$(indx\ indy\ fmin) := prog1_{1,4}$

$prog1_{1,4} = (6\ \ 4\ \ 2.477\times 10^{-3})$

$indx = 6$ $indy = 4$ $fmin = 2.477\times 10^{-3}$

$$fCT - fmin = \begin{pmatrix} 0.2904 & 0.1436 & 0.0864 & 0.0623 & 0.0512 & 0.046 & 0.0436 & 0.0425 \\ 0.1823 & 0.0708 & 0.0341 & 0.0203 & 0.0143 & 0.0117 & 0.0105 & 9.9963\times 10^{-3} \\ 0.1283 & 0.0399 & 0.0152 & 7.3245\times 10^{-3} & 4.353\times 10^{-3} & 3.1694\times 10^{-3} & 2.6787\times 10^{-3} & 2.4737\times 10^{-3} \\ 0.0993 & 0.0248 & 7.1072\times 10^{-3} & 2.6071\times 10^{-3} & 1.3245\times 10^{-3} & 9.7519\times 10^{-4} & 8.8255\times 10^{-4} & 8.5732\times 10^{-4} \\ 0.0831 & 0.017 & 3.5837\times 10^{-3} & 1.1204\times 10^{-3} & 8.4481\times 10^{-4} & 9.9182\times 10^{-4} & 1.1357\times 10^{-3} & 1.2172\times 10^{-3} \\ 0.0737 & 0.012 & 1.2018\times 10^{-3} & 0 & 3.4867\times 10^{-4} & 8.0354\times 10^{-4} & 1.0942\times 10^{-3} & 1.2419\times 10^{-3} \end{pmatrix}$$

Substituting these values of *cx* and *cy* in expression of *ftrunc1(x,y,cx,cy)* leads to the expression of the truncated distribution density of first form that approximate better the experimental data.

Thus, the graphs of the classic and truncated distribution density, for the given experimental values, are shown in Figure 1 and respectively in Figure2.

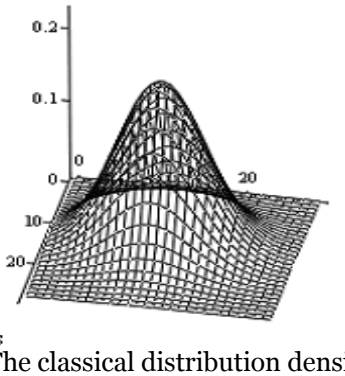

Figure 1. The classical distribution density

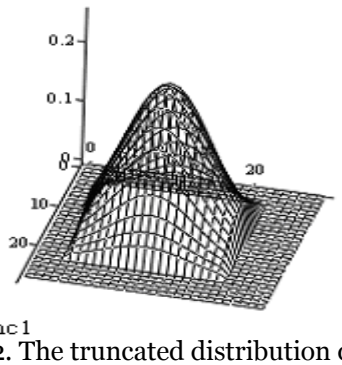

Figure 2. The truncated distribution density *ftrunc1(x,y,cx,cy)*

The correlation coefficients corresponding of the two modeling's are

$$rclas := \sqrt{1 - \frac{\sum_i (u_i - fclas(x_i, y_i))^2}{\sum_i (u_i - mean(u))^2}} \qquad rclas = 0.9631,$$

$$rtrunc1 := \sqrt{1 - \frac{\sum_i (u_i - ftrunc1(x_i, y_i, cxf, cyf))^2}{\sum_i (u_i - mean(u))^2}} \qquad rtrunc1 = 0.9852.$$

The values of dependent variable u, of the distribution density *fclas, ftrunc1* in the points (x_i, y_i), are given, comparatively, in the next table.

$fclas_i := fclas(x_i, y_i)$, $ftrunc1_i := ftrunc1(x_i, y_i, cxf, cyf)$,

$vb := augment(x, y, u, fclas, ftrunc1)^T$.

$vb =$

	1	2	3	4	5	6	7	8	9	10	11	12	13	14	15
1	0.4829	1.0601	1.1437	1.3885	1.574	1.6049	1.8914	2.0392	2.5008	2.6057	2.7279	2.776	2.824	2.8866	3.9726
2	2.0933	2.1323	2.1534	2.2267	2.3801	2.7062	2.7818	3.0022	3.0829	3.1074	3.6696	3.836	4.0711	4.3291	4.5142
3	0.03	0.0639	0.0733	0.1055	0.1802	0.1956	0.2314	0.2294	0.2288	0.2149	0.1492	0.1003	0.0836	0.0501	0.02
4	0.0198	0.0566	0.065	0.0934	0.13	0.1733	0.205	0.2236	0.2026	0.1904	0.1322	0.1066	0.0741	0.0444	$601\cdot10^{-3}$
5	0.0222	0.0633	0.0727	0.1045	0.1454	0.1938	0.2293	0.2501	0.2267	0.2129	0.1479	0.1192	0.0828	0.0497	0

The distribution rate function Fclas(x,y) is given by

$$Fclas(x,y)=\int_{-\infty}^{x}\int_{-\infty}^{y} fclas(u,v)\,dv\,du\,.$$

The rate of the truncated distribution functions is

$$Ftrunc1(x,y,cx,cy)=\int_{-\infty-\infty}^{x\ y} ftrunc1(u,v,cx,cy)\,dv\,du\,.$$

Using the following program, we showed in Figure 5 the function *Ftrunc1* and in Figure 6 the corresponding contours lines.

$nrn := 15$

$k := 1..nrn \qquad xv_k := (min(x)-1)+\frac{(max(x)+1)-(min(x)-1)}{nrn-1}\cdot(k-1)$

$h := 1..nrn \qquad yv_h := (min(y)-1)+\frac{(max(y)+1)-(min(y)-1)}{nrn-1}\cdot(h-1)$

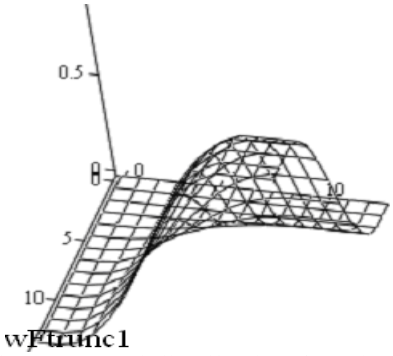

Figure 5.The truncated distribution function *Ftrunc1*

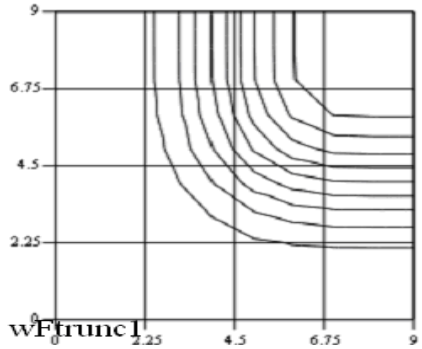

Figure 6. The contour lines of the truncate distribution function *Ftrunc1*

Inserting the notations

$Fclas_i := Fclas(x_i, y_i)$, $\quad Ftrunc1_i := Ftrunc1(x_i, y_i, cxf, cyf)$,

$vb := augmen(Fclas, Ftrunc1)^T$,

the constants that appear as having been previously determined, results the distribution of the values of distribution functions in points corresponding to the experimental system point.

vb=

	1	2	3	4	5	6	7	8	9	10	11	12	13	14	15
1	$54\cdot10^{-3}$	0.0134	0.0165	0.0295	0.0519	0.0904	0.143	0.2161	0.3373	0.367	0.5817	0.6389	0.7024	0.7587	0.9393
2	$43\cdot10^{-4}$	$71\cdot10^{-3}$	0.0123	0.024	0.0461	0.0866	0.1406	0.2184	0.3461	0.3776	0.6121	0.6746	0.7441	0.8056	0.9948

3. CONCLUSIONS

We notice that, for the experimental data presented in the paper, the optimal modeling is given by the distribution density *ftrunc1(x,y,cx,cy)* ($rtrunc1 = 0.9852$).

This modeling are better than the non-truncated modeling fclas(x,y) ($rclas = 0.9631$).
In the practical case these results show us, that is more advantage to use the truncated modeling, because the classical modeling is the practical case of these.

REFERENCES

[1.] Şt. Maksay, D. Stoica – Considerations on Modeling Some Distribution Laws, Applied Mathematics and Computation, Volume 175, Issue 1, 1 April 2006, Pages 238-246;
[2.] Johnson, A.C. (2001), "On the Truncated Normal Distribution: Characteristics of Singly- and Doubly-truncated Populations of Application in Management Science," PhD. Dissertation, Stuart Graduate School of Business, Illinois Institute of Technology, Illinois.
[3.] Şt. Maksay, D. Stoica – Calculul probabilităţilor, Editura Politehnica, Timişoara, 2005;

INTERNATIONAL SYMPOSIUM on
ADVANCED ENGINEERING & APPLIED MANAGEMENT
– 40th ANNIVERSARY in HIGHER EDUCATION (1970-2010)
4 – 5 November, 2010, Hunedoara, ROMANIA

[1.]Ludovic Dan LEMLE, [2.]Tudor BÎNZAR, [3.]Lucian Flavius PATER, [4.]Valentina BALASOIU

RIESZ-DUNFORD REPRESENTATION THEOREM FOR UNIFORMLY CONTINUOUS SEMIGROUPS

[1.] UNIVERSITY "POLITEHNICA" TIMIŞOARA, FACULTY OF ENGINEERING HUNEDOARA, ROMÂNIA
[2-3.] UNIVERSITY "POLITEHNICA" TIMIŞOARA, DEPARTMENT OF MATHEMATICS, ROMÂNIA
[4.] NATIONAL COLLEGE OF INFORMATICS "TRAIAN LALESCU" HUNDEOARA, ROMANIA

ABSTRACT:
This note presents a Riesz-Dunford type representation and a Bromwich type representation for uniformly continuous semigroups on a Banach space.
A.M.S.(2010) Subject Classification: 47D03.
KEYWORDS:
uniformly continuous semigroups, Riesz-Dunford representation, Bromwich representation

1. INTRODUCTION

Let E be a complex Banach space. We denote by $B(E)$ the Banach algebra of bounded linear operators on E. For a closed linear operator A, not necessarily bounded, with domain $D(A)$ in the space E, denote by $\rho(A)$ and $\mathrm{R}(.,\mathrm{A})$ the resolvent set of A and the resolvent of A, respectively.

The family of operators $\{T(t)\}_{t\geq 0} \subset B(E)$ is said to be a *semigroup of bounded linear operators on E* if

(i) T(0)=I (I is the identity operator on E);
(ii) T(t+s)=T(t)T(s) for all t,s≥0 (the semigroup property).

The semigroup $\{T(t)\}_{t\geq 0} \subset B(E)$ is said to be *uniformly continuous* if $t \mapsto T(t)$ is continuous on $[0,\infty)$ in the uniform operator topology. Due to semigroup property this is equivalent to

$$\lim_{t\downarrow 0}\|T(t)-I\|=0 \quad .$$

The most important object associated to a C_0 - semigroup $\{T(t)\}_{t\geq 0}$ is its infinitesimal generator. The linear operator A defined by

$$D(A)=\left\{x\in E:\lim_{t\downarrow 0}\frac{T(t)x-x}{t} \quad exists\right\}$$

and

$$Ax=\lim_{t\downarrow 0}\frac{T(t)x-x}{t} \quad , \quad \forall x\in D(A)$$

is the *infinitesimal generator* of the semigroup $\{T(t)\}_{t\geq 0}$. Clearly the operator $A: D(A)\subseteq E\to E$ is linear but not necessarily bounded unsless $D(A)$ is all of E. Nathan [4] and Yosida [7] proved that the infinitesimal generator of a semigroup is a bounded linear operator in E if and only if the semigroup is uniformly continuous. For more information about C_0 - semigroup we refer to Davies [1], Hille and Phillips [2], Pazy [5], Yosida [8] and the references therein.

This paper is dedicated to the problem of representing the semigroup $\{T(t)\}_{t\geq 0}$ in terms of its infinitesimal generator. We can obtain the semigroup from the resolvent of the generator A by inverting the Laplace transform. Similar results for C_0-semigroups were presented in Lemle and Jiang [3].

2. RIESZ-DUNFORD'S TYPE REPRESENTATIONS

In this section we give a Riesz-Dunford's type representation for uniformly continuous semigroups. For this purpose we use a special class of Jordan's curves for a bounded linear operator defined by Reghiş and Babescu [6].

2.1. Definition. *A Jordan closed smooth curve which surround $\sigma(A)$ is said to be A-spectral if it is homotope to a circle C_r of radius $r > \|A\|$ centered at the origin.*

We have:

2.2. Theorem. *Let A be the infinitesimal generator of the uniformly continuous semigroup $\{T(t)\}_{t\geq 0}$. If Γ_A is an A-spectral curve then*

$$T(t) = \frac{1}{2\pi i}\int_{\Gamma_A} e^{\lambda t} R(\lambda; A)d\lambda \quad , \quad \forall t \geq 0.$$

Proof. Let Γ_A be an A-spectral curve. Then Γ_A is homotope to the circle C_r of radius $r > \|A\|$ centered at the origin. We have:

$$\frac{1}{2\pi i}\int_{\Gamma_A} e^{\lambda t} R(\lambda; A)d\lambda = \frac{1}{2\pi i}\int_{C_r} e^{\lambda t} R(\lambda; A)d\lambda \quad , \quad \forall t \geq 0.$$

But the serie

$$R(\lambda; A) = \sum_{n=0}^{\infty} \frac{A^n}{\lambda^{n+1}}$$

converges uniformly for λ on compacts set of $\{\lambda \in C : |\lambda| > \|A\|\}$, particularly on circle C_r. Then

$$\frac{1}{2\pi i}\int_{C_r} e^{\lambda t} R(\lambda; A)d\lambda = \frac{1}{2\pi i}\int_{C_r} e^{\lambda t}\sum_{n=0}^{\infty}\frac{A^n}{\lambda^{n+1}}d\lambda = \sum_{n=0}^{\infty}\frac{1}{2\pi i}\int_{C_r}\frac{e^{\lambda t}}{\lambda^{n+1}}d\lambda A^n.$$

Using the identities

$$\frac{1}{2\pi i}\int_{C_r}\frac{e^{\lambda t}}{\lambda^{n+1}}d\lambda = \frac{t^n}{n!} \quad , \quad \forall n \in N,$$

we conclude that

$$\frac{1}{2\pi i}\int_{\Gamma_A} e^{\lambda t} R(\lambda; A)d\lambda = \sum_{n=0}^{\infty}\frac{t^n A^n}{n!} = T(t) \quad , \quad \forall t \geq 0. \blacksquare$$

3. BROMWICH'S TYPE REPRESENTATION

Next theorem gives Bromwich's type representation theorem for uniformly continuous semigroups.

3.1. Theorem. *Let A be the infinitesimal generator of a C_0-semigroup $\{T(t)\}_{t\geq 0}$. If $a > \|A\|$, then*

$$T(t) = \frac{1}{2\pi i}\int_{a-i\infty}^{a+i\infty} e^{zt} R(z; A)dz$$

and the integral converges uniformly for t in bounded intervals.

Proof. Let $a > \|A\|$. For $R > 2a$ we consider Jordan's closed smooth curve

$$\Gamma_R = \Gamma'_R \cup \Gamma''_R$$

where

$$\Gamma'_R = \{a + i\tau : \tau \in [-R, R]\}$$

and

$$\Gamma''_R = \left\{a + R(\cos\varphi + i\sin\varphi) : \varphi \in \left[\frac{\pi}{2}, \frac{3\pi}{2}\right]\right\}$$

For $z \in \Gamma'_R$ we have

$$|z| = |a + i\tau| > a > \|A\|$$

and for $z \in \Gamma''_R$ we find

$|z| = |a + R(\cos\varphi + i\sin\varphi)| = |a - [-R(\cos\varphi + i\sin\varphi)]| \geq |a - R| > \|A\|$. Therefore from $z \in \Gamma_R$ it follows $z \in \rho(A)$. Moreover, Γ_R is homotop to the circle C of radius R-a centered at the origin.

Then Γ_R is an A-spectral curve and from theorem 2.2 it follows that

$$T(t) = \frac{1}{2\pi i}\int_{\Gamma_R} e^{zt} R(z; A)dz \quad , \quad \forall t \geq 0$$

for every $R > 2a$. If we denote

$$I'_t(R) = \frac{1}{2\pi i}\int_{\Gamma'_R} e^{zt} R(z; A)dz$$

and

$$I''_t(R) = \frac{1}{2\pi i}\int_{\Gamma''_R} e^{zt} R(z; A)dz$$

we can see that $T(t) = I'(R) + I''(R) \quad , \quad \forall t \geq 0.$

Next we show that

$$\lim_{R\to\infty} \frac{1}{2\pi i}\int_{\Gamma''_R} e^{zt} R(z; A)dz = 0$$

uniformly for t in bounded intervals. To this end we use the serie

$$R(z; A) = \sum_{n=0}^{\infty} \frac{A^n}{z^{n+1}}$$

which converges uniformly for z on compacts set of $\{z \in C : |z| > \|A\|\}$, particularly on Γ''_R. For every $R > 2a$ and every $t \geq 0$ we have

$$I''(R) = \sum_{n=0}^{\infty}\left(\frac{1}{2\pi i}\int_{\Gamma''_R} \frac{e^{zt}}{z^{n+1}} A^n dz\right) =$$

$$= \left(\frac{1}{2\pi i}\int_{\Gamma''_R} \frac{e^{zt}}{z} dz\right) I + \sum_{n=1}^{\infty}\left(\frac{1}{2\pi i}\int_{\Gamma''_R} \frac{e^{zt}}{z^{n+1}} dz\right) A^n .$$

We consider

$$A_t(R) = \left(\frac{1}{2\pi i}\int_{\Gamma''_R} \frac{e^{zt}}{z} dz\right) I$$

and

$$B_t(R) = \sum_{n=1}^{\infty}\left(\frac{1}{2\pi i}\int_{\Gamma''_R} \frac{e^{zt}}{z^{n+1}} dz\right) A^n$$

Changing variables to

$$z = a + R(\cos\varphi + i\sin\varphi) \quad , \quad \varphi \in \left[\frac{\pi}{2}, \frac{3\pi}{2}\right]$$

we obtain

$$A_t(R) = \left[\frac{1}{2\pi i}\int_{\frac{\pi}{2}}^{\frac{3\pi}{2}} \frac{e^{t(a+R\cos\varphi+i\sin\varphi)}}{z} R(-\sin\varphi + i\cos\varphi)d\varphi\right] I =$$

$$= \left[\frac{R}{2\pi}e^{ta}\int_{\frac{\pi}{2}}^{\frac{3\pi}{2}} e^{tR\cos\varphi}e^{itR\sin\varphi}\frac{1}{z}(\cos\varphi + i\sin\varphi)d\varphi\right] I$$

from where one deduce that

$$\left\|A_t(R)\right\| \le \frac{R}{2\pi}e^{ta}\int_{\frac{\pi}{2}}^{\frac{3\pi}{2}} \left|e^{tR\cos\varphi}\right|\left|e^{itR\sin\varphi}\right|\frac{1}{|z|}\left|\cos\varphi + i\sin\varphi\right|d\varphi \le$$

$$\le \frac{R}{2\pi}e^{ta}\int_{\frac{\pi}{2}}^{\frac{3\pi}{2}} e^{tR\cos\varphi}\frac{1}{R-a}d\varphi \le \frac{1}{2\pi}\frac{R}{R-a}\int_{\frac{\pi}{2}}^{\frac{3\pi}{2}} e^{tR\cos\varphi}d\varphi$$

since for $z \in \Gamma''_R$ we have

$$|z| = |a + R(\cos\varphi + i\sin\varphi| > R - a$$

therefore

$$\frac{1}{|z|} < \frac{R}{R-a}.$$

Consider $0 < t_1 < t_2$ and $t \in [t_1, t_2]$. From the inequality $R > 2a$, it follows that $2R - 2a > R$ and therefore

$$\frac{R}{R-a} < 2.$$

Consequently

$$\left\|A_t(R)\right\| \le \frac{1}{\pi}e^{ta}\int_{\frac{\pi}{2}}^{\frac{3\pi}{2}} e^{tR\cos\varphi}d\varphi \le \frac{1}{\pi}e^{t_2 a}\int_{\frac{\pi}{2}}^{\frac{3\pi}{2}} e^{t_1 R\cos\varphi}d\varphi$$

But for every $\varphi \in \left[\frac{\pi}{2}, \frac{3\pi}{2}\right]$ one obtain $e^{t_1 R\cos\varphi} \le 1$ and we have

$$\lim_{R\to\infty} e^{t_1 R\cos\varphi} = 0.$$

By Lebesgue's bounded convergences theorem it follows

$$\lim_{R\to\infty}\int_{\frac{\pi}{2}}^{\frac{3\pi}{2}} e^{t_1 R\cos\varphi}d\varphi = 0$$

so we deduce that

$$\lim_{R\to\infty} A_t(R) = 0$$

and the limit is uniform for $t \in [t_1, t_2]$.

We consider now the integral

$$B_t(R)=\sum_{n=1}^{\infty}\left(\frac{1}{2\pi i}\int_{\Gamma''_R}\frac{e^{zt}}{z^{n+1}}dz\right)A^n$$

For every $t\in[t_1,t_2]$ and $R>2a$ we have

$$e^{tR\cos\varphi}\le 1\quad,\quad \forall\varphi\in\left[\frac{\pi}{2},\frac{3\pi}{2}\right],$$

so that

$$\left|\int_{\Gamma''_R}\frac{e^{zt}}{z^{n+1}}dz\right|\le\frac{\mathrm{Re}^{ta}}{(R-a)^{n+1}}\int_{\frac{\pi}{2}}^{\frac{3\pi}{2}}e^{tR\cos\varphi}d\varphi\le\pi e^{ta}\frac{R}{(R-a)^{n+1}}$$

Since $R>2a>a+\|A\|$, it follows

$$\|B_t(R)\|\le\sum_{n=1}^{\infty}\frac{\|A\|^n}{2\pi}\left|\int_{\Gamma''_R}\frac{e^{zt}}{z^{n+1}}dz\right|\le\frac{e^{ta}}{2}\frac{R}{R-a}\sum_{n=1}^{\infty}\left(\frac{\|A\|}{R-a}\right)^n$$

and because

$$\frac{\|A\|}{R-a}<1$$

one deduce that

$$\|B_t(R)\|\le e^{ta}\frac{\|A\|}{2}\frac{R}{R-a}\frac{1}{R-a-\|A\|}.$$

Consequently

$$\lim_{R\to\infty}B_t(R)=0$$

and the limit is uniform for $t\in[t_1,t_2]$.

Then we have

$$\lim_{R\to\infty}I''(R)=0$$

uniformly for $t\in[t_1,t_2]$ from where we conclude that

$$T(t)=\lim_{R\to\infty}\frac{1}{2\pi i}\int_{\Gamma'_R}e^{zt}R(z;A)dz=\frac{1}{2\pi i}\int_{a-i\infty}^{a+i\infty}e^{zt}R(z;A)dz$$

and the integral converges uniformly for $t\in[t_1,t_2]$.■

REFERENCES

[1.] Davies, E.B. (1980). *One-parameter semigroups.* Academic Press.
[2.] Hille, E. and Phillips, R.S. (1957). *Functional Analysis and Semi-Groups.* A.M.S. Providence.
[3.] Lemle, L.D., Jiang, Y. (2007). Bromwich's type representation for semigroups of linear operators, *The Cyprus Journal of Sciences,* Vol. 5, 107-125.
[4.] Nathan, D.S. (1935). One parameter semigroups of transformations in abstract vector spaces, *Duke Math. J.,* 518-526.
[5.] Pazy, A. (1983). *Semigroups of Linear Operators and Applications to Partial Differential Equations.* Springer Verlag.
[6.] Reghiş, M. and Babescu, Gh. (1980). Cosine and sine functions valued in Banach algebras, *Analele Univ. Timişoara,* Vol. 1, 83-92.
[7.] Yosida, K. (1936). On the group embedded in the metrical complete ring, *Japan J. Math.,* 7-26.
[8.] Yosida, K. (1967). *Functional Analysis.* Springer Verlag.

INTERNATIONAL SYMPOSIUM on
ADVANCED ENGINEERING & APPLIED MANAGEMENT
– 40th ANNIVERSARY in HIGHER EDUCATION (1970-2010)
4 – 5 November, 2010, Hunedoara, ROMANIA

[1.]Imre Zsolt MIKLOS; [2.]Carmen Inge ALIC; [2.]Cristina Carmen MIKLOS

INDEXING DEVICE WITH SPHERICAL ELEMENTS (BALLS)

[1-3] UNIVERSITY POLITEHNICA OF TIMISOARA, FACULTY OF ENGINEERING FROM HUNEDOARA, ROMANIA

ABSTRACT:
In the present paper it's present an indexing device used to protect the blooms tilting mechanisms on rolling train, the modeling and its CAD using Autodesk Inventor Professional, respectively that experimental tests on a laboratory model of the device together with the results analyzes in table and graphically form.

KEYWORDS:
Tilting mechanism, indexing device, experimental trials

1. INTRODUCTION

The proposed device is used to protect the tilting mechanisms from the blooming type rolling train if accidental increase the force from the main tilting rod.

The main rod of the tilting mechanism is a sword-sheath construction; the combination of the two components is accomplished by two bolts, which are designed to break when the force exceeds a value determined by design. The proposed protection device works on the principle of indexing systems with balls, is adaptable to the tilting mechanism rod and serves to eliminate the time when the rolling train not work to change the broken bolts with new ones. Principle sketch of the protection device with balls is shown in fig. 1.

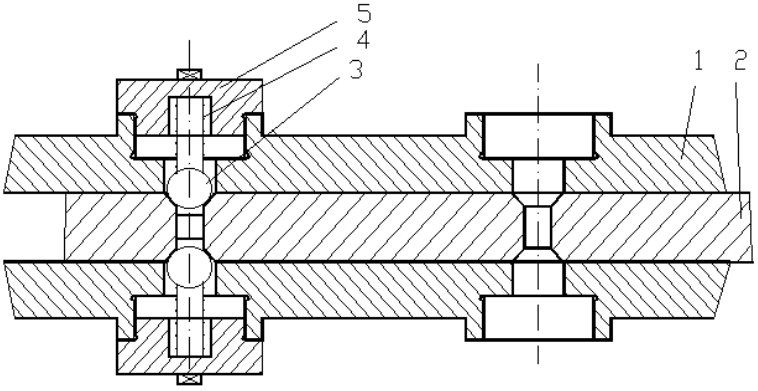

Fig. 1. Protection device with spherical elements. 1 - rod sheath; 2 - sword rod; 3 - spherical locking element (ball); 4 - compression spring; 5 - screw cap
Instead each shear bolt will be mounted a pair of spherical locking elements (balls).

If the force of the rod tilting mechanism exceeds (accidentally) the operation mode corresponding value, the balls from the device construction are retracting in space from the sheath rod, compressing the springs. In a new cycle of the tilting mechanism, in the conditions when the causes that led to accidental increased of the force from rod mechanism stops, the springs will push the balls back into the tapered channels from the sword rod, and the mechanism will still function normally, without the rolling train to be stopped, respectively the rolling process stopped.

Taking into account that the connecting rod's critical force (the spring's pressing force) is very big and because the spring's space is limited (for a little deformation), is recommended to use compression ring springs, which satisfy the conditions below.

2. INDEXING DEVICE DESIGN

The dynamic analysis of the tilting mechanism from the rolling train 1000 mm found that the maximum force (to break the bolts) of the rod mechanism is:

$$F = 475000 \text{ [N]}$$

As noted in the bibliography, for designing the indexing device, the calculation force that this device need to give up, is obtained by amplifying the regime force system with a safety factor from the biggest force in the rod $K_F = 1{,}116$. So, the calculation force that triggers the locking device with spherical bodies is:

$$F_{max} = K_F \cdot F = 1{,}116 \cdot 475000 = 530100[N]$$

Calculation scheme for ball device design is shown in fig. 2.

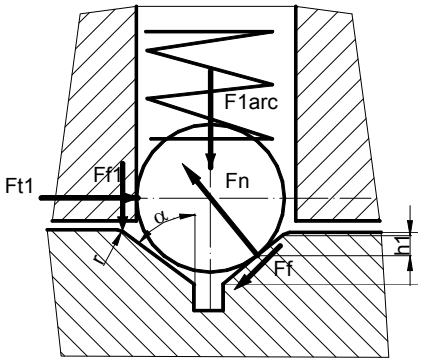

Fig. 2. Indexing device calculation scheme

In order to design the protection device with ball, the constructive choose the following sizes:

- trapezoidal channel opening semiangle, α=30–50 degrees
- ball diameter, depending on indexing device dimension, d_b = 40–50 [mm]
- trapezoidal channel depth, h = (0,2...0,5)d_b
- trapezoidal channel connection radius, r ≤ 0,5d_b
- load uneven distribution coefficient between the ball and lock body, λ=0,8
- Initial deflection for spring assembly, δ_1 = 18 [mm]
- coefficient of friction μ_o = 0,15
- longitudinal MOE E = 215000 [Mpa]
- admissible strength at the balls contact load σ_{ak} = 5000[Mpa]

Then calculate the following sizes:

- spring preloaded force: $F_{1arc} = \frac{F_{max}}{2}\left[\left(1 \quad \mu_0^2\right) \quad tg\alpha \quad 2 \quad \mu_0\right]$

- spring stiffness: $k_a \leqslant \frac{F_{1arc}}{\delta_1}$

- normal force between the balls and trapezoidal channel: $F_n = \frac{F_{1arc}}{\lambda}\left[\left(1 \quad \mu_0^2\right) \quad \sin\alpha \quad 2 \quad \mu_0 \quad \cos\alpha\right]$

- resistance to balls contact load: $\sigma_{k\,max} = 0{,}63\sqrt[3]{\frac{F_n \quad E^2}{d_b^2}} \leqslant \sigma_{ak}$

The above calculations are performed using a computer program written in Visual Basic. Program work interface is shown in fig. 3, together with calculated values displayed (including sizes for ring springs).

Based on the above calculated sizes, automatic protection device with balls was modelled 3D, in Autodesk Inventor Professional program. In fig. 4 is presents the model photo-realistic images.

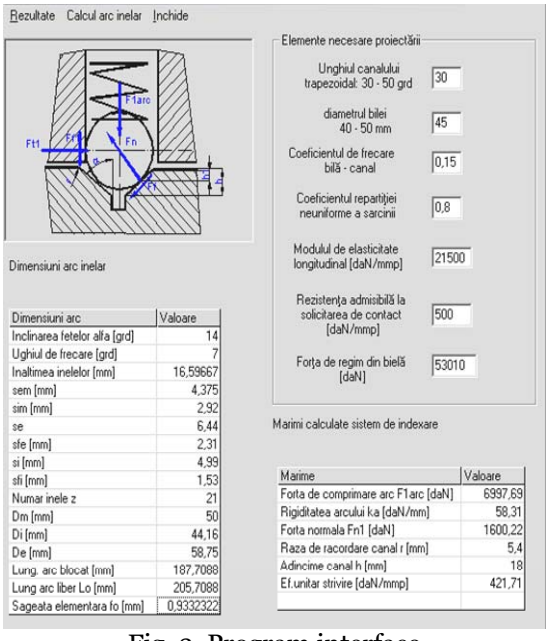

Fig. 3. Program interface

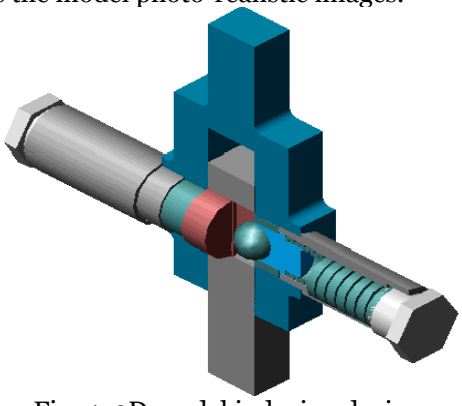

Fig. 4. 3D model indexing device

3. EXPERIMENTAL TESTS ON INDEXING DEVICE

In order to follow the behavior of the indexing device with spherical locking elements whose design and model were presented in paragraph 2, because of rod big dimensions where this system adapts, has been designed and implemented a small dimensions model to be tested under laboratory conditions.

Active elements of the device experimental model with nominal dimensions respectively how to make a contact between trapezoidal channel - ball - ball guide element are presented in fig. 5.

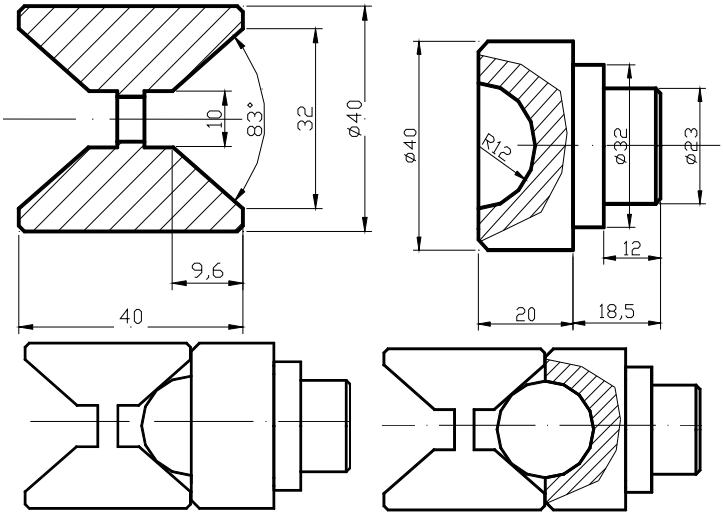

Fig. 5. Active elements geometric dimensions

According to fig.5 trapezoidal channel angle is $\alpha = 83/2 = 41,5$degrees, which is within the range 30-50 degrees, and ball diameter is 24 mm.

The fig. 6 picture presents the active elements of the developed device model.

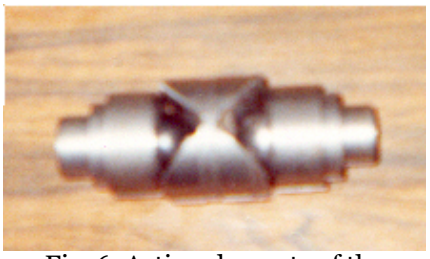

Fig. 6. Active elements of the indexing device

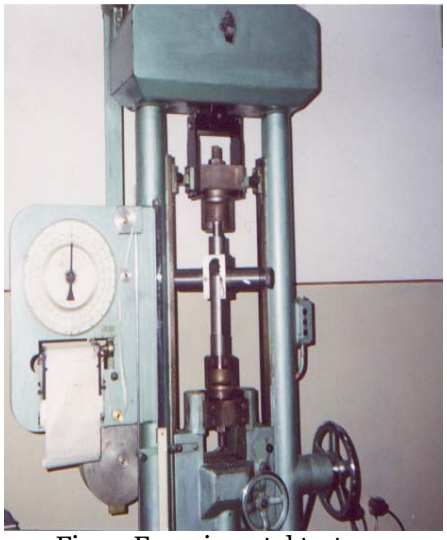

Fig. 7. Experimental tests on experimental model

As a compression spring, for pressing the balls in trapezoidal channels, to the indexing device experimental model studied, does used compression springs, know their calibration curves.

Experimental tests on experimental model of protection device with balls, where made on the universal test machine, according to fig. 7.

Table 1 Arc 1 C_1 = 3,82 [N/mm]

f[mm]	3	6	9	15	18
	4	7,5	11	19	24
	3,5	8	12	18,75	23,6
	4	7,75	12,5	20	23
Fmediu[daN]	3,833333	7,75	11,83333	19,25	23,53333
Farc [daN]	1,2	2,4	3,4	5,8	6,8
F [daN]	3,83	7,75	11,83	19,25	23,53

The experimental tests will pursue a dependency between the preload force of coil springs and the force where device with balls will trigger (read on the test machine dial).

Compression springs preload force, will result from their calibration graphs based on their deformation, determined as the multiplication of the turns number of cover and their thread pitch (p = 1,5 [mm]).

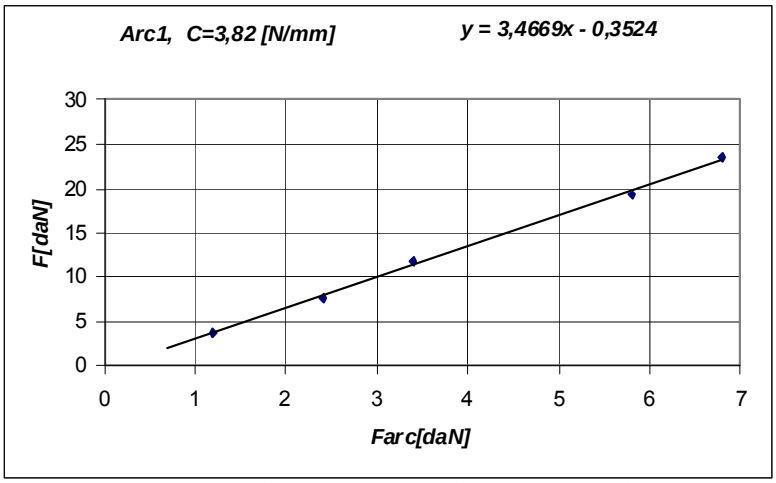

Fig. 8. Trigger force variation of the indexing device

The experimental results are processed into tables and graphics, and an example is shown in table 1 and fig. 8.

4. CONCLUSIONS

Indexing device with balls was bring under stress tension, aiming determining the dependence between the force where the system gives up (read on the test machine dial) and the preload force of the spring coil (determined from their calibration graphs).

We used three pairs of compression springs, different stiffness, respectively C_1 = 3,82 [N/mm], C_2 = 11,25 [N/mm] and C_3 = 6,56 [N/mm].

The construction of the device with spherical locking elements was used two balls with a 24 mm diameter and a tronconical channel with 83 degrees opening angle and a depth of 9.6 mm.

Analyzing the results of experimental tests on an experimental model of ball device, it can say the following conclusions:

- The model on small-scale of indexing device with spherical locking elements work correctly for all three pairs of springs used.
- In the tests it was found a linear increase of the force when the ball device gives up, in relation to the spring's preload force.
- For springs pairs with different stiffness, on the same preload force, the force at which the indexing device with balls starts increases with the spring stiffness.
- The force value in which the device with balls starts, depends on trapezoidal channel dimensions, decreasing with the increasing its angle.

REFERENCES

[1.] Burchard, B., ş.a., Secrete AutoCAD 14, Editura Teora Bucureşti 1998
[2.] Cioată ,V., Miklos, I. Zs., Proiectare asistată de calculator cu Autodesk Inventor, Editura Mirton, Timişoara, 2009
[3.] Drăghici, I., ş.a., Indrumar de proiectare în construcţia de maşini, Vol. I,II Editura Tehnică Bucureşti, 1981.
[4.] Kelly, J., Utilizare, Microsoft Excel 97, Editura Teora, Bucureşti, 1998.
[5.] Miklos I. ZS., Cioată, V., Desenare 2D cu AutoCAD 2002, Editura Mirton Timişoara, 2003
[6.] Miklos, I. ZS., Contribuţii privind îmbunătăţirea performanţelor tehnologice ale mecanismelor de răsturnat blumuri la liniile de laminare, Teză de doctorat, Universitatea din Petroşani, 2001.

INTERNATIONAL SYMPOSIUM on
ADVANCED ENGINEERING & APPLIED MANAGEMENT
– 40th ANNIVERSARY in HIGHER EDUCATION (1970-2010)
4 – 5 November, 2010, Hunedoara, ROMANIA

[1.]Teodor VASIU, [2.]Adina BUDIUL – BERGHIAN

THE PORTABLE GRINDERS BLACK& DECKER RELIABILITY DETERMINATION

[1, 2] FACULTY OF ENGINEERING HUNEDOARA, ROMANIA

ABSTRACT:
In this work is represented the assessment method to real reliability of electromechanic entities. The practical example is doed for a tipo - dimensional portable grinder. The example needs illustrated the interpretation of experimental date (looking the operation/breakdown of grinders) statistically analyzed.
KEYWORDS: reliability, statistical analysis, portable grinders

1. INTRODUCTION

The determination real reliability by portable grinders is done abaft the research of their behavior in exploitation. Were, drew up a program of follow the operation of a breakdown number of seventeen grinders Black& Decker. This program contains the acquest moment of each grinder, who tallies with the first moment of utilization the entity, the breakdown moment and entrance in service and in latter, the duration of maintenance activities. The systematized data are right truncated because pursuit grinders stop after first period of operation and reestablishment. Certainly that the study till be much more former if the studious entities be can be seed on whole their duration of life. This thing presupposes a tight cooperation between provider and user, carry don't always he is obtained on the measure of our desires.

2. METHODOLOGY

For determination the real reliability of portable grinders, the values of their times of good operation were entered in a specialized software, WEIBULL++6 (figure 3. 1), who permits the quick settlement depending on repartition most fit the case, with a coefficient of correlation Rho or ρ.

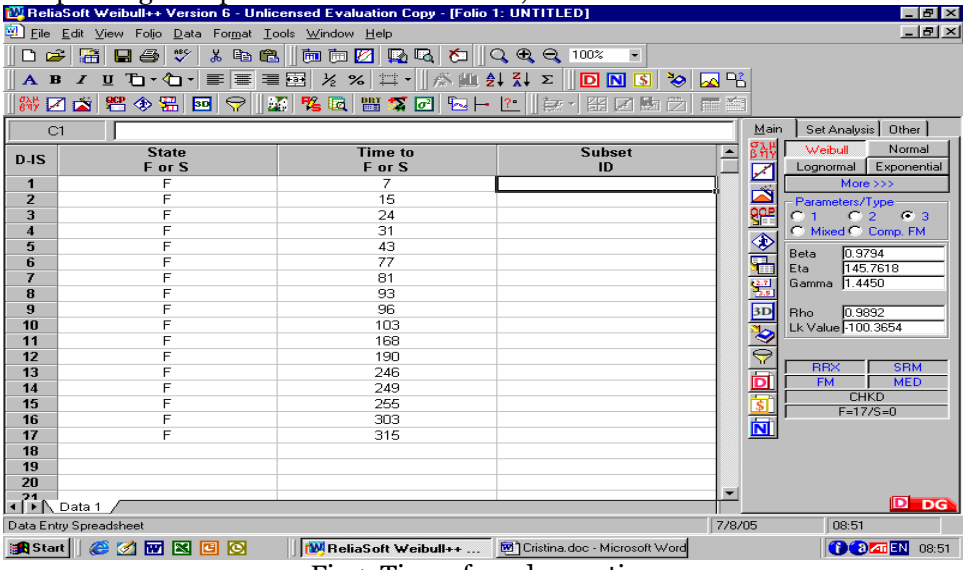

D-IS	State F or S	Time to F or S	Subset ID
1	F	7	
2	F	15	
3	F	24	
4	F	31	
5	F	43	
6	F	77	
7	F	81	
8	F	93	
9	F	96	
10	F	103	
11	F	168	
12	F	190	
13	F	246	
14	F	249	
15	F	255	
16	F	303	
17	F	315	
18			
19			
20			

Fig.1. Time of good operation

For the present case, the distribution law of portable grinders functioning is Weibull with three parameters β = 0,9794, η = 145,7618 and γ = 1,4450. The correlation coefficient is 0,9892. Accordingly these laws the mean time between failures is

$$MTBF = \eta\Gamma\left(\frac{1}{\beta}+1\right) = 145,7618 \times \Gamma(2,021) = 145,7618 \times 1 = 145,7618 \quad \text{days},$$

in which Γ(x) is the Eulerian integral of second kind.

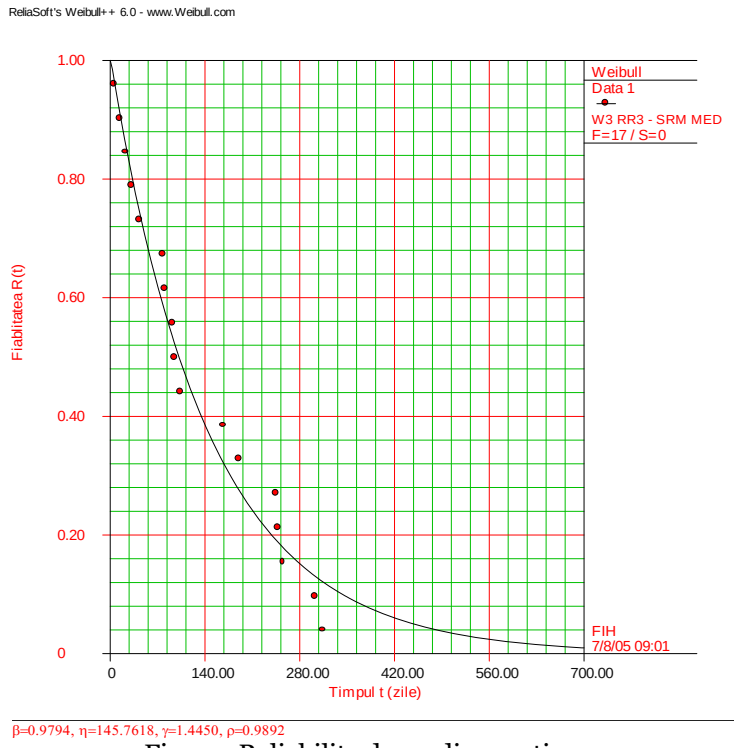

Fig. 3.2 Reliability depending on time

The β value, gated closer to 1 indicated the fact that the abrasive discs with all as the new, there are in the natural period of life. This thing show that the entities are submissive of a proper running in to producer. The positive γ value show that no faultiness appears in the exploitation of grinders giddap of 1,445 days.

The program WEIBULL+ + 6 permits curve-plotting depending on the time of reliability (fig.3.2), percentile(non-reliability) (fig.3.3), density of probability (fig.3.4) and failure rate (fig.3.5), as well as the correlation among the parameters of Weibull law, materialized through the zone with probability of 95% (fig.3.6) and the function Likelihood (fig.3.7).

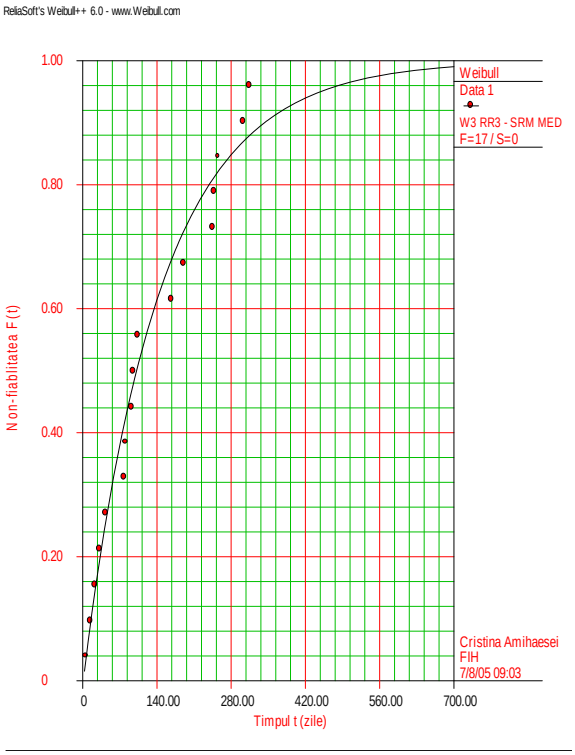

Fig. 3.3 The percentile depending on time

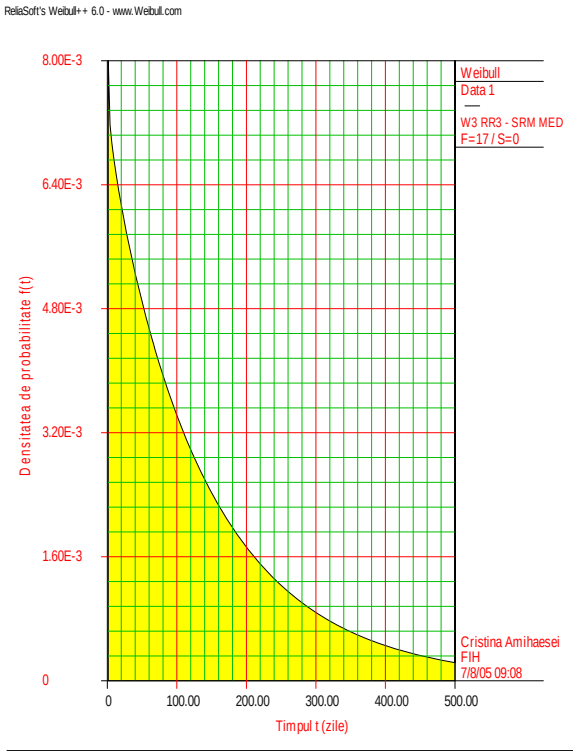

Fig. 3.4. The density of probability depending on time

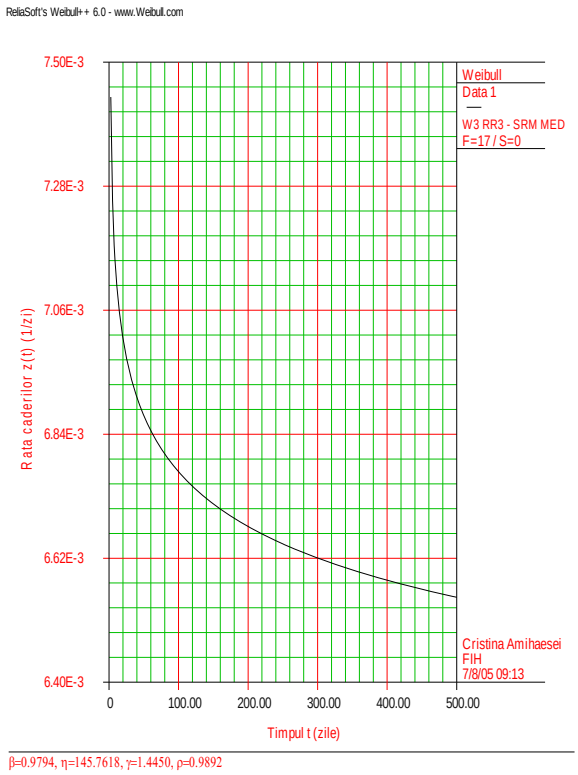

Fig. 3.5 The failure rate depending on time

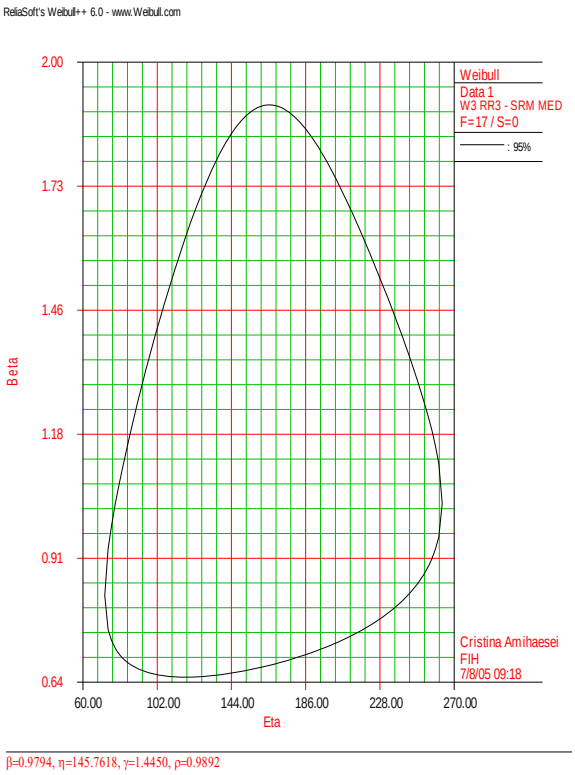

Fig. 3.6 Values β şi η with 95% probability

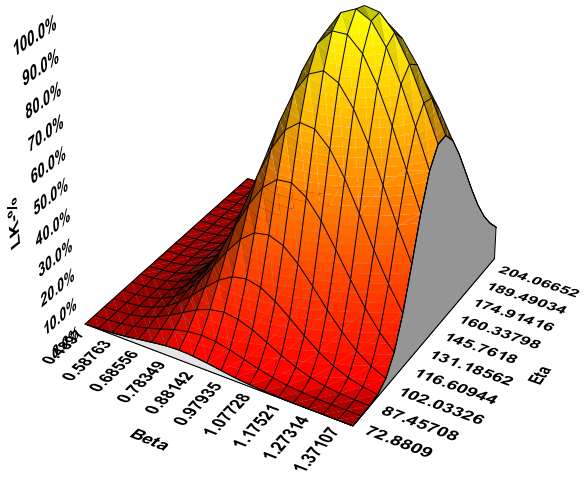

Fig. 3.7. Likelihood function

3. CONCLUSION

Consisted that, figure 3.5, as a starter, failure rate has relative erect values, specify operate of a new entities. He follows a quick diminution, what show that the regime of natural life is installed relatively quick. This thing is strengthened also be β value. Reduce bold the failure rate, specifies the electric components and electronic, is waited directing to the ascertainments concerning the out of order nature of by hand grinder.

The electric defects of portable grinders reduce significantly (fig.3.2) the reliability still of their working setting, what does as the period of established guarantee of producer to is attenuate properly.

REFERENCES

1. Baron, T., ş.a., Calitate şi fiabilitate - manual practic, vol. 1 şi 2, Editura Tehnică, Bucureşti, 1988.
2. Budiul-Berghian, A., Contribuţii privind îmbunătăţirea fiabilităţii mecanismelor tip foarfece pentru debitat produse metalurgice, Teză de doctorat, Petroşani, 2007.
3. Mihoc Gh., Muja A., Diatcu E., Bazele matematice ale teoriei fiabilităţii, Editura Dacia, Cluj-Napoca, 1976.
4. Niculesc, D., Calitate, fiabilitate, mentenanţă, A. M. C., vol. 18-19, Editura Tehnică, Bucureşti, 1975.
5. Roman, I., Determinarea indicatorilor de fiabilitate, în Calitatea producţiei şi metrologie, nr. 1, 1974.
6. Vasiu T., Fiabilitatea sistemelor electromecanice, Editura Bibliofor, Deva, 2000.

INTERNATIONAL SYMPOSIUM on
ADVANCED ENGINEERING & APPLIED MANAGEMENT
– 40th ANNIVERSARY in HIGHER EDUCATION (1970-2010)
4 – 5 November, 2010, Hunedoara, ROMANIA

[1.] Carmen Inge ALIC, [2.]Sorin Aurel RAŢIU, [3.]Vasile ALEXA,
[4.] Cristina Carmen MIKLOS, [5.]Imre Zsolt MIKLOS

CRÉATION DE RESSOURCES PÉDAGOGIQUES INTERACTIVES ORGANISÉES EN BASE DE DONNÉES, POUR DES APPRENTISSAGES EN SOUDAGE

[1.] UNIVERSITY „POLITEHNICA" TIMIŞOARA, FACULTY OF ENGINEERING HUNEDOARA, ROMANIA

ABSTRACT:
Create of interactive learning resources structured in database, for the acquisition of knowledge and skills in the welding field
This publication aims to expose the collaborative work and the experiences of our project team in order to design and implement a training tool in the welding domain, which includes interactive educational resources organized into a database. The training tool is currently in developing progress under a two years European project, funded by the LLP/**L**ifelong **L**earning **P**rogram/Sectorial Program Leonardo da Vinci/Partnerships. The transnational project team consists of four partner organizations, of which AFPA– Lyon, France, ensures the coordination of the project, and *Universitatea „POLITEHNICA" Timisoara-Facultatea de Inginerie Hunedoara,* Romania, the *Institut de Soudure*-Paris, France, and *Le FOREM*-Bruxelles/Charleroi, Belgium, are the partners.
The goal of the project is to design a more attractive multimedia training content, with multimodal character (accessible on keywords-based consultation, or in training route mode), which will contribute to the development of personal and professional autonomy of the employees, students and European people in training and further training activities in welding domain, since the practitioner level until the welding engineer.
This publication was developed to promote the visibility of the project and its progress, and is dedicated, also, to the intent of dissemination and exploitation of the project results.
KEYWORDS:
collaborative work, European project, training resources, welding training

1. CONTEXTE ET MOTIVATION

Dans de nombreux pays de l'Europe, les métiers du soudage font aujourd'hui l'objet d'une définition qui varie considérablement selon l'activité et le type de production réalisée (unitaire ou en série, en entreprise ou sur chantier). Ainsi, pour une partie de l'industrie, il s'agit avant tout d'un métier très spécialisé ; pour l'autre partie du secteur, être soudeur impose une polyvalence et de multiples compétences qui se rapprochent de celles du chaudronnier ou du tuyauteur. De tels éléments contribuent à l'existence d'un marché de l'emploi « éclaté », en pleine évolution au sein des différents pays, distinguant nettement les salariés spécialisés de ceux à qui il est demandé d'être poly-compétents, autonomes et capables de réaliser un travail depuis sa conception jusqu'à sa réalisation. Cet élargissement des tâches, qui s'accentue de plus en plus et impose une mobilité accrue des personnes, entraîne des difficultés de recrutement pour les entreprises, argumentée à la fois par des exigences de qualité de production et la recherche de profils plus ou moins qualifiés, selon les tâches.

Si l'unique réponse fournie reste à ce jour le recours massif aux entreprises de travail temporaire, ces dernières dans leur travail de placement offrent généralement un personnel dont le niveau de formation se limite au passage des licences autorisant le travail du soudage. Cela ne permet pas toujours l'ouverture vers de nouvelles perspectives de production et n'encourage pas non plus une possible réorganisation du travail vers des profils d'exécution. Aussi qu'elle s'adresse à

des soudeurs spécialisés, de « simples » soudeurs ou tout autres praticiens, tantôt sédentarisés, tantôt mobiles, la formation reste l'une des clés d'adaptation à l'évolution technique, technologique et organisationnelle des métiers liés au domaine du soudage.

Problématique généralement commune aux pays européennes, la formation en soudage devrait donc faire l'objet d'un projet permettant de réfléchir ensemble à la modernisation des ressources formatives existantes, et travailler à sa la mise en œuvre pour:

- Former selon des modes diversifiés à différents niveaux d'emploi dans les métiers du soudage;
- Répondre aux besoins en main d'œuvre qualifiée des entreprises et les aider dans leur développement et leur conquête de nouveaux marchés, en formant des salariés capables d'autonomie et de réflexion sur le travail;
- Accompagner et faciliter la transmission des savoirs au sein même des entreprises ;
- Fixer une partie de la main d'œuvre tentée par des secteurs plus attractifs ;
- Apporter un outil de formation adapté aux contraintes (recrutement, compétitivité, formation) des entreprises en termes de flexibilité et de souplesse d'utilisation ;
- Doter d'un outil moderne de formation au soudage à la fois les entreprises et les principaux opérateurs de formation au soudage en Europe ;

Dans le contexte décrit, au sein des organismes de formation on compte aujourd'hui d'un nombre important de ressources formatives attachées à l'apprentissage des gestes et techniques des métiers du soudage. L'essentiel de ces ressources mises à la disposition des personnes en formation, reste principalement constitué de textes et d'images fixes, n'autorisant que peu d'interactivité entre l'utilisateur et les ressources. L'utilisation de l'interactivité sous forme de navigation ou de recherche d'information, reste souvent limitée aux liens internes attachés à des diaporamas réalisés par les personnels enseignants, et si certaines de ces ressources font l'objet d'une animation par l'intégration d'images vidéos, elles sont à la fois peu nombreuses et peu attractives. L'évolution des techniques de soudage, la diversification des contextes d'application, l'exigence de compétences, ainsi que la demande croissante de souplesse au sein de la formation intégrée au travail imposent la nécessité d'une modernisation et/ou d'adaptation des ressources formatives existantes.

2. OBJECTIFS DU PROJET. ÉTAPES ET APPROCHES. ACTIVITÉS.

Les activités du projet ont les objectifs suivants :

- Construire un cadre d'échange et de coopération entre des acteurs de la formation soudage en Europe, Fig.1 ;

Fig.1. Le projet de parteneriat - Cadre européenne d'échange et de coopération entre des acteurs de la formation soudage

- Offrir aux partenaires la possibilité de moderniser et d'harmoniser leurs patrimoines de ressources de formation au soudage (Fig.2) ;

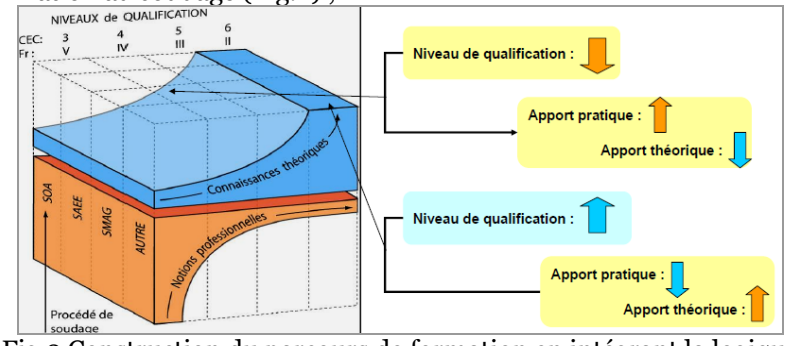

Fig.2 Construction du parcours de formation en intégrant la logique *ECVET - "European Credit for Vocational Education and Training".*

- Concevoir et proposer un support plus attractif de contenus de formation (multimédia), au caractère multimodal (accès en consultation sur mots clé ou en mode parcours de formation), Fig.3, et qui puisse contribuer au développement de l'autonomie personnelle et professionnelle des salariés, des étudiants et des personnes en formation soudage en Europe, depuis le niveau praticien jusqu'à l'ingénieur soudage ;

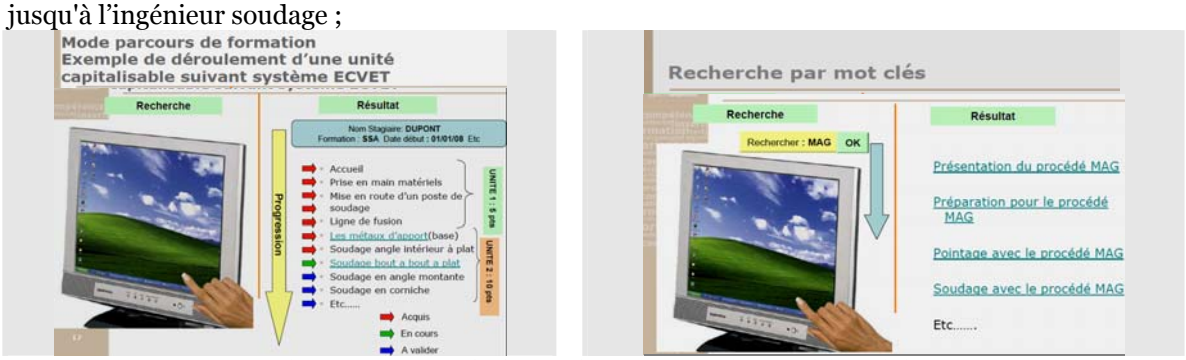

Fig.3. Contenus de formation au caractère multimodal,
accès en mode « parcours de formation » ou en mode « consultation par mots clé »

- Rapprocher formation et lieux de travail en proposant à des utilisateurs de pays différents (formateurs, enseignants, responsable d'atelier, chef d'entreprise, etc.) un outil évolutif de consultation et d'utilisation de ressources en soudage, Fig.4.

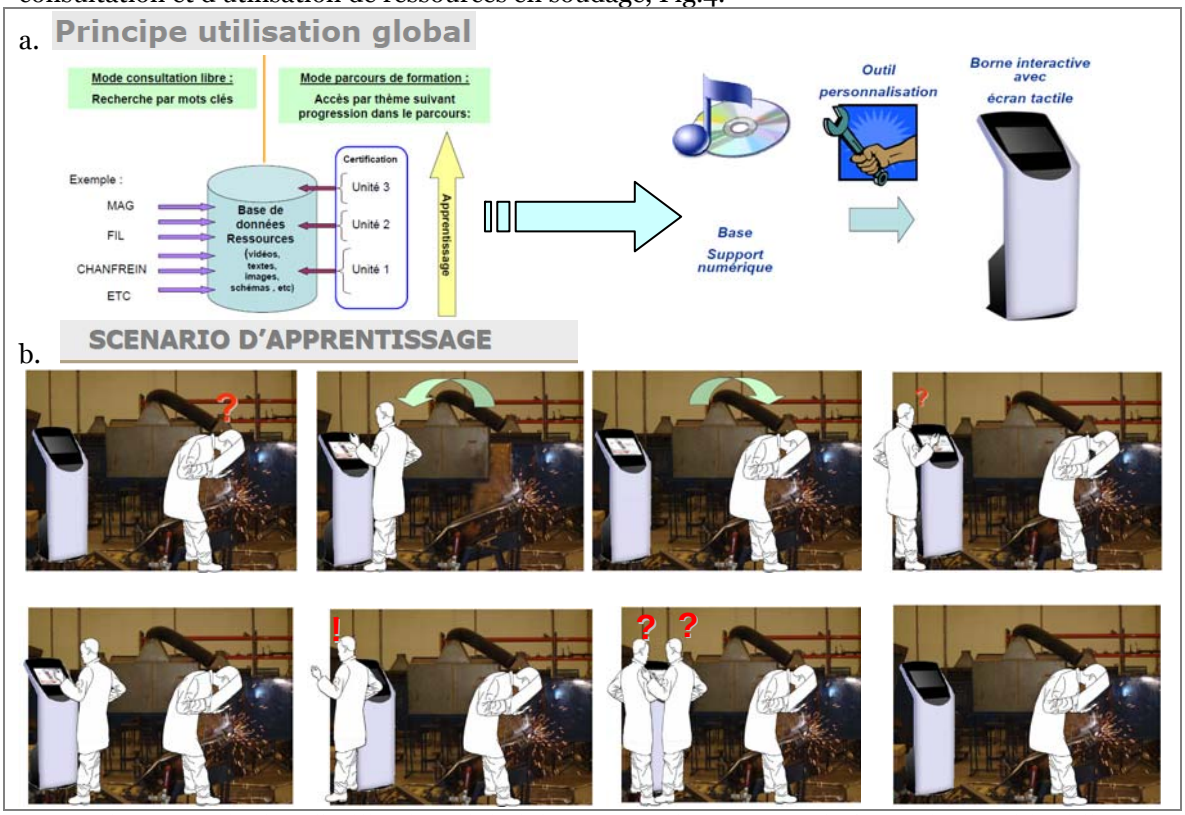

Fig. 4. a. Principe d'utilisation global du support de contenus de formation multimédia,
au caractère multimodal ; b. Scénario d'apprentissage

L'outil de formation en cours d'être réalisé, se différencie des environnements virtuels et autres simulateurs en soudage, en le sens qu'il offre des fonctionnalités différentes, principalement ouvertes sur l'acquisition des connaissances, concepts et techniques nécessaires à l'activité, suivant des niveaux de pratiques différenciés, et qu'il n'est pas orienté sur l'acquisition d'habiletés psychomotrices pour une maîtrise de la manipulation des outils de soudage. Les principaux sujets traités sont : Procédés de soudage ; Rappel d'électricité et de physique ; Métaux d'apport ; Accessoires de soudage ; Environnement de la zone de travail ; Mise en service ; Maintenance ; Réglages de base en soudage ; Influence des paramètres ; Contrôle ; Hygiène, sécurité et développement durable ; Traitement des défauts.

L'approche adoptée afin de mettre en oeuvre le projet va de l'ingénierie pédagogique jusqu'au test en situation réelle et comprend la conception, la réalisation, la validation et

l'évaluation. Ces principales étapes se décomposent en plusieurs étapes durant lesquelles chaque partenaire, compte tenu de ses spécificités et de son degré d'expertise lié à l'apprentissage du soudage, a une part à prendre et donc des tâches à réaliser, [1].

- La première étape des activités a permis aux partenaires de se positionner sur un même niveau de connaissance concernant les objectifs et les modalités de déroulement du projet, et a été consacrée à un travail de *collecte*, de *sélection* et *d'harmonisation* des contenus de formation existants et susceptibles de nourrir l'outil interactif mis en projet;
- La seconde étape, a été de *structurer* les contenus d'apprentissage retenus en *unités indépendantes* (granularisation) répondant à des acquisitions de connaissances et de compétences suivant différents niveaux fixés (opérateur – Technicien - Ingénieur). Cette étape a abouti à la présentation de progressions pédagogiques d'utilisation souple, complète ou partielle et différenciées suivant les niveaux d'emplois retenus ; Fig.5.

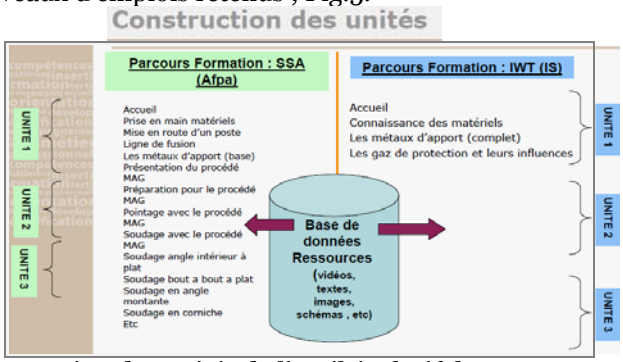

Fig.5. Construction des unités de l'outil évolutif de ressources en soudage

- La troisième étape a eu pour objectifs la *scénarisation des contenus* choisis et structurés en progressions, Fig.6. Elle s'est accompagnée d'une phase *d'essais et d'adaptation* de la méthode auprès des différents environnements représentatifs des partenaires (entreprises, centres de formation, d'enseignement) qui a permis *l'ajustement, l'harmonisation et la stabilisation* en matière de format des scénarii intégrés à la future borne interactive.

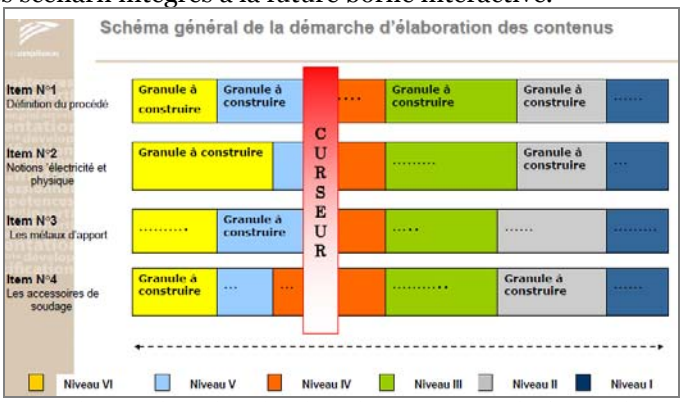

Fig.6. Structuration et de scénarisation des contenus de formation en soudage

- Une quatrième étape a pour objectif de *définir* puis *choisir* les *modalités et moyens techniques* de mise en place de l'outil interactif (modalités pédagogiques, formats multimédias, traduction, etc.) et intègrera une démarche d'assurance qualité.
- La cinquième étape favorisera la mise en œuvre par *expérimentation* de la nouvelle solution de formation finalisée et organisera la *mesure de ses effets*.

3. RÉPARTITION DES TÂCHES. COOPÉRATION ET COMMUNICATION

La répartition des tâches entre les organismes participants assure l'implication active de tous les partenaires et, selon les compétences requises, prévue que chaque partenaire contribue à des degrés différents aux travaux à réaliser. Ainsi :

- L'AFPA (Fig.7a), entité à vocation nationale sur le champ de la formation et de la certification, en complément de sa connaissance des publics en formation, dispose d'une expérience importante dans la pédagogie adaptée aux formations des professionnels qualifiés en soudage. En possédant à ce titre une expertise en matière d'environnement pédagogique et d'outils didactiques, elle assure la coordination du programme d'actions et contribue prioritairement aux étapes de conception et de réalisation de l'outil par l'apport d'un patrimoine ressources et par son expertise en matière d'ingénierie pédagogique.

- L'Institut de Soudure (Fig.7c), outre sa renommée nationale et internationale sur le champ de la formation et de la certification des professionnels d'entreprises, des niveaux soudeurs jusqu'aux niveaux ingénieurs, dispose d'une grande expertise en recherche et développement industriels en soudage, ainsi que dans la conception et le développement de supports et d'outils pédagogiques. A ce titre, il apporte une contribution soutenue à chacune des étapes, allant de la conception à l'évaluation du produit de formation réalisé. Ses compétences en matière de veille normative et documentaire favorisent la mise en place de l'outil au caractère à la fois actualisé et évolutif, et participe à la démarche qualité contenue dans le projet.
- Le FOREM (Fig.7d), outre l'adaptation et l'insertion des travailleurs et des demandeurs d'emploi sur le marché du travail (aide au repérage des compétences et conseils aux dispositifs de recrutement) justifie une très bonne connaissance des entreprises et de leurs besoins en qualifications liées au soudage. A ce titre, son implication dans l'évaluation et la dissémination auprès d'entreprises du produit de formation réalisé, favorisera l'expérimentation et l'exploitation de ce dernier et permettra les ajustements et modifications nécessaires à sa finalisation, tout en facilitant la mesure des effets constatés.

www.industrie.afpa.fr www.fih.upt.ro www.isgroupe.com www.leforem.be

a. b. c. d.

Fig.7. Les organismes participants à la répartition des tâches du projet de parteneriat

- L'Université Polytechnique de Timisoara et la Faculté d'Ingénierie d'Hunedoara (Fig.7b), par leur expertise en recherche, contribuent à la fois à la modélisation de l'outil de formation et aux stratégies argumentatives qui accompagnent un système d'apprentissage interactif. L'apport du travail universitaire permette dans la phase de réalisation, un approfondissement des éléments de réalité virtuelle attachés à l'apprentissage proposé par le nouvel outil interactif, qu'il s'agisse des phases d'apprentissage ou encore de phases d'évaluation. Sa participation à la phase de conception est envisagée pour ce qui concerne les ressources de formation affectées au niveau ingénieur.

Afin d'assurer la cohérence dans la conduite du projet et de permettre un partage optimal des informations relatives aux travaux, chaque partenaire, malgré une répartition préalable des tâches, participe à l'ensemble des étapes constitutives de la démarche, et apport sa contribution par la présence de son référent ou des acteurs repérés pour leur expertise dans le projet. Afin de pouvoir s'assurer d'une plus large possibilité d'expérimentation, donc d'évaluation de l'outil crée, la cinquième étape aura un caractère transverse et mobilisera l'ensemble des partenaires et les contextes d'activité qu'ils représentent. Cela va permettre une évaluation plus juste et va offrir une ouverture en termes de communication externe et de dissémination du produit.

L'un des objectifs majeurs de ce projet est de réaliser un outil commun de formation au soudage, en établissant une collaboration renforcée entre les partenaires. A ce titre, et afin de pouvoir engager efficacement un travail de réflexion et de conception du support de formation, l'équipe a trouvé opportun de mettre en place une organisation collégiale basée sur le partage à la fois des informations, des expériences vécues et des travaux à réalisés. Les partenaires, disposant tous d'outils de communication modernes (site Web, systèmes de messagerie, de vidéoconférences, etc.), l'outil privilégié a été l'Internet, avec toutes les possibilités d'échanges de données. De plus, en qualité de coordonnateur, l'AFPA a déployé l'infrastructure nécessaire à la mise en place d'un outil collaboratif, la *Plateforme informatique "BRIS"*, Fig.8, organisée autour de la technologie *Share Point* de Microsoft.

Les nombreuses fonctionnalités de cette plateforme, applicables au projet, permettent : l'utilisation par les partenaires d'espaces de travail pour la création ; la révision ou la publication de documents de formation attachés au soudage; une gestion plus efficace du projet à l'aide du modèle de liste de tâches; la coordination du travail d'équipe à l'aide des calendriers partagés, des alertes et des notifications ; un renforcement de la communication entre partenaires à l'aide des fonctionnalités de présence et de messagerie instantanée.

Afin de solidifier la communication interne autour du projet, l'utilisation régulière de conférences téléphoniques et de plus, à partir du juin 2010, de vidéoconférences, Fig.8b, la rencontre des référents au sein des réunions du comité de pilotage, comme l'invitation des acteurs (personnels et apprenants) de chaque organisme aux différents groupes de travail, ont renforcé la garantie d'une bonne coopération et d'une circulation des informations efficace.

a.

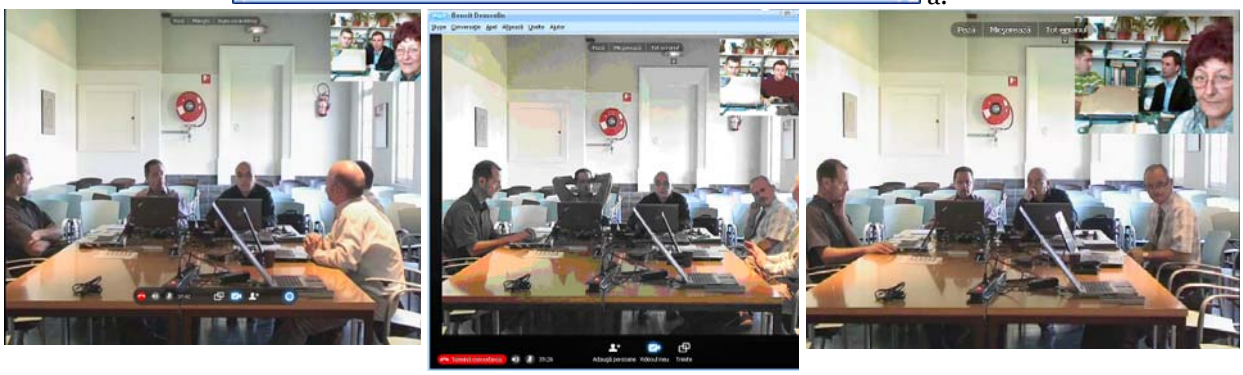

b.

Fig.8. a. Plateforme informatique collaborative (technologie *Share Point*);
b. Vidéoconférence Bruxelles-Paris-Hunedoara, Group de travail, oct.2010

4. IMPACT ET VALEUR AJOUTÉ EUROPÉENNE

L'intérêt de la mise en œuvre du projet réside dans la possibilité pour les apprenants d'accéder à un processus d'apprentissage du soudage individualisé, dynamique et adapté. La mise au point de ce support interactif reprenant l'ensemble des connaissances, gestes et techniques du soudage constitue un guide des pratiques et d'apprentissage spécialement conçu pour les professionnels de l'activité. En leur offrant la possibilité d'un développement des compétences par un accroissement de l'attractivité de la formation proposée, il est possible d'envisager une amélioration de la compétitivité de ces praticiens, leur permettant par là même de faire valoir en entreprises, comme sur le marché du travail, leur capacité d'insertion et d'adaptation aux exigences économiques, technologiques et techniques.

De leurs cotés, les partenaires sont demandeurs d'aide à la mise en place d'une nouvelle ingénierie et/ou d'une nouvelle méthodologie d'apprentissage des gestes et techniques en soudage. En privilégiant la recherche d'une solution innovante, et en proposant une approche pédagogique originale à un niveau européen, les organismes partenaires pourront mettre à profit dans leurs activités (Formation, Enseignement, Insertion) l'expertise combinée issue du projet, et renforceront ainsi leur efficacité en matière de demandes d'amélioration des compétences en soudage. Également, en développent un tel projet, chaque partenaire renforce sa dimension réseau au niveau européen et promeut la coopération en matière d'assurance qualité dans le domaine des apprentissages, et de la formation au soudage, en particulier.

5. PERTINENCE PAR RAPPORT AUX OBJECTIFS DU PROGRAMME LEONARDO da VINCI

Le projet de parteneriat réponde à l'objectif d'améliorer la qualité des partenariats et d'accroître le volume de coopérations entre les organismes proposant des offres d'éducation et de formation, les entreprises, les partenaires sociaux et tous acteurs pertinents de la formation professionnelle dans toute l'Europe. (LEO- Objectif 2). Les mesures et activités envisagées pour répondre aux objectifs fixés sont de deux ordres: *stratégique et opérationnel*.

- *Stratégique*, par l'organisation des séminaires : Réunissant principalement les membres du Comité de Pilotage formé des référents nommés pour le projet, le calendrier prévoit tout au long de la durée du projet (2 ans) une réunion trimestrielle, alternativement chez les différents partenaires (Lyon, Bruxelles, Hunedoara, Paris). Chaque séminaire serve de point étape et permette à la fois le suivi et la coordination des travaux, ainsi que la prévision des recadrages et réajustements

nécessaires à la bonne progression du projet. L'ensemble des informations de ces séminaires traitées est diffusé par le biais de la *Plateforme collaborative.*

- *Opérationnel*, par la mise en place localement ou transnationalement des étapes identifiées : Des temps de regroupement (travail communs), des temps d'échanges entre les équipes de chaque organisme partenaire, ainsi que des temps de travail autonomes, pleinement intégrés aux activités de chacun des partenaires. Les équipes participantes assurent la responsabilité globale de la qualité technique du produit à réaliser.

- Les temps d'échanges sont consacrés à la fois aux réalisations à produire et au partage des informations entre les équipes, en bénéficiant de la *Plateforme collaborative* qui permettent de : gérer le cycle de vie des documents ; créer et contrôler leurs propres espaces de travail ; afficher les relations entre les tâches et l'état du projet ; coordonner le travail d'équipe à l'aide des calendriers partagés ; communiquer avec l'ensemble des « adhérents » au projet.
- Les temps de regroupement, réunirent les personnels mandatés par chaque organisme partenaire qui, en fonction de la répartition des tâches, se regroupent indépendamment en des séminaires afin d'analyser, confronter et mettre en œuvre les réalisations attendues par le projet. On utilise ces temps aussi pour associer des apprenants (étudiants, stagiaires, salariés) suivant la nature des tâches à réaliser.

En répondant aux objectifs opérationnels du programme Leonardo da Vinci, les principaux thèmes du partenariat sont : le développement de contenus et de concepts communs dans le domaine de l'*EFP* (*Tpc-13*), et l'adaptation des compétences nécessaires sur le marché du travail. Le domaine pédagogique et de formation, selon les *VET fields,* est«*540-Industrie et Développement au sens large* ».

6. ÉVALUATION

La méthode utilisée pour évaluer la réalisation des objectifs du partenariat et les moyens qui l'accompagnent, permette la récupération constante des informations liées à la vie du projet, l'identification des bonnes pratiques ainsi que le recensement des productions telles que décrites dans les attendus du projet. Le coordonnateur (AFPA), ainsi que les partenaires, mettent en œuvre une organisation dynamique et un processus permanent de suivi du projet :

- Réalisation et communication des *planifications de travail* qui suivent les réunions de comité de pilotage à l'ensemble des équipes partenaires ;
- *Echanges réguliers* d'informations liées au projet entre le coordonnateur et les différents organismes partenaires par l'intermédiaire du référent nommé (lien direct par la plateforme collaborative) ;
- *Consultation régulière* des éléments d'échange et de travail mis en partage sur la plateforme collaborative ;
- *Invitation* de participants externes lors de certains comités de pilotage (participants aux groupes de travaux, bénéficiaires concernés par le projet ou invités des organismes) ;
- Responsabilisation des partenaires dans l'évaluation des résultats obtenus par la mise en place sur la plateforme collaborative de *questionnaires de suivi* (documents harmonisés) ;
- Établissement de *rapports* (initial, intermédiaire et final), reprenant : les principales réalisations (points forts, points faibles, opportunités, menaces qui prévalent pendant la mise en œuvre du projet ; conclusions et recommandations en vue de favoriser la réalisation des effets durant la période restant à couvrir.

7. INTÉGRATION AUX ACTIVITÉS PÉDAGOGIQUES OU AUX AUTRES ACTIVITÉS EN COURS

Pour les organismes partenaires dont l'activité repose principalement sur l'enseignement et la formation professionnelle (*AFPA, IS, UPT/FIH*), les tâches nécessaires à la mise en œuvre du projet ont été directement intégrées aux activités de chacune des structures. Ainsi, les travaux relevant de la phase de conception et de réalisation du projet sont conduits par des personnels dont les compétences et l'expertise en ingénierie de formation, en pédagogie et en recherche s'expriment quotidiennement dans les activités dont ils ont la charge. Ils réalisent régulièrement : des temps de travail consacrés au projet ; des sollicitations auprès des centres d'enseignement et de formations recevant des publics en formation soudage pour des confrontations régulières au produit en cours de construction (soit pour des expérimentations, soit pour des évaluations ponctuelles des réalisations en cours). Pour ce qui est de la phase de mise au format multimédia des ressources ordonnées, ce temps de travail associe plus spécialement l'université par la conduite d'encadrants qualifiés (enseignants-chercheurs et étudiants impliqués dans la recherche sur les applications multimédias). L'intégration des activités du projet aux enseignements proposés par le cursus des

étudiants de l'Université Polytechnique et de sa Faculté d'Ingénieurs de Hunedoara serve, également, de support à des travaux pratiques.

Comme pour les organismes de formation et d'enseignement, *Le FOREM*, par les sollicitations exprimées auprès des entreprises pour évaluation et validation du produit développé, intègre à ses activités habituelles celles relevant du projet. On envisage ainsi, en fin de programme, un travail d'expérimentation et d'exploitation des résultats qui associerait, sur des bassins d'emplois identifiés par *Le FOREM*, salariés comme demandeurs d'emploi pour une utilisation de l'outil en vue de se former au soudage suivant des niveaux de besoins différenciés. Le suivi de telles activités nécessitera un travail de programmation et de suivi intégrés aux activités habituelles.

8. FINANCEMENT EUROPÉEN. PERSONNEL IMPLIQUÉ. RÉSULTATS

Les organismes participants ont choisi le type de partenariat qui correspond le mieux au plan de travail pour toute la durée de 2 ans, «LEO- 24 M» (nombre min. de 24 mobilités sortantes/partenaire, effectués durant la période contractuelle). Le montant des subventions obtenues variable d'un pays à l'autre, est le maximal : 25.000 Euro pour chaque des partenaires français et roumain, et 20.000 Euro pour le partenaire belge (95 000 Euro/total projet). Le nombre de personnels impliqués dans les activités du partenariat a été établi à 4 pour chacun des organismes participants. La description détaillée des résultats attendus ainsi que les dates afférentes, sont inscrits dans les documents [1], [3], [4], [5].

9. DIFFUSION ET EXPLOITATION DES RÉSULTATS. CONCLUSIONS

Ces activités se réalisent mettant en œuvre le *"Plan de diffusion et exploitation des résultats"*, élaboré au niveau transnational, ainsi qu'au niveau de chaque partenaire. La cohérence des activités de diffusion est facilitée par l'utilisation de la *Plateforme collaborative,* qui assure que l'ensemble des acteurs impliqués bénéficie d'un même niveau d'information sur les avancées et les résultats. Ils mettent à profit ces informations pour en informer leur environnement professionnel, et la mise en lien avec un certain nombre d'entreprises pour l'évaluation et la validation du produit de formation, participe également à la diffusion des résultats par l'intermédiaire des organismes partenaires.

Le projet rapproche formation et lieux de travail, en proposant à des utilisateurs de pays différents un outil évolutif de consultation et d'utilisation de ressources en soudage. A son fin, le projet mettra à la disposition des acteurs de formation en soudage un support plus attractif de contenus de formation, qui contribuera au développement de l'autonomie personnelle et professionnelle des salariés, des étudiants et des personnes en formation soudage en Europe. L'intérêt de la mise en œuvre du projet réside dans la possibilité pour les apprenants d'accéder à un processus d'apprentissage du soudage individualisé, dynamique et adapté. Le développement des compétences par un accroissement de l'attractivité de la formation, envisage une amélioration de la compétitivité de ces praticiens, leur permettant par là même de faire valoir en entreprises, comme sur le marché du travail, leur capacité d'insertion et d'adaptation aux exigences économiques, technologiques et techniques.

A la suite de ce projet, il est envisagé d'exploiter plus largement les résultats obtenus, en établissant un plan de transfert auprès d'autres organismes et établissements traitant de l'apprentissage du soudage, ceci vers des pays européens concernés par le champ traité. Ce transfert pourrait se traduire par la mise en œuvre d'une mesure de transfert d'innovation Leonardo, ayant pour objet la mise en place d'un projet de coopération basé sur la dimension innovante de l'outil élaboré.

REFERENCES/RÉFÉRENCES

[1] Document Candidature. Programme Éducation et Formation Tout au Long de la Vie/EFTLV, Partenariat Leonardo da Vinci 2009, Janvier 2009.
[2] Pachet documente "Reuniune de informare privind implementarea Proiectelor de Parteneriat Leonardo da Vinci", ANPCDEFP, Bucureşti, octombrie 2009.
[3] Synoptique du projet Léonardo - Soudage. Équipe BRIS, Lyon, Décembre 2009.
[4] Projet LdV-Partenariats. Partage des tâches -Équipe BRIS. Lyon, Février 2010.
[5] Proiect LLP-LdV/PAR/2009/RO/003. Plan de implementare la nivel local. Februarie 2010
[6] Cahier des charges - Procédés de soudage. Équipe BRIS. Janvier, 2010.
[7] Pachet Documente Proiect LLP-LdV/PAR/2009/RO/003 pentru "Reuniune coordonatori de proiecte LdV". Timişoara, aprilie 2010.
[8] Proiect LLP-LdV/PAR/2009/RO/003. Raport de progres intermediar şi Anexe. Iunie, 2010.

INTERNATIONAL SYMPOSIUM on
ADVANCED ENGINEERING & APPLIED MANAGEMENT
– 40th ANNIVERSARY in HIGHER EDUCATION (1970-2010)
4 – 5 November, 2010, Hunedoara, ROMANIA

Vasile ALEXA[1], Sorin Aurel RAȚIU[1], Carmen Inge ALIC[1]

DESIGN AND IMPEMENTATION FOR AN INFORMATICS APLICATION TO WORKING-OUT THE MIG-MAG WELDING TECHNOLOGY

[1.] UNIVERSITY POLITEHNICA OF TIMISOARA, FACULTY OF ENGINEERING FROM HUNEDOARA, ROMANIA

ABSTRACT:
This paper work presents the technology development for welding in MIG-MAG shielding gas environment and a new calculation methodology for major welding parameters using an informatics application.

KEYWORDS:
welding, Mig-Mag, informatics, software

1. INTRODUCTION

The information system is a coherently structured assembly, made of electronic computing and communication equipments, software, processes, automated and manual procedures, used as automatic data processing tool within a field of activity.

The designing and developing of computer systems is appropriate in new IT systems, or for developing, upgrading or maintaining the existing ones.

In case of designing, the information system development team must carry out the following successive modelling processes [5], [6]:

- information modelling that provides the critical description of the existing system and defines the functional requirements measured by the objectives to be met by the new information system;
- conceptual modelling that describes the structure and functional solution of the new system to meet in the best possible conditions the required objectives, independent of computer, operating system or data management system;
- technical or detailed modelling that implies the transformation of the functional solution into an operational solution on a particular type of computer and data management system.

In database applications, the tables are updated by means of specialized models, called forms, which provide:

- end-user *friendly interface*, achieved through various controls (buttons, text boxes, etc.) or other embedded graphics;
- *simultaneous updating* of multiple tables through subforms;
- *validation rules in addition* to those defined in the tables.

2. THE MIG-MAG WELDING PROCEDURE

Welding in protective environment is the generic term for all the welding processes in which the weld pool and the metal transferred into it are protected, by a shielding gas, against the action of the atmosphere. The arc between the electrode and work piece burns visible.

The processes of welding in shielding gas environment can be classified according to the type of electrode, shielding gas and the electric arc protection used.

A first classification can be done by electrode type[1], [2]. Thus, the processes can be divided into non-fusible electrode processes and fusible electrode processes.

The non-fusible electrode – or „permanent" – is made of tungsten, and that's why this procedure is called *gas-shielded arc welding with a non-fusible electrode*.

In case of fuse welding electrode, this is simultaneously one of the electric arc poles, and filler. It has the same chemical composition or very close to that of base material. This procedure is called *gas-shielded arc welding with a fusible electrode*.

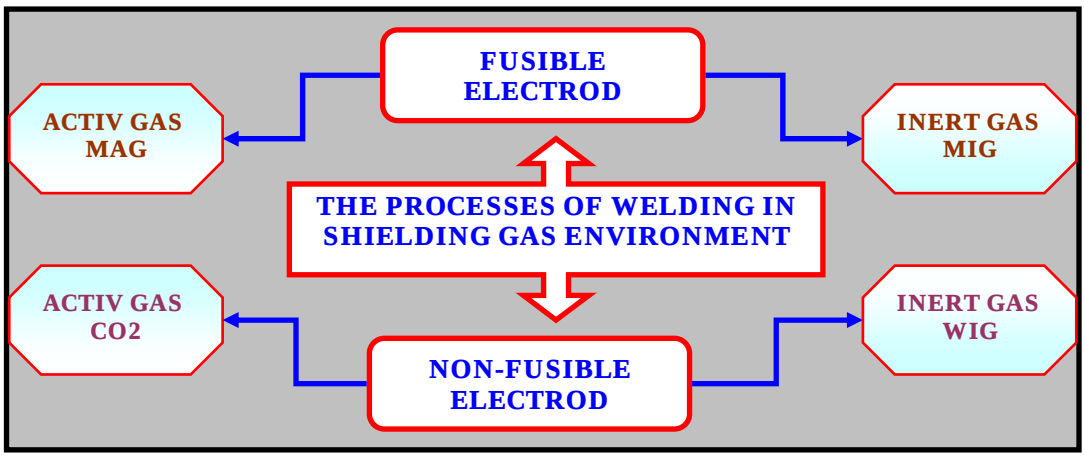

Fig. 1. The processes of welding in shielding gas environment

These two categories can be differentiated by the shielding gas they use [1].

In the process of welding in shielding gas environment with non-fusible electrode, there are used inert or noble gases. The term "inert" comes from Greek and means “indifferent” or „slow in reaction”. Among the noble gases available, for welding in inert gas environment with fusible electrode (WIG) there are mainly used argon or helium, or mixtures thereof.

In the process of welding in shielding gas environment with fusible electrode, there are used either inert or active gases. Therefore, we make the distinction between *welding in an inert gas environment with fusible electrode* (MIG) and *welding in an active gas environment with fusible electrode* (MAG).

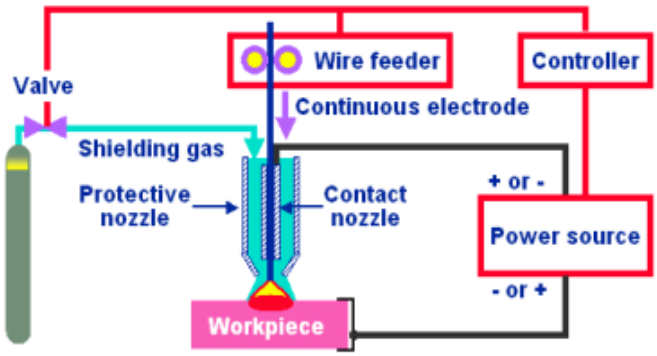

Fig. 2. MIG / MAG welding process

Another distinction is made depending on the type of shielding gas used, i.e. between the MAGM welding, where there are used mixtures of argon-based gasses with addition of active components, as CO2 and O2 (also known as *GMMA* = “*gas-mixture metal arc*” welding), and the MAGC welding, where it is used technical carbon dioxide, CO_2, (also known as *GMA-CO2*).

3. TECHNOLOGY DEVELOPMENT FOR WELDING IN MIG/MAG SHIELDING GAS ENVIRONMENT

Classically, this technology involves the following stages [4], figure 3:

- presentation of backlash shape and establishing the actual sizes;
- choice of welding materials;
- calculation of parameters and welding technology;
- tabulation.

The first stage, *presentation of backlash shape and establishing the actual sizes, figure 5*, will be based on the following features [3]:

- reduced diameter of the electrode wire;
- lack of coating material;
- high current densities.

Fig. 3. User interface

Fig. 4. MIG / MAG welding technologies

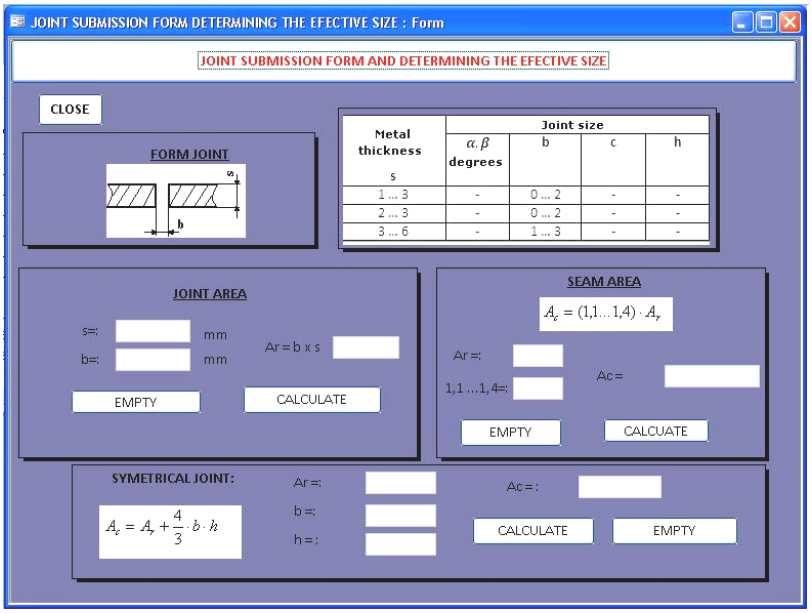

Fig. 5. Joint submission form and determining the effective size

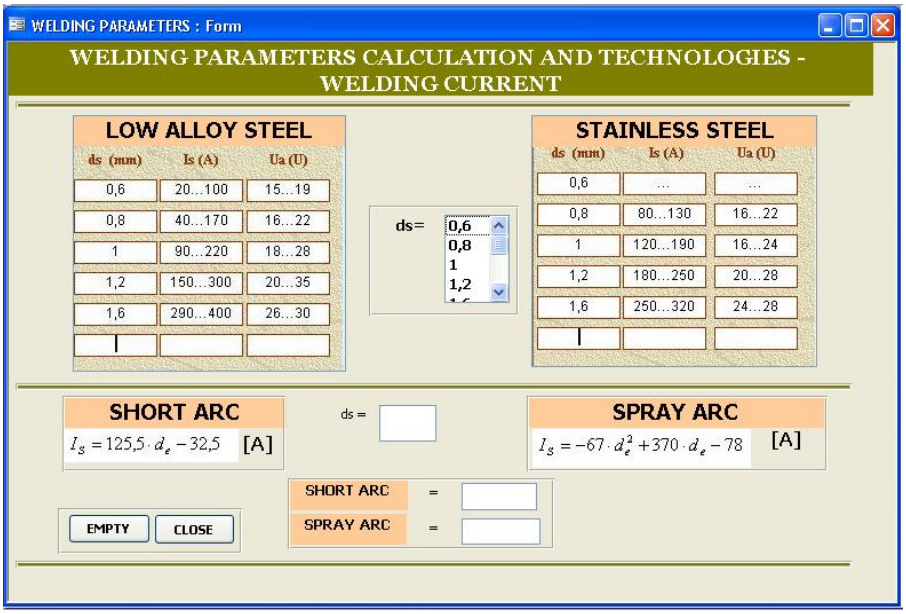

Fig. 6. Strength of the welding current

The inadequately chosen of backlash sizes and the mismatch of technological welding parameters can lead to malfunctions, as follows:

- puncture and drainage of molten metal material at the root;
- electrode wire passing among components without arc ignition, or its discontinuation;
- lack of penetration at the root;
- root unmelting.

The second stage, *choice of welding materials*, includes:

- choosing the wire brand and shielding gas;
- establishing the electrode wire diameter;
- determining the number of passes;
- arrangement of passes.

The third stage, *calculation of parameters and welding technology*, aims to establish, figure 6:

- the welding variance;
- free length of electrode wire;
- current amperage;
- spring tension

The first form of application is called *Interface* and allows the launching of the other options of the application, figure 3.

The program requires data entry in the afferent fields. Then, by pressing the button „CALCULATE", the requested result is automatically displayed.

4. CONCLUSIONS

This type of information system enables the development of welding technology automatically, saving time, because the engineer disposes of a comprehensive database, from where he extracts the values of the imposed welding parameters.

So, the values of the other parameters are going to be calculated based on the extracted values, through an intuitive and friendly interface.

REFERENCES

[1.] M. Burcă, S. Negoiteasa – Sudarea MIG/MAG, Editura SUDURA Timişoara, ediţia a 2- a, 2004.
[2.] G., Aichele, 116 Reguli de sudare în mediu de gaz protector, Editura Sudura, Timişoara, 1999.
[3.] N. I., Trif, Automatizarea proceselor de sudare, Tom V, Vol. 2, Enciclopedie de Sudură, Editura Lux Libris, Braşov, 1996.
[4.] *** Colecţia de standarde comentate, Editura Sudura, Timişoara, 2000-2005.
[5.] P., Norton, ş.a , Microsoft Office 2000 Editura Teora, Bucureşti, 2003.
[6.] J., Habracken, Microsoft Access 2002 pentru începători Editura Teora, Bucureşti, 2003.

INTERNATIONAL SYMPOSIUM on
ADVANCED ENGINEERING & APPLIED MANAGEMENT
– 40th ANNIVERSARY in HIGHER EDUCATION (1970-2010)
4 – 5 November, 2010, Hunedoara, ROMANIA

[1.]Georgeta Emilia MOCUŢA, [2.]Mihaela POPESCU, [3.]Ioan Dănuţ DAN

THE BEST WAY OF WORKING SPACE ROBOT WHICH EQUIPS A FLEXIBLE MANUFACTURING CELL COMPONENT OF WELDED IN RAIL FIELD

[1-2.]POLITEHNICA UNIVERSITY OF TIMISOARA, ROMANIA
[3.] SOCIETATEA NAŢIONALĂ TRANSPORT FEROVIAR MARFĂ, "CFR MARFA"-SA SUCURSALA TIMISOARA, ROMANIA

ABSTRACT:
The industrial robot acts on its operating space under different shapes, namely by manipulating parts, by executing processing technological operations, by measuring specific parameters of products or even of the operating space etc.
Many applications and functions performed by a robot reveal an essential characteristic, namely their versatility.
Studying the movement of a robot consists of a single well-defined problem but a collection of several problems that are more or less than one other option. Exemplification was performed using MSC NASTRAN program.
KEYWORDS:
industrial robot, operating space, movement of a robot, exemplification

1. INTRODUCTION

The industrial robot acts on its operating space under different shapes, namely by manipulating parts, by executing processing technological operations, by measuring specific parameters of products or even of the operating space etc.

Many applications and functions performed by a robot reveal an essential characteristic, namely their versatility.

Versatility defined as the robot's physical ability to perform various functions and to take various actions in a given technological application is closely related to the structure and mechanical ability of the robot, which in turn determines the configuration of the robot workspace.

Since the workspace of a robot has geometry depending on components and structure of its mechanisms, in this space the characteristic point of the robot must execute motions on trajectories imposed by obstacles to avoid collision. In a first analysis of a robot working space should not be dealt with "obstacles" and can be utilized. "Obstacles" are operating in the area of warehouses or other exhaust retrofit devices of flexible robotic cell in which all components must interact.

Trajectory through "obstacles" can be chosen so that we can avoid collisions with maximum probability.

2. THE STUDY

Studying the movement of a robot consists of a single well-defined problem but a collection of several problems that are more or less than one other option.

The robot is becoming a more autonomous mechanical system that increases the need for automatic trajectory planning in its development.

The simplest planning problem assumes that the robot is only moving object in space which does not possess dynamic properties thus avoiding temporal problems.

It also considers that the robot does not come into contact with surrounding objects, thus avoiding problems of mechanical interaction.

These considerations turn the physical planning problem into a purely geometric problem.

Furthermore it is considered that the robot is only moving rigid solid which is limited only by the obstacles.

With these simplifications the basic problem of planning robot trajectories can be formulated as follows:

- let's consider A a single solid or rigid (robot) that moves in a Euclidean space W, called workspace, represented by Rn, n = 2 or 3; it's movement is not limited by any restriction on kinematics.
- let's consider B1,...,Bq fixed rigid objects (obstacles) distributed in well defined positions in working space W;
- knowing the position and orientation, at baseline, the robot, and final finishing position and orientation of this workspace W, generate a path specifying a continuous sequence of positions and orientations of A starting from the initial configuration (position and orientation), avoiding the contact with obstacles Bj and finishing in the final configuration (position and orientation) final;
- if such a path does not exist, "error" must be reported.

It is obvious that although the basic planning problem is super simplified it is still a difficult problem with many solutions and direct extensions to more complicated issues.

Objectively mobile object (the robot the characteristic point) in such a matter is referred to in the literature as "flying objects".

The basic problem involves the robot path planning through exactly the trajectory generated by the planner. It is also assumed that both the geometry and robotics as well as obstacles positions are known with precision. In reality no planning problem meets these assumptions. Moreover, they control their robots and geometric patterns are not precise. Since the robot has no a priori information about the desktop, it must be based on runtime its sensory system for recording information necessary to achieve the task. It must work in exploring space and solve the problem of planning in the presence of uncertainties.

The problem is to calculate the trajectory generation based on data received from the motion planner sizes order to ensure passage of the robot through the established points.

Generation of movement can be made directly in the space coordinates kinematics couplings, or operational area.

Navigation strategy refers to determining how (methods) to move the robot according to the type of task performed.

Modelling space implies establishing navigation maps in the considered space.

Modelling methods known in literature are [1-5]:

- uniform grid method;
- tree method;
- heterogeneous grid method;
- convex polygon method;
- method of crossing points.

Evolution of the robot in the workspace imposes the statement that the space of configurations SC is intrinsically independent of the choice of reference systems SA and SW.

Trajectory planning problem in the presence of obstacles can be expressed as: given a workspace populated with obstacles known through their borders, and by moving objects, must determine a path without collisions with obstacles in bringing mobile objects in the final initial configuration.

The problem can be approached in two ways global or local, hence the two types of planning methods: global and local.

Application of global methods require complete knowledge of the working space "in advance", modelling proper clearance, research and selection of all possible paths of a certain trajectories corresponding to a minimum cost criterion. Such a method guarantees the existence or absence of a solution. Also global planning methods can be easily adapted to the off-line programming.

Applying a local method requires partial knowledge of the workspace.

Such a method does not guarantee reaching the final configuration, but the advantage of good real-time adjustments.

In both cases, solving the planning problem involves solving geometric problems (pure geometry) or combine geometry with kinematics and/or dynamics.

In such situations often are used the results of algorithmic geometry.

In general the application of planning methods must meet certain restrictions such as: the safest way, the shortest path, etc.

3. ANALYSES, DISCUSSIONS, APPROACHES AND INTERPRETATIONS

Analyzing the best methods in place of the theoretical and the application can highlight the road map method, exact cell decomposition method and the potential field method. Of these potential field method treats the robot represented as a point in configuration space, that as a particle under the influence of an artificial potential field U whose local variations reflects ”structure” of the free space.

Potential function is defined as the amount of free space on an attractive potential, which attracts the robot toward the final configuration, and a repulsive potential, which removes the robot from obstacles.

The method was originally developed as an "on line” method to avoid collisions to be applied when there is no model of obstacles, in advance, but they may refer to during the execution of movement. In particular, the procedure can lock in a local minimum of potential function.

This deficiency can be corrected by calculating the finite element method applied to study a potential field.

Starting from the potential field finite element method we propose, as an effective tool for the analysis of optimum road space of the robot.

Thus we suggest that the workspace of a robot to be modelled as a homogenous body which is dependent on structure geometry of components and obstacles.

In this space to work tasks the robot must go through the obstacles imposed trajectories which it has to avoid.

The road through the obstacles can be chosen so that to avoid the maximum probability collisions. If we accept that two neighbouring obstacles behave as two sources of the same physical stationary field and consider that the moving of the characteristic point is carried on the same potential trajectory as that of the resulting field we can select a family of trajectories corresponding to a certain field potential in a given interval.

In the application illustrated in Figure 1 the working space was modelled as a homogeneous body with known thermal characteristics.

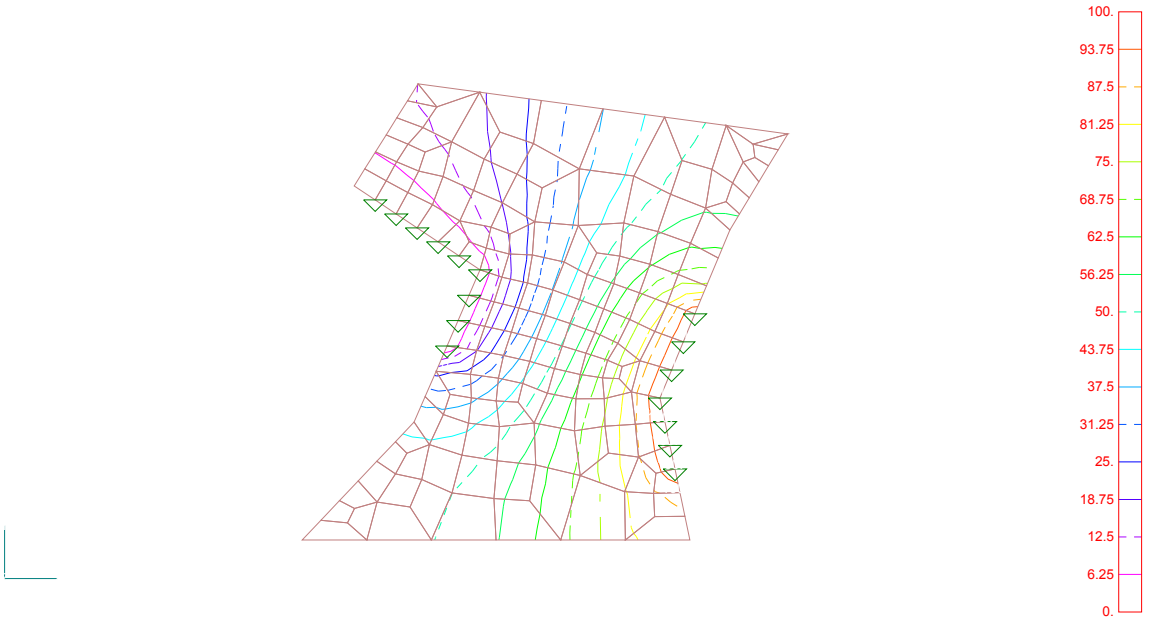

Figure 1 Thermal analysis of a working space modelled as homogeneous body found in a field where the heat source hot / cold data are boundaries of obstacles.

Obstacles are considered as being „hot" or "cold" areas/sources on the boundary of the considered working space as being an homogenous body on which a thermal field is applied from the hot/cold sources (modelled obstacles).

Applying the finite element method analysis facility on the thermal model workspace the outcome is isothermal surfaces. From these areas we can define curves obtained by modelling which can be trajectories of the characteristic point.

Using the family of isothermal surfaces in the average temperature (resulting from thermal finite element analysis) on this can reside optimum trajectories to be passed.

So configurations libraries can be built-up for the working space and trajectories to pass, respectively located on the average temperature isothermal surface.

Illustrated in Figure 1 is a workspace of a robot modelled as homogeneous body found in a field where heat sources hot / cold data are borders of the obstacles that need to avoid in his motion.

Thermal finite element analysis on the isothermal model gives us the results. The treaty was exemplified in the plan but can be generalized in three-dimensional space. Most times one of the 3D motion parameters can be imposed by the kinematics couplings which controls programming. Applications can be treated and depending on who is involved in the process robot. The most complex situation is found in welding rail vehicle structures.

4. CONCLUSIONS

A key issue in the field of industrial robots operation (i.e. programming the optimal path of motion) enjoys the benefits of programs devoted to finite element analysis to allow for applying the ”potential field method” as an analysis of a stationary thermal field.

Exemplification was performed using MSC NASTRAN program.

REFERENCES

1. Gârbea D., Analiză cu elemente finite Editura Tehnică Bucureşti 1990
2. Hubner H. K., "Metoda Elementului Finit Pentru Ingineri" Departamentul de inginerie mecanică, Laboratorul de cercetări Genenral Motors, Wiley-Interscience, John Wiley&Sons, New York, London, Sydney, Toronto, 1990
3. Pires, J. N, Loureiro, A., Bölmsjo, G., Welding Robots - Technology, System Issues and Application, 1st Edition., 2006, XVIII, 180 p. 88 illus., Hardcover, ISBN: 978-1-85233-953-1
4. Staicu, S., Liu, X-J., Wang, J., Inverse dynamics of the HALF parallel manipulator with revolute actuators, Nonlinear Dynamics, Springer, 50, 1-2, pp. 1-12, 2007
5. Staicu,S., Zhang, D., A novel dynamic modelling approach for parallel mechanisms analysis,Robotics and Computer-Integrated Manufacturing, Elsevier, 24, 1, pp. 167-172, 2008

INTERNATIONAL SYMPOSIUM on
ADVANCED ENGINEERING & APPLIED MANAGEMENT
– 40th ANNIVERSARY in HIGHER EDUCATION (1970-2010)
4 – 5 November, 2010, Hunedoara, ROMANIA

[1.] Tamás ENDRŐDY

UNFOLDING THE CONVEX POLYHEDRONS TO A CONNECTED NON-OVERLAPPING POLYGON (PREPARING TOOLS FOR CREATIVE PROOF OF THE DÜRER'S CONJECTURE)

[1.] CAD Expert, Former Scientific Advisor University of Szeged, HUNGARY
and Szent István University, HUNGARY

Abstract:
Albrecht Dürer published his conjecture around 1525: "All the polyhedrons can be unfolded by their suitable cutting edges to a plane so that we can receive a joined polygon-mesh with non-overlapping faces". The author of this article is dealing basically with the suitable positioning of cutting edges for unfolding the convex polyhedrons to a plane, coding the polygon received and its modelling surface.
His aim is to give tools for proving Dürer's conjecture and/or to prepare a creative proof for the essential categories of the convex polyhedrons. The notion of the finite convex polyhedrons has a very large set of solids from tetrahedrons to the arbitrarily complicated polyhedrons —covered by $p \geq 3$ sided convex polygons— which have 1ess and less or nil symmetrics. In the case of the analysed finite convex polyhedrons 2 polygons meet in each edge, in their peak $q \geq 3$ pieces of polygons meet where the angle is alfa $_{pi} < 360°$ in consequence of convexity, otherwise it can be degraded to a plane and can become infinitely big, which was formerly excluded.
The BREP model, an augmented structure of the "Winged edge model" for unfolding the convex polyhedrons and the spherical mosaic/ellipsoid ordered to the polyhedron can help us several times, which can be gained by the projected polyhedron-peaks from an internal point to an external sphere surface which has only mutual points (min.2) with the polyhedron.
The author developed a special complete induction method of the "Winged edge model" for preparing a creative proof of the Dürer's conjecture.
Keywords: Dürer's Conjecture, convex polyhedrons, spherical mosaic/ellipsoid

INTERNATIONAL SYMPOSIUM on
ADVANCED ENGINEERING & APPLIED MANAGEMENT
– 40th ANNIVERSARY in HIGHER EDUCATION (1970-2010)
4 – 5 November, 2010, Hunedoara, ROMANIA

[1.]Vasile George CIOATA, [2.]Imre KISS

SIMULATION OF SOLIDIFICATION PROCESS OF THE PIECES OBTAINED THROUGH DIE FORGING IN SEMI-SOLID STATE

[1.]UNIVERSITY "POLITEHNICA" TIMISOARA, FACULTY ENGINEERING HUNEDOARA,
[2.]UNIVERSITY "POLITEHNICA" TIMISOARA, FACULTY ENGINEERING HUNEDOARA

ABSTRACT:
In paper is presented some considerations regarding the semi-solid processing of alloys and is presented a new variant of the Rheocasting method. Because the simulation of solidification process has become an important tool for semi-solid processing, in paper is developed a simulation model, developed by means of the finite analysis program Ansys 7.6.1, which allows the analysis of the thermal phenomenon. To validate the simulation model, the results is compared with experimental results and is observed slight differences between these, which means that the suggested simulation model can be used with sufficient precision for the analysis of the thermal phenomenon within the process of die-forging in semi-solid state.
KEYWORDS: thixoforming, semi-solid state, solidification, finite element method, heat transfer

1. INTRODUCTION

The basic principle of processing in a semi-solid state consists in obtaining the pieces during the solidification stage of the alloy. Along this time interval, part of the material is still liquid, while other parts are entirely solid. In order to have a thixotropic behavior, the solid phase has to consist in spheroidal (globular) particles, coated in liquid material. This special microstructure can be obtained by rigorous (mechanical, electromagnetic, etc.) mixing during solidification.

The semi-solid state processing knows, generally, two-development route: thixoforming route and rheocasting route.

Thixoforming is the general used term for described of the obtained process of the final parts from the semi-solid state materials, with a help of the metallic dies/forms and the top die. If the part is obtained in a metallic closed form, the method is called thixocasting, and if the part is obtained in a open die, is called thixoforging.

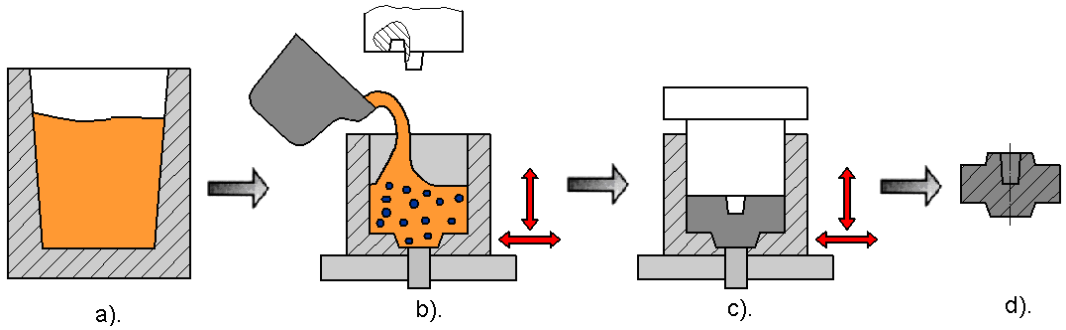

Fig. 1 – Diagram of the new NRC variant [2]
a). alloy elaboration; b). alloy casting into the mould and the obtaining of a structure with thixotropic behavior; c). the formation proper, under vibrations; d). the finished piece

The Rheocasting is other route for development of the processing in the semi-solid state. It is used, still from beginning of the researches like as the technology for obtaining of the material with non-dendrite microstructure for ulterior processing through thixoforming. In 1996, is developed a new rheocasting (NRC) process, which was patented by UBE Industries Ltd. In November 2000, the authors mention this new method in the *Diecasting World* magazine [1].

A variant of the Rheocasting method is presented in [2]. This variant involves the following processing stages: alloy elaboration, feeding the mould with it and mechanically agitating the material by vibration, in order to obtain a structure with a thixotropic behavior (the solid phase has to consist of spheroidal particles coated by the liquid phase) and the formation proper as a result of vibrations. Figure 1 shows a diagram of this variant and points out to the main stages of processing. The red arrows symbolize the mechanical agitation of the metal and mold, by vibration.

2. SIMULATION OF SOLIDIFICATION PROCESS BY FINITE ELEMENT METHOD

2.1. Preliminary

The solidification process is complex in nature and the simulation of such process is required in industry before it is actually undertaken. Finite element method is used to simulate the heat transfer process accompanying the solidification process.

We further introduce a simulation model, developed by means of the finite analysis program Ansys V.6.1, which allows the analysis of the process behavior under the conditions of a variation of the feeding temperature of the mould and of the mould preheating temperature.

By means of this method we managed to determine the temperature field inside the processed alloy, as well as inside the punch mould, during the forging process in a semi-solid state, at certain points. The alloy is poured into the mold in a liquid state, with temperature higher than melting temperature; it solidifies in the range of solidification, followed by cooling.

In order to further validate the simulation model, the points under consideration, used for measuring the temperature, correspond to the position of the thermocouples mounted on the experimental installation, as given in detail in [2]. Their positions are given in figure 2; to be mentioned that they are related to the origin (0,0) of the XOY coordinate system.

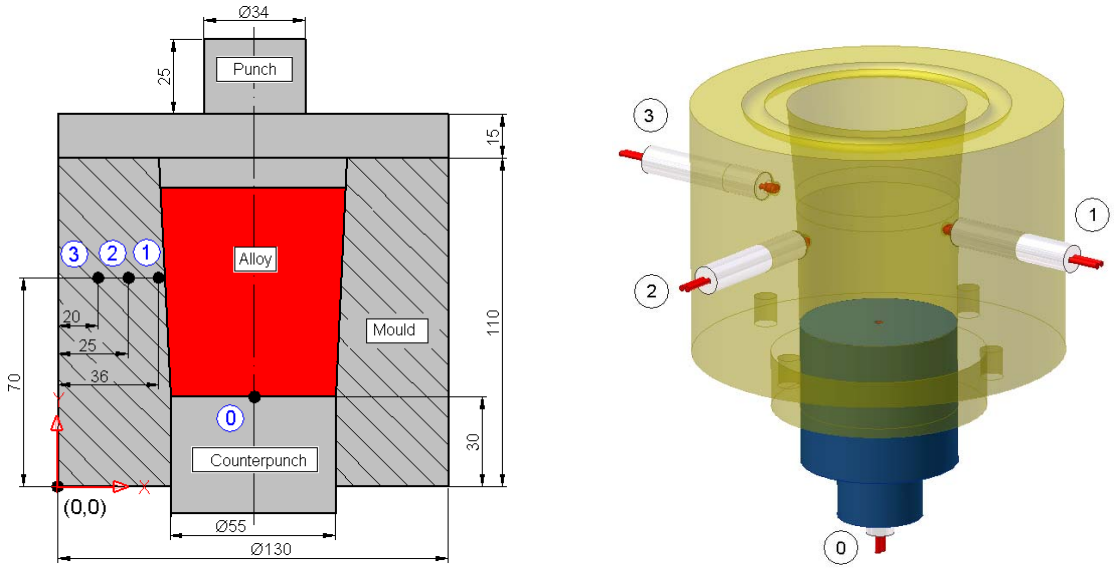

Fig. 2 – Location of thermocouples

After that, it traces the curves T=f(t) (temperature vs. time) for points 0, 1, 2 and 3 for comparison with experimental results.

2.2. Model development

The problem can be modeled in the two-dimensional space, considering the cross section containing the symmetry axis, through the ensemble mould-alloy-punch-counter-punch. Considering the dimensions given in figures 2 and 3, the geometrical model needed by the analysis is obtained by means of the intrinsic modeler of the software, the modeling stages being shown in figure 4.

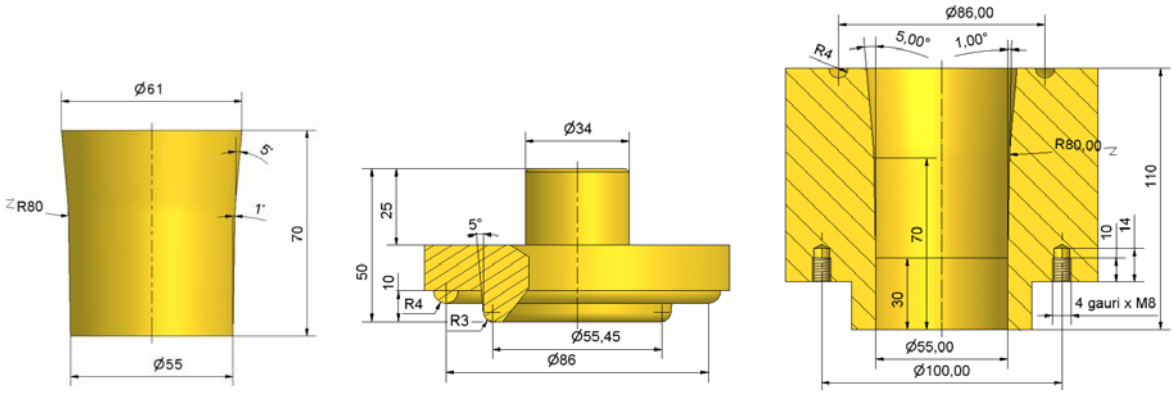

part punch mould

Fig. 3 - Geometrical models and dimensions of the model components

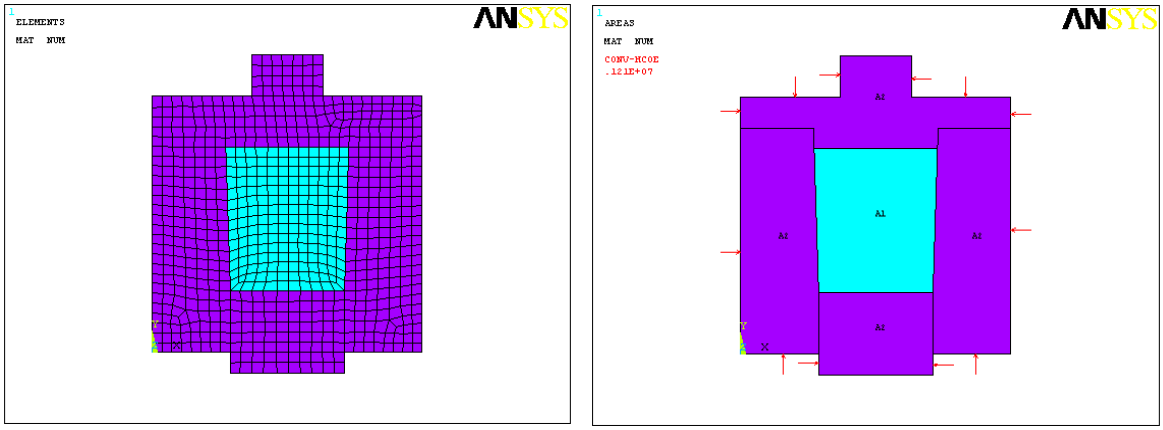

Fig. 4 – Stages of obtaining the geometrical model

For the given analysis, we chose as element of the discretization network, the element type PLANE 55, which is specific to the stationary or transitory thermal analysis, in a two-dimensional plane. At the moment of generating the finite element network we also assigned the corresponding material characteristics.

The materials and their properties are given in table 1 and in figures 5 and 6.

Table 1 – The materials properties

	Material	Density, kg/m^3	Specific heat, J/kg·C	Thermal conductivity, W/mC	Enthalpy, kJ/g
Alloy	AlSi7Mg0,38	2230	1300	As in fig. 5	As in fig.6
Mould, punch and counterpunch	Steel	8000	500	As in fig. 5	-

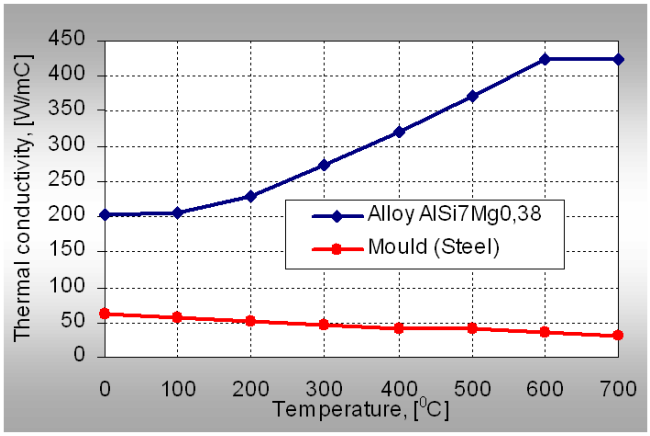

Fig. 5 – Thermal conductivity of the materials

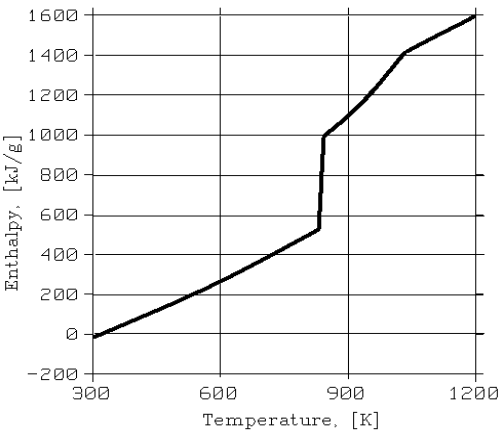

Fig. 6 – The dependency enthalpy – temperature for the alloy AlSi7Mg0,38

The heat transfer between the mould and the environment is done by free convection. This is materialized by the application of certain contour conditions along the lines that make the outer contour of the geometrical model (fig. 4). The parameters of the condition are: the convection coefficient is 12,30 W/m^2·C and the room temperature is: 25^{0}C.

The alloy is cast into the mould in a liquid state, at a higher temperature than the melting one, and it solidifies during the solidification interval, after which it cools down.

The temperature of the alloy and of the mould/punch is time-dependent, so the analysis will be a transitory (non-stationary) one. The chosen analysis time was 300 seconds and the step, 1 second. The initial analysis conditions are:

- The nodes corresponding to the alloy at the initial moment have all the temperature of 630 ^{0}C;
- The nodes corresponding to the mould, punch and counterpunch, at the initial moment, have all the temperature of 100 ^{0}C.

2.3. Results

After the analysis proper (processing) has been done, in the post-process stage one can visualize the temperature fields inside the alloy and mould, at various moments, as shown in figures 7...10.

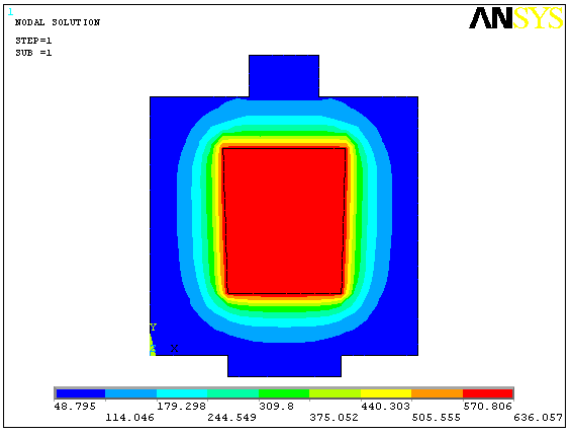

Fig. 7 – The temperature field at moment t=1s

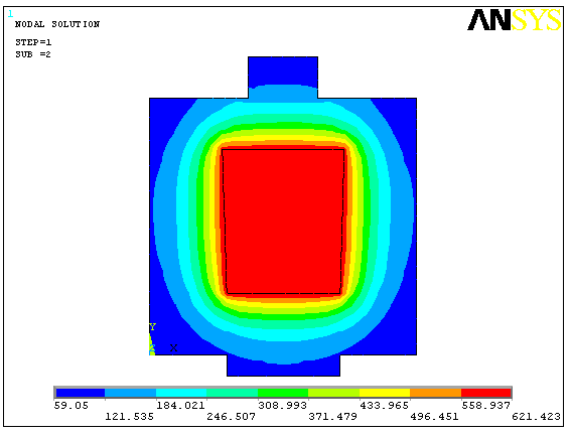

Fig. 8 – The temperature field at moment t=2s

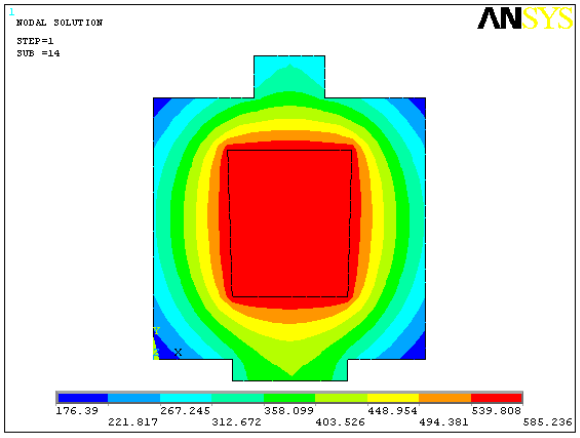

Fig. 9 – The temperature field at moment t=14s

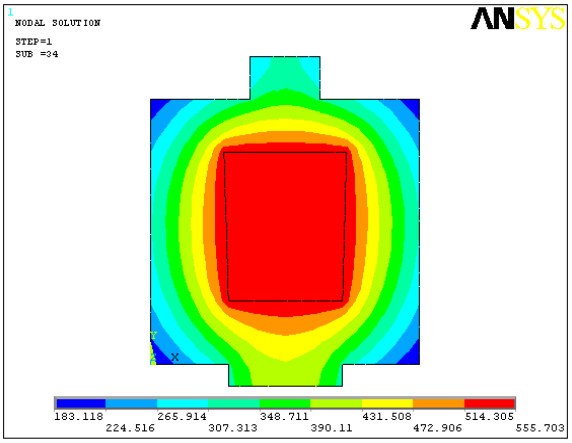

Fig. 10 – The temperature field at moment t=34s

At the same time, one can visualize the evolution of the solidification front inside the piece, at various moments. Thus, in figure 10 we give the evolution of temperature inside the piece and mould, from the casting of the alloy, up to the moment of complete solidification of the piece.

In order to determine the temperatures at the points of interest, at specific times, we identified the node corresponding to the location points of the thermocouples and we defined the variables marked as 0, 1, 2 and 3.

We plotted the curves T=T(t) (temperature depending on time) for points 0, 1, 2 and 3 in order to obtain a comparison with the experimental results.

Temperature variation at the points of interest is given in figure 12. The shape of the curves resembles a lot that of the curves obtained during the experiments.

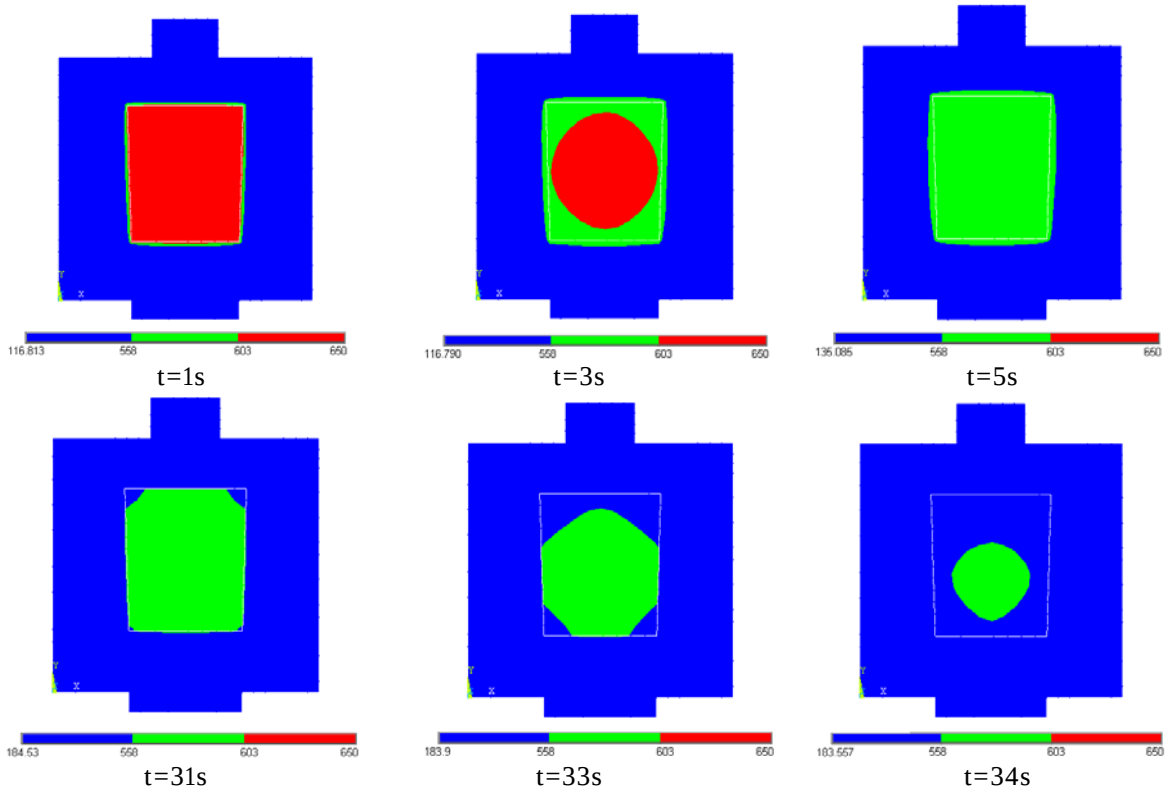

Fig. 11 – The evolution of the solidification front inside the piece

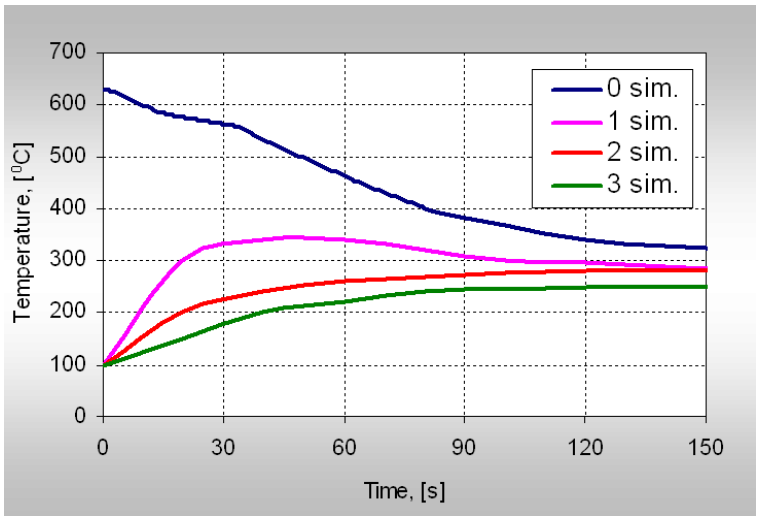

Fig. 12 – The piece cooling curve (0 sim.) and the mould heating curves (1 sim., 2 sim., 3 sim.), obtained by simulation under conditions: T_T=630^{0}C, T_{OM}=100 ^{0}C

The moulding times under various processing situations can be obtained by detailing the cooling curves T=T(t) obtained during the temperature interval T_T-T_S.

3. VALIDATION OF THE SIMULATION MODEL

In order to compare the experimental data with those resulted from simulation, we created the graphical representation given in figure 13, where we showed, in the same diagram, the dependencies T=T(t) – corresponding to points 0, 1, 2 and 3 – obtained experimentally and, respectively, by simulation.

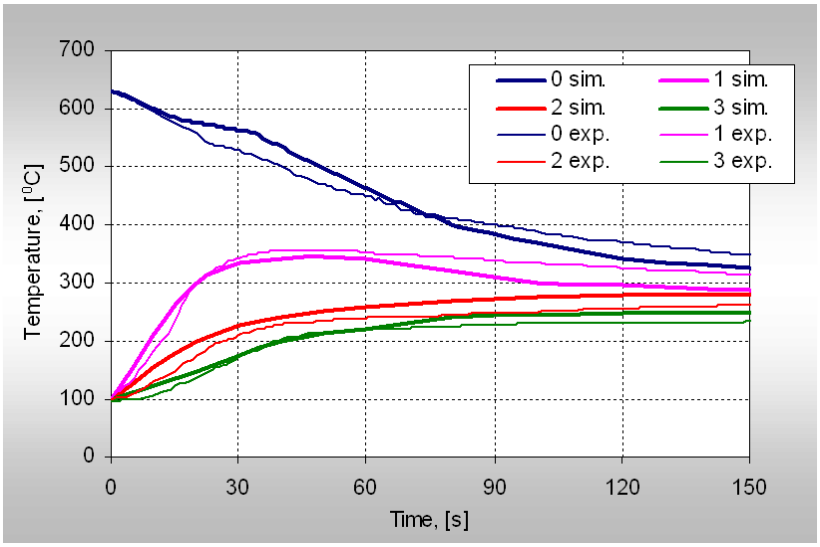

Fig. 13 – Comparison between the experimental results and the ones obtained by simulation, under conditions T_T=630^{0}C, T_{OM}=100^{0}C

One can notice really slight differences between the results to be compared, which means that the suggested simulation model can be used with sufficient precision for the analysis of the thermal phenomenon within the process of forging in a semi-solid state.

REFERENCES

[1.] KAUFMANN, H., et all, New Rheocasting: a novel approach to semi-solid casting, Diecasting World, November 2000, 14 -17
[2.] CIOATA, V. G., Studii si cercetari privind matritarea metalelor si aliajelor in stare semilichida (Studies and researchs on die forging of the metals and alloys in the semi-solid state), Doctorate Thesis, Timişoara "Politehnica" University, 2004, p. 6-7, 83-84, 123-132
[3.] KIRKWOOD, D. H., et.all, Semi-solid Processing of Alloys, Springer, 2010
[4.] HIRT, G., KOPP, R., Thixoforming. Semi-solid Metal Processing, Wiley VCH, 2009

INTERNATIONAL SYMPOSIUM on
ADVANCED ENGINEERING & APPLIED MANAGEMENT
– 40th ANNIVERSARY in HIGHER EDUCATION (1970-2010)
4 – 5 November, 2010, Hunedoara, ROMANIA

[1.]Vasile George CIOATA, [2.]Imre KISS

DETERMINING THE CONTACT FORCES BETWEEN THE WORKPIECE AND FIXTURE USING THE FINITE ELEMENT METHOD

[1.]UNIVERSITY "POLITEHNICA" TIMISOARA, FACULTY ENGINEERING HUNEDOARA,
[2.]UNIVERSITY "POLITEHNICA" TIMISOARA, FACULTY ENGINEERING HUNEDOARA

ABSTRACT: During clamping operations and machining, the forces which act on the workpiece (weight, inertial forces and moments, cutting forces and moments, clamping forces) cause the contact forces between the locators and the workpiece. Because of these contact forces, elastic deformations appear in the contact area between the locators and the workpiece, deformations which are a source of machining errors. If the values of the contact forces is big, these can cause plastic deformations which leads to the destruction of the workpiece in the contact area. Also, the very small values of the contact forces can cause the slipping of the workpiece on the locators or even the loss of the contact between the workpiece and the locators compromising the orientation scheme. Therefore, the evaluation of the contact forces between the workpiece and the locators is an important stage in the design process of the binding devices. In this paper work there is presented an example of using the finite element method in order to determine the contact forces for a real situation of processing.
KEYWORDS: fixture, workpiece, contact force, locators, clamping elements, finite element method

1. INTRODUCTION

In order to execute the different processing operations, the workpiece must be installed in the fixture or directly on the tool-machine in a certain position in comparison with the cutting tool. The installation of a workpiece has two functional phases: the orientation and the clamping. These two phases can be executed successively with orientation elements and clamping elements, or simultaneously, with an auto centered device.

The orientation of a workpiece is the operation which establishes a strictly determined position of the workpiece in comparison with the edges and the trajectory of the cutting tool. An object in the three-dimensional space disposes of six degrees of freedom: three translations through the length of the axes and three rotations around the axes of an orthogonal system of axes. In order to ensure a unique position for the workpiece in comparison with a XYZ axes system, all the six degrees of freedom must be bound. The orientation notion has to be related to the technological system adjusted to the dimension and to the serial production.

During the workpiece's processing action, the workpiece's position has to be maintained, that means that the orientation scheme must be preserved, which corresponds to the clamping phase. Clamping means applying on the workpiece which is oriented on the locators, a clamping forces system built to make the orientation scheme and preserve it during the processing. This forces system must achieve the contact between workpieces and locators and maintain it during the processing, assuring at the same times a maximum rigidity for the workpiece-device system, which has to remove or diminish the vibrations.

In order to determine the clamping force, the most detrimental situations must be considered, even though these situations are unlikely to occur. For example, for a milling device we must consider the next possible situations: milling towards or against the advance, milling with a cylindrical mill or a cylindrical-frontal mill, milling towards the device's locators or in the opposite way, technological indiscipline. Clamping forces are calculated using the workpiece equilibrium under the influence of the forces which act on it (weight, inertial forces and moments, cutting forces and moments) or using the rigidity of the locators and clamping elements of the workpiece.

2. THE CALCULATION OF THE CONTACT FORCES

During clamping operations and machining, the forces which act on the workpiece (weight, inertial forces and moments, cutting forces and moments, clamping forces) cause the contact forces between the locators and the workpiece. Because of these contact forces, elastic deformations appear in the contact area between the locators and the workpiece, deformations which are a source of machining errors. If the values of the contact forces is big, these can cause plastic deformations which leads to the destruction of the workpiece in the contact area.

Also, the very small values of the contact forces can cause the slipping of the workpiece on the locators or even the loss of the contact between the workpiece and the locators compromising the orientation scheme.

Therefore, the evaluation of the contact forces between the workpiece and the locators is an important stage in the design process of the binding devices.

For the fixture design practice, the evaluation of the contact forces between the elements of the workpiece-fixture system is very important because their size is not constant during the processing of the workpiece, depending on the cutting forces and moments, which have a variable feature and a position and direction which vary during the processing.

To the design of the devices for processing of the workpieces, the extreme values of the contact forces are important. The maximum and minimum values of the contact forces are determined according to the next reasons [1, 2]:

- The maximum contact force, $f_{c\,max:}$ the maximum value of the contact pressure (Hertz pressure, p_{max}) is

$$p_{\max} = 3\tau_{\max},$$

where $\tau_{\max}$ is the maximum shear stress. And the indentation will appear when:

$$\tau_{\max} = \frac{\sigma_y}{2},$$

where σ_y is the yield stress of the workpiece material.

Therefore

$$p_{\max} = 1{,}5\sigma_y.$$

The maximum contact force for locators with a plane contact surface is

$$f_{c\max} = p_{\max} \cdot \pi a^2 = 1{,}5\sigma_y \cdot \pi a^2,$$

where *a* is the radius of the contact area.

- The minimum contact force, $f_{c\ min}$. The contact forces must be bigger than this value, to prevent the workpiece from slipping on the locators or lose contact with it. To prevent the loss of the contact between the workpiece and the locators the contact force must be bigger than zero. To prevent the slipping of the workpiece, this condition is required:

$$\sqrt{q_x^2 + q_y^3} \le \mu \cdot f_{c\min},$$

from where the minimum value of the contact force comes out:

$$f_{c\min} \ge \frac{\sqrt{q_x^2 + q_y^3}}{\mu}$$

where q_x and q_y are components on the x and y directions of the tangential forces which act in the contact area and μ is the static friction coefficient between the workpiece and the locators.

3. EVALUATION OF THE CONTACT FORCES WITH THE FINITE ELEMENT METHOD

A quick calculus of the contact forces which appear between the locators and the workpiece to be processed can be made using the finite element method.

Forwards it is presented an example of application of this method for a practical situation of machining.

Considered the machining of a prismatic workpiece into a device formed by 6 locators emplaced in three reciprocal perpendicular planes-which allow locking the workpiece's 6 DOFs- and two clamping systems C1 and C2 (Fig. 2). It is necessary milling a feature to 25±0.002 mm and 12±0.002 mm dimensions, measured from the AC edge. The workpiece is made of aluminum, with the sizes: 220x122x112 mm, with the density 2700 kg/m^3, Young's modulus E_P=70 GPa and Poisson's ratio υ_P=0.334. The locators and the clamping elements have plane surfaces, the diameter is 18 mm and are made of hardened steel with E=207 GPa and υ_P=0.292. Clamping forces of 640 N and 690 N

are applied simultaneously by clamp C1 and clamp C2. The static friction coefficient is assumed to be 0.25 between the workpiece and fixture elements.

The cutting force's constituents and torque used in milling the considered feature are estimated to be Fx=131 N, Fy=232 N, Fz=55 N and M=2.77 N·m as in Fig. 1.

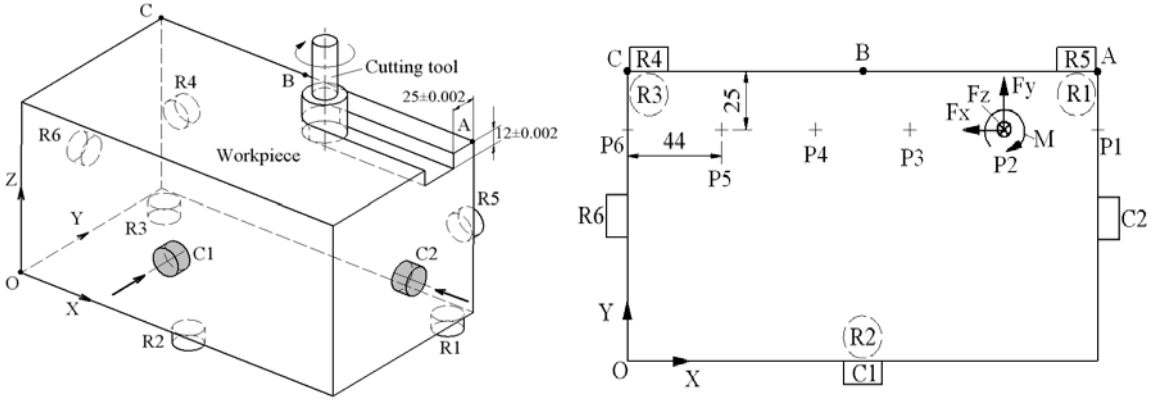

Fig. 1. Scheme of workpiece-fixture system [3]

The coordinates of the locators, of the clamping elements and the application points of the cutting force and moment, related to the OXYZ system are presented in table 1.

Table 1

Coordinates	Locators						Clamps		Points					
	R1	R2	R3	R4	R5	R6	C1	C2	P1	P2	P3	P4	P5	P6
X [mm]	210	110	10	10	210	0	110	220	220	176	132	88	44	0
Y [mm]	112	10	112	122	122	61	0	61	97	97	97	97	97	97
Z [mm]	0	0	0	56	56	56	56	56	0	0	0	0	0	0

4. MODEL DEVELOPMENT

The solid model of the system chosen to be analyzed was realized in Autodesk Inventor Professional and then transferred in Ansys Version 11.0 for the FEA analysis. All the elements of the system have been modeled as isotropic elastic bodies. The locators and the fixture tips have cylindrical shape, the contact surface is plane and has circular shape with the aria assumed to be 254 mm². The 10-node tetrahedral element Solid92 was used to mesh all solid bodies. Contact between the workpiece and fixture was simulated using the quadratic surface-to-surface contact elements Targe170 and Conta174. A constant static coefficient of friction was used to establish contact properties at the interfaces. To simulate the locators being rigidly fixed in place, the surface of each locator tip opposite to the contact was restrained in all three translational degrees of freedom. In order to simulate the clamping force, there have been applied single forces over the surface of both fixture elements, in opposite contact.

In order to determine the contact forces which appear during the processing, the cutting force and moment were applied in 6 equidistant points (P1,..., P6) on the top surface of the workpiece, at a distance of 25 mm from the AC edge.

5. RESULTS

The contact forces between locators and workpiece were determined for each loading situation. Contact forces between the workpiece and the locators were also determined after applying the clamping forces, before the processing, their values are presented in table 2.

Table 2

	Locators					
	R1	R2	R3	R4	R5	R6
Contact forces [N]	11,88	33,1	19,81	217,16	178,69	411,25

The diagrams in fig 2, which present the variation of the contact forces between the locators and the workpiece during the processing, were drawn. The contact forces which appear during the processing are not constant; these have values which depend on the cutting tool position. The extreme values of the contact forces were represented with a discontinued line; these define the recommended area where the contact forces must be situated.

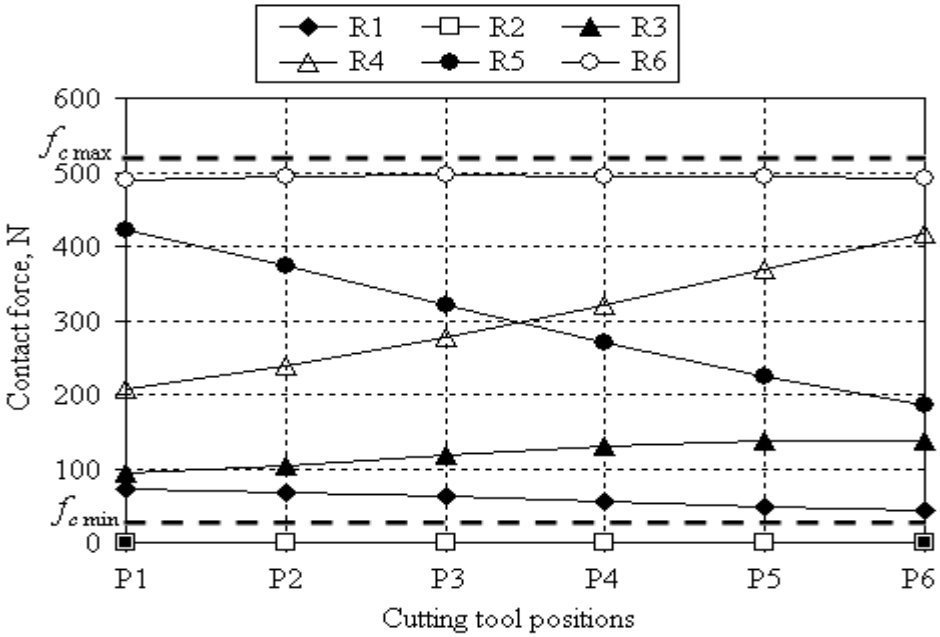

Fig. 2. Contact forces

A value of the contact force which is outside the defined area causes either the instability of the workpiece on the locators, like the case of the contact force between locator R1 and the workpiece, or the destruction of the workpiece in the contact area because of the plastic deformations.

REFERENCES

[1.] JONHSON, K. L., Contact mechanics, Cambridge University Press, Cambridge, 1987

[2.] SANCHEZ, H. T., ESTREMS, M., FAURA, F., Fixturing analysis methods for calculating the contact load distribution and the valid clamping regions in machining processes, Int J Adv Manuf Technol, (2006) 29: 426–435

[3.] CIOATĂ, V. G., Determining the machining error due to workpiece - fixture system deformation using the finite element method, Annals of DAAAM for 2008 & Proceeding of The 19th International DAAAM Symposium "Intelligent Manufacturing & Automation: Focus on Next Generation of Intelligent Systems and Solutions", Published by DAAAM International, Vienna, 2008, 127-128.

[4.] RONG, Y., ZHU, Y., Computer-aided fixture design. Dekker, New York, NY, 1999

[5.] KOŠŤÁL, P., VELÍŠEK, K., ZVOLENSKÝ, R., Intelligent Clamping Fixture in General, In: Lecture Notes in Computer Science. - ISSN 0302-9743. - Vol. 5315 : Intelligent Robotics and Applications. First International Conference, ICIRA 2008, Wuhan, China, October 15-17, 2008.▽ Part II (2008). - ISBN 978-3-540-88516-0, p. 459-465

INTERNATIONAL SYMPOSIUM on
ADVANCED ENGINEERING & APPLIED MANAGEMENT
– 40th ANNIVERSARY in HIGHER EDUCATION (1970-2010)
4 – 5 November, 2010, Hunedoara, ROMANIA

[1.]L. MIHON, [2.]A. NEGOITESCU, [3.]A. TOKAR, [4.]D. OSTOIA

MOTOR AND VEHICLE OPTIMIZATION PROCESS MODELING BY USING THE AVL CRUISE IN STANDARD APPLICATIONS

[1-4.] „POLITEHNICA" UNIVERSITY OF TIMISOARA, ROMANIA

ABSTRACT:
AVL CRUISE is used to perform simulation and analysis of the vehicle propulsion system. It is designed to develop and optimize low-emission engines, power trains and sophisticated engine control systems, cooling systems and transmissions. CRUISE allows modeling the entire optimization process for motor and vehicle in standard applications, such as fuel consumption reduction, acceleration tests, full load tests, traction diagrams and calculation of thermal, mechanical, electrical and control system parameters. In the paper are presented results obtained for a regular simulation of road vehicle behaviour in working conditions.
KEYWORDS: Simulations, vehicle propulsion system

1. INTRODUCTION

CRUISE allows the simulation of vehicle driving performance, fuel consumption and emissions. This concept can be used for modeling all vehicle configurations with scalable fidelity. This approach allows the reuse of models or sub-systems in different optimization phases of a process in order to improve vehicle performances.

The engine operation optimization is done by calculating and optimizing fuel consumption and emissions, road performances (acceleration and deceleration), transmission ratios, braking performances, in order to determine the load for resistance and vibration calculation.

CRUISE allows modeling existing vehicles and new vehicle concepts with single or double traction (cars, trucks, motorcycles, etc) (Fig. 1).

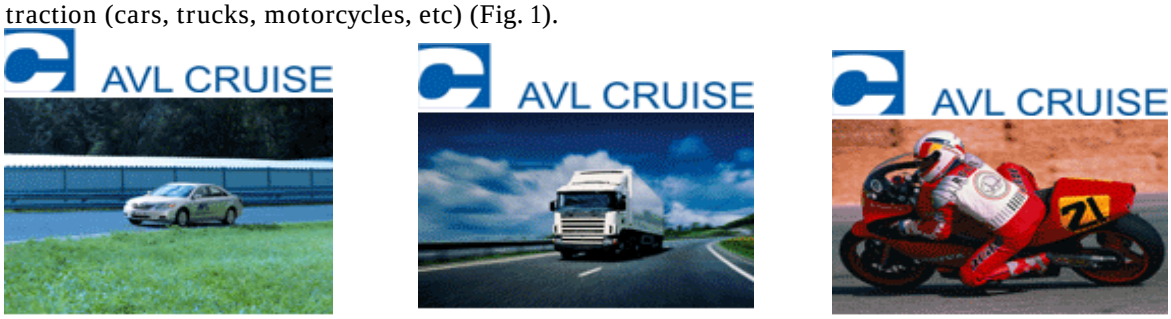

Fig. 1. Vehicle types that can be modeled with AVL CRUISE

AVL CRUISE simulation platform vehicle emphasizes:

- Optimization of vehicle and vehicle components (fuel economy, vehicle performance);
- Extensive range of vehicles and possible propulsion configurations;
- Assessment of new vehicle concepts (i.e., hybrid, electric vehicles, fuel cells);
- Transitory propulsion effects analysis;
- Design of vehicle thermal management systems;
- Smart driving module to reproduce the real vehicle behavior.

2. CALCULATION POSSIBILITIES

The software enables simple or mixed kinematic calculation (dynamic modeling) to study low frequencies, vibrations occurred during vehicle running, the axis torque (power shaft or rear and front axles).

Calculations can be made in quasi-stationary regime or allow the engine real cycle simulation, where the throttle shutter position can be controlled.

The calculation allows the following:

- Fuel consumption and emissions determination under the next driving conditions:
  - *Running cycle* – for driving, a simulated speed profile is imposed to the vehicle. Driving conditions are specified: runway slope, wind speed, the rolling friction coefficient, etc. Speed profile data can be entered as time and distance dependent values.
  - *Cruise* - running on a real route can be simulated. Speed profile based on distance is defined as the maximum speed that cannot be overtaken. Additional maximum values for acceleration and deceleration can be defined. These values can be used by the driver, but does not interact with the maximum load when the speed profile is suddenly changed.
  - *Constant speed* - involves running in all gears.
- Driving performances determination consists of acceleration behavior calculation which indicates the increase of performances and traction force, by following (Fig.2):
  - Running at constant speed;
  - Performances increase;
  - Acceleration at full load;
  - Maximum traction force;
  - Vehicle handling.

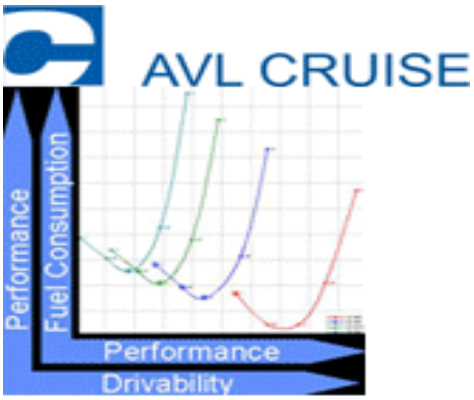

Fig. 2 Fuel consumption, performances and vehicle handling efficiency

CRUISE provides interfaces with MATLAB and Simulink through a DLL created by Real-Time Workshop or through a MATLAB API. The MATLAB API interface enables the user to run Simulink in the background and use scopes as well as variable time step integration methods.

Simulink is an environment for multidomain simulation and Model-Based Design for dynamic and embedded systems.

3. SYSTEM AND SUB-SYSTEM STRUCTURE

Components and their connections can be grouped into sub-systems and can be activated or deactivated so that side-bar configurations of active sub-system can be defined.

All systems contain the same systems; they differ only by their activation status. The structure of the systems/sub-systems and their activation status is shown in the navigation tree and also in the side-bar systems section of the vehicle modeler (Fig. 3, Fig.4). Correlations between AVL Cruise interface and other programs are very easy and allow too modify and interact all the time in the modellation process. A lot of paremeters can be easly monitorized through the interfaces, either AVL Cruise or the other program that waork together with (Fig.5).

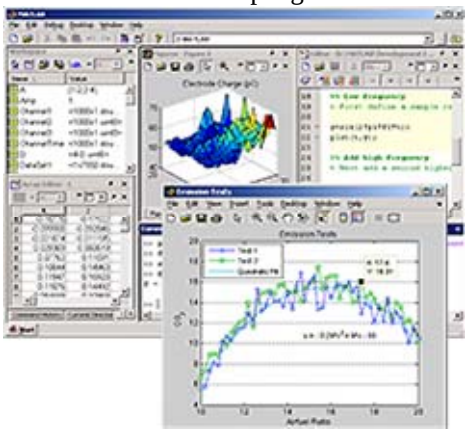
Fig. 3. MATLAB Interface

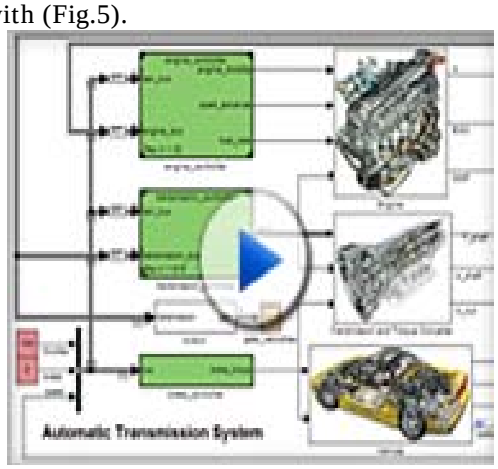

Fig. 4. Simulink simulation environment

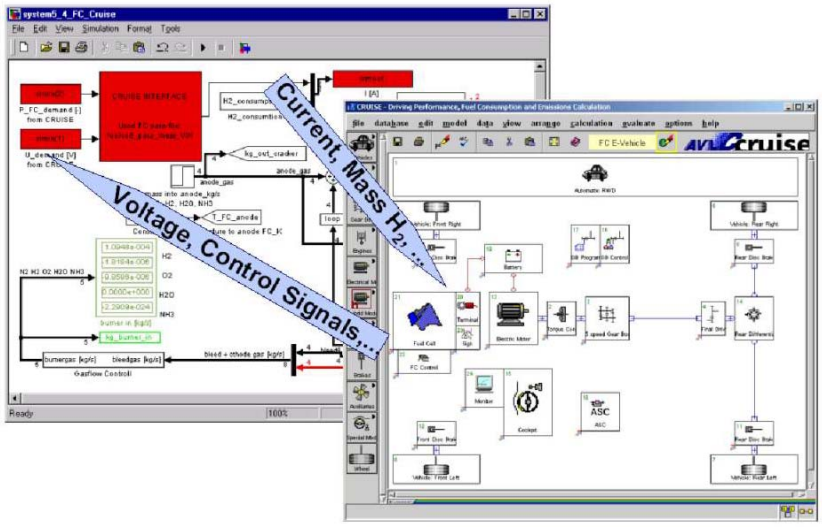

Fig.5. Direct correlation between AVL Cruise Interface and Matlab/Simulink environment

4. ANALYSIS AND SIMULATION RESULTS

The technical data of a BMW 535i E28 vehicle having above 200000 km run and 11 PTI were used for simulation.

After selecting Vehicle in the Main Window, it can be chosen between the following power train configurations: general, manual standard or automatic standard.

For Vehicle Modeling the components are organized into component groups and they can simply be dragged and dropped onto the working area, where they can be linked together to represent the desired power train configuration (Fig.6).

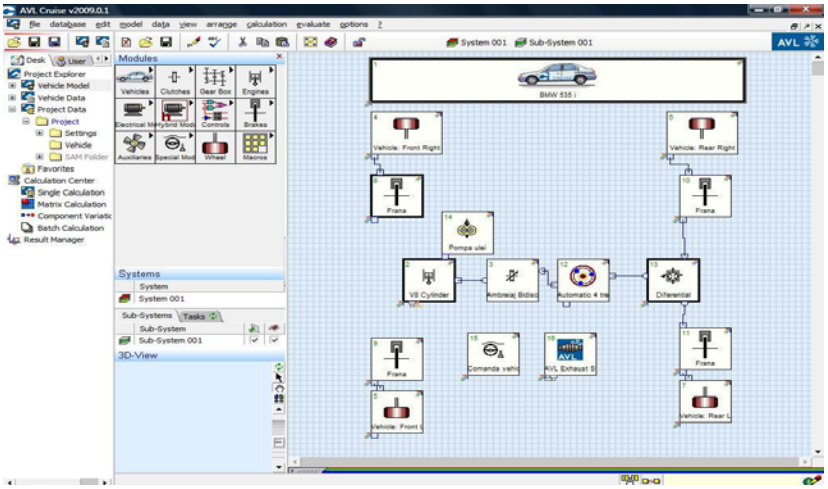

Fig. 6. Vehicle Modeler View

Each component contains the Properties option as is shown in Fig. 7. The calculation can be influenced in the Properties window. With these settings it is also possible to run a calculation with minimal input data (i.e., in prototype phase), as the input fields of the unavailable data can be switched off.

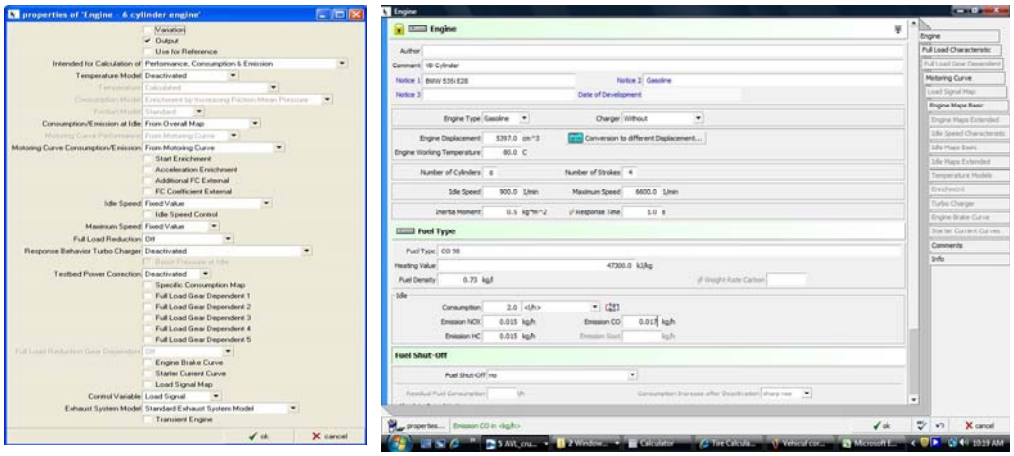

Fig. 7. Engine Properties

After simulation there were obtained: load characteristic (Fig. 8), torque characteristic (Fig. 9) and their dependence in 3D representation (Fig. 10), and also the fuel consumption variation (Fig.11).

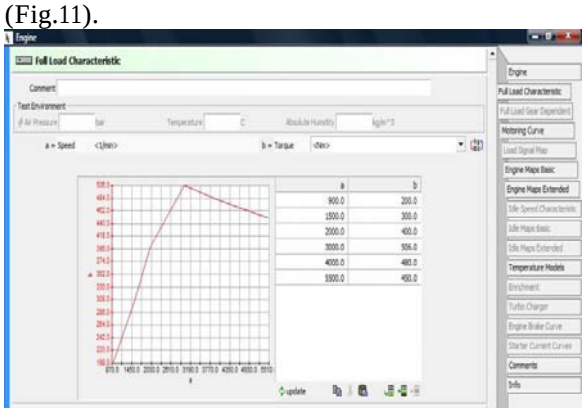

Fig. 8 Load Characteristic

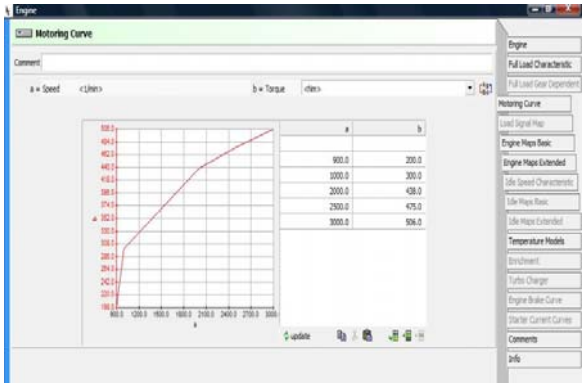

Fig. 9 Torque Characteristic

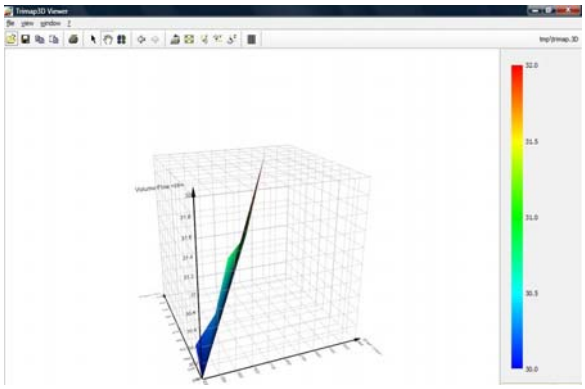

Fig. 10 Engine characteristics in 3D Representation

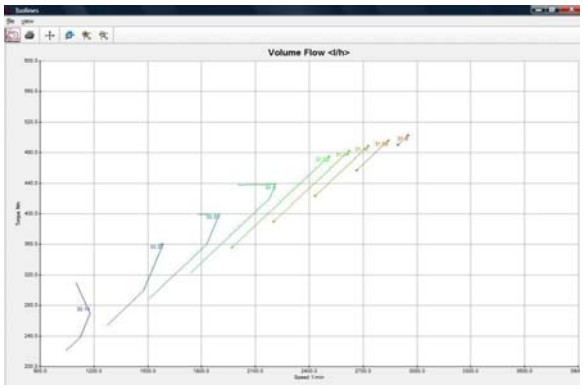

Fig. 11 Fuel Consumption Variation versus Engine Torque and Speed

5. CONCLUSIONS

CRUISE allows the calculation of driving performance, fuel consumption and emissions, the various driving cycle evaluation (i.e., FTP72, ECE-R15, HDC), traction curves, acceleration, maximum speed, hill climbing ability, etc.

The characteristics include the modular concept, the implementation of vehicle simulation, elastic shafts torsion and engine cold start.

Its modularity enables modeling of vehicles running on the basis of the available modules (engine, gearbox, clutch, etc.) as well as novel concepts achievement such as hybrid cars or cars with several engines.

CRUISE enables the characteristic curves and maps interactive modification. The data is represented in a graph and table form at the same time. Modifications are possible in either of these representations. Data map can be directly introduced or can be read from ASCII files. The application of arithmetic functions on certain single points or the entire curve is possible.

REFERENCES

[1.] Gillespie, T.D., Fundamentals of Vehicle Dynamics, SAE International, 1992
[2.] AVL CRUISE v.2009, Technical Documentation
[3.] http://www.mathworks.com/products/connections/product_detail/product_35685.html
[4.] http://www.figes.com.tr/carmaker/dokuman/CarMaker_0702.pdf

INTERNATIONAL SYMPOSIUM on
ADVANCED ENGINEERING & APPLIED MANAGEMENT
– 40th ANNIVERSARY in HIGHER EDUCATION (1970-2010)
4 – 5 November, 2010, Hunedoara, ROMANIA

[1.] Siby ABRAHAM, [2.] Imre KISS, [3.] Sugata SANYAL, [4.] Mukund SANGLIKAR

STEEPEST ASCENT HILL CLIMBING FOR A MATHEMATICAL PROBLEM

[1.] DEPT. OF MATHS & STATS, G. N. KHALSA COLLEGE, UNIVERSITY OF MUMBAI, MUMBAI, INDIA
[2.] DEPT. OF ENG & MANAGEMENT, FACULTY OF ENGINEERING HUNEDOARA,
UNIVERSITY POLITECHNICA TIMISOARA, ROMANIA
[3.] SCHOOL TECH & COMP SC, TATA INST. OF FUNDAMENTAL RESEARCH, MUMBAI, INDIA
[4.] DEPT. OF MATHEMATICS, MITHIBAI COLLEGE, UNIVERSITY OF MUMBAI, MUMBAI, INDIA

ABSTRACT:
The paper proposes artificial intelligence technique called hill climbing to find numerical solutions of Diophantine Equations. Such equations are important as they have many applications in fields like public key cryptography, integer factorization, algebraic curves, projective curves and data dependency in super computers. Importantly, it has been proved that there is no general method to find solutions of such equations. This paper is an attempt to find numerical solutions of Diophantine equations using steepest ascent version of Hill Climbing. The method, which uses tree representation to depict possible solutions of Diophantine equations, adopts a novel methodology to generate successors. The heuristic function used help to make the process of finding solution as a minimization process. The work illustrates the effectiveness of the proposed methodology using a class of Diophantine equations given by $a_1 . x_1^{p1} + a_2 . x_2^{p2} + \ldots\ldots\ldots + a_n . x_n^{pn} = N$ where a_i and N are integers. The experimental results validate that the procedure proposed is successful in finding solutions of Diophantine Equations with sufficiently large powers and large number of variables.
KEYWORDS:
artificial intelligence technique, hill climbing, Diophantine Equations

1. INTRODUCTION

A Diophantine Equation [Cohen 2007] [Rossen 1987] [Zuckerman 1980] is a polynomial equation, given by

$$f(a_1, a_2, \ldots, a_n, x_1, x_2, \ldots, x_n) = N \quad (1)$$

where a_i and N are integers. These equations, which were initially studied in detail by third century BC Alexandrian Mathematician Diophantus [Bashmakova 1997] [Bag 1979], have many different types. The simplest ones are the linear equations given by:

$$ax_1 + bx_2 = c \quad (2)$$

The equations of the form

$$x_1^2 + x_2^2 = x_3^2 \quad (3)$$

are important as they give solutions, which are Pythagorean triplets. In 1665, French Mathematician Fermat popularized such equations by famously stating that equations of the form

$$x_1^n + x_2^n = x_3^n \quad (4)$$

have no solutions for n>2, though the world had to wait till 1994 for an actual proof, which used elliptic curves [Shirali & Yogananda 2003]. An elliptic curve (Stroeker and Tzanakis, 1994; Poonen, 2000) is a particular type of Diophantine equation given by

$$y^2 = x^3 + ax + b, \quad (5)$$

where and b are rational numbers and the right hand side of the equation (5) are given to have distinct roots. There are many such important equations in the collection of Diophantine equations.

Diophantine equations are used extensively in many fields. Elliptic curve based public key cryptosystems [Lin CH 1995][Laih CS 1997] [Koblitz 1984] offer better security provisions

comparing with other cryptosystems. The performance of super computers can be enhanced by parallelizing compilers to check the problem of data usage which can be reduced to characterization of a Diophantine equation [Zhiyu 1989]. Computable economics [Velu 2004] uses decision problems like Diophantine equations to propose a change in the market equilibrium conditions instead of the conventional parameters. Integer factorization [Knuth 1997] uses Diophantine equations in the process of breaking down a composite number into smaller non-trivial divisors. Diophantine equations are also used in other areas like algebraic curves [Ponnen 2000], projective curves [Brown & Myres 2002] [Stroeker & Tzanakis 1994] and theoretical computer science [Ibarra 2004][Guarari 1982]. These application areas make Diophantine equations an important domain not just in the realm of Mathematics but in other fields too.

Though Diophantine equations have a great historical background and have been used in many areas, there does not exist a general method to find solutions of such equations [Davis 1992] [Matiyasevich 1993]. Then, finding numerical solutions to such equations is the only next way out. This is a tough task as the computing complexity involved in such a process is quite high. In this regard, applying artificial intelligence techniques, which are known for maneuvering huge search space, is significant. Literature talks about few attempts to find numerical solutions of Diophantine equations using hard computing and soft computing techniques of Artificial Intelligence. Abraham and Sanglikar [Abraham and Sanglikar 2001] used basic genetic operators like mutation, inversion and crossover [Michalewich 1992] to find numeric solutions of some elementary equations. They [Abraham and Sanglikar 2007 a] later used a procedure called 'host parasite co-evolution' [Hills 1992] [Paredis 1996][Wiegand 2003] in a typical genetic algorithm to find numerical solutions. They also proposed [Abraham and Sanglikar 2007 b] a unique evolutionary and co-evolutionary [Rosin and Belew 1997] computing method to find numerical solutions of such equations. Joya et al [Joya et al., 1991] used higher order Hopfield neural networks to find solutions of Diophantine equations. Abraham and Sanglikar [Abraham and Sanglikar 2008] offered simulated annealing as a possible strategy to find solutions of these equations. Abraham et al [Abraham et al 2010] discussed in detail a particle swarm optimization based method to find numerical solutions of such equations. In addition to these methods based on soft computing, literature also mentions A * search based hard computing mechanism as a possible alternative to find numerical solutions of these equations [Abraham and Sanglikar 2009]. Hard computing methods are significant as they try to explore as many candidate solutions as possible in a systematic way unlike soft computing, which uses randomness in the process and hence risks of 'slipping away' the solutions on the way.

This paper proposes hill climbing as a hard computing artificial intelligence technique to find numerical solutions of Diophantine equations. Hill Climbing is a local search [Russel & Norwig 2003] technique. It starts with an initial solution and steadily and gradually generates neighboring successor solutions. If the neighboring state is better than the current state, we make the neighboring state the current state. The whole process can be taken as an optimization process [Lugar 2006]. There are different variants of hill climbing. They are simple hill climbing, steepest hill climbing, stochastic hill climbing and random restart hill climbing. The paper uses steepest ascent version of the hill climbing to find numerical solution of Diophantine equations. In steepest hill climbing all successor nodes are probed and compared for its relevance and then the best amongst them is taken as the successor node. This results in having an exhaustive local search and identification of the best possible successor of a given node at any instant of time.

2. HILL-DOES Methodology

The system developed to find numerical solutions of Diophantine equations using Hill climbing is based on the Steepest Ascent version of Hill Climbing and is called HILL-DOES. It uses a system of equations given by

$$a_1 . x_1^{p1} + a_2 . x_2^{p2} + ... + a_n . x_n^{pn} = N \quad (6)$$

where a_i and N are integers, for demonstrating the effectiveness of the system proposed.

2.1 Representation

The possible solutions of the Diophantine equation (6) are represented by a tree whose nodes are taken as n-vectors given by $(x_1, x_2, ..., x_n)$. The procedure starts with an initial solution, given to be (1, 1, 1, ... , 1) and uses two queues in its construction. The first queue, which is called PROBE-Q, is used to store the nodes, which have been probed. The second queue, which is referred as NOPROBE-Q, is used to store the nodes, which have been generated but not better than the current node. These two queues help to separate the generated nodes into two distinct classes – 'probed nodes' and 'not-probed nodes'.

2.2 Successor nodes

Successor nodes of the current node are generated in HILL-DOES using specially defined production rules. The production rules applied are given by:

$(x_1, x_2, ..., x_i, ... , x_n) \rightarrow (x_1, x_2, ..., x_{i+1}, ... , x_n)$ for i =1, 2, ..., n (7)

These production rules help to generate all possible nodes in the vicinity of the current node. Hill climbing, being a local search technique, needs to explore all possible nodes within the neighborhood of the current node. The successor nodes generated in this way, take care of this requirement of the search strategy.

2.3 Heuristic function

The heuristic function used to evaluate the effectiveness of a node $(x_1, x_2, x_3, ..., x_n)$ in the search process is given by

$$H(x_{1,} x_{,2 .....,} x_n) = N - (a_1x_1^{p1} + a_2x_2^{p2} + a_3x_3^{p3} + ... + a_nx_n^{pn}) \quad (8)$$

Since the objective of the procedure is to find numerical solutions of equation (6), the problem reduces to find a vector given by $(x_1, x_2, ..., x_n)$ with $H(x_{1,} x_{,2 .....,} x_n) = 0$. The value of 'H' shows how far is a given node away from the goal node. Lower the value of 'H', closer is the node to the solution. However, the negative value of 'H' requires some extra care to make the search process on track. Whenever H value becomes negative, the proposed procedure does not expand the corresponding node even if that has better heuristic function value compared to others. Instead, the node with the next better heuristic function value is expanded and the process is continued. In other words, the nodes having negative H values are replaced with the better nodes from the NO-PROBEQ.

2.4 Backtracking

It is possible to have a current node, with all its successor nodes having inferior heuristic values in comparison with that of the current node. Steepest ascent hill climbing always demands having better nodes as successor nodes to continue the procedure. This drawback of hill climbing is overcome in the procedure by incorporating a strategy of backtracking. As per this, when the procedure fails to produce better nodes as successor nodes, it leaves the current node and goes back or backtracks to the previous best node generated. Then, the exploration process resumes from that node and the process of traversing through the tree in another path is followed. It is quite possible that during the search process, the procedure might hit on such inferior successor nodes on a regular basis. At these instances, the procedure is continued with backtracking at each and every instance. This way an unhindered search procedure is guaranteed always in HILL-DOES.

2.5 Algorithm

The basic steepest ascent hill climbing algorithm is slightly restructured to be acquainted with the constraints of Diophantine equations. The algorithm used in HILL-DOES is explained in the following lines.

Step1: Initialize node, which is usually (1, 1, ... , 1). Evaluate it.
Put it in the PROBE-Q.

Step2: If PROBE-Q is empty, then stop.

Step3: Pick first node from PROBE-Q. Label it as current node: C-Node.

Step4: If C-Node is the goal node then return C-Node as a solution.
(Goal state is reached when $H(x_{1,} x_{,2 .....,} x_n) = 0$

Step5: If C-Node is not a goal node, check whether $H(x_{1,} x_{,2 .....,} x_n) > 0$

a) If yes, generate successors of C-Node and evaluate them.
b) If no, Go to step 2.

Step6: Compare successors of C-node and the better node amongst them.
Store the remaining nodes in the NOPROBE-Q.

a) If the better node is better than C-Node and if it has not been probed before, then make it C-Node. If it has been probed, then pick the first element from NOPROBE-Q and make it as the C-Node. Put C-Node in the PROBE-Q.
b) If the better node is not better than C-Node, then pick the first element from the NOPROBE-Q, make it as the C-Node and put in PROBE-Q. If NOPROBE-Q is empty, then do nothing.

Step6: Go to step 2.

The algorithm as it is used in HILL-DOES is illustrated using a simple Diophantine Equation given by $x_1^2 + x_2^2 = 100$. The initial node is (1, 1) and $H(1, 1) = 100 - (1^2 + 1^2) = 98$.

Step1: Put (1, 1) in PROBE-Q.

Step3: C-Node = (1,1).

Step5: Since it is not a goal node and H(C-Node) = 98 > 0 , generate Successors of it.

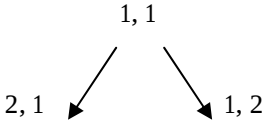

Step6: Both (2,1) and (1, 2) have the same heuristic function value 95. So, choose any one say (2,1). Put (2,1) in PROBE-Q and (1, 2) in NOPROBE-Q. Generate children of (2,1).

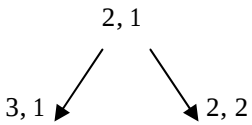

Since the heuristic value of node (3, 1) is 90, which is better than the heuristic value 92 of the node (2, 2) and 95 of (2, 1) we select (3, 1) as the next node to be expanded. Continue this process of generating successors and identifying the best amongst them to be C- Node, which is illustrated in figure 1. If the process gets stuck in not finding a better successor, back track to the previous node and continue the process of exploration until a node with heuristic function value zero is generated. Such a node will be the solution of the given Diophantine equation.

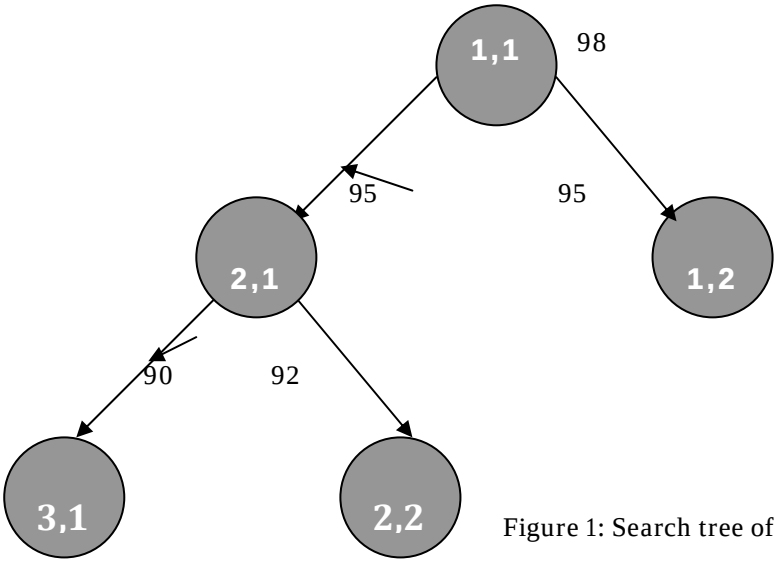

Figure 1: Search tree of $x_1^2 + x_2^2 = 100$

3. ANALYSIS, DISCUSSION AND INTERPRETATION

The procedure discussed in HILL-DOES has been implemented in Java. The user supplies the details of the equation like number of variables involved, coefficients, powers and the value of N. The experimental results have been analyzed and discussed in the following sections.

3.1 Nodes Generated

Figure 2 shows the nodes generated by HILL-DOES for an elementary equation $x_1^2 + x_2^2 = 149$, before finding the first solution (10,4). The process generated 68 nodes during the search process. The figure shows the steady search of the process in the search space. Figure 3 demonstrates the convergence of heuristic function values of the nodes generated in the same demonstration. Initially, there is a sudden reduction of heuristic function values and once the process becomes mature, there is a directed approach towards the value zero, finally resulting in the solution.

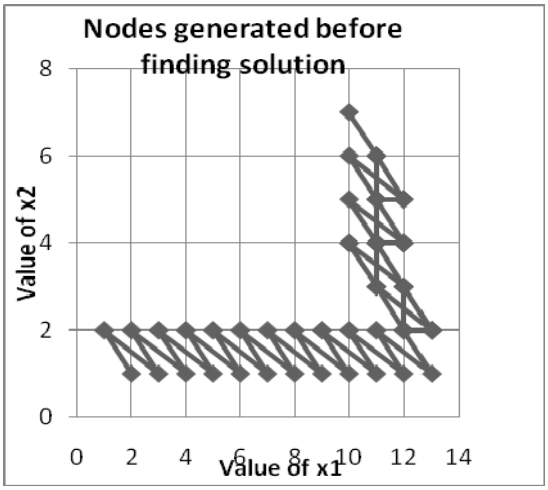

Figure 2: Nodes generated during the search

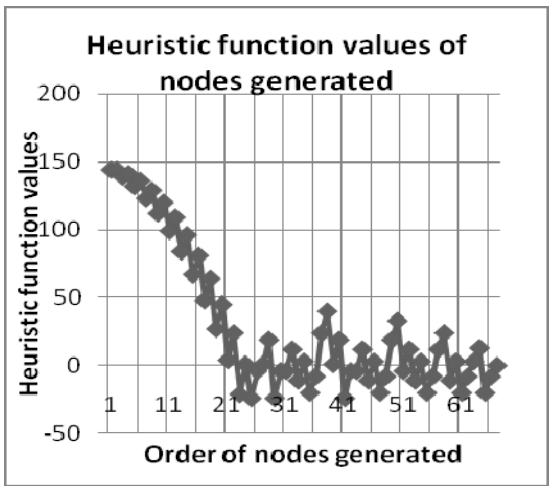

Figure 3: Heuristic function values of nodes

3.2 Results on equations with varying degrees

Table 1 demonstrates the results obtained when the system was run for different Diophantine equations with varying values for the degrees. It shows that irrespective of reasonably large values for degrees and higher values of N, the system could give solutions within a smaller number of iterations. This points out that those large values of N do not affect the efficiency of the system. In addition, the comparatively lesser number of iterations only consumed for finding the solutions also validate the effectiveness of the system in finding solutions of Diophantine equations with larger value of N.

Table 1: Results on equations with varying degrees

No	Diophantine Equation	Degree of equation	Solution found	Iterations
1	$x_1^{\,2} + x_2^{\,2} = 625$	2	24,7	29
2	$x_1^{\,3} + x_2^{\,3} = 1008$	3	10, 2	10
3	$x_1^{\,4} + x_2^{\,4} = 1921$	4	6, 5	9
4	$x_1^{\,5} + x_2^{\,5} = 19932$	5	7, 5	10
5	$x_1^{\,6} + x_2^{\,6} = 47385$	6	6, 3	7
6	$x_1^{\,7} + x_2^{\,7} = 4799353$	7	9, 4	11
7	$x_1^{\,8} + x_2^{\,8} = 16777472$	8	8, 2	8
8	$x_1^{\,9} + x_2^{\,9} = 1000019683$	9	10, 3	11
9	$x_1^{\,10} + x_2^{\,10} = 1356217073$	10	8, 7	13

3.3 Results on equations with varying number of variables

Table 2 shows the results obtained when HILL-DOES was run on Diophantine equations with varying number of variables. This shows that the system provides solutions even when the number of variables is competitively high.

Table 2: Results on equations with varying number of variables

No	Diophantine Equation	Degree of equation	Solution found	Iteration required
1	$x_1^{\,2}+x_2^{\,2} = 149$	2	10, 7	34
2	$x_1^2+x_2^2+x_3^2 = 230$	3	15, 2, 1	15
3	$x_1^2+x_2^2+...+x_4^2= 295$	4	17, 2, 1, 1	17
4	$x_1^2+x_2^2+....+x_5^2= 325$	5	17, 1, 1, 3, 5	22
5	$x_1^2+x_2^2+....+x_6^2= 420$	6	20, 1, 1, 1, 1, 4	22
6	$x_1^2+x_2^2+....+x_7^2= 450$	7	21, 2, 1, 1, 1 ,1	21
7	$x_1^2+x_2^2+....+x_8^2= 590$	8	23, 2, 1, 1, 1,1, 2, 7	86
8	$x_1^2+x_2^2+....+x_9^2= 720$	9	26, 2, 1, 1, 1, 2, 2, 2, 5	42
9	$x_1^2+x_2^2+....+x_{10}^2=956$	10	30, 2, 1, 1, 1,1, 2, 2, 2, 6	48

4. CONCLUSION

The paper presents steepest ascent hill climbing search based procedure to find numerical solution of Diophantine equations. Local optimum points were tackled by resorting to backtracking as and when the procedure hit on such local optimum points. The experimental results showed that the technique work fine for Diophantine equations of varied types. However, the solutions generated, especially when the number of variables is large, have the tendency to have the coordinates closely placed. Further enhancement to the work is directed at addressing this issue.

REFERENCE

[1.] [Abraham & Sanglikar 2001]: Abraham, S and Sanglikar, M; 'Diophantine equation solver-a genetic algorithm application', Mathematical Colloquium Journal, Vol. 15, No 3, pp 16-20, 2001.

[2.] [Abraham & Sanglikar 2007a]: Abraham, S and Sanglikar, M; 'Nature's way of avoiding premature convergence: a case study of Diophantine equations', Proceedings of the International Conference on Advances in Mathematics: Historical Developments and Engineering Applications, Pantnagar, Uttarakhand, India, 19–22 December, pp 182, 2007.

[3.] [Abraham & Sanglikar 2007b]: Abraham, S and Sanglikar, M; 'Finding solution to a hard problem: an evolutionary and co-evolutionary approach' Proceedings of the International Conference on Soft Computing and Intelligent Systems, Jabalpur, India,27–29 December, pp 262-267, 2007.

[4.] [Abraham & Sanglikar 2008]: Abraham, S and Sanglikar, M; 'Finding numerical solution to a Diophantine equation: simulated annealing as a viable search strategy', Proceedings of the International Conference on Mathematical Sciences, United Arab Emirates University, Al Ain, UAE, 3–6, pp 319, March, 2008.

[5.] [Abraham & Sanglikar 2009]: Abraham, S and Sanglikar, M; 'A* search for a challenging problem', Proceedings of the 3rd Internl Confer.on Maths and Computer Science, Loyola College, Chennai, 5th–6th January, pp 453-457, 2009.

[6.] [Abraham et al 2010]: Abraham, S; Sanyal, S and Sanglikar, M; 'Particle Swarm Optimization based Diophantine Equation Solver', International Journal of Bio-inspired Computation, Vol 2, No 2, pp 100-114, 2010.
[7.] [Bag 1979]: Bag A K; 'Mathematics in ancient and medieval India', Chaukhambha Orientalia, Delhi, 1979.
[8.] [Bashmakova 1997]: Bashmakova et al; 'Diophantus and Diophantine Equations, Mathematical Association of America, 1997.
[9.] [Brown & Myers 2002]: Brown, E. and Myers, B; 'Elliptic curves from Model to Diophantus and Back', The Mathematical Association of America Monthly, August–September, Vol. 109, pp.639–649, 2002.
[10.] [Cohen 2007]: Cohen, H; Number Theory, Vol. I: Tools and Diophantine Equations and Vol. II: Analytic and Modern Tools, Springer-Verlag, pp. 239- 240, 2007.
[11.] [Davis 1982]: Davis, M; 'Hilbert's tenth problem is unsolvable', Computability and Unsolvability, Appendix 2, 1999-235, Dover, New York, 1982.
[12.] [Guarari 1982]: Guarari, E.M; 'Two way counter machines and Diophantine equations', Journal of ACM, Vol. 29, No. 3, 1982.
[13.] [Hills 1992]: Hills, W.D; 'Co-evolving parasites improve simulated evolution as an optimization procedure', Artificial Life, Addison Wesley, Vol. 2, 1992.
[14.] [Ibarra et al. 2004]: Ibarra, O.H. et al; 'On two way FA with monotone counters and quadratic Diophantine equations', Theoretical Computer Science, Vol. 312, pp.2–3, 2004.
[15.] [Joya et al 1991]: Joya et al; 'Application of Higher order Hopfield neural networks to the solution of Diophantine equation', Lect. Notes in Comp Sc, Vol.540, Springer, 1991.
[16.] [Knuth D 1997]: Knuth, D; 'The Art of Computer Programming, Volume 2: Semi-numerical Algorithms', Third Edition. Addison-Wesley, 1997.
[17.] [Koblitz 1984]: Koblitz, N; Introduction to Elliptic Curves and Modular Forms, Springer, 1984.
[18.] [Laih. et al., 1997]: Laih, C.S. et al; 'Cryptanalysis of Diophantine equation oriented public key cryptosystem', IEEE Transactions on Computers, April, Vol. 46, 1997.
[19.] [Lin et al. 1995]: Lin, C.H. et al 'A new public-key cipher system based upon Diophantine equations', IEEE Transactions on Computers, January, Vol. 44, 1995.
[20.] [Luger 2006]: Luger, G.L; Artificial Intelligence: Structures and Strategies for Complex Problem Solving, 4e Pearson Education, 2006.
[21.] [Matiyasevich 1993]: Matiyasevich, Y.V; Hilbert's Tenth Problem, MIT press, 1993.
[22.] [Michalewich 1992]: Michalewich, Z; GA + Data Structures = Evaluation Programs, Springer Verlag, 1992.
[23.] [Paredis, J. 1996]: Paredis, J; 'Co-evolutionary computation', Artificial Life Journal, Vol. 2, No. 3, 1996.
[24.] [Poonen 2000]: Poonen, B; 'Computing rational points on curves', Proceedings of the Millennial Conference on Number Theory, 21–26 May, University of Illinois at Urbana-Champaign, 2000.
[25.] [Rosin & Belew 1997]: Rosin, C.D. and Belew, R.K; 'New methods for competitive co-evolution', Evolutionary Computation, Vol. 5, No. 1, pp.1–29, 1997.
[26.] [Rossen, K. 1987]: Rossen, K; Elementary Number Theory and its Applications, Addison, 1987.
[27.] [Russell &Norwig 2003]: Russell, S. and Norwig, P; Artificial Intelligence– A Modern Approach, 2nd ed., Pearson, 2003.
[28.] [Shirali & Yogananda 2003]: Shirali, S. and Yogananda, C.S; 'Fermat's last theorem: a theorem at last', Number Theory: Echoes From Resonance, University Press, 2003.
[29.] [Stroeker & Tzanakis 1994]: Stroeker & Tzanakis,"Solving elliptic Diophantine equations by estimating linear forms in elliptic logarithms, Acta Arithmetica, Vol. 67, No. 2, 1994.
[30.] [Velu 2000]: Velu Pillai K; Computable Economics: The Arne Memorial Lecture Series, Oxford University Press, 2000.
[31.] [Wiegand 2003]: Wiegand, P; 'An analysis of cooperative co-evolutionary algorithms', PhD dissertation, George Mason University, 2003.
[32.] [Zhiyu 1989]: Zhiyu, S., Li, Z., Yew, P.C. 'An empirical study on array subscripts and data dependencies', CSRD Report 840, August, 1989.
[33.] [Zuckerman 1980]: Zuckerman; An Introduction to the theory of numbers', 3rd ed., Wiley, 1980.